RD & W 2005

PS 186 A

ISSN 0968-0462

Bulletin of The Natural History Museum

THE NATURAL HISTORY MUSEUM
27 AUG 2002
PRESENTED
PALAEONTOLOGY LIBRARY

Geology Series

THE NATURAL HISTORY MUSEUM

VOLUME 58 NUMBER 1 27 JUNE 2002

The *Bulletin of The Natural History Museum* (formerly: *Bulletin of the British Museum (Natural History)*), instituted in 1949, is issued in four scientific series, Botany, Entomology, Geology (incorporating Mineralogy) and Zoology.

The Geology Series is edited in the Museum's Department of Palaeontology

Keeper of Palaeontology:	Dr N. MacLeod
Editor of Bulletin:	Dr M.K. Howarth
Assistant Editor:	Mr C. Jones

Papers in the *Bulletin* are primarily the results of research carried out on the unique and ever-growing collections of the Museum, both by the scientific staff and by specialists from elsewhere who make use of the Museum's resources. Many of the papers are works of reference that will remain indispensable for years to come. All papers submitted for publication are subjected to external peer review for acceptance.

SUBSCRIPTIONS Bulletin of the Natural History Museum. Geology Series (ISSN 0968-0462) is published twice a year (one volume per annum) in June and November. Volume 58 will appear in 2002. The 2002 subscription price (excluding VAT) of a volume, which includes print and electronic access, is £88.00 (US $155.00 in USA, Canada and Mexico). The electronic-only price available to institutional subscribers is £79.00 (US $140.00 in USA, Canada and Mexico).

ORDERS Orders, which must be accompanied by payment, may be sent to any bookseller, subscription agent or direct to the publisher: Cambridge University Press, The Edinburgh Building, Shaftesbury Road, Cambridge CB2 2RU, UK; or in the USA, Canada and Mexico: Cambridge University Press, Journals Department, 40 West 20th Street, New York, NY 1011-4211, USA. EU subscribers (outside the UK) who are not registered for VAT should add VAT at their country's rate. VAT registered members should provide their VAT registration number. Japanese prices for institutions (including ASP delivery) are available from Kinokuniya Company Ltd, P.O. Box 55, Chitose, Tokyo 156, Japan. Prices include delivery by air. Postmaster: send address changes in USA, Canada and Mexico to: Bulletin of the Natural History Museum. Geology Series, Cambridge University Press, 110 Midland Avenue, Port Chester, New York, NY 105783-4930. Claims for missing issues should be made immediately on receipt of the subsequent issues.

Orders and enquiries for issues prior to 2002 should be sent to: Intercept Ltd., P.O. Box 716, Andover, Hampshire SP10 1YG, *Telephone*: (01264) 334748, *Fax*: (01264) 334058, *Email*: intercept@andover.co.uk, *Internet*: http:/www.intercept.co.uk

ADVERTISING Apply to the Publisher. Address enquiries to the Advertising Promoter.

COPYRIGHT AND PERMISSIONS This journal is registered with the Copyright Clearance Center, 222 Rosewood Drive, Danvers, MA 01923, USA. Organizations in the USA who are also registered with C.C.C. may therefore photocopy material (beyond the limits permitted by Section 107 and 108 of U.S. Copyright law) subject to payment to C.C.C. of the per-copy fee of $16.00. This consent does not extent to multiple copying for promotional or commercial purposes. Code 0968-0462/2002 $16.00. ISI Tear Sheet Service, 3501 Market Street, Philadelphia, PA 19104, USA, is authorised to supply single photocopies of separate articles for private use only. Organizations authorised by the UK Copyright Licensing Agency may also copy material subject to the usual conditions. For all other use, permission should be sought from Cambridge University Press.

No part of this publication may otherwise be reproduced, stored or distributed by any means without permission in writing from Cambridge University Press, acting for the copyright holder.

ELECTRONIC ACCESS This journal is included in the Cambridge Journals Online service which can be found at: http://journals.cambridge.org

For further information on other Press titles access http://uk.cambridge.org or http://us.cambridge.org

World list abbreviation: Bull. nat. Hist. Mus. Lond. (Geol.)

Copyright © 2002 The Natural History Museum

Geology Series Vol. 58, No. 1, pp. 1–79

ISSN 0968–0462

The Natural History Museum
Cromwell Road
London SW7 5BD

Issued 27 June 2002

Typeset by Ann Buchan (Typesetters), Middlesex
Printed in Great Britain by Henry Ling Ltd, at the Dorset Press, Dorchester, Dorset

Bull. nat. Hist. Mus. Lond. (Geol.) **58**(1): 1–11 Issued 27 June 2002

Gough's Cave 1 (Somerset, England): a study of the axial skeleton

THE NATURAL HISTORY MUSEUM
27 AUG 2002
PRESENTED
PALAEONTOLOGY LIBRARY

STEVEN E. CHURCHILL
Department of Biological Anthropology and Anatomy, Duke University, Durham NC 27708, USA
TRENTON W. HOLLIDAY
Department of Anthropology, Tulane University, New Orleans LA 70118, USA

SYNOPSIS. The postcranial axial skeleton of Cheddar Man (Gough's Cave 1) is represented by seventeen presacral vertebrae, the sacrum, and nineteen ribs, all of which are relatively well-preserved. Cheddar Man derives from early Holocene deposits in Gough's Cave, and the remains of his axial postcranial skeleton are described here. Comparative evaluation of the Gough's Cave 1 remains reveals an axial skeleton that falls within the range of variation in size and shape of males of the same time period, albeit towards the small end of that range (reflecting relatively short stature in Cheddar Man).

INTRODUCTION

The postcranial axial skeleton of Cheddar Man is represented by a single cervical vertebra, eleven thoracic vertebrae, all five lumbar vertebrae, sacrum, and nineteen ribs. The hyoid, manubrium, sternum and xiphoid process were not recovered. The preservation of the recovered vertebrae is generally good, with many being complete. Sequencing of vertebrae was based on size, details of morphology of the articular facets, neural arches, and transverse and spinous processes, and by evaluating the articulation of each element with the identified supra- and subjacent vertebrae (Bass, 1987; Steele & Bramblett, 1988). Prior efforts to reconstruct the entire articulated vertebral column for museum display involved the gluing of fibrous pads (to represent the intervertebral discs) to the bodies of many of the vertebrae, and in some cases elements were glued to 'mocked up' replicas of the missing vertebrae, making observation and measurement of morphology difficult (only the fifth and eighth thoracic and the third lumbar vertebrae could be entirely separated from reconstructive materials: these specimens were thus singled out for photography). The ribs are also in a very good state of preservation overall; more than half of them preserve the head, neck and tubercles proximally and most are complete distally to the area around the anterior angle. Sequencing of ribs was accomplished by examining overall size and shape, the position of the *M. iliocostalis* line, size and shape of the articular facets, and the height of the rib heads (with the inferior bodies held in the same plane) relative to one another (Mann, 1993). A number of the ribs bear cut marks that may be attributable to stone tools.

Each vertebra is briefly described, followed by a discussion of the vertebral morphology of Gough's Cave 1 (the sacrum is described along with the os coxae in Trinkaus, this series). The ribs are then likewise described and their morphology discussed.

MATERIALS AND METHODS

The description of the Gough's Cave 1 axial postcranial remains is augmented by osteometric data and comparisons with various samples of fossil and recent humans. The necessity of accurate identification of vertebral and costal number (i.e., the position of the element in the series) for collection of comparative data presents difficulties in working with fragmentary fossil material (see Franciscus & Churchill, 2002). For vertebral morphology, comparative osteometrics were collected on European terminal Pleistocene specimens (all associated with Late Upper Paleolithic assemblages, and dating between 19,000 and 11,000 ybp) and early Holocene specimens (associated with Mesolithic assemblages and dating between 10,000 and 5,000 ybp). These two samples thus bracket in age the Gough's Cave 1 skeleton. The terminal Pleistocene sample includes Arene Candide 2, 4, 5, 10 and 12, Bichon 1, Bruniquel 24, Cap Blanc 1, Chancelade 1, Grotta Contineza, Grotte des Enfants 3, La Madeleine, Oberkassel 1 and 2, Parabita 1 and 2, Le Peyrat 5 and 6, Romito 4, St. Germain La Rivière 4 and Veyrier 1 (Paoli *et al.*, 1980; Simon & Morel, nd; Genet-Varcin & Miquel, 1967; von Bonin, 1935; Vallois, 1941–46, 1972; Verneau, 1906; de Quatrefages & Hamy, 1882; Verworn *et al.*, 1919; Cremonesi *et al.*, 1972; Patte, 1968; Graziosi, 1962; Vallois, 1972; Pittard & Sauter, 1945). The early Holocene sample is composed of Los Azules, Gramat 1, Hoëdic 8 and 9, Rastel 1, Téviec 1, 11 and 16 (Fernández-Tresguerres, 1976; Lacam *et al.*, 1944; Barral & Primard, 1962; Péquart *et al.*, 1937). Additional comparative data was collected on recent Europeans (n = 125), north Africans (n = 61) and sub-Saharan Africans (n = 26) (details of sample composition are provided in Holliday, 1995). For the ribs, comparative data is limited to a small sample of recent European-Americans (n = 20: Franciscus & Churchill, 2002).

Operational definitions of the measurements employed can be found in Martin (1928) or as footnotes to Tables. Vertebral osteometrics are provided in Tables 1–3, costal osteometrics are in Tables 6–8. All measurements were taken by the authors on the original specimens; measurements quoted in brackets in Tables 1–9 are estimated values.

VERTEBRAL REMAINS

Descriptions

CERVICAL VERTEBRA 6 OR 7 (FIG. 1)

A single cervical vertebra, complete except for some damage to the left side ventral surface of the corpus, is preserved (at bottom of Fig. 1). Based on its size and neural arch morphology (the transverse processes are large and laterally flaring) it appears to be either the 6th or 7th cervical vertebra (this element is attached superiorly to a 'mocked up' cervical vertebral column, thus preventing examination

© The Natural History Museum, 2002

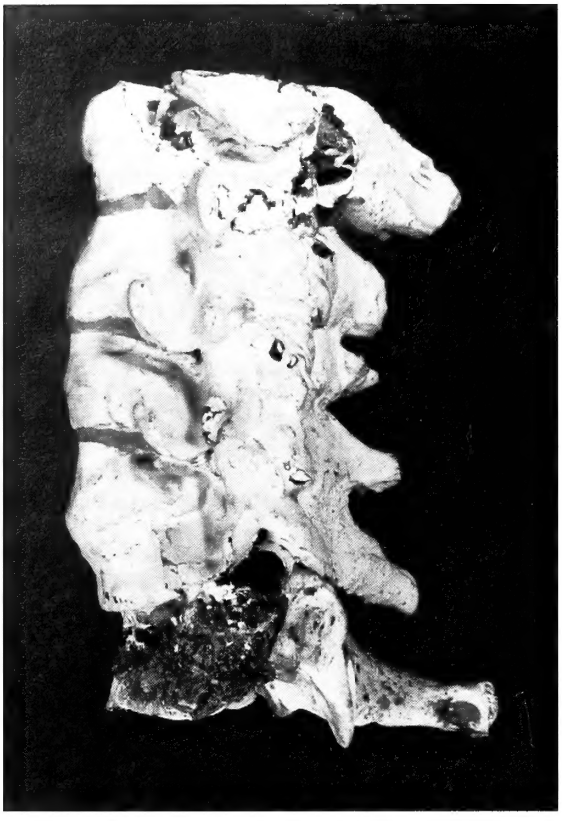

Fig. 1 Gough's Cave 1 sixth or seventh cervical vertebra at bottom of figure, articulated to four reconstructed vertebra above; lateral view; × 1.

Table 1 Dimensions (mm) of the sixth cervical vertebra.

Dorso-ventral diameter[1]	56.8
Superior external transverse articular diameter[2]	51.7
Superior internal transverse articular diameter[3]	(31.5)
Superior transverse articular diameter[4]	41.6
Inferior external transverse articular diameter[5]	48.3
Inferior internal transverse articular diameter[6]	21.8
Inferior transverse articular diameter[7]	35.1
Spinal canal dorso-ventral diameter (M-10)	14.7
Spinal canal transverse diameter (M-11)	21.5
Spinous process length[8]	29.2
Spinous process angle[9]	5°
Body ventral height (M-1)	(12.2)
Body inferior dorso-ventral diameter (M-5)	17.3
Body inferior transverse diameter (M-8)	28.6

[1]From the mid-ventral surface of the body to the dorsal tip of the spinous process.
[2]Maximum distance between the lateral edges of the superior articular facets.
[3]Maximum distance between the medial edges of the superior articular facets.
[4]Average of the external and internal transverse articular diameters of the superior articular facets.
[5]Maximum distance between the lateral edges of the inferior articular facets.
[6] Maximum distance between the medial edges of the inferior articular facets.
[7]Average of the external and internal transverse articular diameters of the inferior articular facets.
[8]From the ventro-superior margin of the intersection of the laminae and the spinous process to the dorsal tip of the spinous process (not including the unfused tubercle).
[9]The angle between the central long axis of the spinous process and the horizontal plane of the superior surface of the body, taken in the median sagittal plane of the vertebra.

of the superior surface of the corpus and making its identification more difficult). The first thoracic vertebra is preserved, and it articulates poorly with this element, suggesting that this is the 6th cervical vertebra. The inferior surface of the body is concave (not flat as is normally found in 7th cervical vertebra: Bass, 1987), and the anterior tubercle of the transverse process is relatively large and thus looks to be the carotid tubercle of C6. In addition, the end of the spinous

Table 2 Dimensions (mm) of the thoracic vertebrae.

	T1	T2/3	T4	T5	T6	T7	T8	T9	T10	T11	T12
Dorso-ventral Diameter[1]	60.2	–	–	–	68.5[11]	69.0[11]	–	–	71.1[11]	67.8[11]	(69.2)[11]
Superior external transverse articular diameter[2]	46.1	–	36.2	–	31.4	32.9	33.1	34.3	35.9	38.3	–
Superior internal transverse articular diameter[3]	21.9	–	15.5	15.2	13.7	–	15.2	14.7	12.5	15.1	–
Superior transverse articular diameter[4]	34.0	–	25.9	–	22.6	–	24.2	24.5	24.2	26.7	–
Inferior external transverse articular diameter[5]	–	38.0	37.1	33.9	34.4	34.5	–	37.5	38.7	–	36.2
Inferior internal transverse articular diameter[6]	–	14.8	13.8	12.9	–	13.6	–	–	10.4	–	17.3
Inferior transverse articular diameter[7]	–	26.4	25.5	23.4	–	24.1	–	–	24.6	–	26.8
Spinal canal dorso-ventral diameter (M-10)	16.7	–	16.5	17.1	15.2	–	17.8	16.8	–	17.3	–
Spinal canal transverse diameter (M-11)	20.9	(18.4)	16.5	17.1	17.4	17.1	17.3	18.2	17.7	20.0	20.3
Spinous process length[8]	31.3[11]	(30)[11]	–	–	36.4[11]	37.8[11]	–	–	36.3[11]	29.1[11]	26.3
Spinous process angle[9]	8°	–	–	–	47°	70°	–	–	55°	45°	16°
Body ventral height (M-1)	13.7	–	17.3	18.0	17.0	18.3	19.4	18.8	19.1	19.4	(20)
Body dorsal height (M-2)	–	–	17.4	18.1	–	–	20.1	–	–	–	–
Body median height (M-3)	–	–	–	15.8	–	–	19.4	–	–	–	–
Body superior dorso-ventral diameter (M-4)	18.4	–	22.0	23.2	25.7	–	28.9	32.8	30.7	32.2	–
Body superior transverse diameter (M-7)[10]	30.2	–	26.7	26.9	29.7	31.1	32.2	36.2	36.5	39.4	–
Body inferior dorso-ventral diameter (M-5)	–	–	21.7	25.6	–	30.2	32.5	–	32.4	–	(34)
Body inferior transverse diameter (M-6)[10]	–	–	28.5	28.7	31.3	32.8	36.4	38.2	39.3	42.3	41.7

[1]From the mid-ventral surface of the body to the dorsal tip of the spinous process.
[2]Maximum distance between the lateral edges of the superior articular facets.
[3]Maximum distance between the medial edges of the superior articular facets.
[4]Average of the external and internal transverse articular diameters of the superior articular facets.
[5]Maximum distance between the lateral edges of the inferior articular facets.
[6]Maximum distance between the medial edges of the inferior articular facets.
[7]Average of the external and internal transverse articular diameters of the inferior articular facets.
[8]From the ventro-superior margin of the intersection of the laminae and the spinous process to the dorsal tip of the spinous process (not including the unfused tubercle).
[9]The angle between the central long axis of the spinous process and the horizontal plane of the superior surface of the body, taken in the median sagittal plane of the vertebra.
[10]Transverse body dimensions did not include the articular facets for the rib head.
[11]Dorsal tubercle of spinous process unfused and missing.

process looks as though it gave rise to a bifid tubercle (the spinous process of the seventh cervical vertebra generally ends in a single tubercle (Williams & Warwick, 1980)), although the secondary centre of ossification is unfused and the process is preserved as a single tubercle. These features suggest that this bone represents the sixth cervical vertebra.

The spinous process projects nearly horizontally from the body (Table 1), as is common in lower cervical vertebrae. The corpus is wide in the transverse dimension relative to its dorso-ventral diameter. As in all lower cervical vertebrae, the spinal canal is wider transversely than dorso-ventrally, and is triangular in outline.

THORACIC VERTEBRA 1 (FIG. 2)

The first thoracic vertebra is largely complete. The right side transverse process is broken off and the left side process is missing a small portion of its lateral end. The posterior tubercle of the spinous process is unfused. A crack runs through the left side neural arch lamina and inferior and superior articular facets. The vertebra cannot be viewed from the inferior perspective due to adherent reconstructive materials.

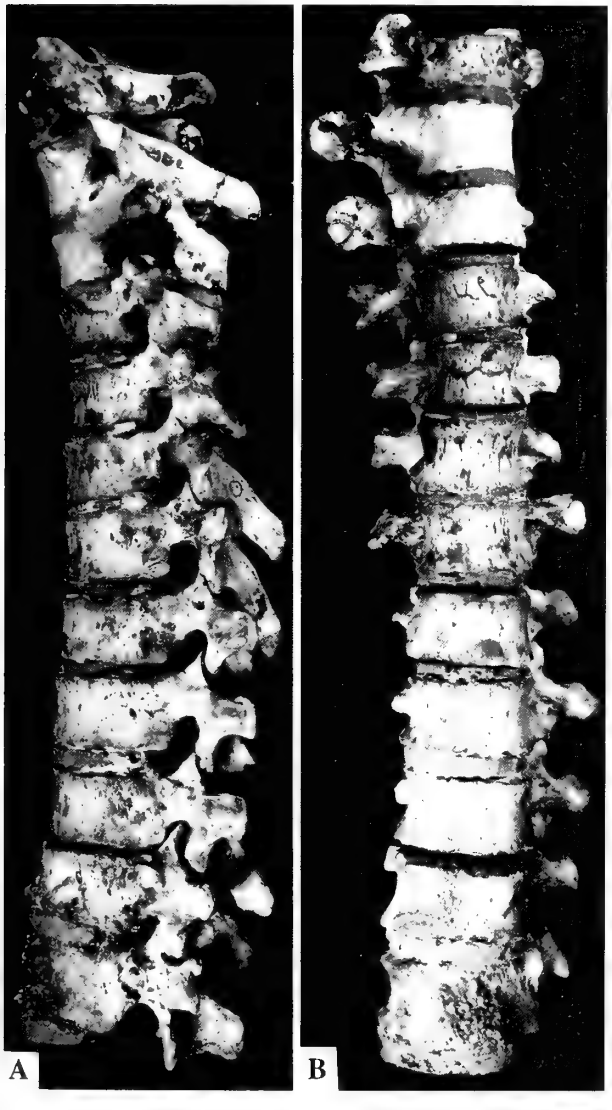

Fig. 2 Gough's Cave 1 thoracic vertebrae 1–12 in articulation. **2a,** lateral; **2b,** ventral; × 0.48. Note that reconstructed intervertebral disks of uniform thickness dorso-ventrally have been inserted between some of the vertebral bodies, probably diminishing the degree of curvature that would have obtained during life.

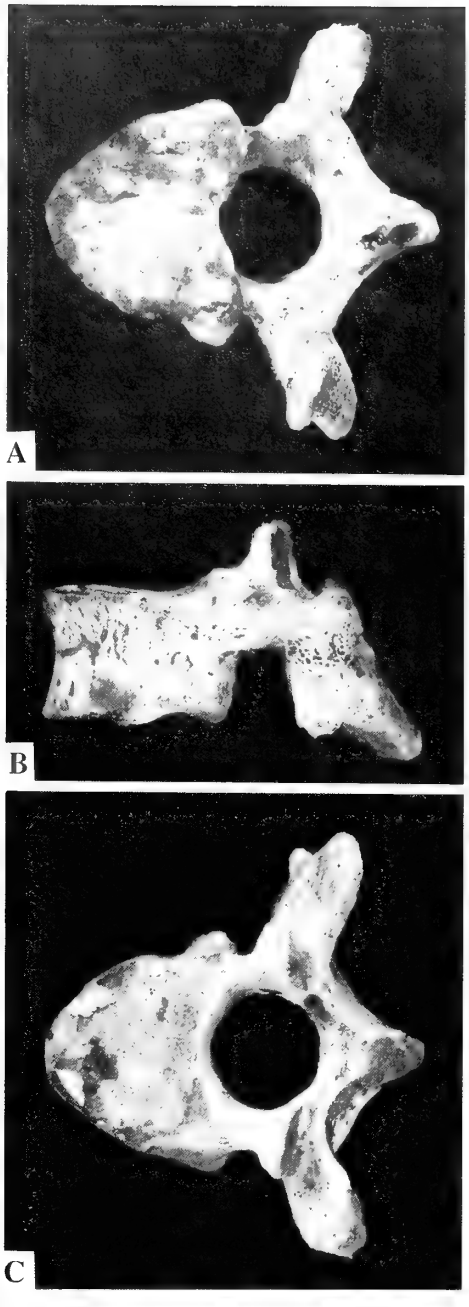

Fig. 3 Gough's Cave 1 fifth thoracic vertebra. **3a,** superior; **3b,** lateral; **3c,** inferior; × 1.

The spinous process projects nearly horizontally from the corpus (Table 2). The dorso-ventral diameter of the spinal canal is somewhat smaller than the transverse diameter.

THORACIC VERTEBRA 2 OR 3

The second or third thoracic vertebra is represented by the posterior portion of a neural arch only. This fragment includes the left side

lamina with the inferior articular facet, spinous process (with the posterior tubercle missing), and the right side lamina with the transverse process and superior and inferior articular facets.

THORACIC VERTEBRA 4

This vertebra is complete except for the posterior half of the spinous process and the left side transverse process (Fig. 2). The superior and inferior surfaces of the body are obscured by reconstructive materials.

The dorsal and ventral supero-inferior heights of the body are equal in this vertebra (Table 2). As with all of the thoracic vertebrae, the corpus has a greater transverse than dorso-ventral diameter (although the difference is not as great as that seen in the preserved [sixth or seventh] cervical vertebra). The dimensions of the spinal canal are equal in the transverse and dorso-ventral directions.

THORACIC VERTEBRA 5 (FIGS 2, 3)

The fifth thoracic vertebra is complete except for most of the spinous process, the dorsolateral surface of the right transverse process, and the lateral end of the left transverse process (Fig. 3)

As with the fourth thoracic vertebra, the dorsal and ventral supero-inferior heights of the body are equal (Table 2). The dimensions of the spinal canal are equal in the transverse and dorso-ventral directions.

THORACIC VERTEBRA 6

This vertebra is complete except for the lateral ends of both transverse processes (Fig. 2). This specimen is attached to the seventh thoracic vertebra inferiorly, and has reconstructive materials adherent to the superior surface of the body.

The spinous process is infero-dorsally oriented (Table 2). The transverse diameter of the spinal canal is slightly greater than the dorso-ventral diameter in this element.

THORACIC VERTEBRA 7

This element is complete except for the very tip of the spinous process and the lateral end of the right transverse process. This vertebra is affixed to the sixth thoracic vertebra superiorly and the inferior surface of the corpus is obscured by reconstructive material.

The spinous process is strongly angled inferiorly (Table 2), and the transverse and dorso-ventral diameters of the body are sub-equal (with the transverse dimension being slightly larger).

THORACIC VERTEBRA 8 (FIGS 2, 4)

This vertebra is mostly complete, lacking only the left side inferior costal facet (on the body), the right transverse process, the left inferior articular facet, and most of the spinous process (Fig. 4). The neural arch is cracked in several places and reconstructed.

The dorsal supero-inferior height of the corpus is slightly greater than that of the ventral body (Table 2). The transverse and sagittal dimensions of the spinal canal are roughly equal in this vertebra.

THORACIC VERTEBRA 9

The ninth thoracic vertebra is complete except for the end of the spinous process. The neural arch is broken off through both pedicles and has been reconstructed. This vertebra is attached to the tenth thoracic vertebra inferiorly and the superior surface of the corpus is covered by reconstructive material.

The spinal canal of this vertebra shows an expansion of the transverse diameter and a diminution of the dorso-ventral diameter of the spinal canal relative to that of the suprajacent vertebra (Table 2).

THORACIC VERTEBRA 10

This vertebra is complete, but displays some slight damage to the right side inferolateral edge of the body. This specimen is attached to the ninth thoracic vertebra superiorly.

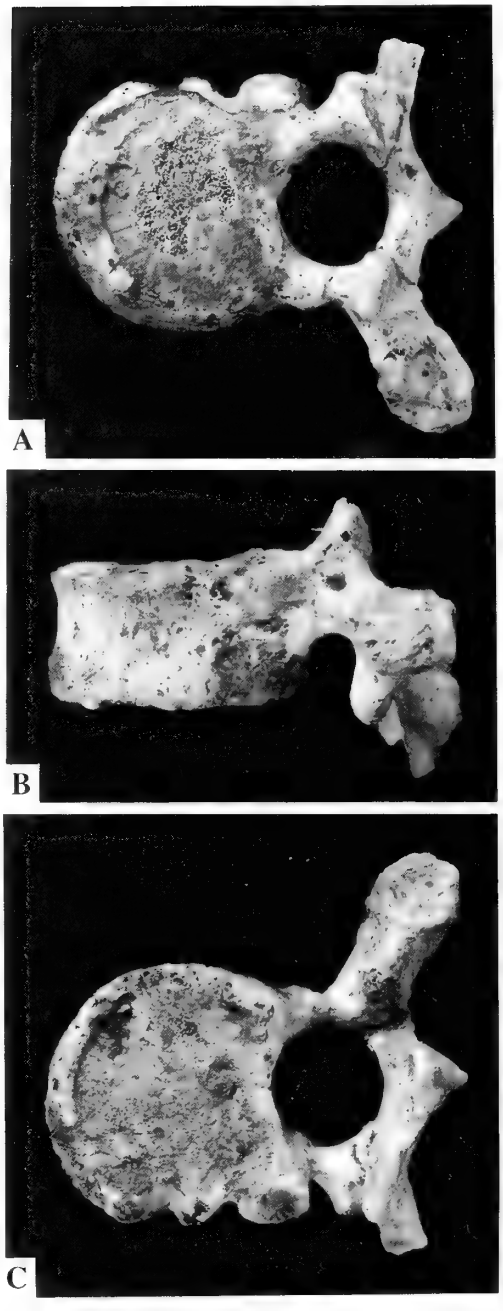

Fig. 4 Gough's Cave 1 eighth thoracic vertebra. **4a,** superior; **4b,** lateral; **4c,** inferior; × 1.

The spinous process is infero-dorsally directed, and is not as sharply inferiorly angled as that of the seventh thoracic vertebra (Table 2).

THORACIC VERTEBRA 11

The eleventh thoracic vertebra is complete except for the very tip of the spinous process. The vertebra has some slight erosion to the inferior left side of the ventral surface of the corpus. The tip of the spinous process appears to be unfused. It is affixed to the twelfth thoracic vertebra inferiorly.

The specimen exhibits slight anterior wedging of its body. The

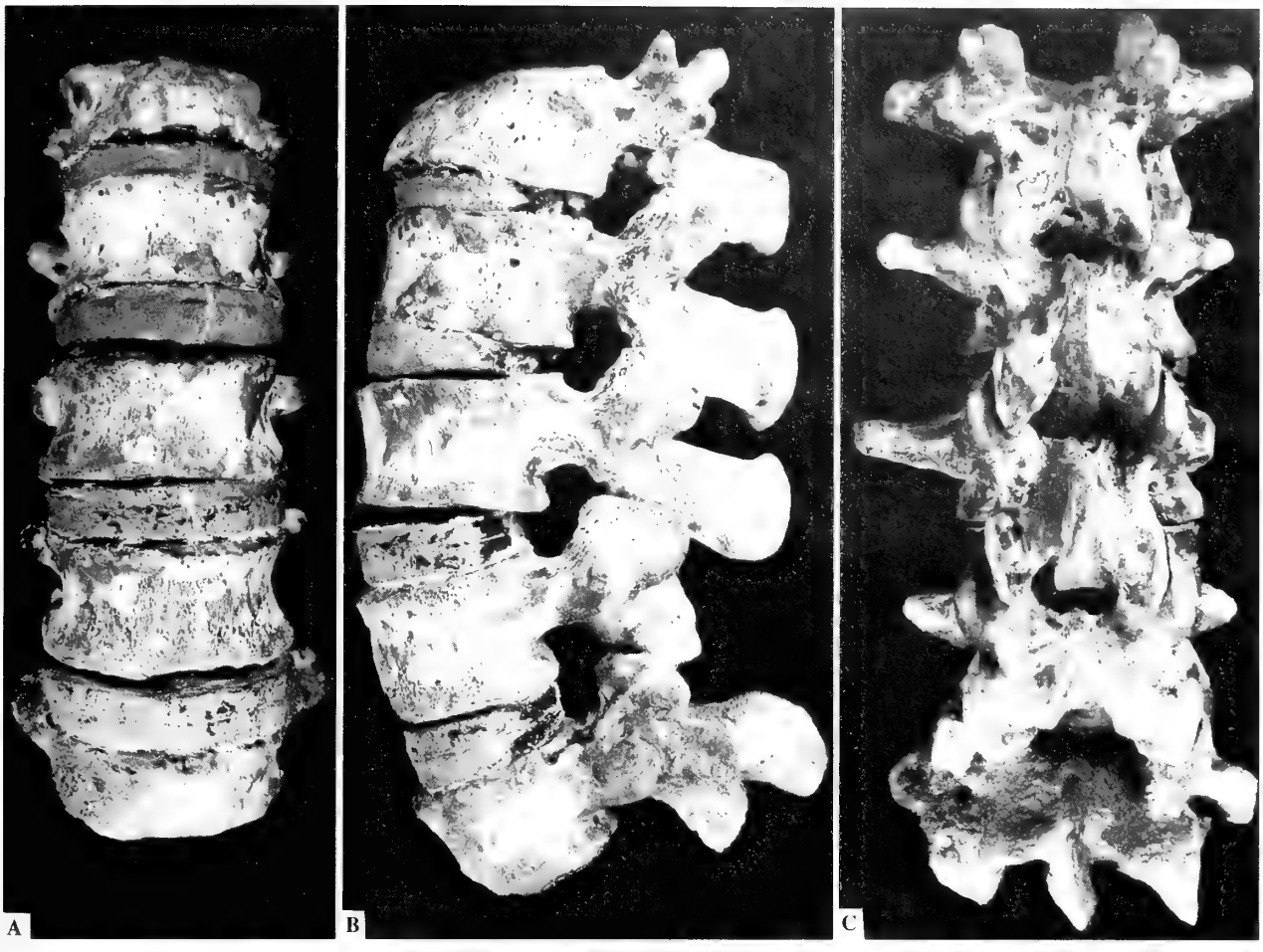

Fig. 5 Gough's Cave 1 lumbar vertebrae in articulation. **5a,** ventral; **5b,** lateral; **5c,** dorsal; × 0.72. Reconstructed intervertebral disks have been inserted between the lumbar bodies.

spinous process has a more moderate inferior projection than that of the suprajacent vertebra (Table 2), and the spinal canal has a greater transverse than dorso-ventral diameter.

THORACIC VERTEBRA 12

The twelfth thoracic vertebra is largely complete. This bone lacks only a portion of the left side ventral and lateral surfaces of the body, and the dorsolateral tip of the transverse process. The tip of the spinous process is unfused and missing, and the annular ring of the inferior surface is not fully fused to the centrum. The specimen is attached to the eleventh thoracic vertebra superiorly and its inferior surface is obscured by reconstructive material.

The spinous process forms a moderate (inferiorly directed) angle with the plane of the body (Table 2). As with the lumbar vertebrae, the transverse diameter of the body is considerably greater than the dorso-ventral dimension.

LUMBAR VERTEBRA 1 (FIG. 5)

The first lumbar vertebra is largely complete, lacking only the right side mammillary process. Some erosional damage is evident on the ventral surface of the body. The posterior tip of the spinous process appears to be unfused and missing (this region is obscured by reconstructive materials making observation of the morphology difficult). The bone is cracked through the right side pedicle and lamina and has been reconstructed. The specimen is attached inferiorly to the second lumbar vertebra.

The body of the first lumbar vertebra exhibits marked anterior wedging (a much greater dorsoventral dimension inferiorly than superiorly: Table 3; Fig. 5). Erosion and damage to the anterior surface precludes measurement of the inferior dorsoventral diameter, and may accentuate the degree of wedging evident in the specimen. The spinous process is short and projects horizontally from the body (Table 3). The spinal canal transverse diameter is the largest of all the lumbar vertebrae, and is considerably greater than the dorso-ventral diameter.

LUMBAR VERTEBRA 2

This specimen is complete except for the lateral part of the right side transverse process (Fig. 5). The secondary centre of ossification for the tubercle of the spinous process is fused but the epiphyseal line is still open along its superior margin. The epiphyseal line between the secondary centre of ossification of the inferior annular ring and the centrum is also evident (but is mostly closed and was undergoing obliteration at the time of death). This bone is attached to the first lumbar vertebra superiorly and its inferior surface is covered by reconstructive material.

Table 3 Dimensions (mm) of the lumbar vertebrae.

	L1	L2	L3	L4	L5
Dorso-ventral Diameter[1]	80.2[11]	85.1	86.4	–	79.3
Superior external transverse articular diameter[2]	35.7	30.3	34.8	37.8	54.7
Superior internal transverse articular diameter[3]	17.4	–	20.9	20.3	21.3
Superior transverse articular diameter[4]	26.6	–	27.9	29.1	38.0
Inferior external transverse articular diameter[5]	29.6	31.0	34.1	46.2	52.4
Inferior internal transverse articular diameter[6]	–	18.8	16.4	19.8	27.9
Inferior transverse articular diameter[7]	–	24.9	25.3	33.0	40.2
Spinal canal dorso-ventral diameter (M-10)	18.9	–	15.2	17.0	18.3
Spinal canal transverse diameter (M-11)	24.2	20.9	21.8	22.6	22.9
Spinous process length[8]	27.8[11]	33.9	37.5	–	34.6
Spinous process angle[9]	2°	2°	16°	–	30°
Body ventral height (M-1)	(20.3)	22.0	23.6	26.2	(25)
Body dorsal height (M-2)	(26.5)	26.0	26.9	25.5	24.0
Body median height (M-3)	–	–	25.0	–	–
Body superior dorso-ventral diameter (M-4)	(31.6)	–	40.3	36.4	34.1
Body superior transverse diameter (M-7)	44.8	45.5	47.5	50.0	52.8
Body inferior dorso-ventral diameter (M-5)	–	39.7	37.2	(36.4)	(30)
Body inferior transverse diameter (M-6)	48.2	50.3	52.1	52.9	(50)
Body sagittal angle[10]	–15°	(–14°)	–10°	–6°	+8°

[1]From the mid-ventral surface of the body to the dorsal tip of the spinous process.
[2]Maximum distance between the lateral edges of the superior articular facets.
[3]Maximum distance between the medial edges of the superior articular facets.
[4]Average of the external and internal transverse articular diameters of the superior articular facets.
[5]Maximum distance between the lateral edges of the inferior articular facets.
[6]Maximum distance between the medial edges of the inferior articular facets.
[7]Average of the external and internal transverse articular diameters of the inferior articular facets.
[8]From the ventro-superior margin of the intersection of the laminae and the spinous process to the dorsal tip of the spinous process (not including the unfused tubercle).
[9]The angle between the central long axis of the spinous process and the horizontal plane of the superior surface of the body, taken in the median sagittal plane of the vertebra.
[10]Angle in the median sagittal plane between the tangents to the median sagittal surfaces of the superior and inferior vertebral disk surfaces (a positive angle has its apex dorsally and opens ventrally).
[11]Dorsal tubercle of spinous process unfused and missing.

The spinous process is of moderate length and is horizontally projecting from the corpus (Table 3). The dorsal supero-inferior body height is greater than that of the ventral surface, and the body is wide in transverse diameter relative to dorso-ventral diameter.

Lumbar vertebra 3 (fig. 6)

The third lumbar vertebra is complete except for the lateral portion of the right side transverse process. The tip of the spinous process is fused but the epiphyseal line is still open along its superior edge. The inferior and superior annular rings appear to be fully fused to the centrum, with the epiphyseal lines completely obliterated.

The spinous process is mildly angled inferiorly relative to the plane of the corpus (Table 3) and is of moderate length. The body is supero-inferiorly higher on its dorsal than ventral aspect. Both the body and spinal canals are wide transversely relative to their dorso-ventral dimensions.

Lumbar vertebra 4

The fourth lumbar vertebra is largely complete. It lacks only the spinous process and the right side transverse process. Slight erosion to the ventral surface of the body is evident. The superior surface of the body is covered by reconstructive material.

The ventral surface of the body is supero-inferiorly higher than the dorsal surface (Table 3). The corpus and spinal canal are transversely wide relative to their dorso-ventral diameters.

Lumbar vertebra 5

This vertebra is largely complete, lacking only the lateral ends of the transverse processes. Matrix is concreted to the left side transverse process, inferior articular facet and lamina. There is some erosion visible on the ventral surface of the body. The superior surface of the corpus is obscured by reconstructive material.

The spinous process is shorter than that of the third lumbar vertebra (Table 3) and is the most inferiorly directed of all the lumbar vertebrae. The ventral surface of the body is higher supero-inferiorly than the dorsal surface. The body and spinal canal are transversely wide relative to their dorso-ventral diameters.

Morphology

When articulated, the thoracic vertebrae show a normal kyphosis (Fig. 2). The sum of the ventral body heights is 196.5 mm (using the average of the ventral heights of the first and third vertebrae for the missing corpus of vertebra 2), considerably shorter than the mean value for recent European males reported by Boule and Vallois (1937) of 243.1 mm, and is closer to the mean value of 221.9 mm obtained for European females (standard deviations and sample sizes not given). This is a reflection of the shorter stature of the Gough's Cave 1 individual relative to recent European males (see Holliday & Churchill, this series). The total ventral body height of Cheddar Man is more similar to, yet still on the small side of, the male and female skeletons from Téviec (male skeletons 2 [217.5 mm] and 16 [231.0], female skeletons 1 [217.5] and 6 [223.5]: Boule & Vallois, 1937). This becomes more apparent when one looks at dorsal body heights, which are more reliable indicators of trunk height than are the ventral heights (which are frequently subject to anterior wedging: Stewart, 1966). Summary statistics for total thoracic column height (summed dorsal body heights for T1–T12) for comparative samples can be found in Table 4. The total thoracic height figure for Gough's Cave 1 and the majority of the fossil sample were predicted via least-squares regressions of total thoracic height on those elements preserved for a recent human series (n=45: Holliday, 1995). The standard error of the estimate for the measurements predicted by this method is very low (Holliday, 1995), providing a reasonable degree of confidence in the predicted values. In no case was a predicted thoracic height used if its standard error of the estimate was greater than 3% of the prediction itself.

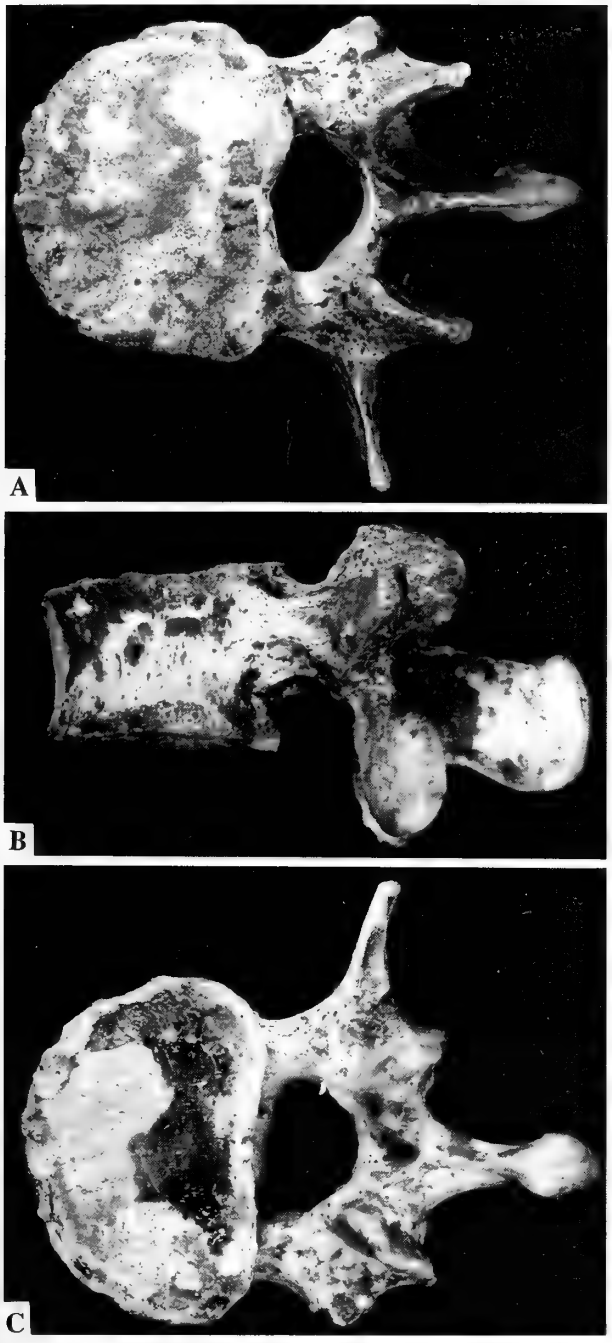

Fig. 6 Gough's Cave 1 third lumbar vertebra. **6a,** superior; **6b,** lateral; **6c,** inferior; × 0.9.

As is evident from Table 4, Gough's Cave 1 has a short thoracic column relative to most of the mean values for males in the comparative samples. The value for his thoracic height is less than that of all the male means, with the exception of the recent sub-Saharan Africans. His value falls within the low end of the male range for most of the samples. Interestingly, his thoracic height falls very close to the mean values of all of the European (Pleistocene, Holocene and recent) female samples. This of course reflects the overall short stature of the Gough's Cave 1 specimen.

Table 4 Summary statistics for thoracic column height (mm) in Recent and Late Pleistocene/Early Holocene samples (mean; SD; n).

	Total Thoracic Height	
	Male	Female
Gough's Cave 1	234.7	
Mesolithic Europeans	251.7; 20.4; 4	233.8; 5.7; 2
Late Upper Paleolithic Europeans	256.8; 18.1; 12	231.8; 10.1; 3
Recent Europeans	259.0; 12.9; 63	238.3; 12.6; 52
Recent North Africans	239.9; 15.8; 26	223.5; 8.4; 28
Recent Sub-Saharan Africans	229.6; 11.0; 9	219.7; 16.2; 15

When articulated, the lumbar vertebrae evince a normal lordosis (Fig. 5). The sum of the ventral body heights is more similar to those observed in the males from Téviec with five lumbar vertebrae (118.5 mm in Téviec 2, 116.0 in Téviec 4). The females from Téviec with five lumbar vertebrae have total ventral body heights that are slightly, but not substantially, shorter (110.0 mm in Téviec 1, 112.0 mm in Téviec 3). Three of the skeletons from Téviec have six lumbar vertebrae, without a reduction in the number of thoracic vertebrae, and thus have lumbar regions that are substantially longer supero-inferiorly (Téviec 16 [male], 155 mm; Téviec 6 [female] 148.5 mm: Boule & Vallois, 1937). As with the thoracic vertebral column, inclusion of the summed dorsal body heights of the lumbar vertebrae allows the comparison of Gough's Cave 1 to several Recent and fossil human samples. As for the thoracic column heights, lumbar column heights were predicted via least-squares regressions; none was used if its standard error of the estimate exceeded 3% of the predicted measurement. Table 5 shows that Cheddar Man has a shorter lumbar column than the male mean of all but one comparative sample (recent North Africans). To some extent, this is due to the marked posterior wedging exhibited in the specimen's L3–L5 vertebrae (see below). However, his relatively small size also plays a role; his lumbar column height falls squarely among the means for all the European female samples. Importantly, the male mean for the Mesolithic sample is high due to the inclusion of Téviec 16, who, as discussed above, has 6 lumbar vertebrae.

In recent Europeans, the ventral body height is typically greater than the dorsal body height in the fourth and fifth, and often in the third, lumbar vertebrae (Boule & Vallois, 1937). In the sample from Téviec, this pattern generally holds only for the fifth vertebra (Boule & Vallois, 1937). Gough's Cave 1 evinces the pattern seen in recent Europeans, with a greater supero-inferior dimension of the ventral body in the third, fourth and fifth lumbar vertebrae (Table 3). The lumbo-vertebral index (100 * [Σ dorsal body heights]/[Σ ventral body heights]) is 110.1 in Cheddar Man, higher than the mean value for the Téviec specimens but not outside their range (mean of six individuals = 103.6, range 96.3–110.1: Boule and Vallois, 1937). The position of the articular facets of the vertebrae indicate a lordotic curvature to the lumbar column (with perhaps greater lordosis created in the lower lumbars: Fig. 5), so there must have been considerable wedging of the intervening intervertebral disks.

Table 5 Summary statistics for lumbar column height (mm) in Recent and Late Pleistocene/Early Holocene samples (mean; SD; n).

	Total Lumbar Height	
	Male	Female
Gough's Cave 1	128.9	
Mesolithic Europeans	137.4; 13.5; 4	126.9; 8.4; 2
Late Upper Paleolithic Europeans	130.1; 8.6; 11	127.9; 2.5; 4
Recent Europeans	134.9; 8.0; 66	128.2; 7.4; 59
Recent North Africans	127.0; 10.5; 29	123.4; 7.3; 32
Recent Sub-Saharan Africans	131.5; 5.9; 11	122.7; 9.0; 15

The spinous processes of the thoracic and lumbar vertebrae are unremarkable and not particularly robust, similar to the condition observed in the Téviec skeletons (Boule and Vallois, 1937). The transverse processes of the lower thoracic vertebrae are, however, relatively large and robust. The insertion areas for the *levator costae* muscles and costotransverse ligaments tend to be well marked on the ribs (see below), suggesting some overall robusticity in the thorax of Cheddar Man (at least with respect to muscles and structures important in respiration). The inferior demi-facets for the rib heads on the centra are quite large in most of the thoracic vertebrae, and tend to form laterally-projecting tubercles with inferiorly directed articular surfaces. The flattening of the left side ventral bodies that usually occurs in thoracic vertebrae 5–8 (from pressure from the aorta) is only slightly apparent in Gough's Cave 1.

COSTAL REMAINS (FIG. 7)

Descriptions

RIB 2

The right second rib is preserved as a 78.8 mm-long fragment from the neck just proximal of the tubercle to the region of the proximal end of the *M. serratus anterior* tubercle (the proximal part of the tubercle is apparent). The left second rib is preserved as a 95.9 mm-long fragment from mid-neck to just distal of the *M. serratus anterior* tubercle, and the superior surface of the distal half of the fragment is covered with a thin layer of matrix (Fig. 7).

The right-side rib has a well developed crest for *M. scalenus posterior* and a distinct groove on the external edge of the inferior surface for the intercostal muscles and membranes. The *M. scalenus posterior* crest is not as strongly developed on the left-side rib (although the difference is slight), but the region just internal of the crest (on the superior surface) is more rugose. The *M. serratus anterior* crest on the left rib is very weakly developed. A piece of the superior surface of the shaft of this rib is missing in the region of the proximal tubercle, and the rest of the tubercle is covered by thin matrix, but it is clear nonetheless that the tubercle is not large. The left rib also displays a distinct groove on the external edge of the inferior surface for the intercostal muscles and membranes, but it is not as well defined as on the right side rib. The non-articular tubercles are relatively slight, with the one on the left rib being slightly larger. The articular facets (measuring 10.2 mm proximodistally (PD) by 6.1 mm supero-inferiorly (SI) on the right and 9.1 PD by 6.3 SI on the left) are dorsoinferiorly directed.

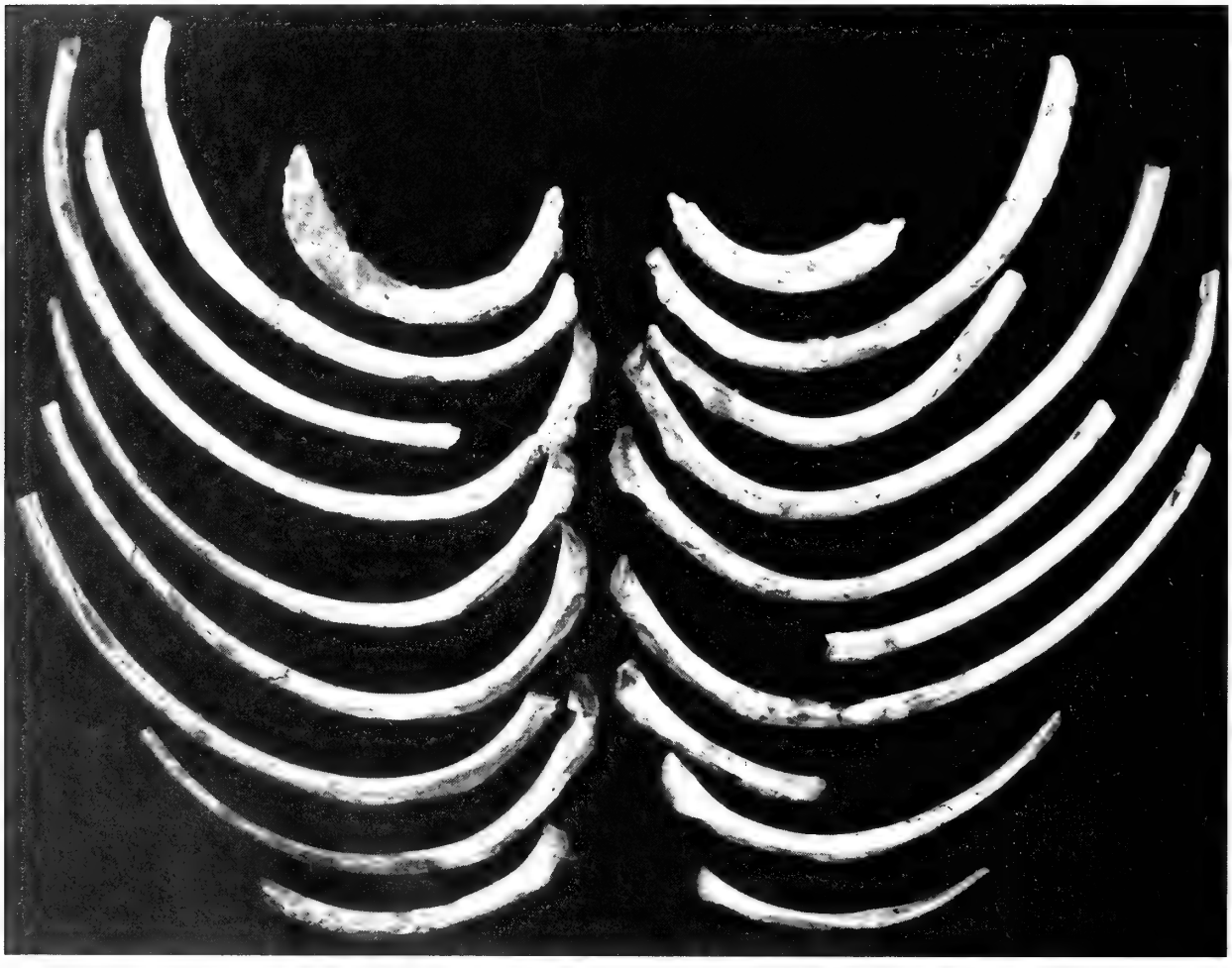

Fig. 7 Gough's Cave 1 ribs in superior view; × 0.43. The ribs are arranged in sequential order with the second ribs at the top and right-side ribs to the right of the photograph.

Table 6 Dimensions (mm) of ribs 2–4.

	R2	L2	R3	L3	R4
Neck length[1]	–	–	–	–	(27.9)[2]
Proximal thickness (M-2)	11.2	12.2	8.8	–	8.9
Proximal height (M-1)	7.3	7.1	8.4	–	9.3
Shaft thickness[3]	(11.7)[4]	(12.3)[4]	8.3	7.7	8.1
Shaft height[3]	(7.1)[4]	(7.3)[4]	11.7	10.1	7.7

[1]Distance from the middle of the head to the middle of the articular tubercle.
[2]Head unfused, measurement taken from middle of epiphyseal surface for head.
[3]Rib thickness (internal-external diameter, measured in the plane of rib curvature) and height (supero-inferior diameter, taken perpendicular to the plane of curvature of the rib) at the point where the *M. iliocostalis* line meets the inferior edge of the rib.
[4]Taken 1 cm distal of where proximal thickness and height were taken.

Rib 3

The right-side third rib is represented by a 154.7 mm-long fragment from mid-neck to just proximal of the anterior angle. The left third rib is preserved as a 171.7 mm-long fragment from the distal end of the posterior angle to just proximal of the sternal end.

The *M. iliocostalis* line[1] in the right rib is not pronounced (a feature of all of the Cheddar Man's ribs). A small portion of the *M. iliocostalis* line is preserved proximally in the left-side rib, and it looks to have been more strongly developed than in the right (however, the rib itself is somewhat slighter). The right rib shows a discernable attachment for *M. levator costae* and both ribs have a distinct sulcus on the superior edge of the rib in the vicinity of the posterior angle (ca. 30 mm long) for the intercostal muscles. There is no discernable subcostal groove on the right rib, and the left side shows a weak subcostal groove for only a few centimeters distal of the posterior angle. The left rib has a supero-inferior flare to the body about 45 mm proximal of the anterior angle, reflecting perhaps a healed fracture. The articular facet on the right side is dorsoinferiorly directed and measures 9.5 mm (proximodistally) by 7.8 mm (supero-inferiorly).

Rib 4

The right fourth rib is a 127.0 mm-long fragment preserved from the head to somewhere proximal of midshaft. The proximal end of the rib is intact. The left fourth rib is a 156.8 mm-long fragment of the rib body, from somewhere distal of the posterior angle to the region of the anterior angle.

On the right side, the surface of the head is rough and irregular, likely representing the subchondral surface of the unfused secondary centre of ossification for the head. There is a small and superiorly directed tubercle on the neck, and from this a crest runs distally along the superior margin of the bone past the non-articular tubercle, most likely representing the attachment of the superior costotransverse ligament. The *M. iliocostalis* line is not pronounced. The articular tubercle is large (9.0 mm proximodistally by 11.5 mm internal-external) and is primarily inferiorly directed. The subcostal groove is weakly developed on both ribs. In the right rib there is a strong bend at the posterior angle (the angle between the head-neck axis and the proximal costal body is approximately 90°).

Rib 5

The right fifth rib is preserved as a 190 mm-long fragment, intact from the head down to the anterior angle, and missing only a portion of the sternal end. The left rib is represented by a 210 mm-long fragment, also intact from the head down to the anterior angle and missing only a part of the sternal end.

The secondary centres of ossification for the heads are only partially fused (and portions are missing) on both sides. As in the right fourth rib, the fifth ribs present small superiorly directed tubercles on the neck that continue distally as crests running along the superior margins of the bones past the non-articular tubercles. These crests, most likely marking the sites of attachment of the superior costotransverse ligaments, are more strongly developed than that on the fourth rib. Both ribs also have a crest on the inferior edge of the neck running from the head to the proximoinferior edge of the articular facet. These crests may represent the attachments of expanded accessory ligaments from the heads and necks of the subjacent ribs (Williams & Warwick, 1980) or distal extensions of the radiate ligaments binding the heads to the adjacent vertebra. The nonarticular tubercles are bulbous and projecting, and the articular tubercles are inferodorsally directed (measuring 7.9 mm PD by 10.3 mm SI on the right, and 7.2 mm PD by 10.5 mm SI on the left). The *M. iliocostalis* lines are not very well developed and it is hard to make out where the lines cross the inferior border of the rib. The subcostal grooves are neither deep nor strongly developed but are clearly visible along most of the body. The angle between the head/neck axis and the axis of the body is about 117° on both sides.

Table 7 Dimensions (mm) of ribs 5–7.

	R5	L5	R6	L6	R7	L7
Rib length (M-4)	–	>200[1]	–	–	–	–
External arc (M-3)	–	>323[1]	–	–	–	–
Neck length[2]	(27.3)[3]	(28.5)[3]	(23.9)[3]	(25.3)[3]	–	(26.9)[3]
Proximal thickness (M-2)	9.2	8.3	8.0	8.6	–	8.9
Proximal height (M-1)	8.6	8.7	10.0	12.0	–	9.3
Shaft thickness[4]	9.3	9.6	8.6	8.7	9.7	9.3
Shaft height[4]	13.0	–	14.5	14.4	13.6	13.5
Chord[5]	–	(213)[1]	–	–	–	–
Subtense[6]	–	(77)[1]	–	–	–	–
Transverse width[7]	–	8.2	–	–	–	–

[1]Rib is missing a small portion of the sternal end.
[2]Distance from the middle of the head to the middle of the articular tubercle.
[3]Head unfused, measurement taken from middle of epiphyseal surface for head.
[4]Rib thickness (internal-external diameter, measured in the plane of rib curvature) and height (supero-inferior diameter, taken perpendicular to the plane of curvature of the rib) at the point where the *M. iliocostalis* line meets the inferior edge of the rib.
[5]Distance from the distal margin of the articular tubercle to the proximal extent of the sternal end, following McCown and Keith (1939: fig. 75).
[6]Maximum perpendicular distance from the chord to the external surface of the rib, following McCown and Keith (1939; fig. 75).
[7]Internal-external diameter of the rib body at the intersection of the subtense.

Rib 6

The right sixth rib is preserved as a 165.3 mm-long fragment, complete from the head to somewhere distal of midshaft. The left-side rib is a 185.1 mm-long fragment, complete from the head to the area of the anterior angle.

The centres of ossification of the heads are incompletely fused and portions of them are missing. The ribs of both sides have short necks with small tubercles on their superior surfaces for the superior costotransverse ligaments. The ribs lack the crests (distal of the tubercles) that are seen on the suprajacent ribs. The inferior edges of

[1]The iliocostal muscles are the lateral-most extensions of the *erector spinae* (*sacrospinalis*) muscle. The *M. iliocostalis lumborum* inserts on the inferior borders of the lower six or seven ribs, at the posterior angle (Williams & Warwick, 1980). *M. iliocostalis thoracis* arises from the superior borders of the angles of the lower six ribs and inserts on the superior margins of the upper six ribs. *M. iliocostalis cervicis* attaches to the superior borders of the third to sixth ribs. Thus various combinations of these muscles, as well as the thoracolumbar fascia, contribute to the formation of the *iliocostalis* lines on the external surface of the posterior angle of the ribs, and will be referred to throughout this description as the *iliocostalis* muscle.

the necks also lack the crests seen on the fifth ribs. The articular tubercles are primarily inferiorly directed and round in shape (right-side 9.7 mm PD by 9.5 mm internal-external (IE), left-side 9.4 mm PD by 9.5 mm IE). The nonarticular tubercles are almost absent, appearing as small dorsosuperior extensions of the articular facets. The *M. iliocostalis* lines are not rugose nor marked. The attachments for *M. levator costae* can be seen as crests on the superior edges of the ribs running distally from the level of the tubercles and blending into the *M. iliocostalis* lines. The subcostal grooves are clear and distinct. The head/neck axis to shaft axis angle is roughly 135° in both ribs.

Rib 7

The right seventh rib is preserved as a 181.1 mm-long fragment of the body, from somewhere distal of the posterior angle to just distal of the anterior angle. Judging from the size and curvature of the left side antimere, the proximal break occurred right at the distal end of the posterior angle. The left-side rib is represented by a 185.0 mm long-fragment, complete from the head to the region of the anterior angle.

The secondary centre of ossification for the head of the left rib is unfused and missing. The neck is short and has a tubercle and crest on its superior surface for the superior costotransverse ligament. The neck has a large foramen or pit (plugged with matrix) on its dorsal surface. The *M. levator costae* crest is pronounced. The articular facet is dorsoinferiorly directed and oval in shape (10.8 mm PD by 8.4 mm IE). The nonarticular tubercle is poorly defined but is larger than that of the 6th rib. The *M. iliocostalis* line is non-rugose and poorly defined. On both sides the proximal bodies are quite thick and form a 'roof' over the subcostal groove along the proximal shaft. The subcostal grooves are very clearly defined along the proximal portions of the shafts. In the left-side rib, the head/neck axis to body axis angle is strong (approximately 109°).

Rib 8

The right eighth rib is preserved as a 198 mm-long fragment, complete from the head to the area of the anterior angle. The left rib is preserved as a 190.3-mm long fragment of the body, retaining a small portion of the nonarticular tubercle proximally. Distally the left-side rib is broken somewhere proximal of the anterior angle.

On the right rib the head is unfused and missing. The neck is short and has a tubercle and crest on its superior surface for the superior costotransverse ligament. This crest is continuous with the insertion of *M. levator costae* and blends with the superior portion of the *M. iliocostalis* line distally. The same morphology can be seen in the left-side rib from the area of the *M. levator costae* insertion (the most proximally preserved portion of the shaft) down to the *M. iliocostalis* line. The inferior surface of the right-side neck also has a clearly defined crest, perhaps reflecting the attachment of an expanded accessory ligament from the head and neck of the subjacent rib (Williams & Warwick, 1980) or a distal extension of the radiate ligament. The neck has a foramen or pit on the dorsal surface just proximal to the articular facet. The articular facet is oval (11.6 mm PD by 9.3 mm IE) and is primarily inferiorly directed. The nonarticular tubercle is poorly defined and blends with the proximal end of the *M. iliocostalis* line. The *M. iliocostalis* lines are non-rugose and poorly defined on both ribs. Small, mildly rugose depressed areas can be seen on the superior margins of the shafts just distal to the *M. iliocostalis* lines, likely marking the proximal extent of the insertion of the intercostal muscles. The subcostal grooves are very clear along the proximal halves of the ribs. The head/neck axis to body axis angle of the right-side rib is 122°.

Table 8 Dimensions (mm) of ribs 8–11.

	R8	L8	R9	L9	R11	L11
Neck length[1]	(26.7)[2]	–	(22.5)[2]	(23.1)[2]	–	–
Proximal thickness (M-2)	10.2	9.3	8.4	8.2	–	–
Proximal height (M-1)	9.8	9.2	9.7	9.1	–	–
Shaft thickness[3]	–	10.6	–	7.9	6.9	6.3
Shaft height[3]	–	11.4	–	15.3	13.2	13.8

[1]Distance from the middle of the head to the middle of the articular tubercle.
[2]Head unfused, measurement taken from middle of epiphyseal surface for head.
[3]Rib thickness (internal-external diameter, measured in the plane of rib curvature) and height (supero-inferior diameter, taken perpendicular to the plane of curvature of the rib) at the point where the *M. iliocostalis* line meets the inferior edge of the rib.

Rib 9

The right ninth rib is a 79.6 mm-long fragment of the proximal end, complete from the head to the region of the posterior angle. The left rib is preserved as a 150.5 mm-long fragment, complete from the head to somewhere below midshaft.

The centres of ossification for the heads are unfused and missing. The necks are relatively short. In the right-side rib, a small tubercle is evident on the superior surface of the neck, perhaps reflecting an attachment for an accessory ligament that ran superiorly to the crest on the inferior surface of the neck of the right eighth rib. The crests for *M. levator costae* are clearly defined on both ribs. The articular facets are oval shaped (measuring 8.9 mm PD by 7.7 mm IE on the right, 8.9 mm PD by 8.0 mm IE on the left) and are inferodorsally directed. The nonarticular tubercles arise from the articular tubercles and are relatively small. The *M. iliocostalis* lines are not pronounced. The costal grooves are wide supero-inferiorly and shallow. The head/neck axis to shaft axis angle is 116° in both ribs.

Rib 11

The right eleventh rib is represented by a 130.5 mm-long fragment, complete from the head to somewhere near the anterior angle. The left-side rib is preserved as a 102.5 mm-long fragment, complete from the head to 37 mm below the posterior angle. The shaft of the left rib is eroded and damaged.

The heads are unfused and missing on both sides. The ribs present neither articular nor nonarticular tubercles, but crests for the costotransverse ligaments are visible on the superior margins of the proximal bodies. Narrow, oval insertion scars for the intercostal muscles are visible on both the inferior and superior edges at the posterior angle. The *M. iliocostalis* lines are indistinct, but bulging tubercles are visible at the posterior angle in each rib for the attachment of this muscle.

Rib 12

The right twelfth rib is complete, and has a total length of 96.6 mm. The area of the internal intercostal muscle attachment on the superior edge is eroded away, but otherwise the bone is well preserved.

The head appears to be unfused. The rib has a clear crest on the superior surface of the neck for the costotransverse ligament. There is also a sulcus on the inferior edge of the internal surface of the proximal shaft for *M. quadratus lumborum*. The diaphragm attachment is indistinct. There is a long (19 mm), narrow scar on the inferior edge of the distal shaft for *M. serratus posterior inferior*, and on the superior external surface some rugosity is visible that may represent the attachment site of *M. latissimus dorsi*. The right twelfth rib is 95.9 mm long (M-4: Martin, 1928) and has an external arc length (M-3: Martin, 1928) of 54 mm.

Unidentified shaft fragment

This is a 58.2 mm-long fragment of the distal end of a rib body, including the sternal end. The subcostal groove is not preserved, and thus the side cannot be determined. The fragment is somewhat damaged and has some areas of plaster reconstruction. The supero-

inferior height of the body is 14.4 mm. Based on the size and shape of the fragment, it appears to be part of an upper rib.

Morphology

The overall size (Tables 6–8), shape, robusticity and muscularity of the Gough's Cave 1 ribs fall within the range of variation of recent human samples. In terms of rib shaft height and thickness the Gough's Cave 1 ribs generally fall within one standard deviation of the mean values obtained in the comparative sample (Table 9). Rib shaft shape, as measured by the ratio of thickness to height, is also generally within one standard deviation of the EuroAmerican means. The notable exceptions concern the fourth and eighth ribs, both of which are markedly shorter in the supero-inferior dimension, resulting in shaft shape ratios that are elevated (indicating a 'rounder' shaft cross-section) relative to the comparative sample.

The *M. iliocostalis* lines are generally poorly marked in the entire series of ribs. Other muscle markings and ligamentous insertions tend to be more pronounced. Most of the ribs exhibit a distinct crest for *M. levator costae* and clear attachment areas for the superior costotransverse ligament. However, the insertions on the external surfaces of the rib necks for the costotransverse ligaments are not pronounced, and, with the exception of the fifth rib, the non-articular tubercles (upon which the lateral costotransverse ligaments attach) are slight. Evidence of expanded accessory or radiate ligaments can be seen in several of the ribs. The subcostal grooves tend to be weakly developed in the upper ribs of the series, but are distinct in the middle ribs. The insertion sites of the intercostal muscles are well defined in a number of the ribs. The insertion of *M. scalenus posterior* is evident in both second ribs, yet the *M. serratus anterior* tubercle is relatively slight in the left side rib (this region is not preserved in the right-side rib). In the preserved right twelfth rib, an obvious sulcus for *M. quadratus lumborum* can be seen, and the attachment areas of *M. serratus posterior inferior* and *M. latissimus dorsi* are clearly evident. The presence of crests for the *levator costae* muscles, along with the visible insertion sites of the intercostal muscles in some ribs and the development of the attachment areas of the ligaments that bind the ribs to vertebrae suggest a moderately high level of respiratory activity in this individual. However, this general robusticity does not extend to all of the muscles of the back and trunk that arise from or attach to the ribs.

Table 9 Rib shaft dimensions (mm) in Gough's Cave 1 and recent European-American males (mean, SD).

RIB		Gough's Cave 1	EuroAmerican Males (n = 20)
2	Thickness	(11.7)[1]	12.7 ± 1.1
	Height	(7.1)[1]	7.3 ± 0.8
	T/H ratio	1.65	1.73 ± 0.2
3	Thickness	8.3	7.8 ± 1.1
	Height	11.7	11.2 ± 1.7
	T/H ratio	0.71	0.71 ± 0.1
4	Thickness	8.1	8.6 ± 0.9
	Height	7.7	11.7 ± 1.9
	T/H ratio	1.05	0.74 ± 0.1
5	Thickness	9.3	9.0 ± 1.0
	Height	13.0	12.8 ± 1.6
	T/H ratio	0.72	0.71 ± 0.1
6	Thickness	8.6	9.2 ± 1.0
	Height	14.5	13.9 ± 1.5
	T/H ratio	0.59	0.67 ± 0.1
7	Thickness	9.7	9.0 ± 1.0
	Height	13.6	15.0 ± 1.9
	T/H ratio	0.71	0.61 ± 0.1
8[2]	Thickness	10.6	8.6 ± 0.8
	Height	11.4	15.5 ± 2.5
	T/H ratio	0.93	0.57 ± 0.1
9[2]	Thickness	7.9	8.0 ± 0.8
	Height	15.3	17.0 ± 2.8
	T/H ratio	0.52	0.48 ± 0.1
11	Thickness	6.9	6.1 ± 1.0
	Height	13.2	12.9 ± 1.6
	T/H ratio	0.52	0.48 ± 0.1

[1]Taken 1cm distal of location of proximal thickness and height measurements.
[2]Taken on left-side rib for Gough's Cave 1.

REFERENCES

Barral, L. & Primard, S. 1962. L'Homme de Rastel, Commune de Peillon (A.M.). *Bulletin du Museé Anthropologique et Préhistorique du Monaco*, **9:** 171–190.

Bass, W. M. 1987. *Human Osteology*. Columbia, MO.

Bonin, G. von 1935. The Magdalenian Skeleton from Cap-Blanc in the Field Museum of Natural History. *University of Illinois Bulletin*, **34:** 1–76.

Boule, M. & Vallois, H. 1937. Anthropologie. *In*: M. Péquart, S.-J. Péquart, M. Boule and H. Vallois (eds), *Téviec: Station-nécropole Mésolithique du Morbihan. Archives de l'Institute de Paléontologie Humaine*, Mémoire **18:** 111–227.

Cremonesi, G., Parenti, R. & Romano, S. 1972. Scheletri paleolitici della grotta delle Veneri presso Parabita (Lecce). *Atti, XIV Riunione, Istituto Italiano Preistoria e Protoistoria*, **1972:** 105–116.

Fernández-Tresguerres, J. 1976. Enterramiento aziliense de la Cueva de Los Azules I (Cangas de Onis, Oviedo). *Boletín del Instituto de Estudios Asturianos*, **87:** 273–290.

Franciscus, R. G. & Churchill, S. E. 2002. The costal skeleton of Shanidar 3 and a reappraisal of Neandertal thoracic morphology. *Journal of Human Evolution*, **42:** 303–356.

Genet-Varcin, E. & Miquel, M. 1967. Contribution à l'étude du squelette magdalénien de l'abri Lafaye à Bruniquel (Tarn et Garonne). *Anthropologie, Paris*, **71:** 467–478.

Graziosi, P. 1962. Découverte de gravures rupestres de type paléolithique dans l'Abri del Romito (Italie). *Anthropologie, Paris*, **66:** 262–268.

Holliday, T. W. 1995. *Body Size and Proportions in the Late Pleistocene Western Old World and the Origins of Modern Humans*. Ph.D. thesis, University of New Mexico.

Lacam, R., Niederlender, A. & Vallois, H. V. 1944. Le gisement mésolithique du Cruzoul de Gramat. *Archives de l'Institute de Paléontologie Humaine*, **Mémoire 21:** 1–92.

Mann, R. W. 1993. A method for siding and sequencing human ribs. *Journal of Forensic Sciences* **38:** 151–155.

Martin, R. 1928. *Lehrbuch der Anthropologie*. 2nd Edition. Jena.

McCown, T. D. & Keith, A. 1939. *The Stone Age of Mount Carmel II: The Fossil Human Remains from the Levalloiso-Mousterian*. Oxford.

Paoli, G., Parenti, R. & Sergi, S. 1980. Gli Scheletri Mesolitici della Caverna delle Arene Candide (Liguria). *Memorie dell'Istituto Italiano di Paleontologia Umana*, No. 3, Rome.

Patte, E. 1968. L'homme de la femme de l'Azilien de Saint Rabier. *Mémoire du Muséum d'Histoire Naturel, Série C*, **19:** 1–56.

Péquart, M., Péquart, St. -J., Boule, M. & Vallois, H. V. 1937. Téviec: Station-nécropole Mésolithique du Morbihan. *Archives de l'Institute de Paléontologie Humaine*, Mémoire **18:** 1–228.

Pittard, E. & Sauter, M. R. 1945. Un squelette magdalénien provenant dc la station des Grenouilles (Veyrier, Haute-Savoie). *Archives suisses d'Anthropologie générale*, **11:** 149–200.

Quatrefages, A. de & Hamy, E. T. 1882. Les races humaines fossiles. *Crania Ethica, Paris*, **1:** 52–54, 82–83.

Simon, C. & Morel, P. (nd) L'Homme du Bichon. Manuscript in preparation.

Steele, D. G. & Bramblett, C. A. 1988. *The Anatomy and Biology of the Human Skeleton*. College Station, TX.

Stewart, T. D. 1966. Some problems in human paleopathology. *In*: S. Jarcho (ed), *Human Palaeopathology*: 43–55. New Haven.

Vallois, H. V. 1941–1946. Nouvelles recherches sur le squelette de Chancelade. *Anthropologie, Paris*, **50:** 65–202.

—— 1972. Le gisement et le squelette de Saint-Germain-la-Rivière – Troisième Partie – Anthropologie. *Archives de l'Institute de Paléontologie Humaine*, Mémoire **34**.

Verneau, R. 1906. *Les Grottes de Grimaldi. Anthropologie*. Monaco.

Verworn, M., Bonnet, R. & Steinmann, G. 1919. *Der diluviale Menschenfund von Oberkassel bei Bonn*. Wiesbaden.

Williams, P. L. & Warwick, R. 1980. *Gray's Anatomy, 36th Edition*. Philadelphia.

Bull. nat. Hist. Mus. Lond. (Geol.) **58**(1): 13–79 Issued 27 June 2002

Upper Ordovician brachiopods from the Anderken Formation, Kazakhstan: their ecology and systematics

L.E. POPOV
Department of Geology, National Museum of Wales, Cardiff CF10 3NP
L.R.M. COCKS
Department of Palaeontology, The Natural History Museum, Cromwell Road, London SW7 5BD
I.F. NIKITIN
Institute of Geological Sciences, Almaty 480100, Kazakhstan

CONTENTS

SYNOPSIS. The brachiopod fauna from the Anderken Formation (Lower to Middle Caradoc) of the Chu-Ili Range, south-eastern Kazakhstan, is revised and described systematically. It consists of 62 species in 55 genera, of which the genera *Tesikella*, *Olgambonites* and *Zhilgyzambonites* (all Plectambonitoidea) and *Ilistrophina* (Camarelloidea) are new, and the species *Bellimurina (Bellimurina) sarytumensis*, *Teratelasmella chugaevae*, *Foliomena prisca*, *Acculina kulanketpesica*, *Dulankarella larga*, *Kajnaria rugosa*, *Anoptambonites convexus*, *Olgambonites insolita*, *Zhilgyzambonites extenuata*, *Gacella institata*, *Placotriplesia spissa*, *Grammoplecia wrighti*, *Dolerorthis pristina*, *Austinella sarybulakensis*, *Plectorthis? burultasica*, *Bowanorthis? devexa*, *Pionodema opima*, *Parastrophina iliana*, *Ilistrophina tesikensis*, *Liostrophia pravula*, *Plectosyntrophia unicostata*, *Rhynchotrema akchokense* and *Nikolaispira guttula* are new. Six brachiopod-dominated assemblages are recognised and defined, termed the *Ectenoglossa*, *Tesikella*, *Mabella–Sowerbyella*, *Acculina–Dulankarella*, *Parastrophina–Kellerella* and *Zhilgyzambonites–Foliomena* Associations. The relationships with contemporary faunas are assessed, and the Anderken brachiopods appear to have much in common with those of north-west China.

INTRODUCTION

The global geography of the Lower Palaeozoic has been the subject of widespread international discussion in recent years (references in Cocks 2001), but much is not yet clear. In the Ordovician, the large area of what is today Kazakhstan was then divided into many separate crustal fragments of variable size. The relative positions of these fragments are contentious; some authors, notably Sengor & Natalin (1996), consider that most of the fragments made up an enormous island arc, termed the Kipchak Arc, which stretched in a long curve all the way from the substantial craton of Baltica to the central Siberian Angaran craton. Others, for example Nikitin, have subdivided Kazakhstan in other ways, with a more conservative

© The Natural History Museum, 2002

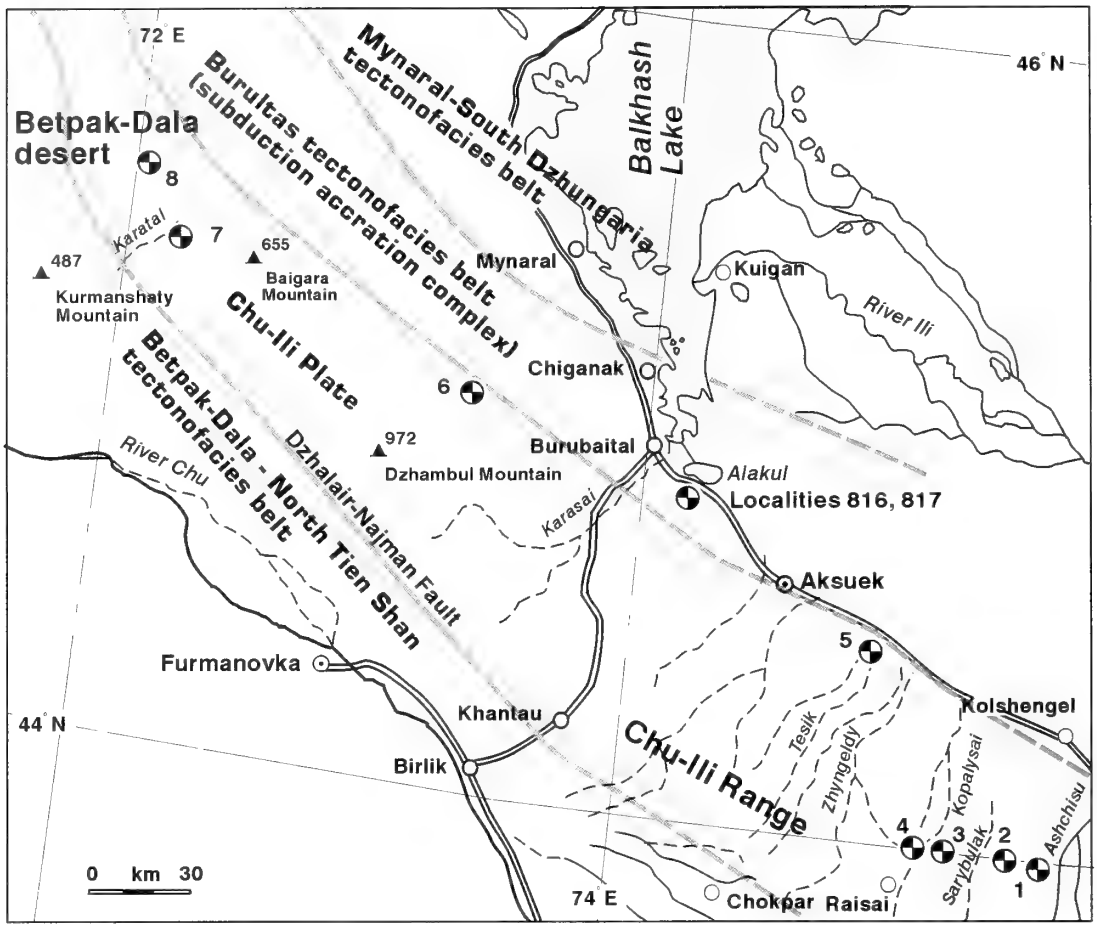

Fig. 1 Generalised map of the Chu-Ili Range and West Balkhash Region (including the southern part of Lake Balkhash), showing the boundaries of the Early Palaeozoic tectonofacies belts, mainly after Nikitin *et al.* (1991), and the position of the brachiopod localities discussed in the text: **1**, Anderkenyn-Akchoku; **2**, Kujandysai; **3**, east side of Kopalysai River; **4**, Buldubai-Akchoku Mountain; **5**, Tesik River; **6**, Burultas Valley; **7**, south-east side of Karatal River near Sorbulak spring; **8**, 7 km southwest of Karpkuduk Well, Kotnak Mountains.

palaeogeography. Up until now, little assessment of the faunas contained within these tectonic plates has been made, particularly in relationship to contemporary faunas from other areas. One such plate is that forming the Chu-Ili Range, and termed here the Chu-Ili Plate (Fig. 1). Within the Chu-Ili Plate the successions have been known for some time (e.g. Nikitin 1972, 1973). However, although a number of papers have been published on aspects of some of the contained Ordovician faunas, much remains to be done. A central formation within the unit is the Anderken Formation of early Caradoc age. This immediately underlies the Dulankara Formation, whose brachiopods from its lowest Otar Member we have recently revised (Popov *et al.* 2000). Although some pioneering descriptions of some of the Anderken brachiopods were published by Rukavishnikova (1956) and some individual species have been published in a number of publications, e.g. Popov (1980, 1985) and Nikitin & Popov (1983), the whole brachiopod fauna from the formation has never been published, and this is the chief purpose of the present paper. In addition, six brachiopod-dominated associations can be identified from the Anderken Formation. LEP and LRMC are responsible for the whole paper and IFN for input into the systematic palaeontology and biofacies sections.

OUTLINE OF GEOLOGY AND FOSSIL LOCALITIES

The Chu-Ili Plate (Fig. 1), as recognised here, is a small part of Asia today, and is traceable from the Zailiyskiy Alatau Range in the southeast to the northern Betpak-Dala Desert in the northwest, where it disappears under late Palaeozoic and Mezo-Cenozoic deposits. To the southwest it is bordered by the large Dzhalair-Najman Fault and northward-dipping homoclinal sequences of Upper Cambrian and Lower to Middle Ordovician age which are mainly siliciclastic slope rise deposits (e.g. the Dzhambul Formation), indicating passive margin development, and several thrust sheets consisting of dismembered ophiolites of the early Palaeozoic Ashchisu Formation (Toporova *et al.* 1971). The Dzhalair-Najman Fault mainly follows an early Palaeozoic suture which separates the Lower Palaeozoic Chu-Ili Plate from the Middle to Upper Ordovician volcanic island-arc association traceable along the northeastern margin of the Betpak-Dala-North Tien Shan tectonofacies belt of Nikitin (Nikitin *et al.*1991), which is the same as the Djezkazaan-Kirgiz (4.1) tectonofacies unit of Sengör & Natalin (1996). To the

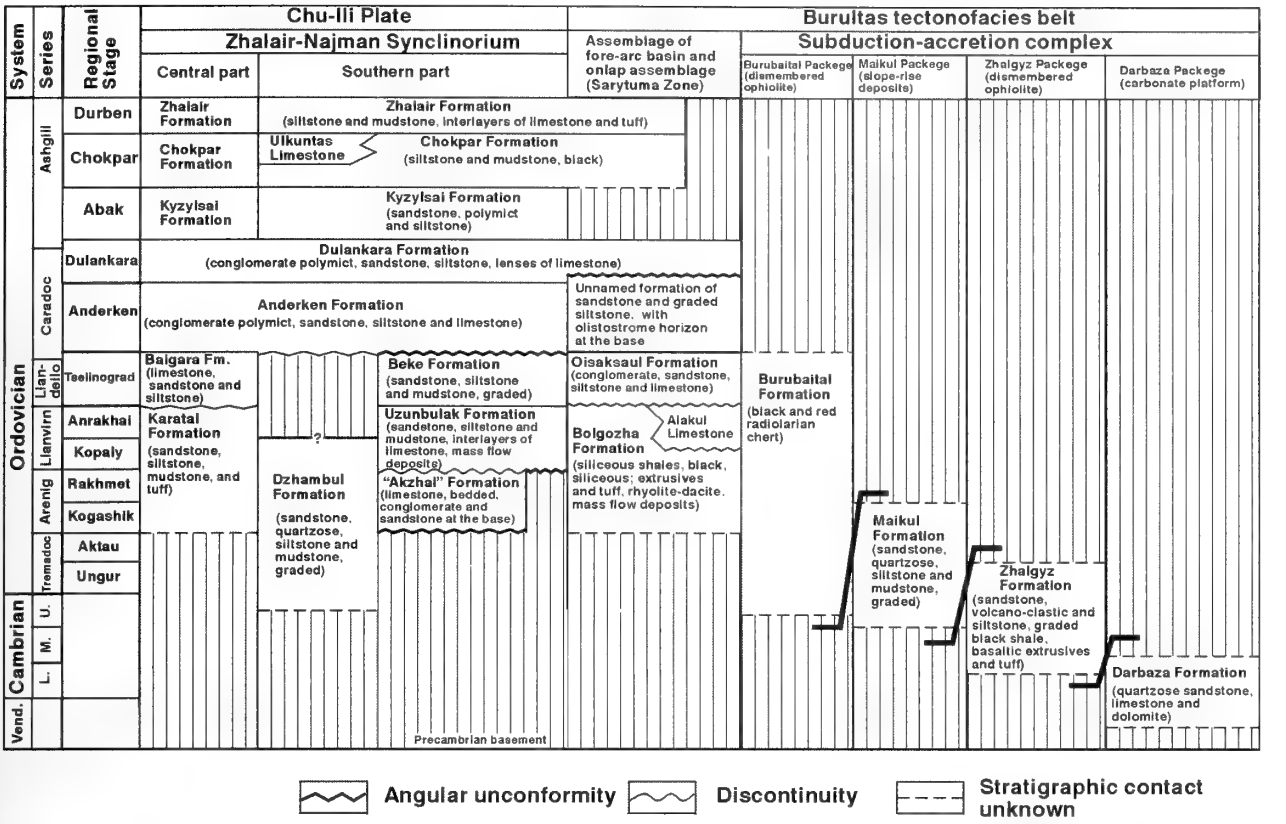

Fig. 2 Chart showing the correlation between the Lower Palaeozoic lithostratigraphic units in the Chu-Ili Plate and the Burultas tectonofacies belt.

north-east of the Chu-Ili Plate lies the Burultas tectonofacies belt (Fig. 2), which represents an accretionary wedge suggesting active margin development, island arc volcanism and subduction of the oceanic crust under the Chu-Ili Plate from the early Arenig to the Llandeilo *Pygodus anserinus* Biozone (Koren *et al.* 1993). By the Caradoc, subduction and volcanism had ceased as a result of the docking of a small terrane or island arc, the Mynaral-South Dzhungaria tectonofacies belt of Nikitin *et al.* (1991).

The Ordovician deposits in the central part of the Chu-Ili Plate, the Dzhalair-Najman Synclinorium, form a nearly continuous sequence of siliciclastic and carbonate rocks from Arenig to Ashgill in age (Fig. 2), which are relatively unmetamorphosed and chiefly dip gently to the northeast. They are covered conformably by Silurian deposits (Nikitin *et al.* 1980) or unconformably by the Devonian. The Ordovician stratigraphy and major lithostratigraphic units were described by Keller (1956) and Nikitin (1972).

The Lower to Middle Caradoc deposits, which are the main source of the brachiopods described here, are termed the Anderken Formation, which is a transgressive sequence of mainly siliciclastic deposits that contain variably developed lens-like carbonate units in the upper part representing mud mounds or algal build-ups (Nikitin *et al.* 1974; 1996). They are best developed in the following eight general localities (Figs 1, 3):

Localites 1–2. Area between the Ashchisu and Sarybulak rivers.

In the south-eastern part of the Chu-Ili Range the best sections of the Anderken Formation are located in a block with faulted margins between the rivers Ashchisu and Sarybulak (Fig. 1, localities 1–2; Figs 3, 4). Here the Anderken Formation overlies, with a slight angular unconformity, graded sandstones, siltstones and mudstones of the Beke Formation, which is Llandeilo to early Caradoc in age, dated by numerous graptolites of the *Hustedograptus teretiusculus* and *Nemagraptus gracilis* Biozones (Tsai 1976). The Anderken comprises six lithostratigraphic units traceable up to 40 km along strike, overlain unconformably by Devonian deposits. These units are (in ascending order):

Unit 1. Polymict, pebbly conglomerate, with sandy matrix and with some beds of sandstone and gritstone. Thickness from 45 m to 120 m, with maximum values in the Anderkenyn-Akchoku section.

Unit 2. Coarse- to medium-grained sandstone with subhorizontal stratification alternating with abundant cross-bedded sets. Lenses of polymict, pebbly conglomerate represent shallow channels formed by tidal currents. Thickness varying from 52 m in the Kujandysai section in the west to 180 m in the Anderkenyn-Akchoku section (Figs 3, 5). The upper part contains the lingulide *Ectenoglossa sorbulakensis*, the trilobite *"Isotelus" romanovskyi* Weber and gastropods (Samples 8130-1, 7612). The middle part of the unit in the Anderkenyn-Akchoku section contains a carbonate mud-mound up to 16 m thick with a core built of light grey micritic limestone. On the flanks there is bedded biomicrite with the brachiopods *Skenidioides* sp., *Christiania* sp. and *Kellerella misiusi*, the trilobites *Mesotaphraspis spinosus* Lisagor, *Selenoharpes* sp., *Acrolichas* sp. *Eokosovopeltis romanovskyi* and *Sphaerexochus* aff. *hisingeri* Warburg. *Illaenus* sp. was noted from about 1.0–1.5 m below the top of the mud-mound in the eastern part of its exposure (Sample 8226). Cystoid and crinoid columnals are abundant.

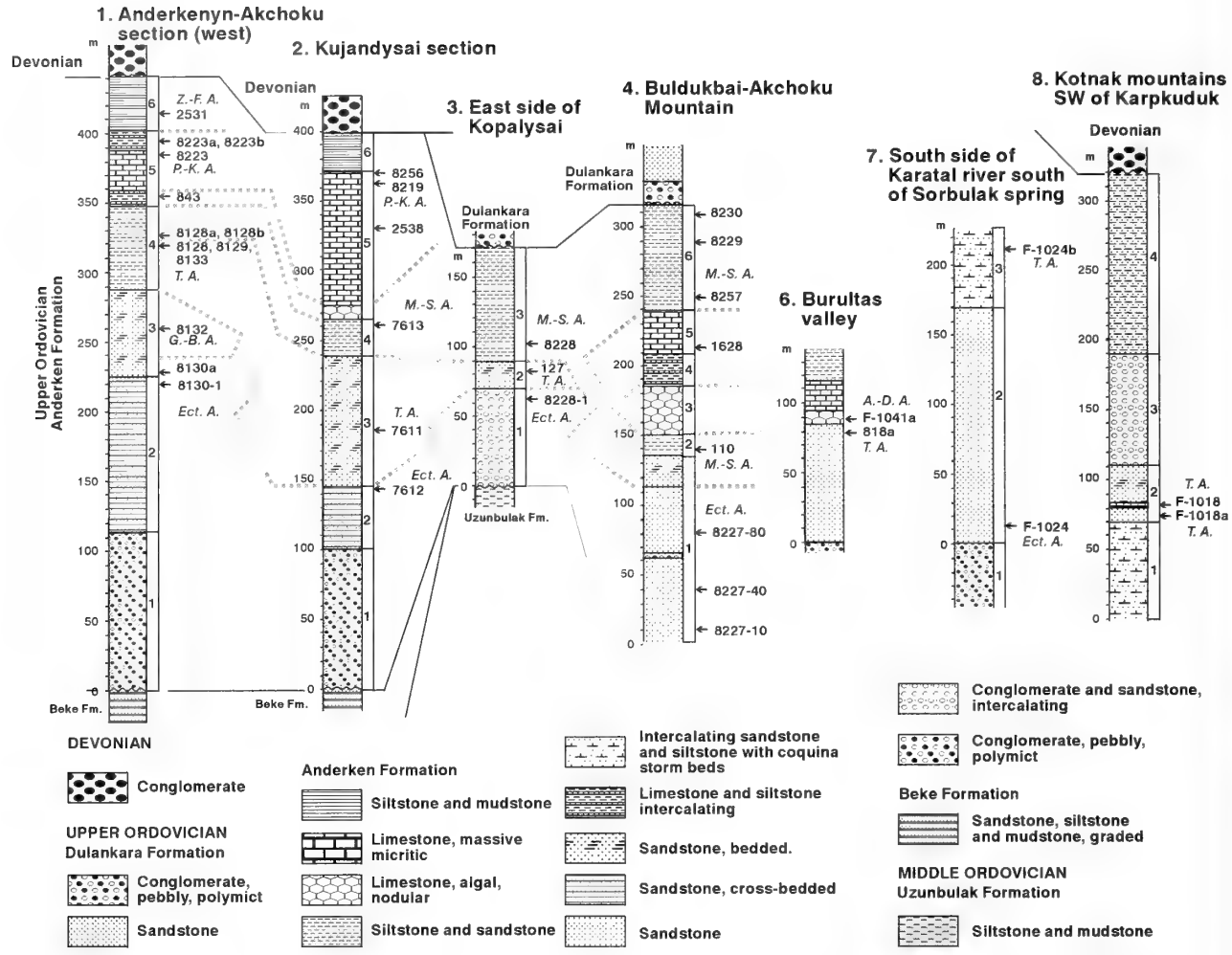

Fig. 3 Columnar sections through the Anderken Formation showing informal units, stratigraphic positions of samples and brachiopod associations: *Ect. A.-Ectenoglossa* Association, *T. A., Tesikella* Association, *M.-S. A., Mabella–Sowerbyella* Association, *A.-D. A., Acculina–Dulankarella* Association, *P.-K. A., Parastrophina–Kellerella* Association, *Z.-F. A., Zhilgyzambonites–Foliomena* Association, *G.-B. A,* Gastropod-Bivalved Molluscs Association. The numbers of the sections are the same as those on Fig. 1.

Unit 3. Coarse- to medium- grained sandstone with mostly subhorizontal stratification, about 40–62 m thick in the Anderkenyn-Akchoku section and up to 97 m thick in the Kujandysai section, with some storm beds of coquinas up to 20 cm thick with concentrations of gastropods and the disarticulated bivalved molluscs *Edmondia fecunda* Khalfin, *Ctenodonta* sp. and *Orthonota*? sp. (Sample 8130a). Gastropods, bivalved molluscs and the trilobite *Eokosovopeltis romanovskyi* become increasingly abundant in the flank deposits in the upper 20 m of the unit (Samples 8130, 8134). In the Kujandysai section concentrations of bivalved molluscs occur in the middle part in association with the rare brachiopod *Tesikella necopina* and the pelmatozoan columnals *Clivosocystis clivosus* Stukalina and *Ordinacrinus punctatus* Stukalina (Sample 7611).

Unit 4. Medium- to fine-grained sandstone replaced gradually upwards by siltstone with numerous trace fossils and symmetrical ripple marks. Thickness varies from 22 to 80 m in the Anderkenyn-Akchoku section and is about 28 m in the Kujandysai section. The lower part contains local concentrations of the coalified plant *Akdalaphyton caradoci* Senkevich, and gastropod and bivalved molluscs in association with the brachiopod *Tesikella necopina* (Samples 8127-2b, 8129, 8133, 8138). The upper part contains an abundant brachiopod fauna of the *Sowerbyella–Mabella* Association (Samples 100b, 7613, 8128a, 8128b, 8135, 8137) and the trilobites *Dulanaspis laevis anderkensis* Chugaeva, *Lonchodomas tecturmasi* Weber, *Pliomerina* sp., *Remopleurides* sp., *Styginella macrophtalma* Pribyl & Vanek, *Bronteopsis extraordinaris* Chugaeva, the cystoid and crinoid columnals *Clivosocystis clivosus*, *Digiticrinus levis* Stukalina, *Ordinaricrinus punctatus* Stukalina and *Communicrinus communis* Stukalina and the starfish *Stenaster obtusus* (Forbes).

Unit 5. Limestones varying in thickness from 8 to 98 m forming a chain of carbonate build-ups between the Uzunbulak and the Ashchisu rivers (Fig. 3). The cores of these build-ups rest on a bed of nodular limestone from 2–10 m thick with abundant dasyclad algae *Cyclocrinites nikitini* Gnilovskaya and *Mastopora reticulata* Gnilovskaya (Nikitin *et al.* 1974). A bed of nodular, algal limestone with dasyclad algae is usually present in the interspaces between the carbonate build-ups and contains brachiopods of the *Acculina–Dulankarella* Association (Samples 100, 8251, 85258), the rare

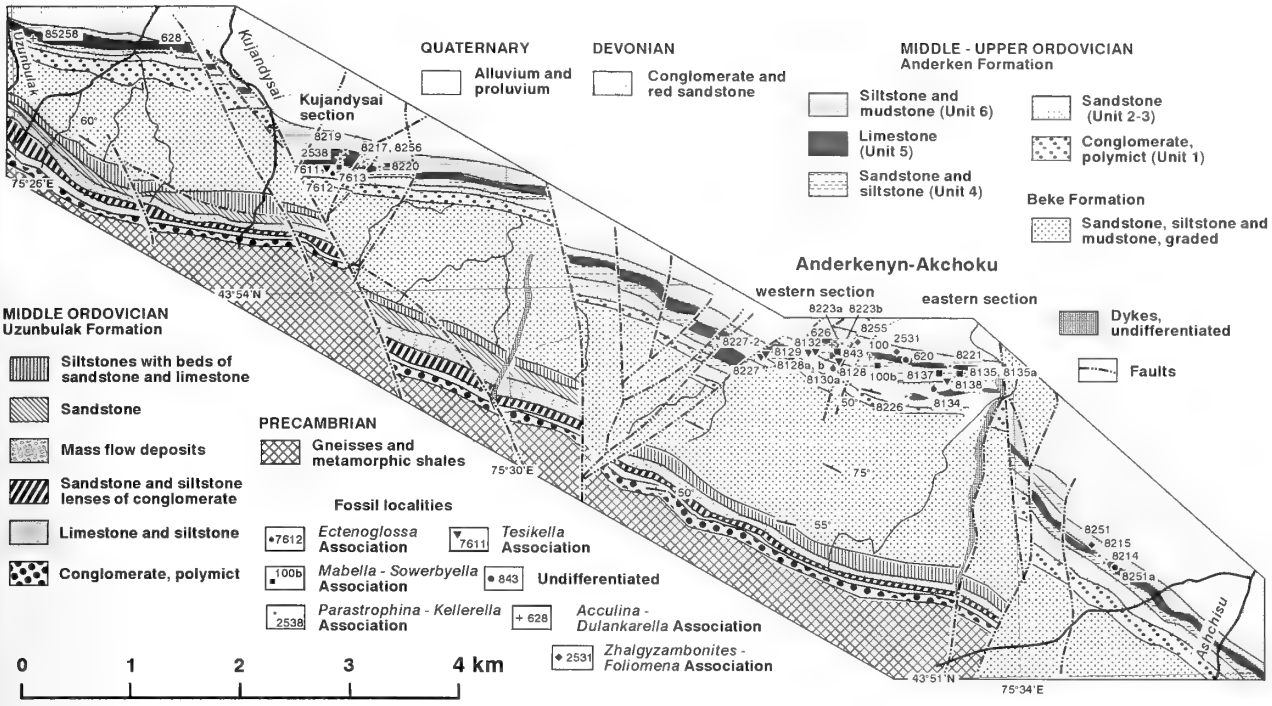

Fig. 4 Geological map showing distribution of the Middle and Upper Ordovician rocks and the positions of measured sections and fossil localities that yielded brachiopods in the area between the Uzunbulak and Ashchisu Rivers, south-eastern Chu-Ili Range (after Nikitin 1972, modified).

tabulate corals *Lichenaria*? sp. and *Amsassia* sp., stromatoporoids, and various trilobites and echinoderms. Locally between the Kujandysai and Sarybulak rivers, and on both sides of the Ashchisu River in the eastern part of outcrop area, carbonate build-ups disappear and the unit comprises bedded limestone varying from biomicrite to biosparite intercalating with siltstone and mudstone, with brachiopods of the *Parastrophina–Kellerella* Association (Tables 4–5, Samples 628, 8223, 8223a, 8223b). Brachiopods of this association also occur in pockets of bioclastic limestone in the mud-mound core and the overlying bedded limestone together with large spherical or ellipsoidal ooids of radiaxial calcite up to 1 cm across (Samples 2538, 8217, 8219, 8256).

Unit 6. Siltstone and mudstone with up to 6 interlayers of bentonite up to 0.3 m thick in the lower part, total about 50–60 m thick, containing brachiopods of the *Zhilgyzambonites–Foliomena* Association (Samples 8231, 8251, 8255). Abundant trilobites are *Granulatagnostus granulatus* Kolobova, *Sphaeragnostus* sp., *Microparia speciosa* Hawle & Corda, *Hammatocnemis* sp., *Birmanites almatiensis* (Chugaeva), *Cyclopyge* sp., *Cybele weberi* Chugaeva and *Ovalocephalus* sp., and graptolites include *Dicranograptus nicholsoni*, *Diplograptus anderkenensis*, *Glyptograptus trubinensis* and *Pseudoclimacograptus scharenbergi*, suggesting the Lower to Middle Caradoc *Diplograptus multidens* Biozone (Keller 1956).

Locality 3. East side of Kopalysai River

On the east side of the Kopalysai River (Fig. 1) the Anderken Formation is about 160 m thick and rests unconformably on the siliciclastic Llandeilo Beke Formation (Fig. 2). Detailed description of this section was provided by Keller (1956: 26), who recognised three units (Fig. 3): (1) bed of intercalating polymict conglomerate and coarse- to medium-grained sandstone up to 70 m thick with bivalves, rare *Ectenoglossa sorbulakensis* (Sample 8223-1) and numerous plant remains of *Akdalaphyton caradoci*; (2) intercalating fine-grained sandstone and siltstone about 15–20 m thick with brachiopods of the *Tesikella* Association (Sample 127), the trilobites *Dulanaspis levis anderkensis* and *Lonchodomas tecturmasi*; and (3) mudstones with some siltstones and fine-grained sandstones about 70–80 m thick with abundant brachiopods of the *Mabella–Sowerbyella* Association (Sample 8228). The deposits overlying the Anderken Formation are polymict pebbly conglomerates and sandstones of the Dulankara Formation.

Locality 4. Buldukbai-Akchoku Mountain

On the west side of the River Kopalysai, the Anderken Formation includes a large carbonate mud-mound which forms the top of Buldukbai-Akchoku Mountain. The lower part of the formation is exposed on the south-western slope of the mountain, north of an east-west fault (Figs 1, 3, 5–7). It includes, in ascending order:

Unit 1. Medium- to fine-grained sandstone up to 120 m thick with *Ectenoglossa sorbulakensis*.

Unit 2. Dark green, bedded siltstones, about 14 m thick with a few layers of fine grained sandstone 3–10 cm thick, containing *Mabella conferta* and *Shlyginia fragilis* of the *Sowerbyella–Mabella* Association.

Unit 3. Siltstones with nodules of algal limestone gradually changing into beds of nodular limestone with dasyclad algae towards the top, 38 m thick in total.

Unit 4. Nodular algal limestone intercalating with siltstone about 0.5–1.5 m thick, up to 22 m thick in total, with brachiopods of the *Acculina–Dulankarella* Association (Sample 8231-40).

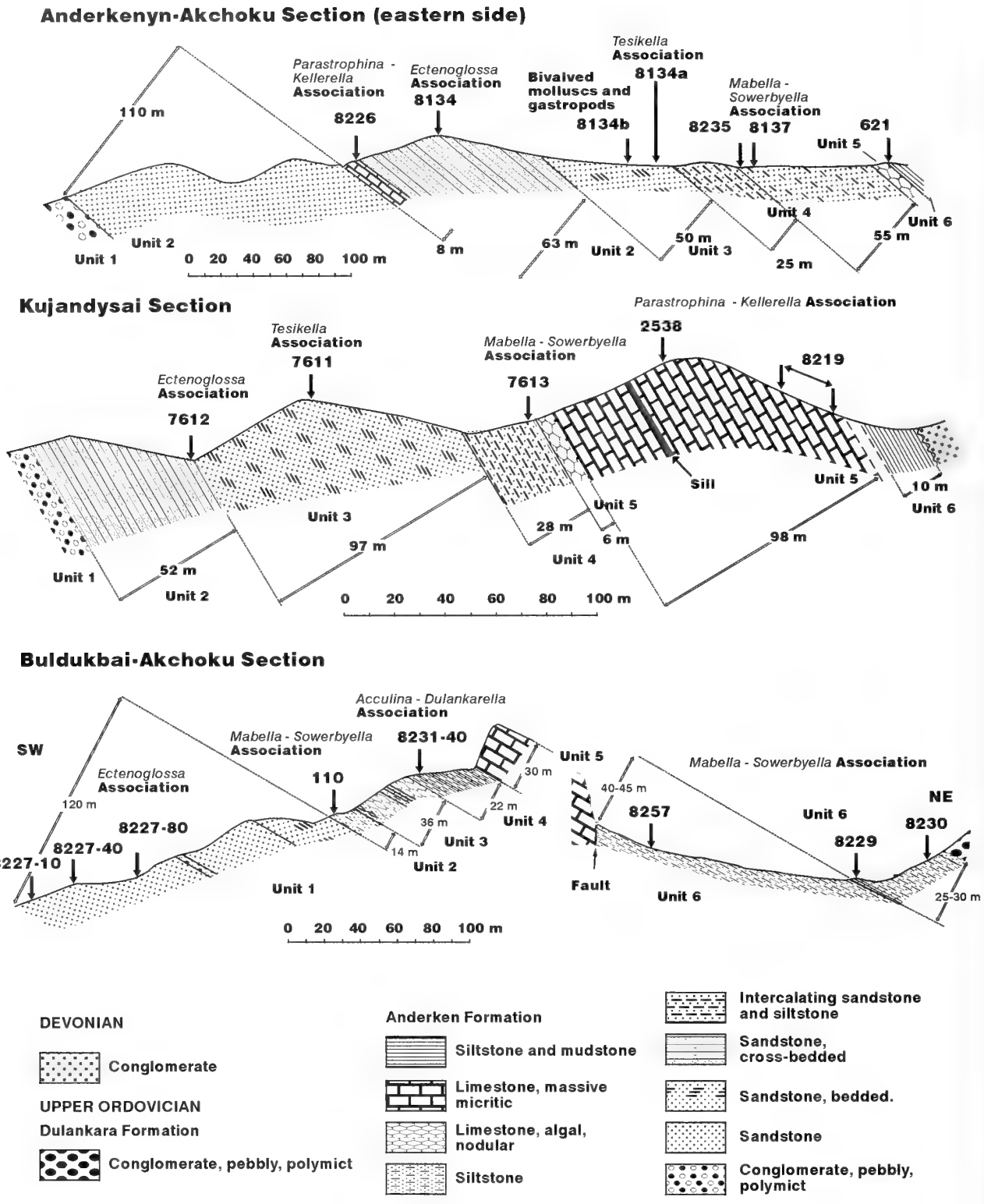

Fig. 5 Schematic stratigraphic sections of the Anderken Formation in the Chu-Ili Range, showing the position of samples and distribution of brachiopod associations.

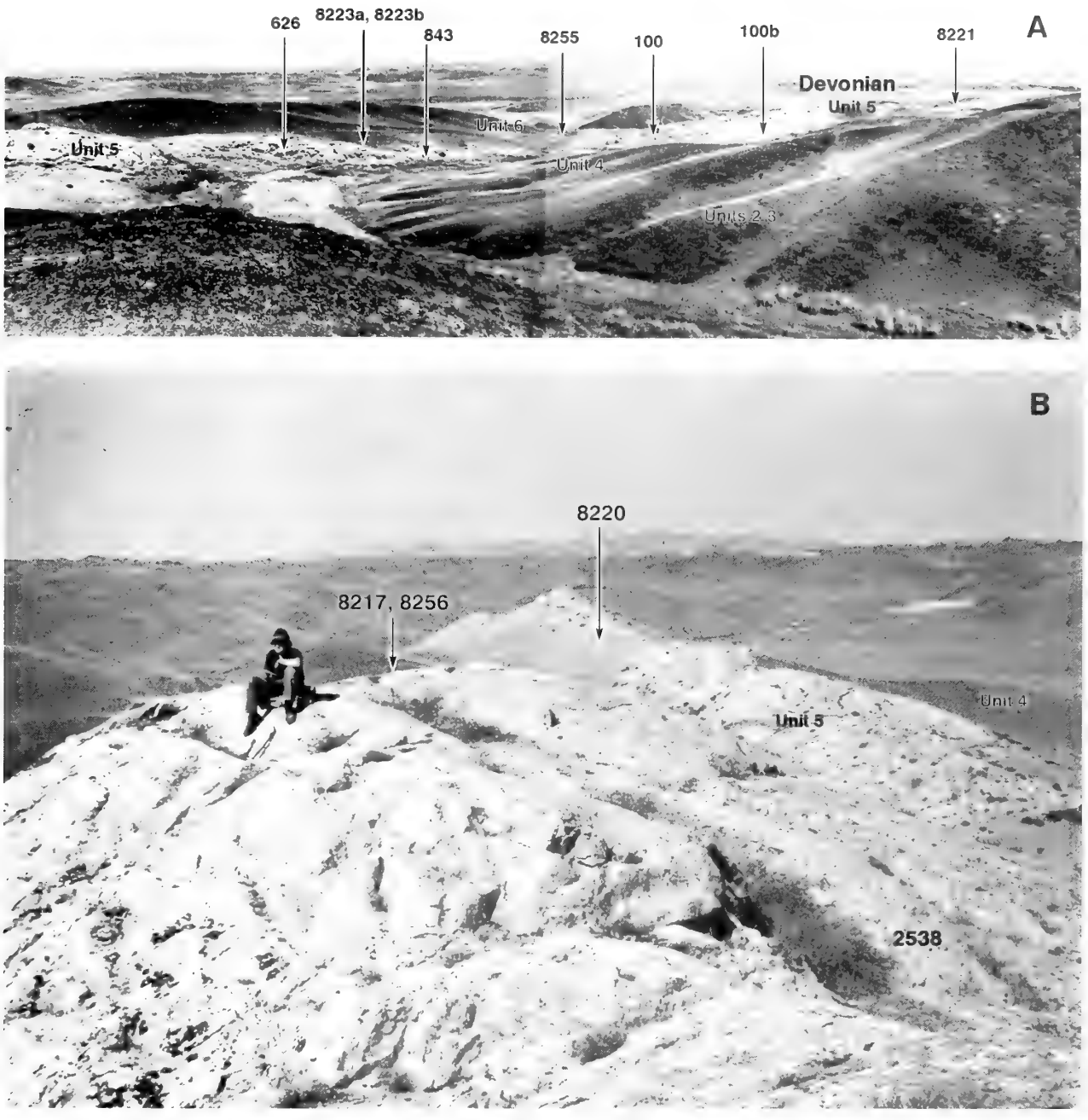

Fig. 6 **A**, general view of the Anderken Formation at the Anderkenyn-Akchoku section, showing informal lithostratigraphic units discussed in the text and the position of brachiopod localities. **B**, view of large complex carbonate buildup at Akchoku Mountain in the upper part of the Kujandysai section. Photographs by Igor Nikitin.

Unit 5. Massive micritic limestone forming the core of the carbonate mud-mound at the top of the mountain, about 30 m thick.

The upper part of the Anderken Formation outcrops along the north-eastern slope of Buldukbai-Akchoku Mountain. It includes:

Unit 6. Laminated, dark green siltstone up to 70 m thick with storm beds of calcareous sandstone rich in brachiopod coquinas about 10–15 cms thick and crinoid columnals. The top is a characteristic bed of laminated brownish-violet siltstone about 0.5 m thick overlain by polymict conglomerate of the Dulankara Formation (Fig. 7B). The unit contains numerous coalified plant remains of *Akdalaphyton caradoci* concentrated on several bedding surfaces, brachiopods of the *Sowerbyella–Mabella* Association (Samples 8229, 8230) and the echinoderms *Clivosocystis* sp., *Digitocrinus levis* and *Ristnacrinus bifidus* Stukalina.

Locality 5. Tesik River

This locality is on the southern side of the River Tesik about 1.5 km upstream of the bridge crossing the river on the highway from

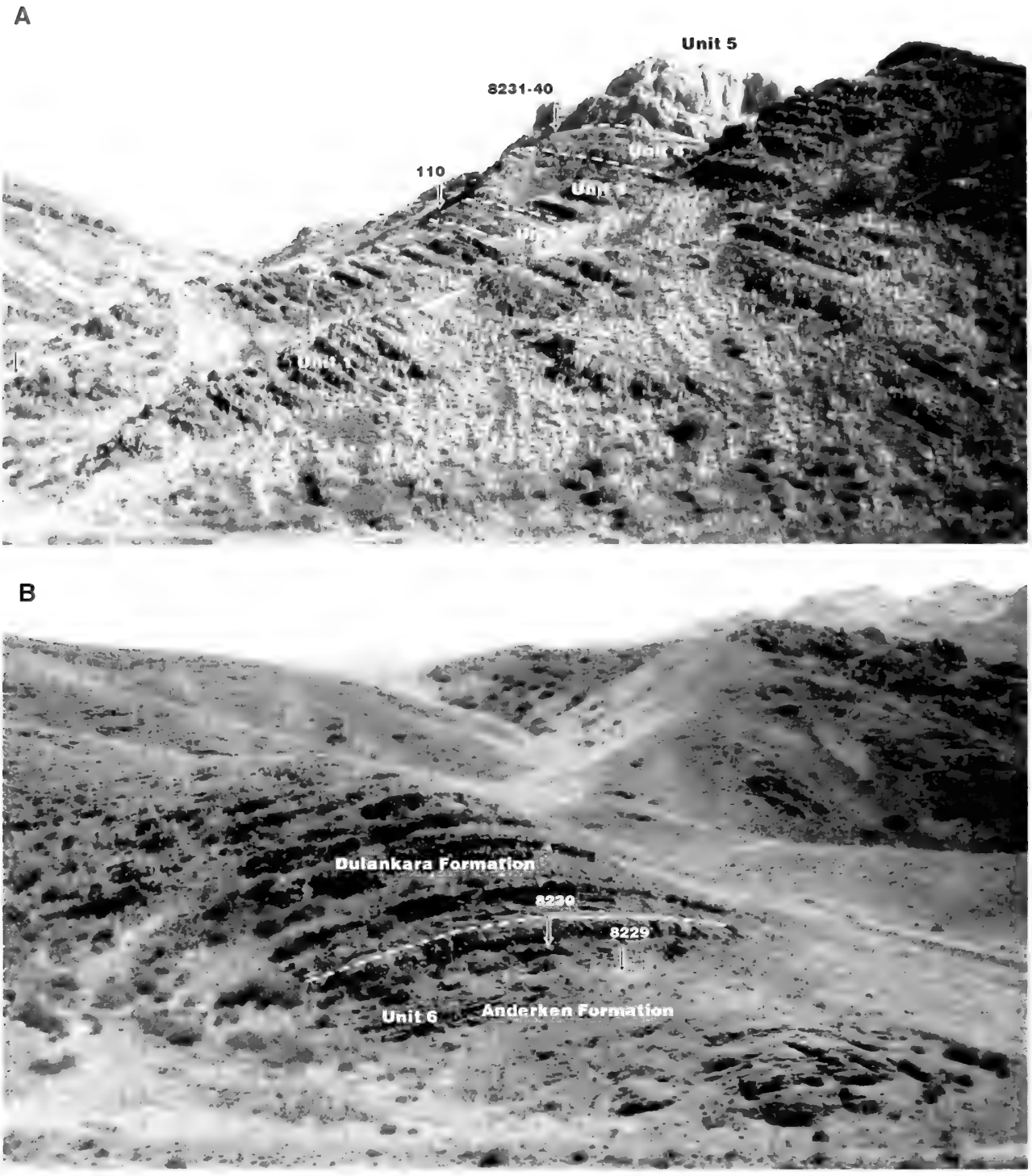

Fig. 7 The Anderken Formation on the south-western slope of Buldukbai-Akchoku Mountain. **A,** Units 1 to 5, and Sample localities 8227–80, 110 and 8231–8240; **B,** Unit 6 and the contact with the overlying Dulankara Formation and Sample localities 8229 and 8230. Photographs by Lars Holmer.

Almaty to Balkhash (Fig. 1, locality 5). It is an isolated natural exposure of about 20 m of pink to light red rocks of massive micritic limestone forming the core of a mud-mound with lens-like beds of biosparite at the base of the exposure. Most of the bioclasts are fragmented large cystoid columnals. It contains an abundant *Parastrophina–Kellerella* Association (Sample 948).

Locality 6. Burultas Valley

The Burultas Valley (Fig. 1, locality 6) is about 42–45 km west of Chiganak on the western Balkhash coast (northeastern part of

Quadrangle 73°22'30" to 73°30' E; 45° to 45°05' N). A summary of the Ordovician geology and lithostratigraphy of this locality is in Nikitin *et al.* (1980, text-figs 18, 20). The Anderken Formation consists mainly of siliciclastic rocks with a thick unit of polymict conglomerates at the base and a number of carbonate mud-mounds in the upper part (Fig. 3). The carbonate unit in the top of the sequence is a bed of nodular algal limestone about 6–10 m thick with numerous *Girvanella* sp., *Cyclocrinites nikitini* and *Mastopora reticulata* and brachiopods of the *Acculina–Dulankarella* Association (Locality 1041a of Nikitin = Sample 390/76 of Kovalevskii), which underlies a lens of massive, micritic limestone up to 20 m thick which forming the mud-mound core. The unit thins about 200 m westward from Locality 1041a, where it is represented by bedded and nodular limestone with the brachiopods *Pionodema opima*, *Dulankarella larga* and *Mabella conferta* (Sample 818). The uppermost 10 m of the underlying unit, of fine-grained sandstone intercalating with siltstone, contains a different brachiopod assemblage with *Tesikella necopina* (Sample 818a), in association with abundant cystoid columnals.

Locality 7. Sorbulak spring on the east side of the River Karatal

In the south Betpak-Dala Desert, about 20 km west of Baigara Mountain, the Anderken Formation is well exposed on both sides of the River Karatal (Fig. 1, locality 7). Here it rests on the graded sandstones and siltstones of the Llandeilo to Lower Caradoc upper Baigara Formation (Fig. 2), or is in contact with intrusives. About 2 km south-east of the Karatal river, south of Sorbulak spring, it comprises (1) polymict conglomerates more than 50 m thick, (2) medium- to fine-grained sandstones 169–170 m thick with *Ectenoglossa sorbulakensis* about 10–15 m above the base of the unit (Fig. 3, Sample 1024); and (3) intercalating fine-grained slightly calcareous sandstones and siltstones about 60 m thick with the *Tesikella* Association in the upper 20 m of the unit. The upper part of the section is an unfossiliferous unit of intercalating fine-grained sandstones, lilac and red siltstones and mudstones several hundred metres thick, which is overlain by the basal conglomerate of the Dulankara Formation.

Locality 8. Kotnak Mountains

This incomplete section of the Anderken Formation is situated west of the Kotnak Mountains, about 7 km SW of Karpkuduk Well. There, about 1.5 km north-east of the salt marsh (Figs 1, 3, 8), the formation consists of: (1) siltstone about 70 m thick with some storm beds of calcareous sandstone about 10–20 cm thick with a coquina of the bivalve *Ctenodonta* sp. (Samples 1017, 1019); (2) sandstone intercalating with siltstone in the upper part, total 40 m thick, with brachiopods of the *Tesikella* Association in the lower 10 m of the unit

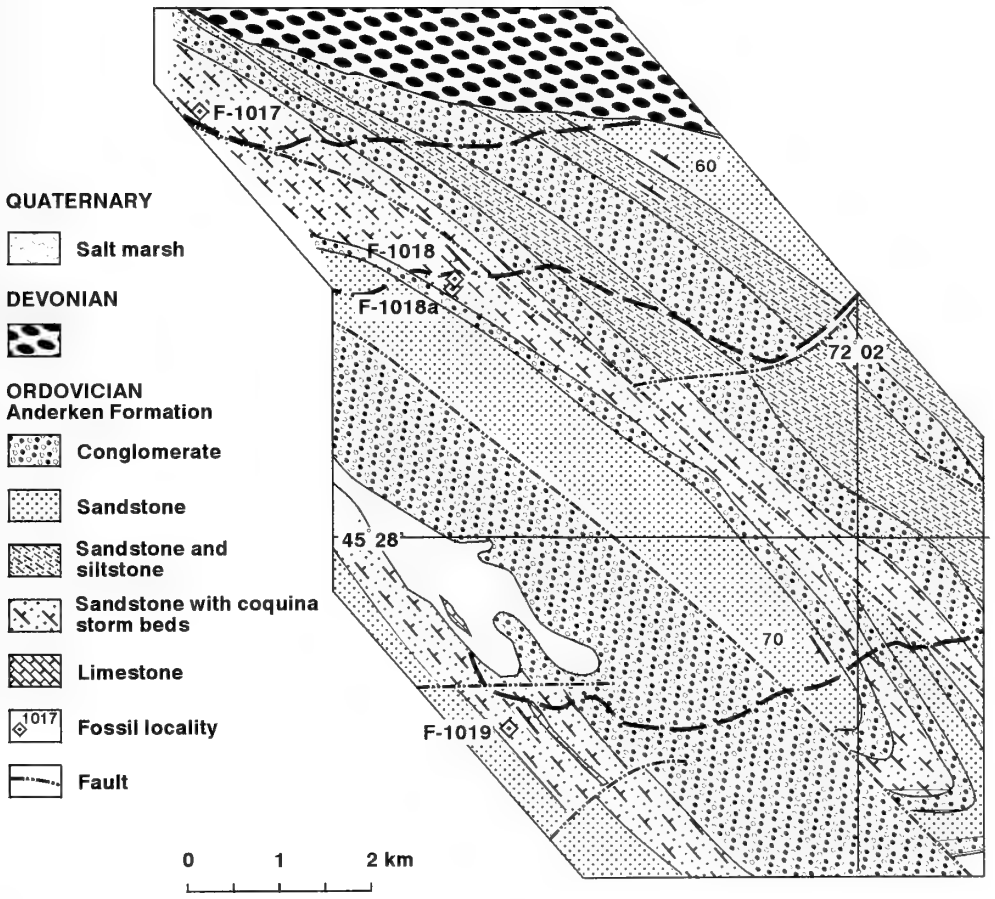

Fig. 8 Geological map showing the distribution of the Anderken Formation and the position of fossil localities in the area about 7 km south-west of Karpkuduk well, Kotnak Mountains.

Table 1 Composition of *Ectenoglossa* Association from the Anderken Formation showing number of complete shells, ventral and dorsal valves respectively.

Sample number	7612	8130a	8130–1	8223–1	8227–10	8227–40	8227–80	F–1024
Number of specimens	27	1	2	1	6	4	3	12
Ectenoglossa sorbulakensis	24:3:2	0:1:0	0:2:0	0:1:1	6:0:0	0:3:4	0:3:3	0:8:12

(Sample 1018a) below a bed of skeletal calcareous sandstone about 5 m thick with an allochthonous brachiopod fauna with a mixture of taxa of the *Tesikella* and *Mabella–Sowerbyella* Associations (Sample 1018); (3) intercalating beds of sandstone and pebbly polymict conglomerate about 80–90 m thick; and (4) siltstone with a few beds of fine-grained sandstone, total 130 m thick and overlain unconformably by Devonian conglomerate.

FAUNAL ASSOCIATIONS

The Anderken Formation is a transgressive sequence from near shore to outer shelf deposits with predominantly siliciclastic deposition. The lower part of the formation, below the main horizon with carbonate build-ups in theAnderkenyn-Akchoku, Kujandysai, Buldukbai-Akchoku and Burultas sections, was formed in tide-dominated environments of mostly tidal flat deposits with characteristic sets of pebbly conglomerates, cross-bedded and laminated sands, coquina storm beds and traces of tidal currents. Carbonate build-ups in the upper part of the formation preserve numerous traces of photosynthetic activity and contain a diverse flora of green and red algae (Nikitin *et al.* 1974); suggesting formation in shallow depths within the euphotic zone. The outer shelf deposits are recorded only in the south-eastern Chu-Ili Range and consist of silt and mud containing graptolites. The benthic fauna is dominated by trilobites but includes one of the earliest records of the *Foliomena* brachiopod fauna. Apollonov (1975) has described the trilobite associations of the middle and late Ordovician of the Chu-Ili Plate.

A matrix based on the distribution of about 1800 brachiopod specimens from 33 samples within the Anderken Formation was subjected to Principal Component Analysis (Etter 1999). Plots of eigenvectors corresponding to three maximum directions of variation (F1–F3) are illustrated on two two-dimensional diagrams (Fig. 9). The Diversity Index is calculated as the number of species minus 1 divided by the natural logarithm of the number of brachiopod individuals in the sample (for details see Williams *et al.* 1981).The analysis of taxonomic composition and relative abundance of brachiopod taxa from numerous localities and samples in the Anderken Formation allows recognition of six brachiopod associations characterised below. They are interpreted within the Benthic Assemblage (BA) scheme of Boucot (1975).

1. The *Ectenoglossa* Association. This is a monospecific lingulide association of BA-1 with *Ectenoglossa sorbulakensis* in the Anderkenyn-Akchoku, Kujandysai and Buldukbai-Akchoku sections, the east side of the Kopalysai River and on the southern side of the Karatal River south of Sorbulak spring (Table 1).The assemblage shows patchy distribution in lithologies of coarse- to medium-grained sands with subhorizontal and cross-bedded stratification. In most of the localities shells are disarticulated on the bedding surfaces and only in Sample 7612 do conjoined valves predominate (89% of individuals). A cluster of six articulated shells preserved in life position inclined from 62°–80° to the bedding surface was recovered from Sample 8227-40 in the Buldukbai-Akchoku section, which confirms the infaunal mode of life of this lingulide. The gastropods *Lophospira* sp. and *Latitenia kasachstanica* Vostokova and the bivalved molluscs *Endomionia fecinda*, *Ctenodonta* sp. and *Cyrtodonta*? *subcentralis* (Khalfin 1958), which are widespread in similar lithologies and form coquina storm beds, do not co-occur together with the lingulides; for example, in Sample 8130 a bedding surface with *Ectenoglossa sorbulakensis* and a storm bed with molluscs and the trilobite *Eokosovopeltis romanovskyi* are separated by an interval only about 2.5 m thick. It is likely that *Ectenoglossa*

Table 2 Composition of *Tesikella* Association from the Anderken Formation showing number of complete shells, ventral and dorsal valves respectively.

Sample numbers	127	818a	F-1018a	7611	8128	F-1018	F-1024b	8127-2b	8138
Number of specimens	18	22	32	7	18	172	20	1	2
Diversity index	0.33	0.65	0.58	0.51	1.38	3.11	2.16		
Trematis sp.	0:0:1								
Tesikella necopina	3:14:12	0:13:12	0:16:7	1:5:5	0:4:2	1:4:3	0:2:2	0:1:0	0:2:0
Longvillia lanx			0:4:5			2:7:3			
Glyptomena onerosa						0:1:5			
Christiania egregia						0:7:18	0:2:7		
Limbimurina sp.						0:1:1			
Isophragma imperator						1:36:34			
Acculina kulanketpesica					0:0:1	0:1:2			
Mabella conferta		1:0:0				0:1:2			
Shlyginia fragilis						0:6:4			
Anaptambonites orientalis						1:4:3			
Sowerbyella rukavishnikovae			0:10:11			0:8:17	0:9:10		
Bicuspina rukavishnikovae						3:1:9			
Plectorthis burultasica					0:0:1	1:6:7			
Dolerorthis expressa						1:12:9			
Phragmorthis conciliata						0:4:4	0:1:0		
Eodalmanella extera		4:4:0		0:0:1		1:28:22			
Pionodema opima					2:8:5				
Rhynchotrema sp. nov.					1:0:0				
Didymelasma cf. *transversa*						0:0:1			

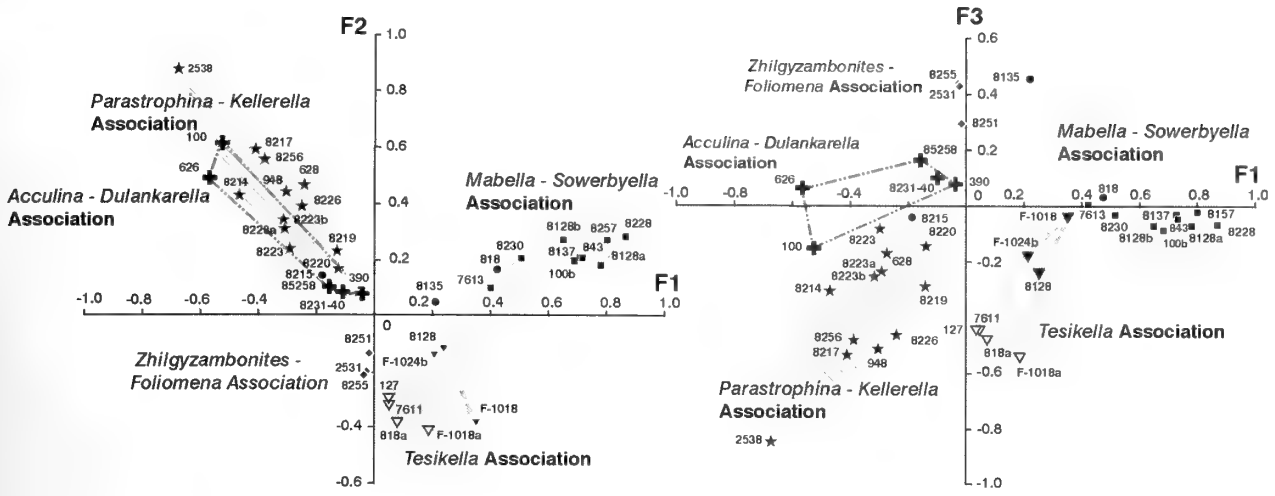

Fig. 9 Two-dimensional principal component analysis plots on first (F1), second (F2) and third (F3) eigenvectors of selected brachiopod samples from the Anderken Formation shown on Tables 1–6.

sorbulakensis formed a separate monotaxic community which inhabited a mobile sandy bottom in peritidal environments, perhaps tidal flats.

2. The *Tesikella* Association (average Diversity Index 1.18; observed range 0.33–2.16, N=7). This is a low-diversity strophomenide-dominated brachiopod association. It is widespread in shallow marine environments of BA-2, which are mainly fine-grained sands with subhorizontal stratification, occasional storm beds with mollusc coquinas and locally abundant plant remains of *Akdalaphyton caradoci*. This association is defined by the index species *Tesikella necopina*, an endemic species and genus restricted only to the Lower Anderken Formation. This species pursued an opportunistic life strategy and expanded into environments inhabited mostly by gastropod and bivalved mollusc communities, in which rhynchonelliformean brachiopods, if they occur, are an insignificant component of the assemblage and show patchy distribution. Traces of tidal currents, ripple marks and occasional storm beds suggest rather turbulent environments occasionally affected by seasonal storms. Shells in all the samples are mostly disarticulated (Table 2) and some contamination by allochthonous shells from adjacent associations cannot be excluded. However, results of the Principal Component Analysis show that all the samples referred to the *Tesikella* Association form a distinct cluster and are characterised by low positive values of F1 and negative values of the two other maximum directions of variation (F2 and F3). Sample 1018, which may be contaminated by allochthonous shells, shows low negative values of F3 similar to the samples of the *Mabella–Sowerbyella* Association (Fig. 9).

In its pioneer stage, the *Tesikella* Association is characterised by the appearance of *Tesikella necopina* in mollusc-dominated environments, where it is the only brachiopod (Samples 127, 7611, 8127–2b, 8138), or where it comprises more than 50% of the brachiopod fauna together with *Longvillia lanx*, *Sowerbyella rukavishnikovae* (up to 34%) and *Eodalmanella extera* (up to 18%). At its mature stage the association includes four to eight species usually common in the *Sowerbyella–Mabella* Association, e.g. *Christiania egregia* (up to 35%), *Sowerbyella rukavishnikovae* (up to 50%) and *Pionodema opima* (56% in one sample). All the other taxa constitute less than 5% of individuals in any particular sample. Among other groups bivalved molluscs, the trilobites *"Isotelus" romanovskyi*, *Lonchodomas tecturmasi* and *Dulanaspis levis anderkensis* occur. The echinoderm fauna is dominated by the cystoidean *Clivosocystis minusculus* Stukalina which is known only from columnals. The abundance of coquinas and plant remains suggests biogenic fixation of a sandy substrate.

Sample 1018 from the Kotnak Mountains is placed within the field of the *Tesikella* Association (Fig. 9), but differs in high taxonomic diversity and the occurrence of taxa characteristic of the *Sowerbyella–Mabella* and *Acculina–Dulankarella* associations, e.g. *Anoptambonites orientalis*, *Glyptomena onerosa*, *Limbimurina* sp. and *Acculina kulanketpesica*. This sample came from a bed of bioclastic sandy limestone, which is an atypical lithology for the *Tesikella* Association, more likely to have been deposited within a bar system, and contains an allochthonous brachiopod coquina representing a mixture of several life associations. The abundance of coarse clastics and storm beds formed mostly by the bivalve *Ctenodonta* sp. (Samples 1017, 1019) in the Anderken Formation of this section suggest turbulent depositional environments within a shore-face zone comparable with the lower part of the Otar beds in the Dulankara Formation of the Dulankara section in the south-eastern Chu-Ili Range (Popov *et al.* 2000).

3. *Mabella–Sowerbyella* Association (average Diversity Index 1.30; observed range 0.83–1.86, N=9) is another low diversity association of BA-2 dominated by strophomenides. It is recognised in the Anderkenyn-Akchoku, Kopalysai and Buldukbai-Akchoku sections by the predominance of *Mabella conferta* and *Sowerbyella rukavishnikovae* which together comprise 40–80% of individuals in the assemblage. *Glyptomena onerosa*, *Shlyginia fragilis* and *Anoptambonites orientalis* mainly occur in this association (Table 3). As in the mature *Tesikella* Association, orthides are represented only by *Eodalmanella extera* and *Pionodema opima*, which do not usually co-occur. This association is confined to a fine clastic substrate of silts and fine-grained sands, usually with traces of bioturbation and locally abundant concentrations of the plant *Akdalaphyton caradoci*. In samples from the Anderkenyn-Akchoku section brachiopods are preserved disarticulated, but in the Kopalysai and Buldukbai-Akchoku sections the number of articulated specimens increases up to 50 percent, suggesting rapid burial and lack of significant post-mortem displacement of the shells. The most common trilobites in the associated faunal assemblage are *Lonchodomas*

Table 3 Composition of *Mabella–Sowerbyella* Association from the Anderken Formation showing number of complete shells, ventral and dorsal valves respectively.

Sample number	100b	7613	8128a	8128b	8137	8257	8228	8229	110	8230	843
Number of individuals	248	50	9	27	10	21	41	5	11	36	75
Diversity index	1.09	1.79	1.82	1.21	1.73	1.31	1.62	1.86	0.83	1.13	1.39
Trematis sp.							0:0:1				
Paracraniops sp.			0:0:1								
Glyptomena onerosa	0:5:9	0:1:2			0:2:2	0:0:2		0:1:0			0:3:4
Christiania egregia		0:0:1									
Foliomena prisca							0:1:0				
Dulankarella larga							0:1:0				
Mabella conferta	0:115:7	1:0:0	0:1:2	0:11:14	0:1:2	6:2:0	13:10:2	1:1:0	7:1:0	1:24:13	0:15:24
Shlyginia fragilis	0:15:10	0:10:16	0:3:1	0:2:0	0:3:2	4:3:1			0:2:0	0:1:2	0:0:1
Anoptambonites orientalis	0:9:20			0:0:2						1:1:1	
Olgambonites insolita					0:0:1						
Sowerbyella rukavishnikovae	0:28:79	0:2:2	0:0:2	0:4:5	0:2:2	0:2:1	0:5:2	0:1:0		0:2:2	
Triplesia sp.							0:2:3				
Phragmorthis conciliata		1:0:0								0:0:1	
Plectorthis burultasica											0:1:2
Eodalmanella extera	0:3:10		0:1:0	0:2:4							0:6:12
Pionodema opima		1:24:24				1:1:0	2:8:5	1:1:1	0:0:1	0:4:4	1:24:24
Rhynchotrema akchokense		0:2:1									2:3:5

Table 4 Composition of *Acculina–Dulankarella* and *Parastrophina–Kellerella* associations from the Anderken Formation showing number of complete shells, ventral and dorsal valves respectively.

	Acculina–Dulankarella Association					*Parastrophina–Kellerella* Association	
Sample number	F-100	F-1041a	626	85258	8231–40	628	8219
Number of individuals	168	113	112	32	11	40	2
Diversity index	5.07	1.91	4.87	2.60	1.25	5.42	
Mezotreta? sp.	0:1:0						
Schizotreta sp.			1:0:0			0:0:1	
Bellimurina sarytumensis		1:4:0				0:0:1	
Teratelasmella chugaevae	12:0:0		4:0:2			0:0:1	
Furcitellinae gen. et sp. indet.	1:1:1	2:1:2	1:0:1			0:0:1	
Limbimurina? sp.	0:0:1					0:1:1	
Christiania aff. *sulcata*						1:6:4	
Christiania egregia	1:4:1	2:1:3	0:2:0	5:1:0			
Craspedelia tata	7:2:0		6:4:0		0:1:0	1:0:1	
Acculina kulanketpesica	12:1:3	32:3:1	1:1:1	4:2:1	1:5:1		
Dulankarella larga	25:1:0	47:0:0	11:1:0		1:1:1		
Kajnaria rugosa	2:0:0	3:1:0	1:0:0			2:1:0	
Mabella conferta	1:0:0	3:0:0				0:1:0	
Shlyginia fragilis				0:1:0		0:1:0	
Glyptambonites sp.	0:2:0						
Sortanella aff. *quinquecostata*	1:1:2		2:3:2			0:1:1	
Anoptambonites convexus	12:1:3		13:6:3	1:2:1	1:0:1		
Sowerbyella aff. *ampla*	0:2:3		2:8:0	0:1:4			
Gacella institata	3:1:4		5:1:3	2:0:0		0:0:1	
Placotriplesia spissa	2:1:0	3:2:1	1:1:3	1:0:0			
Triplesia aff. *subcarinata*						0:0:2	
Bicuspina rukavishnikovae	1:0:0		1:0:0				
Grammoplecia wrighti			1:0:1			0:0:2	
Skenidioides sp.							
Dolerorthis pristina	1:4:2		0:1:0			0:2:2	
Glyptorthis sp.			1:0:0			0:2:1	
Austinella sarybulakensis				3:1:1			
Plectorthis burultasica		1:1:0				1:0:0	
Phragmorthis conciliata			0:1:0				
Parastrophina iliana	5:1:1	4:0:0	7:0:0	2:0:0		2:0:1	
Parastrophina plena	7:0:0						1:0:0
Liostrophia pravula	3:0:2					1:0:4	
Plectosyntrophia? unicostata	2:0:0		4:0:0				
Schizostrophina margarita	1:3:0		2:0:0			1:0:0	1:0:0
Rhynchotrema akchokense	2:0:0		1:0:0			1:0:0	
Pectenospira pectenata			1:1:1				
Kellerella misiusi	3:0:0		1:0:0				
Nikolaispira guttula	2:0:0						

tecturmasi, *Dulanaspis levis anderkensis* and *Styginella macrophtalma*, whereas *Bronteopsis extraordinaris*, *Pliomerina* sp. and *Remopleurides* sp. are relatively rare. Bivalved molluscs include *Anderkenia ledomorpha*, *Clionichia crispa*, *Edmondia obliqua* and *Praemyophoris? antiqua* (Khalfin 1958), and gastropods are represented mostly by *Lophospira cribrosa* Vostokova. Other fossils include unidentified fenestrate and ramose bryozoans of at least three different species, cystoid and crinoid columnals identified by Stukalina (1988) as *Clivosisystis clivosus*, *Communicystis communis*, *Digiticrinus levis*, *Ordinacrinus punctatus*, *Ristnacrinus bifidus* and *Shizocrinus lentiformis*, the cystoidean *Polycosmites?* sp. and the starfish *Stenaster obtusus*.

4. *Acculina–Dulankarella* Association (Diversity Index 3.14; observed range 1.25–5.07, N=5) is characteristic of a nodular algal limestone with abundant dasyclad algae which was deposited in the base and flanks of carbonate build-ups in the upper Anderken Formation. It is a medium to high diversity association defined by the occurrence of the plectambonitoideans *Acculina kulanketpesica* and *Dulankarella larga*. Other brachiopods include *Teratelasmella chugaevae*, *Kajnaria rugosa*, *Gacella institata* and *Austinella sarybulakensis* which do not exceed 5% in other associations. Other components of the assemblage are taxa common in the *Parastrophina–Kellerella* Association (Tables 4–5), whereas *Christiania egregia* is the only abundant species characteristic also of the *Mabella–Sowerbyella* Association. *Mabella conferta* and *Shlyginia fragilis* occur sporadically and do not exceed 5% in a particular sample. There are abundant green algae: *Apidium parvulum*, *Cyclocrinites nikitini*, *Mastopora reticulata*, *Mastopora nana* and *Sinuatipora bucera* and the red alga *Contexta binaria* (Gnilovskaya *in* Nikitin *et al.* 1974). Small organic build-ups up to 30 cm across of the algae *Girvanella* and *Renalcis* are also characteristic and encrust brachiopod shells and green algae. The substrate was mainly of silt and lime mud with patches of hardground and numerous bioclasts. The abundance of brachiopods preserved as conjoined valves (45–64%) in combination with the abundant flora of algae suggests quiet environments within the euphotic zone of BA-3. Strophomenides (61–90%) constitute the most diverse and abundant component of the brachiopod fauna. The second most abundant group is the camarelloideans (4–14%), mostly *Parastrophina iliana* and relatively rare *Parastrophina plena*, *Eoanastrophia unicostata*, *Liostrophia pravula* and *Schizotretina margarita*, which do not exceed 5% in a particular sample; and orthides, rhynchonellides and spire-bearing groups form an insignificant part of the association. Among other groups trilobites are the most abundant. These were partly studied by Weber (1948) and Chugaeva (1958), but details remain inadequate. The most characteristic taxa are: *Illaenus* sp., *Acrolichas punctata*, *Cheirurus* sp., *Eokosovopeltis romanovskyi*, *Mesotaphraspis spinosus*, *Pliomerina sulcifrons* and *Sphaerexochus* sp. A diverse echinoderm fauna was identified mostly from cystoid and crinoid columnals (Stukalina 1988). Among molluscs the most characteristic is the cephalopod *Discoceras kazakhstanensis* Barskov. The rare corals *Amsassia* sp. and *Lichenaria* sp., clathrodictyid stromatoporoids, gastropods and bivalved molluscs are also reported, but remain poorly known.

Table 5 Composition of *Parastrophina–Kellerella* Association from the Anderken Formation showing number of complete shells, ventral and dorsal valves respectively.

Sample number	948	2538	8214	8226	8217	8223	8223a	8223b	8256
Number of individuals	200	200	33	12	13	15	18	9	31
Diversity index	2.64	4.91	2.63	1.61	2.34	2.58	3.11	2.76	2.33
Nushbiella dubia		0:1:1					0:1:0		
Bellimurina sp.	0:2:1	0:1:0	1:2:0						0:1:0
Limbimurina sp.		0:0:1						0:0:2	
Christiania aff. *sulcata*		0:2:1	1:4:1	0:1:0	0:1:0	0:2:0	0:1:1	0:2:1	
Foliomena prisca						0:0:1			
Craspedelia tata	2:2:1	8:4:3	1:2:0				0:1:0	0:1:0	
Kajnaria rugosa						1:1:0			
Sortanella aff. *quinquecostata*	3:2:1	4:0:2							
Anoptambonites convexus		9:6:2				0:3:1			1:3:4
Sowerbyella aff. *ampla*	2:2:1	3:1:1	2:2:2		0:2:0		3:1:0	1:0:0	
Triplesia aff. *subcarinata*		2:0:0							
Placotriplesia spissa		3:1:7	0:2:1			1:1:0			0:0:1
Grammoplecia wrighti			0:2:1						
Skenidioides sp.			1:0:0	0:1:0				0:1:0	
Dolerorthis pristina	4:5:7	0:1:1	2:1:3		0:0:1	0:0:1		0:1:0	
Glyptorthis sp.	0:2:1	2:2:1	3:1:1				0:1:1		0:0:1
Plectorthis burultasica		3:1:1							
Phaceloorthis sp.		1:0:0							
Bowanorthis? devexa	7:0:0	5:0:0							
Phragmorthis conciliata		2:0:1					0:0:1		
Parastrophina iliana	15:0:0	15:0:1							2:0:0
Parastrophina plena	62:0:0	17:0:1	3:0:0	2:1:1	2:0:0		1:0:0	1:0:0	5:0:0
Ilistrophina tesikensis	14:0:0								
Liostrophia pravula	7:0:0	13:0:1				3:0:0			3:0:0
Plectosyntrophia? unicostata		1:0:0			0:0:1				
Schizostrophina margarita		16:0:0			0:0:1	0:0:1			5:3:2
Didymelasma cf. *transversa*		1:0:0							
Rhynchotrema akchokense	2:0:0	2:0:0							
Pectenospira pectenata	14:1:1	3:0:0	1:0:0				3:0:0		
Kellerella misiusi	15:0:1	39:0:0		2:0:0	5:0:0		2:0:0		5:0:0
Nikolaispira guttula	13:0:0	20:0:0		1:0:0			2:0:0		
Acculina sp.		0:1:1							

5. *Parastrophina–Kellerella* Association (Diversity Index 3.17, observed range 1.61–5.42, N=10) is closely associated with carbonate build-ups and also belongs to BA-3. These build–ups were interpreted by Nikitin *et al.* (1974) as a chain of bioherms with a frame built by the cyanobacterians *Girvanella* and *Renalcis*: however, micritic limestone usually comprises the most significant part of the volume of the rock in the core of a build-up. According to Nikitin *et al.* (1974), these build-ups form a low ridge, raised about 1.5–3 m above surrounding areas with fine clastic sedimentation. Fossils are usually concentrated in pockets of bioclastic limestone between individual bioherms and mounds (Samples 948, 2538, 8223a, 8256). Composition of this association is essentially similar to the *Acculina–Dulankarella* Association, with more than 80% of recorded species in common. However, the abundance of camarelloideans increases up to 49% (Sample 948) and the archaic spire-bearing brachiopods *Pectenospira pectenata*, *Kellerella misiusi* and *Nikolaispira guttula* constitute a significant part of the association (21–42% in the most representative samples), whereas in the *Acculina–Dulankarella* Association they are less than 2% (Table 5). The relative abundance of strophomenides decreases significantly and such genera as *Acculina*, *Dulankarella*, *Mabella* and *Shlyginia* disappear completely. *Christiania* is represented by the species *C.* aff. *sulcata*, which is closely linked to this association. Diminution in the sizes of the strophomenides might reflect the predominance of hard grounds. Taxonomic composition of the association is modified in the bedded bioclastic limestone which has large ooids (up to 1 cm across) on the top and flanks of the core (Samples 8214, 8217, 8223, 8223b). Brachiopods are relatively rare and dispersed through the rock. Relative abundance of strophomenides, and especially *Christiania* aff. *sulcata*, increases, whereas spire-bearing brachiopods become rare or completely disappear in some samples (8214, 8223, 9223b). According to the Principal Component Analysis these occupy an intermediate position between the cluster formed by samples of the *Acculina–Dulankarella* Association and samples 948, 2538, 8256, which represent the fully developed *Parastrophina–Kellerella* Association (Fig. 8B).

The associated trilobite fauna is only partly known and includes such taxa as *Illaenus* sp., *Acrolichas punctata*, *Amphilichas punctata*, *Eokosovopeltis romanovskyi*, *Glaphurina weberi*, *Mesotaphraspis spinosus*, *Pliomerina sulcifrons*, *Selenoharpes* sp. and *Sphaerexochus* aff. *hisingeri* (Weber 1948, Chugaeva 1958, Kolobova & Popov, 1986). Crinoid columnals usually represent the most important source of bioclasts in the rock. They mostly belong to *Webericrinus variabilis*, *Ordinacrinus ordinaris*, *Malovicrinus depressus*, *Tatjanicrinus crusciformis*, *Flexicrinus flexus*, *Communicrinus communis* and *Multifidocrinus mulrifidus* (Stukalina 1988).

In the eastern part of the Anderkenen-Akchoku section (Sample 8226), isolated carbonate build-ups up to 16 m thick appear within Unit 2, which is mostly cross-bedded sandstone containing lingulide and mollusc associations. It is likely that these build-ups formed almost intertidally, but, except for a much lower diversity, the brachiopod assemblage retains a relative abundance of spire-bearers (*Kellerella misiusi*) and camerelloideans (*Parastrophina plena*) typical of the *Parastrophina–Kellerella* Association, whereas trilobites such as *Acrolichas* sp., *Eokosovopeltis romanovskyi*, *Sphaerexochus* aff. *hisingeri* and *Illaenus* sp. also show close similarity to the assemblage from the carbonate unit in the upper part of the Anderken Formation.

6. *Zhilgyzambonites–Foliomena* Association (Diversity Index 1.21; observed range 1.14–130, N=3) is known from three samples collected from the unit of mudstones and siltstones in the uppermost Anderken Formation in the Anderkenyn-Akchoku section (Figs 3, 5, Unit 6, Table 6). Brachiopods are a minor part of a trilobite-dominated benthic assemblage, which includes *Amphitrion* cf. *radians*, *Ampixinella* sp., *Birmanites almatiensis*, *Bronteopsis extraordinaris*, *Cheraurus kassini*, *Cybele weberi*, *Dionide kazachstanica*, *Dindymene* sp., *Hammatocnemis* sp., *Microparia speciosa*, *Ovalocephalus* sp., *Granulatagnostus granulatus* and *Sphaerognostus* sp. (Chugaeva 1958, Nikitin *et al.* 1974). Co-occurrence of agnostids, cyclopygids and *Ovalocephalus* allows us to refer this assemblage to the *Ovalocephalus* fauna of Fortey (1997) which is characteristic of outer shelf trilobite biofacies corresponding to BA 4–5. Co-occurrence of the *Foliomena* and the *Ovalocephalus* faunas is common in late Caradoc to early Ashgill deep water benthic communities in South China (Rong *et al.* 1994). The *Zhilgyzambonites–Foliomena* Association includes only six strophomenide genera. Two of them (*Olgambonites* and *Zhilgyzambonites*) are Kazakhstan endemics, whereas *Anisopleurella* and *Kassinella* are characteristic of early *Foliomena* faunas in the Caradoc of China (Rong *et al.* 1999) and elsewhere.

Table 6 Composition of *Zhilgyzambonites–Foliomena* Association from the Anderken Formation showing number of complete shells, ventral and dorsal valves respectively.

Sample number	2531	8251	8255
Number of specimens	4	4	15
Diversity index	1.44	0.72	1.48
Foliomena prisca	1:0:0	0:1:0	1:3:3
Olgambonites insolita			0:3:2
Zhilgyzambonites extenuata	0:2:1	0:3:3	2:5:5
Kassinella? sp.			0:0:1
Chonetoidea sp.			1:0:0
Anisopleurella sp.	0:1:1		

OVERALL PALAEOECOLOGY

The sequence of brachiopod associations in the Anderken Formation shows an onshore-offshore pattern with a monotaxic lingulide community inhabiting mobile sand nearshore, low diversity mollusc and brachiopod associations of BA-2 on a shallow clastic shelf, medium to high diversity faunas of BA-3 linked with carbonate build-ups, and a deep water *Foliomena* fauna as part of a trilobite-dominated benthic assemblage in BA 4–5. In terms of abundance, diversity and taxonomic composition, the five associations formed by rhynchonelliformean brachiopods can be subdivided into three groups, which show little interaction and apparently evolved independently. They are: 1, low-diversity strophomenide-dominated *Tesikella* and *Mabella–Sowerbyella* Associations of shallow clastic shelf corresponding to BA-2; 2, medium to high diversity *Acculina–Dulankarella* and *Parastrophina–Kellerella* Associations closely linked to carbonate build-ups; and 3, a deeper-shelf *Zhilgyzambonites–Foliomena* Association representing an early *Foliomena* Fauna.

The predominance of strophomenides in environments corresponding to BA-2, which is usually dominated by rhynchonellides and spire-bearing taxa in the late Ordovician and Silurian (Boucot 1975; Ziegler *et al.* 1968), is a distinctive feature of the Anderken sequence of communities. The *Tesikella* and *Mabella–Sowerbyella* Associations share eight brachiopod species but *Tesikella necopina* (the index species of the former association) does not usually co-occur with *Mabella conferta* and *Shlyginia fragilis*. The *Tesikella necopina* Association also demonstrates significant variations in

Table 7 Additional list of brachiopod taxa from localities in the Anderken Formation not referred to a particular association

Sample number	42	818	1628	8215	620	8251a	8135
Number of specimens	3	4	4	10	13	2	2
Glyptomena onerosa							0:1:0
Christiania aff. *sulcata*				1:4:1			
Craspedelia tata				0:1:0			
Dulankarella larga		1:0:0					
Mabella conferta					0:1:0		
Shlyginia fragilis	0:1:0	0:0:1			5:7:2		0:1:0
Anaptambonites orientalis							
Sowerbyella? aff. *ampla*			1:3:0				
Sowerbyella rukavishnikovae							
Triplesia aff. *subcarinata*						2:0:0	
Placotriplesia spissa				2:1:0			
Grammoplecia wrighti				1:0:0	2:1:8		
Plectorthis burultasica					1:0:1		
Eodalmanella extera					2:0:1		
Dolerorthis pristina	2:0:0						
Pionodema opima		2:0:0					

relative abundance and taxonomic composition from one sample to another, which may reflect its opportunistic character and higher environmental stress, whereas the *Mabella–Sowerbyella* Association, in spite of its low diversity (4 to 8 genera per sample), shows a relatively constant taxonomic composition in most samples (Table 3), and this association forms a compact cluster in the Principal Components Analysis (Fig. 9). Comparison with somewhat younger *Ctenodonta–Sowerbyella*, *Altaethyrella-Nalivkinia (Pronalivkinia)* and *Dinorthis* Associations of the lower Dulankara Formation which inhabited similar environments on the shallow clastic shelf on the Chu-Ili Plate in the late Caradoc-early Ashgill (Popov *et al.* 2000), suggest a rapid faunal turnover. In these younger faunas *Sowerbyella* and *Shlyginia* retained their dominant position and *Anoptambonites* also remained a characteristic minor component, but most of the Anderken genera disappeared (e.g. *Tesikella*, *Eodalmanella* and *Pionodema*) or moved into the middle shelf (*Mabella* and *Glyptomena*) and were replaced by rhynchonellides such as *Altaethyrella* and atrypides such as *Nalivkinia (Pronalivkinia)*. In contrast, the orthides (e.g. *Plaesiomys*, *Bokotorthis* and *Dinorthis*) became increasingly abundant.

The diverse *Acculina–Dulankarella* and *Parastrophina–Kellerella* Associations, which were closely linked with carbonate build-ups, have little in common with the faunas which inhabited shallow clastic shelves nearby. In the *Acculina–Dulankarella* Association strophomenides remain the most abundant brachiopods but they are mostly different genera, such as *Bellimurina*, *Teretelasmella*, *Craspedelia*, *Acculina*, *Dulankarella*, *Kajnaria* and *Sortanella*. *Anoptambonites* occurs in both associations, but as different species. *Mabella* and *Shlyginia* are mostly confined to the *Mabella–Sowerbyella* Association, as well as occurring in a few samples of the *Acculina–Dulankarella* Association, but as less than 5% of the sample (Table 4). They disappear in the *Parastrophina–Kellerella* Association (Table 5), which is possibly the earliest known brachiopod assemblage in which pentamerides together with spire-bearing taxa come to a dominant position. In contrast to the brachiopod fauna of the shallow clastic shelf, assemblages associated with carbonate build-ups did not undergo any significant taxonomic change during the Caradoc. The late Caradoc to early Ashgill brachiopod fauna of the Dulankara carbonate mud-mound in the north Betpak-Dala Desert (Nikitin *et al.* 1996), which was also on the same Chu-Ili Plate, retained a close similarity to the Anderken fauna and contained 14 genera in common including *Parastrophina* and the early athyridides *Kellerella* and *Nikolaispira*. The strophomenide component was largely unchanged and such genera as *Bellimurina*, *Limbimurina*, *Christiania*, *Craspedelia*, *Sortanella* and *Anoptambonites* are common to both faunas.

The significance of the *Foliomena* fauna was discussed by Cocks & Rong (1988) and Rong *et al.* (1994, 1999). In the Lower to Middle Caradoc it was confined mostly to South China and only in the Ashgill did it become cosmopolitan. In Kazakhstan there are no previous reports of the occurrence of *Foliomena*, but the associated *Ovalocephalus* trilobite fauna occurs in many outer shelf environments from the Middle Caradoc (Apollonov 1975; Nikitin *et al.* 1974). In the Anderken Formation *Foliomena* itself is not restricted to BA 4–5, but occurs occasionally in the *Parastrophina–Kellerella* (Sample 8223) and *Mabella–Sowerbyella* (Sample 8228) Associations. However, the other taxa, which include the two new genera and species *Olgambonites insolita* and *Zhilgyzambonites extenuata* together with rare *Anisopleurella, Chonetoidea* and *Kassinella,* are not present in shallow shelf associations. In addition. there are seven localities (Table 7) whose brachiopods cannot be referred with confidence to any of the six named associations.

Although comprehensive comparisons of the Anderken faunas with other contemporary brachiopods from elsewhere are beyond the scope of this paper, it is worth noting here that the total Anderken assemblage has much in common with that described from north-west China (Fu 1982).

SYSTEMATIC PALAEONTOLOGY

Figured and cited specimens are housed in the Natural History Museum, London (BB and BC collection numbers), Institute of Geological Sciences, Almaty, Kazakhstan (IGNA collection numbers), and in the CNIGR Museum, St. Petersburg, Russia (CNIGR collection numbers). All the quoted sample numbers are from the Anderken Formation except where stated. Bibliographical references to families and above are omitted if they are in the *Treatise on Invertebrate Paleontology* (Kaesler 2000).

Abbreviations given in tables of measurements and in the text are: Lv, Ld – sagittal ventral and dorsal valve length; W – maximum width; T – maximum thickness; Ml, Mw – length and width of the muscle field; Sw, St – width and height of tongue in the ventral valve; BBl, BBw length and distance between outer margins of brachiophores or socket ridges; Sl – length of median ridge; LPl,

LPw length and width of lophophore platform; X – mean; S – standard deviation from the mean; r – coefficient of correlation; OR – observed range; max. – maximum value; min. – minimum value; N – number of measured or counted specimens.

Order **LINGULIDA** Waagen, 1885
Superfamily **LINGULOIDEA** Menke, 1828
Family **OBOLIDAE** King, 1846
Subfamily **GLOSSELLINAE** Cooper, 1956
Genus ***ECTENOGLOSSA*** Sinclair, 1945

TYPE SPECIES. *Lingula lesueueri* Rouault, 1850, from the Arenig of Normandy, France.

Ectenoglossa sorbulakensis Popov, 1980 Pl. 1, figs 1–4

1980 *Ectenoglossa sorbulakensis* Popov: 142, pl. 1, figs 1–4.
1984 *Ectenoglossa sorbulakensis* Popov; Nikitin & Popov *in* Klenina *et al.*: 142, pl. 1, figs 1–4.

HOLOTYPE. CNIGR 1/11523, ventral internal mould, from the Anderken Formation, locality 1024, east side of Karatal valley.

MATERIAL. Six pairs of conjoined valves, 26 ventral and 31 dorsal valves from Sample 8130a, Anderkenyn-Akchoku; Samples 8227–10, 8227–40 (BC 57370–73), 8227–80, Buldukbai Akchoku; 8228a, east side of Kopalysai; all Chu-Ili Range; Sample 1024, east side of Karatal Valley, south Betpak-Dala.

DESCRIPTION. Shell equivalved, elongate, subrectangular in outline, about 190% as long as wide with maximum width at mid-length, ornamented by fine concentric fila about 13–15 per mm. Ventral valve very gently convex with narrow, triangular pseudointerarea, mainly occupied by deep pedicle groove and small propareas crossed by flexure lines. Dorsal valve gently convex, lacking pseudointerarea. Ventral interior with pair of slightly diverging, elongate, suboval umbonal muscle scars flanked laterally by pair of short diverging ridges; pedicle nerve impression well defined. Dorsal interior with weak median ridge.

DISCUSSION. *Ectenoglossa sorbulakensis* closely resembles *Ectenoglossa minor* Zhan & Cocks (1998: 14) from the Lower Ashgill of South China in having a strongly elongate equivalved shell with subparallel lateral margins, rudimentary ventral pseudointerarea and propareas with well defined flexure lines. However, the interiors of both valves are weakly impressed in the Chinese species, which makes precise comparison difficult. The main difference of the Kazakh species from the latter is the less elongate shell outline, which is no more than twice as long as wide. A detailed description, discussion and the basic statistics of this species was provided by Popov (1980).

Superfamily **DISCINOIDEA** Gray, 1840
Family **TREMATIDAE** Schuchert, 1893
Genus ***TREMATIS*** Sharpe, 1848

TYPE SPECIES. *Orbicula terminalis* Emmons, from the Trenton Group (Caradoc), New York, U.S.A.

Trematis? sp Pl. 1, figs 5, 6

MATERIAL. Figured dorsal valve, BC 57375 (L=14.8, W=14.4) and another dorsal valve, Samples 127, 8228, Kopalysai.

DESCRIPTION. Shell subcircular, ornamented by radial capillae of about 5 per 1 mm enlarged in number by intercalation and with radially arranged rounded or transversely suboval pits in the interspaces between capillae. Ventral valve unknown. Dorsal valve gently and unevenly convex in transverse profile with maximum height about one-third of the valve length from the marginal umbo. Dorsal interior unknown.

DISCUSSION. These specimens are similar to the shells described by Cooper (1956: 275) as *Trematis* sp. 3 from the *Cyrtonotella* Zone of the Edinburg Formation (Caradoc) of Virginia in their pits and radial ornament. The ventral valve in both unnamed species remains unknown, and therefore the generic attribution is provisional.

Family **DISCINIDAE** Gray, 1840
Subfamily **ORBICULOIDEINAE** Schuchert, 1929
Genus ***SCHIZOTRETA*** Kutorga, 1848

TYPE SPECIES. *Orbicula elliptica* Kutorga, presumably Volkhov or Kunda Stage (Upper Arenig-Lower Llanvirn), vicinity of St. Petersburg, Russia.

Schizotreta sp. Pl. 1, figs 7–10

MATERIAL. One pair of conjoined valves, one ventral and two dorsal valves from Samples 100 (BC 57590) and 626, Anderkenyn-Akchoku section; Samples 628 (BC 56825), 2538, Kujandysai section

PLATE 1

Figs 1–4 *Ectenoglossa sorbulakensis* Popov. Sample 8227–40, Buldukbai-Akchoku section, west side of Kopalysai. **1,** BC 57370, ventral exterior, × 2. **2,** BC 57372, dorsal internal mould, × 2. **3,** BC 57371, dorsal exterior, × 2. **4,** BC57373, ventral internal mould, × 2.

Figs 5, 6 *Trematis* ? sp. Sample 8228, east side of Kopalysai, BC 57375, dorsal exterior and surface ornament, × 6, × 2.

Figs 7–10 *Schizotreta* sp. Sample 100, Anderkenyn-Akchoku section, BC 57590, conjoined valves, posterior, dorsal, lateral and ventral views, × 2.

Fig. 11, 12 *Mesotreta*? sp. Sample 100, Akchoku Mountain, Anderkenyn-Akchoku section, CNIGR 1/12361, ventral exterior and lateral view, × 8.

Figs 13, 14 *Nushbiella dubia* Popov. Sample 2538, Akchoku Mountain, Kujandysai section, BC 57591; **13,** dorsal exterior, × 8; **14,** ventral exterior, × 8.

Fig. 15 *Paracraniops* sp. Sample 8128a, Anderkenyn-Akchoku section, BC 57377, dorsal internal mould, × 5.

Figs 16–21 *Longvillia lanx* (Popov), Sample 1018, area 7 km southwest of Karpkuduk well, Kotnak mountains, south Betpak-Dala. **16, 17,** CNIGR 27/11989, latex cast of cardinalia and dorsal interior, × 5, × 2. **18–20,** CNIGR 27/11989, dorsal, ventral and lateral views of conjoined valves, × 1. **21,** CNIGR 30/11989, **holotype,** ventral internal mould, × 2.

Figs 22–28 *Bellimurina (Bellimurina) sarytumensis* sp. nov. **22, 23**, Sample 8214, BC 57379, **holotype**, Anderkenyn-Akchoku section, ventral exterior and lateral view, × 2. **24, 25**. Sample 2538, Akchoku Mountain, Kujandysai section, BC 57378, conjoined valves, dorsal and ventral views, × 3. **26**, Sample 1041a, Burultas Valley, BC 57364, dorsal internal mould, × 2. **27**, Sample 100, Anderkenyn-Akchoku section, BC 57380, ventral exterior, × 3. **28,** Sample 2538, CNIGR 10/12361, dorsal external mould, × 3.

Fig. 29 *Dolerorthis expressa* Popov. Sample 1018, 7 km southwest of Karpkuduk well, Kotnak Mountains, BC 57368, ventral internal mould, × 1.5.

Figs 30, 31 Furcitellinae gen. et sp. indet. Sample 628, west side of Kujandysai, BC 57381, ventral and dorsal views of conjoined valves, × 1.5.


1


2


3

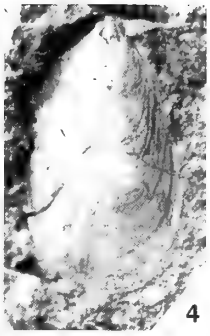
4


5

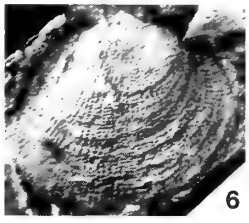
6


7

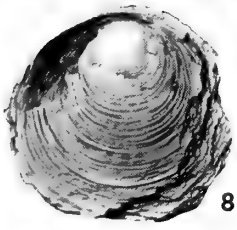
8


9

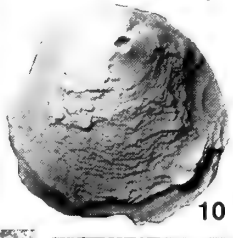
10

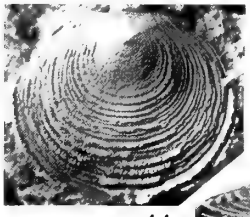
11

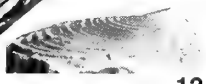
12

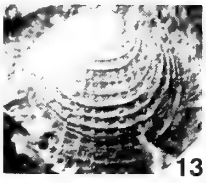
13

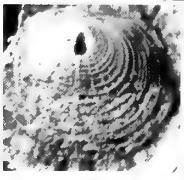
14

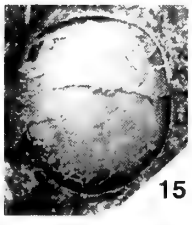
15

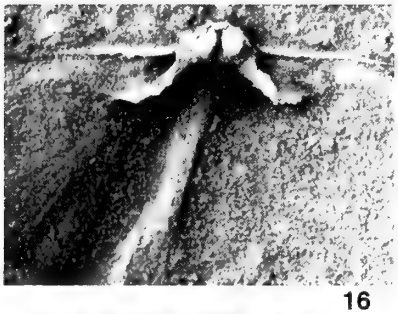
16

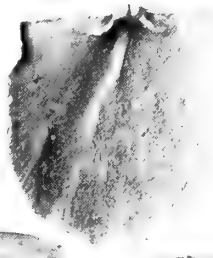
17

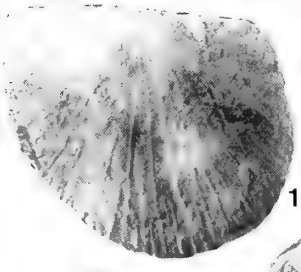
18

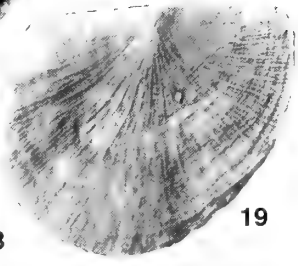
19

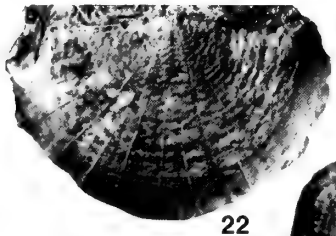
22

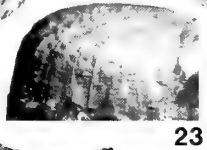
23

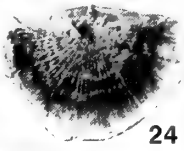
24


20

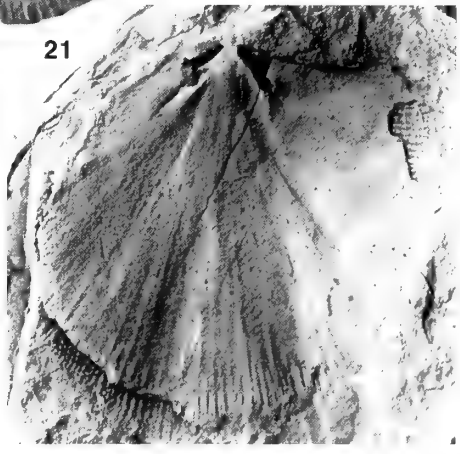
21

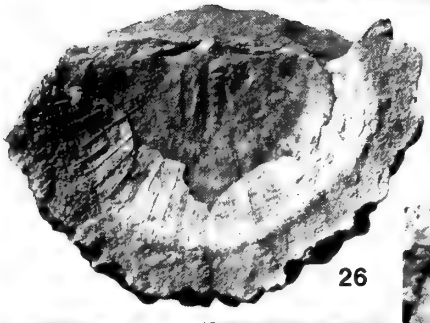
26

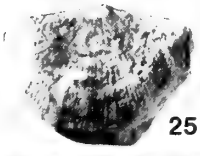
25

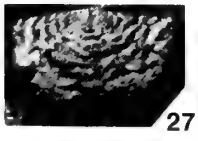
27

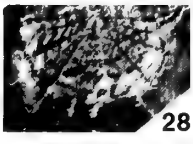
28

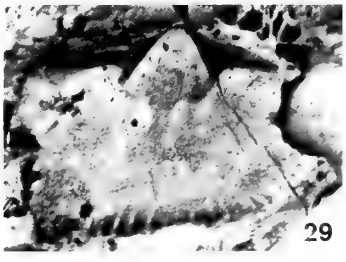
29

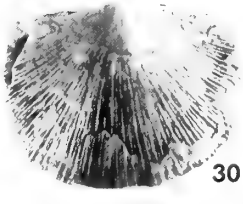
30


31

DESCRIPTION. Shell planoconvex, subcircular, ornamented by strong rounded irregular concentric rugellae of 10–11 per 3 mm. Ventral valve low, subconical with maximum height at the umbo which is situated about 10% of the valve length from the posterior margin. Pedicle foramen small, rounded, located at the end of narrow pedicle track covered by listrium. Dorsal valve flat with submarginal umbo. Interior of both valves not observed.

MEASUREMENTS. BC 57590, conjoined valves, L=14.8, W=14.4, T=4.8.

DISCUSSION. These specimens resemble *Schizotreta triangularis* Popov (Nikitin *et al.* 1996: 85) from the late Caradoc Dulankara Regional Stage of the northern Betpak-Dala Desert, Central Kazakhstan, but differ in their subcircular valve outline, ventral umbo situated close to the posterior margin and strong, irregular concentric rugellae. In concentric ornament they somewhat resemble *Schizotreta corrugata* Cooper (1956: 277) from the Llandeilo Pratt Ferry Formation of Alabama, USA, but can be distinguished in having a larger size, more circular shell outline and more densely spaced concentric rugellae.

Order **SIPHONOTRETIDA** Kuhn, 1949
Superfamily **SIPHONOTRETOIDEA** Kutorga, 1848
Family **SIPHONOTRETIDAE** Kutorga, 1848
Genus ***MESOTRETA*** Kutorga, 1848

TYPE SPECIES. *Siphonotreta tentorium* Kutorga, 1848: 270, from the Arenig (Volkhov Regional Stage), north-western Russia.

DISCUSSION. The type material of *Mesotreta tentorium* is lost and its taxonomic position within the Siphonotretoidea is unclear. At present, our knowledge of the type species of this genus is based on a single incomplete ventral valve from the Upper Volkhov Stage (Holmer & Popov 2000: Fig. 79,2). *Mesotreta* is unique among the Siphonotretida because of its low conical ventral valve with small, slightly eccentric pedicle foramen, but it possesses the hollow spines characteristic of this order. The ventral interior and dorsal valve of *Mesotreta* remain unknown.

Mesotreta? sp. Pl. 1, figs 11, 12

1986 *Nushbiella dubia* (Popov); Kolobova & Popov: pl. 1, fig. 1, *non* fig. 2.

MATERIAL. One ventral valve (CNIGR 1/12361) from Sample 100, Anderkenyn-Akchoku section.

DESCRIPTION. Valve slightly transverse, elliptical in outline; low, subconical with eccentric umbo at 20% of valve length from the posterior margin. Foramen small, slightly elongate, suboval. Concentric ornament of up to 16 thin, evenly spaced, crowded growth lamellae and numerous fine hollow spines. Ventral interior and dorsal valve unknown.

DISCUSSION. This unnamed species resembles *Siphonotreta tentorium* in having a low conical ventral valve lacking a well-defined pseudointerarea and small umbonal pedicle foramen, but the Kazakhstanian specimen differs in its strongly developed lamellose ornament and more posterior ventral umbo.

Genus ***NUSHBIELLA*** Popov *in* Kolobova & Popov, 1986

TYPE SPECIES. *Multispinula? dubia* Popov, 1977; from the Bestamak Formation, Tselinograd Regional Stage (Llandeilo), Chingiz Range, Kazakhstan.

Nushbiella dubia (Popov, 1977) Pl. 1, figs 13, 14

1977 *Multispinula? dubia* Popov: 104, pl. 25, figs 8–11.
1986 *Nushbiella dubia* (Popov) Kolobova & Popov: 251, pl. 1, fig. 2, *non* fig. 1.
2000 *Nushbiella dubia* (Popov) Holmer & Popov: fig. 79, 6a, b.

HOLOTYPE. CNIGR 1/10847, ventral valve, Bestamak Formation (Llandeilo), locality 553a, east side of Chagan River near Konur-Aulie cave, Chingiz Range, Kazakhstan.

MATERIAL. One ventral and one dorsal valve from Sample 8223a, Anderkenyn-Akchoku section; Sample 2538 (BC 57591), Kujandysai section.

DISCUSSION. The specimens from the Anderken Formation have no significant differences from the rather older topotypes in ornament and external shell morphology.

Order **CRANIOPSIDA** Gorjansky & Popov, 1985
Superfamily **CRANIOPSOIDEA** Williams, 1963
Genus ***PARACRANIOPS*** Williams, 1963

TYPE SPECIES. *Craniops pararia* Williams, 1962, from the Lower Ardmillan Series (Caradoc), Girvan, Scotland.

Paracraniops sp. Pl. 1, fig. 15

MATERIAL. One dorsal internal mould, BC 57377, from Sample 8128a, Anderkenyn-Akchoku section.

DISCUSSION. A single specimen represents the earliest record of craniopsides from Kazakhstan. There is little doubt of the generic attribution, but there is insufficient material to allow detailed comparison with other named species of the genus.

Order **STROPHOMENIDA** Öpik, 1934
Superfamily **STROPHOMENOIDEA** King, 1846
Family **STROPHOMENIDAE** King, 1846
Subfamily **STROPHOMENINAE** King, 1846
Genus ***LONGVILLIA*** Bancroft, 1933

TYPE SPECIES. *Orthis grandis* J.de C. Sowerby, 1839, from the Cheney Longville Flags (Lower Caradoc), Shropshire, England.

Longvillia lanx (Popov, 1985) Pl.1, figs 16–21

1985 *Strophomena lanx* Popov: 58; pl. 1, fig. 13; pl. 2, figs 12, 13; pl. 3, fig. 1.
1985 *Strophomena digna* Popov: 67 *nomen erratum.* pl. 1, fig. 13.

HOLOTYPE. CNIGR 30/11989, ventral internal mould, from the Anderken Formation, Sample 1018a, 7 km south-west of Karpkuduk well, Kotnak Mountains, refigured here (Pl. 1, fig. 21).

MATERIAL. Two pairs of conjoined valves, 11 ventral and 8 dorsal valves from Samples 1018, 1018a, 7 km south-west of Karpkuduk well, Kotnak Mountains.

DESCRIPTION. Shell very gently convexiconcave, slightly transverse, subrectangular in outline with maximum width about one-quarter of the valve length from the hinge line. Anterior commissure rectimarginate. Ventral valve gently and evenly concave in profile with a slightly raised, pointed umbo and steeply apsacline ventral interarea bearing large, convex pseudodeltidium. Dorsal valve evenly convex with flattened umbonal area. Radial ornament

unequally parvicostellate in posterior half of mature valves with 2–4 parvicostellae between accentuated ribs, becoming near equally parvicostellate anteriorly with 5–8 ribs along the anterior margin. Ventral interior with strong teeth and low, diverging dental plates continuing anteriorly as straight muscle bounding ridges bordering posteriorly the open subtriangular muscle field which is about 30% as long as the valve. Adductor scars narrow, weakly impressed, flanked laterally by slightly longer diductor scars. Dorsal interior with cardinal process, low, widely diverging, oblique socket ridges and a short median ridge up to 40% valve length. Adductor field weakly impressed.

MEASUREMENTS. CNIGR 29/11989, conjoined valves, L=22.5, W=26.4, Iw=23.6, T=5.1; CNIGR 30/11989, ventral internal mould, holotype, L=26.8, W=28.3, Ml=8.8, Mw=9.6; CNIGR 35/11989, dorsal internal mould, L=16.7, W=18.5, T=3.5, Sl=7.8.

DISCUSSION. This species was originally referred to *Strophomena*, but it is characterised by an open ventral muscle field bounded posterolaterally by dental plates and short, diverging bounding ridges, a short dorsal median ridge and the absence of side septa, all suggesting attribution to *Longvillia*. It differs from the type species *Longvillia grandis* in its less transverse outline, with the maximum width slightly anterior to the hinge line, the radial ornament becoming nearly regular in the anterior half of the shell, and in possessing a somewhat stronger median ridge.

Subfamily **FURCITELLINAE** Williams, 1965

Genus ***BELLIMURINA (BELLIMURINA)*** Cooper, 1956

TYPE SPECIES. *Leptaena charlottae* Winchell & Schuchert, from the Caradoc of Minnesota, U.S.A.

Bellimurina (Bellimurina) sarytumensis sp.nov. Pl. 1, figs. 22–28.

1986 *Bellimurina rudis* [sic] Lu; Kolobova & Popov: pl. 1, fig. 10.

ETYMOLOGY. After Sarytuma Well in the Betpak-Dala Desert.

HOLOTYPE. BC 57379, Pl. 1, figs 22, 23, a ventral valve from Sample 8214, Anderkenyn-Akchoku section.

MATERIAL. Two pairs of conjoined valves, ten ventral and four dorsal valves from Samples 100 (BC 56826, BC 57380), 620 (BC 56827–28) and 626 (BC 56829–31), Anderkenyn-Akchoku section; Sample 8214 (BC 56839–40, BC 57379), west side of Ashchisu River; Samples 628 (BC 56837), 2538 (BC 56838, BC 57378) and 8256 (BC 56841), Kujandysai section; Sample 948 (BC 56832–36), Tesik River; Samples 390 (BC 57365), 1041a (BC 57364), Burultas Valley.

DESCRIPTION. Shell concavoconvex, slightly transverse, subrectangular in outline, about 70% as long as wide with maximum width at mid-length with rounded cardinal extremities and rectimarginate anterior commissure. Ventral valve convex with maximum height at geniculation (about three-quarters valve length). Ventral interarea apsacline with well developed pseudodeltidium perforated apically by a minute foramen. Dorsal valve flattened with geniculation near the anterior margin. Dorsal interarea low, linear, anacline with a well-developed chilidium. Radial ornament unequally parvicostellate with 6–7 accentuated ribs originating at the umbo and up to 7 strong ribs in interspaces. About 4–7 fine parvicostellae per mm along the anterior margin. Concentric ornament of fine, slightly uneven rugellae about 2 per mm, covering all the posterior half of the shell.

Table 8 Measurements of ventral valves of *Beillimurina sarytumensis* sp. nov from samples 100, 626 and 8214 from Anderkenyn-Akchoku section, Sample 2538 from Kujandysai section and Sample F-1041a from Burultas valley.

	Lv	W	L/W
N	6	6	6
X	7.8	11.1	69.4%
S	3.62	4.35	6.8
MIN	5.2	8	56.5%
MAX	14.8	19.5	75.9%

Ventral interior with small teeth supported by low, divergent dental plates and small, weakly impressed subtriangular muscle field. Dorsal interior with bilobed cardinal process, widely flaring socket plates, poorly impressed median septum extending about one-third valve length, poorly impressed pair of side septa subparallel to the median septum and not extending beyond it.

MEASUREMENTS. (435/12375) conjoined valves, L=6.4, W=8.3, T=3.0; (436/12375) ventral valve, L=15.4, W=21.3, T=5.4.

DISCUSSION. These shells are most similar to, and possibly conspecific with, the specimens described by Nikitin & Popov (1996: 16, figs 6J–N) as *Bellimurina*? sp. from the Dulankara Regional Stage of north Betpak-Dala in general shell shape and radial ornament with 6–7 accentuated primary ribs, but the dorsal interior in specimens from the Dulankara Stage remains unknown. The Kazakh shells are similar to the specimens described as *Kiaeromena longxianensis* Fu, 1982 from the Pinling Formation of northwest China in size, ornament and weakly geniculated lateral profile, but further comparison is difficult because of poor description and insufficient illustrations of that species, although it is unlikely to belong to *Kiaeromena*, which is known only from the Baltic. Cooper (1956) described eight species of *B. (Bellimurina)* from the Caradoc of Laurentia, of which he named six, but the dorsal interiors do not match *B. (B.) sarytumensis*, nor do those of *B. (B.) rudis* Xu, Rong & Liu (1974) from the early Caradoc Shitzupu Formation of South China. *B. (B.) quadrata* Fu (1982) appears more quadrate in outline and its interior is not illustrated (see also under *Limbimurina?* sp. below).

Genus ***TERATELASMELLA*** Laurie, 1991

TYPE SPECIES. *Teratelasmella plicata* Laurie, 1991, from the Upper Cashions Creek Limestone (Lower Caradoc), Tasmania, Australia.

Teratelasmella chugaevae sp. nov. Pl. 2, figs 10–20; Figs 10, 11.

ETYMOLOGY. In memory of the late Marina Chugaeva to honour her outstanding trilobite work.

HOLOTYPE. BC 57392, Pl. 2, figs 14–18, conjoined valves, from the Anderken Formation, Sample 626, Anderkenyn-Akchoku section.

MATERIAL. 16 pairs of conjoined valves and 3 dorsal valves from the Anderkenyn-Akchoku section, Samples 100 (BC 56842–51, BC 57390–91) and 626 (BC 56853–57, 57392); Kujandysai section, Samples 628 (BC 56858) and 85258 (BC 56852).

DESCRIPTION. Shell strongly dorsibiconvex, transverse, suboval, about 70% as long as wide, with maximum width at mid-length, and

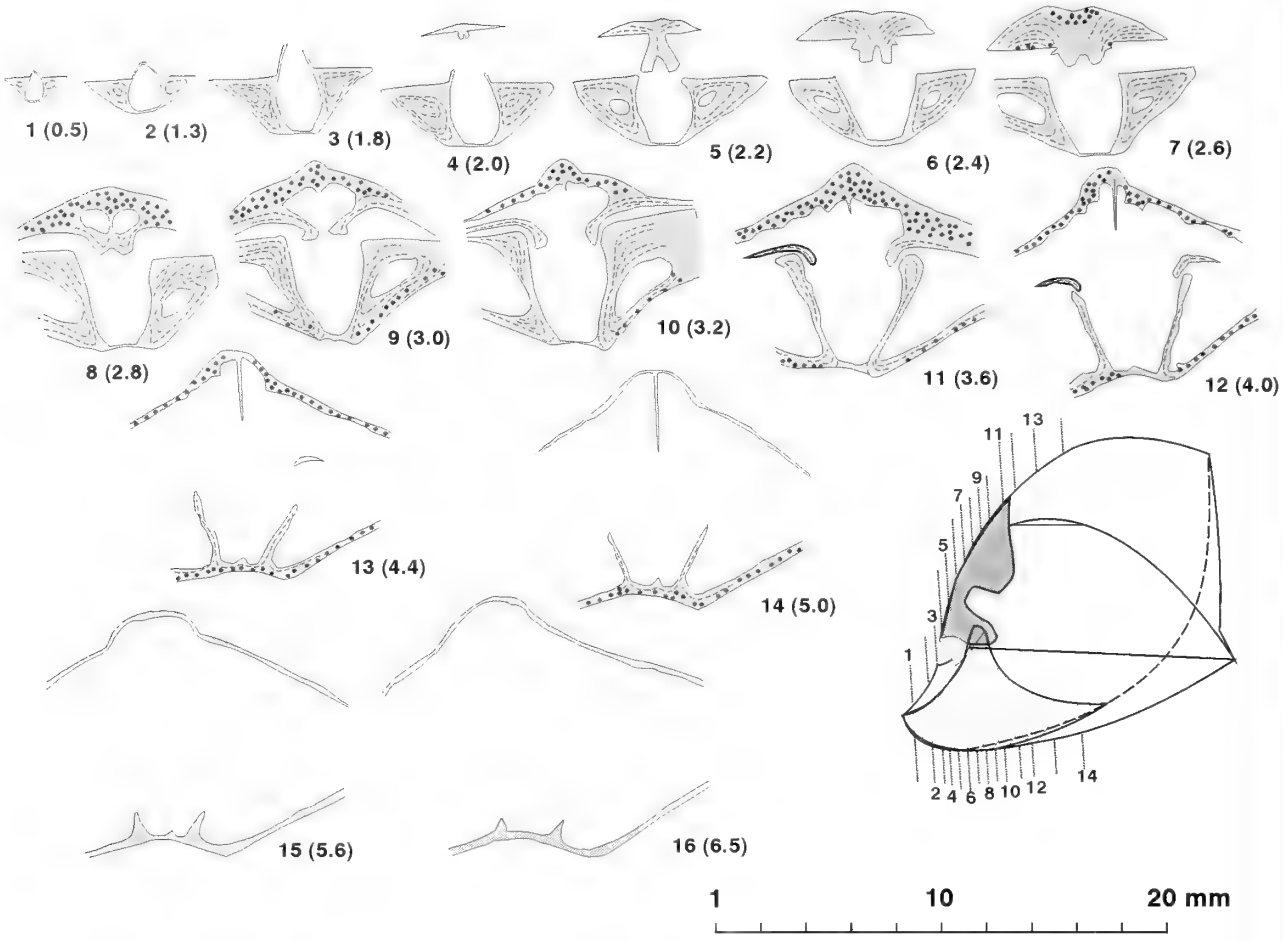

Fig. 10 Transverse serial sections of conjoined valves of *Teratelasmella chugaevae* sp. nov. from Sample 100. Distance in mm is measured from the posterior tip of ventral beak. Dorsal valve uppermost. Also lateral view to show section positions and schematic reconstruction.

90% as thick as long. Anterior commissure strongly uniplicate. Ventral valve moderately convex with maximum thickness near quarter valve length. Interarea high, triangular, apsacline with delthyrium completely covered by pseudodeltidium perforated by a small umbonal foramen. Ventral sulcus originating at the umbonal area, strongly deepening anteriorly and ending with prominent, semielliptical tongue inclined at less than a right angle to the commissural plane. Flanks of the valve flattened, slightly inclined to the commissural plane. Dorsal valve very strongly convex, with a low, anacline interarea. Strong median fold, rounded in cross-section, with steep lateral slopes originating near the beak. Very weak and narrow dorsal median sulcus in the umbonal area of some specimens. Radial ornament coarsely parvicostellate with 5 ribs per 3 mm along the posterior margin of mature specimens.

Interiors of both valves were studied in transverse sections (Figs 10, 11). Ventral valve with strong teeth supported by high dental plates continuing anteriorly as muscle bounding ridges. Low median ridge in the anterior half of the ventral muscle field. Dorsal valve interior with bilobed cardinal process and low, curved socket ridges. Median septum high, triangular, blade-like, extending anteriorly to mid-valve, flanked laterally by a pair of short side septa. Adductor field raised anteriorly and bordered by a high rim.

DISCUSSION. This species is similar only to *Teratelasmella plicata* Laurie, 1991, but it can be distinguished in being larger (up to 25.6 mm wide), with a strongly dorsibiconvex lateral profile, a deep ventral sulcus, a high dorsal median fold originating in the umbonal area rather than at the mid-valve as in the type species, and coarser radial ornament.

Furcitellinae gen. et sp. indet.

Pl. 1, figs 30, 31, Pl. 2, figs 1–4

MATERIAL. Four pairs of conjoined valves, two ventral and six dorsal valves from Samples 100 (BC 56859, 57382, 57384) and 626, Anderkenyn-Akchoku section; Sample 628 (BC 56577, 56863, 57381) and 8220 (BC 56578), Kujandysai section; Sample 1041a (BC 56860–62, 57383), Burultas Valley.

DESCRIPTION. Shell convexoplane, transverse, subrectangular in outline with maximum width near mid-length. Cardinal extremities nearly right angled. Anterior commissure rectimarginate. Ventral valve almost flat with acute and slightly erect beak. Ventral interarea low apsacline with convex pseudodeltidium. Dorsal valve evenly convex with low, orthocline interarea and well-developed chilidium. Radial ornament parvicostellate. Up to 10 mm from the umbo the ribs are nearly equal in size and are 7–9 per 3 mm. In larger specimens 2–5 finer costellae become inserted between the larger

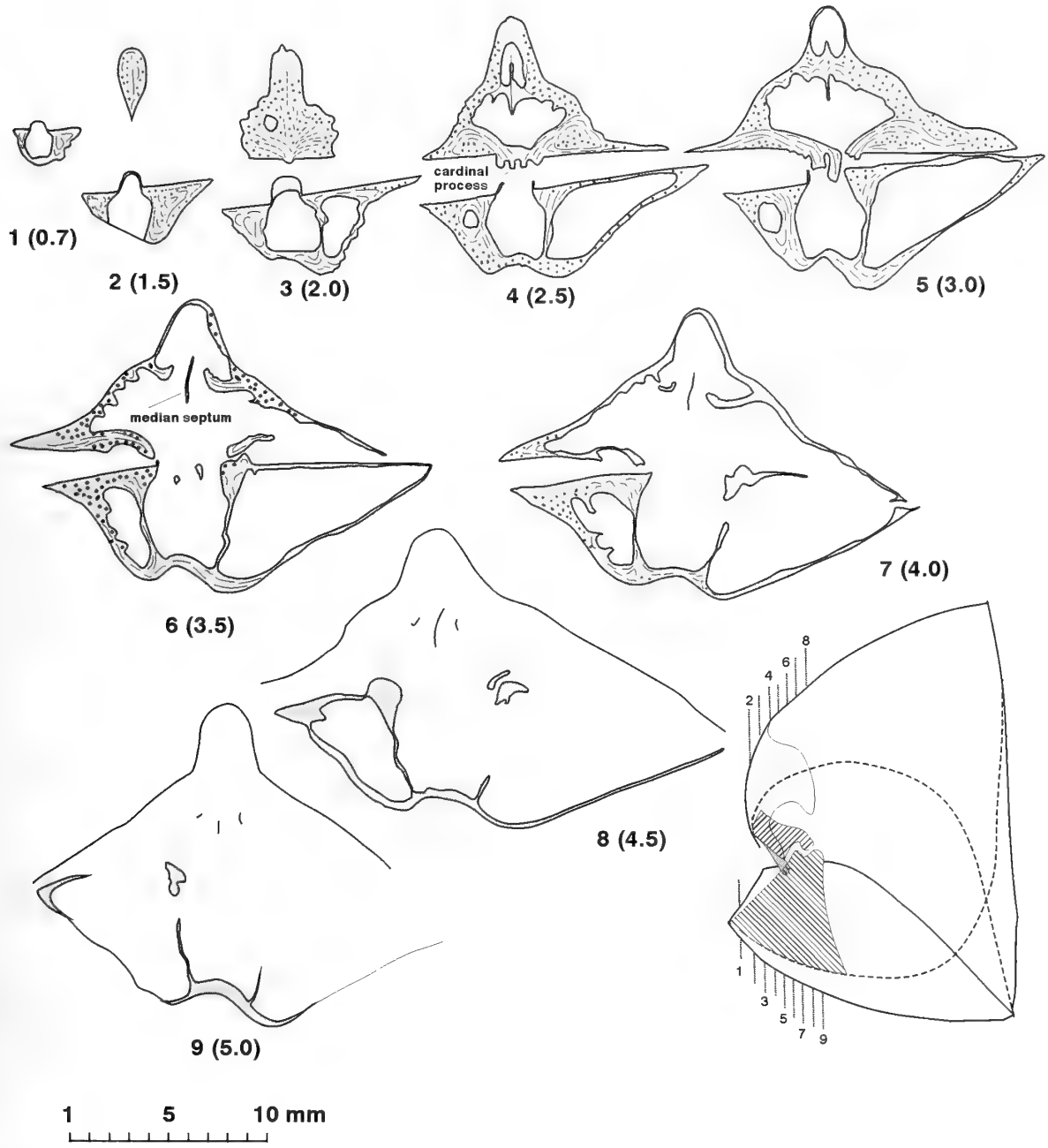

Fig. 11 Transverse serial sections of *Teratelasmella chugaevae* sp. nov. from Sample 100. Distance in mm is measured from the posterior tip of ventral beak. Dorsal valve uppermost. Also lateral view to show section positions and schematic reconstruction.

ribs and ornament becomes unequally parvicostellate, with up to 4 accentuated ribs and 9–15 parvicostellae per 3 mm along the anterior margin.

Ventral interior with delicate teeth and long, divergent dental plates. Ventral muscle field subtriangular, open anteriorly. Dorsal interior with bilobed cardinal process. Other characters of dorsal interior unknown.

DISCUSSION. Within the Furcitellidae as revised by Cocks & Rong (2000) these shells are comparable with *Quondongia* (Percival 1991:151) and *Molongcola* (Percival 1991:153) from the Caradoc of Australia in their planoconvex lateral shell profile and in the absence of geniculation, but they differ from *Molongcola* in possessing parvicostellate ornament. The absence of information on the dorsal interior makes precise generic attribution impossible.

Family **GLYPTOMENIDAE** Cooper, 1956
Genus ***GLYPTOMENA*** Cooper, 1956

TYPE SPECIES. *Glyptomena sculpturata* Cooper, 1956, from the Chatham Hill Formation (Llandeilo), Virginia, U.S.A.

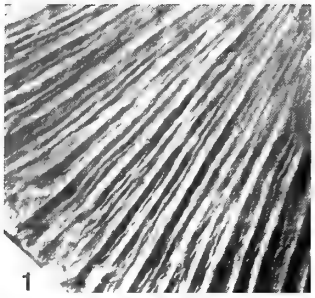
1

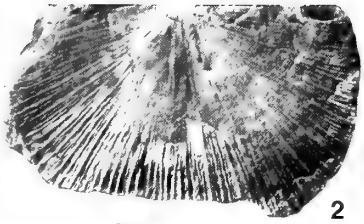
2


4

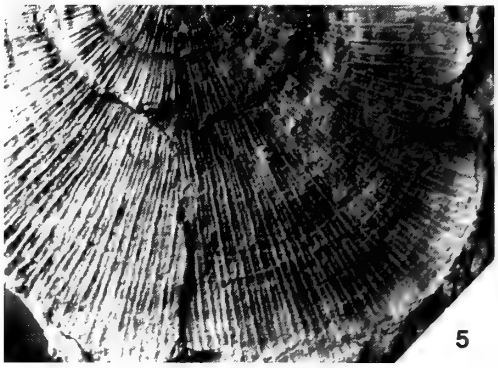
5


3


6


7

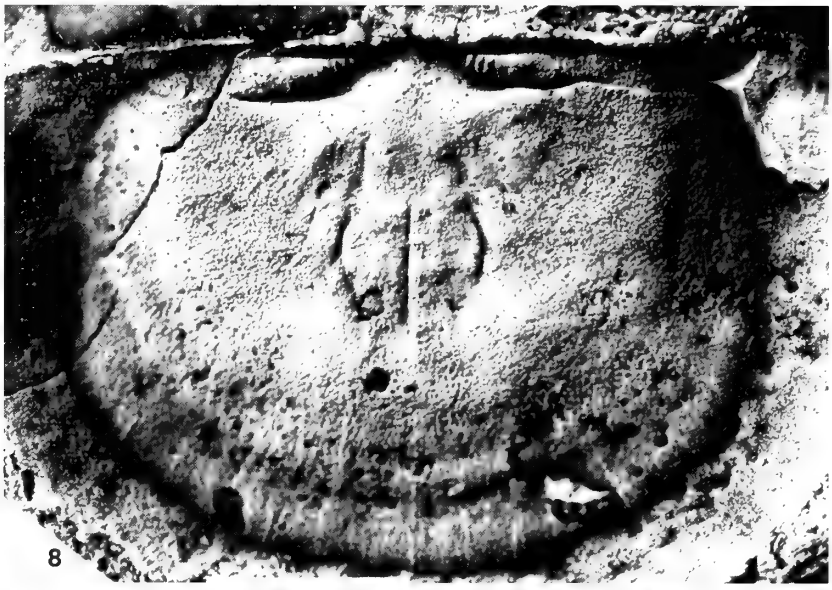
8

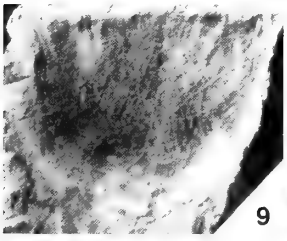
9

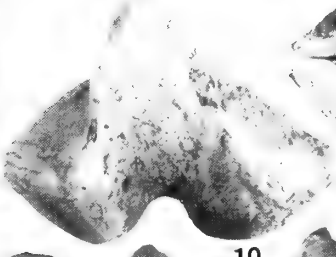
10


11


12


17

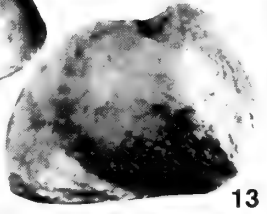
13

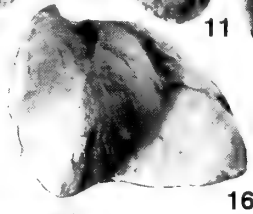
16


14


15

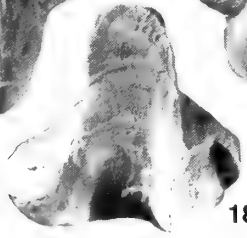
18

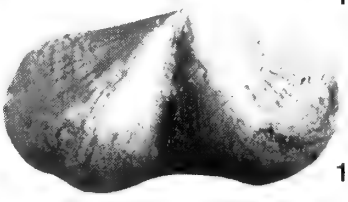
19


20

Glyptomena onerosa Popov, 1980 Pl. 2, figs 5–9

1980 *Glyptomena onerosa* Popov: 152, pl. 2, figs 5–7.

HOLOTYPE. CNIGR 50/11523, Anderken Formation, from Sample 100b, Anderkenyn-Akchoku section.

MATERIAL. 14 ventral and 24 dorsal valves from Samples 100b, 843 (BC 57387), 8135, 8137, 8235 (BC 57386), Anderkenyn-Akchoku section; Sample 7613 (BC 57388), Kujandysai section; Samples 8229 (BC 57385), 8257 (BC 56864–65), Buldukbai-Akchoku section; Sample 1018, 7 km SW of Karpkuduk well, Kotnak Mountains.

DESCRIPTION. Shell concavoconvex, semielliptical in outline, about 60% as long as wide, with maximum width at the hinge line. Cardinal extremities slightly acute. Anterior commissure rectimarginate. Ventral valve moderately convex in lateral profile with maximum thickness at about one-third valve length. Ventral interarea low, apsacline, with small apical pseudodeltidium. Dorsal valve flattened with dorsal geniculation at about 75% of valve length from the umbo. Dorsal interarea low, anacline with well developed, broad, convex chilidium. Radial ornament inequally parvicostellate with up to three generations of accentuated ribs separated by 2–5 parvicostellae in the interspaces. Number of ribs along the anterior margin of mature specimens varying from 11 to 15 per 3 mm. Concentric ornament of fine, regularly spaced concentric fila, about 20–25 per mm.

Ventral interior with strong teeth bearing rows of crenulations on the outer side and long, widely divergent dental plates. Ventral muscle field heart-shaped about one-third as long as the valve with strongly impressed diductor scar somewhat longer, but not enclosing slightly raised, narrow triangular adductor track. Dorsal interior with bilobed cardinal process on a low notothyrial platform and widely diverging socket ridges subparallel to the hinge line. Sockets deep, transverse, bearing strong vertical ridges on the anterior slope. Adductor scars weakly impressed, bisected by the fine median septum extending anteriorly about 60% of valve length. Pair of inner side septa about the same length as the median septum, slightly divergent proximally and curved towards the anterior of the median ridge near the mid-valve. Outer side septa very fine or completely absent in some specimens.

DISCUSSION. This species is similar to *Glyptomena sculpturata* Cooper, 1956, but differs in having a geniculated dorsal valve and more densely accentuated ribs.

***Limbimurina*? sp.** Pl. 3, fig. 1

MATERIAL. One ventral and five dorsal valves from Samples 100, 626 (BC 57395), 8223b (BC 56867–68), Anderkenyn-Akchoku section; Samples 628 and 2538 (BC 56866), Kujandysai section.

DESCRIPTION. Shell flattened, transverse, subrectangular in outline; strongly geniculate ventrally with a trail up to 4 mm long inclined at nearly right angles to the commissural plane. Cardinal extremities nearly right angled. Ventral valve strongly flattened posteriorly to the geniculation, with gently convex umbonal area. Ventral interarea low, planar, apsacline with apical pseudodeltidium. Dorsal valve with strong angular concentric rugae accentuating the geniculation. Dorsal interarea anacline. Radial ornament unequally parvicostellate with 4–5 parvicostellae per mm along the anterior margin. Concentric ornament of oblique rugellae crossing each other at less than 30–40° and covering all the valve surface between hinge line and geniculation. Interior of both valves unknown.

MEASUREMENTS. dorsal valve, L=14.1, W=29.0.

DISCUSSION. Generic assignment of the Kazakh specimens to *Limbimurina* is based mostly on the distinctive shell shape, with strong geniculation enhanced by the characteristic concentric frill and the irregular oblique rugellae forming an interference pattern with concentric rugae in the posterior half of the shell. The specimens from the Anderken Formation differ from *Limbimurina brevilimbata* Cooper, 1956 from the Edinburg Formation of Virginia and *L. insueta* Cooper, 1956 from the Rodman Formation of Pennsylvania in the strongly transverse outline of the shell. The trail in the Kazakh shells is considerably higher than in *L. insueta*, but not as high as in *L. brevilimbata*.

Similar shells were also described as *Limbimurina*? sp. from the Dulankara Regional Stage (Upper Caradoc) of north Betpak-Dala (Nikitin & Popov 1996). They differ from the Anderken specimens in their more densely spaced parvicostellae, which vary from 11 to 14 per mm along the anterior margin.

A similar species is *Bellimurina quadrata* Fu, 1982, from the Pinling Formation of Northwest China, which also possesses a geniculation as well as a characteristic concentric frill, and irregular oblique rugellae forming characteristic interference patterns; but precise comparision is difficult because of the short description and insufficient illustrations. It most likely belongs to *Limbimurina*, but no detailed information was provided on the dorsal interior (Fu 1982:122, pl. 35, figs 20–21).

Family **LEPTAENIDAE** Hall & Clarke, 1894
Genus ***LIMBIMURINA*** Cooper, 1956

TYPE SPECIES. *Limbimurina insueta* Cooper, 1956, from the Nealmont Formation (Caradoc), Pennsylvania, U.S.A.

Family **CHRISTIANIIDAE** Williams, 1952
Genus ***CHRISTIANIA*** Hall & Clarke, 1892

TYPE SPECIES. *Leptaena subquadrata* Hall, 1883, from the Caradoc of the U.S.A.

PLATE 2

Figs 1–4 Furcitellinae gen. et sp. indet. **1, 2, 4.** Sample 100, Anderkenyn-Akchoku section; **1, 2**, BC 57382, dorsal radial ornament and exterior, × 5, × 2; **4**, BC 57384, ventral internal mould, × 2. **3**, Sample 1041a, Burultas Valley, BC 57383, ventral exterior, × 2.5.

Figs 5–9 *Glyptomena onerosa* Popov. **5,** Sample 7613, Akchoku Mountain, Kujandysai section, BC 57388, dorsal valve ornament, × 3. **6**, Sample 8229, Buldukbai-Akchoku section, west side of Kopalysai, BC 57385, ventral internal mould, × 2. **7,** Sample 8235, Anderkenyn-Akchoku section, BC 57386, ventral internal mould, × 3. **8,** Sample 100b, Anderkenyn-Akchoku section, CNIGR Museum, dorsal internal mould, × 4. **9**, Sample 843, Anderkenyn-Akchoku section, BC 57387, dorsal exterior, × 1.5.

Figs 10–20 *Teretelasmella chugaevae* sp. nov. Anderkenyn-Akchoku section. **10–13, 19, 20,** Sample 100; **10–13, 19,** BC 57391, conjoined valves, anterior, posterior, dorsal, lateral and ventral views, × 1.5; **20**, BC 57390, conjoined valves, posterior view, × 2. **14–18,** Sample 626, BC 57392, conjoined valves, **holotype**, dorsal, posterior, lateral, ventral and anterior views, × 1.5.

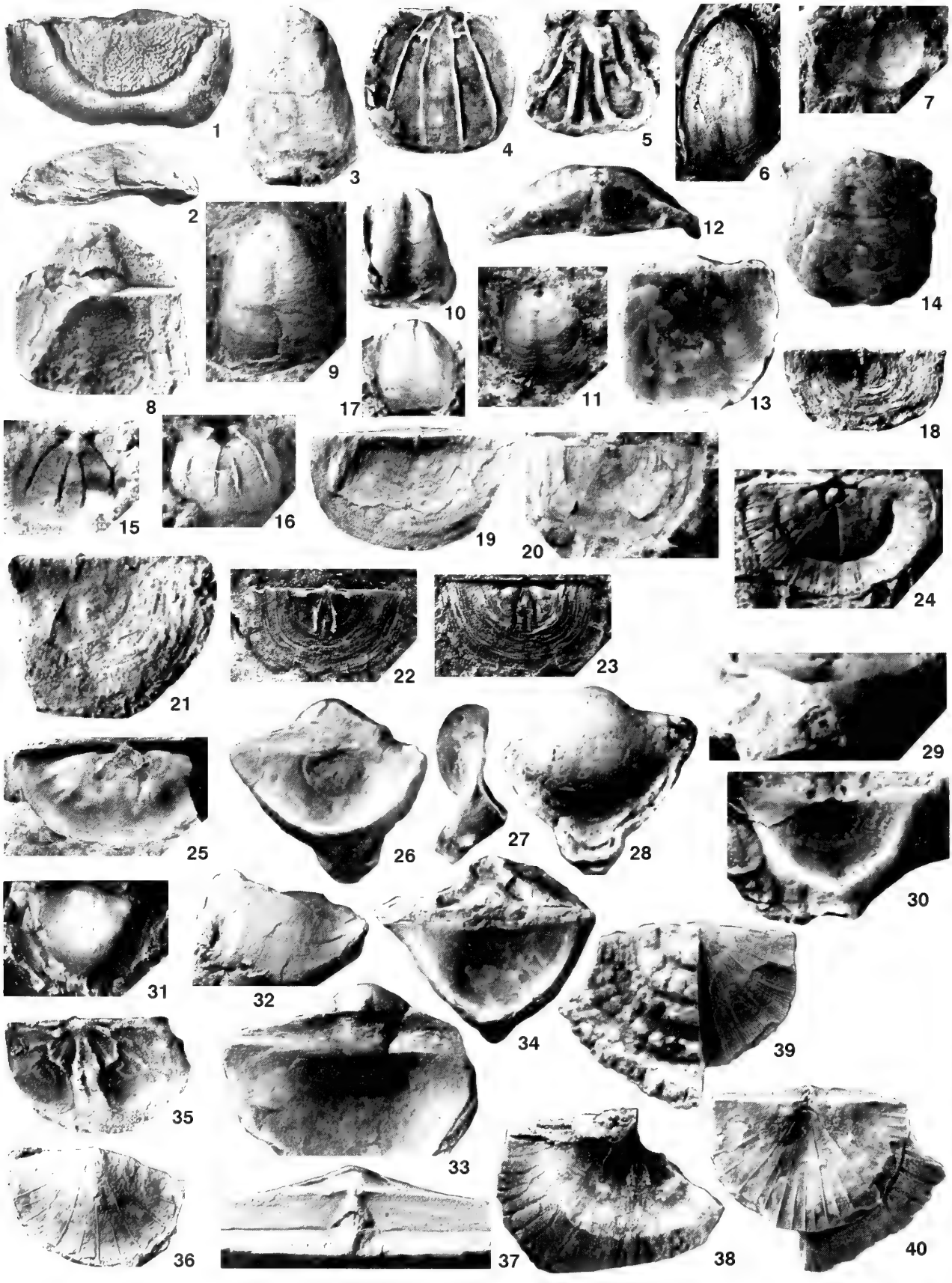
1
2
3
4
5
6
7
8
9
10
11
12
13
14
15
16
17
18
19
20
21
22
23
24
25
26
27
28
29
30
31
32
33
34
35
36
37
38
39
40

Cristiania egregia Popov, 1985 Pl. 3, figs 2–6, 8

1985 *Christiania egregia* Popov: 60, pl. 2, figs 7–11.

HOLOTYPE. CNIGR 25/11989, dorsal internal mould from the Anderken Formation, Sample 1018, 7 km south-west of Karpkuduk Well, Kotnak Mountains.

MATERIAL. Eight pairs of conjoined valves, 17 ventral and 30 dorsal valves from Samples 100 (BC 56875–81), 843, 626 (BC 56869–70), 8214 (BC 56871–2), Anderkenyn-Akchoku section; Samples 7613, 628 (BC 56587, 56886–89), Kujandysai section; Sample 1041a (BC 57396–98), Burultas Valley; Sample 1024b, east side of Karatal River near Sorbulak well; Sample 1018 (BC 56873–74), 7 km south-west of Karpkuduk well, Kotnak Mountains.

DESCRIPTION. Shell concavoconvex, strongly elongated, suboval in outline, about 160% as long as wide with maximum width about two-thirds valve length from the hinge line. Cardinal extremities subrectangular, usually slightly alate. Anterior commissure broadly uniplicate. Ventral valve moderately convex in lateral profile with maximum thickness at about one-third valve length, about 20% as thick as long. Ventral interarea strongly apsacline to orthocline with a large convex pseudodeltidium perforated apically by a minute, circular foramen. Very weak ventral sulcus originating at the umbonal area. Dorsal valve gently concave with hypercline interarea and complete, convex chilidium. Radial ornament finely parvicostellate, rarely preserved.

Ventral interior with strong, transverse teeth and low, widely diverging dental plates. Muscle field weakly impressed, bilobate, with short, linear adductor scars bisected by a fine median ridge. Dorsal interior with bilobed cardinal process, low, curved socket ridges subparallel to the hinge line and two pairs of strong side septa. Dorsal median septum very fine, about 61% as long as the valve. Adductor scars bordered anteriorly by strong muscle bounding ridges curved posteriorly.

DISCUSSION. Detailed discussion of this species was provided by Popov (1980: 61). Among the Kazakh species it is most similar to *Christiania tortuosa* Popov, 1980 from the Lidievka Formation (Llandeilo-Lower Caradoc) of north-central Kazakhstan, but differs in having a weak ventral sulcus, very fine radial ornament and a long dorsal median ridge extending far beyond the mid-valve. There are a large number of nominal *Christiania* species known globally, and the genus as a whole is due for revision.

Christiania aff. ***sulcata*** Williams, 1962 Pl. 3, figs 7, 9–17

MATERIAL. Three pairs of conjoined valves, 23 ventral and 10 dorsal valves from Samples 8223 (BC 56585–6), 8223a, 8223b (BC 57399, 57401), Anderkenyn-Akchoku section; Sample 8215 (BC 56583–4), west side of Ashchisu River; Samples 628 (=K-107/1970) (BC 56593), 2538 (BC 56579, 81, 89), 8217 (BC 57400), 8220 (BC 56592), Kujandysai section.

DESCRIPTION. Shell concavoconvex, elongate and subtrapezoidal in outline, as long as wide with maximum width at three-quarters valve length. Hinge line about 85% of maximum shell width. Cardinal extremities near right-angled and slightly alate. Lateral commissures near straight, slightly diverging anteriorly. Anterior commissure gently uniplicate. Ventral valve strongly convex in profile with maximum thickness at about one-third valve length. Ventral interarea strongly apsacline to near orthocline with narrow convex pseudodeltidium perforated apically by a minute rounded foramen. Lateral sides of the valve steep inclined near right angle towards the commissural plane. A shallow sulcus v-shaped in cross-section originating near the umbo and flanked by two distinct plications rounded in cross-section. Dorsal valve moderately concave with low and narrow median fold. Dorsal interarea hypercline with a convex chilidium. Shell surface finely and equally parvicostellate with 16 to 18 parvicostellae along the anterior margin of mature specimens.

Ventral interior with small, bilobed muscle field, fine teeth and rudimentary dental plates. Dorsal interior with a double cardinal process, low, curved socket ridges, thin median septum extending somewhat anterior of mid-valve and two pairs of strong side septa.

MEASUREMENTS. (457/12375) ventral valve, L=8.2, Iw=5.7, W=6.8, T=3.8, Sw=3.2; 458/12375), dorsal valve, L=5.6, Iw=5.2, W=5.3, Sw=2.2

DISCUSSION. These specimens resemble *Christiania sulcata* Williams, 1962, from the Stinchar Limestone (Upper Llandeilo-

PLATE 3

Fig. 1 *Limbimurina* sp. Sample 626, Anderkenyn-Akchoku section, BC 57395, ventral exterior, × 1.5.

Figs 2–6, 8 *Christiania egregia* Popov. **2, 3**, Sample 1041a, Burultas Valley, BC 57396, lateral and ventral views of exterior, × 2. **4,** Sample 1018, area 7 km west of Karpkuduk well, Kotnak Mountains, south Betpak-Dala, CNIGR 22/11989, latex cast of dorsal interior, × 2. **5,** Sample 1041a, BC 57397, dorsal valve interior, × 2. **6,** Sample 1018, CNIGR 23/11989, ventral internal mould, × 2. **8,** Sample 1041a, BC 57398, conjoined valves dorsal view showing interareas, × 4.

Figs 7, 9–17 *Christiania* aff. *sulcata* Williams. **7,** Sample 628, west side of Kujandysai, BC 56593, dorsal exterior, × 4. **9,** Sample 8223b, Anderkenyn-Akchoku section, BC 57399, ventral exterior, × 3. **10,** Sample 8217, BC 57400, ventral exterior, × 3. **11–16,** Sample 2538, Akchoku Mountain, Kujandysai section; **11,** BC 56589, dorsal external mould, × 3; **12–14**, BC 56579, conjoined valves, posterior view, × 8, dorsal and ventral views, × 6; **15, 16,** BC 56581, dorsal internal mould and latex cast, × 5. **17**, Sample 8223b, BC 57401, ventral internal mould, × 3.

Figs 18–23, 25 *Foliomena prisca* sp. nov. **18, 19, 21–23**, Sample 8255, Anderkenyn-Akchoku section; **18**, BC 57402, latex cast of dorsal exterior, × 4; **19**, BC 57403, latex cast of dorsal exterior, × 4; **21**, BC 57404, latex cast of dorsal exterior, × 4; **22, 23**, BC 57405, **holotype**, latex cast and dorsal internal mould, × 4. **20,** Sample 100, Anderkenyn-Akchoku section, BC 57407, dorsal exterior, × 4. **25,** Sample 8217, Kujandysai section, BC 57408, ventral internal mould, × 4.

Fig. 24 *Kassinella (Kassinella)?* sp. Sample 2531, Anderkenyn-Akchoku section, BC 56497, dorsal internal mould, × 8.

Figs 26–34 *Craspedelia tata* Popov. **26–28**, Sample 626, Anderkenyn-Akchoku section, BC 57409, conjoined valves, dorsal, lateral and ventral views, × 4. **29–30**, Sample 100, BC57410, dorsal exterior and anterior views, × 3. **31**, Sample 8238, CNIGR 9/12361, ventral exterior, × 2. **32–34,** Sample 626; **32, 34,** BC 57411, dorsal anterior and exterior view, × 3; **33**, BC 57412, conjoined valves, dorsal view, × 5.

Fig. 35 *Isophragma imperator* Popov, Sample 1018, 7 km southwest of Karpkuduk well, Kotnak Mountains, south Betpak-Dala, CNIGR 22/11522, latex cast of dorsal interior, × 2.

Figs 36–40 *Acculina kulanketpesica* sp. nov. **36**, Sample 8231–40, Buldukbai-Akchoku section, BC 57416, ventral exterior, × 2. **37–40,** Sample 1041a, Burultas Valley; **37,** BC 57415, posterior view of ventral and dorsal interareas, × 5; **38,** BC 12903, ventral interior, × 2; **39, 40,** BC 12904, **holotype**, conjoined valves, ventral and dorsal views, × 3.

Table 9 Measurements of ventral valves of *Christiania* aff. *sulcata* Williams, *Parastrophina–Kellerella* Association, Anderkenyn-Akchoku and Kujandysai sections.

	Lv	W	Iw	Sw	Lv/W	Iw/W	Sw/W
N	9	9	6	5	9	6	5
X	6.5	5.6	4.8	2.5	115.0%	87.8%	42.9%
S	1.91	1.15	0.85	0.73	16.1	6.4	12.4
MIN	4.0	4.4	3.9	1.7	90.9%	82.8%	23.0%
MAX	9.4	7.4	6.3	3.2	147.5%	100.0%	54.2%

Lower Caradoc) of Girvan, Scotland, but differ in having an elongate subtrapezoidal shell outline and two rounded plications flanking the ventral sulcus. A characteristic feature of the Kazakh specimens is the absence of high ridges bordering the dorsal adductor field anteriorly, which also appear to be absent in *C. sulcata* (Williams 1962: pl. 18, fig. 36). *Christiania* aff. *sulcata* also differs from *C. egregia* in having a stronger ventral median sulcus which is v-shaped in cross-section, a distinctive dorsal median fold and significantly smaller size.

Family **FOLIOMENIDAE** Williams, 1965
Genus ***FOLIOMENA*** Havlíček, 1952

TYPE SPECIES. *Strophomena folium* Barrande, 1879, from the Králův Dvůr Formation (Ashgill) of Bohemia.

Foliomena prisca sp. nov. Pl. 3, figs 18–23, 25

ETYMOLOGY. After *priscus*, Latin – old.

HOLOTYPE. BC 57405, Pl. 3, figs 22, 23, a dorsal valve, from the Anderken Formation, Sample 8255, Anderkenyn-Akchoku section.

MATERIAL. 2 pairs of conjoined valves, 4 ventral and 3 dorsal valves from Samples 100 (BC 57407), 2531, 8221 (BC 56890), 8223b, 8251, 8255 (BC 57402–06, 08), Anderkenyn-Akchoku section; 628, 2538, 8217, Kujandysai section.

DESCRIPTION. Shell flat and gently resupinate, transverse, subrectangular in outline, about 60% as long as wide, with maximum width at hinge line. Cardinal extremities near right angled. Anterior commissure rectimarginate. Ventral valve gently convex in the posterior half and weakly concave anteriorly. Ventral interarea apsacline with a minute, apical pseudodeltidium. Dorsal valve with lateral profile flat to slightly concave in the posterior half and convex posteriorly, with maximum thickness at about three-quarters valve length in mature specimens. Dorsal interarea linear, anacline, with separate chilidial plates flanking narrow notothyrium. Radial ornament of fine capillae rarely preserved. Concentric ornament of numerous slightly uneven fine rugellae.

Ventral interior with delicate teeth lacking dental plates and an open, weakly impressed muscle field. Dorsal interior with a small bilobed cardinal process in the low notothyrial platform and thin widely diverging socket ridges. Thin median septum, about half the length of the pair of strong curved side septa.

MEASUREMENTS. (463/12375) ventral valve, L=6.0, W=11.7; (464/12375) ventral valve, L=6.4, W=11.4; (466/12375) dorsal valve, L=4.3, W=7.2; (468/12375) dorsal valve, L=4.6, W=8.5; (469/12375) dorsal valve, L=3.6, W=6.3.

DISCUSSION. Cocks & Rong (1988:65) discussed the variation in the ornament of *Foliomena* and noted that, although all the shells from the type locality in Bohemia were devoid of radial ornament, occasional costae or costellae can be present sporadically in some populations. The presence of fine capillae is a key feature in our new species, as is the resupinate shell shape and the separate chilidial plates, although the features within the interarea are poorly known in *Foliomena folium*. It is difficult to make a precise comparison of our shells with *F. inelegans* Fu, 1982 from the Pingliang Formation (Upper Caradoc) of North China, because of inadequate information on the interior of the latter species. From *F. jielingensis*, described by Zeng (1987) from the Miapo Formation (Lower Caradoc) of the Yangtze Gorge area, south China, *F. prisca* differs in the presence of the fine ornament, the resupinate shell shape and in the absence of the ventral internal tuberculae seen in *F. jielingensis*.

Superfamily **PLECTAMBONITOIDEA** Jones, 1928
Family **PLECTAMBONITIDAE** Jones, 1928
Subfamily **TAPHRODONTINAE** Cooper, 1956
Genus ***ISOPHRAGMA*** Cooper, 1956

TYPE SPECIES. *Isophragma ricevillense* Cooper, 1956, from the Lower Caradoc of Tennessee, U.S.A.

Isophragma imperator Popov, 1980 Pl. 3, fig. 35

1980 *Isophragma imperator* Popov: 147, pl. 2, figs 8–12.

Holotype. CNIGR 25/11523, from Sample 1018, 7 km south-west of Karpkuduk Well, Kotnak Mountains.

MATERIAL. One pair of conjoined valves, 36 ventral and 34 dorsal valves from Sample 1018.

DISCUSSION. Popov (1980) provided detailed description and discussion of this species.

Family **BIMURIIDAE** Cooper, 1956
Genus ***CRASPEDELIA*** Cooper, 1956

TYPE SPECIES. *Craspedelia marginata* Cooper, 1956: 773, pl. 213, figs. 1–20, from the Pratt Ferry Formation (Landeilo), Alabama, U.S.A.

Craspedelia tata Popov, 1980 Pl. 3, figs 26–34

1980 *Craspedelia tata* Popov: 55, pl. 17, figs 6–9.
1986 *Craspedelia tata* Popov; Kolobova & Popov: pl. 1, fig. 9.

HOLOTYPE. CNIGR 8/11098, from the Lidievka Formation (Lower Caradoc), Belyi Kardon, north-central Kazakhstan.

MATERIAL. 25 pairs of conjoined valves, 18 ventral and 5 dorsal valves from Samples 100 (BC 56900–03, 57410, 57597) (=K98/1970), 626 (BC 56532, 56907–10, 57409, 57411–12), 8223a (BC 56935), 8223b, Anderkenyn-Akchoku section; Samples 8214 (BC 56925–30, 56932–33, 57598), 8215b (BC 56931), west side of Ashchisu River; Samples 628 (BC 56911), 2538 (BC 56917–24), Kujandysai section; Sample 8231–40, Buldukbai-Akchoku; Sample 948 (BC 56912–16), Tesik River.

DESCRIPTION. Shell smooth, concavoconvex posteriorly, strongly geniculated ventrally with a trail up to 8 mm long which curves back postero-ventrally; semielliptical in outline, about 80% as long as wide, with maximum width slightly anterior to hinge line. Cardinal extremities rounded. Anterior commissure uniplicate. Ventral valve strongly convex posteriorly with maximum thickness about one-third anteriorly. Narrow and shallow sulcus anterior to the

geniculation. Dorsal valve strongly concave with low, planar interarea and notothyrium covered by joined apical chilidial plates. Weak median fold originating anterior to the geniculation. Shell surface smooth with fine growth lines. Ventral interior with strong teeth and *vascula media* subparallel. Dorsal interior with simple, undercut cardinal process, divided bema, low median ridge and a pair of slightly diverging side ridges bisecting the bema.

DISCUSSION. This species differs from *Craspedelia marginata* Cooper (1956) and *C. gabata* Williams (1962: 179), from the Lower Ardwell Formation (Middle Caradoc) of Girvan, in its high (up to 8 mm) ventrally directed trail with a well-defined ventral sulcus and dorsal median fold. It differs from *C. intonsa* Potter, 1991, from Member 1 of the Gregg Ranch Unit (Llandeilo), of California, USA, in having a larger shell, up to 12 mm long, with a less transverse outline and a high trail, which exceeds the thickness of the ventral valve in mature specimens.

Family **LEPTELLINIDAE** Ulrich & Cooper 1936
Subfamily **LEPTELLININAE** Ulrich & Cooper 1936
Genus ***ACCULINA*** Misius, in Misius & Ushatinskaya,1977

TYPE SPECIES. *Acculina acculica* Misius *in* Misius & Ushatinskaya, 1977, from the Tabylgaty Formation (Lower Caradoc: *gracilis* Zone), Moldo-Too Range, North Kirgyzstan.

Acculina kulanketpesica sp. nov. Pl. 3, figs 36–40, Pl. 4, figs 1–5

ETYMOLOGY. After Kulanketpes ('donkey cannot escape' in Kazakh) Valley on the way from Lake Balkhash to the type locality.

HOLOTYPE. BC 12904, Pl. 3, figs 39, 40, conjoined valves, from the Anderken Formation, Sample 1041a, Burultas section.

MATERIAL. 50 pairs of conjoined valves, 13 ventral and 10 dorsal valves from Samples 100 (=K98/1970) (BC 56493–5, 56485–90, BC 57414), 620 (BC 56937–39), 626, 8128, Anderkenyn-Akchoku section; Sample 8231–40 (BC 57416, 18), Buldukbai-Akchoku; Sample 1041a (BC 12900–7, 57413, 15, 19), Burultas Valley; Samples 85258 (BC 56491–2, 56941–6), 2538 (BC 56501–02), Kujandysai.

DESCRIPTION. Shell resupinate, transverse, semielliptical in outline, about 70% as long as wide and 35% as thick as long. Cardinal extremities near right-angled or slightly acute. Anterior commissure rectimarginate. Ventral valve gently to moderately concave in the anterior half and slightly convex posterior to the mid-valve. Ventral interarea apsacline with a narrow, convex pseudodeltidium. Dorsal valve flat and gently sulcate between the umbo and mid-length, becoming moderately convex anteriorly. Interarea anacline with a narrow, convex chilidium completely covering the notothyrium. Radial ornament unequally parvicostellate with 7 accentuated costae in the umbonal area and 27–30 accentuated costellae along the anterior and lateral margins in full grown specimens. Interspaces between the accentuated costellae occupied by fine parvicostellae about 7–10 per mm along the anterior margin. Fine, closely spaced growth lamellae form comae crossed by accentuated ribs in the anterior half of the shell.

Table 10 Basic statistics of complete shells of *Acculina kulanketpesica* sp. nov. from Sample F-1041a, Burultas valley.

	Lv	Ld	W	T	Lv/W	Ld/W	T/Lv
N	6	5	6	5	6	5	5
X	15.5	14.7	22.6	5.4	68.9%	65.6%	34.5%
S	0.89	0.92	0.85	1.13	1.9	2.1	7.0
MIN	14.0	13.5	21.3	3.8	65.7	63.4	24.1
MAX	16.4	16.1	23.5	7.0	71.2%	68.5%	42.9%

Ventral valve with strong teeth with central grooves; lacking dental plates. Ventral muscle field small, rounded pentagonal with strongly impressed diductor scars completely divided by slightly shorter, narrow, triangular adductor scars. Ventral mantle canals saccate with slightly diverging vascula media. Dorsal valve interior with trifid cardinal process situated on the low notothyrial platform. Socket ridges low, widely diverging and slightly incurved posteriorly. Dorsal adductor muscle field subquadrate, bordered laterally by low, subparallel ridges. Median ridge high and strongly thickened, extended anteriorly to the mid-valve, merging with high diaphragm bordering the lophophore platform. Dorsal mantle canals lemniscate.

DISCUSSION. This species also occurs in Betpak Dala, Kazakhstan (the locality in Nikitin & Popov 1996). It differs from *Acculina acculica* Misius (*in* Misius & Ushatinskaya 1977: 114) in its significantly larger shell, strongly convex anteriorly transverse profile of the dorsal valve and numerous comae (Pl. 3, fig. 39) in the anterior part of full grown specimens. It is also similar to *A. villosa* Nikitina (1985: 24) from the Rgaity Formation (Llandeilo-Lower Caradoc) of the Kendyktas Range, south Kazakhstan, in the development of comae, but can be distinguished in having a well-defined peripheral rim in the ventral valve, a somewhat smaller dorsal lophophore platform, which has a subrectangular, not a flabellate outline, and a pair of fine transmuscle ridges dividing the anterior and posterior adductors. *Acculina* is the only plectambonitoid in the Anderken Formation to possess comae, and its exterior is also normally covered by encrusting girvanellid algae. Two specimens (BC 56502–3, Pl. 4, figs 7, 8) from the Kujandysai section from Sample 2538 differ from other *Acculina* in having a geniculate shell with the lophophore platform less than half the valve length, and probably represent a separate species.

Genus ***DULANKARELLA*** Rukavishnikova, 1956

TYPE SPECIES. *Dulankarella magna* Rukavishnikova 1956, from the Dulankara Formation (late Caradoc), Kazakhstan, Chu-Ili Range, Kazakhstan.

Dulankarella larga sp. nov. Pl. 4, figs 9–25, Pl. 5, figs 1–3

ETYMOLOGY. After *largus*, Latin – rich.

HOLOTYPE. BC 57421, Pl. 4, figs 9, 10, a dorsal valve interior from Anderken Formation, Sample 8231-40, Buldukbai-Akchoku section.

MATERIAL. 86 pairs of conjoined valves, 3 ventral and 2 dorsal valves, from Samples 100 (=K98/1970) (BC 56514, 16–18, 25–29, 57422, 24, 26), 626 (BC 56522–4), 8223a (BC 56511, 56975), Anderkenyn-Akchoku; Sample 8231–40 (BC 57421, 23), Buldukbai-Akchoku; Sample 8228 (BC 56986), east side of Kopalysai River; Samples 1041a (BC 56512, 19–21, 56947–57), 818a, 1041a (BC 56967, 57425), Burultas Valley.

DESCRIPTION. Shell strongly concavoconvex, transverse and semielliptical in outline, on average 73% as wide as long, with maximum width at the hinge line and 45% as thick as long. Cardinal extremities slightly acute. Anterior commissure weakly sulcate. Ventral valve strongly and evenly convex in lateral profile, subcarinate posteriorly in transverse profile. Ventral interarea low, planar, anacline


1

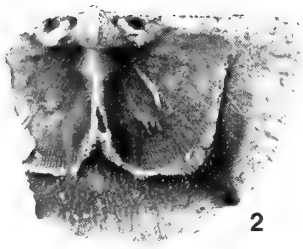
2

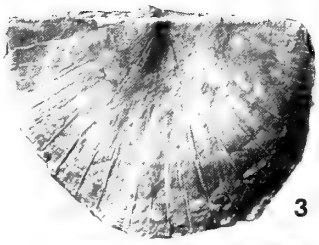
3

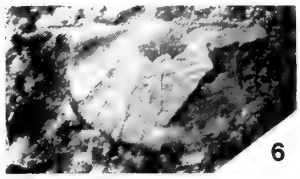
6

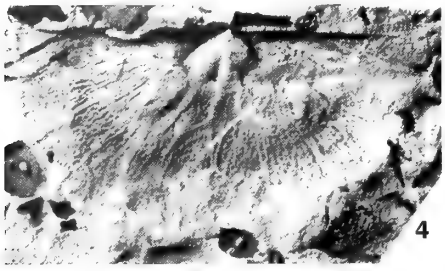
4


5

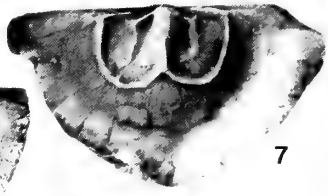
7

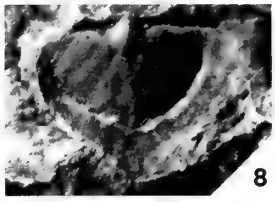
8

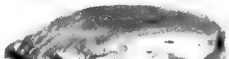
12

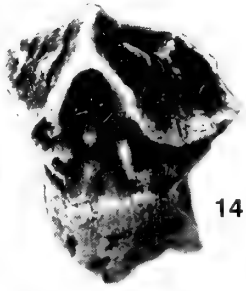
14

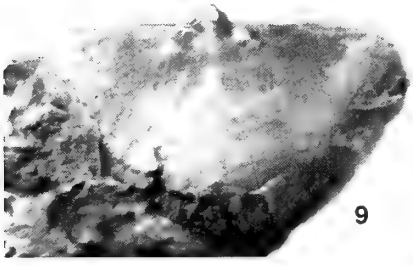
9

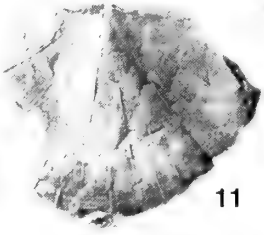
11

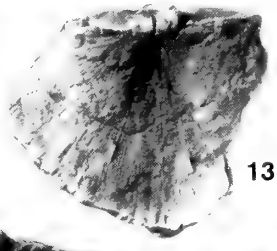
13

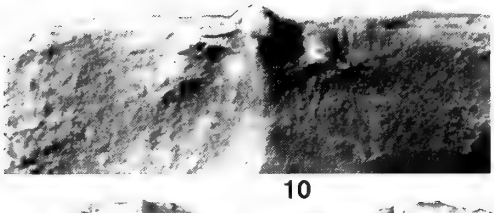
10


15

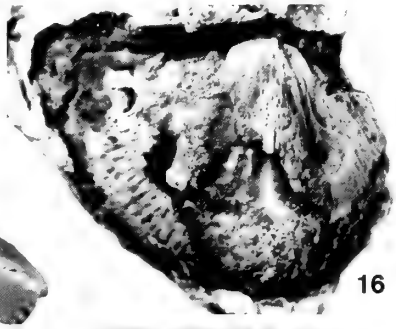
16

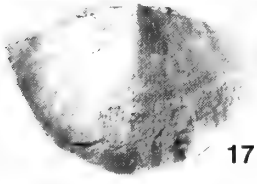
17

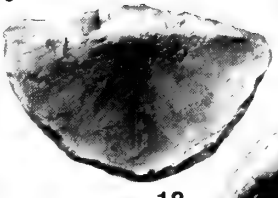
18


19

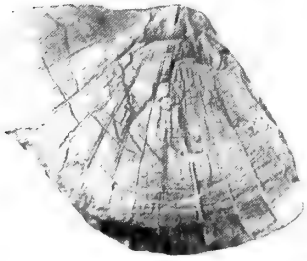
20

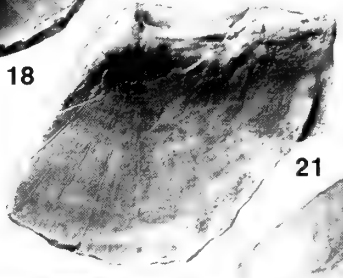
21

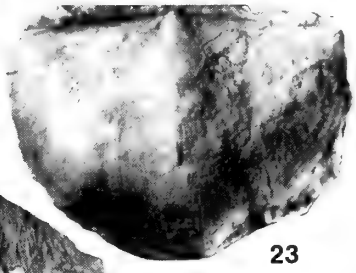
23

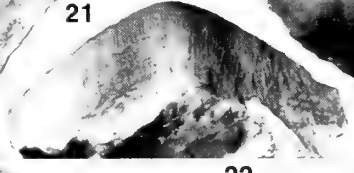
22

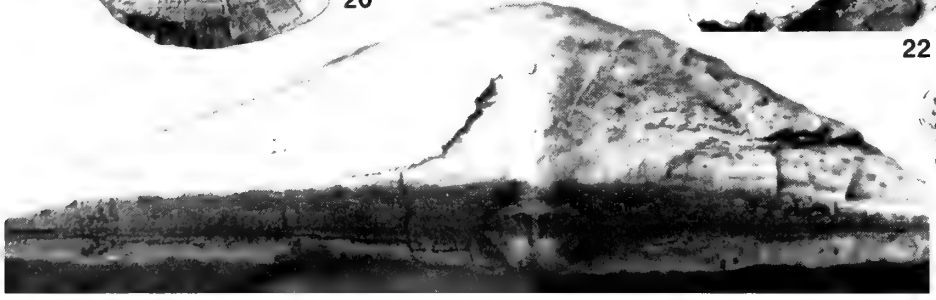
24

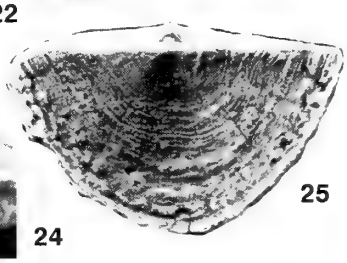
25

Table 11 Basic statistics of complete shells of *Dulankarella larga* sp. nov. from Sample F-1041a, Burultas valley.

	Lv	W	T	Lv/W	T/Lv
N	9	9	7	9	7
X	16.9	24.6	7.7	69.7%	46.1%
S	2.10	3.57	1.19	10.2	3.2
MIN	13.5	19.1	5.7	51.9%	41.5%
MAX	18.8	31.6	9.2	81.3%	50.0%

with delthyrium partly covered by a convex pseudodeltidium. Dorsal valve strongly concave and slightly geniculate anteriorly. Dorsal interarea hypercline with chilidial plates joined apically. Sulcus broad and shallow, originating near mid-valve. Radial ornament unequally parvicostellate with 5–7 accentuated ribs originating at the umbo and two or three generations of accentuated costellae, totaling 31–38 in number in full grown specimens. Parvicostellae between accentuated ribs very fine and closely spaced, about 12–16 per mm along the anterior margin.

Ventral valve interior with strong teeth supported by short dental plates, thickened at the base. Muscle field bilobed with strongly impressed, rounded subrhomboidal diductor scars separated by short, elongate subtriangular adductor scars. Paired nodose swellings anterolateral to the muscle field. Ventral mantle canals saccate with short, divergent *vascula media*. Dorsal interior with trifid cardinal process bearing a strong, ridge-like median lobe and up to 6 fine ridges on the lateral lobes. Socket ridges narrow, widely diverging. Median septum strongly raised and thickened anteriorly with the maximum height at the point of junction with the outer boundary of the lophopore platform accentuated by geniculation of the valve.

DISCUSSION. This species resembles the later *Dulankarella magna* Rukavishnikova (1956:139) in size and transverse profile, but differs in having a finer radial ornament with 5–7 strongly accentuated primary ribs and a characteristic rounded subrhomboidal outline of the ventral diductor scars, which only slightly touch each other anteriorly to the adductor scars. The differences from *Dulankarella? partita* Percival (1979b: 103) are in having a less transverse outline, evenly convex ventral valve, the ventral muscle field lacking a median ridge, and the rhomboidal outline of the ventral diductor scars.

Genus *KAJNARIA* Nikitin & Popov, 1984

TYPE SPECIES. *Kajnaria derupta* Nikitin & Popov *in* Klenina *et al.* (1984), from the Bestamak Formation (Lower Caradoc), Chingiz Range, Kazakhstan.

Kajnaria rugosa sp. nov. Pl. 5, figs 6–18

ETYMOLOGY. After *rugosus*, Latin – wrinkled.

HOLOTYPE. BC 56551, Pl. 5, figs 12, 13, a dorsal internal mould from Sample 628, Kujandysai section.

MATERIAL. 9 pairs of conjoined valves and three ventral valves from Samples 100 (BC 56545–47, 57436, 37), 626 (BC 56548), 8223a, Anderkenyn-Akchoku section; Sample 628 (=K107/1970) (BC 56551, 57439), Kujandysai section; Sample 1041a (BC 56543, 44), Burultas Valley: Sample 816 (BC 56549–50, 57438), Alakul lake.

DESCRIPTION. Shell strongly concavoconvex, semielliptical in outline, about 67–82% as long as wide with maximum width at the hinge line. Cardinal extremities acute and slightly alate in adult specimens. Ventral valve strongly convex in lateral profile, weakly geniculate in some specimens, with maximum thickness posterior to mid-length. Relatively weak umbo. Interarea anacline with narrow convex pseudodeltidium. Dorsal valve moderately and evenly convex with hypercline interarea. Notothyrium completely covered by convex chilidium. Radial ornament unequally parvicostellate with 5–7 primary accentuated ribs and two to three generations of accentuated costellae, with the interspaces between them covered by fine closely-spaced parvicostellae, about 7–14 per mm. Concentric ornament of up to 9 undulated rugellae in the posterior half of both valves.

Ventral interior with strong teeth lacking dental plates. Ventral muscle field small, strongly supported by raised muscle bounding ridges which merge centrally and anteriorly. A further pair of strong curved ridges originate posteriorly at one-third of the length of the hinge line on each side of the valve, and curve anterolaterally to form a w-shaped structure which terminates near the end of the bounding ridges at about quarter valve length. Mantle canals saccate with *vascula media* subparallel in the proximal part and diverging anteriorly. Dorsal interior with erect trifid cardinal process fused anteriorly to a strong median ridge. Sockets large. The median ridge merges near the mid-length with a high subperipheral rim bordering the lophophore platform.

DISCUSSION. This species differs from *Kajnaria derupta* in the twice as large shell size and the well defined concentric rugellae in the posterior half of the valves.

Genus *MABELLA* Klenina, 1984

TYPE SPECIES. *Leptellina (Mabella) semiovalis* Klenina *in* Klenina *et al.* (1984), from the Taldyboy Formation, Dulankara Regional Stage (Upper Caradoc), Chingiz Range, Kazakhstan.

PLATE 4

Figs 1–5 *Acculina kulanketpesica* sp. nov. **1,** Sample 1041a, Burultas Valley, BC 57413, dorsal interior, × 2. **2**, Sample 8137, Anderkenyn-Akchoku section, BC 57417, latex cast of dorsal interior, × 3. **3,** Sample 100, Anderkenyn-Akchoku section, BC 57414, dorsal exterior view of conjoined valves, × 2. **4,** Sample 1018, area 7 km SW of Karpkuduk well, Kotnak Mountains, ventral internal mould, × 3. **5,** Sample 85258, east of Uzunbulak River, BC 56491, ventral internal mould, × 2.

Fig. 6 *Glyptambonites* sp., Sample 628 (=K-107/70), west side of Kujandysai, BC 56510, ventral exterior, × 3.

Figs 7, 8 *Acculina* sp. Sample 2538, Akchoku Mountain, Kujandysai section. **7,** BC 56502, latex cast of dorsal interior, × 2. **8,** BC 56501, ventral internal mould, × 1.5.

Figs 9–25 *Dulankarella larga* sp. nov. **9, 10, 16**, Sample 8231–40 , Buldukbai-Akchoku section, west side of Kopalysai; **9, 10**, BC 57421, **holotype**, dorsal interior, × 2.7; cardinal process and socket plates, × 5; **16,** BC 57423, ventral internal mould, × 2. **11–13, 19–21, 24, 25**, Sample 1041a, Burultas Valley; **11–13**, conjoined valves, lateral, ventral and dorsal views, × 2; **19–21**, BC 57425, conjoined valves, ventral, dorsal and lateral views, × 2; **24**, Sample 1041a, BC 56512, conjoined valves, posterior view showing interareas, × 6; **25**, BC 56967, dorsal view of conjoined valves, × 2. **14, 15, 17, 18, 22, 23**, Sample 100, Anderkenyn-Akchoku section; **14**, BC 56514, incomplete dorsal valve interior, × 3; **15,** BC 57422, ventral internal mould, × 2; **17, 18**, BC 57424, conjoined valves, ventral and dorsal views, × 1.5; **22, 23**, BC 57426, ventral valve exterior, anterior and ventral views, × 2.

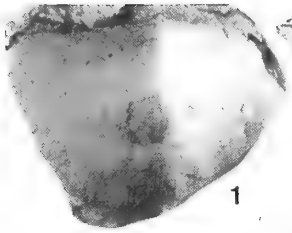
1

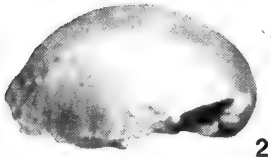
2

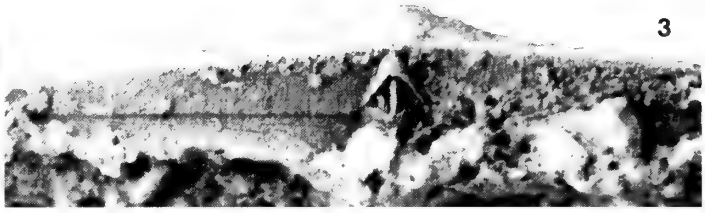
3


4

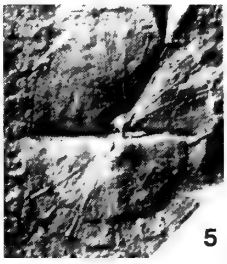
5


6

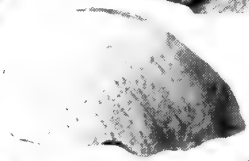
7

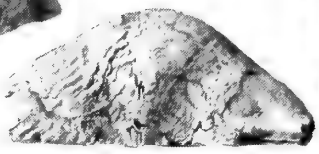
8

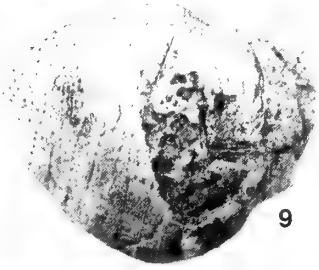
9

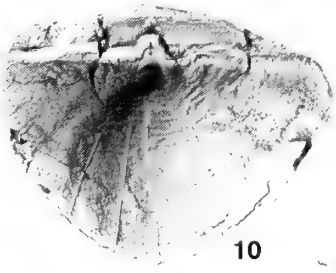
10

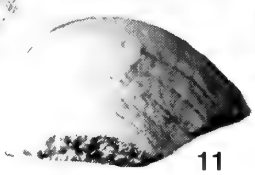
11

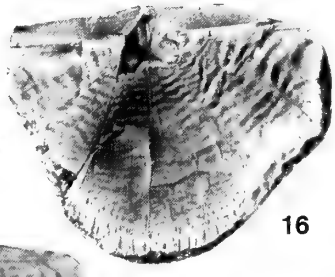
16


12


13

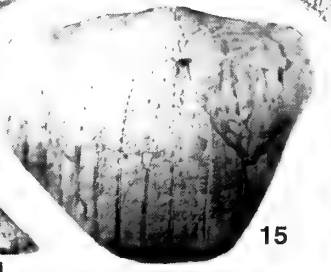
15


14

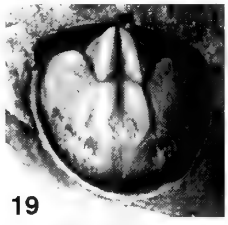
19

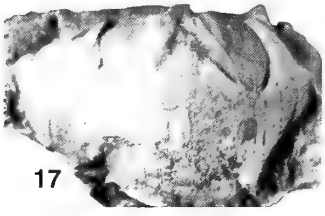
17


18

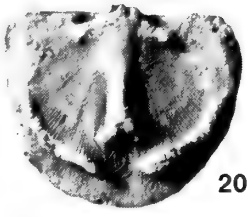
20

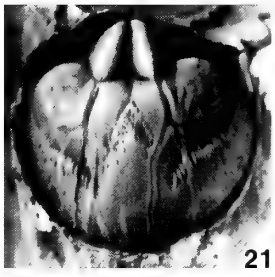
21

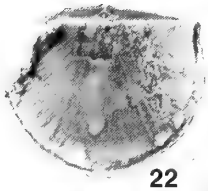
22


23


27

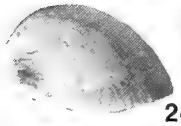
24

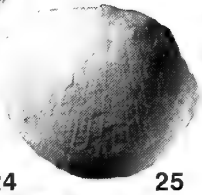
25


26

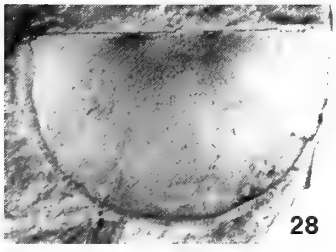
28

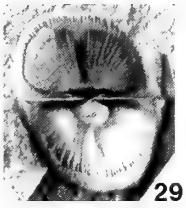
29

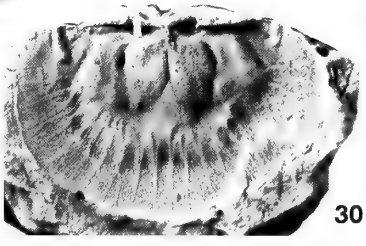
30

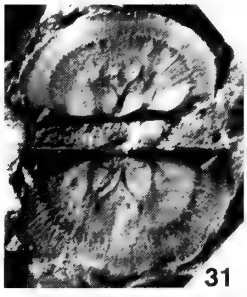
31

SPECIES INCLUDED. *Leptellina (Mabella) semiovalis* Klenina, *in* Klenina *et al.* 1984: 69, pl. 5, figs. 1, 3, 4; pl. 9, figs 4, 7 (=*Leptellina (Mabella) obtusa* Klenina, *in* Klenina *et al.* 1984: 71, pl. 5, figs 5, 6; pl. 6, fig.2; =*Leptellina (Mabella) incurvata* Klenina, *in* Klenina *et al.* 1984: 72, pl. 5,fig. 2), Upper Caradoc, beds tb_{II-V} of Taldyboi Formation, Chingiz Range, Kazakhstan; *Leptellina? conferta* Popov, 1985: 56, pl. 2, figs 1–6, Lower Caradoc, Anderken Formation, Chu-Ili Range; *Leptelloidea multicostata* Rukavishnikova, 1956: 132; *Wiradjuriella halis* Percival, 1991: 138, fig. 12A–Z, Aa–Al, Upper Caradoc, New South Wales, Australia; *Leptellina* sp., Percival, 1979b, Ordovician, Goonumbla Volcanics, New South Wales, Australia.

DISCUSSION. *Mabella* differs from *Leptellina* in the distinctive median septum which enlarges anteriorly, and is sometimes bifurcating and tubular. However, *Wiradjuriella*, from the Caradoc of Australia (Percival 1991), has this same structure as *Mabella* and can be considered congeneric with it (Cocks & Rong 2000).

Mabella conferta (Popov, 1985) Pl. 5, figs 19–29

1985 *Leptellina? conferta* Popov: 56, pl. 2, figs 1–6, text-figs 1, 2.
1991 *Wiradjuriella conferta* (Popov) Percival: 140.

HOLOTYPE. CNIGR 17/11989, ventral internal mould from the Anderken Formation, Sample 100b, Anderkenyn-Akchoku section.

MATERIAL. 35 pairs of conjoined valves, 183 ventral and 66 dorsal valves from Samples 100, 100b, 843, 8128a, 8128b, 8137 (BC 56982–84), Anderkenyn-Akchoku section; Sample 7613, Kujandysai section; Samples 110, 8229, 8230 (BC 57440), 8257, Buldukbai-Akchoku; Sample 8228 (BC 57441, 43–46), east side of Kopalysai River; Samples 818a (BC 57442), 1041a (BC 56978–81), Burultas Valley; Samples 1018, 1018a, 7 km south-west of Karpkuduk well, Kotnak Mountains.

DESCRIPTION. Shell concavoconvex, transverse, semioval in outline, length about three-quarters of the width, with maximum width at the hinge line. Anterior commissure rectimarginate. Ventral valve strongly convex in transverse and lateral profiles with the maximum thickness slightly posterior to mid-length. Planar strongly apsacline interarea and small, convex pseudodeltidium. Dorsal valve gently concave to almost flat, with a planar, anacline interarea and disjunct chilidial plates. Radial ornament very fine, unequally parvicostellate, with up to five accentuated parvicostellae per 3 mm along the anterior margin of mature specimens.

Ventral interior with strong teeth lacking dental plates. Cordate muscle field with short, ridge-like adductor scars completely separating strongly impressed diductor scars. Strong, slightly divergent, saccate mantle canals. Dorsal interior with low, trifid cardinal process facing posteriorly, short socket ridges subparallel to the hinge line. Lophophore platform about 90% valve length and 87% as wide as maximum valve width, bordered by a high, ridge-like rim divided medially. High median septum about three-quarters as long as the valve, not joined anteriorly with the subperipheral rim.

DISCUSSION. This species was originally assigned to *Leptellina* and later referred by Percival (1991) to *Wiradjuriella*. Percival also listed and discussed the differences between the various species of the genus, which is so far known only from Australia and Kazakhstan.

Genus ***SHLYGINIA*** Nikitin & Popov, 1983

TYPE SPECIES. *Shlyginia declivis* Nikitin & Popov, 1983, from the Andriushino Formation, Tselnograd Regional Stage (Llandeilo-Lower Caradoc), north-central Kazakhstan.

DISCUSSION. The affinities of *Shlyginia* and its differences from *Dulankarella* were discussed by Nikitin & Popov (1996).

Table 12 Measurements of complete shells of *Shlyginia fragilis* (Rukavishnikova) Sample 8228 and 8257 from Kopalysai section.

	Lv	W	T	L/W	T/L
N	16	16	16	16	16
X	10.4	16.3	4.2	64.0%	40.4%
S	1.04	1.34	0.54	6.2	4.5
MIN	8.5	13.6	2.9	50.0%	31.2%
MAX	12.2	19	5.1	72.1%	51.8%

Table 13 Measurements of ventral valves of *Shlyginia fragilis* (Rukavishnikova) Sample 8228 from Kopalysai section.

	Lv	W	Ml	Mw	Lv/W	M//L	Ml/Mw
N	6	6	6	6	6	6	6
X	9.4	12.8	3.6	4.3	75.2%	37.6%	83.5%
S	2.47	3.61	1.13	1.05	11.2	4.5	16.3
MIN	5.3	5.8	1.8	2.6	60.0%	30.5%	67.9%
MAX	12.8	15.5	5.3	5.6	91.4%	41.4%	110.4%

Table 14 Measurements of dorsal valves of *Shlyginia fragilis* (Rukavishnikova) Sample 8228 from Kopalysai section and sample 8229 from Buldukbai-Akchoku.

	Ld	W	Sl	BBl	BBw	Ld/W	Sl/L	BBw/W
N	6	6	3	6	6	6	3	6
X	8.1	12.1	5.5	1.2	3.8	67.7%	79.2%	31.7%
S	1.87	2.55	1.25	0.42	0.93	13.2	8.6	8.5
MIN	6.2	7.8	4.3	0.6	2.8	49.7%	69.4%	23.6%
MAX	10.8	14.8	6.8	1.8	5.0	82.1%	84.4%	43.6%

PLATE 5

Figs 1–3 *Dulankarella larga* sp. nov. **1, 2,** Sample 100, Anderkenyn-Akchoku, BC 57427, ventral exterior and lateral views, × 2. **3,** Sample 1041a, Burultas Valley, BC 56513, interareas of conjoined valves, × 8.

Figs 4, 5 *Chonetoidea* sp. Sample 8255, Anderkenyn-Akchoku section, BC 56537, external and internal moulds of conjoined valves, × 8.

Figs 6–18 *Kajnaria rugosa* sp. nov. **6**, unnamed Lower Caradoc formation, about 4 km south-west of Lake Alakul, Sample 816, BC 57438, ventral internal mould, × 1.5. **7–11, 14–16**, Sample 100, Anderkenyn-Akchoku; **7–10,** BC 57436, conjoined valves, lateral, posterior, ventral and dorsal views, × 2; **11, 14–16,** BC 57437, conjoined valves, lateral, posterior, ventral and dorsal views, × 2. **12, 13, 17, 18**, Sample 628, west side of Kujandysai River; **12, 13,** BC 56551, latex cast and dorsal internal mould, **holotype**, × 2; **17, 18,** BC 57439, ventral internal mould, oblique posterior and oblique anterior views, × 2.

Figs 19–29 *Mabella conferta* (Popov). **19, 21, 26, 28, 29,** Sample 8228, east side of Kopalysai; **19,** BC 57445, ventral internal mould, × 3; **21,** BC 57443, ventral internal mould, × 4; **26,** BC 57444, ventral internal mould, × 4; **28**, BC 57446, dorsal exterior, × 4; **29**, BC 57441, internal mould of conjoined valves of juvenile specimen, × 4. **20**, Sample 8230, Buldukbai-Akchoku section, west side of Kopalysai, BC 57440, latex cast of dorsal interior, × 3. **22–25**, Sample 818a, Burultas Valley, BC 57442, conjoined valves, dorsal, posterior, lateral and ventral views, × 4. **27**, Sample 7613, Akchoku Mountain, Kujandysai section, CNIGR 20/11989, latex cast of dorsal interior of juvenile, × 3.

Figs 30, 31 *Tesikella necopina* (Popov, 1980), Kopalysai, Rukavishnikova. **30,** Sample 34, BC 56881, ventral internal mould, × 2. **31**, Sample 818a, Burultas Valley, BC 57435, × 2.5.

Shlyginia fragilis (Rukavishnikova, 1956) Pl. 6, figs 11–25

1956 *Dulankarella fragilis* Rukavishnikova: 136, pl. 2, figs 16–23.
1996 *Shlyginia fragilis* (Rukavishnikova) Nikitin & Popov: 7.

HOLOTYPE. IGNA 28/1369, conjoined valves; Anderken Formation, east side of Kopalysai River.

MATERIAL. Eight pairs of conjoined valves, 57 ventral and 53 dorsal valves from Samples 100b (BC 56989), 620 (BC 56991–99), 843, 8128a, 8128b, 8135, 8137 (BC 57450), Anderkenyn-Akchoku section; Samples 628, 7613, 8258, Kujandysai section; Samples 110, 8230 (BC 57453), 8257, Buldukbai-Akchoku; Sample 8228 (BC 12881–88, 57447, 48, 52), east side of Kopalysai River; Samples 390, 818 (BC 57451), 1041a, Burultas Valley; Sample 1018, area 7 km south-west from Karpkuduk well, Kotnak Mountains, south Betpak-Dala.

DESCRIPTION. Shell concavoconvex, transverse, semielliptical in outline, length about two-thirds of the width, with maximum width slightly anterior to hinge line or at the hinge line, and 40% as thick as long. Cardinal extremities acute to slightly rounded. Anterior commissure rectimarginate. Ventral valve moderately convex in transverse profile with maximum thickness at about one-third of valve length. Interarea low, planar, apsacline with small triangular delthyrium, covered apically by the minute pseudodeltidium. Dorsal valve moderately convex, slightly geniculate anteriorly with low, planar, hypercline interarea and notothyrium covered laterally by disjunct chilidial plates. Radial ornament finely parvicostellate with 8–11 parvicostellae per mm at the anterior margin and 4–8 parvicostellae between the accentuated costellae which originate in the umbonal area, near the mid-valve and anterior to mid-valve in full grown specimens.

Ventral valve interior with small teeth lacking dental plates. Muscle field flabellate, on average 80% as long as wide and 40% as long as the valve. Diductor scars large, suboval, deeply impressed and completely enclosing small lanceolate adductor scars bisected by a fine median ridge. Ventral mantle canals saccate with short diverging *vascula media.* Dorsal interior with a trifid cardinal process widely diverging, low and short socket ridges and strong median ridge joined anteriorly with the peripheral rim. Dorsal adductor field large, subquadrate.

DISCUSSION. This species differs from the type species *Shlyginia declivis* Nikitin & Popov (1983: 238, pl. 3, figs 1–5) in its larger size and moderately concave lateral profile of the dorsal valve, which is also weakly geniculate anteriorly.

Subfamily **PALAEOSTROPHOMENINAE** Cocks & Rong, 1989
Genus ***GLYPTAMBONITES*** Cooper, 1956

TYPE SPECIES. *Glyptambonites musculosus* Cooper, 1956, from the Oranda Formation (Caradoc) of Virginia, U.S.A.

Glyptambonites sp. Pl. 4, fig. 6

MATERIAL. Three ventral valves, from Sample 628 (BC 56510), Kujandysai, Sample 100, Anderkenyn-Akchoku section.

DISCUSSION. *Glyptambonites* is a rare genus in the Anderken Formation and also uncommon in the overlying Dulankara Formation of the Chu-Ili Range. Its internal features are known from specimens from the latter, but not from the Anderken Formation. The exterior of our material appears similar to *Glyptambonites glyptus* Cooper, 1956 from the Llandeilo to early Caradoc of Virginia and Alabama.

Genus ***TESIKELLA*** gen. nov.

ETYMOLOGY. After the River Tesik.

TYPE SPECIES. *Palaeostrophomena necopina* Popov, 1980, from the Anderken Formation, Chu-Ili Range.

DIAGNOSIS. Shell profile resupinate, ventral valve with low interarea; chilidial plates disjunct; radial ornament unequally parvicostellate; ventral interior with double teeth lacking dental plates; ventral muscle field enclosed by bilobed bounding ridges: adductor scars short; ventral subperipheral rim variably developed; dorsal interior with strong median septum coalescing anteriorly with platform.

DISCUSSION. The subfamily Palaeostrophomeninae has the genera *Palaeostrophomena*, *Apatomorpha*, *Glyptambonites*, *Ishimia*, *Lepidomena*, *Titanambonites* and *Toquimia* definitely attributed to it, and *Goniotrema* is possibly a member (Cocks & Rong 2000). Of these, all are of normal convexity apart from *Palaeostrophomena* which is generally resupinate and *Toquimia*, in which resupination develops anteriorly in larger specimens. *Tesikella* is also resupinate and in external features resembles *Palaeostrophomena* apart from the irregular rugae, which are variable in the latter. However, internally *Tesikella* has a dorsal platform which is absent in *Palaeostrophomena*, and also has a variably developed subperipheral rim in the ventral valve which in some specimens is fully developed but in others consists only of semi-continuous papillae. The ventral muscle field is enclosed by bilobed bounding ridges, which are not present in other members of the subfamily, but are developed in other Leptellinidae.

PLATE 6

Figs 1–6 *Tesikella necopina* (Popov, 1980), Sample 8129, Anderkenyn-Akchoku section. **1,** BC 57433, ventral internal mould, × 2. **2**, BC 57434, ventral exterior, × 2. **3, 4**, BC 57604, latex cast, × 3, and dorsal internal mould, × 2. **5, 6**, BC 57432, latex cast, × 3, and ventral internal mould, × 2.

Figs 7–10 *Sowerbyella (Sowerbyella) rukavishnikovae* Popov. **7,** Sample 100b, Anderkenyn-Akchoku section, CNIGR 41/11522, latex cast of dorsal exterior, × 5. **8**, Sample 110, Buldukbai-Akchoku section, BC 57801, ventral internal mould, × 4. **9,** Sample 1018a, 7 km southwest of Karpkuduk well, Kotnak Mountains, south Betpak-Dala, CNIGR 44/11522, dorsal interior, × 2.5. **10,** Sample 100b, CNIGR 38/11989, dorsal interior, × 2.5.

Figs 11–25 *Shlyginia fragilis* (Rukavishnikova). **11, 12, 17–19, 21, 23, 24**, Sample 8228, east side of Kopalysai; **11,** BC 57448, ventral internal mould, × 2; **12**, BC 12882, ventral internal mould, × 3; **17–19**, BC 57447, ventral, dorsal and lateral views of conjoined valves, × 2; **21, 23, 24**, BC 57452, conjoined valves, lateral, dorsal and ventral views, × 2. **13–16**. Sample 818, Burultas Valley, BC 57451, conjoined valves, ventral, dorsal and lateral views, × 4; posterior view of interareas, × 6. **20,** Sample 8230, BC 57453, dorsal internal mould, × 3. **22,** Sample 8137, Anderkenyn-Akchoku section, BC 57450, ventral internal mould, × 3. **25,** Sample 620, Anderkenyn-Akchoku section, BC 57449, ventral internal mould, × 3.

Figs 26–33 *Sortanella* aff. *quinquecostata* Nikitin & Popov. **26–30,** Sample 2538, Akchoku Mountain, Kujandysai section; **26,** BC 57488, ventral internal mould, × 2; **27–29,** BC56771, conjoined valves, dorsal, ventral and lateral views, × 4; **30**, BC 57460, ventral internal mould, × 4. **31**, Sample 626, Anderkenyn-Akchoku section, BC 57458, dorsal exterior, × 2. **32, 33**, Sample 100, Anderkenyn-Akchoku section, BC 57459, conjoined valves, dorsal and ventral views, × 2.


1


2


3

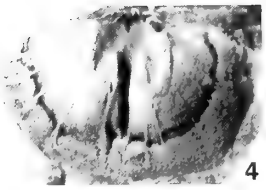
4


5

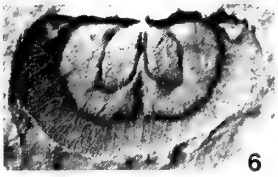
6

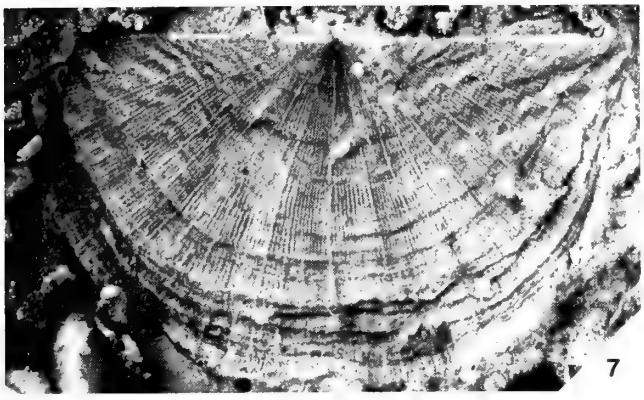
7

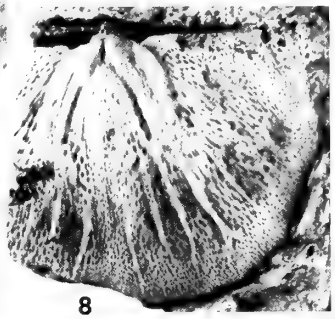
8

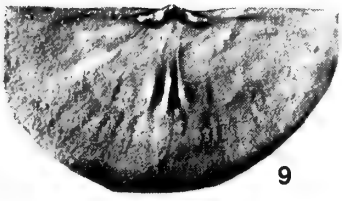
9


10


11

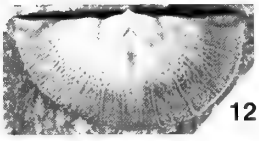
12

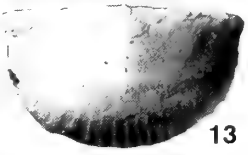
13

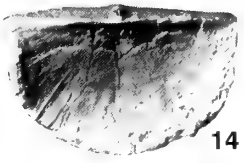
14

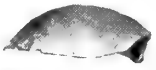
15


16

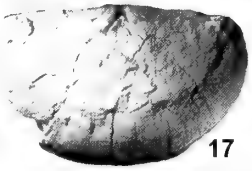
17

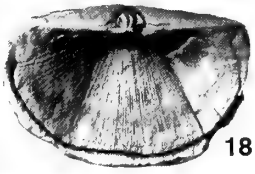
18

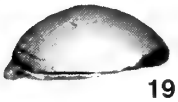
19


20

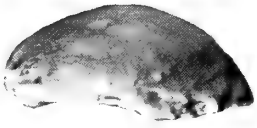
21

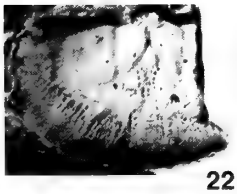
22

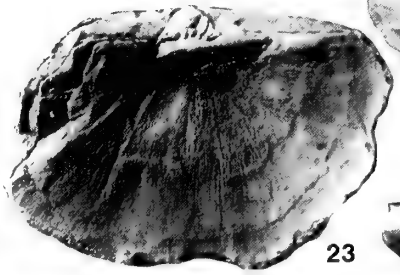
23

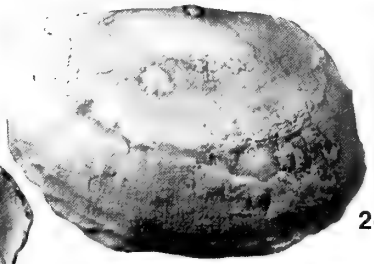
24

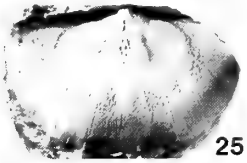
25

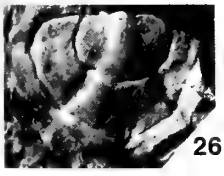
26

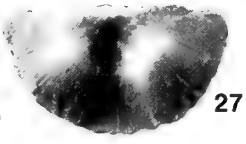
27

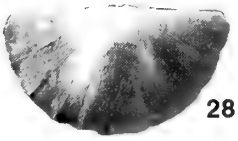
28


29

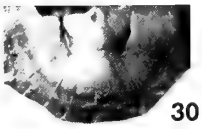
30

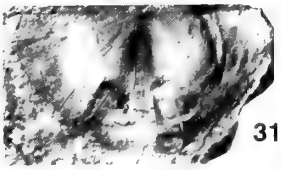
31

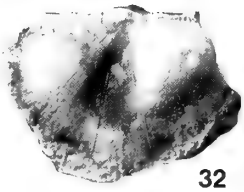
32

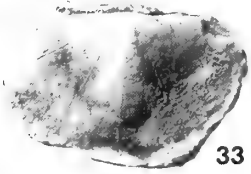
33

Tesikella necopina (Popov, 1980)
Pl. 5, figs 30, 31, Pl. 6, figs 1–6

1980 *Palaeostrophomena necopina* Popov: 145, pl. 1, figs 8–11.

HOLOTYPE. CNIGR 15/11523 (L=11.4, W=16.8), dorsal internal mould, Anderken Formation, east side of Kopalysai, Sample 127/K-1970.

MATERIAL. Five pairs of conjoined valves, 60 ventral and 43 dorsal valves from Samples 8128, 8129 (BC 57432–34, 57604), 8138, Anderkenyn-Akchoku section; Sample 7613, Kujandysai section; Sample 127/K-1970 and Rukavishnikova (1956) Sample 34 (BC 56881), east side of Kopalysai; Sample 818a (BC 57435), Burultas Valley; Sample 1024b, east side of Karatal near Sorbulak well; Samples 1018, 1018a, area 7 km south-west of Karpkuduk well, Kotnak Mountains.

DESCRIPTION. Shell profile resupinate, transversely subrectangular outline, about 55–60% as long as wide with maximum width at the hinge line. Cardinal extremities slightly acute to near right angled. Anterior commissure rectimarginate, broadly rounded. Ventral valve with lateral profile slightly convex in the umbonal area, gently concave anteriorly. Ventral interarea low, planar, catacline with a well developed, narrow pseudodeltidium. Dorsal valve with moderately convex lateral profile, flattened posteriorly with low anacline interarea and separate chilidial plates. Radial ornament parvicostellate with 10–12 parvicostellae per mm in mature specimens and accentuated costellae of two-three generations.

Ventral interior with strong, double teeth lacking dental plates and large divided musle field with strong diductor scars and muscle bounding ridges extending anteriorly to the mid-valve. Adductor scars small, strip-like, divided by a fine median ridge, about half the length of the diductor scars. Subperipheral rim variably developed, posterior to which is a weak median ridge. Mantle canals saccate with very short *vascula media* branching just beneath the anterior margin of the diductor scars. Dorsal interior with trifid cardinal process on a low notothyrial platform and low, widely diverging socket ridges. Median septum strong and narrow, about 75% as long as the valve and joined anteriorly to a low subperipheral rim. Adductor scars radially arranged with smaller anterior pair extending anteriorly to mid-valve.

DISCUSSION. Popov (1980) originally attributed the species to *Palaeostrophomena*, but since then the internal characteristics, particularly of the ventral valve, have become known, and it is clear that this species cannot properly be attributed to that genus.

Family **XENAMBONITIDAE** Cooper, 1956
Subfamily **XENAMBONITINAE** Cooper, 1956
Genus ***SORTANELLA*** Nikitin & Popov, 1996

TYPE SPECIES. *Sortanella quinquecostata* Nikitin & Popov, 1996, from the Dulankara Regional Stage (Upper Caradoc), north Betpak-Dala, Kazakhstan.

Sortanella aff. ***quinquecostata*** Nikitin & Popov, 1996
Pl. 6, figs 26–33

MATERIAL. Ten pairs of conjoined valves, 7 ventral and 8 dorsal valves from Samples 100 (=K98/1970) (BC 57459), 626 (BC 57000, 57006–9, 57458), Anderkenyn-Akchoku section; Samples 628, 2538 (BC 56771, 56810, 57010–03, 57460, 88), Kujandysai section; Tesik River, Sample 948 (BC 57002–5).

DISCUSSION. These specimens closely resemble *Sortanella quinquecostata* Nikitin & Popov (1996: 9) in radial ornament, posteriorly subcarinate ventral valve and gently uniplicate anterior commissure. The type locality is about 400 km to the north-west of our localities, and occurs in the overlying Dulankara Regional Stage which is late Caradoc rather than early to middle Caradoc. Because no dorsal interiors are known, the species cannot yet be identified from the Anderken Formation with certainty.

Subfamily **AEGIROMENINAE** Havlíek, 1961
Genus ***CHONETOIDEA*** Jones, 1928

Chonetoidea sp. Pl. 5, figs 4, 5

TYPE SPECIES. *Plectambonites papillosa* Reed, 1905, from the Slade and Redhill Mudstone Formation (Middle Ashgill), Pembrokeshire, Wales.

MATERIAL. One internal and one external mould of a pair of conjoined valves, BC 56537 (L=3.2, W=5.1) from Sample 8255, Anderkenyn-Akchoku section.

DESCRIPTION. Shell planoconvex, transverse, semielliptical in outline with maximum width at the hinge line. Cardinal extremities acute. Anterior commissure rectimarginate. Ventral valve gently convex in lateral profile with maximum thickness slightly anterior to the apex. Interarea low, planar, anacline with minute apical pseudodeltidium. Dorsal valve flat with a low, anacline interarea. Chilidial plates separate. Radial ornament finely and unequally parvicostellate with five accentuated primary ribs and four secondary costellae originating at about mid valve length.

Ventral interior with small, bilobate muscle field bisected posteriorly by low median ridge. Dorsal interior with simple undercut cardinal process joined to minute socket ridges subparallel to the hinge line. Median ridge originating anterior to the deep alveolus and extending to mid-valve. Six septulae lateral to the anterior part of the median ridge near the mid-valve.

DISCUSSION. These specimens resemble *Chonetoidea virginica* Cooper (1956: 805), from the Edinburg Formation of Virginia, in the size and outline of the planoconvex shell, unequally parvicostellate radial ornament, and number and arrangement of septulae in the dorsal valve.

Family **HESPERONOMIIDAE** Cooper, 1956
Genus ***ANOPTAMBONITES*** Williams, 1962

TYPE SPECIES. *Leptaena grayae* Davidson, 1883, from the Craighead Limestone (Upper Caradoc) of Girvan, Scotland.

Anoptambonites convexus sp. nov.
Pl. 7, figs 5–26; Figs 12.1–12.6

1986 *Anoptambonites* sp.; Kolobova & Popov, pl. 1, figs 7, 8.

ETYMOLOGY. After *convexus*, Latin – convex.

HOLOTYPE. BC 57462, Pl. 7, figs 5, 6, a dorsal interior from Sample 100, Akchoku Mountain.

MATERIAL. 36 pairs of conjoined valves, 21 ventral and 14 dorsal valves from Samples 100 (=K98/1970) (BC 56540, 57014–32, 57462, 64, 69, 71), 626 (BC 57466, 68), 8214 (BC 57480), 8223 (BC 57063–68), 8223b (BC 57467), Anderkenyn-Akchoku section; Samples 628 (BC 56530, 42, 57043–51), 2538 (BC 56531, 57052–61,

Table 15 Measurements of complete shells and ventral valves of *Anoptambonites convexa* sp. nov., *Acculina–Dulankarella* Association, samples 100 and 626 from Anderkenyn-Akchoku section.

	Lv	W	T	Lv/W	T/Lv
N	18	17	8	17	8
X	12.1	16.5	6.9	71.6%	47.1%
S	4.24	5.26	1.86	7.5	6.3
MIN	5.8	8.2	3.5	57.8%	39.4%
MAX	18.0	23.9	9.6	86.5%	58.9%

Table 16 Measurements of complete shells and ventral valves of *Anoptambonites convexa* sp. nov., *Parastrophina–Kellerella* Association, samples 2538, 8217 and 8256 from Kujandysai section.

	Lv	W	T	Lv/W	T/Lv
N	11	11	4	11	4
X	6.4	9.9	2.8	65.5%	44.8%
S	1.13	2.33	0.57	7.6	6.1
MIN	5.2	6.6	2.0	57.0%	38.5%
MAX	9.0	15.3	3.2	79.3%	51.6%

57461, 63, 65), 8217, 8256 (BC 57070–73), Kujandysai section; Samples 8230 (BC 57069), 8231–40, Buldukbai-Akchoku.

DESCRIPTION. Shell concavoconvex, transverse, semielliptical in outline, about 72% as long as wide with maximum width at hinge line and thickness 47% of valve length. Cardinal extremities slightly acute to rectangular. Anterior commissure rectimarginate. Ventral valve carinate posteriorly, strongly convex in lateral profile with the maximum thickness at the point of geniculation somewhat anterior to mid-length. Beak pointed and slightly erect posterior to the hinge line. Ventral interarea steeply apsacline to procline with mainly open delthyrium covered apically by the minute pseudodeltidium. Dorsal valve gently and unevenly concave in lateral profile, flat to mid-length. A shallow sulcus originates at the umbo and fades towards the anterior margin. Dorsal interarea anacline with convex chilidium. Radial ornament finely and near equally multicostellate with 28–43 primary ribs originating near the umbo and 4–6 ribs per mm at the anterior margin. Concentric ornament of fine, evenly spaced fila.

Ventral valve with teeth lacking dental plates. Muscle field small, cordate, bisected by fine median ridge separating small, lanceolate adductor scars. *Vascula media* short, widely diverging. Dorsal interior with undercut cardinal process bearing up to 8 ridges on both sides of strong central lobe. Lophophore platform semielliptical, bordered by a high rim joined to the median septum. Dorsal adductor muscle field subrectangular, about one-third as long as the valve.

VARIABILITY. The average size of *Anoptambonites convexus* from the *Acculina–Dulankarella* Association, which typically occurs within the nodular limestone deposited on the flanks of carbonate mud mounds (Sample 100), is one and half to two times larger than the average size of the shells from the pockets in the mud mound core (Samples 2538 and 8231–40) and the overlying bedded limestone (Samples 628, 8217, 8223, 8256) in which the *Parastrophina–Kellerella* Association characteristically occurs. However, the specimens from the *Parastrophina–Kellerella* Association retain a similar outline, transverse and lateral profile of the shells from the *Acculina–Dulankarella* Association and are also characterized by their multicostellate ornament which consists of 26 to 36 primary ribs and 4 to 6 ribs along the anterior margin of full grown specimens.

DISCUSSION. This species differs from *Anoptambonites grayae* (Davidson), as revised by Williams (1962: 171) from the Craighead

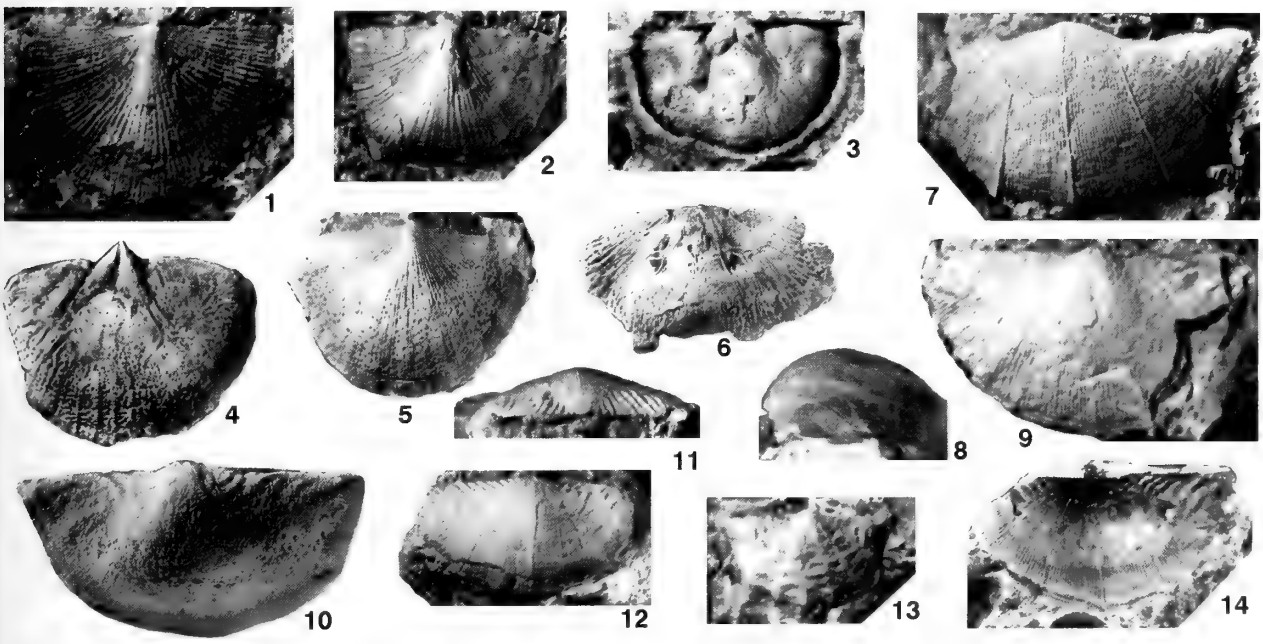

Fig. 12 **1–6.** *Anoptambonites convexus* sp. nov. **1, 4, 5,** Anderkenyn-Akchoku section, **1,** Sample 8223b, BC 57467, ventral exterior, × 3; **4, 5,** Sample 100, **4,** BC 57470, ventral internal mould, × 2; **5**, BC 57472, ventral exterior, × 2. **3, 6,** Buldukbai section, **3,** Sample 8230, BC 57069, ventral internal mould, × 3, **6**, Sample 8231, BC 57473, ventral internal mould, × 1.5. **2**, Kujandysai section, Sample 8256, ventral exterior, × 2.
7–14, *Sowerbyella (Sowerbyella)* aff. *ampla* (Nikitin & Popov), **7–13**, Kujandysai section, Sample 2538, **7**, BC 57082, ventral exterior, × 3; **8,9**, BC 57482, lateral and ventral views of ventral exterior, × 4; **10**, BC 57081, ventral internal mould, × 3; **11, 12**, BC 57479, anterior and ventral views of ventral exterior, × 3; **13**, BC 57481, ventral exterior, × 3. **14**, Anderkenyn-Akchoku section, Sample 8214, BC 57480, dorsal exterior, × 2.5.

Limestone (Upper Caradoc) of Girvan, in having a strongly concavo-convex lateral profile, a cardinal process with up to 8 vertical ridges on the lateral lobes, a shorter median septum and a relatively small lophophore platform extending anteriorly only to the mid-valve. *Anoptambonites convexus* differs from two somewhat younger Kazakh species, *A. subcarinatus* Nikitin & Popov (1996:10) from the north Betpak-Dala and *A. kovalevskii* Popov, Nikitin & Cocks (2000), from the Dulankara Mountains, both from the Dulankara Regional Stage (Upper Caradoc to lowermost Ashgill), in having equally multicostellate radial ornament and a weakly geniculate ventral valve profile, with the maximum height anterior to the mid-valve and near the point of geniculation. It also differs from the former species in having a rectimarginate anterior commissure.

Anoptambonites orientalis Popov, 1980 Pl. 7, figs 1–4, 27

1980 *Anoptambonites orientalis* Popov:149; pl. 2, figs 12–17.

HOLOTYPE. CNIGR 30/11523, dorsal internal mould, from the Anderken Formation, Anderkenyn-Akchoku section, Sample 100b.

MATERIAL. Two pairs of conjoined valves, 14 ventral and 26 dorsal valves from Samples 100b, 8128a (BC 56533, 57476), 8128b, 8137 (BC 57478), Anderkenyn-Akchoku section; Sample 8230, Buldukbai-Akchoku section, and Sample 1018, about 7 km south-west of Karpkuduk well, Kotnak Mountains.

DISCUSSION. Detailed description of this species was provided by Popov (1980). It differs from the contemporaneous *Anoptambonites convexus* sp. nov. as well as from the somewhat younger *A. subcarinatus* Nikitin & Popov, 1996 and *A. kovalevskii* Popov, Nikitin & Cocks, 2000 in having a flattened shell, a carinate ventral valve with gently and evenly convex lateral profile lacking geniculation, a very weakly concave dorsal valve, and in the presence of a small but well-defined pseudodeltidium. The platform in mature specimens of *A. orientalis* reaches up to 75% of the valve length, whereas in *A. convexus* and *A. kovalevskii* it barely exceeds half the valve length.

Genus ***KASSINELLA (KASSINELLA)*** Borissiak, 1956

TYPE SPECIES. *Kassinella globosa* Borissiak, 1956, from the Lower Ashgill Kulunbulak Formation, Tarbagatai Range, Kazakhstan.

Kassinella (Kassinella)? sp. Pl. 3, fig. 24

MATERIAL. One dorsal internal mould, BC 56497, from Sample 2531, Anderkenyn-Akchoku section.

DISCUSSION. A single dorsal valve shows the undercut cardinal process and lack of both bema and side septa characteristic of the Hesperomenidae. It possesses an evenly semicircular platform and a median septum not extending anterior of the platform. This evenly semicircular platform is unlike most species of *Hesperomena, Anoptambonites, Aulie* and *Chaganella*: within the family only *Kassinella (Kassinella)* has such a platform. However, without knowledge of the ventral interior and the exterior of both valves, generic assignment can only be provisional. *Kassinella (Kassinella)* is known from the late Caradoc and Ashgill of Kazakhstan, South China, Australia, Scotland, Bohemia and Sweden (Zhan & Cocks 1998:36), but if the record from the Anderken Formation is confirmed then this may be its earliest occurrence.

Family **SOWERBYELLIDAE** Öpik, 1930
Subfamily **SOWERBYELLINAE** Öpik, 1930
Genus ***SOWERBYELLA (SOWERBYELLA)*** Jones, 1928

TYPE SPECIES. *Leptaena sericea* J. de C. Sowerby, 1839, from the Horderley Sandstone (Lower Caradoc) of Shropshire, England.

Sowerbyella (Sowerbyella) rukavishnikovae Popov, 1980 Pl. 6, figs 7–10

1980 *Sowerbyella rukavishnikovae* Popov: 151, pl. 2, figs 1–4.
1984 *Sowerbyella rukavishnikovae* Popov; Nikitin & Popov *in* Klenina *et al.*:150, pl. 16, figs 17–22.

HOLOTYPE. CNIGR 40/11523, a dorsal internal mould from the Anderken Formation, Anderkenyn-Akchoku section, Sample 100b.

MATERIAL. 70 ventral and 133 dorsal valves. Samples 100b (BC 56554–5), 848, 8128a, 8128b, 8137, Anderkenyn-Akchoku section; Sample 7613, Kujandysai section; Samples 110 (BC 57801), 8229, 8230, 8257, Buldukbai-Akchoku; Sample 8228, east side of the Kopalysai River; Sample 1024b, east side of Karatal Valley, near Sorbulak well; Samples 1018, 1018a, 7 km south-west of Karpkuduk well, Kotnak Mountains.

DISCUSSION. Description, discussion and basic statistics of this species were provided by Popov (1980). Some further specimens from the Anderken Formation are illustrated here. This species is also reported from the upper Bestamak and lower Sargaldak Formations of the Chingiz Range (Nikitin & Popov *in* Klenina *et al.* 1984).

Sowerbyella (Sowerbyella) aff. *ampla* (Nikitin & Popov, 1996) Figs 12.7–12.14

1986 *Anisopleurella* sp. Kolobova & Popov: pl. 1, fig. 6.
aff.1996 *Anisopleurella ampla* Nikitin & Popov: 12, figs 5K–R.

MATERIAL. 14 pairs of conjoined valves, 25 ventral and 8 dorsal valves from Samples 100 (=K98/70), 626, 2531, 8214 (BC 57480), 8215, 8223a, 8223b, Anderkenyn-Akchoku section; Samples 628, 2538 (BC 57081, 82, 57479, 81, 82), Kujandysai section; Sample 948 (BC 57084–85), Tesik River.

PLATE 7

Figs 1–4, 27 *Anoptambonites orientalis* Popov. **1–3,** Sample 8128a, Anderkenyn-Akchoku section; **1**, BC 56533, latex cast of dorsal interior, × 4; **2, 3,** BC 57476, ventral internal mould and latex cast, × 2. **4, 27,** Sample 8137, Anderkenyn-Akchoku section, BC 57478, latex cast and dorsal internal mould of immature specimen, × 4.

Figs 5–26 *Anoptambonites convexus* sp. nov. **5, 6. 9, 10, 18, 20–22,** Sample 100, Anderkenyn-Akchoku section; **5, 6,** BC 57462, **holotype**, dorsal internal mould and latex cast, × 2; **9, 10,** BC 57464, posterior view of conjoined valves showing interareas, × 1.5 and × 5; **18,** BC 57469, ventral exterior, × 2; **20–22,** BC 57471, conjoined valves, ventral, lateral and dorsal views, × 2. **7, 8, 11-16,** Sample 2538, Akchoku Mountain, Kujandysai section; **7,** BC 57461, ventral internal mould, × 3; **8**, CNIGR 7/12361, ventral exterior, × 3; **11, 12,** BC 57465, latex cast and dorsal internal mould, × 3; **13–16,** BC 57463, conjoined valves, dorsal, lateral, ventral and posterior views, × 3. **17, 23–26**, Sample 626, Anderkenyn-Akchoku section; **17,** BC 57466, ventral internal mould, × 1.5; **23–26,** BC 57468, conjoined valves, dorsal, posterior, lateral and ventral views, × 2. **19,** Sample 628 (=K-107/70), west side of Kujandysai, BC 56542, ventral internal mould, × 2.

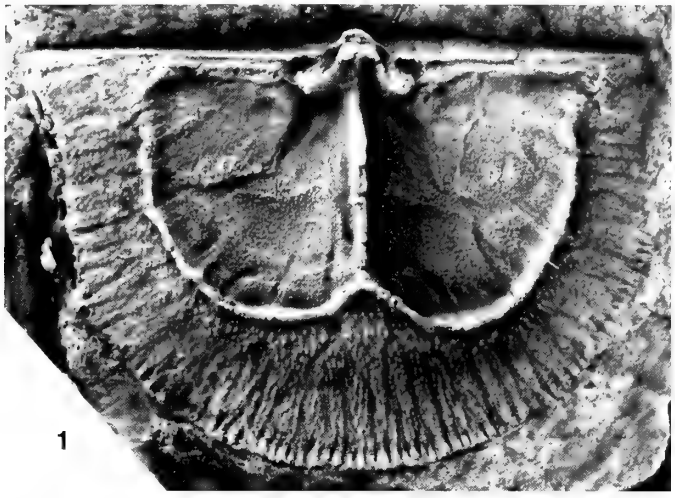
1

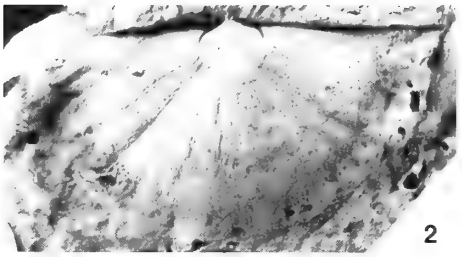
2

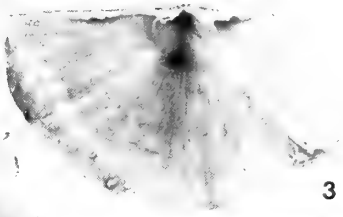
3


4

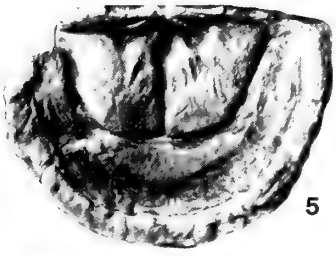
5


6

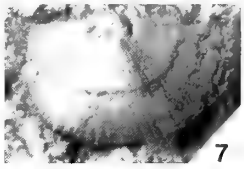
7


10

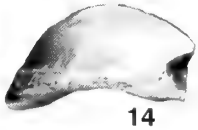
14

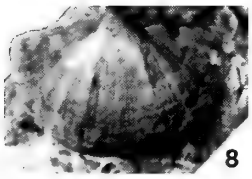
8

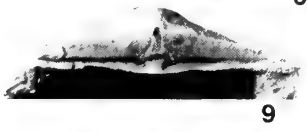
9

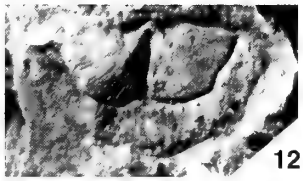
12


11

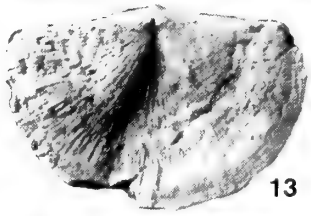
13

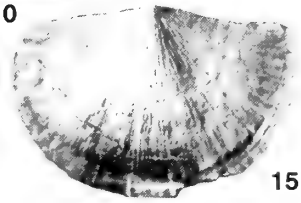
15


16

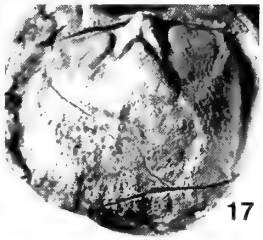
17

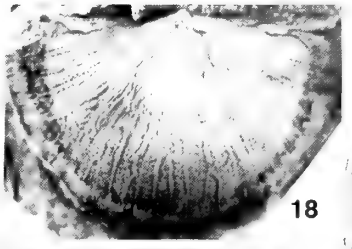
18

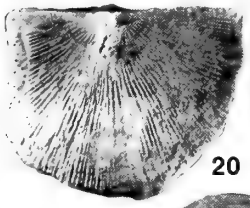
20


25

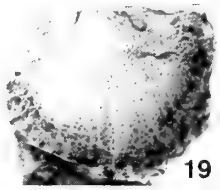
19

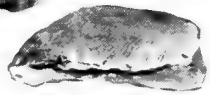
21

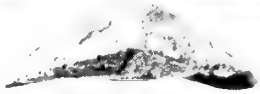
24

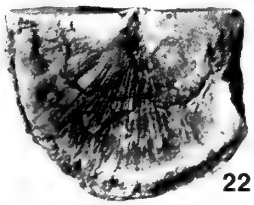
22

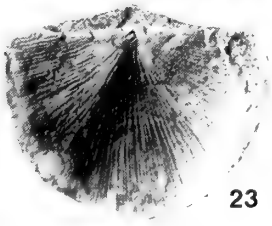
23

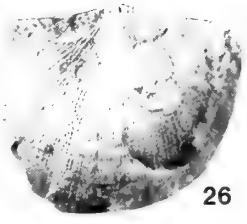
26

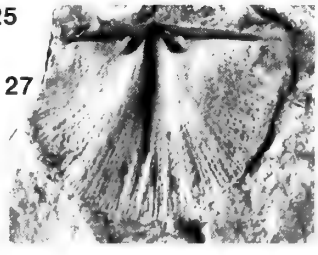
27

DESCRIPTION. Shell concavoconvex, transverse, semielliptical in outline, about 56% as long as wide, with maximum width at hinge line. Cardinal extremities acute and slightly alate. Anterior commissure broadly rounded and rectimarginate. Ventral valve moderately and unevenly convex in profile with the maximum thickness at about quarter valve length. Ventral interarea strongly apsacline and slightly curved in cross-section, with small triangular delthyrium covered apically by pseudodeltidium. Dorsal valve moderately concave, with hypercline interarea; notothyrium covered laterally by chilidial plates. Radial ornament unequally and finely parvicostellate with closely-spaced parvicostellae varying from 9 to 12 per mm. Five accentuated ribs originating at the umbo and four accentuated costellae inclined between them in the mid-valve. Indistinct radial plications developed sometimes along the accentuated ribs. About 6–9 strong concentric rugellae inclined below 30–40° towards the hinge line.

Ventral interior with small teeth lacking dental plates and small bilobate muscle field with flabellate diductor scars completely surrounding small lanceolate adductor scars. Dorsal interior with undercut cardinal process, small curved socket ridges, bilobed bema, short median ridge and two widely divergent side septa.

DISCUSSION. The Anderken specimens strongly resemble *Anisopleurella ampla* Nikitin & Popov (1996) from the slightly younger Dulankara Regional Stage of north Betpak-Dala, Central Kazakhstan, in size and general shell shape, but differ slightly in having a finer radial ornament with 9–12 parvicostellae per mm instead of 7–10 in the Dulankara specimens, and an uneven ventral valve lateral profile. *Anisopleurella ampla* is reassigned here to *Sowerbyella (Sowerbyella)* mainly because it has two pairs of side septa including a closely-spaced more prominent pair. In the variable development of strong concentric ornament it is similar to the subgenus *S. (Rugosowerbyella)*, but differs in having a median septum and the two pairs of side septa, and in the small, weakly impressed ventral muscle field.

Genus *ANISOPLEURELLA* Cooper, 1956

TYPE SPECIES. *Anisopleurella tricostellata* Cooper, 1956, from the Pratt Ferry Formation (Llandeilo) of Alabama, U.S.A.

DISCUSSION. The relationships of *Anisopleurella* and other genera are unresolved. The Ordovician genera within the subfamily are *Sowerbyella, Anisopleurella, Eochonetes, Eoplectodonta, Gunningblandella* and our new genera *Olgambonites* and *Zhilgyzambonites*. *Eochonetes* and *Eoplectodonta* may be interpreted as *Sowerbyella* with hinge lines modified to form denticles (which resulted in the subsequent loss of dental plates), and *Gunningblandella* and *Olgambonites* are resupinate modifications of *Sowerbyella*, which was a very plastic stock. *Anisopleurella* has a much more distinctive and erect dorsal median septum and side septa than *Sowerbyella*, with the side septa bisecting the divided bema but not reaching to the anterior edge of it. Both genera occur in rocks of Llandeilo age, but which of the two was ancestral is not known.

Anisopleurella sp. Pl. 8, figs 1, 2, 5

MATERIAL. One ventral and one dorsal internal mould from Samples 2531 (BC 57489), 8255 (BC 56539), Anderkenyn-Akchoku section.

DISCUSSION. These specimens can be firmly assigned to *Anisopleurella* because they have the characteristic parvicostellate ornament with three accentuated ribs, a dorsal median ridge and a pair of widely diverging prominent side septa bisecting a bilobed bema. They are somewhat comparable to, and may be conspecific with, *Anisopleurella yichangensis* Zeng, 1987 from the early Caradoc Miaopo Formation of Hubei, South China, but the absence of well-preserved exteriors of the Chinese species makes detailed comparison impossible.

Genus *OLGAMBONITES* gen. nov.

ETYMOLOGY. After the late Olga Ivanova Nikiforova, a pioneer in brachiopod studies.

TYPE SPECIES. *Olgambonites insolita* sp. nov. from the Anderken Formation, Chu-Ili Range.

DIAGNOSIS. Shell convexiconcave; anterior commissure rectimarginate to weakly uniplicate; ventral interarea procline to slightly apsacline with apical pseudodeltidium; dorsal interarea anacline with separate chilidial plates; radial ornament unequally parvicostellate; ventral interior with small teeth lacking dental plates and small bilobed muscle field with short adductor scars completely separating larger diductor scars; ventral mantle canals lemniscate; dorsal interior with simple undercut cardinal process joined to narrow socket ridges; fine median ridge and bilobed bema bordered by rim and crossed by up to 8 side septa.

DISCUSSION. *Olgambonites* possesses an undercut cardinal process, divided bema and side septa in the dorsal valve; all characteristic of the Sowerbyellidae, but it differs from most genera in the family in having a convexiconcave shell. The only other resupinate genus is *Gunningblandella* (Percival 1979b) from the Caradoc of Australia, but *Olgambonites* differs from that genus in having a dorsal median septum and numerous side septa.

PLATE 8

Figs 1, 2, 5 *Anisopleurella* sp. **1, 2,** Sample 8255, Anderkenyn-Akchoku section, BC 56539, dorsal internal mould and latex cast, × 12. **5**, Sample 2531, Anderkenyn-Akchoku section, BC 57489, ventral internal mould, × 7.

Figs 3, 4, 6–10, 12, 13 *Zhilgyzambonites extenuata* gen. et sp. nov. Anderkenyn-Akchoku section. **3, 9, 10, 12, 13,** Sample 8255; **3,** BC 57493, ventral internal mould, × 6; **9**, BC 56538, latex cast of conjoined ventral and dorsal interiors, × 4; **10**, BC 57494, ventral internal mould, × 6; **12, 13**, BC 12915, **holotype**, latex cast and internal mould of dorsal interior, × 5.5. **4, 7, 8,** Sample 2531; **4,** BC 57490, latex cast of ventral exterior, × 6; **7, 8**, BC 57492, dorsal internal mould and latex cast, × 5. **6**, Sample 8215, BC 57491, latex cast of dorsal exterior, × 6.

Figs 11, 14–20 *Olgambonites insolita* gen. et sp. nov. Sample 8255, Anderkenyn-Akchoku section. **11,** BC 56535, dorsal external mould, × 4. **14, 15,** BC 56534, latex cast and ventral internal mould, × 4. **16, 17,** BC 56664, latex cast and ventral internal mould, × 4. **18,** BC 57592, ventral exterior, × 4. **19, 20**, BC 56663, **holotype**, internal mould and latex cast of dorsal valve, × 4.

Figs 21–33 *Gacella institata* sp. nov. **21–25, 32, 33**. Sample 100, Anderkenyn-Akchoku section; **21–25**, BC 57496, conjoined valves, posterior, anterior, dorsal, ventral and lateral views, × 2; **32, 33**, BC 57500, conjoined valves, **holotype**, dorsal and ventral internal moulds, × 2. **26, 27**, Sample 85258, Kujandysai section, BC 56576, latex cast and dorsal internal mould, × 3. **28–31**. Sample 626, Anderkenyn-Akchoku section, BC 57497, conjoined valves, anterior, ventral, lateral and dorsal views, × 2.


1


2

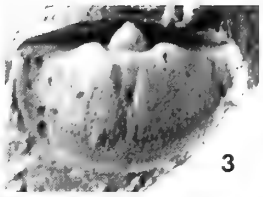
3

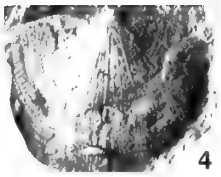
4

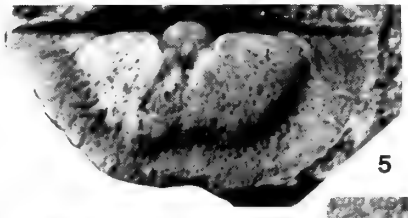
5

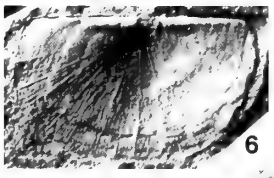
6


7


12

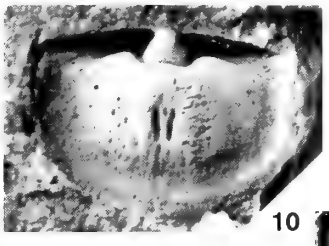
10


8

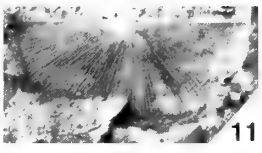
11


13

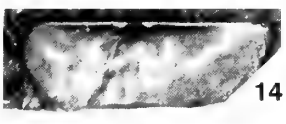
14

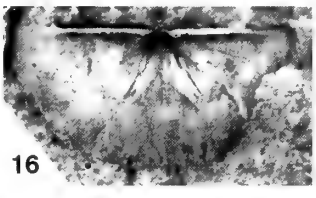
16


18

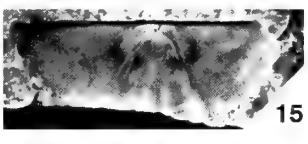
15

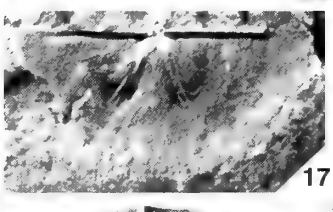
17

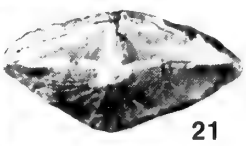
21

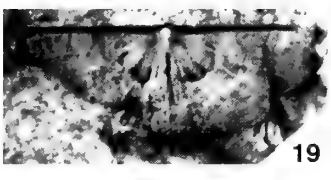
19

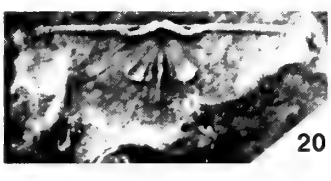
20

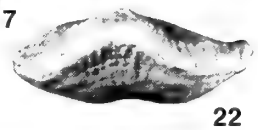
22

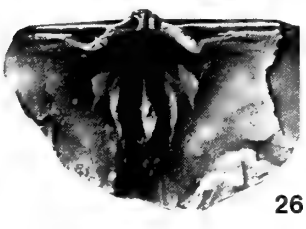
26


23

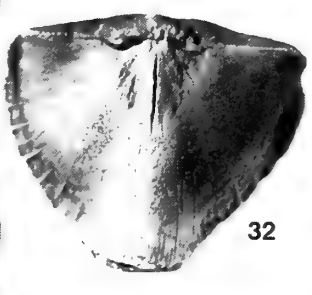
32

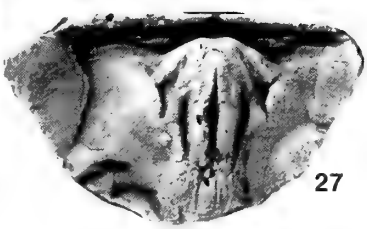
27


24


28

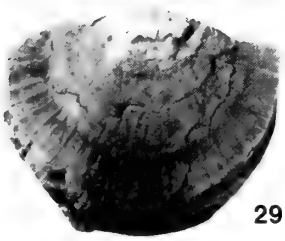
29

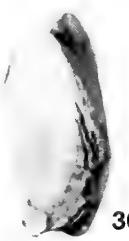
30

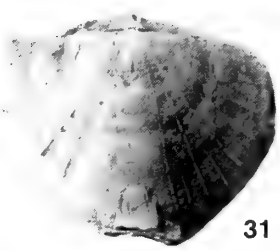
31

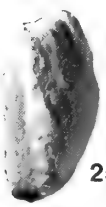
25

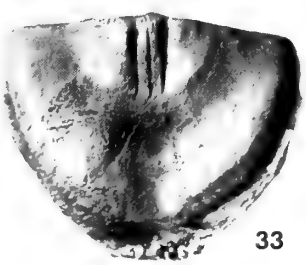
33

Olgambonites insolita sp. nov. Pl. 8, figs 11, 14–20

ETYMOLOGY. After *insolitus*, Latin –extraordinary.

HOLOTYPE. BC 56663, a dorsal valve (Pl. 8, figs 19, 20) from the Anderken Formation, Sample 8255, Anderkenyn-Akchoku section.

MATERIAL. 3 ventral (BC 56534–36, BC 56664) and 2 dorsal valves (BC 56538, BC 56663) from the type locality.

DESCRIPTION. Shell convexoconcave, semielliptical in outline, about half as long as wide, with maximum width at the hinge line, and acute cardinal extremities. Ventral valve gently concave in lateral profile with apsacline interarea and narrow convex pseudodeltidium. Dorsal valve gently convex with anacline pseudointerarea. Radial ornament inequally parvicostellate with 7–9 primary accentuated ribs and two generations of accentuated costellae. Very fine parvicostellae, about 10–11 per mm. Concentric ornament of fine evenly spaced rugellae and very fine crowded growth lamellae in the anterior half of the shell.

Ventral interior with small teeth and highly raised, rounded, subrectangular muscle field bordered anteriorly by the steep rim. Dorsal interior with simple undercut cardinal process joined to the socket ridges and small alveolus. Bema entire, highly raised anteriorly and bordered by a steep rim. Short median ridge originating anterior to bema and joined to the subperipheral rim.

DISCUSSION. The new species is known only from the type locality.

Genus ***ZHILGYZAMBONITES*** gen. nov.

ETYMOLOGY. After Zhilgyz well, Betpak-Dala Desert.

TYPE SPECIES. *Zhilgyzambonites extenuata* sp. nov. from the Anderken Formation, Chu-Ili Range.

DIAGNOSIS. Shell concavoconvex, with rectimarginate posterior commissure, ventral interarea apsacline with delthyrium completely covered by pseudodeltidium; dorsal interarea anacline with complete chilidium; radial ornament finely and unequally parvicostellate; ventral valve with small teeth lacking dental plates; ventral muscle field small, highly raised anteriorly; dorsal interior with undercut cardinal process joined to socket ridges, deep alveolus and strongly elevated, entire bema; median ridge fine, originating anteriorly to bema and joined anteriorly to the subperipheral rim.

DISCUSSION. *Zhilgyzambonites* is somewhat similar to *Aulie* (Nikitin & Popov *in* Klenina *et al.* 1984), which is within the Hesperomenidae, in the characteristic pseudodeltidium and chilidium, the ventral valve, which lacks dental plates and has a small muscle field which is strongly raised anteriorly, and the dorsal interior with the deep alveolus and an undercut cardinal process; but it differs in having an elevated bema and a short median ridge between the anterior margin of the bema and the subperipheral rim. However, the presence of a bema in *Zhilgyzambonites* places it within the Sowerbyellidae on the criteria established by Cocks & Rong (1989). The dorsal interior of the new genus somewhat resembles *Diambonioidea* (Zeng 1987), but the Kazakh genus differs from the latter in having a strongly raised ventral muscle field, a ventral median ridge anterior to the muscle field, and an undercut cardinal process; the simple, not undercut, cardinal process of *Diambonioidea* places it within the Grorudiidae (Cocks & Rong 2000).

Table 17 Measurements of ventral valves of *Zhilgyzambonites extenuata* sp. nov., Samples 2531, 8251, 8255, from Anderkenyn-Akchoku section.

	Lv	W	Lv/W
N	7	7	7
X	3.7	5.2	70.9%
S	0.78	0.97	5.4
MIN	2.2	3.2	61.1%
MAX	4.4	6.2	78.6%

Zhilgyzambonites extenuata sp. nov. Pl. 8, figs 3, 4, 6–10, 12, 13

ETYMOLOGY. After *extenuatus*, Latin – little, weak.

HOLOTYPE. BC 12915, a dorsal valve (Pl. 8, figs 12, 13) from the Anderken Formation, Sample 8255, Anderkenyn-Akchoku section.

MATERIAL. 2 pairs of conjoined valves, 10 ventral and 10 dorsal valves from Samples 2531 (BC 57490, 92), 8255 (BC 12915–21, 57493, 94) and possibly 8215 (BC 57089, 91, 57491), Anderkenyn-Akchoku section.

DESCRIPTION. Shell concavoconvex, semielliptical in outline, on average 70% as long as wide with maximum width at the hinge line. Cardinal extremities nearly right angled. Ventral valve moderately and evenly convex in lateral profile with apsacline interarea and narrow convex pseudodeltidium completely covering the delthyrium. Dorsal valve moderately concave with linear, anacline interarea and convex chilidium. Radial ornament unequally parvicostellate with 7–9 accentuated primary ribs and two generations of accentuated costellae. Parvicostellae very fine, about 10–11 per mm. Concentric ornament of fine evenly spaced rugellae and very fine crowded growth lamellae in the anterior half of the shell.

Ventral valve interior with small teeth and highly raised, rounded, subrectangular muscle field about 20% valve length and bordered anteriorly by a steep rim. Dorsal interior with simple undercut cardinal process joined to narrow, strongly curved socket ridges; small alveolus. Dorsal adductor scars with anterior pair slightly larger than posterior, strongly impressed, divided by a pair of transmuscle septa. Bema entire, strongly raised anteriorly and bordered by a steep rim. Short median ridge originating anteriorly to bema and joined to the subperipheral rim.

DISCUSSION. As far as is yet known, this is the only species within the new genus. The material from Sample 8215 does not include valve internals and is thus only doubtfully referred to the species.

Table 18 Measurements of dorsal valves of *Zhilgyzambonites extenuata* sp. nov., Samples 2531, 8251, 8255, from Anderkenyn-Akchoku section.

	Ld	W	Ml	Mw	LPl	LPw	BBl	BBw	Ld/W	Ml/Ld	Ml/Mw	PLl/Ld	LPw/W	BBw/W
N	8	8	3	3	3	3	3	3	8	3	3	3	3	3
X	3.8	6.1	1.5	2.6	2.9	4.8	0.3	2.3	62.5%	35.1%	58.6%	67.4%	73.9%	35.7%
S	0.53	0.67	0.17	0.40	0.21	0.20	0.06	0.72	6.0	2.4	10.3	7.2	0.3	12.6
MIN	3	5.2	1.4	2.2	2.7	4.6	0.3	1.7	54.0%	33.3%	46.7%	62.2%	73.5%	26.2%
MAX	4.5	6.8	1.7	3	3.1	5	0.4	3.1	71.7%	37.8%	65.4%	75.6%	74.2%	50.0%Order

ORTHOTETIDA Waagen, 1884
Suborder **ORTHOTETIDINA** Waagen, 1884
Superfamily **CHILIDIOPSOIDEA** Boucot, 1959
Family **CHILIDIOPSIDAE** Boucot, 1959
Subfamily **GACELLINAE** Williams & Brunton, 2000
Genus ***GACELLA*** Williams, 1962

TYPE SPECIES. *Gacella insolita* Williams, 1962, from the Stinchar Limestone (Lower Caradoc), Girvan, Scotland.

Gacella institata sp. nov. Pl. 8, figs 21–33, Pl. 9, figs 1–4

ETYMOLOGY. After *institа*, Latin – a swathe.

HOLOTYPE. BC 57500, Pl. 8, figs 32, 33, from the Anderken Formation, Sample 100, Anderkenyn-Akchoku section.

MATERIAL. 10 pairs of conjoined valves, 2 ventral and 8 dorsal valves, from Samples 100 (=K-98/1970) (BC 57496, 98, 99, 57500), 626 (BC 57497), Anderkenyn-Akchoku section; Samples 628, 85258 (BC 57092–3, 56576), Kujandysai Section..

DESCRIPTION. Shell subequally biconvex, transverse, semielliptical in outline about 80% as long as wide, with maximum width at hinge line. Cardinal extremities acute to rectangular. Anterior commissure gently uniplicate. Ventral valve convex in lateral profile with maximum thickness slightly anterior to the umbo and with flattened sides. Sulcus shallow, originating about 2–3 mm from the umbo. Ventral interarea planar, apsacline with a broad, convex pseudodeltidium perforated apically by a minute foramen. Lateral profile of the dorsal valve gently convex with maximum thickness near the anterior margin. Dorsal median fold low, rounded in cross-section, originating in the umbonal area but very weakly defined until the mid-valve. Dorsal interarea planar, anacline, with convex chilidium. Radial ornament unequally parvicostellate with two to three generations of acentuated ribs, about 4–5 per 3 mm along the anterior margin of mature specimens. Concentric ornament of numerous fine growth lamellae anteriorly.

Ventral interior with teeth supported by long subparallel but slightly divergent dental plates and narrow, elongate subtriangular muscle field divided by median ridge. Numerous fine crenulations on the outer surface of the teeth. Dorsal interior with bilobed cardinal process on a high notothyrial platform: adductor scars elongated slightly, shorter than half valve length, crossed by two pairs of short transmuscle septa. Median ridge fine and faint, originating some distance from the notothyrial platform.

MEASUREMENTS. (471/12375) conjoined valves, L=14.0, W=16.9, T=6.3, Sw=8.9; (474/12375) conjoined valves, L=20.4, W=21.0, T=11.2, Sw=8.7; (475/12375) conjoined valves, L=22.9, W=24.5, T=10.2, Sw=12.8; (476/12375) conjoined valves, L=16.5, W=19.8, T=6.5, Sw=11.2; (479/12375) conjoined valves, L=10.5, T=6.7, Sw=6.7.

DISCUSSION. This species differs from others of the genus in having a concentric ornament of strong growth lamellae and coarser accentuated ribs. It can be compared to *Gacella ponderosa* Williams, 1962, from the Confinis Formation (Llandeilo) of Girvan, south Scotland, in the general shape and size of the shell, but differs in having a less convex lateral profile in both valves in addition to the patterns of radial and concentric ornament.

Gacella institata differs from *G. sulcata* Misius (*in* Misius & Ushatinskaya 1977), from the Tabylgaty Formation (Upper Caradoc) of the Moldo-Too Range, Kyrgizstan, in having a shallow ventral median sulcus and low dorsal median fold usually originating in the umbonal region; the convex, not flat, lateral profile of the ventral valve, and in the absence of geniculation in the dorsal valve.

Suborder **TRIPLESIIDINA** Moore, 1952
Superfamily **TRIPLESIOIDEA** Schuchert, 1913
Family **TRIPLESIIDAE** Schuchert, 1913
GENUS ***TRIPLESIA*** Hall, 1859

TYPE SPECIES. *Atrypa extans* Emmons, from the Trenton Group (Caradoc), New York, U.S.A.

Triplesia sp. Pl. 9, figs 22–26

MATERIAL. Two ventral and three dorsal valves (BC 57512) from Sample 8228, Kopalysai.

DESCRIPTION. Shell dorsibiconvex, transverse suboval in outline, about 80% as long as wide with uniplicate anterior commissure. Ventral valve moderately convex, with maximum thickness at about one-third valve length. Ventral interarea anacline. Sulcus originating near mid-valve, strongly deepening anteriorly, flanked laterally by angular plications. Dorsal valve moderately convex with swollen umbo. Strong median fold with steep sides, originating anteriorly of mid-valve, bisected medianly by fine groove. Shell surface smooth with rare, slightly irregular growth lamellae anteriorly. Ventral interior with teeth supported by short subparallel dental plates. Dorsal interior with forked cardinal process on a short shaft.

MEASUREMENTS. (488/12375) dorsal valve, L=16.2, W=16.9, T=4.5.

DISCUSSION. These shells are comparable with large specimens of *Triplesia* aff. *subcarinata*, but differ in having a narrow groove bisecting the dorsal median fold and a ventral sulcus which is more rounded in cross-section and a dorsal median fold. However, the shape of the dorsal fold and ventral sulcus varies significantly and it is difficult to evaluate observed morphological differences in this species because of the small number of shells available.

Triplesia* aff. *subcarinata Cooper, 1956
Pl. 10, figs 1–8, 19

MATERIAL. 6 conjoined valves, 2 ventral and 3 dorsal valves from Samples 100 (=K-98/1970), 626 (BC 57515), 8251a (BC 57514), Anderkenyn-Akchoku section; Samples 85258 (BC 57094–5), Kujandysai section; Sample 1041a, Burultas Valley.

DISCUSSION. This species resembles *Triplesia carinata* Cooper, 1956, from the Pratt Ferry Formation of Alabama and *T. subcarinata* Cooper, 1956, from the Lebanon Formation of Tennessee, as well as specimens of that species from the Bestamak Formation (Llandeilo-Lower Caradoc) of the Chingiz range, Kazakhstan (Nikitin & Popov *in* Klenina *et al.*1984), in having a well-developed sulcus and a carinate dorsal median fold originating near the mid length, but it differs from both in having a larger shell, a strongly convex lateral profile in the dorsal valve with maximum height near the anterior margin, and a variable transverse profile of the dorsal median fold which has a tendency to be rounded in most specimens. *Triplesia* aff. *subcarinata* differs from *T. ainca* Severgina, 1978, from the Lower Ashgill Gurianovka Formation and Marinikha Limestone of the Sayano-Altai Mountain Region in having a strongly dorsibiconvex lateral profile with a slightly accentuated ventral beak erect posteriorly, a narrow ventral sulcus and a dorsal median fold usually rounded in cross-section.

GENUS ***BICUSPINA*** Havlíček, 1950

TYPE SPECIES. *Orthis cava* Barrande, 1848, from the Lower Caradoc of Bohemia.

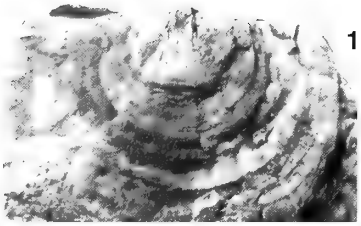
1

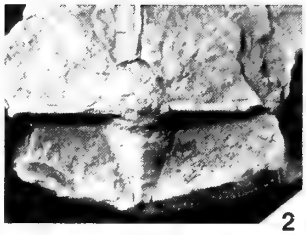
2


4

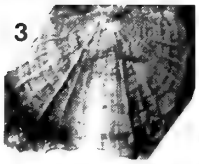
3


5

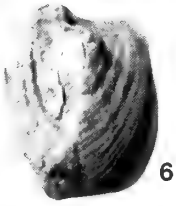
6

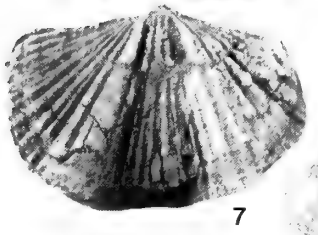
7

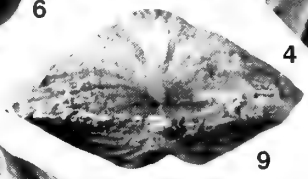
9


8

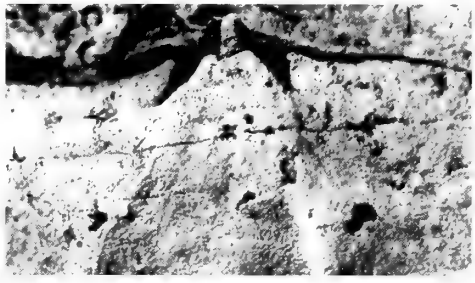
10

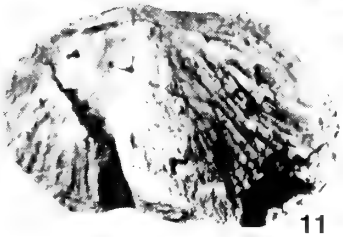
11

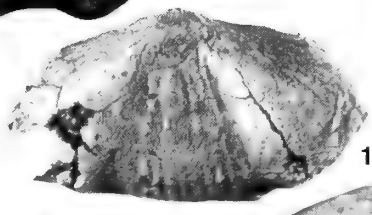
12


13

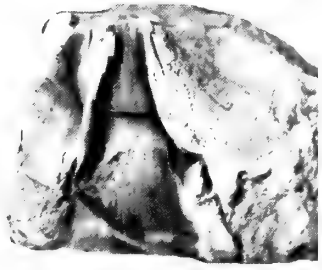
14

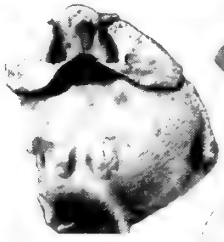
15

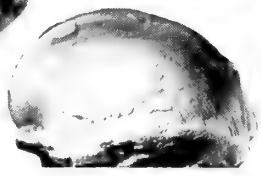
18

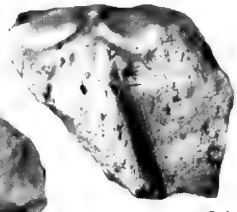
21

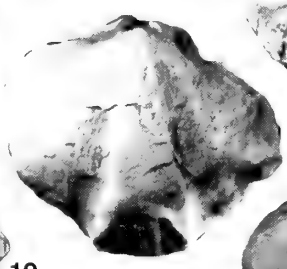
20

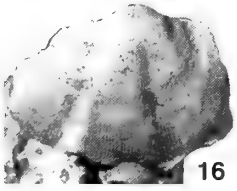
16


17

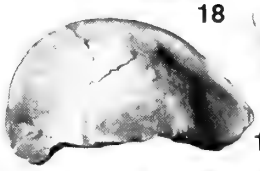
19

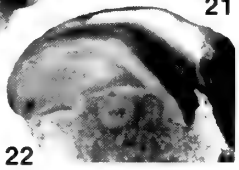
22


23

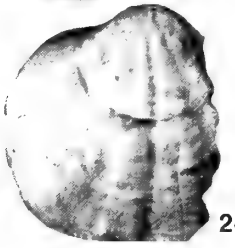
24

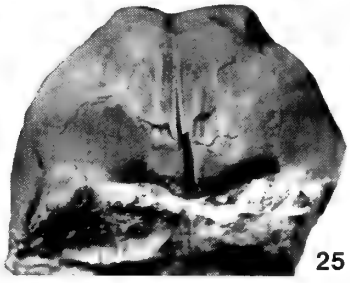
25

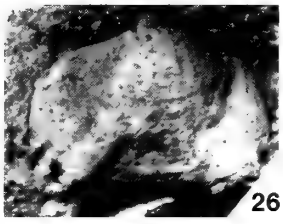
26

Bicuspina rukavishnikovae Klenina, 1984 Pl. 9, figs 5–13

1984 *Bicuspina rukavishnikovae* Klenina *in* Klenina *et al.*: 62, pl. 5, figs 7, 8.

1985 *Bicuspina attrita* Popov: 61, pl. 3, figs 2–4.

HOLOTYPE. IGNA 411/89, conjoined valves, from the Abai Formation (Lower Caradoc), Ordotas Mountains, Chingiz Range, Kazakhstan.

MATERIAL. Five conjoined valves, one ventral and 9 dorsal valves from Samples 100 (=K-98/1970) (BC 57505), 626, Anderkenyn-Akchoku section; Sample 1018 (including the holotype of *B. attrita* CNIGR 32/11989), area 7 km southwest of Karpkuduk well, Kotnak Mountains.

DESCRIPTION. Shell dorsibiconvex, about half as thick as long and about 90% as long as wide. Hinge line short, about two-thirds maximum width. Ventral valve gently convex in lateral profile with maximum thickness at about one-third valve length. Beak small, slightly curved. Ventral interarea low, planar, apsacline with small pseudodeltidium bisected by monticulum. Ventral median sulcus originating in umbonal area with flattened bottom and steep lateral sides about 60% valve width. Well-developed semioval tongue. Dorsal valve strongly convex with maximum thickness at mid-length and flattened umbonal area. Median fold high, originating near umbo, with steep lateral slopes. Radial ornament costellate with 6–11 ribs in the fold and sulcus and 13–21 ribs on the lateral sides of mature shells.

Ventral interior with small teeth supported by short diverging dental plates. Ventral muscle field open anteriorly, weakly impressed. Umbonal area with a short internal pedicle tube (Pl. 9, fig.10). Dorsal interior with forked cardinal process on a short, thickened shaft, and small curved socket ridges.

MEASUREMENTS. (471/12375) conjoined valves, L=14.0, W=16.9, T=6.3, Sw=8.9; (474/12375) conjoined valves, L=20.4, W=21.0, T=11.2, Sw=8.7; (475/12375) conjoined valves, L=22.9, W=24.5, T=10.2, Sw=12.8; (476/12375) conjoined valves, L=16.5, W=19.8, T=6.5, Sw=11.2; (479/12375) conjoined valves, L=10.5, T=6.7, Sw=6.7.

DISCUSSION. Coarsely ribbed triplesiides are characteristic of the Caradoc of West Gondwana (Havlíček 1950; Melou 1990) and Avalonia (Williams 1963; 1974), but they are apparently absent from China and Australia and very rare in Kazakhstan. Specimens from the Chu-Ili Range were previously known as *Bicuspina attrita* Popov (1985). They differ from *Bicuspina rukavischnikovae,* described by Klenina (*in* Klenina *et al.* 1984) from the Abai Formation of the Chingiz Range, only in having a slightly uneven lateral profile of the ventral valve with maximum height posterior to mid-length, and in a more apsacline ventral interarea. These differences are regarded here as intraspecific, and specimens of *Bicuspina* from the Chu-Ili and Chingiz ranges are therefore conspecific. Klenina mentioned the presence of a forked cardinal process and internal pedicle tube in the original description of the species, but the interiors of both valves were not illustrated.

The published Llanvirn age of *B. rukavischnikovae* in the Ordotas Mountains of the Chingiz Range, which is the type locality, is not supported by analysis of the associated brachiopod assemblage. It co-occurs with *Hesperorthis karaadirensis* Klenina, which is probably synonymous with *Paralenorthis numerosa* (Nikitin & Popov) and rhynchonellids, suggesting that the age of the assemblage is not older than Llandeilo to early Caradoc.

Genus ***GRAMMOPLECIA*** Wright & Jaanusson, 1993

TYPE SPECIES. *Grammoplecia triplesioides* Wright & Jaanusson, 1993, from the Boda Limestone (Ashgill) of Dalarna, Sweden.

Grammoplecia wrighti sp. nov. Pl. 9, figs 14–21

ETYMOLOGY. After A.D. Wright, to honour his triplesioid studies.

HOLOTYPE. BC 57509, Pl. 9, figs 17, 18, a dorsal valve from the Anderken Formation, Sample 8214, Anderkenyn-Akchoku section.

MATERIAL. Three pairs of conjoined valves, three ventral and 9 dorsal valves, from Samples 620 (BC 57100–04, 57506, 07, 10, 11), 626 (BC 57105–6), Anderkenyn-Akchoku section; Samples 8214 (BC 57099, 57508–11), 8215b (BC 57107), west side of Ashchisu River; Sample 628, Kujandysai Section,.

DESCRIPTION. Shell dorsibiconvex, slightly transverse, subrectangular to suboval in outline, about 83% as long as wide. Hinge line straight, not exceeding two-thirds shell width. Anterior commissure uniplicate. Ventral valve moderately convex with low, apsacline interarea and flat pseudodeltidium bisected by monticulum. Ventral sulcus originating about 3–5 mm from the umbo, ending in wide, trapezoidal tongue about 83% as wide as the valve. Dorsal valve strongly convex with maximum thickness at about one-third valve length. Strong dorsal median fold, flat centrally with steep lateral slopes. Lateral slopes convex in cross-section, strongly inclined to the commissural plane. Radial ornament of fine capillae about 5–7 per mm crossed by fine, closely-spaced concentric fila.

Ventral interior with strong teeth and long, diverging, widely spaced dental plates. Ventral muscle field large, about two-fifths valve length, slightly raised anteriorly with wide, subtriangular adductor track dividing narrow, strip-like diductor scars. Dorsal interior with forked cardinal process on strong short shaft joined to low and short socket plates. Adductor field quadripartite with anterior and posterior pairs separated by strong, transverse ridges. Low

PLATE 9

Figs 1–4 *Gacella institata* sp. nov., Sample 100, Anderkenyn-Akchoku section. **1**, BC 57498, ventral valve, umbonal area, × 5. **2**, Sample 100, BC 57502, enlargement of interarea of conjoined valves, × 3. **3, 4**, BC 57499, dorsal valve exterior, × 2, and umbonal area showing radial ornament, × 6.

Figs 5–13 *Bicuspina rukavishnikovae* Klenina, 1984. **5–9**, Sample 100, Anderkenyn-Akchoku section, BC 57505, conjoined valves, dorsal, lateral, ventral anterior and posterior views, × 2. **10–13**, Sample 1018, area 7 km southwest of Karpkuduk well, Kotnak Mountains; **10**, CNIGR 31/11989, ventral internal mould showing internal pedicle tube, × 5; **11**, CNIGR 32/11989, dorsal exterior, × 2; **12, 13**, CNIGR 33/11989, conjoined valves, ventral view, × 2, posterior view, × 5.

Figs 14–21 *Grammoplecia wrighti* sp. nov. Anderkenyn-Akchoku section. **14, 15, 19–21**, Sample 620; **14**, BC 57506, ventral internal mould, × 2; **15**, BC 57507, conjoined valves, oblique posterior view of internal mould showing cardinal process, × 2; **19, 20**, BC 57510, dorsal and lateral views of exterior, × 2; **21**, BC 57511, dorsal internal mould, × 2. **16–18**, Sample 8214; **16**, BC 57508, dorsal exterior, × 2; **17, 18**, BC 57509, **holotype**, dorsal exterior and lateral views, × 2

Figs 22–26 *Triplesia* sp. Sample 8228, east side of Kopalysai. **22, 23, 25**, dorsal internal mould, lateral and dorsal views, × 2, posterior view showing cardinal process, × 3. **24**, BC 57512, latex cast of dorsal exterior, × 2. **26**, ventral internal mould, × 2.

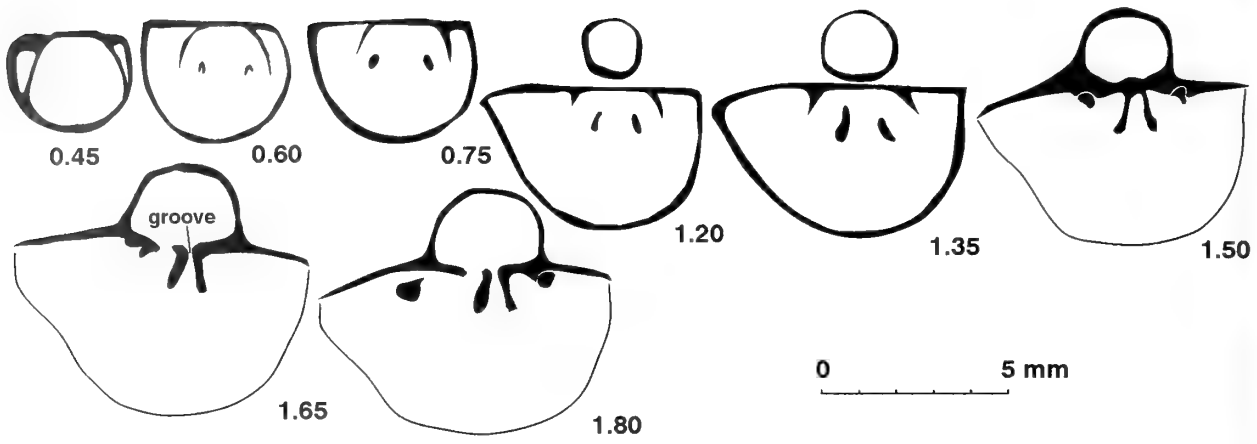

Fig. 13 Transverse serial sections of *Placotriplesia spissa* sp.nov., BC 57605 from Sample 628. Distance in mm is measured from the posterior tip of ventral beak. Dorsal valve uppermost.

and narrow median ridge extending to anterior border of the muscle field.

MEASUREMENTS. (490/12375) dorsal valve, L=17.2, W=19.2, T=8.2, Sw=9.6; (491/12375) dorsal valve, L=17.2, W=21.0, T=8.6, Sw=8.2; (495/12375) dorsal valve, L=10.2, W=15.3, T=7.8, Sw=4.6.

DISCUSSION. This species differs from *Grammoplecia triplesioides* Wright & Jaanusson, 1993, *G. globosa* (Nikitin & Popov, 1985), from the Andryushinka Formation (Llandeilo-Lower Caradoc) of north-central Kazakhstan, *G. krotovi* (Chernyschev, 1887) from the Upper Caradoc to Lower Ashgill of Novaya Zemlya, Vaigach and the Urals (Bondarev 1968) and *G. sibirica* (Nikiforova, 1955) from the Upper Caradoc of Siberia, in having a more transverse shell outline, a ventral sulcus and dorsal median fold with steep lateral sides and flat centrally, a strongly and evenly convex dorsal profile with maximum height at mid-length and a broader hinge line.

Genus ***PLACOTRIPLESIA*** Amsden, 1968

TYPE SPECIES. *Triplesia praecipta* Ulrich & Cooper, 1936a, from the Wenlock of Arkansas, U.S.A.

Placotriplesia spissa sp. nov.

Pl. 10, figs 9–18; Figs 13, 15

HOLOTYPE. BC 57517, Pl. 10, figs 9–13, from Sample 2538, Anderken Formation, Akchoku Mountain, Kujandysai section.

MATERIAL. 9 pairs of conjoined valves, 6 ventral and 12 dorsal valves from Samples 8214, 8215, 8223, Anderkenyn-Akchoku section; Samples 628, 2538 (BC 57517), 8219, 8256, Kujandysai section.

DESCRIPTION. Shell smooth, dorsibiconvex profile, about 80% as thick as long and 75% as long as wide, transverse and suboval in outline, with maximum width at mid-length. Hinge-line short, less than half valve width. Anterior commissure strongly uniplicate. Ventral valve moderately convex, with an erect beak and minute apical foramen. Ventral interarea high, planar, apsacline with flat pseudodeltidium. Ventral sulcus originating from quarter to half valve length, strongly deepening anteriorly, with strong geniculated tongue about 75% valve width, and inclined at less than a right angle towards commisural plane. Lateral sides of sulcus accentuated by angular plications. Dorsal valve strongly convex, with swollen incurved beak; dorsal median fold strong and rounded in cross-section. Ventral interior with delicate teeth and short divergent dental plates. Dorsal interior with grooved forked cardinal process with strongly curved prongs posteriorly with distal parts subparallel to commisural plane, separated proximally and fused with narrow curved socket ridges.

DISCUSSION. This species represents the earliest record of

PLATE 10

Figs 1–8, 19 *Triplesia* aff. *subcarinata* Cooper. Anderkenyn-Akchoku section. **1–4, 19**, Sample 8251a, BC 57514, conjoined valves, ventral, dorsal, posterior and anterior views, × 2, dorsal view of the umbonal area showing pseudodeltidium with monticulus, × 4. **5–8**, Sample 100, BC 57515, conjoined valves, × 2.

Figs 9–18 *Placotriplesia spissa* sp.nov. **9–14**, Sample 2538, Akchoku Mountain, Kujandysai section. **9–13,** BC 57517, **holotype**, conjoined valves, ventral, dorsal, anterior, posterior and lateral views, × 2. **14**, CNIGR 3/12361, conjoined valves showing ventral interarea with pseudodeltidium lacking monticulum, × 5. **15–18**, Sample 8214, Anderkenyn-Akchoku section, CNIGR 3/12361, conjoined valves, ventral, dorsal, anterior and lateral views, × 2.

Figs 20–22 *Skenidioides* sp. Sample 8214, west side of Ashchisu River, BC 57518, conjoined valves, ventral, dorsal and posterior views, × 6.

Figs 23–29, 31–36 *Dolerorthis pristina* sp. nov. **23–25, 32, 34**, Sample 626, Anderkenyn-Akchoku section. **23–25, 32**, BC 57519, conjoined valves, ventral, lateral and dorsal views, × 2, detail of the shell surface, × 8; **34**, BC 57522, ventral internal mould, × 2. **26–29, 31**, Sample 620, Anderkenyn-Akchoku section, BC 57520, **holotype**, conjoined valves, dorsal, ventral, lateral, posterior and anterior views, × 2. **33, 35**, Sample 2538, Akchoku Mountain, Kujandysai section; **33**, BC 57521, ventral exterior, × 2; **35**, BC 56768, dorsal interior, × 3. **36**, Sample 8214, Anderkenyn-Akchoku section, BC 57523, dorsal internal mould, × 2.

Figs 37–42 *Glyptorthis* sp., Kujandysai section. **37,** Sample 2538, BC 57524, ventral internal mould, × 3. **38–42,** Sample 628 (=K-107/70), west side of Kujandysai, BC 57525, conjoined valves, anterior, dorsal, lateral and ventral views, × 3, dorsal view, × 6.

Fig. 43 *Plectorthis? burultasica* sp. nov. Sample 1018, area 7 km SW of Kotnak mountains, south Betpak-Dala, CNIGR 2/11989, latex cast of ventral interior, × 2.

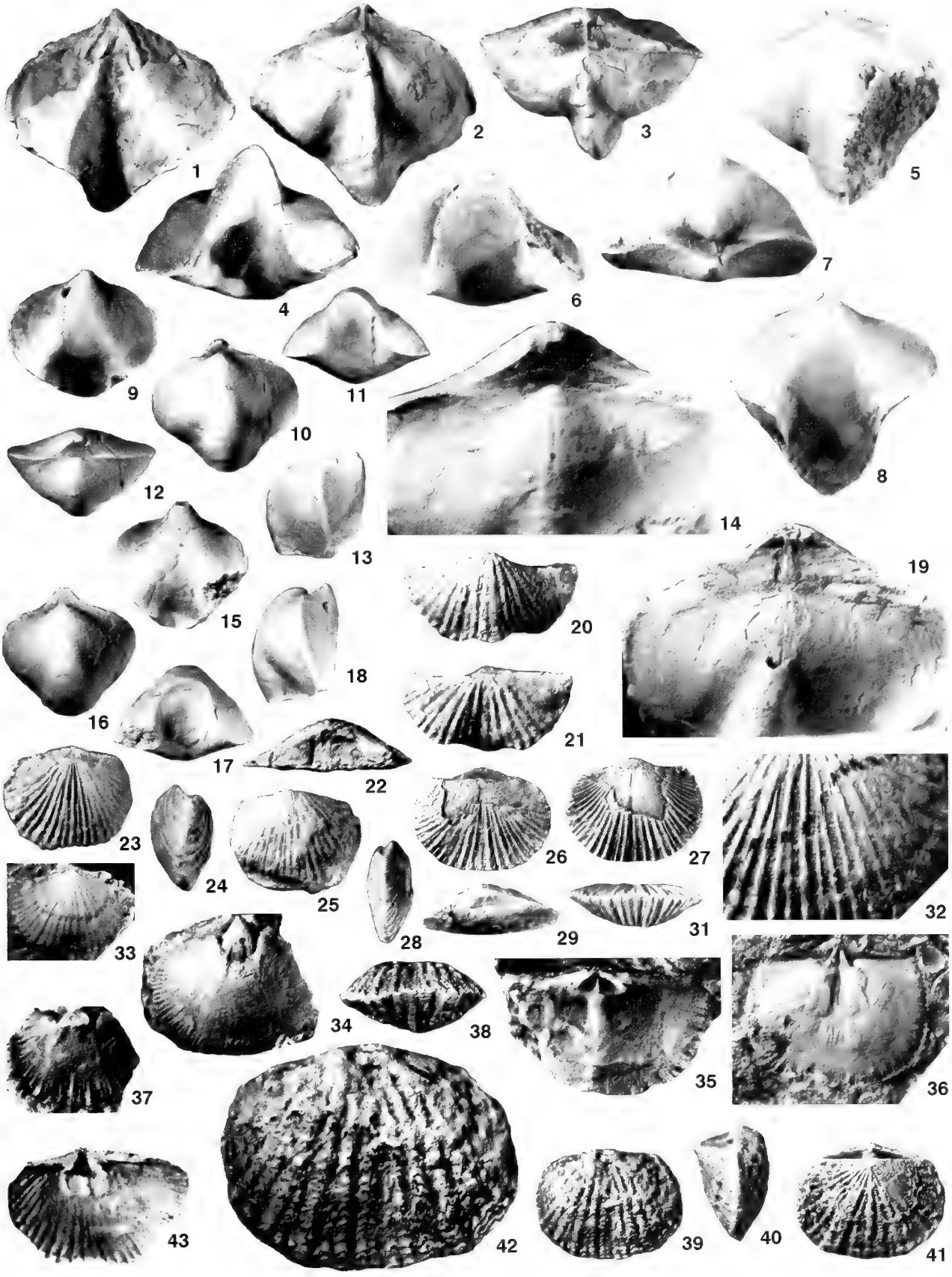
1
2
3
5
4
6
7
9
11
10
8
12
14
13
19
15
20
18
16
21
17
22
23
26
27
32
24
25
28
29
31
33
34
38
35
36
37
43
42
39
40
41

Table 19 Measurements of complete shells of *Placotriplesia spissa* sp. nov., Sample 2538. Kujandysai section, 8221 from Anderkenyn-Akchoku section and Sample F-1041a from Burultas valley.

	L	W	T	Sw	St	L/W	T/L	Sw/W	St/Sw
N	7	7	7	7	3	7	7	7	3
X	13.9	19.0	11.5	10.4	7.7	73.9%	81.6%	75.5%	73.2%
S	2.61	4.27	3.13	1.43	3.04	7.9	12.7	6.1	22.3
MIN	10.5	13.6	6.8	8.2	3.3	60.4%	61.7%	67.9%	37.5%
MAX	16.3	24.5	14.7	11.5	7.6	83.9%	90.2%	83.0%	69.1%

Placotriplesia, which is otherwise known only from the Silurian. It differs from *P. praecipta, P. juvenis* Ulrich & Cooper (1936a), *P. waldronensis* (Miller & Dyer), and *P. rostellata* (Ulrich & Cooper 1936a) in having a strongly dorsibiconvex shell, high dorsal median fold and deep ventral median sulcus originating at some distance from the umbo. It also differs from *P. praecipta*, as redefined by Amsden (1968), in having a strongly curved cardinal process with posteriorly-directed prongs.

Order **PROTORTHIDA** Schuchert & Cooper, 1931
Superfamily **PROTORTHOIDEA** Schuchert & Cooper, 1931
Family **SKENIDIIDAE** Kozlowski, 1929
Genus ***SKENIDIOIDES*** Schuchert & Cooper, 1931

TYPE SPECIES. *Skenidioides billingsi* Schuchert & Cooper, 1931, from the Caradoc of Ontario, Canada.

Skenidioides sp. Pl. 10, figs 20–22

MATERIAL. One pair of conjoined valves (L=2.7, W=5.4, T=1.7), one ventral and one dorsal valves from Samples 8223b and 8226, Anderkenyn-Akchoku section; Sample 8214 (BC 57518), west side of Ashchisu River.

DISCUSSION. The shells from the Anderken Formation closely resemble *Skenidioides anthonensis* (Sardeson), as redescribed and illustrated by Cooper (1956: 491), in the general shape of the shell, narrow median sulcus in the dorsal valve, carinate ventral valve and characters of radial ornament, but differ somewhat in having a more flattened dorsal valve. Although the exterior is characteristic of *Skenidioides*, the absence of known interiors in the specimens from the Anderken Formation precludes specific identification.

Order **ORTHIDA** Schuchert & Cooper, 1932
Suborder **ORTHIDINA** Schuchert & Cooper, 1932
Superfamily **ORTHOIDEA** Woodward, 1852
Family **HESPERORTHIDAE** Schuchert & Cooper, 1931
Genus ***DOLERORTHIS*** Schuchert & Cooper, 1931

TYPE SPECIES. *Orthis interplicata* Foerste, from the Niagara Group (Silurian) of Indiana, U.S.A.

Dolerorthis expressa Popov, 1980
Pl. 1, fig. 29, Pl. 11, figs 1, 2

1980 *Dolerorthis expressa* Popov: 144, pl. 1, figs 5–7.

HOLOTYPE. CNIGR 11/11523, ventral internal and external moulds (L=18.4, W=24,7), from the Anderken Formation, Sample 1018, 7 km southwest of Karpkuduk well, Kotnak Mountains.

MATERIAL. One pair of conjoined valves, 12 ventral and 11 dorsal valves, internal and external moulds, from Sample 8137 (BC 57526), Anderkenyn-Akchoku; Sample 817, about 4 km south-west of Alakul Lake; Sample 1018 (BC 57368),7 km southwest of Karpkuduk well, Kotnak Mountains, south Betpak-Dala.

DESCRIPTION. Shell subequally biconvex, transverse, subrectangular in outline, about 75% as long as wide with maximum width anterior to hinge line. Cardinal extremities slightly rounded; anterior commissure weakly unisulcate; ventral valve gently convex in lateral profile with maximum thickness at about one-third from anterior margin; ventral interarea apsacline, slightly curved in cross-section with open triangular delthyrium. Dorsal valve moderately convex with shallow sulcus originating at the umbo. Interarea low, planar, anacline. Radial ornament variably multicostellate with costellae of two to three generations. 4–6 ribs per 3 mm along the posterior margin of adult specimens. Concentric ornament of fine, ridge-like, evenly spaced fila, 3–4 per mm.

Ventral interior with strong teeth supported by diverging dental plates continuing anteriorly as elevated muscle bounding ridges enclosing an elongate, subrhomboidal muscle field about two-fifths as long as the valve. Adductor scars narrow, strip-like, completely separating large, deeply impressed diductor scars of about equal length. Mantle canals saccate with subparallel to slightly converging *vascula media*. Dorsal interior with simple, ridge-like cardinal process on the high notothyrial platform slightly inclined posteriorly. Brachiophores high, triangular with slightly diverging bases. Weakly impressed dorsal adductor scars divided posteriorly by a very short median ridge.

DISCUSSION. This species is somewhat similar to *Dolerorthis tenuicostata* Williams (*in* Whittington & Williams 1955: 406) from the Lower Caradoc of Wales, but differs in having a more transverse shell outline, lateral profile of the ventral valve with maximum thickness anterior to the mid-length in full grown specimens and a weak dorsal sulcus continuing towards the anterior margin. It differs from *Dolerorthis* aff. *hubeiensis* Zeng, which occurs in the Dulankara Regional Stage of north Betpak-Dala, Kazakhstan (Nikitin *et al.* 1996), in having a subequally biconvex transverse shell, finer radial ornament and more widely spaced concentric fila.

Dolerorthis pristina sp. nov. Pl. 10, figs 23–29, 31–36

ETYMOLOGY. After *pristinus*, Latin – former.

HOLOTYPE. BC 57520, Pl. 10, figs 26–29, 31, conjoined valves (L=9.7, W=12.6, T=4.2) from the Anderken Formation, Sample 620, Anderkenyn-Akchoku section.

MATERIAL. 8 pairs of conjoined valves, 15 ventral and 18 dorsal valves from Samples 100 (=K-98/1970) (BC 57110–7), 620 (BC 57520), 626 (BC 57130–32, 57519), 8223a (BC 57158, 59), 8223b, Anderkenyn-Akchoku; Sample 8214 (BC 57150–54, 57523), Ashchsu River; Samples 628 (BC 57133–5), 2538 (BC 56768, 57141–45, 57521, 22), 8217 (BC 57156–7), Kujandysai near Akchoku Mountain; Sample 948 (BC 57136–40), Tesik River.

Table 20 Measurements of complete shells of *Dolerorthis pristina* sp. nov., Samples 100 and 626 from Anderkenyn-Akchoku section.

	Lv	W	T	Iw	Lv/W	T/L	Iw/W
N	10	10	6	10	10	6	9
X	10.0	11.8	4.2	10.3	85.2%	47.6%	87.9%
S	3.04	3.36	1.11	2.63	10.0	6.5	9.5
MIN	5.9	7.5	2.8	6.5	70.2%	40.0%	75.0%
MAX	14.2	18.2	5.5	13.7	103.6%	56.3%	100.0%

DESCRIPTION. Shell weakly ventribiconvex, slightly transverse, suboval in outline, on average 82% (S=7.0, N=10) as long as wide and 48% (S=6.0, N=6) as high as long. Anterior commissure slightly shorter than maximum shell width at mid-length. Cardinal extremities obtuse. Anterior commissure rectimarginate or weakly sulcate. Radial ornament costellate with up to 17 primary costae and costellae branching near the mid-length and near the anterior and lateral margins. 6–8 costellae per 3 mm along the anterior margin and varying from 31 to 54 in full-grown specimens.

Ventral valve moderately and unevenly convex with maximum thickness at about one-third valve length from the small, pointed beak. Ventral interarea apsacline, slightly curved in cross-section with open, narrow delthyrium. Dorsal valve weakly convex with maximum thickness slightly anterior from the beak. Interarea low, planar, linear. Shallow sulcus usually well defined in the posterior half of the dorsal valve, but fading anteriorly.

Ventral interior with small teeth and low, divergent dental plates. Muscle field small, slightly elongate, subpentagonal in outline. Adductor scars narrow, completely separating diductor scars of about equal length. Mantle canals saccate with slightly divergent proximal parts of *vascula media*. Dorsal valve interior with high, subtriangular brachiophores diverging anteriorly. Cardinal process ridge-like with crenulated myophore, situated on a low subtriangular notothyrial platform. Adductor muscle field subrectangular with anterior adductor scars slightly larger than posterior. Median ridge low and broad, bisecting the entire adductor muscle field.

DISCUSSION. *Dolerorthis pristina* differs from *D. expressa* (Popov 1980) in its less convex dorsal valve, much smaller size (less than half *D. expressa*), and in its evenly convex ventral profile, in contrast to *D. expressa* in which the ventral profile is relatively flat near the umbo, but increases greatly anteriorly. In addition, *D. pristina* has finer radial ornament.

Zeng (1987) erected *Paradolerorthis* as a subgenus within *Dolerorthis*. However, his quoted distinctions and equivocal illustrations do not allow us to recognize his subgenus as useful, but the type species *D.* (*Paradolerorthis*) *calla* appears similar to *D. pristina*.

Family **GLYPTORTHIDAE** Schuchert & Cooper, 1931
Genus ***GLYPTORTHIS*** Foerste, 1914

TYPE SPECIES. *Orthis insculpta* Hall, 1847, from the Richmondian (Ashgill), New York, U.S.A.

Glyptorthis sp. Pl. 10, figs 37–42

MATERIAL. Five pairs of conjoined valves, 7 ventral and 6 dorsal valves from Samples 620 (BC 57163, 64), 8223a, Anderkenyn-Akchoku; Sample 8214, Ashchisu River; Samples 2538 (BC 57166–69, 57524), 8256, Kujandysai near Akchoku Mountain; Sample 628 (BC 57165, 57525), east side of Kujandysai; Sample 948, Tesik River.

DESCRIPTION. Shell slightly ventribiconvex, transverse, rounded subrectangular in outline, about 80% as long as wide. Hinge line slightly narrower than maximum shell width at mid-length. Cardinal extremities slightly obtuse. Anterior commissure varying from slightly sulcate to rectimarginate. Ventral valve moderately convex with maximum thickness at umbo. Interarea moderately high, triangular, planar, catacline, divided by narrow triangular, open delthyrium. Dorsal valve gently convex with maximum thickness at about one-quarter valve length from the beak. Dorsal sulcus shallow and narrow, originating at umbo and fading anteriorly. Dorsal interarea low, linear, orthocline. Radial ornament coarsely costellate with up to 16 primary ribs and 25–30 costellae (up to 5 costellae per 3 mm) in adult specimens. Secondary costellae in the median part of the dorsal valve bifurcate internally. Concentric ornament of crowded, evenly spaced growth lamellae.

Ventral interior with teeth supported by short and high dental plates. Muscle field small, situated entirely within delthyrial chamber. Mantle canals saccate with straight, slightly diverging anteriorly *vascula media*. Dorsal interior not observed.

DISCUSSION. These specimens closely resemble *Glyptorthis balcletchiensis* (Davidson, 1883) from the Upper Caradoc of the Girvan District, Scotland (Williams 1962) in the size, general outline and convexity of the shell, as well as in the number and bifurcation of the costellae. It differs from another coarsely ribbed Kazakh species *Glyptorthis? bestamaki* Nikitin & Popov (*in* Klenina *et al.* 1984) from the lower Bestamak Formation (*Nemagraptus gracilis* Zone) of the Chingiz Range in having a rectimarginate or slightly sulcate anterior commissure and a dorsal sulcus not reversed anteriorly into the median fold.

Family **PLAESIOMYIDAE** Schuchert, 1913
Genus ***AUSTINELLA*** Foerste, 1909

TYPE SPECIES. *Orthis kankakensis* McChesney, from the Maquoketa Formation (Ashgill) of Iowa, U.S.A.

Austinella sarybulakensis sp. nov. Pl. 11, figs 15–22

ETYMOLOGY. After Sarybulak River, 10 km west of the type locality.

HOLOTYPE. BC 56507, Pl. 11, figs 15–18, conjoined valves; Anderken Formation, Sample 85258, east side of Uzunbulak River.

MATERIAL. Three conjoined valves, one ventral and one dorsal valve from Sample 85258 (BC 56505–8), east side of Uzunbulak River; Sample 818a, Burultas Valley.

DESCRIPTION. Shell subequally biconvex, transverse, subrectangular in outline about 93–97% as long as wide and 54–60% as thick as long. Hinge line somewhat shorter than maximum shell width at the mid-length. Anterior commissure uniplicate. Ornament costellate with 8–9 costellae per 5 mm along the anterior margin and 25–28 primary ribs near the umbo. Ventral valve moderately convex with maximum thickness slightly anterior to the umbo. Ventral pseudointerarea high, triangular with open, triangular delthyrium. Shallow sulcus originating at about 7 to 9 mm anterior to the beak, widening and deepening anteriorly. Lateral sides of the valve gently and evenly convex in transverse section. Dorsal valve moderately and unevenly convex. Dorsal interarea low, planar, orthocline. Shallow dorsal sulcus in the umbonal area reverses into a median fold at 5–7 mm from the umbo.

Ventral interior with strong teeth and short, slightly divergent dental plates. Muscle field strongly raised anteriorly in a form of pseudospondylium, rounded subtriangular in outline, about two-

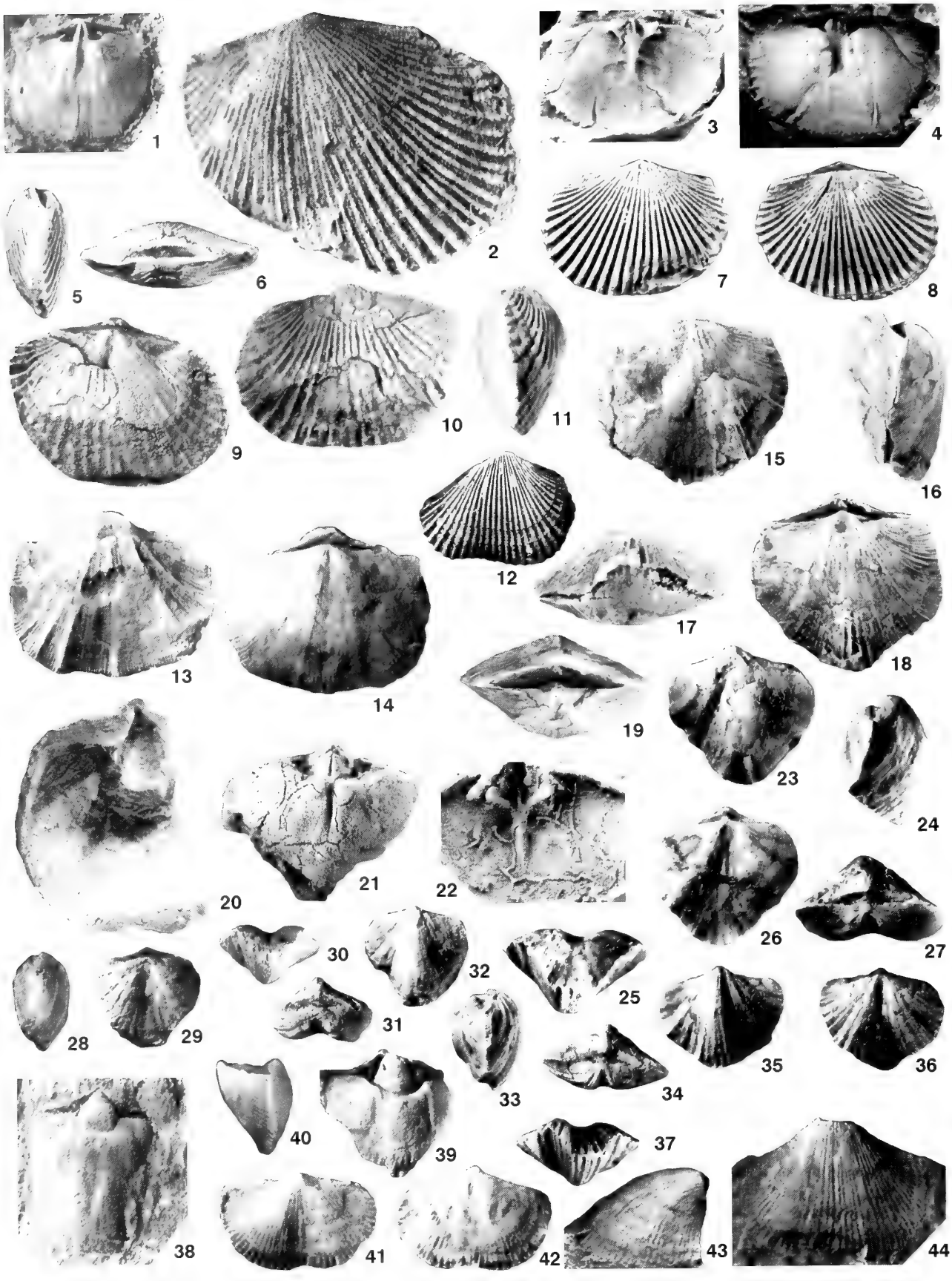
1
2
3
4
5
6
7
8
9
10
11
15
16
12
17
18
13
14
19
23
24
20
21
22
26
27
30
32
25
28
29
31
35
36
33
34
40
39
37
38
41
42
43
44

fifths as long as the valve. Mantle canal system saccate with short, diverging *vascula media*. Dorsal interior with blade-like cardinal process situated on a high subtriangular notothyrial platform. Brachiophores high, subtriangular with strongly thickened, slightly divergent bases. Adductor field weakly impressed, quadripartite, bisected by a low median ridge. Anterior adductors larger than posterior ones.

MEASUREMENTS. Conjoined valves; [BC 56507, L=22.2, W=24.0, T=12.2, Sw=14.4, St=6.4; BC 56508, L=25.1, W=26.3, T=14.8, Sw=14.6, St=6.8].

DISCUSSION. This species can be distinguished from other species of the genus such as *Austinella whitfieldi* (Winchell & Schuchert) and *A. kankakensis* (McChesney), re-described by Wang (1949) from the Ashgill Maquoketa Formation of Iowa, by its uniplicate anterior commissure with the dorsal sulcus reversed into the median fold posterior to the mid-valve.

Superfamily **PLECTORTHOIDEA** Schuchert, 1929
Family **PLECTORTHIDAE** Schuchert, 1929
Subfamily **PLECTORTHINAE** Schuchert, 1929
Genus ***PLECTORTHIS*** Hall & Clarke, 1892

TYPE SPECIES. *Orthis plicatella* Hall, from the Cincinnatian (Lower Ashgill), of the U.S.A.

Plectorthis*? *burultasica sp. nov. Pl. 10, fig. 43, Pl. 11, figs 3–12

1985 *Plectorthis* aff. *altaica* Severgina; Popov: 51, pl. 1, figs 1, 2.

ETYMOLOGY. After the type locality in the Burultas Valley.

HOLOTYPE. BC 57528, Pl. 11, figs 3–4, dorsal valve, Anderken Formation, Sample 7613, Akchoku Mountain, Kujundysai section.

MATERIAL. Five conjoined valves, 8 ventral and 9 dorsal valves from Samples 2538, 7613 (BC 57528), Kujandysai near Akchoku Mountain; Sample 626 (BC 57170, 71), 843, 8128 (BC 57530), Anderkenyn-Akchoku; all Chu-Ili Range; Sample 1041a (BC 57529), Burultas Valley; Sample 1018 (BC 57367), 7 km southwest of Karpkuduk well, Kotnak mountains, south Betpak-Dala.

DESCRIPTION. Shell subequally biconvex, transversely subrectangular in outline, about 60% as thick as long and three-quarters as long as wide, with maximum width at mid-length. Cardinal extremities obtuse to slightly rounded. Anterior commissure rectimarginate. Ventral valve moderately and gently convex in lateral profile with low, strongly apsacline interarea slightly curved in cross-section. Dorsal valve moderately and evenly convex in lateral profile with low, linear, orthocline interarea and shallow umbonal sulcus fading at mid-length. Radial ornament of 28–32 rounded costellae bifurcating at the posterior half of the shell and separated by interspaces of about equal width as ribs. Radial rows of fine rounded exopunctae on both sides of each rib.

Ventral valve with teeth supported by thin diverging dental plates about one-third shorter than length of the elongate subpentagonal muscle field. Adductor scar narrow triangular, slightly raised anteriorly, about the same length as strongly impressed diductor scars. Dorsal valve interior with high, triangular brachiophores with bases converging anteriorly. Notothyrial platform high and narrow, crossed by ridge-like cardinal process with crenulated myophore. Median ridge strong, extending anteriorly to mid-valve. Dorsal anterior and posterior adductor scars about equal size, separated by fine, slightly oblique, transverse ridges.

DISCUSSION. Criteria for generic separation amongst the Plectorthidae require revision. The type species of *Plectorthis*, *P. plicatella*, has never been fully revised, although Schuchert & Cooper (1932, pl. 11, figs 4, 9) illustrated ventral and dorsal interiors from the Maysville Formation of Cincinnati, Ohio. Material labelled as *P. plicatella* in the Natural History Museum (eg. BB 14835) from Cincinnati includes well preserved exteriors with no trace of exopunctae. However, our new species has well-developed rows of exopunctae on both sides of each costa, as have other species attributed to *Plectorthis*, e.g. *Plectorthis*? *punctata* illustrated by Cooper (1956), *P. obesa*, mentioned but not illustrated by Cooper (1956), and the *Plectorthis* sp. of Neuman (1971:21). Thus, until comparable exopunctae have been found in true *P. plicatella*, we attribute the exopunctate species to *Plectorthis* with a query.

Plectorthis? *burultasica* resembles *Plectorthis altaica* Severgina, 1967 from the Khankhara Formation (Caradoc) of Gornyi Altai in radial ornament, size and outline, but differs in having a weak umbonal dorsal sulcus fading to the mid-valve and a more ventribiconvex profile. *Plectorthis*? *punctata* has a slightly sulcate dorsal valve by comparison with *P.*? *burultasica* as well as fewer rib bifurcations. It is also considerably smaller. In addition, *P.*? *obesa* has a more strongly convex dorsal valve and fewer bifurcations in the ribbing.

PLATE 11

Figs 1, 2 *Dolerorthis expressa* Popov, Sample 8137, Anderkenyn-Akchoku section, BC 57526, dorsal internal mould, × 2, and latex of external mould, × 6.

Figs 3–12 *Plectorthis? burultasica* sp. nov. **3, 4**, Sample 7613, Akchoku Mountain, Kujandysai section. BC 57528, **holotype**, dorsal latex cast and internal mould, × 2. **5–8**, Sample 1041a, Burultas, BC 57529, conjoined valves, lateral, posterior, ventral and dorsal views, × 2. **9–11**, Sample 1018, area 7 km SW of Kotnak mountains, south Betpak-Dala, CNIGR 1/11989, conjoined valves, dorsal, ventral and lateral views, × 2. **12**, Sample 8128, Anderkenyn-Akchoku section, BC 57530, ventral exterior, latex cast, × 2.

Figs 13, 14 *Phaceloorthis*? sp. Sample 2538, Akchoku Mountain, Kujandysai section, BC 57531, conjoined valves, ventral and dorsal views, × 1.5.

Figs 15–22 *Austinella sarybulakensis* sp. nov. Sample 85258, east side of Kujandysai. **15–18,** BC 56507, conjoined valves, **holotype**, ventral, lateral, anterior and dorsal views, × 1.5. **19,** BC 56508, conjoined valves, posterior view, × 1.5. **20**, BC 56505, ventral interior, × 2. **21, 22,** BC 56506, dorsal internal mould and latex cast, × 2.

Fig. 23–37 *Bowanorthis? devexa* sp. nov. Sample 2538, Akchoku Mountain, Kujandysai section. **23–27,** BC 57532, conjoined valves, **holotype**, ventral, lateral, anterior, dorsal and posterior views, × 3. **28–32,** BC 57533, conjoined valves, lateral, dorsal anterior, posterior, and ventral views, × 3. **33–37,** BC 57534, conjoined valves, lateral, posterior, ventral, dorsal and anterior views, × 3.

Figs 38–44 *Phragmorthis conciliata* Popov. **38**, Sample 1018, area 7 km SW of Kotnak mountains, south Betpak-Dala, CNIGR 11/11989, ventral internal mould, × 4. **39**, Sample 7613, Akchoku Mountain, Kujandysai section. BC 57535, ventral internal mould, × 5. **40–42**, Sample 2538, Akchoku Mountain, Kujandysai section, BC 57536, conjoined valves, lateral, dorsal and ventral views, × 4. **43, 44**, Sample 626, Anderkenyn-Akchoku section, BC 57537, ventral exterior and lateral view, × 4.

Genus ***PHACELOORTHIS*** Percival, 1991

TYPE SPECIES. *P. decoris* Percival, 1991, from the Quondong Limestone (Caradoc) of New South Wales, Australia.

Phaceloorthis? sp. Pl. 11, figs 13, 14

MATERIAL. One pair of conjoined valves (BC 57531) (L=20.8, W=25.6, T=9.8) from Sample 2538, Kujandysai, near Akchoku Mountain.

DESCRIPTION. Shell subequally biconvex, transversely subrectangular in outline with hinge line somewhat shorter than maximum shell width at mid-length. Anterior margin rectimarginate. Ventral valve moderately convex in lateral profile with maximum thickness at one-third valve length. Ventral interarea almost orthocline, slightly curved in cross-section with open, narrow triangular delthyrium. Dorsal valve moderately convex with maximum thickness near the mid-valve. Umbonal area with shallow sulcus fading towards mid-valve. Dorsal interarea anacline, planar, linear. Shell surface with 9 low, angular radial plications and superimposed finely fascicostellate ribs 7–9 per 3 mm along the anterior margin. Interior of both valves unknown.

DISCUSSION. The interior of this species remains unknown, which makes its generic attribution highly provisional, but there are only a few impunctate mid and late Ordovician orthide genera with fascicostellate ornament and they are mostly related to the family Giraldiellidae. Otherwise fascicostellate ribbing is characteristic of the plectorthid genus *Phaceloorthis*. This single specimen somewhat resembles *Phaceloorthis recondita* Popov, Nikitin & Cocks, 2000 from the Otar Member (Upper Caradoc) of the Dulankara Moutains in its general shell shape and size and fascicostellate ornament, but differs in having an orthocline ventral interarea and weak radial plications.

Family **WANGYUIIDAE** Zeng, 1989
Genus ***BOWANORTHIS*** Percival, 1991

TYPE SPECIES. *Bowanorthis fragilis* Percival, 1991, from the Caradoc of New South Wales, Australia.

Bowanorthis? ***devexa*** sp. nov. Pl. 11, figs 23–37; Fig. 14

ETYMOLOGY. After *devexus*, Latin – hollow.

HOLOTYPE. BC 57532, Pl. 11, figs 23–27, conjoined valves, from the Anderken Formation, Sample 2538, Kujandysai, near Akchoku Mountain.

MATERIAL. Twelve conjoined valves from Samples 2538 (BC 57178, 57532–34), 8217 (BC 57179) Kujandysai, near Akchoku Mountain; Sample 948 (BC 57172–77), Tesik River.

DESCRIPTION. Shell ventribiconvex, slightly transverse and semioval, about 85–98% as long as wide with hinge line slightly shorter than maximum width at one-quarter shell length. Anterior commissure sulcate. Ventral valve carinate posteriorly, strongly convex in lateral profile with maximum thickness at about one-third valve length. Beak small, erect. Ventral interarea apsacline, incurved in cross-section, with small subtriangular delthyrium. Ventral median fold originating at the umbonal area with steep lateral slopes flanked by folds. Lateral sides of the valves less convex. Dorsal valve evenly convex with linear, anacline interarea and deep, V-shaped median sulcus originating at the beak and ending in a low semioval tongue occupying slightly less than half of the valve length. Radial ornament fascicostellate with three strong angular ribs and 4–5 costellae per mm along the anterior margin of mature specimens. Interior of both valves unknown.

MEASUREMENTS. Conjoined valves; (58/12375) L=6.4, W=6.7, T=3.8, Sw=3.3; (59/12375), L=4.5, W=4.6, T=2.7, Sw=2.6; (60/12375), L=4.8, W=5.6, T=3.1, Sw=2.4.

DISCUSSION. This species is provisionally included within *Bowanorthis* because of the small ventribiconvex shell with strongly sulcate anterior commissure, carinate ventral valve, fascicostellate ornament and receding dental plates, all resembling *B. fragilis* from the Caradoc of New South Wales (Percival 1991); however, it differs in having a strongly apsacline ventral interarea and a less transverse shell outline. The general morphology of the cardinal process and brachiophores in the Kazakh species looks similar to *B. fragilis*, but the presence of the characteristic sigmoidal plates is impossible to

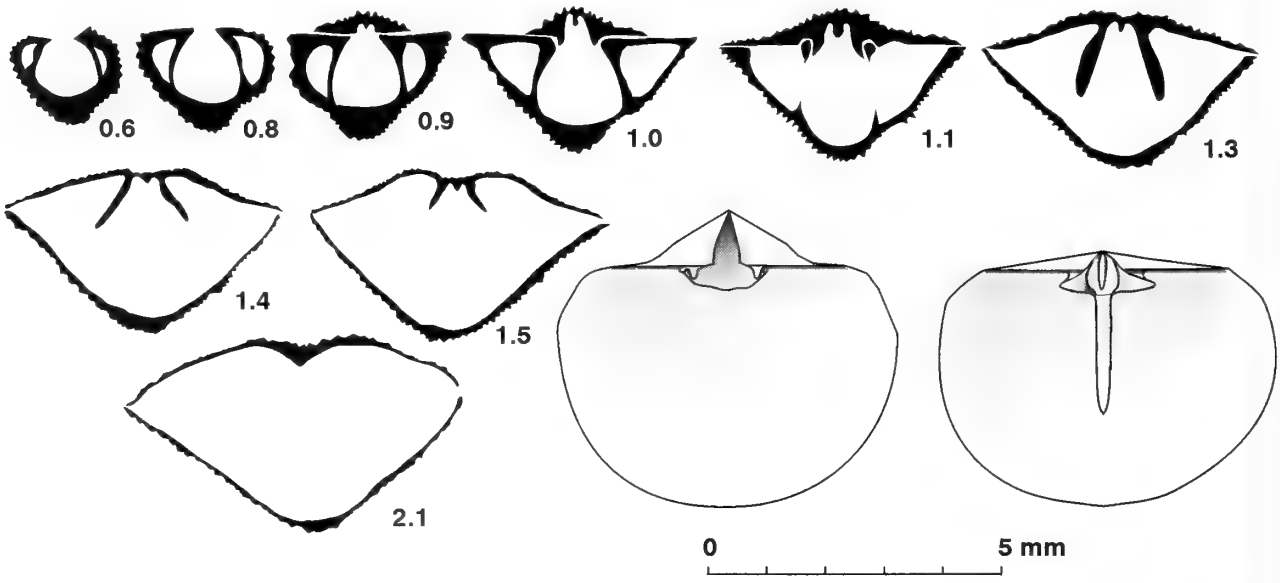

Fig. 14 Transverse serial sections of *Bowanorthis*? *devexa* sp.nov. from Sample 2538, Kujandysai section. Distance in mm is measured from the posterior tip of ventral beak. Dorsal valve uppermost. Also reconstructions of the ventral and dorsal interiors.

confirm from our sections (Fig. 14). In general shell shape and fascicostellate radial ornament the Anderken material is similar to *Ranorthis* Öpik (1939) from the Volkhov and Kunda Stages of Baltica. However, the generic attribution of *devexa* is tentative and it may represent an undescribed genus.

Family **RANORTHIDAE** Havlíček, 1949
Genus ***EODALMANELLA*** Havlíček, 1950

TYPE SPECIES. *Orthis socialis* Barrande, 1879; from the Sarká Formation (Llanvirn) of Bohemia.

Eodalmanella extera Popov, 1985 Pl. 12, figs 10–12, 15

1985 *Eodalmanella extera* Popov: 54, pl. 1, figs 3–8.

HOLOTYPE. CNIGR 4/11989, ventral internal mould (L=4.1, W=6.1), from the Anderken Formation, Anderkenyn-Akchoku section, Sample 843.

MATERIAL. Five pairs of conjoined valves, 42 ventral and 48 dorsal valves, internal and external moulds, from Samples 100b, 620 (BC 57189), 843, Anderkenyn-Akchoku section; Sample 1018, 7 km southwest of Karpkuduk well, Kotnak Mountains.

DESCRIPTION. Shell ventribiconvex, transverse, subrectangular in outline, about 85% as wide as long with maximum width at mid-length. Anterior commissure gently sulcate. Ventral profile moderately convex, about one-third as thick as long, with maximum thickness at about one-quarter valve length. Dorsal valve gently convex in transverse profile with maximum thickness slightly anterior to the umbo and with shallow median sulcus originating in the umbonal area. Dorsal interarea linear, strongly anacline. Radial ornament multicostellate with 3–6 ribs per mm along the anterior margin of mature specimens. Concentric ornament of very fine ridge-like, evenly spaced fila, often branching anteriorly.

Ventral interior with teeth supported by short, divergent dental plates and rounded subtriangular, slightly elongate muscle field about 37% as long as the valve. Ventral adductor scars narrow, subtriangular, slightly shorter than diductor scars. Cardinal process ridge-like with bilobed, crenulated miophore. Brachiophores high, triangular, with widely diverging bases. Fulcral plates well developed. Dorsal adductor scars quadripartite, extending anteriorly to mid-valve, bordered laterally by low ridges.

DISCUSSION. This species strongly resembles *Scaphorthis? aulacis* Percival (1979a) from the Caradoc Goonumbla Volcanics of New South Wales in the impunctate shell, radial ornament and internal morphology of both valves. The Kazakh species differs in having longer dental plates, a cardinal process with a long shaft crossing all the bottom of the notothyrial cavity and well defined lateral ridges bordering the dorsal adductor field. A detailed discussion and basic statistics of this species were provided by Popov (in Nikitin & Popov 1985).

Family **CREMNORTHIDAE** Williams, 1963
Genus ***PHRAGMORTHIS*** Cooper, 1956

TYPE SPECIES. *Phragmorthis buttsi* Cooper, 1956, from the Effna-Rich Valley Formations (Llandeilo-Lower Caradoc) of Virginia, U.S.A.

Phragmorthis conciliata Popov, 1985
Pl. 11, figs 38–44; Pl. 12, figs 1–9

1985 *Phragmorthis conciliata* Popov: 52, pl. 1, figs 9–12.

HOLOTYPE. CNIGR 10/11989 (Pl. 12, figs 1, 2), dorsal valve internal mould (L=4.5, W=7.2), from the Anderken Formation, 7 km south-west of Karpkuduk well, Kotnak Mountains, Sample 1018.

MATERIAL. Two pairs of conjoined valves, 6 ventral and 8 dorsal valves, internal and external moulds, from Samples 626 (BC 57537), 8223a, Anderkenyn-Akchoku section; Samples 2538 (BC 57536), 7613 (BC 57535), Kujandysai section; Sample 8230, Buldukbai-Akchoku section; Sample 1018, 7 km southwest of Karpkuduk well Kotnak Mountains; Sample 1024b, south side of Karatal River, south of Sorbulak spring.

DIAGNOSIS. Shell ventribiconvex, transverse, subrectangular outline about 77% as wide as long with maximum width at mid-length, anterior commissure gently unisulcate; ventral valve strongly convex with maximum thickness between the umbo and mid-valve; ventral interarea high triangular, apsacline with narrow open delthyrium; dorsal valve moderately and evenly convex with narrow and shallow sulcus originating at the umbo; radial ornament finely and equally multicostellate with 5 ribs per mm along the anterior margin of mature specimens. Ventral interior with elongate subtriangular muscle field on pseudospondylium 21–26% as long as the valve. Dorsal interior with simple, ridge-like cardinal process on the high notothyrial platform which is strongly raised anteriorly; high, blade-like median septum 88% valve length; large, deeply impressed adductor scars, radially arranged, about 66% valve length.

DISCUSSION. This species differs from *Phragmorthis buttsi* Cooper (1956: 510) in its transverse subrectangular outline and lesser convexity of both valves. It is on average about half the size of *Phragmorthis crassa* Cooper (1956: 511) and has finer radial ornament. Both *P. buttsi* and *P. crassa* have a subcarinate ventral valve, which is another difference from the Kazakh species.

Table 21 Measurements of ventral valves of *Pionodema opima* sp. nov., Sample 8228 from Kopalysai Section, sample 8230 from Buldukbai-Akchoku and Sample 7613 from Kujandysai section.

	Lv	W	Ml	Mw	Lv/W	Ml/L	Iw/W
N	9	9	5	6	9	5	5
X	7.6	9.4	3.2	3.5	81.2%	38.5%	90.5%
S	1.38	2.16	0.63	1.26	8.6	4.9	14.9
MIN	5.0	7.3	2.6	2.3	68.5%	34.2%	64.9%
MAX	9.8	13.8	4.1	5.7	93.2%	46.6%	103.6%

Table 22 Measurements of dorsal valves of *Pionodema opima* sp. nov., Sample 8228 from Kopalysai Section, sample 8229 from Buldukbai-Akchoku and Sample 7613 from Kujandysai section.

	Ld	W	BBl	BBw	Ml	Mw	Lv/W	Ml/L	BBw/W
N	7	7	5	5	3	3	4	3	5
X	7.6	9.5	1.6	2.6	3.4	3.1	82.8%	41.2%	60.4%
S	2.36	2.86	0.15	0.34	0.32	0.10	10.7	2.9	9.9
MIN	3.2	4.0	1.4	2.3	3.2	3.0	70.1%	38.8%	50.0%
MAX	10.5	12.9	1.7	3.1	3.8	3.2	96.1%	44.4%	73.9%

Suborder **DALMANELLIDINA** Moore, 1952
Superfamily **ENTELETOIDEA** Waagen, 1884
Family **DRABOVIIDAE** Havlíček, 1950
Subfamily **DRABOVIINAE** Havlíček, 1950
Genus ***PIONODEMA*** Foerste, 1912

TYPE SPECIES. *Orthis subaequata* Conrad, from the Caradoc of Missouri, U.S.A.

Pionodema opima sp. nov. Pl. 12, figs 13, 14, 16–27

ETYMOLOGY. After *opimus*, Latin – fat.

HOLOTYPE. BC 57545, Pl 12, figs 17–18, internal mould of conjoined valves, from the Anderken Formation, Sample 7613, Kujandysai section.

MATERIAL. Nine pairs of conjoined valves, 70 ventral and 64 dorsal valves from Sample 7613 (BC 57545), Kujandysai section; Sample 8128, Anderkenyn-Akchoku; Sample 8228 (BC 57185, 57547, 48), east side of Kopalysai; Samples 110, 8229 (BC 57546), 8230 (BC 57803), 8257 (BC 57544), Buldukbai-Akchoku section; Sample 818a (BC 57802), Burultas Valley.

DESCRIPTION. Shell slightly dorsibiconvex, transverse, suboval in outline, about 84% as long as wide and 53% as thick as long. Hinge line slightly shorter than the maximum shell width at mid-length. Anterior commissure uniplicate. Ventral valve gently convex with maximum thickness at the umbonal area. Beak curved, pointed and slightly erect posterior to hinge line. Ventral interarea subtriangular, apsacline, weakly curved in cross-section, with open triangular delthyrium. Shallow sulcus originating near mid-valve. Dorsal valve moderately convex with maximum thickness at quarter valve length. Umbonal area with shallow V-shaped sulcus reversed into a low and narrow median fold flanked laterally by weak plications. Radial ornament multicostellate with 28–30 primary ribs and about 3–5 costellae per mm along the anterior margin of full grown specimens. Growth lines fine, ridge-like, crowded, evenly spaced.

Ventral interior with teeth and long, diverging dental plates continuing into ridges bordering laterally slightly elongate suboval muscle field. Ventral adductor scars narrow and subtriangular, raised anteriorly and somewhat shorter than the strongly impressed elongate suboval diductor scars. Ventral mantle canals lemniscate, straight, widely diverging. Dorsal interior with high, triangular brachiophores with slightly diverging bases. Fulcral plates variably developed. Cardinal process ridge-like with crenulated myophore. Dorsal adductor scars bisected by fine median ridge and bordered laterally by subparallel ridges starting from the ends of the brachiophore bases.

DISCUSSION. This species is characterised by a uniplicate anterior commissure with low dorsal median fold and shallow ventral sulcus, which is unusual for *Pionodema* (Cooper 1956), and can be compared only with *P. uniplicata* Cooper, but differs from that species in its more transverse outline and the weak umbonal dorsal sulcus reversing into a median fold at about mid-length. The Anderken specimens also lack the prominent ridge anterior to the ventral muscle field of *P. uniplicata* (Cooper 1956: pl. 154, figs 31–32).

Order **PENTAMERIDA** Schuchert & Cooper, 1931
Suborder **SYNTROPHIIDINA** Ulrich & Cooper, 1936
Superfamily **CAMARELLOIDEA** Hall & Clarke, 1894
Family **CAMARELLIDAE** Hall & Clarke, 1894
Genus ***PARASTROPHINA*** Schuchert & LeVene, 1929

TYPE SPECIES. *Atrypa haemiplicata* Hall, 1847, from the Trenton Limestone (Caradoc), New York, U.S.A.

Parastrophina iliana sp. nov.
Pl.13, figs 30–50; Figs 15, 16

1956 *Camerella haemiplicata* (Hall) var. *rotunda* (Winchell & Schuchert); Rukavishnikova: 129, pl. 2, figs 1, 3 (*non* fig. 2).
1975 *Parastrophina haemiplicata* (Hall); Sapelnikov & Rukavishnikova: 25, pl. 1, figs 1–8.
1986 *Parastrophina haemiplicata* (Hall); Kolobova & Popov; pl. 1, fig. 4.

HOLOTYPE. BC 57557, Pl. 13, figs 38–42, conjoined valves from Sample 100, Anderkenyn-Akchoku section.

MATERIAL. 52 pairs of conjoined valves, one ventral and 3 dorsal valves from Samples 100 (=K-98/1970) (BC 56643–46, 57557), 626 (BC 56634–6), Anderkenyn-Akchoku section; Samples, 628 (BC 56633, 56642, 57559), 2538 (BC 56637–41), 8217 (BC 57556), 8256 (BC 57558), 85258, Kujandysai Section; Sample 948 (BC 57192–99), Tesik River; Sample 1041a, Burultas Valley.

DESCRIPTION. Shell dorsibiconvex to biconvex, transverse, semielliptical in outline, about 90% as long as wide and 75% as thick as long. Anterior commissure uniplicate. Ventral valve gently convex with maximum thickness somewhat posterior to mid-valve. Sulcus originating about 5–6 mm from the umbo, deepening anteriorly and terminating in broad, semioval tongue

PLATE 12

Figs 1–9 *Phragmorthis conciliata* Popov. **1, 2**, Sample 1018, area 7 km SW of Karpkuduk well, Kotnak Mountains, CNIGR 10/11989, **holotype**, latex cast and dorsal internal mould, × 4. **3, 5–9,** Sample 2538, Akchoku Mountain, Kujandysai section; **3**, BC 57538, dorsal exterior, × 4; **5–8**, BC 57539, conjoined valves lateral, dorsal, posterior and ventral views, × 4; **9**, CNIGR 12/11989, latex cast of dorsal exterior, × 4. **4**, Sample, 8230, Buldukbai-Akchoku section, west side of Kopalysai, BC 57603, dorsal internal mould, × 5.

Figs 10–12, 15 *Eodalmanella extera* Popov. **10**, Sample 1018, area 7 km SW of Karpkuduk well, Kotnak Mountains, CNIGR 9/11989, ventral exterior, × 4. **11,** Sample 620, Anderkenyn-Akchoku section, BC 57189, dorsal exterior latex cast, × 5. **12, 15**, Sample 843, Anderkenyn-Akchoku section; **12**, CNIGR 5/11989, dorsal internal mould, × 4; **15**, CNIGR 3/11989, ventral internal mould, × 4.

Figs 13, 14, 16–27 *Pionodema opima* sp. nov. **13, 14**, Sample 8257, Buldukbai-Akchoku section, west side of Kopalysai, BC 57544, internal mould, dorsal and ventral views, × 3. **16,** Sample 8230, east side of Kopalysai, BC 57803, latex cast of dorsal external mould, × 2.7. **17, 18**, Sample 7613, Akchoku Mountain, Kujandysai section, BC 57545, **holotype**, internal mould of conjoined valves, dorsal and ventral views, × 3. **19–24**, Sample 818a, Burultas valley, BC 57802, conjoined valves, detail of radial ornament, × 8, and lateral, ventral, dorsal, posterior and anterior views, × 4. **25,** Sample, 8229, Buldubai-Akchoku section, west side of Kopalysai, BC 57546, dorsal internal mould, × 3. **26, 27**, Sample 8228, east side of Kopalysai; **26**, BC 57548, ventral internal mould, × 3; **27**, BC 57547, ventral internal mould, × 2.

Figs 28–35 *Ilistrophina tesikensis* gen. et sp. nov., Sample 948, Tesik River. **28–31**, BC 56824, conjoined valves, lateral, anterior, ventral and dorsal views, × 4. **32–35**, BC 56823, conjoined valves, **holotype**, dorsal, ventral, lateral and anterior views, × 4.

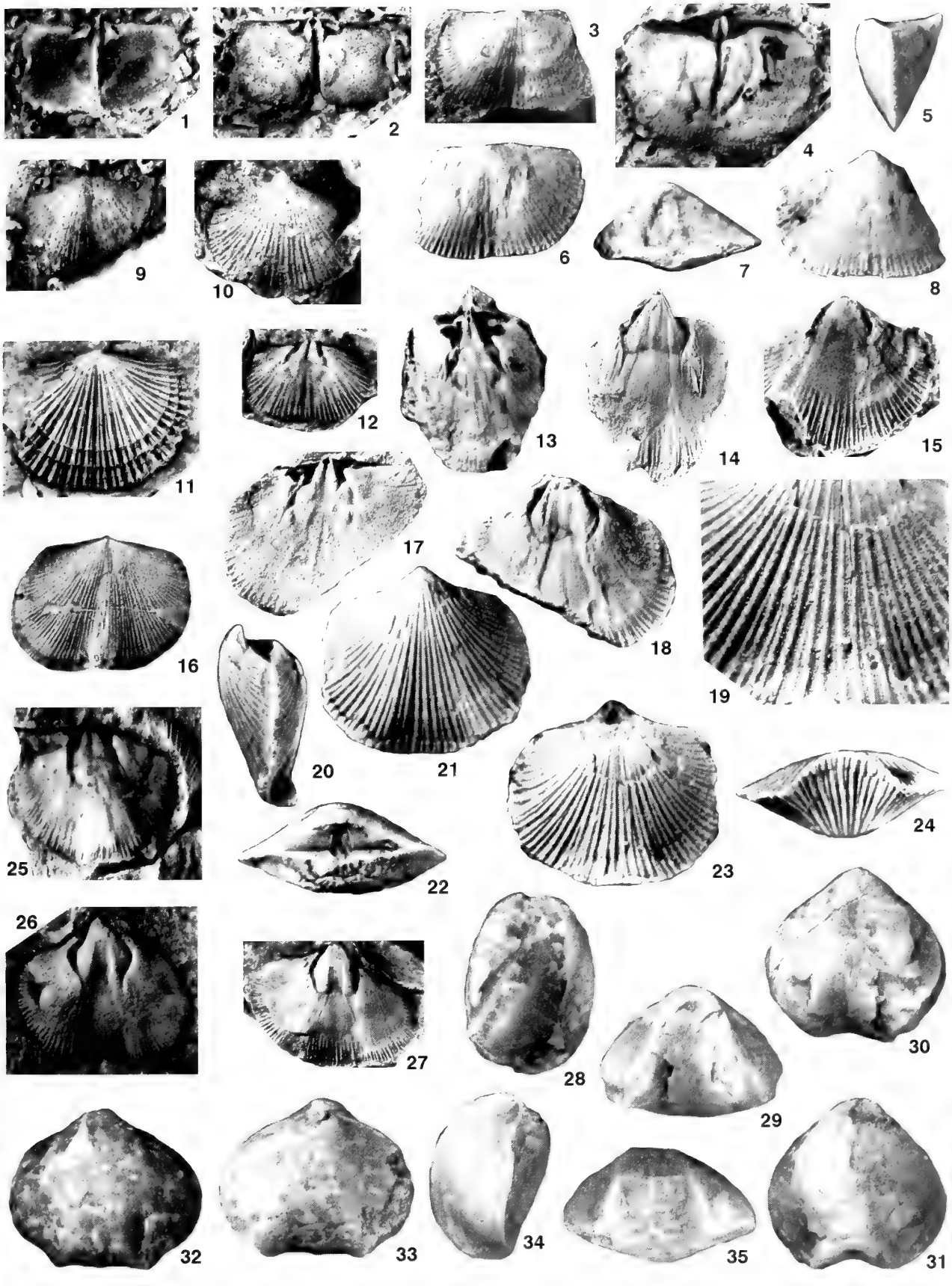
1
2
3
4
5
6
7
8
9
10
11
12
13
14
15
16
17
18
19
20
21
22
23
24
25
26
27
28
29
30
31
32
33
34
35

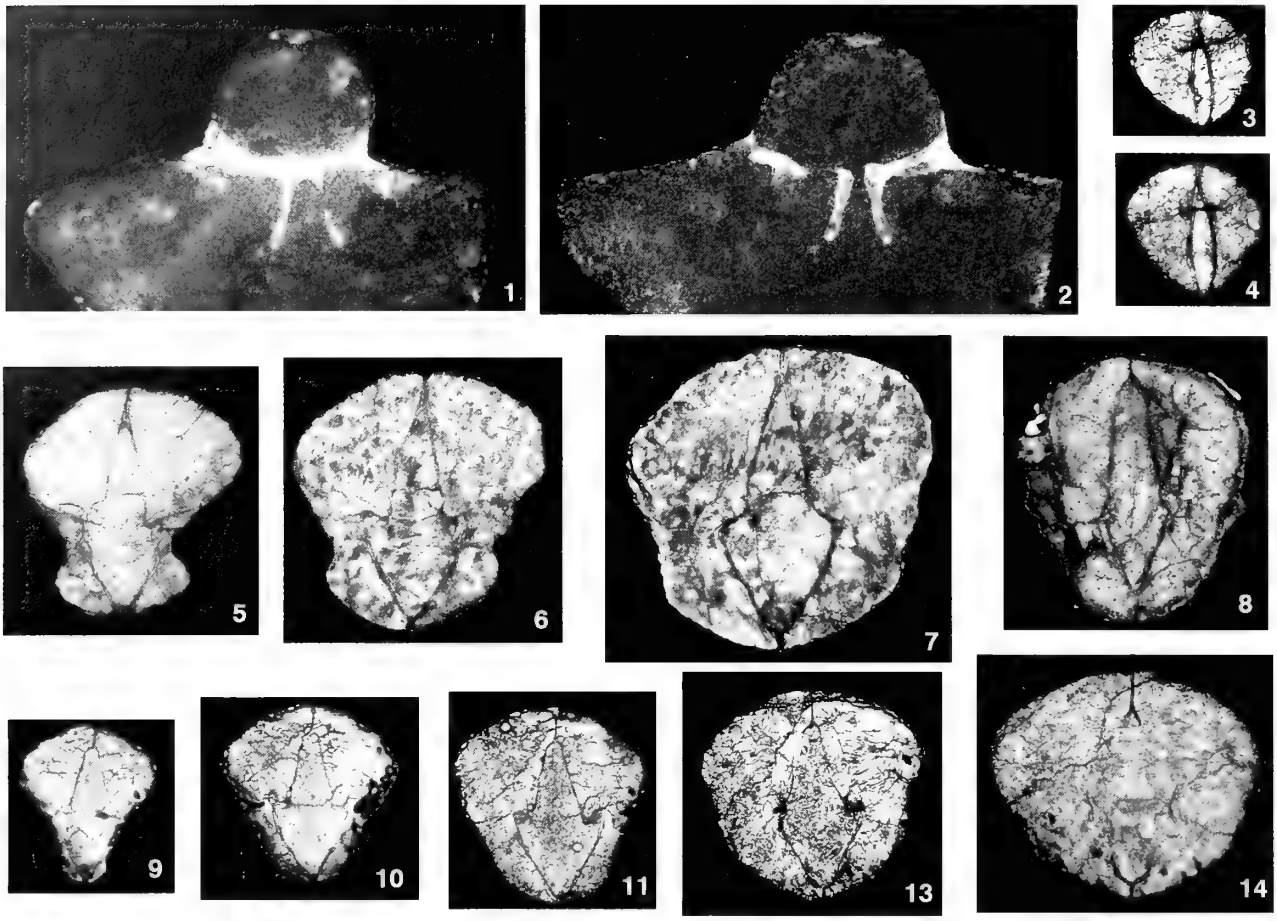

Fig. 15 Photographs of transverse serial sections, × 12. Distance in mm is measured from the posterior tip of ventral beak. Dorsal valve uppermost. **1–2,** *Placotriplesia spissa* sp.nov., BC 57605, Sample 628, Kujandysai section; **1,** 1.5 mm; **2,** 1.8 mm. **3, 4, 9–14**, *Ilistrophina tesikensis* gen. et sp. nov., Sample 948, Tesik River, **3,4,** BC 57606, 0.3 and 0.4 mm; **9–14**, BC 57607, 0.4, 0.6, 0.8, 1.0 and 1.4 mm; **5–7,** *Parastrophina iliana* sp. nov., BC 56560, Sample 948, Tesik River; 0.6, 0.8 and 1.2 mm; **8**, *Parastrophina plena* Sapelnikov & Rukavishnikova, BC 57564, Sample 948, Tesik River, 1.0 mm.

about 66% valve width. Dorsal valve strongly convex with maximum thickness at mid-valve or slightly anteriorly. Umbonal area strongly swollen. Broad median fold originating near mid-valve. Radial ornament of coarse rounded-angular ribs originating anterior to mid-valve in mature specimens with 1–3 ribs in the sulcus, 2–4 on the median fold and up to 6 on the flanks of both valves.

Ventral interior with small teeth and narrow spondylium on a low median septum extending anteriorly to mid-valve. Dorsal interior with narrow cruralium on the low median septum. Alate plates small, projecting anteriorly as short brachial processes. Inner plates narrow, gently curved. Outer plates nearly straight in cross-section, converging towards a thin median septum.

MEASUREMENTS. (471/12375) conjoined valves, L=14.0, W=16.9, T=6.3, Sw=8.9; (474/12375) conjoined valves, L=20.4, W=21.0, T=11.2, Sw=8.7; (475/12375) conjoined valves, L=22.9, W=24.5, T=10.2, Sw=12.8; (476/12375) conjoined valves, L=16.5, W=19.8, T=6.5, Sw=11.2; (479/12375) conjoined valves, L=10.5, T=6.7, Sw=6.7.

DISCUSSION. The Kazakh shells are comparable to *Parastrophina haemiplicata* (Hall), and in particular with specimens described and illustrated by Cooper (1956: 606, pl. 106, figs 33–44; pl. 117, figs 19–27) from the lower Martinsburg Formation of Virginia, in outline and profile of both valves, as well as in the characters of the radial ornament, dorsal median fold and ventral sulcus, but they differ in having more conspicuous ribbing on the flanks of mature shells, which may possess up to 7 ribs; however, the number of ribs is

Table 23 Measurements of complete shells of *Parastrophina iliana* sp. nov., Sample 948, Tesik river.

	L	W	T	Ld	Sw	St	L/W	T/L	Ld/W	Sw/W
N	11	10	10	11	10	10	10	10	10	9
X	8.2	9.1	5.8	8.1	6.1	3.6	89.2%	74.0%	87.7%	65.6%
S	2.05	2.87	1.16	2.10	1.65	1.52	6.3	10.4	5.2	6.5
MIN	5.5	5.6	4.2	5.3	3.2	1.6	80%	62%	79%	57%
MAX	11.9	14.8	7.4	11.7	8.5	6.6	98%	95%	95%	78%

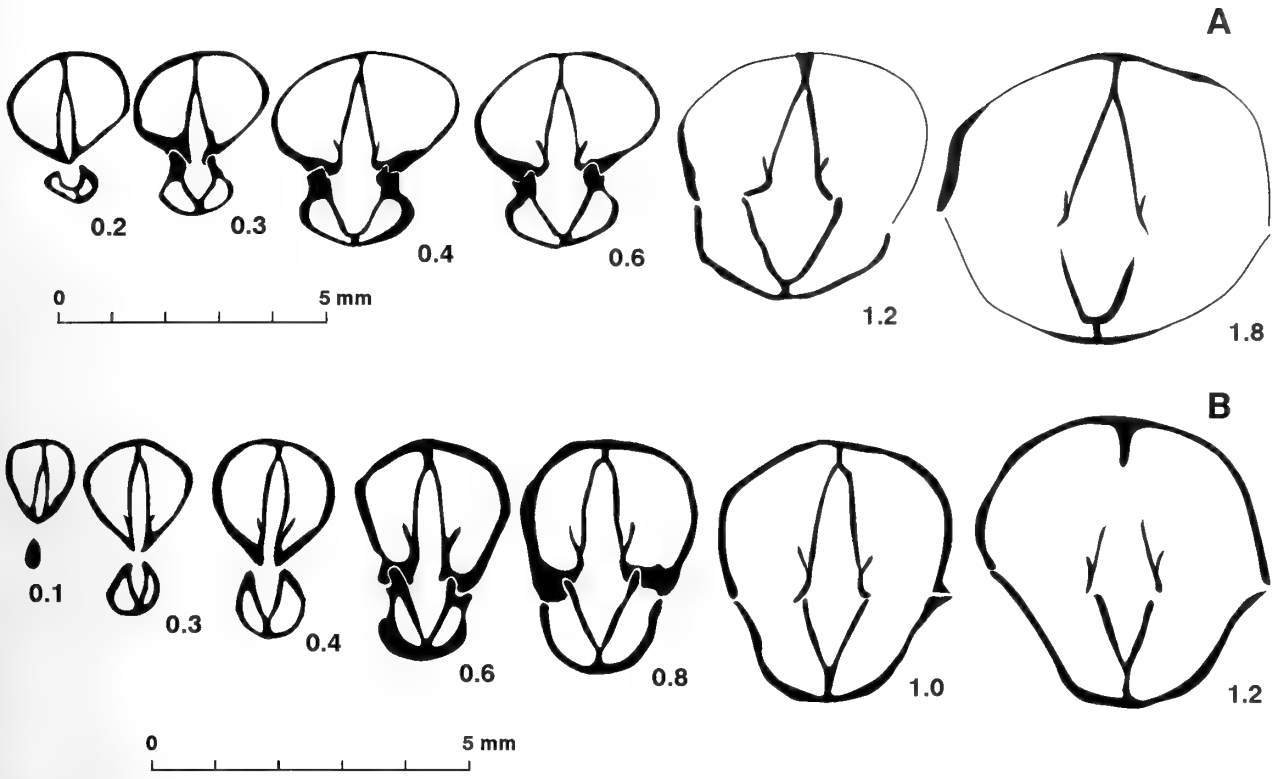

Fig. 16 Transverse serial sections from Sample 948, Tesik River. **A,** *Parastrophina iliana* sp. nov., BC 57560; **B,** *Parastrophina plena* Sapelnikov & Rukavishnikova, BC 57564. Distance in mm is measured from the posterior tip of ventral beak. Dorsal valve uppermost.

variable in the studied samples. There is also a strong tendency to asymmetry in the anterior commissure of the Kazakh shells. However, as mentioned by Cooper, his specimens were somewhat different from Hall's types and the species needs more substantial revision. Specimens from the Anderken Formation described by Rukavishnikova (1956) as *Camerella haemiplicata* (Hall) var. *rotunda* seem likely to represent a mixture of several taxa. In particular, the specimens illustrated on her pl. 2, fig. 2 may belong to *Liostrophia*, but others appear to be conspecific with ours. It is possible that the Kazakh shells are conspecific with the specimens described as *Parastrophina haemiplicata* by Fu (1982: 129, pl. 36, fig. 16) from the Jinhe Formation (Caradoc) of northwest China. The only illustrated specimen is similar to some of the juvenile Kazakh shells in ribbing and in the lateral profile of both valves, but it is impossible to estimate the limits of morphological variation in the Chinese population of *Parastrophina* from the published illustrations and description. There is remarkable general similarity between the brachiopod assemblage from the Jinhe Formation and the fauna from the carbonate mud-mounds in the upper Anderken Formation. In particular, both assemblages contain distinctive genera such as *Schizostrophina* and *Pectenospira* (Popov *et al.* 1999) which are otherwise unknown elsewhere.

Parastrophina plena Sapelnikov & Rukavishnikova, 1975
Pl. 13, figs 51–58; Figs 15, 16

1975 *Parastrophina plena* Sapelnikov & Rukavishnikova: 27, pl. 1, figs 12–14.
1982 *Parastrophina uniplicata* Fu:130, pl. 36, fig. 17.

HOLOTYPE. IGNA 436/1861, conjoined valves, from the Anderken Formation, Sample 302 of Keller (1956), Anderkenyn-Akchoku section.

MATERIAL. 102 pairs of conjoined valves, 1 ventral and 2 dorsal valves from Samples 100 (=K-98/1970), 8223a (BC 56595), 8223b (BC 57248–52), 8226, Anderkenyn-Akchoku section; Samples 8214 (BC 57216–37, 57563), 8215 (BC 57238–47), west side of Ashchisu River; Samples 628 (BC 56598–600), 2536 (BC 56605–10), 2538 (BC 57562), 8217, 8219, 8256 (BC 56603–4), Kujandysai Section; Sample 948 (BC 57200–15), Tesik River.

Table 24 Measurements of ventral valves of *Parastrophina plena* Sapelnikov and Rukavishnikova, Sample 948, Tesik river.

	L	W	T	Ld	Sw	St	L/W	T/L	Ld/W	Sw/W
N	34	34	34	34	31	33	34	34	34	31
X	6.6	7.1	4.8	6.7	4.3	3.1	93.6%	72.7%	94.3%	60.7%
S	0.74	0.95	0.91	0.75	0.55	0.82	5.7	8.7	5.5	5.3
MIN	5.5	5.8	3	5.5	3.4	1.4	83.0%	52.6%	83.6%	52.9%
MAX	9	9.7	7.5	9	5.4	4.8	107.5%	87.7%	107.5%	76.8%

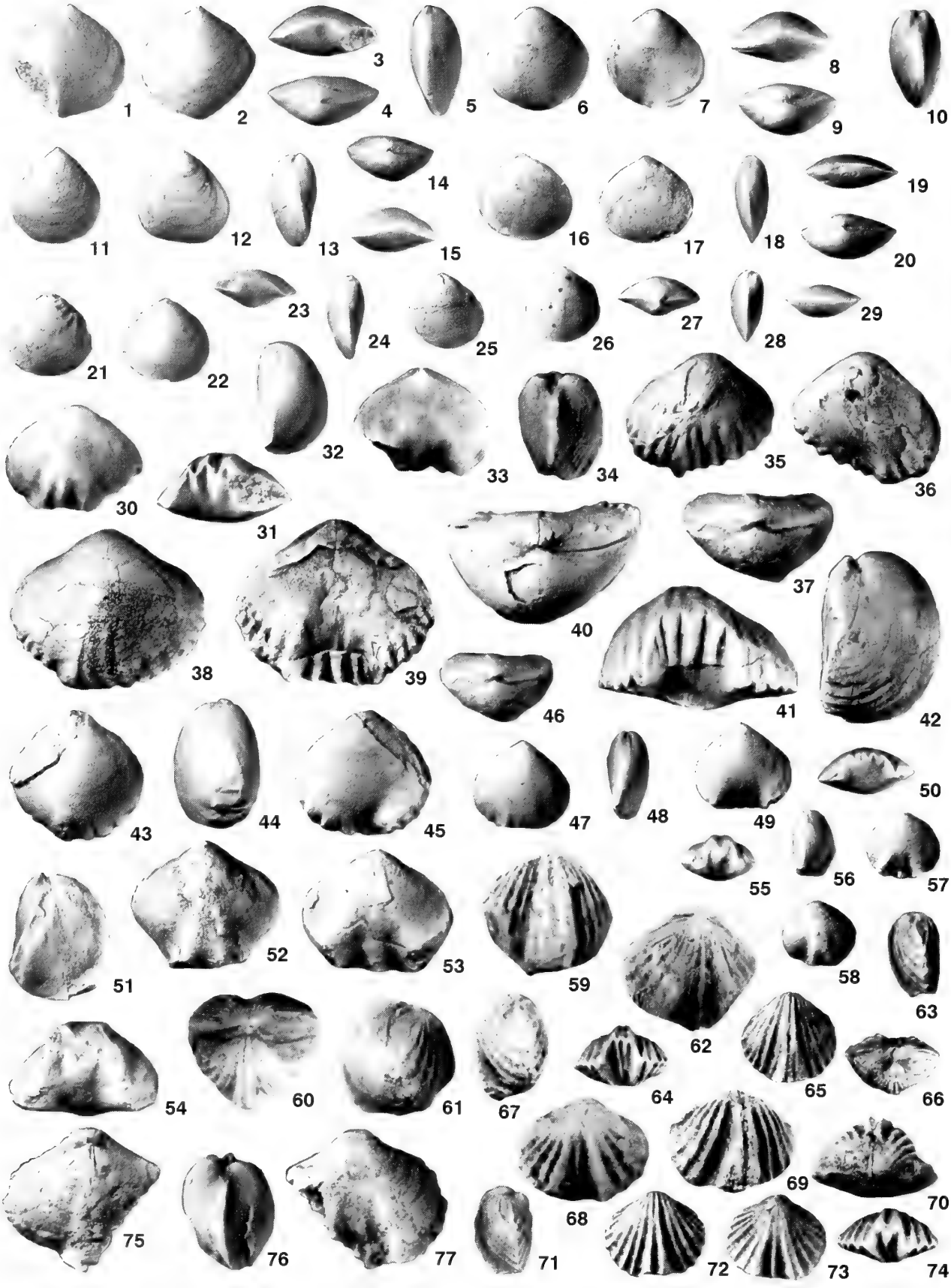
1
2
3
4
5
6
7
8
9
10
11
12
13
14
15
16
17
18
19
20
21
22
23
24
25
26
27
28
29
30
31
32
33
34
35
36
37
38
39
40
41
42
43
44
45
46
47
48
49
50
51
52
53
54
55
56
57
58
59
60
61
62
63
64
65
66
67
68
69
70
71
72
73
74
75
76
77

DESCRIPTION. Shell smooth, dorsibiconvex, subpentagonal in outline, about 70% as thick as long and 95% as long as wide. Anterior commisure sulciplicate. Ventral valve gently convex in lateral profile with maximum thickness about one-third valve length from the small, slightly erect pointed beak posterior to the hinge line. Sulcus about 60% as wide as the valve, originating in the umbonal area at about 4–5 mm from the beak, strongly deepening anteriorly and divided medianly by high angular costa originating near mid-valve. Dorsal valve strongly and evenly convex with maximum thickness at mid-valve with median fold originating slightly anterior to mid-valve and bearing two strong angular ribs.

Ventral interior with small teeth and deep, narrow spondylium on the low median septum. Dorsal interior with narrow cruralium raised anteriorly on a low median septum extending anteriorly not more than 1.5 mm in adults. Inner plates small, thickened, slightly curved in cross-section. Brachial processes short.

MEASUREMENTS. (471/12375) conjoined valves, L=14.0, W=16.9, T=6.3, Sw=8.9; (474/12375) conjoined valves, L=20.4, W=21.0, T=11.2, Sw=8.7; (475/12375) conjoined valves, L=22.9, W=24.5, T=10.2, Sw=12.8; (476/12375) conjoined valves, L=16.5, W=19.8, T=6.5, Sw=11.2; (479/12375) conjoined valves, L=10.5, T=6.7, Sw=6.7.

DISCUSSION. This species usually occurs in the upper Anderken Formation together with *Parastrophina iliana*, but can be easily distinguished in being half the size, in the smooth shell with a single costa in the sulcus and two in the fold of mature specimens, and in the sulciplicate anterior commissure.

Parastrophina plena closely resembles *Parastrophina uniplicata* Fu, 1982 from the Jinhe Formation (Caradoc) of northwest China in its smooth shell, sulciplicate anterior commissure, and in the characters of the dorsal fold and ventral sulcus. They may be conspecific.

Genus ***ILISTROPHINA*** Gen.nov.

TYPE SPECIES. *Ilistrophina tesikensis* sp.nov.

DIAGNOSIS. Shell smooth, ventribiconvex with well-developed dorsal median fold and ventral sulcus; ventral interior with spondylium sessile posteriorly, raised anteriorly on low median septum; dorsal interior with cruralium supported by high median septum; well defined alate plates and long brachial processes.

DISCUSSION. Externally *Ilistrophina* is most similar to *Eostrophina* (Zhan & Rong 1995) but differs in having a narrow spondylium sessile posteriorly, raised anteriorly on a low median septum and well developed alate plates. It differs from *Liostrophia* in having strongly raised cruralium supported by a median septum instead of a sessile cruralium or separated outer plates; however, present knowledge of the interior of type species of the former remains inadequate. *Ilistrophina* resembles *Parastrophina* and *Parastrophinella* in the interior morphology of both valves, but differs in having a smooth shell and a sessile spondylium posteriorly. Jin and Copper (1997) demonstrated that in *Parastrophinella* the cruralium is supported by the median septum along its entire length, but, in contrast to *Ilistrophina*, the dorsal median septum in *Parastrophinella* is very low and buried within secondary shell in the apical area.

Ilistrophina tesikensis sp. nov.

Pl. 12. figs 28–35; Figs 15, 17

ETYMOLOGY. After the type locality.

HOLOTYPE. BC 56823, Pl. 12, figs 32–35, conjoined valves, from Sample 948, Tesik River.

MATERIAL. 14 pairs of conjoined valves (including BC 56823–24) and one dorsal valve, all from Sample 948, Tesik River.

DESCRIPTION. Shell smooth, dorsibiconvex, subcircular in outline,

Table 25 Measurements of ventral valves of *Ilistrophina tesikensis* sp. nov., Sample 948, Tesik river.

	L	W	T	Ld	Sw	St	L/W	T/L	Ld/W	Sw/W
N	9	9	9	9	9	8	9	9	9	9
X	7.5	8.2	5.1	7.5	5.7	3.9	92.3%	68.2%	92.2%	70.2%
S	1.01	1.46	0.82	0.98	0.96	0.94	4.7	6.6	4.9	5.4
MIN	6.2	6.4	4.2	6.2	4.6	2.4	83.8%	58.3%	82.9%	63.9%
MAX	9.8	11.7	6.8	9.7	7.8	5	97.5%	79.4%	97.5%	80.7%

PLATE 13

Figs 1–29 *Liostrophia pravula* sp. nov., Akchoku Mountain, Kujandysai section. **1–15**, Sample 8256; **1–5,** BC 57550, conjoined valves, ventral, dorsal, anterior, posterior and lateral views, × 2; **6–10**, BC 57551, conjoined valves, dorsal, ventral, anterior, posterior and lateral views, × 2; **11–15**, BC 57552, conjoined valves, dorsal , ventral, lateral, posterior and anterior views, × 2. **16–29**, Sample 2538; **16–20,** BC 57553, **holotype**, conjoined valves, dorsal, ventral, lateral, anterior and posterior views, × 2; **21–24**, BC 57554, conjoined valves, ventral, dorsal, anterior and lateral views, × 2; **25–29**, BC 57555, conjoined valves, ventral, dorsal, posterior, lateral and anterior views, × 2.

Figs 30–50 *Parastrophina iliana* sp.nov. **30–33**, Sample 8217, Kujandysai section, BC 57556, conjoined valves, dorsal, anterior, lateral and ventral views, × 2. **34–37**, Sample 2538, Kujandysai section, CNIGR 4/12361, conjoined valves, lateral, dorsal, ventral and posterior views, × 2. **38–42**, Sample 100, Anderkenyn-Akchoku section, BC 57557, **holotype**, conjoined valves, dorsal, ventral, posterior, anterior and lateral views, × 2. **43–46**, Sample 8256, Kujandysai section, BC 57558, conjoined valves, dorsal, lateral, ventral and posterior views, × 2. **47–50**, Sample 628, Kujandysai section, BC 57559, conjoined valves, dorsal, lateral, ventral and anterior views, × 2.

Figs 51–58 *Parastrophina plena* Sapelnikov & Rukavishnikova, 1975. **51–54**, Sample 2538, Kujandysai section, BC 57562, conjoined valves, lateral, dorsal, ventral and anterior views, × 2. **55–58**, Sample 8214, Anderkenyn-Akchoku section, BC 57563, conjoined valves, anterior, lateral, ventral and dorsal views, × 2.

Figs 59–74 *Plectosyntrophia unicostata* sp. nov., Anderkenyn-Akchoku section. **59–62, 67–70**, Sample 626; **59–62,** BC 57568, conjoined valves, dorsal, posterior, lateral, and ventral views, × 2; **67–70**, BC 57570, conjoined valves, **holotype**, lateral, ventral, dorsal and posterior views, × 2. **63–66, 71–74**, Sample 100; **63–66,** BC 57569, conjoined valves, lateral, anterior, dorsal and posterior views, × 2; **71–74**, BC 57571, conjoined valves, lateral, dorsal ventral and anterior views, × 2.

Figs 75–77 *Didymelasma* cf. *transversa* Fu, Sample 2538, Kujandysai section, BC 57573, conjoined valves, dorsal, lateral and ventral views, × 2.

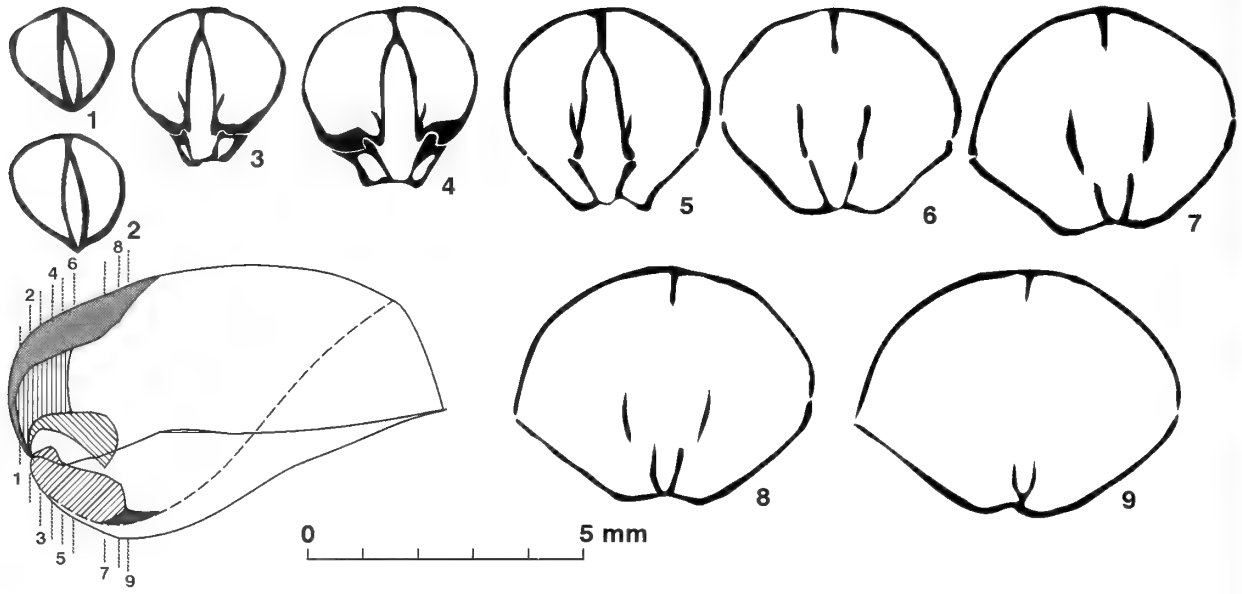

Fig. 17 Transverse serial sections of *Ilistrophina tesikensis* gen. et sp. nov., BC 57606, Sample 948, Tesik River. Distance in mm is measured from the posterior tip of ventral beak (dorsal valve uppermost), also an axial diagram showing the plates.

about 65% as high as long and 90% as long as wide with maximum width at mid-length. Anterior commissure strongly uniplicate. Ventral valve gently convex in lateral profile with maximum thickness somewhat posterior to mid-length. Beak small, curved towards the hinge line. Sulcus originating about 4–5 mm from the umbo, strongly deepening anteriorly and terminating with a high semioval tongue about 70% valve width. Dorsal valve with moderately convex lateral profile. Beak slightly swollen, curved. Dorsal median fold originating anterior to mid-length, semioval in cross-section.

Ventral interior with small teeth and narrow spondylium, bell-shaped in cross-section, sessile posteriorly and raised anteriorly on a low, thick median septum extending to mid-valve length. Dorsal interior with cruralium supported by high median septum along its entire length. Inner plates present.

MEASUREMENTS. conjoined valves, Lv=9.8, W=11.7, T=6.8, Sw=7.8, St=4.0; conjoined valves, Lv=7.8, W=8.2, T=5.7; Sw=5.5, St=4.7.

DISCUSSION. This species is externally comparable to *Eostrophina uniplicata* from the Middle Ashgill Xiazhen Formation of South China, but can be easily distinguished in its smaller size, which does not exceed 10 mm in length in the largest specimens, and in having a dorsal median fold evenly rounded in cross-section and originating anteriorly to the mid-valve.

Genus ***LIOSTROPHIA*** Cooper & Kindle, 1936

TYPE SPECIES. *Liostrophia glabra* Cooper & Kindle, 1936, from the Ashgill of Canada.

Liostrophia pravula sp. nov. Pl. 13, figs 1–29; Fig. 18

ETYMOLOGY. After *pravus*, Latin – bowed.

HOLOTYPE. BC 57553, pl. 13, figs 16–20, conjoined valves, from the Anderken Formation, Sample 2538, Akchoku Mountain, Kuyandysai section.

MATERIAL. 30 pairs of conjoined valves, one ventral and 7 dorsal valves, from Samples 100 (=K-98/1970) (BC 57253–56), 626 (BC 57263–65), 8223, Anderkenyn-Akchoku section; Samples 2538 (BC 57266–69, 57553–55), 8256 (BC 57550–52), Kuyandysai section; Sample 948 (BC 57257–62), Tesik River.

DESCRIPTION. Shell slightly dorsibiconvex, transverse, subcircular in outline, about 51% as thick as long and 90% as long as wide, with maximum width at mid-length. Anterior commissure gently uniplicate. Ventral valve gently convex in lateral profile, with maximum thickness somewhat posterior to mid-length. Small, pointed beak, slightly erect and posterior to hinge line. Broad shallow sulcus, originating near the anterior margin, usually asymmetrical in cross-section. Dorsal valve moderately and evenly convex in profile with slightly swollen, curved beak. Dorsal median fold usually absent but weakly developed anteriorly in mature specimens. Shell surface smooth with one or two ribs in the fold and sulcus near the anterior margin of the largest specimens.

Ventral interior with teeth and spondylium supported anteriorly by very low septum enclosed posteriorly by a secondary shell thickening (Fig. 18). Dorsal interior with sessile cruralium formed by high outer plates joined at the valve floor. Alate plates small, appearing at some distance from the umbo. Inner plates small, slightly thickened, strongly curved in cross-section with the outer parts located almost within comissural plane. Brachial processes thin and relatively long.

MEASUREMENTS. (518/12375) conjoined valves, L=7.6, W=7.9,

Table 26 Measurements of ventral valves of *Liostrophia pravula* sp. nov., Sample 2538, Kujandysai section.

	L	W	T	Sw	St	L/W	T/L	Sw/W
N	11	11	11	10	10	9	9	9
X	5.7	6.3	2.9	4.1	1.5	89.7%	50.9%	61.8%
S	1.45	1.56	1.05	0.75	0.18	7.6	6.3	3.7
MIN	3.3	3.5	1.3	3.2	1.2	81.5%	42.6%	57.1%
MAX	8.2	9.2	5.1	5.7	1.8	103.8%	62.2%	70.2%

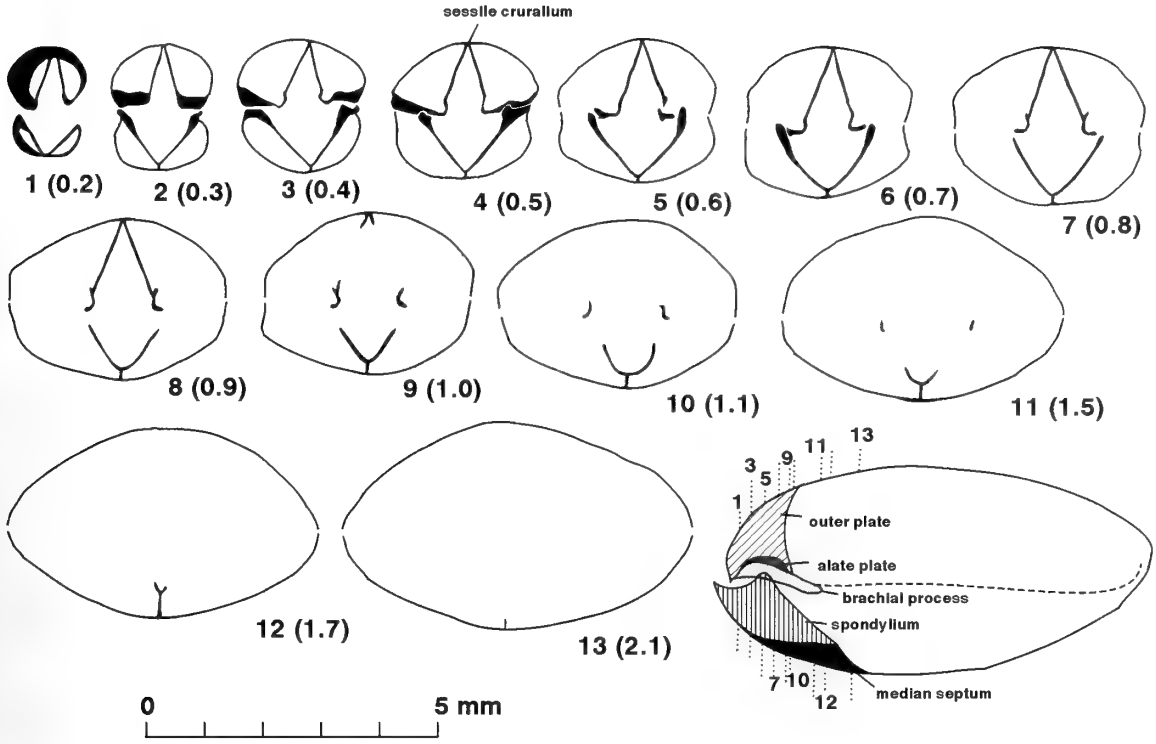

Fig. 18 Transverse serial sections of *Liostrophia pravula* sp.nov., Sample 2538, Kujandysai section. Distance in mm is measured from the posterior tip of ventral beak. Dorsal valve uppermost. Also lateral view to show section positions and schematic reconstruction.

T=3.4; (519/12375) conjoined valves, L=5.2, W=5.7, T=2.0; (520/12375) conjoined valves, L=7.9, W=7.9, T=3.2; (521/12375) conjoined valves, L=8.7, W=8.2, T=4.1; (522/12375) conjoined valves, L=5.8, T=6.3, Sw=3.7.1; (523/12375) conjoined valves, L=10.6, T=10.5, Sw=4.7.

DISCUSSION. This species differs from *Liostrophia glabra* Cooper & Kindle in having a subcircular outline, weak ventral sulcus and in the absence of a dorsal median fold. The characters of the dorsal interior in the type species remain inadequately known. In particular it is unclear from the existing illustrations whether or not it has a sessile cruralium or if it is supported anteriorly by a very short septum. In external morphology, particularly in the smooth, rounded shell with an uniplicate anterior commissure but without a distinct dorsal median fold, *Liostrophia pravula* resembles *Psilocamera planisulcata* Fu, 1982 from the the Jinhe Formation (Caradoc) of north-west China. However, in the single transverse section provided by Fu (1982, text-fig. 18A) the outer plates appear to be completely separate and there are no alate plates or inner plates illustrated.

Liostrophia pravula differs from juvenile specimens of *Ilistrophina tesikensis* not only in its larger size and sessile cruralium (which hardly exceeds half the maximum length), but also in the absence of a dorsal median fold. A ventral sulcus is present in *Ilistrophina tesikensis* when specimens are 4–5 mm long, whereas in *Liostrophia pravula* it is visible only in mature specimens which exceed the average shell size of about 6 mm.

Table 27 Measurements of ventral valves of *Plectosyntrophia unicostata* sp. nov., samples 100 and 626 from Anderkenyn-Akchoku section.

	L	W	T	St	Sw	L/W	T/L	Sw/W
N	6	6	6	6	6	6	6	6
X	9.5	10.7	7.2	4.0	5.8	89.4%	74.1%	156.2%
S	1.37	2.10	2.77	1.87	1.82	4.6	18.3	28.4
MIN	7.8	8.4	4.6	2.2	3.5	82.9%	59.0%	119.6%
MAX	11	13.2	11.2	6.5	7.9	92.9%	101.8%	177.1%

Subfamily **ANASTROPHIINAE** Nikiforova, 1960
Genus ***PLECTOSYNTROPHIA*** Fu, 1982

TYPE SPECIES. *Plectosyntrophia qilianshanensis* Fu, 1982, from the Yingou Group (Middle Ordovician) of North China.

Plectosyntrophia unicostata sp. nov.
Pl. 13, figs 59–74; Fig. 19

HOLOTYPE. BC 57570, Pl. 13, figs 67–70, conjoined valves from Sample 626, Anderkenyn-Akchoku section.

MATERIAL. Seven pairs of conjoined valves and one dorsal valve from Samples 100 (=K-98/1970) (BC 57569, 71), 620 (BC57360), 626 (BC 57271–73, 57568, 70, 72), 8214 (BC 57361), Anderkenyn-Akchoku section; Samples 2538, 8217 (BC 57362), Kujandysai Section.

DESCRIPTION. Shell subequally biconvex, transverse, subpentagonal in outline, about 75% as thick as long and about 89% as long as wide with maximum width slightly anterior to mid-length. Anterior commissure uniplicate. Ventral valve moderately convex with curved beak slightly raised above a narrow triangular, apsacline interarea. Ventral sulcus narrow and shallow, but with steep lateral

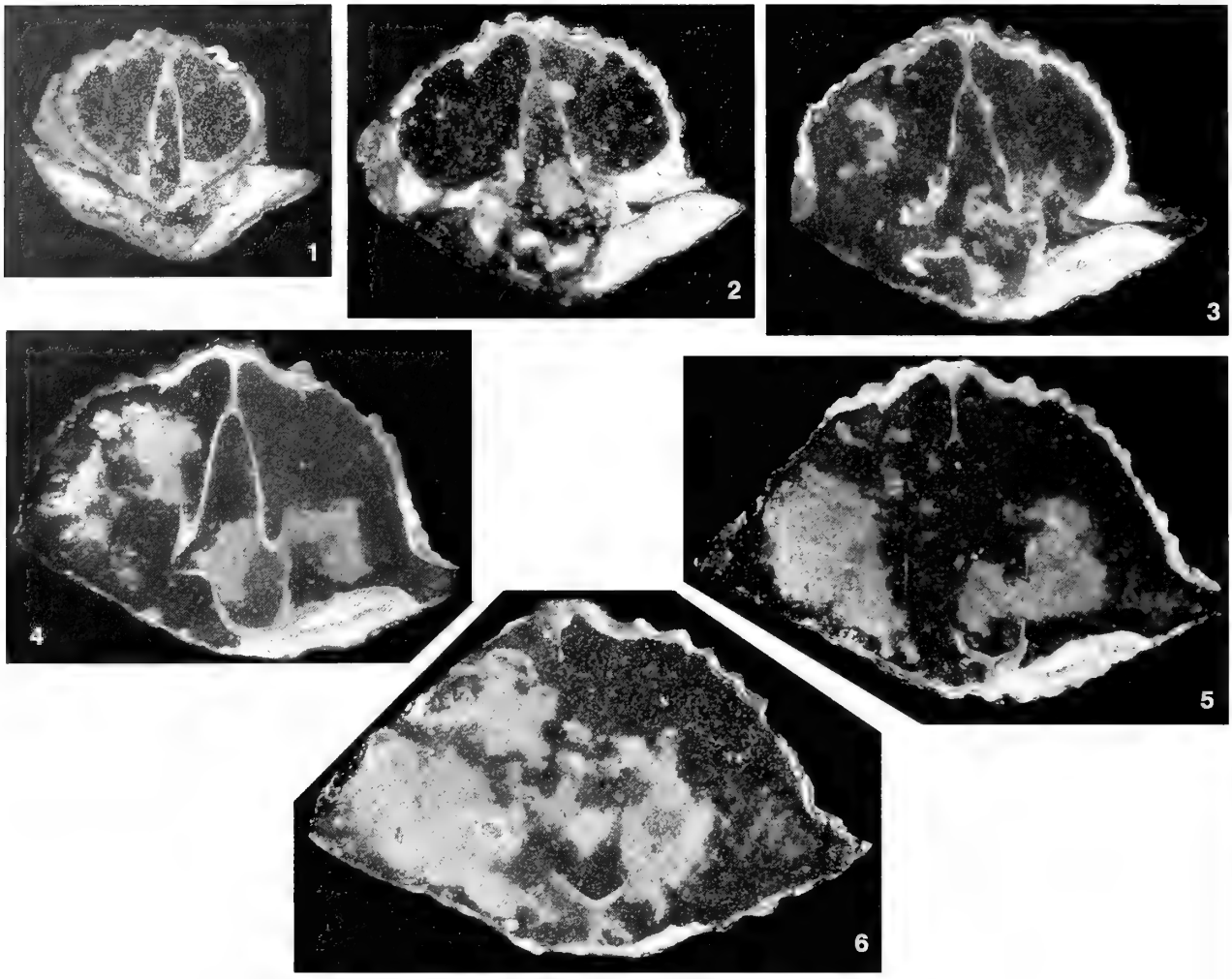

Fig. 19 Photographs of transverse serial sections of *Plectosyntrophia unicostata* sp. nov., BC 57572, from Sample 626, Anderkenyn-Akchoku section; × 12. Distance in mm is measured from the posterior tip of ventral beak. Dorsal valve uppermost.

slopes, originating slightly posteriorly to mid-valve, and ending with a shallow, narrow, trapezoidal tongue about 40% valve width. Dorsal valve strongly convex in lateral profile with maximum thickness near mid-length. Beak slightly swollen and strongly curved towards the hinge line. A low, flattened median fold originates from the umbo. Radial ornament mainly costate, with occasional bifurcating ribs and with 1 primary rib in the sulcus, 2 primary ribs in the median fold and 6–9 on the lateral slopes of the valves. In some specimens one or two small secondary costellae originate in the median fold and dorsal sulcus between the umbo and mid-length. Ventral interior with strong teeth; bell-shaped spondylium in transverse section, sessile posteriorly and raised anteriorly on a low median septum partly covered by secondary shell (Fig. 19). Dorsal interior with narrow cruralium on a high median septum extending anteriorly up to 3 mm in adults. Inner plates narrow, curved; alate plates narrow, bordered laterally by a pair of high subparallel muscle bounding ridges.

MEASUREMENTS. (CNIGR 471/12375) conjoined valves, L=14.0, W=16.9, T=6.3, Sw=8.9; (474/12375) conjoined valves, L=20.4, W=21.0, T=11.2, Sw=8.7; (475/12375) conjoined valves, L=22.9, W=24.5, T=10.2, Sw=12.8; (476/12375) conjoined valves, L=16.5, W=19.8, T=6.5, Sw=11.2; (479/12375) conjoined valves, L=10.5, T=6.7, Sw=6.7.

DISCUSSION. The generic attribution of *unicostata* is tentative because the interior of *Plectostrophia qilianshanensis* is inadequately known. In particular, there is no record of the presence of alate plates in the type species, but some illustrations provided in the original description (Fu 1982, text-fig. 17) suggest their presence. The characters of the ventral interior, in particular the presence of a sessile spondylium slightly raised near its anterior margin on a short septum, also needs confirmation, because Fu's illustrations are schematic and it could be a preservational pattern. In the Kazakh species alate plates are well defined, whereas the sessile spondylium is present only in the earliest ontogenetic stages and is characterised by a spondylium supported by a low median septum partly covered by secondary shell. *Plectosyntrophia qilianshanensis* has 3 ribs in the ventral sulcus and 4 in the dorsal fold, which makes it more similar to *Eoanastrophia kurdaica* than to our species.

P. unicostata differs from *Eoanastrophia kurdaica* Sapelnikov & Rukavishnikova (1975) from the Keskentas Formation (Caradoc), of the Kendyktas Range, south Kazakhstan, in having a more pronounced dorsal median fold with two primary ribs and a ventral

sulcus with a single accentuated primary rib originating in the umbonal area. The coarsely ribbed radial ornament, well defined dorsal median fold and ventral sulcus resembles numerous species of *Plectocamara* described by Cooper (1956) from the Caradoc of North America, but there is no evidence of the presence of alate plates in the former genus.

Family **PARALELLELASMATIDAE** Cooper, 1956
Genus ***SCHIZOSTROPHINA*** Fu, 1982

TYPE SPECIES. *Schizostrophina margarita* Fu, 1982, from the Jinhe Formation (Caradoc), northwest China.

DIAGNOSIS (emended). Shell equally biconvex with parasulcate anterior commissure; shallow ventral median sulcus and dorsal median fold originating in umbonal area; radial ornament of variably developed coarse angular ribs in posterior half of the shell; ventral interior with delicate teeth and spondylium supported posteriorly and free anteriorly; dorsal interior with separated outer plates, slightly diverging distally, and well-defined brachial processes.

DISCUSSION. *Schizostrophina* was erected originally by Fu (1982) without proper illustrations and detailed description of the interior in the type species. However, the very distinctive exterior morphology of the shell, which is unique in late Ordovician syntrophiidines, leaves no doubt that the Kazakh shells from the Anderken Formation belong to the same genus and species. Their internal morphology confirms the original assignment of the genus to the Paralellelasmatidae and suggests a close affinity to *Paralellelasma*, but *Schizostrophina* lacks the radial capillae and the characteristic truncated margins of the ribs along the commissure of the former genus. Another difference is the parasulcate anterior commissure.

Schizostrophina margarita Fu, 1982
Pl. 14, figs 2–27; Fig. 20

1982 *Schizostrophina margarita* Fu: 132, pl. 37, fig. 5.
1982 *Schizostrophina shaanxiensis* Fu: 133, pl. 37, fig. 6.

MATERIAL. 26 pairs of conjoined valves, 6 ventral and 4 dorsal valves from Samples 100 (=K-98/1970) (BC 57275–7), 626 (BC 57279–81), 8223, Anderkenyn-Akchoku section; Samples 628, 2538 (BC 57282–92, 57574–78), 8219 (BC 57294), 8220 (BC 57295), 8256 (BC 57296–9), Kujandysai Section.

DESCRIPTION. Shell equally biconvex, subpentagonal to subtriangular in outline; about as long as wide, with maximum width anterior to mid-valve. Anterior commissure parasulcate. Beaks of both valves swollen and strongly curved. Ventral valve moderately

Table 28 Measurements of ventral valves of *Schizostrophina margarita* Fu, Samples 626, 2538, 8256 from Anderkenyn-Akchoku and Kujandysai sections.

	L	W	T	Sw	St	L/W	T/L	Sw/W	Ld/W	Sw/W
N	18	18	18	17	3	18	18	17	9	9
X	5.8	6.2	4.2	4.3	4.3	94.8%	71.4%	71.7%	92.2%	70.2%
S	1.24	1.68	1.25	1.55	0.92	6.0	9.3%	14.5	4.9	5.4
MIN	3.6	3.7	2.1	2.6	3.2	79.6%	54.5%	45.2%	82.9%	63.9%
MAX	8.0	9.8	6.2	7.8	4.8	102.2%	90.4%	100.0%	97.5%	80.7%

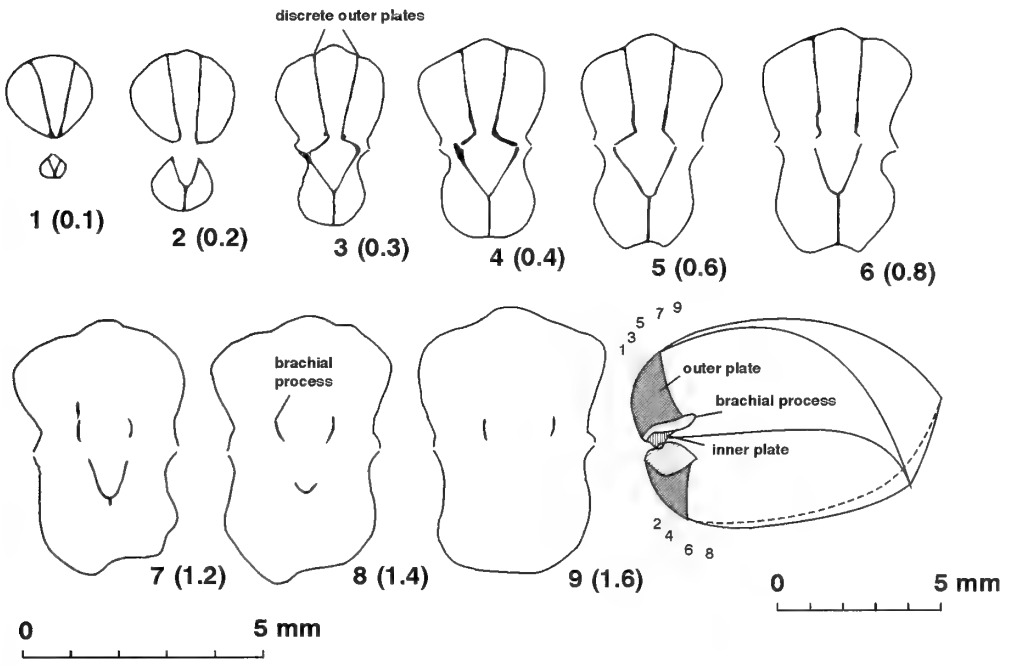

Fig. 20 Transverse serial sections of *Schizostrophina margarita* Fu, Sample 2538, Kujandysai section. Distance in mm is measured from the posterior tip of ventral beak. Dorsal valve uppermost. Also lateral view to show section positions and schematic reconstruction.

convex in lateral profile with maximum thickness slightly posterior to mid-valve. Ventral sulcus originating near the umbo, broad and shallow with low trapezoidal tongue slightly inclined anteriorly. Lateral slopes steep, slightly convex in cross-section. Dorsal valve with moderately convex lateral profile strongly curved posteriorly. Median fold shallow, slightly rounded in transverse section, originating near the beak, flanked by two strong plications. Radial ornament with angular ribs originating near mid-length, 1–3 ribs in the sulcus and 2–4 in the median fold. Pair of ribs occasionally on the lateral slopes of both valves. Ventral interior with deep, narrow spondylium about one-sixth valve length, supported posteriorly by high median septum, free anteriorly. Dorsal interior with separated outer plates, slightly diverging distally, short subtriangular brachial plates and well-defined brachial processes.

MEASUREMENTS. conjoined valves, L=7.9, W=8.6, T=5.9, Sw=6.9; conjoined valves, L=9.8, W=11.2, T=6.7, Sw=8.2; conjoined valves, L=7.8, W=8.2, T=6.2, Sw=6.8; conjoined valves, L=6.8, W=7.2, T=6.2, Sw=5.4; conjoined valves, L=5.7, W=5.8, T=3.4, Sw=4.6.

DISCUSSION. *Schizostrophina margarita*, the type species of the genus, came from the same unit and locality, the Jinhe Formation (Lower Caradoc) of north-west China, as *S. shaanxiensis* and differs from the latter in having a single poorly defined rib in the ventral sulcus and smooth lateral sides of the valve. The Kazakh shells demonstrate a strong variability in the number and characters of radial ornament with growth. The small shells (about 5–6 mm long) usually lack ribs on the lateral sides of the shell, and the radial ornament in the ventral sulcus and dorsal fold is poorly developed or absent (Pl.14, figs 22–24), whereas mature specimens possess a radial ornament closely comparable to one of the specimens referred by Fu (1982) to *S. shaanxiensis*. This suggests that all the shells described by Fu represent a single species, which should be termed *S. margarita*. Since there appear to be no constant morphological differences between the Kazakh and Chinese specimens of *Schizostrophina*, they are regarded here as conspecific.

Genus ***DIDYMELASMA*** Cooper, 1956

TYPE SPECIES. *Didymelasma longicrurum* Cooper, 1956 from the Lebanon Formation (Caradoc), Tennessee, U.S.A.

Didymelasma* cf. *transversa Fu, 1982
Pl. 13, figs 75–77, Pl. 14, fig. 1

MATERIAL. One pair of conjoined valves, BC 57573, from Sample 2538, Kujandysai Section; one dorsal internal mould (BC 57366) from Sample 1018, 7 km southwest of Karpkuduk well, Kotnak Mountains.

DESCRIPTION. Shell smooth, subequally biconvex, transverse to suboval in outline with uniplicate posterior commissure. Ventral valve lateral profile moderately convex with maximum thickness about one-third valve length. Ventral beak swollen and slightly curved. Sulcus originating near mid-length, strongly deepening towards the anterior margin, with low median rib. Tongue semielliptical. Dorsal valve moderately convex in lateral profile with maximum thickness at about two-thirds valve length. Median fold originating somewhat posteriorly to mid-valve, clearly separated from the slightly convex lateral sides of the valve. Ventral interior unknown, except for median septum, possibly supporting spondylium. Dorsal interior with separated, long, subparallel outer plates.

MEASUREMENTS. conjoined valves, L=13.4, T=8.2.

DISCUSSION. The Kazakh specimens closely resemble *Didymelasma transversa* Fu, 1982, from the Caradoc Jinhe Formation of northwest China, in the external features of their smooth shells, including the shape of the dorsal median fold and ventral sulcus, but our material is insufficient to make a precise attribution to this species. Fu (1982, text-fig. 23) also demonstrated the presence of separated, subparallel outer plates in the Chinese shells, which supports their assignation to *Didymelasma*.

Order **RHYNCHONELLIDA** Kuhn, 1949
Superfamily **RHYNCHOTREMATOIDEA** Schuchert, 1913
Family **RHYNCHOTREMATIDAE** Schuchert, 1913
Genus ***RHYNCHOTREMA*** Hall, 1860

TYPE SPECIES. *Atrypa increbescens* Hall, 1847, from the Trenton Formation (Caradoc), New York, U.S.A.

Rhynchotrema akchokense sp. nov. Pl. 14, figs 28–42

ETYMOLOGY. After Akchoku Mountain on the east side of Kopalysai.

HOLOTYPE. BC 57579, Pl. 14, figs 28–32, conjoined valves, from the Anderken Formation, Sample 626, Anderkenyn-Akchoku section.

MATERIAL. 11 conjoined valves, five ventral and six dorsal valves

PLATE 14

Fig. 1 *Didymelasma* cf. *transversa* Fu, Sample 1018, area 7 km SW of Karpkuduk well, Kotnak Mountains, BC 57366, dorsal internal mould, × 2.

Figs 2–27 *Schizostrophina margarita* Fu, Sample 2538, Kujandysai section. **2–6**, BC 57574, conjoined valves, dorsal, ventral, posterior, lateral and anterior views, × 3. **7–9, 11, 14**, BC 57575, conjoined valves, anterior, dorsal, ventral, lateral and posterior views, × 3. **10, 12, 15–17**, BC 57576, conjoined valves, anterior, posterior, dorsal, lateral and ventral views, × 3. **13,** CNIGR 5/12361, dorsal exterior, × 3. **18–22**, BC 57577, conjoined valves, lateral , dorsal, ventral, anterior and posterior views, × 3. **23–27**, BC 57578, conjoined valves, ventral , dorsal, lateral, posterior and anterior views, × 3.

Figs 28–42 *Rhynchotrema akchokense* sp. nov. **28–32, 38–41**, Sample 626, Anderkenyn-Akchoku section; **28–32,** BC 57579, conjoined valves, **holotype**, ventral, lateral, dorsal, posterior and anterior views, × 2; **38–41**, BC 57582, conjoined valves, dorsal, ventral, anterior and lateral views, × 3. **33–36**, Sample 2538, Kujandysai section, BC 57580, conjoined valves, anterior, dorsal, ventral and lateral views, × 2. **37, 42**, Sample 843, Anderkenyn-Akchoku section; **37,** BC 57581, ventral internal mould, × 3; **42**, BC 57583, dorsal internal mould, × 5.

Figs 43–46 *Pectenospira pectenata* Popov, Nikitin & Sokiran, Sample 948, Tesik River, BC 57320, dorsal, anterior, ventral and lateral views of conjoined valves, × 5.5.

Figs 47–57 *Nikolaispira guttula* sp.nov. **47–53**, Sample 2538, Kujandysai section; **47–49,** BC 57584, conjoined valves, anterior, dorsal and ventral views, × 3; **50–53**, BC 57585, conjoined valves, **holotype**, ventral, anterior, lateral and dorsal views, × 3. **54–57**, Sample 8221, Anderkenyn-Akchoku section, BC56770, conjoined valves, anterior, ventral, dorsal and lateral views, × 4.

Figs 58–61 *Kellerella misiusi* Popov, Nikitin & Sokiran, Sample 8214, Anderkenyn-Akchoku section. BC 56773, conjoined valves, anterior, ventral, lateral and dorsal views, × 3.

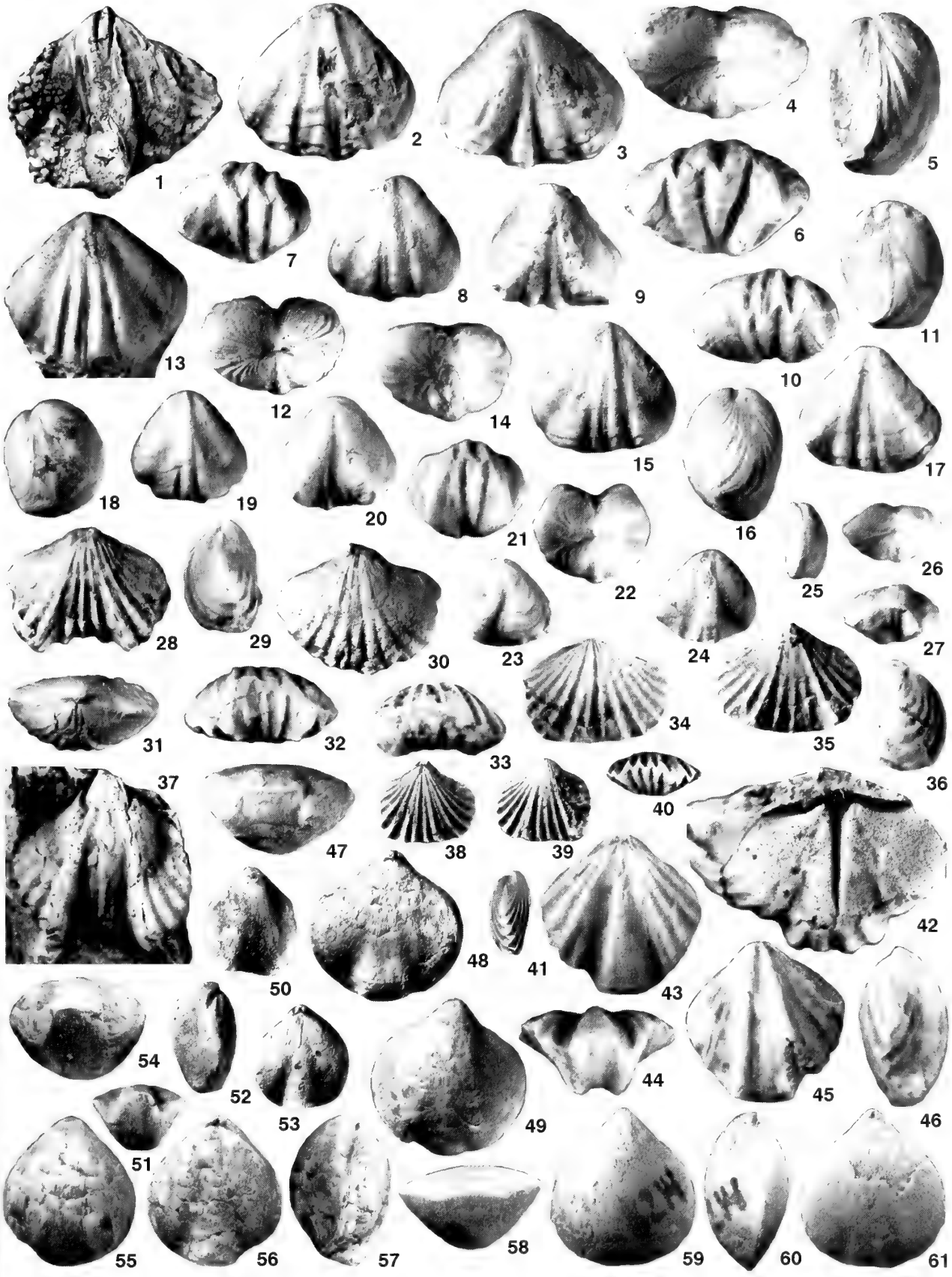
1
2
3
4
5
6
7
8
9
10
11
12
13
14
15
16
17
18
19
20
21
22
23
24
25
26
27
28
29
30
31
32
33
34
35
36
37
38
39
40
41
42
43
44
45
46
47
48
49
50
51
52
53
54
55
56
57
58
59
60
61

from Samples 100 (=K-98/1970) (BC 56656–9), 626, 843 (BC 57581–83), Anderkenyn-Akchoku section; Samples 628 (BC 56661), 2538 (BC 57580), 7613 (BC 56649–55), Kujandysai Section; Sample 948 (BC 57311–2), Tesik River.

DESCRIPTION. Shell dorsibiconvex to biconvex, slightly transverse, about 73% as thick as long and about 75% as long as wide with maximum width at mid-length. Anterior commissure uniplicate. Ventral valve moderately convex in lateral profile with maximum thickness at quarter valve length from the slightly curved, pointed beak. Delthyrium open, narrow triangular. Ventral sulcus originating 2–3 mm from the umbo, very shallow posterior to mid-valve, but deepening anteriorly and terminating in low, trapezoidal tongue about 79% valve width. Dorsal valve moderately and evenly convex in lateral profile with shallow umbonal sulcus inverting into a low flattened median fold with steep lateral slopes. Radial ornament of coarse angular ribs, usually with 4 ribs in the dorsal median fold, 3 ribs in the sulcus and 6–8 on flanks of both valves.

Ventral interior with cyrtomatodont teeth and short, thin dental plates flaring close to the sides of the valve. A pedicle base impression occupies the floor of the delthyrial cavity; large, weakly impressed ventral muscle field with small, lanceolate adductor scars completely surrounded by diductor scars anteriorly. Dorsal interior with disjunct hinge plate and narrow cruralium bearing a simple, ridge-like cardinal process and long, high median ridge extending anteriorly to mid-valve. Adjustor scars weakly impressed with posterior and anterior pair of about equal size, separated by fine, oblique transmuscle ridges.

MEASUREMENTS. (471/12375) conjoined valves, L=14.0, W=16.9, T=6.3, Sw=8.9; (474/12375) conjoined valves, L=20.4, W=21.0, T=11.2, Sw=8.7; (475/12375) conjoined valves, L=22.9, W=24.5, T=10.2, Sw=12.8; (476/12375) conjoined valves, L=16.5, W=19.8, T=6.5, Sw=11.2; (479/12375) conjoined valves, L=10.5, T=6.7, Sw=6.7.

DISCUSSION. Rhynchonellides are widespread in the mid and late Ordovician shallow-water benthic assemblages of Kazakhstan, but with few exceptions are represented exclusively by ancystrorhynchids and oligorhynchids (Nikiforova & Popov 1981; Nikitin & Popov *in* Klenina *et al.* 1984). All other Kazakh rhynchonellide species previously described as *Rhynchotrema* by Rukavishnikova (1956) and Klenina (*in* Klenina *et al.*1984) belong in reality to the ancystrorhynchid *Altaethyrella* or atrypides related to *Nalivkinia* (Popov *et al.* 2000). This species represents the earliest known record of rhynchonellides with the cruralium supported by the dorsal median septum in Kazakstan. Externally it is similar to *Rostricellula sarysuica* Nikitin & Popov (Nikitin *et al.* 1996) from the Upper Caradoc to Lower Ashgill Dulankara Regional Stage of the northern Betpak-Dala Desert, Kazakhstan, but differs in the less convex lateral profile of the dorsal valve, with maximum height at mid-length, the relatively shallow ventral sulcus, and in the presence of a ridge-like cardinal process.

Rhynchotrema akchokense is similar in radial ornament to two Australian species of the genus, *R. oepiki* Percival, 1991, from the Upper Caradoc of New South Wales, and *R. bailliei* Laurie, 1991, from the Caradoc of Tasmania, in having a more transverse shell outline, a less convex dorsal valve profile, with maximum height near the mid-length, a relatively shallow ventral sulcus and a low dorsal median fold. *R. bailliei* is also characterized by its poorly developed cardinal process, which makes its generic assignment somewhat questionable, although we refer it to *Rhynchotrema*.

Order **ATRYPIDA** Rzhonsnitskaya, 1960
Superfamily **LISSATRYPOIDEA** Twenhofel, 1914
Family **PROTOZYGIDAE** Copper, 1986
Genus ***PECTENOSPIRA*** Popov, Nikitin & Sokiran, 1999

TYPE SPECIES. *Pectenospira pectenata* Popov, Nikitin & Sokiran, 1999, from the Anderken Formation, Chu-Ili Range.

Pectenospira pectenata Popov, Nikitin & Sokiran, 1999
Pl. 14, figs 43–46

1999 *Pectenospira pectenata* Popov, Nikitin & Sokiran: 648, pl. 4, figs 21–32, text-fig.10.

HOLOTYPE. CNIGR 23/12986, conjoined valves, from the Anderken Formation, Sample 2538, Kujandysai section.

MATERIAL. 23 conjoined valves, two ventral and one dorsal valve, from Samples 100 (=K-98/1970), 626 Anderkenyn-Akchoku section; Samples 628, 2538 (BC57363), 8257, Kujandysai Section; Sample 948 (BC 57314–20), Tesik River.

DISCUSSION. This species was described and discussed in detail by Popov *et al.* (1999).

Order **ATHYRIDIDA** Boucot, Johnson & Staton, 1964
Suborder **ATHYRIDIDINA** Boucot, Johnson & Staton, 1964
Superfamily **MERISTELLOIDEA** Waagen, 1883
Family **MERISTELLIDAE** Waagen, 1883
Genus ***KELLERELLA*** Nikitin & Popov *in* Nikitin, Popov & Holmer, 1996

TYPE SPECIES. *Kellerella ditissima* Nikitin & Popov *in* Nikitin *et al.* (1996), from the Dulankara Regional Stage (Upper Caradoc), north Betpak-Dala, Kazakhstan.

Kellerella misiusi Popov, Nikitin & Sokiran, 1999
Pl. 14, figs 58–61

HOLOTYPE. CNIGR 26/12986, conjoined valves from the Anderken Formation, Sample 2538, Kujandysai section.

MATERIAL. 72 pairs of conjoined valves and one dorsal valve, from Samples 100 (=K-98/1970), 626, Anderkenyn-Akchoku section; Sample 8214 (BC56773, 57334–9), west side of Aschisu River; Samples 628, 2538, Kujandysai Section.

Table 29 Measurements of ventral valves of *Nikolaispira guttula* sp. nov., Sample 948, Tesik river.

	L	W	T	Ld	Sw	St	L/W	T/L	Sw/W
N	13	13	13	13	13	13	13	13	13
X	6.5	5.6	4.2	6.0	2.9	1.2	117%	64%	52%
S	0.72	0.57	0.66	0.70	0.45	0.29	5.2	5.1	5.8
MIN	5.6	4.9	2.8	5.0	2.2	0.5	110%	50%	42%
MAX	7.6	6.7	5.3	7.2	3.6	1.6	127%	70%	62%

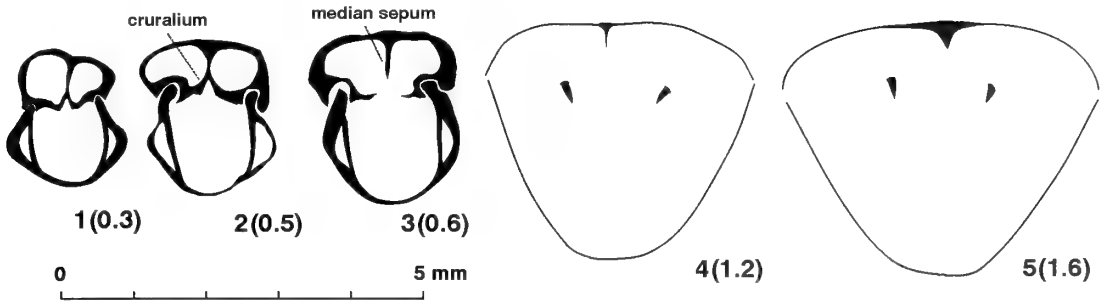

Fig. 21 Transverse serial sections of *Nikolaispira guttula* sp. nov., 1–3, BC 57588; 4–5, BC 57589, Sample 948, Tesik River. Distance in mm is measured from the posterior tip of ventral beak. Dorsal valve uppermost.

DISCUSSION. This species was described and discussed in detail by Popov *et al.* (1999).

Genus ***NIKOLAISPIRA*** Nikitin & Popov *in* Nikitin, Popov & Holmer, 1996

TYPE SPECIES. *Nikolaispira rasilis* Nikitin & Popov in Nikitin *et al.*, 1996, from the Dulankara Regional Stage (Upper Caradoc), north Betpak-Dala, Kazakhstan.

Nikolaispira guttula sp. nov. Pl. 14, figs 47–57; Fig. 21

ETYMOLOGY. After guttula, Latin – small drop.

HOLOTYPE. BC 57585, Pl. 14, figs 50–53, conjoined valves, from the Anderken Formation, Sample 2538, Kujandysai section.

MATERIAL. 38 conjoined valves from Samples 100 (=K-98/1970), 626, 8221 (BC 56770, 37857–58), Anderkenyn-Akchoku section; Samples 628, 2538 (BC 57584, 85), 8257, Kujandysai Section; Sample 948 (BC 57588, 89), Tesik River.

DESCRIPTION. Shell smooth, ventribiconvex, slightly elongate, subpentagonal in outline, about 64% as thick as long and 117% as long as wide. Anterior commissure parasulcate. Ventral valve profile strongly and evenly convex with maximum thickness near the mid-valve. Delthyrium small, open, narrow triangular. Beak slightly acuminate, erect posteriorly. Shallow ventral sulcus originating slightly posterior of the mid-valve, flanked by two low, rounded plications and terminating in a narrow, semicircular tongue. Dorsal valve gently convex with maximum thickness slightly posterior to mid-length. Median fold low and narrow, originating near mid-valve. Ventral interior with delicate teeth and short, thin dental plates placed closely to the lateral sides of the valve. Dorsal interior with small cruralium on a thin, long median septum extending anteriorly to mid-valve (Fig. 21). Spiralia laterally directed comprising up to three whorls. Jugal processes short, situated near the bese of spiralia.

DISCUSSION. This species differs from *Nikolaispira rasilis* Nikitin & Popov (*in* Nikitin, Popov & Holmer 1996), which occurs in the Dulankara Stage (Upper Caradoc to Lower Ashgill) of north Betpak-Dala, Kazakhstan, in having a more elongate outline, like the most elongate specimens of the latter species, and smaller number of whorls of the spiralia.

ACKNOWLEDGMENTS. We thank Rong Jia-yu (Nanjing) for discussion on Chinese material and M.G. Bassett for helpful comments on the manuscript. LEP acknowledges support from the Royal Society of London and the National Museum of Wales. LRMC acknowledges travel funds from The Natural History Museum.

REFERENCES

Amsden, T.W. 1968. Articulate brachiopods of the St.Clair Limestone (Silurian), Arkansas, and the Clarita Formation (Silurian), Oklahoma. *Memoirs of the Paleontological Society*, **1**: 1–117.

Apollonov, M. K. 1975. Ordovician trilobite assemblages of Kazakhstan. *Fossils and Strata*, **4**: 375–380.

Bancroft, B.B. 1933. Correlation tables of the stages Costonian-Onnian in England and Wales. Privately printed, Blakeney, Gloucestershire; 4 pp.

Barrande, J. 1879. *Systeme Silurien du Centre de la Boheme, Volume 5, Classe des Mollusques, Ordre des Brachiopodes.* Prague & Paris, 226 pp., 153 pls.

Bondarev, V.I. 1968. Stratigraphy and characteristic brachiopods of the Ordovician deposits of southern Novaya Zemlya, the island of Vaigach and northern Pai- Khoi. *Nauchno-Issledovatelskii Institut Geologii Arkitiki (NIIGA) Trudy*, **157**: 3–144.

Borissiak, M.A. 1956. The genus *Kassinella*. *Materiali vsesoyuznovo nauchno-issledovatelskii Geologisckeskova Instituta, Moskva*, **12**: 50–52.

Boucot, A. J. 1975. *Evolution and extinction rate controls*. Developments in Paleontology and Stratigraphy, 427 pp., Elsevier, Amsterdam.

Chernyschev, T.N. 1887. Fauna of the middle and upper Devonian of the western slopes of the Urals. *Trudy Geolicheskovo Komiteta, St Petersburg*, **3**: 1–208.

Chugaeva, M. N. 1958. Trilobites from the Ordovician of Chu-Ili Range. *Trudy geologicheskogo Instituta Akademii Nauk SSSR*, Moscow, **9**: 5–138.

Cocks, L.R.M. 2001. Ordovician and Silurian global geography. *Journal of the Geological Society, London*, **158**: 197–210.

—— **& Rong Jia-yu** 1988. A review of the late Ordovician *Foliomena* brachiopod fauna with new data from China, Wales, and Poland. *Palaeontology*, **31**: 53–67, pls 8, 9.

—— **&** —— 1989. Classification and review of the brachiopod Superfamily Plectambonitacea. *Bulletin of the British Museum (Natural History), London, Geology*, **45**: 77–163.

—— **&** —— 2000. Strophomenida. *In* Kaesler, R. (ed.) *Treatise on Invertebrate Paleontology, H, Brachiopoda (Revised)*. Volume 2, University of Kansas Press: 216–348.

Cooper, G.A. 1956. Chazyan and related brachiopods. *Smithsonian Miscellaneous Collections*, **127**:1–1245, pls 1–269.

—— **& Kindle, C.H.** 1936. New brachiopods and trilobites from the Upper Ordovician of Perce, Quebec. *Journal of Paleontology*, **10**: 348–372.

Davidson, T. 1883. A Monograph of the British Fossil Brachiopoda, Vol. V, Silurian Supplement, part 2: 135–242, pls 8–17. *Palaeontographical Society Monographs.*

Etter, W. 1999. Community Analysis: 285–360. *In* Harper, D. A. T. (ed.) *Numerical palaeobiology. Computer-based modelling and analysis of fossils and their distributions*. John Wiley & Sons, Chichester & New York, 468 pp.

Foerste, A.F. 1909. Preliminary notes on Cincinnatian fossils. *Bulletin of the Denison University Scientific Laboratories*, **14**: 209–228, pl. 4.

—— 1912. *Strophomena* and other fossils from Cincinnatian and Mohawkian horizons, chiefly in Ohio, Indiana and Kentucky. *Bulletin of the Denison University Science Laboratories*, **17**: 17–173, pls 1–8.

—— 1914. Notes on the Lorraine faunas of New York and the province of Quebec. *Bulletin of the Denison University Science Laboratories*, **17**: 247–328, pls 1–5.

Fortey, R. A. 1997. Late Ordovician trilobites from southern Thailand. *Palaeontology*, **40**: 451–459.

Fu Li-pu 1982. Brachiopoda. *In* Xian Institute of Geology and Mineral Resources (ed), *Paleontological Atlas of Northwest China, Shaanxi-Gansu-Ningxia Volume, Part 1, Precambrian and Early Paleozoic*. Geological Publishing House, Beijing: 95–178, pls 30–45.

Hall, J. 1847. *Palaeontology of New York, vol. 1. Containing descriptions of the organic remains of the lower division of the New-York System*. van Benthuysen, New York. 338 pp.,100 pls.

—— 1859. Observations on genera of Brachiopoda. *Contributions to the Palaeontology of New York, New York State Cabinet of Natural History, 12th Annual Report,* Albany: 8–110.

—— 1860. Observations on Brachiopoda. *Contributions to the Palaeontology of New York, New York State Cabinet of Natural History, 13th Annual Report,* Albany: 65–75.

—— 1883. Brachiopoda plates and explanations. *New York State Geologists 2nd Annual Report for 1882.* Albany, New York. 17pp., 6 pls.

—— **& Clarke, J.M.** 1892. An introduction to the study of the genera of Palaeozoic Brachiopoda. *Natural History of New York, Palaeontology*, **8**: 1–367, pls 1–20.

Havlíček, V. 1950. The Ordovician Brachiopoda from Bohemia. *Rozpravy Ústředního ústavu geologického*, **13**: 1–72, pls 1–13.

—— 1952. On the Ordovician representatives of the Family Plectambonitidae (Brachiopoda). *Sborník Ústředního ústavu geologického*, **19**: 397–428, pls 1–3.

Holmer, L.E. & Popov, L.E. 2000. Class Lingulata. *In*, Kaesler, R. (editor), *Treatise on Invertebrate Paleontology, Vol. H, Brachiopoda (Revised), Vol. 2:* 30–146. University of Kansas Press.

Jin Jisuo & Copper, P. 1997. *Parastrophinella* (Brachiopoda): its paleogeographic significance at the Ordovician/Silurian boundary. *Journal of Paleontology*, **71**: 369–380.

Jones, O.T. 1928. *Plectambonites* and some allied genera. *Memoirs of the Geological Survey of Great Britain, Palaeontology*, **1**: 367–527, pls 21–25.

Kaesler, R. (editor). 2000. *Treatise on Invertebrate Paleontology, Vol. H, Brachiopoda (Revised), Vols 2, 3.* University of Kansas Press. 919 pp.

Keller, B.M. 1956. General survey of the Ordovician stratigraphy of the Chu-Ili Mountains. *In, Ordovician of Kazakhstan, Part I,* Nauk, Alma-Ata.

Khalfin, L. L. 1958. Plastinchatozhabernyye mollyuski Chu-Iliiskikh gor [Bivalved molluscs of Chu-Ili mountains]. *Trudy geologicheskogo Instituta Akademii Nauk SSSR*, **9**:139–156, pls 1–7. [In Russian.]

Klenina, L.N., Nikitin, I.F. & Popov, L.E. 1984. *Brachiopods and biostratigraphy of the Middle and Upper Ordovician of the Chinghiz Ranges.* Nauka, Alma-Ata. 196 pp., pls 1–20.

Kolobova, I.M. & Popov, L.E. 1986. Faunal characteristics of the Middle Ordovician Anderken Regional Stage in the Chu-Ili Range (Southern Kazakhstan). *Ezhegodnik Vsesojuznogo Paleontologicheskovo Obshchestva*, **29**: 246–261.

Koren, T.N., Lytochkin, V.N., Popov, L.E. & Tolmacheva, T.J. 1993. *Biostratigraficheskii analiz pelagicheskikh strukturno-veshchestvennykh komplexov paleozoja dlja tselej GSR-50 i-200.* VSEGEI, St Petersburg, 79 pp.

Kutorga, S.S. 1848. Ueber die Brachiopoden-Familie der Siphonotretaceae. *Russisch-Kaiserliche Mineralogische Gesellschaft zu St.Petersburg Verhandlungen* [for 1847]: 250– 286, pls 6,7.

Laurie, J.R. 1991. Articulate brachiopods from the Ordovician and Lower Silurian of Tasmania. *Association of Australasian Palaeontologists Memoir*, **11**: 1–106.

Melou, M. 1990. Brachiopodes articules de la Coupe de l'Isle de Rosan (Crozon, Finistère); Formation des Tufs et Calcaires de Rosan (Caradoc-Ashgill). *Geobios*, **23**: 539–560, pls 1–10.

Misius, P.P. & Ushatinskaya, G.T. 1977. New Ordovician and Silurian strophomenids from Kazakhstan and northern Kirgiz. *Novye Vidy Drevnikh Rastenii i Bespozvonochnykh SSSR*, **4**: 113–116.

Neuman, R. B. 1971. An early middle Ordovician brachiopod assemblage from Maine, New Brunswick and northern Newfoundland. *Smithsonian Contributions to Paleobiology*, **3**: 113–124, pls 1,2.

Nikiforova, O.I. & Popov, L.E. 1981. New species of Ordovician rhynchonelloids from Kazakhstan and Central Asia. *Paleontologeski Zhurnal*, **1981**: 54–67.

Nikitin, I.F. 1972. *The Ordovician of the Chingiz Range.* Nauka, Alma-Ata: 126–166, pls 13–20.

—— 1973. *The Ordovician of Kazakhstan, Part 2, Palaeogeography, Palaeotectonics.* Nauka, Alma-Ata, 100 pp.

—— **, Apollonov, M. K., Tsai, D. T., & Rukavishnikova. T. B.** 1980. Ordovician System: 44–78. *In*, Abdulin, A. A. (editor) *Chu-Iliiskii rudnyi poyas. Part 1. Geologiya Chu-Iliiskogo regiona.* Nauka, Alma-Ata.

—, **Frid, N. M. & Zvontsov, V. S.** 1991. Paleogeography and main features of volcanicity in the Ordovician of Kazakhstan and North Tien-Shan. *Geological Survey of Canada Paper*, **90** (9): 259–270.

—, **Gnilovskaya, M.B., Zhuravleva, I.T., Luchinina, V.A. & Myagkova, E.I.** 1974. Anderken bioherm range and history of its origin. *Trudy Instituta Geologii i Geofyziki (IGIG), Akademii Nauk SSSR, Sibirskoe Otlodenie*, **84**: 122–159.

—— **& Popov, L.E.** 1983. Middle Ordovician orthides and plectambonitaceans from the northern Pri-Ishim and the Akzhar River Basin in central Kazakhstan (brachiopods). *Ezhegodnik vsesoyuznovo Paleontologicheskovo Obshchestva*, **26**: 228–247, pls 1–3.

—— **&** —— 1985. Ordovician strophomenids (Brachiopods) from north Priishim (central Kazakhstan). *Ezhegodnik vsesoyuznovo Paleontologicheskovo Obshchestva*, **28**: 34–49, pls 1–3.

—— **&** —— 1996. Strophomenid and triplesiid brachiopods from an Upper Ordovician carbonate mound in central Kazakhstan. *Alcheringa*, **20**: 1–20.

—, —— **& Holmer, L.E.** 1996. Late Ordovician brachiopod assemblage of Hiberno-Salairian type from Central Kazakhstan. *GFF*, **117**: 83–96.

Nikitina, O.I. 1985. A new brachiopod association from the Middle Ordovician of southern Kazakhstan. *Paleontologeski Zhurnal*, **1985** (4): 21–29.

Öpik, A.A. 1939. Brachiopoden und Ostrakoden aus dem Expansusschiefer Norwegens. *Norsk Geologisk Tidsskrift*, **19:** 117–142, pls 1–6.

Percival, I.G. 1979a. Late Ordovician articulate brachiopods from Gunningbland, central western New South Wales. *Proceedings of the Linnean Society of New South Wales*, **103**: 175–187.

—— 1979b. Ordovician plectambonitacean brachiopods from New South Wales. *Alcheringa*, **3**: 91–116.

—— 1991. Late Ordovician articulate brachiopods from central New South Wales. *Memoirs of the Association of Australasian Palaeontologists,* **11**:107–177.

Popov, L.E. 1977. New species of Ordovician inarticulate brachiopods from the Chinghiz Range (East Kazakhstan). *Novye Vidy Drevnik Rastenii i Bespozvonochnych SSSR*, **4**: 102–105, pls 1,2.

—— 1980. New brachiopod species from the Middle Ordovician of the Chu-Ili Hills. *Ezhegodnik Vsesoyuznovo Palaeontologicheskovo Obshchestva*, **23**: 139–158.

—— 1985. Brachiopods of the Anderken horizon of the Chu-Ili Hills (Kazakhstan). *Ezhegodnik Vsesoyuznovo Palaeontologicheskovo Obshchestva*, **28**: 50–68, pls 1–3.

—, **Nikitin, I.F. & Cocks, L.R.M.** 2000. Late Ordovician brachiopods from the Otar Member of the Chu-Ili Range, Kazakhstan. *Palaeontology*, **43**: 833–870, pls 1–6.

—, — **& Sokiran, E.V.** 1999. The earliest atrypides and athyrides (Brachiopoda) from the Ordovician of Kazakhstan. *Palaeontology*, **42**: 625–661, pls 1–4.

Potter, A.W. 1991. Discussion of the systematic placement of the Ordovician brachiopod genera *Cooperea* and *Craspedelia* by Cocks and Rong (1989). *Journal of Paleontology*, **65**: 742–755.

Reed, F.R.C. 1905. New fossils from the Haverfordwest district IV. *Geological Magazine*, **5**: 433–436, 444–454, pls 14, 23.

Rong Jia-yu, Harper, D. A. T., Zhan Ren-bin & Li Rong-yu 1994. *Kassinella-Christiania* Associations in the early Ashgill *Foliomena* fauna of South China. *Lethaia*, **27**: 19–28.

—, **Zhan Ren-bin & Harper, D. A. T.** 1999. Late Ordovician (Caradoc–Ashgill) brachiopod faunas with *Foliomena* based on data from China. *Palaios*, **14**: 412–431.

Rouault, M. 1850. Note preliminaire sur une nouvelle formation découverte dans le terrain Silurien de la Bretagne. *Bulletin de la Societé géologique de France,* (2) **7**: 724–744.

Rukavishnikova, T.B. 1956. Ordovician brachiopods from Kazakhstan. *Trudy Akadeemia Nauk SSSR Geologicheskii Institut*, **1**: 105–168, pls 1–5.

Sapelnikov, V.P. & Rukavishnikova, T.B. 1975. *Upper Ordovician, Silurian and Lower Devonian pentamerids of Kazakhstan.* Nauka, Moscow. 226 pp., 43 pls.

Schuchert, C. & Cooper, G.A. 1931. Synopsis of the brachiopod genera of the suborders Orthoidea and Pentameroidea, with notes on the Telotremata. *American Journal of Science,* (5), **22**: 241–255.

—— **&** —— 1932. Brachiopod genera of the suborders Orthoidea and Pentameroidea. *Memoirs of the Peabody Museum of Natural History*, **4**: 1–270, pls 1–29.

—— **& LeVene, C.M.** 1929. Brachiopoda (generum et genotyporum index et bibliographia). *In*, Pompeckj, F. (ed.) *Fossilium Catalogus, Vol. 1, Animalia, Pars 42.* Junk, Berlin. 140 pp.

Sengor, A.M.C. & Natalin, B.A. 1996. Paleotectonics of Asia: fragments of a synthesis. *In*, Yin, A. & Harrison, M. (eds) *The tectonic evolution of Asia.* Cambridge University Press: 486–640.

Severgina, L.G. 1967. New species and genera of Ordovician brachiopods from the Sayano-Altai Hill District. *Nekotoryie Voprosy Geologii Zapadnoi Sibiri*, **63:** 120–140, pls 1–5.

—— 1978. Brachiopods and stratigraphy of the Upper Ordovician of the Gornoi Altai, Salair and Gornoi Shoria. *Trudy Akademiia Nauk SSSR, Sibirskoe Otdelenie, Institut Geologii i Geofyziki (IGIG)*, **405**: 3–41.

Sharpe, D. 1848. On *Trematis*, a new genus belonging to the family of brachiopodous Mollusca. *Quarterly Journal of the Geological Society of London*, **4**: 66–69.

Sinclair, G.W. 1945. Some Ordovician lingulid brachiopods. *Transactions of the Royal Society of Canada*, **39**: 55–82, pls 1–4.

Sowerby, J. de C. 1839. Shells. *In*, Murchison, R.I. *The Silurian System.* John Murray, London: 579–712, pls 1–29.

Stukalina, G.A. 1988. Studies in Paleozoic crinoid-columnals and stems. *Palaeontographica*, **A204**: 1–66, pls 1–15.

Toporova, R.P., Malitskii, N.P., Mikhailov, N.P. & Moskaljeva, N.V. 1971. Magmatizm i metamorfism, Chu-Baikashskii Rayon. *Geologya SSSR*, **40** (2): 34–46.

Tsai, D. T. 1976. *Graptolity srednego ordovika Kazakhstana* [Graptolites of the Middle Ordovician of Kazakhstan]: 76 pp. Nauka, Alma-Ata [In Russian].

Ulrich, E.O & Cooper, G.A. 1936a. New Silurian brachiopods of the family Triplesiidae. *Journal of Paleontology*, **10**: 331–347, pls 48–50.

—, —— 1936b. New genera and species of Ozarkian and Canadian brachiopods. *Journal of Paleontology*, **10**: 616–631.

Wang Yu 1949. Maquoketa Brachiopoda of Iowa. *Geological Society of America Memoir*, **42**: 1–55, pls 1–12.

Weber, V. N. 1948. Trilobity siluriiskikh otlozhenii SSSR. Vyp. 1. Nizhnesiluriiskie trilobity [Trilobites of the Silurian deposits of USSR. Vol. 1. Lower Silurian trilobites.]. *Monografii po paleontologii SSSR*, **69**: 1–113. [In Russian].

Whittington, H.B. & Williams, A. 1955. The fauna of the Derfel Limestone of the Arenig District. *Philosophical Transactions of the Royal Society of London,* **B238:** 397–430, pls 1–3.

Williams, A. 1962. The Barr and Lower Ardmillan Series (Caradoc) of the Girvan District, southwest Ayrshire. *Geological Society of London Memoir*, **3**: 1–267, pls 1–25.

—— 1963. The Caradocian brachiopod faunas of the Bala District, Merionethshire. *Bulletin of the British Museum (Natural History)*,Geology, **8**: 327–471, pls 1–16.

—— 1974. Ordovician Brachiopoda from the Shelve District, Shropshire. *Bulletin of the British Museum (Natural History)*, Geology Supplement, **11**: 1–163, pls 1–28.

—— **Lockley, M.G. & Hurst, J.M.** 1981. Benthic palaeocommunities represented in the Ffairfach Group and coeval Ordovician successions of Wales. *Palaeontology*, **24**: 661–694.

Wright, A.D. & Jaanusson, V. 1993. New genera of Upper Ordovician triplesiid brachiopods from Sweden. *Geologiska Foreningens i Stockholm Forhandlingar*, **115**: 93–118.

Xu Han-kui, Rong Jia-yu & Liu Di-yong 1974. Ordovician brachiopods. *In*, Nanjing Institute of Geology and Palaeontology, Academia Sinica (editors), *Handbook of Stratigraphy and Palaeontology in Southwest China*, Beijing, 144–154, pls 64–66 (in Chinese).

Zeng Quing-luan 1987. Brachiopoda. *In*, Wang Xiao-feng *et al*, *Biostratigraphy of the Yangste Gorge Area 2, Early Palaeozoic Era*. Geological Publishing House, Beijing. 614 pp (English summary pp. 489–555), pls 8–18.

Zhan Ren-bin & Cocks, L.R.M. 1998. Late Ordovician brachiopods from the South China Plate and their palaeogeographical significance. *Special Papers in Palaeontology*, **59**: 1–70, pls 1–9.

—— **& Rong Jia-yu** 1995. Four new Late Ordovician brachiopod genera from the Zhejiang-Jiangxi border region, east China. *Acta Palaeontologica Sinica*, **34**: 549–574, pls 1–4.

Ziegler, A.M., Cocks, L.R.M. & Bambach, R.K. 1968. The composition and structure of Lower Silurian marine communities. *Lethaia*, **1**: 1–27.

Bulletin of The Natural History Museum
Geology Series

Earlier Geology *Bulletins* are still in print. The following can be ordered from Cambridge University Press or Intercept (addresses on inside front cover). Where the complete backlist is not shown, this may also be obtained from the same addresses.

Volume 51

No. 1 A synopsis of neuropteroid foliage from the Carboniferous and Lower Permian of Europe—The Upper Cretaceous ammonite *Pseudaspidoceras* Hyatt, 1903, in north-eastern Nigeria—The pterodactyloids from the Purbeck Limestone Formation of Dorset. 1995. Pp. 1–88. **£37.50**

No. 2 Palaeontology on the Qahlah and Simsima Formations (Cretaceous, Late Campanian-Maastrichtian) of the United Arab Emirates-Oman Border Region—Preface—Late Cretaceous carbonate platform faunas of the United Arab Emirates-Oman border region—Late Campanian-Maastrichtian echinoids from the United Arab Emirates-Oman border region—Maastrichtian ammonites from the United Arab Emirates-Oman border region—Maastrichtian nautiloids from the United Arab Emirates-Oman border region—Maastrichtian Inoceramidae from the United Arab Emirates-Oman border region—Late Campanian-Maastrichtian Bryozoa from the United Arab Emirates-Oman border region—Maastrichtian brachiopods from the United Arab Emirates-Oman border region—Late Campanian-Maastrichtian rudists from the United Arab Emirates-Oman border region. 1995. Pp. 89–305. **£37.50**

Volume 52

No. 1 Zirconlite: a review of localities worldwide, and a compilation of its chemical compositions—A review of the stratigraphy of Eastern Paratethys (Oligocene–Holocene)—A new protorichthofenioid brachiopod (Productida) from the Upper Carboniferous of the Urals, Russia—The Upper Cretaceous ammonite *Vascoceras* Choffat, 1898 in north-eastern Nigeria. 1996. Pp. 1–89. **£43.40**

No. 2 Jurassic bryozoans from Baltów, Holy Cross Mountains, Poland—A new deep-water spatangoid echinoid from the Cretaceous of British Columbia, Canada—The cranial anatomy of *Rhomaleosaurus thorntoni* Andrews (Reptilia, Plesiosauria)—The first known femur of *Hylaeosaurus armatus* and re-identification of ornithopod material in The Natural History Museum, London—Bryozoa from the Lower Carboniferous (Viséan) of County Fermanagh, Ireland. 1996. Pp. 91–171. **£43.40**

Volume 53

No. 1 The status of '*Plesictis' croizeti*, '*Plesictis' gracilis* and '*Lutra' minor:* synonyms of the early Miocene viverrid *Herpestides antiquus* (Mammalia, Carnivora)—*Baryonyx walkeri*, a fish-eating dinosaur from the Wealden of Surrey—The Cretaceous-Miocene genus *Lichenopora* (Bryozoa), with a description of a new species from New Zealand. 1997. Pp. 1–78. **£43.40**

No. 2 Ordovician trilobites from the Tourmakeady Limestone, western Ireland—Ordovician Bryozoa from the Llandeilo Limestone, Clog-y-fran, near Whitland, South Wales—New Information on Cretaceous crabs. 1997. Pp.79–139. **£43.40**

Volume 54

No. 1 The Jurassic and Lower Cretaceous of Wadi Hajar, southern Yemen—Ammonites and nautiloids from the Jurassic and Lower Cretaceous of Wadi Hajar, southern Yemen. 1998. Pp. 1–107. **£43.40**

No. 2 Caradoc brachiopods from the Shan States, Burma (Myanmar)—A review of the stratigraphy and trilobite faunas from the Cambrian Burj Formation in Jordan—The first Palaezoic rhytidosteid: *Trucheosaurus major* (Woodward, 1909) from the late Permian of Australia, and a reassessment of the Rhytidosteidae (Amphibia, Temnospondyli)—The rhynchonellide brachiopod *Isopoma* Torley and its distribution. 1998. Pp.109–163. **£43.40**

Volume 55

No. 1 Latest Paleocene to earliest Eocene bryozoans from Chatham Island, New Zealand. 1999. Pp. 1–45. **£43.40**

No. 2 A new stylophoran echinoderm, *Juliaecarpus milnerorum*, from the late Ordovician Upper Ktaoua Formation of Morocco—Late Cretaceous-early Tertiary echinoids from northern Spain: implications for the Cretaceous-Tertiary extinction event. 1999. Pp 47–137. **£43.40**

Volume 56

No. 1 A review of the history, geology and age of Burmese amber (Burmite—A list of type and figured specimens of insects and other inclusions in Burmese amber—A preliminary list of arthropod families present in the Burmese amber collection at The Natural History Museum, London—The first fossil prosopistomatid mayfly from Burmese amber (Ephemeroptera; Prosopistomatidae)—The most primitive whiteflies (Hemiptera; Aleyrodidae; Bernaeinae subfam. nov.) from the Mesozoic of Asia and Burmese amber, with an overview of Burmese amber hemipterans—A new genus and species of Lophioneuridae from Burmese amber (Thripida (=Thysanoptera): Lophioneurina),—*Burmapsilocephala cockerelli*, a new genus and species of Asiloidea (Diptera) from Burmese amber—Phantom midges (Diptera: Chaoboridae) from Burmese amber—An archaic new genus of Evaniidae (Insecta: Hymenoptera) and implications for the biology of ancestral evanioids—Digger Wasps (Hymenoptera, Sphecidae) in Burmese Amber—*Electrobisium acutum* Cockerell, a cheiridiid pseudoscorpion from Burmese amber, with remarks on the validity of the Cheiridioidea (Arachnida, Chelonethi). 2000. Pp. 1–83. **£43.40**

No. 2 *Terebratula californiana* Küster, 1844, and reappraisal of west coast north American brachiopod species referred to the genus *Laqueus* Dall, 187—Late Campanian-Maastrichtian corals from the United Arab Emirates-Oman border region—*Rhombocladia dichotoma* (M'Coy, 1844) [Fenestrata, Bryozoa]: designation of a lectotype—The Gough's Cave human fossils: an introduction—The Creswellian (Pleistocene) human axial skeletal remains from Gough's Cave (Somerset, England)—The Creswellian (Pleistocene) human lower limb remains from Gough's Cave (Somerset, England). 2000. Pp. 85–161. **£43.40**

Volume 57

No. 1 Fossil pseudasturid birds (Aves, Pseudasturidae) from the London Clay—*Novocrania*, a new name for the genus *Neocrania* Lee & Brunton, 1986 (Brachiopoda, Craniida), preoccupied by *Neocrania* Davis, 1978 (Insecta, Lepidoptera)—The Creswellian (Pleistocene) human upper limb remains from Gough's Cave (Somerset, England)—Gough's Cave 1 (Somerset, England): a study of the hand bones—A revision of the English Wealden Flora, III: Czekanowskiales, Ginkgoales & allied Coniferales. 2001. Pp. 1–82. **£43.40**

No. 2 The Cenozoic Brachiopod *Terebratula*: its type species, neotype, and other included species. D.E. Lee, C.H.C. Brunton, Emma Taddei Ruggiero, Massimo Caldara & Oronzo Simone.
Gough's Cave 1 (Somerset, England): a study of the pectoral girdle and upper limbs. S.E. Churchill.
Systematic affinity of *Acroporella assurbanipali* Elliott (Dasycladaceae), with notes on the genus *Neomeris*. Filippo Barattolo & Roberta Romano.
Palynological zonation of Mid-Palaeozoic sequences from the Cantabrian Mountains, NW Spain: implications for inter-regional and interfacies correlation of the Ludford/Přídolí and Silurian/Devonian boundaries, and plant dispersal patterns. John B. Richardson, Rosa M. Rodriguez, Stuart J. E. Sutherland. 2001. Pp. 83–162. **£43.40**

CONTENTS

CAMBRIDGE
UNIVERSITY PRESS

0968-0462(200206)58:1;1-U

Bulletin of The Natural History Museum
GEOLOGY SERIES
Vol. 58, No. 1, June 2002

Bulletin of The Natural History Museum

THE NATURAL HISTORY MUSEUM
PALAEONTOLOGY LIBRARY

Geology Series

THE NATURAL HISTORY MUSEUM

VOLUME 58 NUMBER 2 28 NOVEMBER 2002

The *Bulletin of The Natural History Museum* (formerly: *Bulletin of the British Museum (Natural History)*), instituted in 1949, is issued in four scientific series, Botany, Entomology, Geology (incorporating Mineralogy) and Zoology.

The Geology Series is edited in the Museum's Department of Palaeontology

Keeper of Palaeontology:	Dr N. MacLeod
Editor of Bulletin:	Dr M.K. Howarth
Assistant Editor:	Mr C. Jones

Papers in the *Bulletin* are primarily the results of research carried out on the unique and ever-growing collections of the Museum, both by the scientific staff and by specialists from elsewhere who make use of the Museum's resources. Many of the papers are works of reference that will remain indispensable for years to come. All papers submitted for publication are subjected to external peer review before acceptance.

SUBSCRIPTIONS *Bulletin of the Natural History Museum*, Geology Series (ISSN 0968-0462) is published twice a year (one volume per annum) in June and November. Volume 58 will appear in 2002. The 2002 subscription price (excluding VAT) of a volume, which includes print and electronic access, is £88.00 (US $155.00 in USA, Canada and Mexico). The electronic-only price available to institutional subscribers is £79.00 (US $140.00 in USA, Canada and Mexico).

ORDERS Orders, which must be accompanied by payment, may be sent to any bookseller, subscription agent or direct to the publisher: Cambridge University Press, The Edinburgh Building, Shaftesbury Road, Cambridge CB2 2RU, UK; or in the USA, Canada and Mexico: Cambridge University Press, Journals Department, 40 West 20th Street, New York, NY 1011-4211, USA. EU subscribers (outside the UK) who are not registered for VAT should add VAT at their country's rate. VAT registered members should provide their VAT registration number. Japanese prices for institutions (including ASP delivery) are available from Kinokuniya Company Ltd, P.O. Box 55, Chitose, Tokyo 156, Japan. Prices include delivery by air. Postmaster: send address changes in USA, Canada and Mexico to: Bulletin of the Natural History Museum. Geology Series, Cambridge University Press, 110 Midland Avenue, Port Chester, New York, NY 105783-4930. Claims for missing issues should be made immediately on receipt of the subsequent issues.

Orders and enquiries for issues prior to 2002 should be sent to: Intercept Ltd., P.O. Box 716, Andover, Hampshire SP10 1YG, *Telephone*: (01264) 334748, *Fax*: (01264) 334058, *Email*: intercept@andover.co.uk, *Internet*: http:/www.intercept.co.uk

ADVERTISING Apply to the Publisher. Address enquiries to the Advertising Promoter.

COPYRIGHT AND PERMISSIONS This journal is registered with the Copyright Clearance Center, 222 Rosewood Drive, Danvers, MA 01923, USA. Organizations in the USA who are also registered with CCC may therefore photocopy material (beyond the limits permitted by Section 107 and 108 of US Copyright law) subject to payment to CCC of the per-copy fee of $16.00. This consent does not extend to multiple copying for promotional or commercial purposes. Code 0968-0462/2002 $16.00. ISI Tear Sheet Service, 3501 Market Street, Philadelphia, PA 19104, USA, is authorised to supply single photocopies of separate articles for private use only. Organizations authorised by the UK Copyright Licensing Agency may also copy material subject to the usual conditions. For all other use, permission should be sought from Cambridge University Press.

No part of this publication may otherwise be reproduced, stored or distributed by any means without permission in writing from Cambridge University Press, acting for the copyright holder.

Copyright © 2002 The Natural History Museum

ELECTRONIC ACCESS This journal is included in the Cambridge Journals Online service which can be found at: http://journals.cambridge.org

For further information on other Press titles access http://uk.cambridge.org or http://us.cambridge.org

World list abbreviation: *Bull. nat. Hist. Mus. Lond.* (Geol.)

ISSN 0968–0462

The Natural History Museum
Cromwell Road
London SW7 5BD

Geology Series
Vol. 58, No. 2, pp. 81–168
Issued 28 November 2002

Typeset by Ann Buchan (Typesetters), Middlesex
Printed in Great Britain by Henry Ling Ltd, at the Dorset Press, Dorchester, Dorset

Bull. nat. Hist. Mus. Lond. (Geol.) **58**(2): 81–152 Issued 28 November 2002

The Lower Lias of Robin Hood's Bay, Yorkshire, and the work of Leslie Bairstow

...AL
...EUM
PALA...OLOGY ...ARY

M.K. HOWARTH
Department of Palaeontology, The Natural History Museum, Cromwell Road, London SW7 5BD

CONTENTS

SYNOPSIS. Rocks of Lower Liassic (Sinemurian and Lower Pliensbachian) age exposed in Robin Hood's Bay, near Whitby, north Yorkshire, are described from the mapping, stratigraphical descriptions and ammonite collections made by Mr Leslie Bairstow in the years 1927–1970, and preserved in the Palaeontology Department, The Natural History Museum, London. His large-scale map of the geology of the foreshore is published on five sheets at a scale of approximately 1:5000. The stratigraphical sequence from bed 418 at the base up to bed 600.5 at the top of the Lower Pliensbachian is 163.74 m thick, and consists of the Redcar Mudstone Formation, for which four members are formally defined – the Calcareous Shale (at the base), Siliceous Shale, Pyritous Shale and Ironstone Shale Members – overlain by the lower part of the Staithes Sandstone Formation. The lowest beds exposed by the lowest spring tides are Sauzeanum Subzone, Semicostatum Zone, in age; ammonites occur in all subzones, and the only uncertain boundary is that between the Masseanum and Valdani Subzones (Ibex Zone), where there are few characteristic ammonites. Bairstow's ammonite collection consists of more than 2360 specimens, all from recorded horizons, and is notably rich in *Promicroceras, Asteroceras, Eparietites* and *Oxynoticeras* from the Obtusum and Oxynotum Zones, Echioceratids, *Eoderoceras* and *Apoderoceras* from the Oxynotum, Raricostatum and Jamesoni Zones, and Liparoceratids from the Davoei Zone, making it a primary source for Sinemurian and Lower Pliensbachian ammonite biostratigraphy. The recently proposed selection of Wine

© The Natural History Museum, 2002

Haven at the south-eastern end of the bay as the Global Stratotype Section and Point (GSSP) for the base of the Pliensbachian Stage (ie. the world standard definition), is supported by the sequence of ammonites across the Sinemurian/Pliensbachian boundary. All previously figured ammonites from Robin Hood's Bay are listed in a systematic section that includes the evidence on which the ammonite identifications in the paper are based, and 56 of the best preserved ammonites are figured. *Eparietites bairstowi* sp. nov. is proposed for an early species of *Eparietites* and a Sowerby Collection ammonite from the Aplanatum Subzone, Raricostatum Zone, in the bay, is designated neotype of *Eoderoceras armatum* (J. Sowerby).

INTRODUCTION

The geology of Robin Hood's Bay (Fig. 1) has received the attention of many geologists since the 1820s. One such geologist was Leslie Bairstow, who decided to make the description of the outcrops of the Lower Lias on the foreshore of the bay (Fig. 2) the main scientific work of his life. He started serious investigations in 1928 and worked in the bay for the next 50 years. Dr L.F. Spath, a colleague at the British Museum (Natural History) (now the Natural History Museum, London), identified the many ammonites that he collected and brought to the Museum. As long ago as 1956 Spath (1956: 147) referred to 'the (still undescribed) collections made by Mr L. Bairstow in Robin Hood's Bay', but Bairstow was never able to finish a detailed account for publication, and finally he left his work for me to complete. That completion has involved more fundamental work than mere editing: complete rewriting of the stratigraphical section, revision of the maps, preparation of many tables and diagrams not envisaged by Bairstow, and revision of the determinations in order to produce an up-to-date account of the ammonites and the biostratigraphy, were all found to be necessary. The final result is eminently worth publishing, if only because it would be very difficult to duplicate the ammonite collection, which is the core of the paper and the biostratigraphy, at the present time. I had many conversations with Bairstow during the period 1956 to 1965, and less frequently up to the early 1980s, and quotations from a few of them are given here. This paper is not the same as Bairstow would have written – his account would have had more local details of the outcrops in the bay as they were in the 1920s and 1930s, while the paper now presented is more orientated towards correlation by ammonites, for which his accurately documented sequence in the bay is of major international importance. The comparison that it will afford with rocks of the same age and the sequence of zones and subzones on the Dorset coast is long overdue. Such comparison is too lengthy to be included here – it would involve much collation and reidentification of the many separate collections of Dorset ammonites that now exist, in order to produce a consistent set of determinations, and hence biostratigraphy, that could be compared with the sequence in Yorkshire.

The term Lower Lias is used in the title of this paper and elsewhere as an exact equivalent of Hettangian + Sinemurian + Lower Pliensbachian. This is the sense in which it was widely used and understood by palaeontologists when Bairstow worked in the 1920s and 1930s. Even in those days a different usage by those geologists more interested in lithology and sedimentation led to confusion on occasions: the boundary between Lower and Middle Lias was placed by them at a position that best marked the change from dominantly clayey beds below to dominantly sandy beds above. Such a change in lithology occurs at different horizons in different parts of Britain, so their usage of Lower and Middle Lias did not have an accurate date or age connotation. So much confusion resulted from these disparate usages that the terms are rarely used now-a-days. Lower Lias is retained here, in the sense given above, in deference to Bairstow and the long history of Robin Hood's Bay geology, where it is well understood as being the Sinemurian + Lower Pliensbachian, there being no Hettangian exposed in the bay. In this usage the Middle Lias is exactly equivalent to the Upper Pliensbachian, and the Upper Lias to the Toarcian.

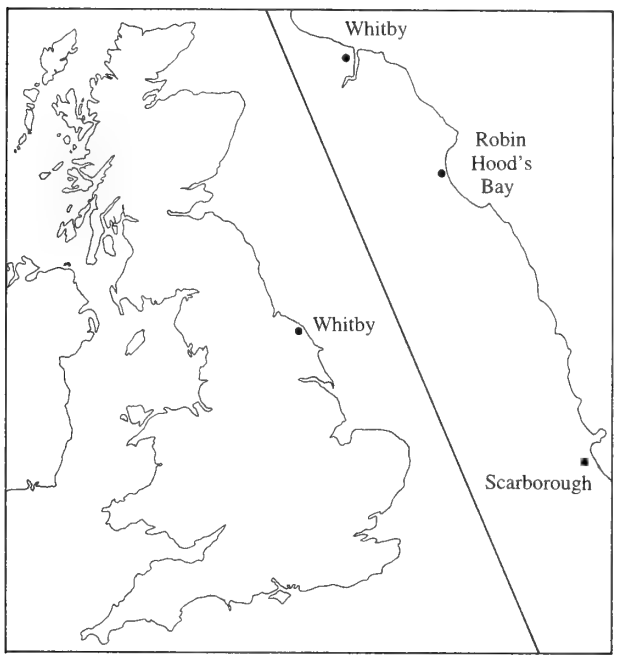

Fig. 1 Map showing the location of Robin Hood's Bay on the north-east coast of England, 10 km south-east of Whitby.

LESLIE BAIRSTOW

Biography

Leslie Bairstow (Fig. 3) was born in Halifax, Yorkshire, on 14 August 1907. After attending Ackworth School (1918–22) and Bootham School, York (1922–25), he went to King's College, Cambridge, where he obtained a degree in Geology in 1928. He started research on the Lower Lias of Robin Hood's Bay in the summer of 1928, supported by college scholarships. He had become interested in collecting fossils from the Yorkshire Lias during his school and undergraduate years, and in getting his ammonites identified he came into contact with Dr L.F. Spath at the British Museum (Natural History). It was at Spath's suggestion that he decided to undertake serious research on the Lower Lias of Robin Hood's Bay, and Dr W.D. Lang, also at the Museum, was keen to get another Lower Lias section accurately documented for comparison with his own work on the Lower Lias of Dorset. He also consulted S.S. Buckman, who advised him to record the location of every ammonite he

Fig. 2 The Robin Hood's Bay foreshore at low tide, looking north-west from the top of Ravenscar (above Peak) at the south-eastern end of the bay. Robin Hood's Bay town is immediately above the foreshore in the centre-right of the photograph. M.K. Howarth photograph, 28 September 1999.

collected with sufficient accuracy to enable the sequences of ammonite 'hemerae' to be compared at the north-western and south-eastern ends of Robin Hood's Bay. Initially the project was intended to be a thesis for a higher degree at Cambridge University, but the detailed mapping, bed-by-bed description and collecting during 1928–1930 were submitted as a dissertation in support of a fellowship application at King's College in late 1930. This was not successful, and Bairstow was preparing for a second application in 1931, when the offer of a permanent post at The Natural History Museum in South Kensington (then the British Museum (Natural History)), with the opportunity to continue work indefinitely on the Lower Lias of Robin Hood's Bay, appealed to him more than a fellowship at Cambridge of six years duration. In fact, during his early years at the Museum he was elected to a three-year visiting Fellowship at King's College in 1932–35. He started at the Museum in October 1931, and although initially put in charge of fossil echinoderms and later Coleoidea (including belemnites), he was able to continue work on Robin Hood's Bay until his retirement in June 1965. He continued to work at the Museum until 1985, when he moved to Todmorden, Yorkshire, where he died on 10 August 1995.

The meticulous attention to detail that Bairstow lavished on the description, collecting and mapping of the Lower Lias of Robin Hood's Bay, made it unlikely that he would produce a final description with which he would be satisfied. It is fortunate, therefore, that for the Cambridge fellowship dissertation of 1930 he produced a finished manuscript version of the map and a stratigraphical description of the whole succession, which are the basis of the present paper. His most useful collecting occurred during the period 1928–34, and work during the following 40 years did not greatly enhance that original burst of activity. His ammonite collection of about 2,360 specimens is housed in The Natural History Museum, and is a prime record of the sequence of ammonite faunas for the upper two-thirds of the Lower Lias. Such a collection would be difficult to repeat today, because so many of the accessible ammonites have been removed from the Bay. Bairstow conducted field parties to the Bay for the 18th International Geological Congress in 1948 and the William Smith Jurassic Symposium in 1969, and gave brief summaries of the zonal sequence and his bed numbering in the guide books for those meetings (Bairstow, 1948, 1969). Apart from a summary in a guide to the fossils of the Scarborough district (Bairstow, 1953), he left no other published account.

The geological map of Robin Hood's Bay, the description of the stratigraphy and basic biostratigraphy formed the first half of his dissertation for the fellowship at King's College, Cambridge, in 1930. The second half of that dissertation consisted of a description of the Lower Lias belemnites of Robin Hood's Bay, and included an assessment of the 19 specific names proposed by Simpson (1855: 22–31; 1884: 47–54) and partly revised by Phillips (1863–1909), for belemnites from the bay. This part of his work was also destined never to be published, but it did give Bairstow an interest in belemnites and related groups, which led to him being put in charge of fossil Coleoidea at the Natural History Museum. In fact, he did much valuable investigation into the early generic nomenclature of fossil Coleoidea, especially the non-belemnite groups, and his detailed notes were passed on first to Dr J.A. Jeletzky, then to later *Treatise* authors, for incorporation in the Coleoid volume of the *Treatise on Invertebrate Paleontology* (not yet published). In these and other matters, especially the geology of Robin Hood's Bay and general identification of specimens sent to the Museum, colleagues found him helpful and were always enlightened by his views. He had a long

Fig. 3 Leslie Bairstow, aged 46; taken from a group photograph of the Palaeontology Department, the Natural History Museum, 1954.

association with the Palaeontographical Society, first as Treasurer for the years 1948 to 1955, then as Vice President from 1966 until 1969, and he was a Trustee of that Society for several years during the same period. [Other biographies on Bairstow can be found in the obituary notices published by the Geological Society (Howarth, 1996) and King's College, Cambridge (Annual Report, October 1996: 27–29).]

Bairstow's unpublished work

The originals of the unfinished and unpublished manuscripts left by Bairstow will be deposited in the Earth Sciences Library of The Natural History Museum, London. They can be divided into three main parts, which will now be described in sequence:

1. The geological map of Robin Hood's Bay.
2. The stratigraphical description of the Lower Lias.
3. His collection of ammonites and other fossils, and his list of the determinations of the ammonites.

GEOLOGICAL MAPS

Bairstow drew his geological map of Robin Hood's Bay in 1928–30 and the top copy formed part of his fellowship submission, now preserved in the archives of King's College, Cambridge. The map was drawn at a scale of 1:2500, and consists of eight sheets, each measuring 320 × 343 mm. Bairstow took (and variously modified) a few geographical lines from the 1:2500 sheets of the Ordnance Survey: these were mainly the top and bottom of the cliffs, some paths and field boundaries at the top of the cliffs, a few roads and prominent buildings, and the line of low tide mark. The latter is the low tide mark of ordinary tides on Ordnance Survey maps (ie. approximately half way between low water mark of spring and neap tides), but Bairstow modified the line to be that of low water mark of spring tides, when the maximum amount of rock is exposed on the foreshore. On some low lying areas low water of spring tides exposes much larger areas of rock than ordinary or neap tides, eg. the area occupied by beds 505–530 north of Robin Hood's Bay town.

Before submission to King's College, Bairstow made machine copies of his map, which he kept throughout his working life and they form the basis of the maps reproduced here. These copies differ from the original maps only in Bairstow's addition of 'datum lines' for locating the ammonites he collected (see the account of his ammonite collection, p. 117 below). I considered the possibility of reproducing Bairstow's original maps in the King's College archives, but the small size of the lettering of the bed numbers, the colour, thinness and lack of sufficient boldness of some of the lines, and logistical difficulties of reproducing maps that are larger than A3 (in one direction), were all against direct reproduction of the originals. After consideration of scale and legibility at the final printed size, it was decided to copy the maps at a different scale, and to divide them into the five sheets (see Fig. 4) that give a better division of the outcrops in Robin Hood's Bay than the original eight maps. Tracing was done with great care, so that the geological lines on the resulting maps reproduced here as Figs 5, 6, 8, 11 and 15 are as close as possible to the lines originally drawn by Bairstow. No alterations were made, and in those parts that were checked, such as the seaward edge of outcrops opposite the mouth of Mill Beck, south of Stoupe Beck, and in Wine Haven, the maps appear to be still accurate, 70 years after they were drawn.

Bairstow did not, however, include the lowest and highest beds on his map: the lowest bed he mapped was the seaward edge of bed 422, Low Balk, though he collected ammonites from lower beds down to bed 421.1. The outcrops of beds 418–421, seaward of Low Balk, were added to the map of Fig. 11 from observations made at the lowest spring tide of the year on 9 September 1991, when they were easily accessible. Similarly, at the top of the succession, the highest bed mapped by Bairstow was bed 590.3, on the south side of Bulmer Steel Hole, even though this is 250 m south of Castle Chamber, which is usually taken as marking the northern boundary of the bay. The higher beds northwards past Castle Chamber and up to the boundary between the Lower and Upper Pliensbachian (ie. the Lower/Middle Lias boundary) were also added to the map of Fig. 5 in September 1991. Thus, the mapping was completed between the lowest bed exposed by the lowest spring tides and the upper boundary of the Lower Pliensbachian. The five large-scale maps are printed here at a scale of 1:5315.

Map 1 (Fig. 5) is the northernmost map and starts from the highest beds outside the bay to the north-west at the junction with the Upper Pliensbachian. The main geographical feature is the cave of Castle Chamber, where the hard shelly sandstones of beds 599 and 601.1 form the floor and roof of the cave. The outcrop is fairly narrow along the whole of this east facing part of the bay, and is subject to aggressive wave action that results in relatively clean rock surfaces and good exposures.

Map 2 (Fig. 6) covers the whole sweep of the scars north and south of Robin Hood's Bay town, from the ironstone shales at the top of the map, down through the softer, pyritous shales opposite Dungeon Hole and Ground Wyke (Fig. 7), to the hard siliceous shales that form prominent scars opposite Robin Hood's Bay town. These are Landing

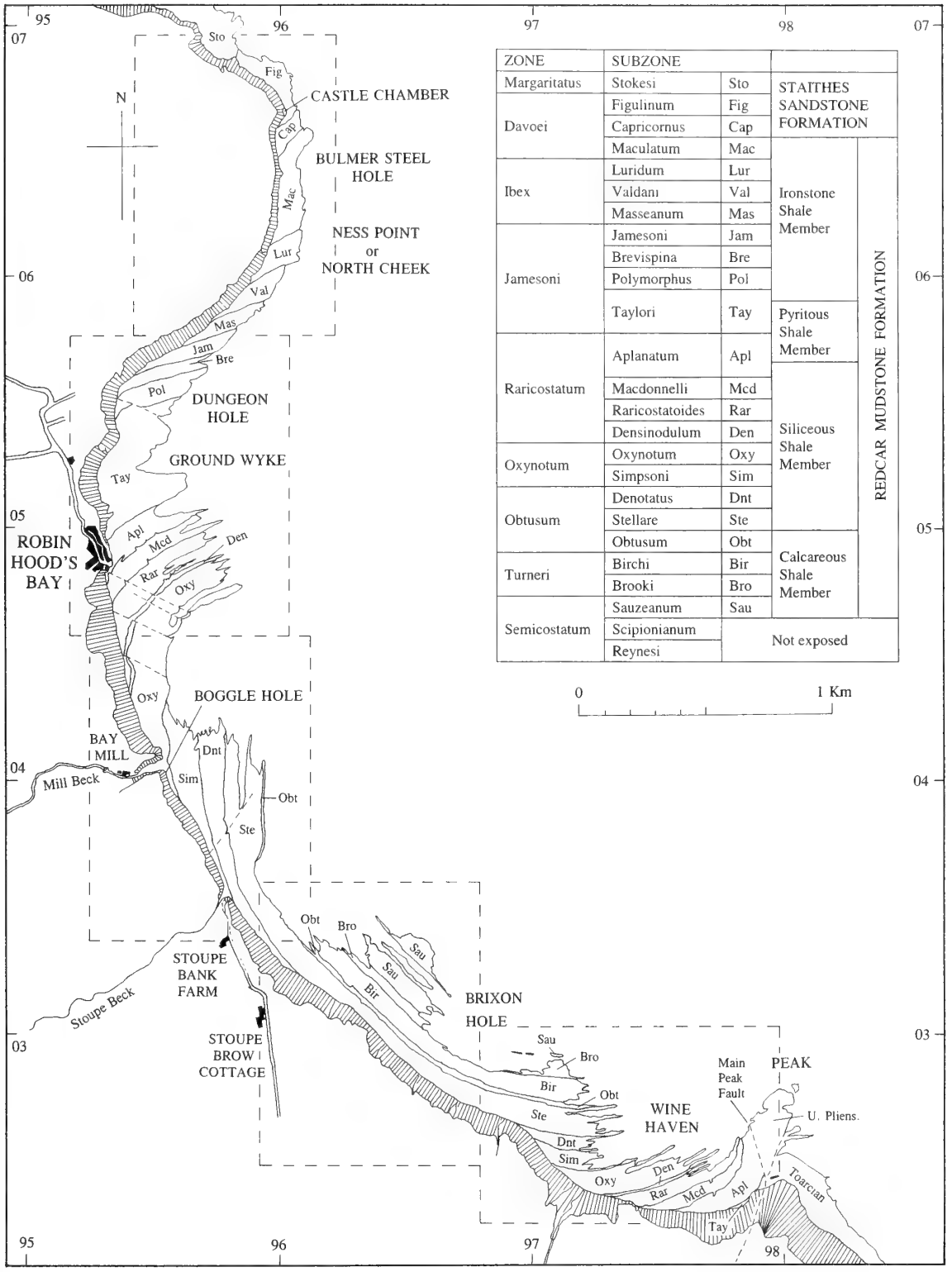

ZONE	SUBZONE		
Margaritatus	Stokesi	Sto	STAITHES SANDSTONE FORMATION
Davoei	Figulinum	Fig	
	Capricornus	Cap	
	Maculatum	Mac	Ironstone Shale Member / REDCAR MUDSTONE FORMATION
Ibex	Luridum	Lur	
	Valdani	Val	
	Masseanum	Mas	
Jamesoni	Jamesoni	Jam	
	Brevispina	Bre	
	Polymorphus	Pol	
	Taylori	Tay	Pyritous Shale Member
Raricostatum	Aplanatum	Apl	Siliceous Shale Member
	Macdonnelli	Mcd	
	Raricostatoides	Rar	
	Densinodulum	Den	
Oxynotum	Oxynotum	Oxy	
	Simpsoni	Sim	
Obtusum	Denotatus	Dnt	
	Stellare	Ste	
	Obtusum	Obt	Calcareous Shale Member
Turneri	Birchi	Bir	
	Brooki	Bro	
Semicostatum	Sauzeanum	Sau	
	Scipionianum	Not exposed	
	Reynesi		

Fig. 4 Summary geological map of the foreshore in Robin Hood's Bay, showing the main geographical features. The geological divisions shown are the subzones, and the areas covered by the five main maps of Figs 5, 6, 8, 11 and 15 are indicated by the rectangles of dashes. The cliff is indicated by vertical lines showing approximately the steepest direction of the face. The table containing the key to the subzones is a summary of Table 1.

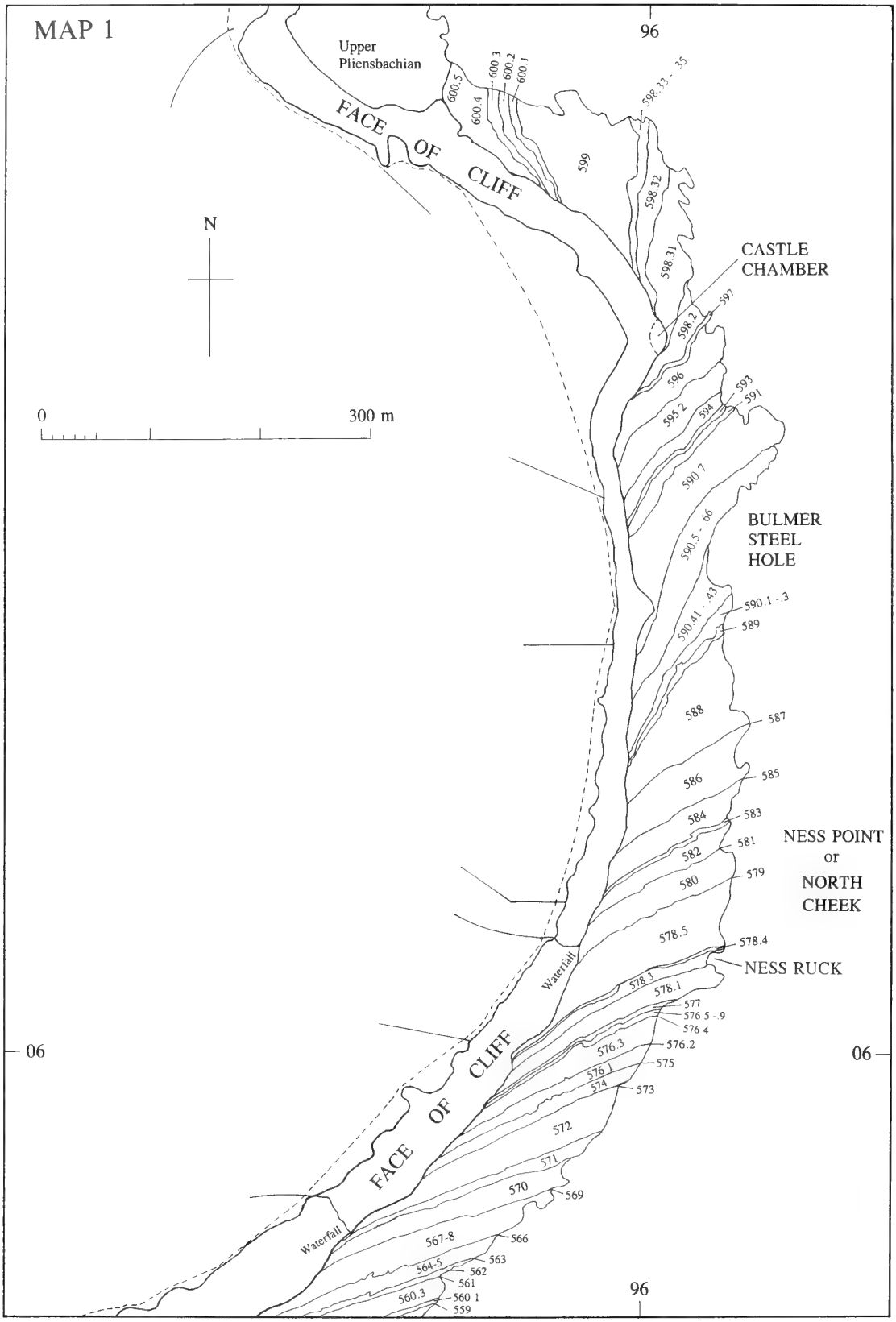

Fig. 5 Map 1, the northernmost part of Robin Hood's Bay, showing the outcrops up to the north-west corner of the bay round to the junction with the Upper Pliensbachian (Middle Lias).

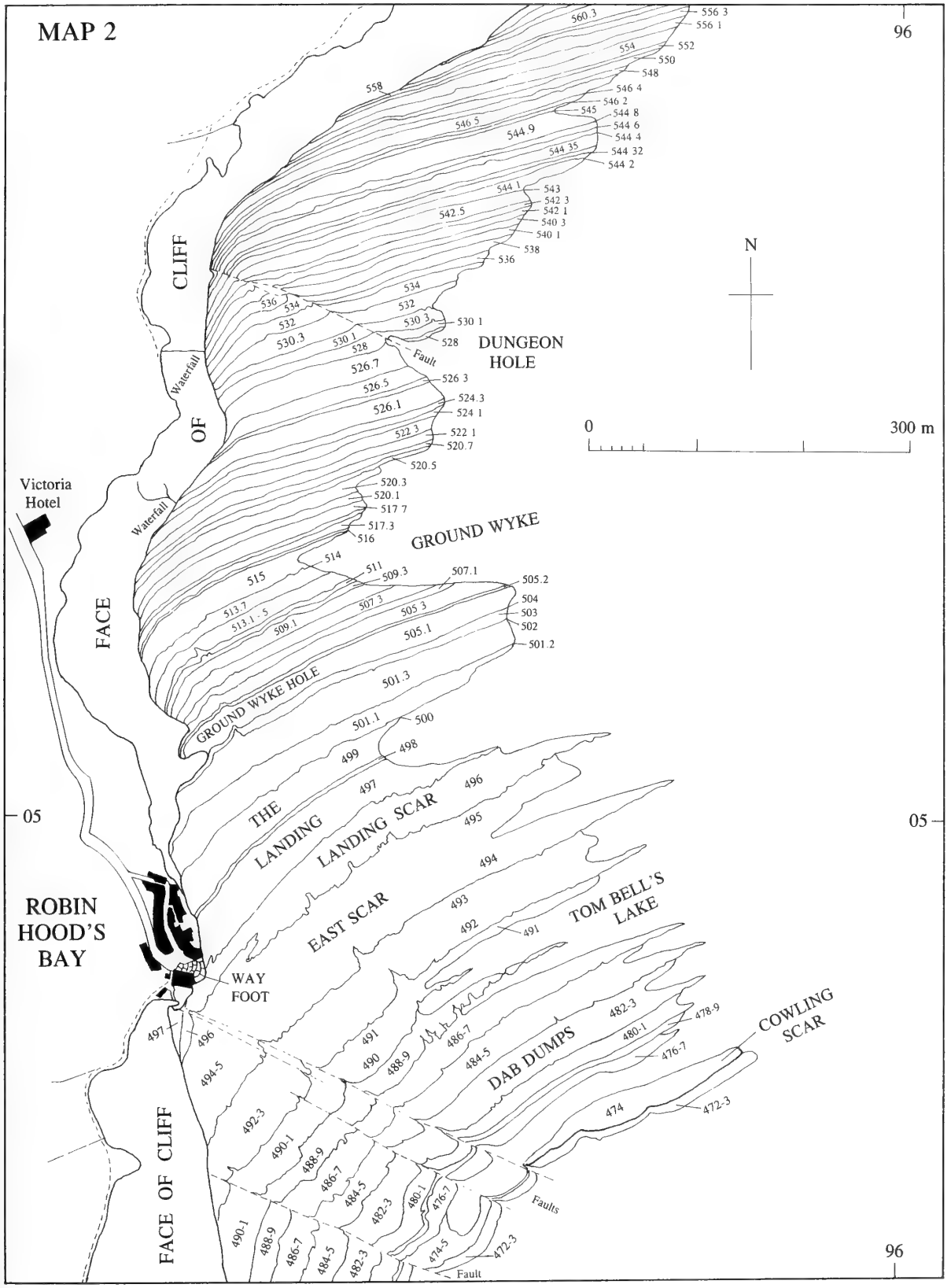

Fig. 6 Map 2, showing outcrops down to the bottom of the Lower Pliensbachian and into the top of the Upper Sinemurian in the rock scars southwards past Robin Hood's Bay town.

Fig. 7 The foreshore at low tide north of Robin Hood's Bay town. L. Bairstow photograph, 1952, taken from the top of the cliff near the northern edge of Fig. 6. The rock outcrops can be seen to have been relatively clean and free of algae and beach deposits at this time.

Scar[1] (bed 496) and East Scar (bed 494) opposite the town, and Cowling Scar (bed 474, Double Band) farther out to sea near the bottom edge of the map. The relatively soft beds of the Pyritous Shales around Ground Wyke are the wettest and lowest (relative to sea level) exposed part of the foreshore in the bay, where there is now little or poor rock exposure owing the seaweed, barnacle and mussel bed cover.

Map 3 (Fig. 8) shows an interesting entity of outcrops around the mouth of Mill Beck, the cliffs that make up 'The Nab', and the major rock scars on the foreshore to the east. There are three prominent scars here – Low Scar, Middle Scar and High Scar, being the hard, calcified silty shales of beds 447, 449 and 455 respectively. Also notable on this map are Tinkler's Stone and Strickland's Dumps, north of the mouth of Stoupe Beck, and both are named on the larger scale Ordnance Survey maps. Tinkler's Stone lies on bed 462 and is a boulder of very hard grey-brown massive limestone, of undetermined origin, but not derived from the Lower Lias. Strickland's Dumps are small, but relatively deep, excavated pools in the dip slope of beds 455.1 and 455.2. The area around Bay Mill and The Nab is shown on a larger scale in Fig. 9. High tides penetrate well into the mouth of Mill Beck between The Nab and the road on the south side of the beck, and sometimes large masses of dead algae partly block or divert the outflow of Mill Beck. However, when the mouth and bed of Mill Beck are clear of algae, the underlying beds can be seen from bed 475 at the mouth of the beck, past Bay Mill and up to bed 494 in front of the weir. They were mapped by Bairstow as shown on Fig. 9 in an amount of detail that is too great to be shown clearly on the main map. The face of The Nab, with some individual beds identified, is shown in Fig. 10.

Map 4 (Fig. 11) features the foreshore north-east of Peter White Cliff where there are exposures down to the lowest beds in Robin Hood's Bay (Fig. 12). At low tides the scars of Low Balk (bed 422; see Fig. 13) and the slightly less conspicuous Pseudo Low Balk (bed 424.2) are prominent rock platforms, both of which can normally be reached only by wading through the shallow channels between beds 424 and 425 and along the middle part of bed 422.2, which never dry out, even at the lowest spring tides. Bed 447 forms a long scarp face across the whole width of the map in front of Peter White Cliff (Fig. 14). On the Ordnance Survey maps, the name High Scar is used for two different beds: one for this bed 447 in front of Peter White Cliff, the other for bed 455 east of Mill Beck. So bed 447 forms both Low Scar east of Mill Beck and the Ordnance Survey's 'High scar' at Peter White Cliff. In view of the possible confusion, the latter use of 'High Scar' is not perpetuated here.

Map 5 (Fig. 15) reaches the south-east corner of the bay, where the Lower Lias succession is truncated by the Peak Fault complex. The Main Peak Fault has a downthrow to the east and a large lateral movement, resulting in Upper Pliensbachian and Toarcian beds on the east abutting the top beds of the Sinemurian and bottom beds of the Lower Pliensbachian on the west. There is a narrow zone of severely shattered beds immediately west of the fault, and minor faults and cracks for some distance farther west. The highest bed exposed on the rock platforms below the cliffs is bed 501.1, the

[1]'Scar' is a term frequently used in descriptions of Yorkshire coast geology for rock outcrops on the foreshore, which are usually below (but may sometimes be above) the level reached by normal high tides. In Robin Hood's Bay several scars are given formal names on some larger scale maps of the Ordnance Survey, and a few others are newly named in this paper. Such scars are formed by, or at least topped by, single beds of hard rock, and all are intertidal in Robin Hood's Bay.

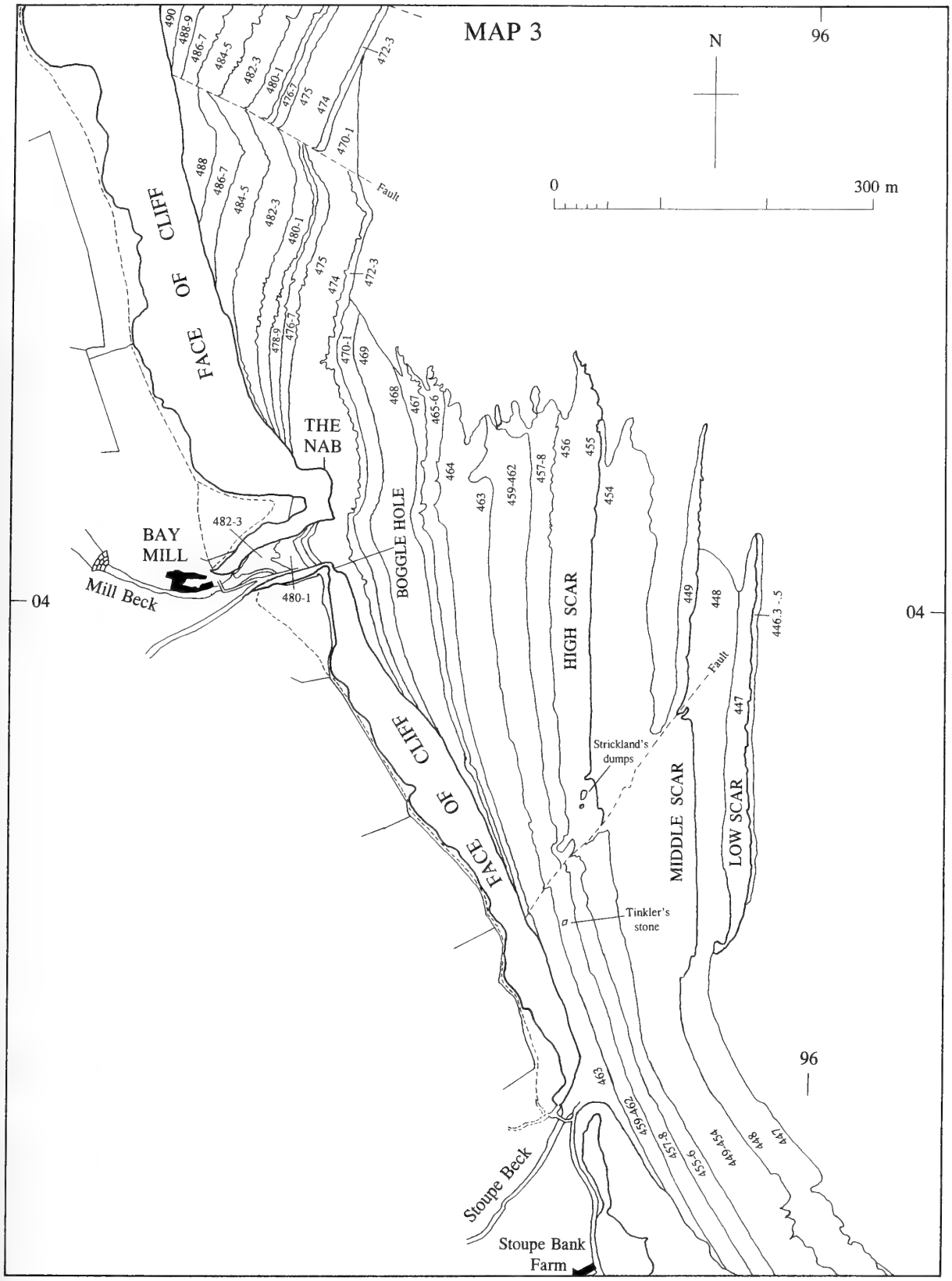

Fig. 8 Map 3, the middle map of the bay, showing the prominent scars on the foreshore east of The Nab and the mouth of Mill Beck, down to the mouth of Stoupe Beck at the bottom of the map.

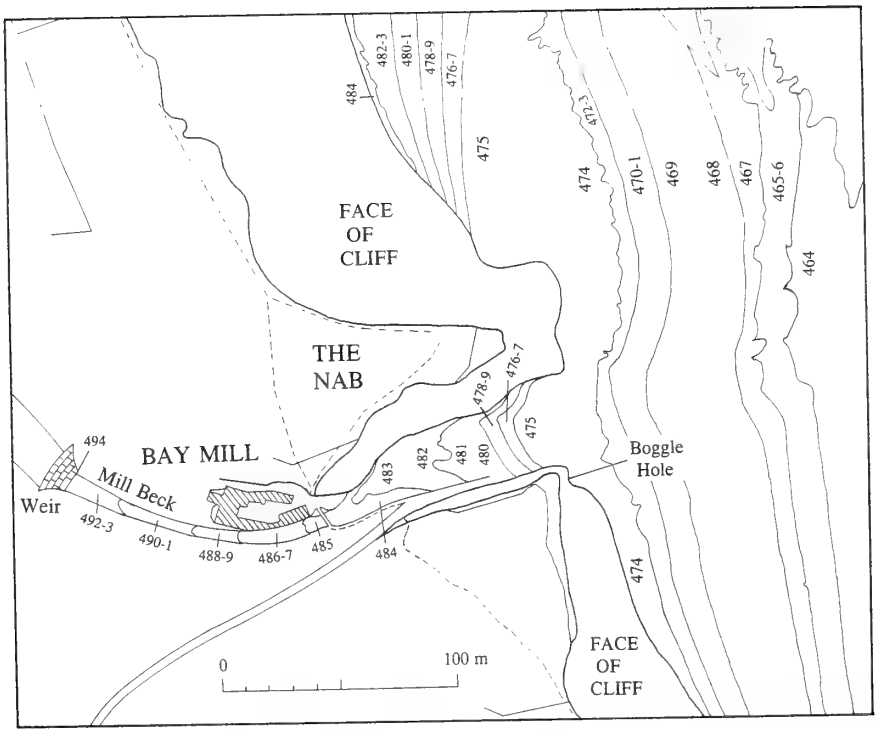

Fig. 9 Details of the outcrops of beds 475–494 in the bed of Mill Beck from the mouth of the beck up to the weir west of Bay Mill.

Fig. 10 The seaward face of The Nab immediately north of the mouth of Mill Beck. M.K. Howarth photograph, 11 September 1991. The beds here are the middle part of the Siliceous Shale Member and belong to the Oxynotum to basal Raricostatoides Subzones; the main beds are identified on the right hand side of the photograph.

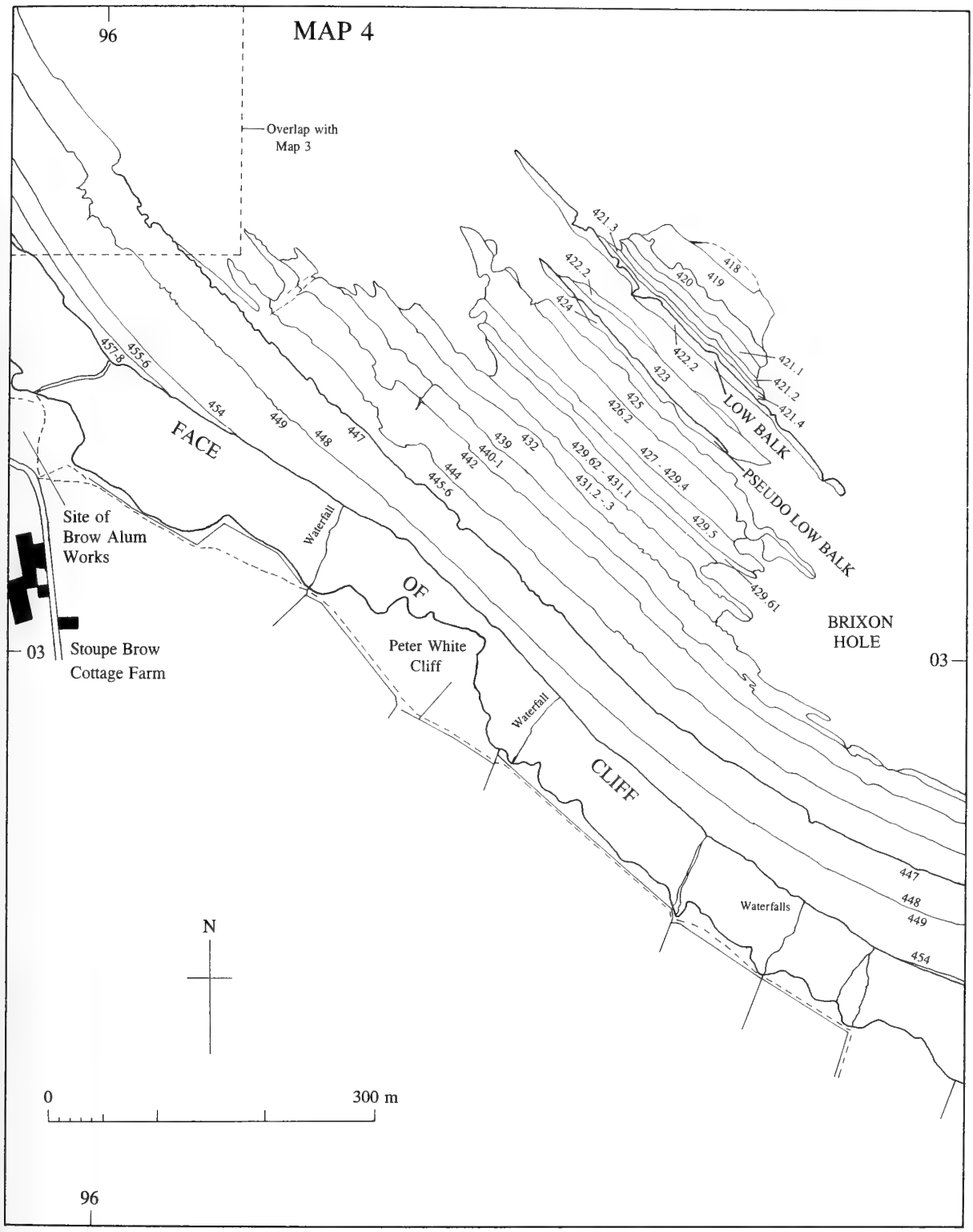

Fig. 11 Map 4, showing outcrops down to the lowest beds exposed in the bay north-east of Peter White Cliff.

Fig. 12 Oblique aerial view of the foreshore in front of Peter White Cliff at low tide. Air Ministry photograph, 10 October 1938, formerly Crown Copyright. The line of Low Balk (bed 422.2) is the lowest bed visible farthest from the cliff (see Fig. 13), and the long outcrop of the prominent bed 447 can be seen just below the cliff (see Fig. 14).

Fig. 13 Low Balk (bed 422.2) at low water of spring tide, almost the farthest accessible point north-east of Peter White Cliff. M.K. Howarth photograph, 10 September 1991.

Fig. 14 The prominent hard calcified shale of bed 447 in front of Peter White cliff. M.K. Howarth photograph, 10 September 1991.

lowest bed of the Lower Pliensbachian. The most prominent bed on the map is bed 474, Double Band, which forms Billet Scar (see Fig. 16). The narrow excavation through beds 476–486 known as The Dock, was originally made for fishing and smuggling purposes.

GEOLOGICAL STRUCTURE OF ROBIN HOOD'S BAY

The pattern of the outcrops on the foreshore of the bay as seen in Fig. 4 is determined by the structure of the rocks (Fig. 17). That structure was first alluded to by Tate & Blake (1876: 27, 196) who described Robin Hood's Bay as 'a complete inlier . . . in the form of a mound, dipping in all directions from the centre . . . the centre of elevation beneath the sea, nearly opposite the centre of the bay'. In the Geological Survey memoir, Fox-Strangways & Barrow (1915: 3, 115) referred to the Lias as 'curving over in a gentle arch or anticline'. Versey (1939: pl. 15) plotted the contours of the base of the Grey Limestone (=Scarborough Formation; Lower Bajocian) over a wide area and showed that around the southern and western sides of Robin Hood's Bay they formed the outer part of a north-west to south-east elongated dome. According to Versey (1939) the dome was produced by tectonic movements probably in the late Pliocene. Kent (1974: 25, 26) and de Boer (1974: 281) accepted the date of formation of the dome as later than the mid-Tertiary Alpine movements and probably Pliocene.

The central part of the Robin Hood's Bay dome can be defined by the outcrops of the Lower Lias on the foreshore of the bay. Fig. 17 shows contours on the outcrop at 10 m bed-thickness intervals, with the 0 m contour starting at the top of bed 422.2, Low Balk. Because the outcrop on the foreshore is essentially flat, the contours approximate closely to strike lines, and they form the pattern of a dome, with a NW to SE axis of elongation in approximately the position shown on the figure. The dip of the beds is at right angles to each contour line away from the centre of the dome. In the northern part of the bay the beds dip NW, and from the 50 m to the 150 m contours the average distance between adjacent contours is 128 m; this gives an average dip of 4.5° for the beds. Between the 20 m and 40 m contours the beds dip to the west, while the lowest beds between the 0 m and 20 m contours dip between west and south at an average of 3.2°. In the south-east corner of the bay near the Peak Fault the beds curve round to dip south-easterly. The Peak Fault throws down on its eastern side and has a lateral movement of several kilometres. Its northern continuation across Robin Hood's Bay, passing close to the shore at the northern end of the bay, is shown on Fig. 17 in accordance with data on the latest map of the British Geological Survey that includes off-shore geology (British Geological Survey, 1995, Tyne Tees, sheet 54°N–02°W, 1:250,000, solid geology).

STRATIGRAPHICAL SUCCESSION

Bairstow drew up a description of the succession in Robin Hood's Bay in 1928–30 and the detailed sequence of beds formed an

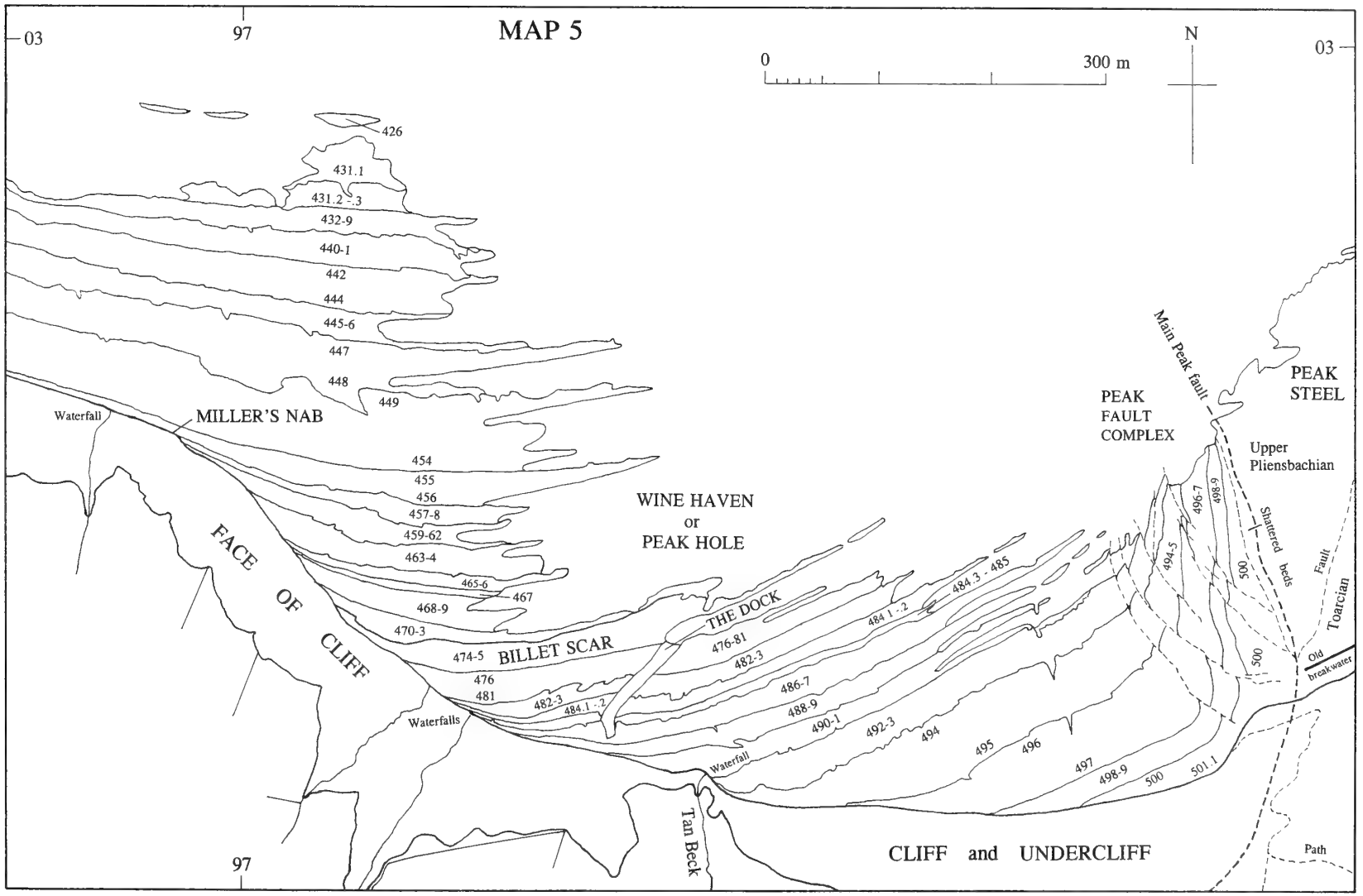

Fig. 15 Map 5, showing the outcrops of Sinemurian and basal Pliensbachian beds in the south-eastern end of the bay, up to their junction with the Peak Fault, which throws them against Upper Pliensbachian and Toarcian to the east.

Fig. 16 The foreshore at low tide in Wine Haven looking eastwards towards Peak and the bottom of the cliff below Ravenscar. L. Bairstow photograph, 1929 or 1930. This view looks along the prominent outcrop of Billet Scar (bed 474) in the middle of the photograph, and 'The Dock' crosses the beds obliquely to the right.

important part of his fellowship submission to King' College. He kept carbon copies of the 85 typed pages of the sequence, and during subsequent years up to 1975 he made alterations, additions and notes on the originals until the final size of the manuscript was about 230 pages. Many alterations were made to the bed numbering, especially at the top, and to the bed thicknesses and details of the lithology, none of which were fully finalized at the time of his fellowship submission. This manuscript is the basis for the much edited version of the stratigraphical succession given below, where as much of the lithological description as necessary has been retained to describe and identify individual beds in the sequence. Bairstow measured bed thicknesses on both the foreshore scars and in the cliffs in order to arrive at figures he considered accurate, and his measurements in feet and inches have been converted to metric units for this paper.

The lithostratigraphical divisions given in the succession below are not those of Bairstow. They are based on more recent work described below in a separate section. Similarly, the zone and subzone divisions given in the succession are based on revisions of the identifications of all Bairstow's ammonites, also as described in a separate section. Table 1 shows a detailed correlation between the zones and subzones, the bed numbers and the lithostratigraphical divisions.

Bed numbers

Bairstow started his detailed description of the beds in 1928 by giving the bed number 500 to the nodules that form the northern boundary of The Landing at Bay Town, and worked up and down the succession from that level. That bed number was selected because he did not know what his lowest and highest numbers would be, and also to 'prevent confusion with the numbers [1–132] given by Lang to Lower Lias beds of similar age on the Dorset coast'. After several changes to his various schemes, especially in the top part of the succession, he finalized his numbering with bed 418 as the horizon exposed at the lowest level reached by spring tides in the bay, and bed 601 as the highest he described in the Staithes Sandstone Formation just beyond the northern end of the bay. In various places he subdivided individual beds by giving numbers after a decimal point (eg. beds 485.1, 485.2, 485.3), and a few beds were subdivided to two places of decimals (eg. beds 464.31, 464.32, 464.33). In bed 590,

STAGE	ZONE	SUBZONE	m	BED NO		
U. Pliensbachian	Margaritatus	Stokesi (part)		600.6-601.2	STAITHES SANDSTONE FORMATION	
Lower Pliensbachian	Davoei 32.63 m	Figulinum	9.70	596.2-600.5		
		Capricornus	3.04	591-596.1		
		Maculatum	19.89	581-590.7	Ironstone Shale Member 62.73 m	REDCAR MUDSTONE FORMATION, 151 m
	Ibex 20.39 m	Luridum	7.24	578.1-580		
		Valdani	7.66	571-577		
		Masseanum	5.49	560.3-570		
	Jamesoni 44.46 m	Jamesoni	5.66	550-560.3		
		Brevispina	3.72	544.6-549		
		Polymorphus	7.05	538-544.5		
		Taylori	28.03	527-537		
				501.1-526.7	Pyritous Shale Member, 26.18 m	
Upper Sinemurian	Raricostatum 17.26 m	Aplanatum	5.57	497-500		
				496	Siliceous Shale Member 38.74 m	
		Macdonnelli	4.48	494-495.7		
		Raricostatoides	6.21	488-493.5		
		Densinodulum	1.00	486.3-487		
	Oxynotum 14.91 m	Oxynotum	9.19	472.1-486.2		
		Simpsoni	5.72	463-471		
	Obtusum 12.45 m	Denotatus	3.37	455.2-462		
		Stellare	7.37	447-455.1		
		Obtusum	1.71	446.31-446.5	Calcareous Shale Member 23.35 m exposed	
Lower Sinemurian (part)	Turneri 7.75 m	Birchi	5.89	433.3-446.2		
		Brooki	1.86	429.7-433.2		
	Semicostatum 13.89 m	Sauzeanum	13.89	418-429.64		
		Scipionianum		Not exposed		
		Reynesi				

Table 1 Summary of the bed numbers used in Robin Hood's Bay, and their grouping into zones and subzones (including thicknesses), and members and formations, showing the detailed correlation between biostratigraphical and lithostratigraphical divisions.

however, he used three places of decimals (eg. bed 590.433) and in bed 598 he used four places of decimals (eg. bed 598.4322). Three and four places of decimals are considered here to be too cumbersome to be acceptable, so they have all been replaced in this description with the minimum amount of renumbering necessary to achieve single and double decimal numbering in beds 590 and 598. Unfortunately, it was not possible to replace all the double decimal numbering in the succession, because there are more than 9 divisions in beds 429, 495, 544 and 590, and to replace them would have involved renumbering the whole succession. This was not practicable in view of the large number of entries of the original bed numbers on specimen labels, index cards and original manuscripts and maps. It should be noted, however, that the subdivisions that Bairstow used for bed 600 are not in a decimal system like those in all the lower beds – subdivisions of bed 600 use the 13 suffix numbers 1–13 after the decimal point; as these are at the top of the succession extending out of Robin Hood's Bay to the north, they are retained here without alteration.

DETAILED SUCCESSION IN ROBIN HOOD'S BAY

In the following detailed succession records of all the ammonites and nautiloids in Bairstow's collection are included for each bed; the first number in brackets following each species is the total number of specimens, and is followed by their registration numbers, then by a reference to any specimens figured here; in a few cases the number of registration numbers quoted is less than the total number of specimens recorded, because specimens were lost, destroyed, poorly preserved, uncollectable (but observed by Bairstow), or too numerous to be worth registering all of them. The thickness of each bed is given in the right hand column in metres (m).

Specimen register numbers are identified here and in the remainder of the paper by the following prefixes: C. and CA – The Natural History Museum, London; GSM – British Geological Survey (Geological Survey Museum), Keyworth, Nottinghamshire; OUM – Oxford University Museum; SM – Sedgwick Museum, Cambridge; WM – Whitby Museum, Yorkshire.

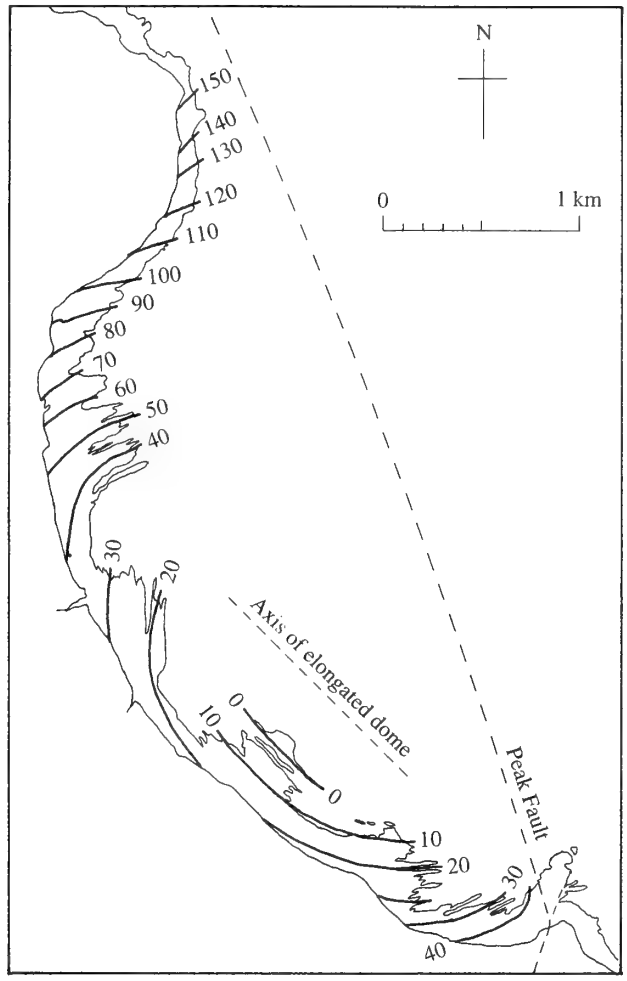

Fig. 17 Map showing contours at 10 m bed thickness intervals in the Lower Lias on the foreshore of Robin Hood's Bay, from which the elongated dome geological structure can be deduced. The only geographical features shown are the line of the base of the cliff and the low tide mark. See text for further explanation.

STAITHES SANDSTONE FORMATION (PART)

Zone of *Amaltheus margaritatus*
Subzone of *Amaltheus stokesi* (lower part)

Bed no.		*m*
601.2	Sandstone, soft, micaceous, laminated	0.66
601.1	Sandstone, hard, shelly in parts; many *Gryphaea* sp.; forms the roof of Castle Chamber at north-west end of Robin Hood's Bay	0.81
600.13	Sandstone, soft, silty	0.33
600.12	Shale, silty	0.38
600.11	Limestone nodules	0.10
600.10	Shale, silty	0.08
600.9	Shale, sandy	0.38
600.8	Shale, silty, with horizon of limestone nodules near top *Amaltheus stokesi* (J. Sowerby) 0.3 m above base (1; CA 4605)	0.53
600.7	Shale, sandy, laminated; forms the most conspicuous positive feature between floor and roof of Castle Chamber	0.25
600.6	Flat limestone nodules *Amaltheus stokesi* (J. Sowerby) (1; MKH Coll, lost).	0.13

Zone of *Prodactylioceras davoei*
Subzone of *Aegoceras (Oistoceras) figulinum*

600.5 Shale, silty, pale grey 0.36
600.4 Limestone nodules (= bed v of Howarth, 1955: 155) 0.06
Aegoceras (Oistoceras) figulinum (Simpson) (11; SM J35968, SM J44776-85).
600.3 Shale, silty 0.91
600.2 Limestone, sideritic, forming a continuous bed (= bed iii of Howarth, 1955: 155) 0.18
Aegoceras (Oistoceras) angulatum (Quenstedt) (9; SM J44790, CA 4595–4602).
600.1 Shale, silty 0.15
599 Sandstone, flaggy, with ripple marks and oyster bands; the top surface forms the floor of Castle Chamber (= bed i of Howarth, 1955: 155) 1.42
Aegoceras (Oistoceras) angulatum (Quenstedt) (1; SM J44789)
598.35 Shale, silty, laminated 0.33
598.34 Limestone nodules 0.08
598.33 Shale, silty, laminated 1.00
598.32 Limestone, grey, weathering yellow; forms continuous tabular bed 0.10
598.31 Shale, silty, soft, but harder near top 2.79
598.2 Shale, silty, hard; forms a conspicuous feature in the cliff and on the scar 0.15
598.1 Shale, silty, soft, darker than the two beds above; occasional sideritic mudstone nodules in middle and upper part 0.67
Aegoceras (Oistoceras) sinuosiforme Spath (5; C.38930, C.39556, C.39579, CA 4594; Pl. 7, fig. 14).
597 Limestone nodules 0.13
Aegoceras (Oistoceras) sinuosiforme Spath (42; C.39398, C.39418-36 [C.39421/22 and C. 39429/30 are single specimens], C.39499-39502, C.39505-07, C.39561, C.39568-77, CA 4588-93).
596.3 Shale, silty, with 0.09 m thick limestone nodules, especially in a band 0.3m below the top 1.22
Aegoceras (Oistoceras) sinuosiforme Spath (28; C.39396-97, C.39399-39417, C.39437-38, C.39504, C.39549, C.39559, CA 4586-87), *Liparoceras (L.) divaricosta* (Trueman) (1; C.39455; Pl. 8, fig. 1).
596.2 Hard, calcified shale, with occasional sideritic mudstone nodules 0.15
Aegoceras (Oistoceras) sinuosiforme Spath (18; C.39503, C.39508-10, C.39560, C.39562-67, C.39578, CA 4580-85).

Subzone of *Aegoceras (A.) capricornus*

596.1 Shale, soft; occasional calcareous mudstone nodules 0.85
595.2 Shale, silty, lower half soft, upper half harder; some lenses of oysters 0.56
595.1 Scattered calcareous mudstone nodules in hard silty shale 0.10
594 Shale, silty, with a few calcareous mudstone nodules 0.61
Aegoceras (A.) lataecosta (J. de C. Sowerby) (1, lost), *Aegoceras (A.)* sp. indet. (10; CA 4579).
593 Sideritic mudstone nodules; conspicuous on the scars at Bulmer Steel Hole 0.13
Aegoceras (A.) artigyrus (Brown) (4; CA 4604).
592 Shale, silty, laminated with some hard bands; a few sideritic mudstone nodules 0.61
591 The Oyster Bed. Hard, silty shale, with flat sideritic mudstone nodules; many oysters and other bivalves 0.18
Aegoceras (A.) lataecosta (J. de C. Sowerby) (1; C.39395).

REDCAR MUDSTONE FORMATION
IRONSTONE SHALE MEMBER

Subzone of *Aegoceras (A.) maculatum*

590.7 Shale, silty 1.42
590.66 Spherical sideritic mudstone nodules 0.10
590.65 Shale, silty, with scattered sideritic mudstone nodules 0.23
590.64 Sideritic mudstone nodules 0.08
590.63 Shale, silty, with scattered sideritic mudstone nodules near the base 0.20
Aegoceras (A.) maculatum (Young & Bird) (8; C.38881, C.38886-90, C.38893, CA 4578), *Aegoceras (A.) maculatum* (Young & Bird) var. *leckenbyi* Spath (1; C.38880).
590.62 Shale, silty 0.41
590.61 Shale, silty, with many sideritic mudstone nodules 0.46
Aegoceras (A.) maculatum (Young & Bird) (8; C.38882-85, C.38891-92, C.38894, C.38896; Pl. 7, fig. 13).
590.5 Shale, silty 1.30
590.43 Shale, silty, with a few sideritic mudstone nodules near the top 0.23
590.42 Calcareous mudstone nodules 0.08
590.41 Shale, silty, with a few sideritic mudstone nodules near the base 0.20
590.3 Shale, silty, with occasional very large (up to 1 m diameter) sideritic mudstone nodules 0.5–1.5 m below the top; seen on the scar on the south side of Bulmer Steel Hole 3.58

590.2 Hard silty shale, with many small sideritic mudstone nodules 0.41
590.1 Shale, silty, with occasional sideritic mudstone nodules 0.51
Aegoceras (A.) maculatum (Young & Bird) (7; C.38895, CA 4573-77), ?*Androgynoceras* sp. indet. (1; CA 4603).
589 Large sideritic mudstone nodules; a strongly marked band crossing the shore south of Bulmer Steel Hole 0.15
588 Shale, silty; one very large sideritic mudstone nodule 1 m below top 4.95
Aegoceras (A.) maculatum (Young & Bird) (5; C.39136, C.38878-79, CA 4571-72), *Androgynoceras heterogenes* (Young & Bird) (1; C.39136), *Liparoceras (L.)* sp. indet. (2; CA 4562-63).
587 Flat septarian sideritic mudstone nodules, some with domed upper surfaces 0.13
586 Shale, silty 2.29
585 Flat septarian sideritic mudstone nodules, some with domed upper surfaces, and sometimes forming a continuous bed 0.13
Aegoceras (A.) maculatum (Young & Bird) (1; C.38877).
584 Shale, silty 1.45
?*Lytoceras* sp. indet. (1; CA 2795), *Aegoceras (A.) maculatum* (Young & Bird) (2; C.38876, CA 4570).
583.2 Shale, with scattered sideritic and calcareous mudstone nodules 0.08
Aegoceras (A.) maculatum (Young & Bird) (2; C.38871-72), *Aegoceras (A.) maculatum* (Young & Bird) var. *atavum* Spath (2; C.38873-74; Pl. 7, fig. 8), *Androgynoceras heterogenes* (Young & Bird) (1; C.38875).
583.1 Continuous bed of sideritic mudstone 0.08
582 Shale, silty, with small scattered spherical sideritic mudstone nodules 0.25 m below top 1.27
Liparoceras (L.) cf. *naptonense* Spath (1; C.39140), ?*Aegoceras* s.l. sp. indet. (1; not registered).
581 Flat sideritic mudstone nodules 0.15
Aegoceras (A.) maculatum (Young & Bird) (2; C.41307, CA 4569; Pl. 7, fig. 12).

Zone of *Tragophylloceras ibex*
Subzone of *Aegoceras (Beaniceras) luridum*

580 Shale 1.30
Aegoceras (Beaniceras) cf. *luridum* (Simpson) (1; CA 4568), *Liparoceras (L.)* cf. *naptonense* Spath (1; C.39141).
579 Flat sideritic mudstone nodules 0.15
Liparoceras (L.) sp. indet. (1; lost).
578.5 Shale 3.40
Aegoceras (Beaniceras) luridum (Simpson) (6; CA 4565-67), *Liparoceras (L.)* sp. indet. (1; CA 4561), *Lytoceras fimbriatum* (J. Sowerby) (1; lost); many large *Inoceramus*.
578.4 Sideritic shale, with many large (0.6 m diameter, or up to 0.5 m × 1.2 m) flat, septarian, sideritic mudstone nodules; forms a conspicuous bed on the scar just north of Ness Ruck; occasional logs of fossil wood 0.23
Lytoceras fimbriatum (J. Sowerby) (8; CA 2787-94).
578.3 Shale 0.76
Lytoceras fimbriatum (J. Sowerby) (2; CA 2785-86).
578.2 Shale, sideritic, with scattered sideritic mudstone nodules 0.08
Lytoceras fimbriatum (J. Sowerby) (3; CA 2782-84).
578.1 Shale, grey, with a paler and harder middle band; contains several pieces of fossil wood 1.32
Aegoceras (Beaniceras) luridum (Simpson) (1; CA 4564).

Subzone of *Acanthopleuroceras valdani*

577 Sideritic shale, with occasional sideritic mudstone nodules; crosses the scar to reach low tide mark at Ness Ruck 0.13
Liparoceras (L.) cf. *heptangulare* (Young & Bird) (1; CA 4560).
576.9 Shale 0.18
576.8 Scattered sideritic mudstone nodules in shale 0.08
576.7 Shale 0.18
576.6 Scattered sideritic mudstone nodules in shale 0.08
Lytoceras fimbriatum (J. Sowerby) (3; CA 2779-81).
576.5 Shale 0.30
576.4 Scattered flat sideritic mudstone nodules in shale 0.05
Lytoceras fimbriatum (J. Sowerby) (1; CA 2778; Pl. 1, fig. 3).
576.3 Shale; contains fossil wood 1.17
576.2 Widely scattered sideritic mudstone nodules in shale 0.10
576.1 Shale 1.02
575 Sideritic mudstone nodules, sometimes septarian 0.15
Liparoceras (L.) heptangulare (Young & Bird) (1; CA 4559), *Lytoceras fimbriatum* (J. Sowerby) (3; CA 2775-77).
574 Shale; contains fossil wood 0.74
573 Sideritic mudstone nodules 0.08
572 Shale 2.59

571 Shale, with many scattered oval sideritic mudstone nodules up to 0.15m thick 0.81
Liparoceras (L.) heptangulare (Young & Bird) (1; C.39137), *Lytoceras fimbriatum* (J. Sowerby) (1; CA 2774).

Subzone of *Tropidoceras masseanum*

570 Shale, with occasional sideritic mudstone nodules that contain gastropods and poorly preserved Crustacea 1.73
Lytoceras fimbriatum (J. Sowerby) (3; CA 2771-73).
569 Continuous bed of sideritic mudstone; outcrops in a gully on the scars, and forms a conspicuous datum line in the cliff 0.08
Tragophylloceras loscombi (J. Sowerby) (2; CA 2761-62).
568 Shale, in 7 or 8 pale and dark bands 1.68
Lytoceras sp. indet. near top of bed (1; lost); *Tropidoceras futtereri* Spath near base of bed (1; CA 4545; Pl. 7, fig. 11); *Tropidoceras masseanum* (d'Orbigny) var. *rotundum* (Futterer) at boundary of beds 567 and 568 (11; CA 4546-55).
567 Shale, hard and silty; forms a slight feature on the scar 0.15
566 Shale 0.28
Liparoceras (L.) sp. indet. (1; lost).
565 Shale, hard and silty; forms a slight feature on the scar 0.08
564 Shale, with harder silty bands at the base and the middle; the higher silty band contains occasional sideritic mudstone nodules 0.56
Liparoceras (L.) sp. indet. (1; lost).
563 Sideritic mudstone nodules; contains large logs of fossil wood 0.08
562 Shale, with occasional sideritic mudstone nodules 0.69
Tropidoceras sp. indet. (3; CA 4556-58), *Liparoceras (L.) cheltiense* (Murchison) (2; C.39138-39).
561 Flat sideritic mudstone nodules 0.08
Tropidoceras sp. indet. or ?*Uptonia* cf. *jamesoni* (J. de C. Sowerby) (2, lost).
560.3 Shale, with shelly layers (top 0.08 m only) 0.08
Tropidoceras futtereri Spath (1; CA 4544; Pl. 7, fig. 10).

Zone of *Uptonia jamesoni*
Subzone of *Uptonia jamesoni*

560.3 Shale, with shelly layers (all below the top 0.08 m) 1.32
Tragophylloceras sp. indet. (1; CA 2770), *Polymorphites bronni* (Roemer) (7; CA 4224-30; Pl. 7, fig. 5), *Uptonia lata* (Quenstedt) (1; CA 4538) and *Uptonia* cf. *jamesoni* (J. de C. Sowerby) (1; CA 4532).
560.2 Flat sideritic mudstone nodules; together with bed 559, forms a distinctive pair of nodule beds on the scar 0.08
Uptonia jamesoni (J. de C. Sowerby) (1; CA 4531), *Polymorphites bronni* (Roemer) (2; CA 4222-23).
560.1 Shale 0.15
Polymorphites bronni (Roemer) (1; CA 4221).
559 Flat sideritic mudstone nodules 0.08
Uptonia jamesoni (J. de C. Sowerby) (1; CA 4530), *Uptonia* sp. indet. (1; CA 4543), *Polymorphites bronni* (Roemer) (1; CA 4220).
558 Shale, with occasional sideritic mudstone nodules at about the middle of the bed 0.66
Uptonia lata (Quenstedt) (5; CA 4533-37), *Uptonia* sp. indet. (4; CA 4539-42), *Polymorphites bronni* (Roemer) (16; CA 4204-19), *Tragophylloceras* sp. indet. (1; CA 2769).
557 Flat sideritic mudstone nodules; conspicuous in the cliff 0.13
Uptonia cf. *jamesoni* (J. de C. Sowerby) (1; CA 4529).
556.3 Shale 0.41
Uptonia jamesoni (J. de C. Sowerby) (1; CA 4528).
556.2 Small spherical, grey, calcareous mudstone nodules, with a few larger flat sideritic mudstone nodules 0.08
Uptonia jamesoni (J. de C. Sowerby) (5; CA 4523-27), *Polymorphites bronni* (Roemer) (3; CA 4201-03).
556.1 Shale 0.71
Polymorphites bronni (Roemer) (5; CA 4196-4200).
555 Grey calcareous mudstone nodules mixed with larger sideritic mudstone nodules 0.10
Uptonia jamesoni (J. de C. Sowerby) (1; CA 4522), *Polymorphites polymorphus* (Quenstedt) (2; CA 4316-17; Pl. 7, fig. 3).
554 Shale 0.76
Uptonia jamesoni (J. de C. Sowerby) (2; CA 4520-21), *Polymorphites bronni* (Roemer) (1; CA 4195), *Parinodiceras parinodum* (Quenstedt) (1; C.39142).
553 Flat sideritic mudstone nodules mixed with a few smaller grey calcareous mudstone nodules 0.13
Tragophylloceras sp. indet. (1; CA 2768).
552 Shale 0.33
551 Scattered sideritic mudstone nodules, mixed with smaller grey calcareous mudstone nodules, in shale 0.08

Uptonia jamesoni (J. de C. Sowerby) (5; CA 4515-19).

550 Shale 0.64
Uptonia jamesoni (J. de C. Sowerby) (5; CA 4510-14), *Platypleuroceras* cf. *brevispina* (J. de C. Sowerby) (3; CA 4469-71).

Subzone of *Platypleuroceras brevispina*

549 Flat sideritic mudstone nodules 0.10
548 Shale 0.36
Parinodiceras parinodum (Quenstedt) (1; C.39144), *Platypleuroceras brevispina* (J. de C. Sowerby) (2; CA 4467-68), *Radstockiceras* sp. indet. (1; CA 3761).
547 Flat sideritic mudstone nodules 0.10
546.5 Shale, with occasional small siderite mudstone nodules in the lower part 1.02
Platypleuroceras aureum (Simpson) (7; CA 4489-95), *Platypleuroceras brevispina* (J. de C. Sowerby) (2, lost), *Polymorphites* sp. indet. (1; lost).
546.4 Scattered sideritic mudstone nodules in shale 0.08
Platypleuroceras brevispina (J. de C. Sowerby) (9; CA 4458-66), *Platypleuroceras* cf. *aureum* (Simpson) (1; CA 4488), *Tragophylloceras* sp. indet. (2; CA 2766-67).
546.3 Shale 0.23
Platypleuroceras brevispina (J. de C. Sowerby) (11; CA 4448-57), *Platypleuroceras aureum* (Simpson) (5; CA 4483-87), *Platypleuroceras* sp. indet. (8; CA 4502-09), *Polymorphites trivialis* (Simpson) (1; CA 4396), *Parinodiceras parinodum* (Quenstedt) (1; C.39143).
546.2 Sideritic mudstone nodules 0.08
Platypleuroceras brevispina (J. de C. Sowerby) (2; CA 4446-47), *Platypleuroceras aureum* (Simpson) (4; CA 4479-82; Pl. 7, fig. 6), *Polymorphites trivialis* (Simpson) (1; CA 4395).
546.1 Shale 0.33
Platypleuroceras brevispina (J. de C. Sowerby) (10; CA 4436-45), *Platypleuroceras aureum* (Simpson) (6; CA 4473-78), *Platypleuroceras* sp. indet. (6; CA 4496-4501), *Polymorphites trivialis* (Simpson) (1; CA 4394).
545 Flat sideritic mudstone nodules; forms a minor feature in a conspicuous gully on the scar 0.15
Platypleuroceras brevispina (J. de C. Sowerby) (1; CA 4435).
544 Shale with horizons of nodules, 4.27 m thick; forms a cambered pavement on the scar, bordered on north and south by conspicuous gullies; might be called the '*Polymorphites* Bed'.
544.9 Shale 0.71
Platypleuroceras brevispina (J. de C. Sowerby) (4; CA 4431-34), *Polymorphites trivialis* (Simpson) (13; CA 4381-93).
544.8 Scattered flat sideritic mudstone nodules in shale 0.10
Polymorphites trivialis (Simpson) (3; CA 4378-80).
544.7 Shale 0.36
Platypleuroceras obsoleta (Simpson) (1; CA 4472), *Platypleuroceras brevispina* (J. de C. Sowerby) (38; CA 4398-4430), *Polymorphites trivialis* (Simpson) (3; CA 4375-77), *Radstockiceras buvignieri* (d'Orbigny) (2; CA 3749-50).
544.6 Flat sideritic mudstone nodules 0.10
Polymorphites trivialis (Simpson) (5; CA 4370-74), *Platypleuroceras brevispina* (Simpson) (1; CA 4397), *Radstockiceras* sp. indet. (1; CA 3760).

Subzone of *Polymorphites polymorphus*

544.5 Shale 0.33
Polymorphites trivialis (Simpson) (25; CA 4347-69), *Tragophylloceras* cf. *numismale* (Quenstedt) (1; CA 2760).
544.4 Scattered flat sideritic mudstone nodules in shale 0.10
Polymorphites trivialis (Simpson) (20; CA 4327-46), *Radstockiceras sphenonotum* (Monke) (2; CA 3757-58; Pl. 5, fig. 4), *Radstockiceras* sp. indet. (1; CA 3759).
544.35 Shale, with a few grey calcareous mudstone nodules 0.93
Polymorphites trivialis (Simpson) (11; CA 4319-26; Pl. 7, fig. 7).
544.34 Small grey calcareous mudstone nodules 0.08
544.33 Shale 0.32
544.32 Scattered flat sideritic mudstone nodules in shale 0.05
544.31 Shale 0.40
Tragophylloceras cf. *numismale* (Quenstedt) (1; CA 2759).
544.2 Small grey calcareous mudstone nodules 0.08
544.1 Shale, with two horizons of small spherical grey calcareous mudstone nodules 0.71
543 Continuous bed of sideritic mudstone; forms the northern boundary of a deep gully 0.15
542.5 Shale 0.71
Polymorphites caprarius (Quenstedt) (10; CA 4306-15), *Radstockiceras sphenonotum* (Monke) (2; CA 3755-56).

542.4 Scattered small dark grey calcareous mudstone nodules in shale 0.04
Epideroceras sp. indet. (2; CA 4071-72), *Polymorphites caprarius* (Quenstedt) (15; CA 4292-4305), *Polymorphites trivialis* (Simpson) (1; CA 4318), *Radstockiceras sphenonotum* (Monke) (3; CA 3752-54), *Tragophylloceras* sp. indet. (1; CA 2765).

542.3 Shale 0.33
Polymorphites caprarius (Quenstedt) (6; CA 4286-91).

542.2 Scattered small grey calcareous mudstone nodules in shale 0.04
Polymorphites caprarius (Quenstedt) (5; CA 4281-85).

542.1 Shale 0.58
Polymorphites caprarius (Quenstedt) (8; CA 4273-80), *Radstockiceras sphenonotum* (Monke) (1; CA 3751).

541 Flat sideritic mudstone nodules 0.08
Polymorphites caprarius (Quenstedt) (4; CA 4269-72), *Tragophylloceras numismale* (Quenstedt) (1; CA 2758).

540.3 Shale 0.53
Polymorphites caprarius (Quenstedt) (11; CA 4258-68).

540.2 Scattered sideritic mudstone nodules in shale 0.08
Polymorphites caprarius (Quenstedt) (6; CA 4253-57).

540.1 Shale 0.64
Polymorphites caprarius (Quenstedt) (14; CA 4239-52), *Hyperderoceras* sp. indet. (1; CA 4053).

539 Flat or spherical sideritic mudstone nodules 0.06
Polymorphites caprarius (Quenstedt) (2; CA 4237-38; Pl. 7, fig. 9).

538 Shale 0.81
Polymorphites caprarius (Quenstedt) (6; CA 4231-36).

Subzone of *Phricodoceras taylori*

537 Scattered flat or spherical sideritic mudstone nodules in shale 0.08

536 Shale 0.74

535 Flat or spherical sideritic mudstone nodules 0.08

534 Shale 0.86

533 Flat sideritic mudstone nodules 0.08

532 Shale, with occasional sideritic mudstone nodules 1.22

531 Large flat sideritic mudstone nodules; forms the northern boundary of a gully cut by the Dungeon Hole fault 0.15

530.3 Shale 0.91

530.2 Grey calcareous mudstone nodules 0.05
Phricodoceras cornutum (Simpson) (1; CA 4060).

530.1 Shale 0.81
Gemmellaroceras rutilans (Simpson) (2; CA 4179-80); *Pinna folium* (Young & Bird) abundant.

529 Widely scattered sideritic mudstone nodules in shale; the lowest nodule bed exposed on the northern side of the Dungeon Hole fault 0.05
Apoderoceras sp. indet. (1; CA 4052).

528 Shale 0.81
Gemmellaroceras sp. indet. (1; CA 4194).

527 Continuous bed of sideritic mudstone; weathers red-brown, and is yellow-brown when broken; a distinctive bed forming a scarp face on the northern boundary of a gully 0.18

PYRITOUS SHALE MEMBER

526.7 Shale, with occasional masses of pyrites, and a few calcareous mudstone nodules 1.57
Apoderoceras sp. indet. (1; CA 4051), *Tragophylloceras* sp. indet. (1; CA 2764).

526.6 Septarian calcareous mudstone nodules 0.10
Apoderoceras cf. *aculeatum* (Simpson) (4; CA 4032-35).

526.5 Shale, with occasional masses of pyrites, and a few calcareous mudstone nodules 1.02
Apoderoceras aculeatum (Simpson) (3; CA 4029-31; Pl. 6, fig. 2).

526.4 Calcareous mudstone nodules 0.06
Apoderoceras sp. indet. (2; CA 4049-50).

526.3 Shale, with many masses of pyrites and 'nests' of pyrites with a radiating structure 0.25
Apoderoceras cf. *aculeatum* (Simpson) (1; CA 4028).

526.2 Calcareous mudstone nodules, some with circular septarian jointing 0.05
Apoderoceras cf. *aculeatum* (Simpson) (1; CA 4027).

526.1 Shale, with a few 'nests' of pyrites, and some calcareous mudstone nodules, especially in the lower part 1.32
Phricodoceras cornutum (Simpson) (5; CA 4055-59), *Gemmellaroceas rutilans* (Simpson) (2; CA 4177-78; Pl. 7, fig. 4), *Apoderoceras aculeatum* (Simpson) (3; CA 4024-26), *Apoderoceras* sp. indet. (1; CA 4048).

525 Large flat sideritic mudstone nodules, with a very irregular top surface which weathers dark red; a very conspicuous bed crossing the scar south of the Dungeon Hole fault (see bed 520.4) 0.10

Apoderoceras aculeatum (Simpson) (1; CA 4023), *Phricodoceras cornutum* (Simpson) (1; CA 4070; Pl. 7, fig. 2).

524.3 Shale, with a few calcareous or sideritic mudstone nodules, and some 'nests' of pyrites 0.51
Phricodoceras cf. *cornutum* (Simpson) (1; CA 4054), *Apoderoceras aculeatum* (Simpson) (1; CA 4022; Pl. 7, fig. 1).

524.2 Sideritic mudstone nodules; some pyrites 0.04

524.1 Shale 0.52
Phricodoceras cf. *taylori* (J. de C. Sowerby) (1; CA 4069), *Apoderoceras* sp. indet. (1; CA 4047).

523 Flat sideritic mudstone nodules 0.06
Apoderoceras aculeatum (Simpson) (1; CA 4021).

522.3 Shale, with occasional sideritic mudstone nodules 0.74

522.2 Flat sideritic mudstone nodules, with circular septarian jointing 0.04

522.1 Shale, with occasional sideritic mudstone nodules, some with viens of pyrites, and some 'nests' of pyrites 0.66
Apoderoceras subtriangulare (Young & Bird) (1; CA 4020).

521 Flat sideritic mudstone nodules, with circular septarian jointing 0.05
Tragophylloceras numismale (Quenstedt) (1; CA 2757).

520.7 Shale 0.48
Apoderoceras subtriangulare (Young & Bird) (2; CA 4018-19; Pl. 6, fig. 4).

520.6 Sideritic mudstone nodules 0.07
Apoderoceras subtriangulare (Young & Bird) (2; CA 4016-17), *Tragophylloceras* cf. *numismale* (Quenstedt) (1; CA 2756).

520.5 Shale, with many scattered sideritic mudstone nodules 0.36
Apoderoceras subtriangulare (Young & Bird) (1; CA 4015), *Apoderoceras* sp. indet. (4; CA 4043-46), *Phricodoceras* cf. *nodosum* (Quenstedt) (1; CA 4061), *Gemmellaroceras* sp. indet. (2; CA 4192-93), *Tragophylloceras numismale* (Quenstedt) (4; CA 2752-55).

520.4 Sideritic mudstone nodules, with an irregular top surface; similar to bed 525 about 50 m to the north, but less conspicuous 0.10
Apoderoceras sp. indet. (1; CA 4042).

520.3 Shale, with many sideritic mudstone nodules 0.82
Apoderoceras subtriangulare (Young & Bird) (1; CA 4014), *Tragophylloceras numismale* (Quenstedt) (3; CA 2749-51).

520.2 Sideritic mudstone nodules 0.04
Tragophylloceras numismale (Quenstedt) (1; CA 2748).

520.1 Shale 0.64
Apoderoceras subtriangulare (Young & Bird) (3; CA 4011-13), *Tragophylloceras numismale* (Quenstedt) (1; CA 2747).

519 Clay; forms a conspicuous parting in the cliff, but difficult to recognize on the scars 0.03

518 Band of sideritic mudstone, with irregular top surface; outcrops at the foot of a low scarp face that forms the northern side of a gully 0.04

517.7 Shale 0.66
Apoderoceras subtriangulare (Young & Bird) (1; CA 4010), *Tragophylloceras numismale* (Quenstedt) (1; CA 2746).

517.6 Flat sideritic mudstone nodules 0.05

517.5 Shale 0.15

517.4 Sideritic mudstone nodules 0.05

517.3 Shale 0.23
Gemmellaroceras sp. indet. (2; CA 4190-91).

517.2 Sideritic mudstone nodules 0.05
Gemmellaroceras sp. indet. (1; CA 4189).

517.1 Shale 0.23

516 Large flat sideritic mudstone nodules 0.06

515.7 Shale 0.26

515.6 Sideritic mudstone nodules 0.08

515.5 Shale 0.26
Tragophylloceras cf. *numismale* (Quenstedt) (1; CA 2745).

515.4 Occasional sideritic mudstone nodules in shale 0.08

515.3 Shale 0.26

515.2 Flat sideritic mudstone nodules 0.08

515.1 Shale 0.26

514 Flat sideritic mudstone nodules 0.04

513.7 Shale 0.58
Apoderoceras sp. indet. (1; CA 4041).

513.6 Sideritic mudstone nodules 0.08
Apoderoceras sp. indet. (1; CA 4040).

513.5 Shale, with a few sideritic mudstone nodules 0.13

513.4 Sideritic mudstone nodules 0.10

513.3 Shale 0.08

513.2 Occasional sideritic mudstone nodules in shale 0.05

513.1 Shale, with occasional sideritic mudstone nodules 0.33
Apoderoceras subtriangulare (Young & Bird) (1; CA 4009).
512 Scattered flat sideritic mudstone nodules in shale 0.04
511 Shale 0.25
Apoderoceras cf. *subtriangulare* (Young & Bird) (1; CA 4008).
510 Band of elongated sideritic mudstone nodules up to 1 m long, with two sets of joints at 60° 0.04
509.3 Shale 0.18
509.2 Scattered sideritic mudstone nodules in shale 0.08
509.1 Shale 0.53
Apoderoceras cf. *subtriangulare* (Young & Bird) (1; CA 4007), ?*Gemmellaroceras* sp. indet. (1; CA 4188).
508 Irregular, septarian sideritic mudstone nodules, set in pale silty shale 0.10
507.3 Shale 0.43
507.2 Scattered sideritic mudstone nodules in shale 0.05
Phricodoceras cf. *taylori* (J. de C. Sowerby) (1; CA 4068).
507.1 Shale, with a few sideritic mudstone nodules 0.30
Apoderoceras subtriangulare (Young & Bird) (3; CA 4004-06).
506 Sideritic mudstone nodules, set in pale silty shale 0.08
Apoderoceras subtriangulare (Young & Bird) (4; CA 4000-03), *Tragophylloceras* sp. indet. (1; CA 2763).
505.3 Shale 0.64
Apoderoceras subtriangulare (Young & Bird) (2; CA 3998-99).
505.2 Shale, with many scattered sideritic mudstone nodules 0.20
Apoderoceras subtriangulare (Young & Bird) (2; CA 3996-97), *Radstockiceras buvignieri* (d'Orbigny) (1; CA 3748), *Tragophylloceras numismale* (Quenstedt) (1; CA 2744; Pl. 1, fig. 1).
505.1 Shale 1.30
Apoderoceras subtriangulare (Young & Bird) (2; CA 3994-95), *Gemmellaroceras tubellum* (Simpson) (1; CA 4176), *Cenoceras striatum* (J. Sowerby) (1; CN 87).
504 Sideritic mudstone nodules set in pale silty shale 0.08
Phricodoceras taylori (J. de C. Sowerby) (1; CA 4067), *Apoderoceras subtriangulare* (Young & Bird) (2; CA 3992-93).
503 Shale; 0.51 m thick in Wine Haven 0.41
?*Gemmellaroceras* sp. indet. (6; CA 4182-87).
502 Occasional grey calcareous mudstone nodules, set in pale silty shale 0.08
Phricodoceras cf. *taylori* (J. de C. Sowerby) (3; CA 4064-66), *Apoderoceras subtriangulare* (Young & Bird) (6; CA 3986-91; Pl. 6, fig. 5).
501.3 Shale 1.52
Phricodoceras cf. *taylori* (J. de C. Sowerby) (2; CA 4062-63), *Apoderoceras* sp. indet. (5; CA 4036-39), *Gemmellaroceras* sp. indet. (4; CA 4181).
501.2 Occasional grey calcareous mudstone nodules in shale 0.05
Apoderoceras cf. *subtriangulare* (Young & Bird) (3; CA 3983-85), *Gemmellaroceras tubellum* (Simpson) (63; CA 4113-75).
501.1 Shale; with calcareous mudstone nodules, 0.05 m thick, at about the middle, which is the highest nodule bed on the foreshore on the west side of the Peak Fault complex in Wine Haven 1.83
Bifericeras donovani Dommergues & Meister (18; CA 3793-3810; Pl. 8, fig. 3), *Apoderoceras subtriangulare* (Young & Bird) (3; CA 3980-82; Pl. 5, fig. 8).

Zone of *Echioceras raricostatum*
Subzone of *Paltechioceras aplanatum*

500 Flat sideritic mudstone nodules; forms the north-western boundary of The Landing at Bay Town 0.08
499 Shale, with a few large calcareous mudstone nodules; forms the north-western part of the floor of The Landing at Bay Town; 1.83 m thick in Wine Haven 1.57
Paltechioceras tardecrescens (Hauer) (2; CA 4607-08), *Eoderoceras armatum* (J. Sowerby) (7; CA 3885-91; Pl. 8, fig. 2), *Gleviceras guibalianum* (d'Orbigny) (1; CA 4606).
498 Shale, with numerous septarian sideritic mudstone nodules; runs down the middle of The Landing 0.23
Paltechioceras tardecrescens (Hauer) (72; CA 3573-3643; Pl. 4, fig. 6), *Eoderoceras armatum* (J. Sowerby) (8; CA 3878-84), *Gemmellaroceras tubellum* (Simpson) (15; CA 4098-4112).
497 Shale, dark grey with 3 paler stripes of silty shale; contains at least one log of fossil wood 2 m long; forms the south-eastern part of the floor of The Landing at Bay Town 2.29
Paltechioceras tardecrescens (Hauer) (154; CA 3428-3572; Pl. 4, fig. 3), *Paltechioceras regustatum* (Buckman) (2; CA 3426-27), *Eoderoceras armatum* (J. Sowerby) (44; CA 3834-77), *Gleviceras guibalianum* (d'Orbigny) (6; CA 3735-40), *Gemmellaroceras tubellum* (Simpson) (24; CA 4074-97).

SILICEOUS SHALE MEMBER

496 Hard calcified, silty shale; forms the capping to Landing Scar at Bay Town 1.40

Gleviceras guibalianum (d'Orbigny) (2; CA 3733-34), *Paltechioceras regustatum* (Buckman) (16; CA 3410-25), *Paltechioceras* sp. indet. (6; CA 3644-49).
In Wine Haven bed 496 caps a conspicuous scar running from 130 m east of Tan Beck waterfall into the west side of the Peak Fault complex, where it can be divided into:
496c Hard calcified, silty shale ..... 0.28 m
496b Shale, with a few large sideritic mudstone nodules ..... 0.21 m
496a Hard calcified, silty shale, especially hard near base ..... 0.91 m

Subzone of *Leptechioceras macdonnelli*

495.7 Shale 0.84
Gemmellaroceras tubellum (Simpson) (1; CA 4073), *Leptechioceras* cf. *macdonnelli* (Portlock) (1; CA 3404).
495.6 Harder shale, with a few sideritic mudstone nodules 0.13
Gleviceras guibalianum (d'Orbigny) (3; CA 3730-32).
495.5 Shale 0.15
Eoderoceras armatum (J. de C. Sowerby) (1; CA 3833).
495.4 Harder calcified shale 0.15
495.3 Shale 0.30
495.2 Hard calcified shale 0.36
495.15 Shale 0.43
Eoderoceras armatum (J. de C. Sowerby) (1; CA 3832).
495.14 Harder shale 0.13
495.13 Shale, with rare sideritic mudstone nodules in Wine Haven 0.33
Leptechioceras cf. *macdonnelli* (Portlock) (1; CA 3403).
495.12 Harder shale 0.13
495.11 Shale 0.53
494 Hard calcified, silty shale; forms the capping of East Scar at Bay Town, and forms a well-marked scar in Wine Haven running eastwards from Tan Beck waterfall, where a few sideritic mudstone nodules occur in the top 0.20 m 1.00
Leptechioceras aff. *macdonnelli* (Portlock) (3; CA 3400-02), *Eoderoceras armatum* (J. Sowerby) (1; CA 3831), *Radstockiceras buvignieri* (d'Orbigny) (4; CA 3744-47; Pl. 5, fig. 1).

Subzone of *Echioceras raricostatoides*

493.5 Shale 0.86
Paltechioceras planum (Trueman & Williams) (1; CA 3409).
493.4 Hard calcified, silty shale; two 0.08 m partings of softer shale seen in the Wine Haven cliff 0.91
Paltechioceras planum (Trueman & Williams) (3; CA 3406-08).
493.3 Shale 0.38
Paltechioceras planum (Trueman & Williams) (1; CA 3405).
493.2 Hard calcified, silty shale; contains a few sideritic mudstone nodules in Wine Haven 0.33
Echioceras intermedium (Trueman & Williams) (5; CA 3383-87), *Eoderoceras hastatum* (Young & Bird) (4; CA 3892-95; Pl. 6, fig. 3).
493.1 Shale 0.22
492 Hard calcified, silty shale; 0.28 m in Wine Haven; caps a strong scar south of East Scar, and a conspicuous scar in Wine Haven where it passes from cliff to scars at the foot of Tan Beck waterfall 0.23
491.3 Shale 0.37
491.2 Harder shale 0.48
Echioceras intermedium (Trueman & Williams) (2; CA 3381-82).
491.1 Shale, with one or two slightly harder bands 1.19
Echioceras raricostatoides Vadasz (1; CA 3399).
490 Hard calcified, silty shale; forms the highest scar that passes in front of Tan Beck waterfall in Wine Haven; crosses Mill Beck just west of Bay Mill 0.18
Echioceras raricostatoides Vadasz (5; CA 3394-98).
489 Shale, soft, laminated; 0.88 m in Wine Haven 0.91
Echioceras raricostatoides Vadasz (8; CA 3389-93; Pl. 4, fig. 2).
488 Hard calcified, silty shale; has a softer central part and is 0.22 m thick in Wine Haven; crosses Mill Beck beside Bay Mill 0.15
Echioceras raricostatoides Vadasz (1; CA 3388), *Crucilobiceras densinodulum* Buckman (1; CA 3830).

Subzone of *Crucilobiceras densinodulum*

487 Shale, with two 0.09 m slightly harder bands 0.92
Crucilobiceras densinodulum Buckman (2; CA 3829) in lower part.

486.3 Hard calcified, silty shale, with many small calcareous mudstone nodules; the '*Crucilobiceras* Bed' *0.08*
Crucilobiceras densinodulum Buckman (18; CA 3812-28; Pl. 6, fig. 1).

Zone of *Oxynoticeras oxynotum*
Subzone of *Oxynoticeras oxynotum*

486.2 Shale 0.06
Bifericeras cf. *vitreum* (Simpson) (1; CA 3811).
486.1 Hard calcified, silty shale; 0.33 m in Wine Haven, where there is a softer central 0.10m parting 0.25
485.3 Shale; a few lenticles of calcareous mudstone in Wine Haven 0.55
485.2 Harder shale; 0.17 m in Wine Haven 0.22
Gleviceras doris (Reynès) (1; CA 3727), *Angulaticeras* sp. indet. (1; CA 2801).
485.1 Shale 0.43
484 Hard calcified, silty shale, with a central parting about 0.09 m thick; similar to, but less conspicuous than, bed 474, the Double Band; 0.56 m thick in Wine Haven 0.44
Gleviceras cf. *guibalianum* (d'Orbigny) (2; CA 3728-29).
483.5 Shale 0.13
483.4 Harder shale 0.46
483.3 Shale, with a few harder lenticles near the base in Wine Haven 0.43
Oxynoticeras sp. indet. (1; CA 3722), ?*Gleviceras* sp. indet. (1; CA 3743).
483.2 Harder shale; 0.09 m in Wine Haven 0.48
483.1 Shale; 0.25 m in Wine Haven 0.18
?*Gleviceras* sp. indet. (1; CA 3742), *Bifericeras bifer* (Quenstedt) (5; CA 3788-92).
482.5 Hard calcified, silty shale; forms the capping to the main Dab Dumps scar; 0.08 m in Wine Haven 0.10
482.4 Shale 0.10
?*Gleviceras* sp. indet. (1; CA 3741).
482.3 Hard calcified, silty shale; 0.10 m in Wine Haven 0.08
Oxynoticeras sp. indet. (1; CA 3721).
482.2 Shale; 0.10 m in Wine Haven 0.08
482.1 Hard calcified, silty shale; caps a fairly prominent scar on Dab Dumps; crosses Mill Beck nearly opposite the foot of Mill Bank where the road reaches the shore 0.13
Oxynoticeras sp. indet. (1; CA 3720).
481 Shale; 0.43 m in Wine Haven 0.38
Oxynoticeras oxynotum (Quenstedt) (1; CA 3716; Pl. 4, fig. 4).
480 Hard calcified, silty shale; 0.89 m in Wine Haven, where the upper half is less hard 0.80
Oxynoticeras sp. indet. (2; CA 3718-19).
479 Shale 0.20
Oxynoticeras cf. *oxynotum* (Quenstedt) (1; CA 3715).
478 Hard calcified, silty shale 0.14
477 Shale, with some thin slightly harder bands 0.42
476 Hard calcified, silty shale; 0.14 m in Wine Haven; crosses Mill Beck just inside the mouth of the valley 0.10
Gleviceras doris (Reynès) (2; CA 3725-26; Pl. 4, fig. 7).
475.6 Shale, slightly indurated in places 0.13
475.5 Hard calcified mudstone lenticles 0.02
475.4 Shale, slightly harder in basal 0.05 m 0.77
475.3 Blue or red-weathering calcareous mudstone nodules 0.05
Oxynoticeras oxynotum (Quenstedt) (1; CA 3714).
475.2 Shale, slightly harder in top 0.13 m 0.43
475.1 Harder shale; 0.10 m in Wine Haven 0.08
474 The Double Band. Hard calcified, silty shale, with a softer central parting, forming a conspicuous double band; caps Cowling Scar in the middle of the bay, forms a terrace in front of Mill Beck Nab and Boggle Hole, and caps Billet Scar in Wine Haven in the south of the bay.
474.3 Hard calcified, silty shale; 0.25 m in Wine Haven, where there are some patches of pyrites 0.20
?*Paroxynoticeras salisburgense* (Hauer) (2; CA 3723-24).
474.2 Shale, softer, only partially calcified 0.08
474.1 Hard calcified, silty shale 0.15
473 Shale, soft, but a partially calcified band in the middle 0.25
Oxynoticeras sp. indet. (1; lost).
472.3 Partly calcified shale 0.13
472.2 Hard calcified, silty shale 0.13
472.1 Shale, slightly calcified in places 0.61
Oxynoticeras oxynotum (Quenstedt) (1; CA 3713).

Subzone of *Oxynoticeras simpsoni*

471 Shale, with occasional calcareous mudstone 'cheese' doggers and masses of pyrites; 0.91 m near Miller's Nab 0.86

470 Calcareous mudstone nodules enveloped in cone-in-cone structures, some 'cheese' doggers and a few strings of pyrites .. 0.08
Gagaticeras exortum (Simpson) (1; CA 3297), *Gagaticeras neglectum* (Simpson) (35; CA 3348-64), *Oxynoticeras simpsoni* (Simpson) (2; CA 3711-12).

469 Shale, with scattered calcareous mudstone 'cheese' doggers 1.83

468 Shale, with many calcareous mudstone nodules about 0.08 m thick enveloped in cone-in-cone structures, and thin lenticles of shelly limestone 0.13
Gagaticeras exortum (Simpson) (5; CA 3292-96; Pl. 2, fig. 7), *Gagaticeras finitimum* Blake (3; CA 3306-08), *Gagaticeras neglectum* (Simpson) (28; CA 3325-47; Pl. 2, fig. 6), *Gagaticeras* sp. indet. (10; CA 3372-80), *Oxynoticeras simpsoni* (Simpson) (22; CA 3689-3710; Pl. 4, fig. 5), *Cenoceras striatus* (J. Sowerby) (1; CN 93).

467 Calcified shale 0.10
Oxynoticeras simpsoni (Simpson) (29; CA 3660-88), *Gagaticeras exortum* (Simpson) (9; CA 3283-91), *Gagaticeras finitimum* Blake (8; CA 3298-3305), *Gagaticeras gagateum* (Young & Bird) (2; CA 3309-10), *Gagaticeras neglectum* (Simpson) (14; CA 3311-24), *Gagaticeras* sp. indet. (7; CA 3365-71), *Palaeoechioceras* sp. indet. (3; CA 3280-82).

466 Shale, with two thin partially calcified bands; 0.48 m thick between Peter White Cliff and Miller's Nab 0.57
Oxynoticeras cf. *simpsoni* (Simpson) (2; CA 3658-59).

465 Hard sandy and micaceous calcified shale 0.08
Oxynoticeras cf. *simpsoni* (Simpson) (2; CA 3656-57).

464.33 Shale, with indurated patches and scattered 'cheese' doggers of lenticular limestone up to 0.2 m thick and up to 2.5 m diameter 0.39
Oxynoticeras simpsoni (Simpson) (1; CA 3655), *Oxynoticeras* sp. indet. (1; CA 3717), *Angulaticeras* sp. indet. (1; CA 2800), *Cymbites* sp. indet. (1; CA 3783).

464.32 Band of irregularly-shaped limestone nodules in a shale matrix 0.35
Oxynoticeras simpsoni (Simpson) (3; CA 3652-54; Pl. 4, fig. 8), *Eparietites impendens* (Young & Bird) (14; CA 3262-75), *Cymbites* sp. indet. (1; CA 3782), *Cenoceras striatus* (J. Sowerby) (1; CN 86).

464.31 Shale 0.10
Eparietites impendens (Young & Bird) (2; CA 3260-61).

464.2 Harder calcified shale 0.06

464.1 Shale, with scattered calcareous mudstone nodules 1.12
Eparietites impendens (Young & Bird) (13; CA 3248-59), *Cymbites laevigatus* (J. de C. Sowerby) (1; CA 3776), *Angulaticeras* sp. indet. (1; CA 2799).

463 Calcareous mudstone nodules; many *Cardinia* 0.05
Oxynoticeras simpsoni (Simpson) (2; CA 3650-51), *Eparietites impendens* (Young & Bird) (3; CA 3245-47).

Zone of *Asteroceras obtusum*
Subzone of *Eparietites denotatus*

462 Shale, with occasional sideritic mudstone 'cheese' doggers; 0.91 m thick between Peter White Cliff and Miller's Nab 0.97
Eparietites impendens (Young & Bird) (16; CA 3229-44; Pl. 4, fig. 1), *Cymbites laevigatus* (J. de C. Sowerby) (7; CA 3769-75), *Angulaticeras* sp. indet. (2; CA 2797-98). 'Tinkler's Stone' is a boulder of very hard grey-brown massive limestone, not derived from the Lower Lias, resting on bed 462 about 150 m north of the mouth of Stoupe Beck; it measures 1.8 m × 1.3 m × 0.85 m high and weighs about 6000 kg.

461 Partly calcified shale 0.05
Eparietites impendens (Young & Bird) (3; CA 3226-28; Pl. 1, fig. 6), *Angulaticeras* sp. indet. (1; CA 2796).

460 Shale 0.29
Eparietites cf. *impendens* (Young & Bird) (2; CA 3224-25).

459 Partly calcified shale, with occasional calcareous mudstone nodules in the lower part 0.10
Eparietites impendens (Young & Bird) (2; CA 3222-23).

458.3 Shale 0.18
Aegasteroceras crassum Spath (2; CA 3051-52), *Aegasteroceras* sp. indet. (2; CA 3177-78), *Eparietites impendens* (Young & Bird) (1; CA 3221), *Cymbites* sp. indet. (1; CA 3781).

458.2 Partly calcified shale 0.23
Aegasteroceras crassum Spath (4; CA 3047-50; Pl. 2, fig. 4), *Aegasteroceras* sp. indet. (1; CA 3176).

458.1 Shale; with occasional calcareous mudstone nodules 0.20
Aeger laevis (Blake) (Decapod crustacean; Withers, 1933); *Aegasteroceras sagittarium* (Blake) (4; CA 3172-75).

457 Calcified shale 0.08
Aegasteroceras sagittarium (Blake) (4; CA 3168-71), *Eparietites impendens* (Young & Bird) (1; CA 3220).

456 Shale, with scattered small calcareous mudstone nodules in the lower half 0.66
Aegasteroceras crassum Spath (1; CA 3046), *Aegasteroceras sagittarium* (Blake) (60; CA 3108-67; Pl. 1, fig. 7), *Cymbites* sp. indet. (2; CA 3779-80).

455 Hard calcified shale, with two softer partings; bed 455 caps High Scar north of Stoupe Beck, and it also forms the highest scar in front of Miller's Nab, west of Wine Haven; the dip slope of beds 455.1 and 455.2 is pierced by several small excavated pools known as Strickland's Dumps (after Sir Charles Strickland), 285 m north of the mouth of Stoupe Beck.

455.5 Hard calcified shale, with occasional small calcareous mudstone nodules near the top 0.15
Aegasteroceras crassum Spath (1; CA 3045), *Aegasteroceras sagittarium* (Blake) (1; CA 3107), *Eparietites bairstowi* sp. nov. (2; CA 3218-19; Pl. 2, fig. 8).

455.4 Shale 0.23
Asteroceras cf. *blakei* Spath (2; CA 3008-09), *Cymbites laevigatus* (J. de C. Sowerby) (2; CA 3767-68).

455.3 Partially calcified shale 0.10
Asteroceras blakei Spath (4; CA 3004-07).

455.2 Shale 0.13
Asteroceras blakei Spath (1; CA 3003), ?*Cymbites* sp. indet. (1; CA 3778), *Eparietites bairstowi* sp. nov. (1; CA 3217; Pl. 3).

Subzone of *Asteroceras stellare*

455.1 Partially calcified shale 0.10
Aegasteroceras sagittarium (Blake) (4; CA 3103-06), *Asteroceras* cf. *blakei* Spath (1; CA 3002).

454.2 Shale with occasional calcareous mudstone nodules 1.04
Aegasteroceras sagittarium (Blake) (49; CA 3054-3102), *Cymbites laevigatus* (J. de C. Sowerby) (1; CA 3766).

454.1 Shale with many small calcareous mudstone nodules; more calcified in lower part 0.10
Promicroceras planicosta (J. Sowerby) (31; C.49425-31, CA 3953-75), *Asteroceras blakei* Spath (4; CA 2999-3001), *Aegasteroceras sagittarium* (Blake) (1; CA 3053), *Cymbites laevigatus* (J. de C. Sowerby) (1; CA 3765).

453.3 Calcified shale 0.25
Promicroceras planicosta (J. Sowerby) (10; C.49418-21, C.49423-24, CA 3950-51), *Xipheroceras* sp. indet. (1; C.49422).

453.2 Shale 0.13
?*Cymbites* sp. indet. (1; CA 3777), *Promicroceras planicosta* (J. Sowerby) (18; C.49406-14, C.49417, CA 3944-49), *Xipheroceras* sp. indet. (1; C.49405), *Asteroceras blakei* Spath (3; CA 2996-98).

453.1 Calcified shale, with many calcareous mudstone nodules 0.08
Promicroceras planicosta (J. Sowerby) (12; C.49402-03, C.49415-16, CA 3936-43), *Xipheroceras ziphus* (Zieten) (1; C.49404), *Asteroceras* sp. indet. (4; CA 3040-43), *Asteroceras blakei* Spath (2; CA 2994-95).

452 Shale 0.43
Xipheroceras ziphus (Zieten) (2; C.49400-01), *Promicroceras planicosta* (J. Sowerby) (27; C.49383-99), *Asteroceras blakei* Spath (12; CA 2982-93; Pl. 2, fig. 2).

451 Calcified shale, with occasional small calcareous mudstone nodules 0.10
Promicroceras planicosta (J. Sowerby) (158; C.49369-82, CA 3918-35; Pl. 5, fig. 3), *Xipheroceras ziphus* (Zieten) (2; CA 3784-85; Pl. 5, fig. 5), *Xipheroceras* sp. indet. (1; C.49368), *Cymbites laevigatus* (J. de C. Sowerby) (1; CA 3764), *Asteroceras stellare* (J. Sowerby) (7; CA 3028-34), *Asteroceras* sp. indet. (2; CA 3038-39).

450.3 Partially calcified shale; the top 0.3 m of this bed is the lowest horizon present in the cliff; it occurs in the base of Peter White Cliff, and all lower beds outcrop on the wave-cut platform of the foreshore only 0.91

450.2 Shale, with many calcareous mudstone nodules and a few 'cheese' doggers 0.10
Asteroceras stellare (J. Sowerby) (1; CA 3027).

450.1 Shale, with some partly calcified lenticles and a few red-weathering 'cheese' doggers 0.82
Asteroceras stellare (J. Sowerby) (2; CA 3025-26), *Promicroceras planicosta* (J. Sowerby) (1; CA 3917), both species 0.3 m above the base.

449 Hard calcified silty shale, with well-marked jointing in two directions; forms the capping to Middle Scar between Stoupe Beck and Mill Beck; 0.19 m thick near Miller's Nab 0.15
Asteroceras stellare (J. Sowerby) (7; CA 3018-24), *Aegasteroceras crassum* Spath (1; CA 3044).

448.5 Shale; 0.73 m on Miller's Nab scars 0.56
Promicroceras planicosta (J. Sowerby) (2; CA 3915-16), *Asteroceras* sp. indet. (1; CA 3037).

448.4 Harder, partially calcified silty shale 0.10
Asteroceras sp. indet. (1; CA 3036).

448.3 Shale; 0.41 m on Miller's Nab scars 0.33
Asteroceras stellare (J. Sowerby) (1; CA 3017).

448.2 Grey calcareous mudstone nodules 0.09

448.1 Shale 1.52
Promicroceras planicosta (J. Sowerby) (3; CA 3912-14), *Epophioceras landrioti* (d'Orbigny) (2; CA 3277-78), *Cymbites laevigatus* (J de C. Sowerby) (1; CA 3763; Pl. 5, fig. 6).

447 Hard indurated, well-jointed, silty, calcified shale; a very conspicuous bed, forming the capping to Low Scar between Mill Beck and Stoupe Beck, and the capping to the most prominent scar between Stoupe Beck and Miller's Nab 0.56
Asteroceras stellare (J. Sowerby) (1; CA 3016).

CALCAREOUS SHALE MEMBER

Subzone of *Asteroceras obtusum*

446.5 Shale, with occasional cone-in-cone enveloped grey calcareous mudstone nodules, especially in a band from 0.10 m to 0.25 m below the top 0.56
Epophioceras landrioti (d'Orbigny) (1; CA 3276), *Xipheroceras ziphus* (Zieten) (1; C.49360), *Cymbites laevigatus* (J. de C. Sowerby) (1; CA 3762), *Promicroceras planicosta* (J. Sowerby) (20; C.49343-59, C.49366-67).

446.4 Harder, partially calcified shale 0.15
Epophioceras sp. indet. (1; CA 3279), *Xipheroceras* cf. *ziphus* (Zieten) (1; C.49337), *Promicroceras planicosta* (J. Sowerby) (1; C.49338).

446.33 Shale, with widely scattered calcareous nodules 0.25
Promicroceras planicosta (J. Sowerby) (7; C.49362-65, CA 3909-11), *Asteroceras confusum* Spath (3; CA 3012-14), *Xipheroceras dudressieri* (d'Orbigny) (1; C.49336; Pl. 5, fig. 2), *Xipheroceras* sp. indet. (2; C.49361, CA 3787).

446.32 Large scattered calcareous nodules in a shale matrix 0.15
Promicroceras capricornoides (Quenstedt) (4; C.49340-42, CA 3908), *Asteroceras confusum* Spath (2; CA 3010-11; Pl. 1, fig. 4), *Asteroceras obtusum* (J. Sowerby) (1; CA 3015), *Xipheroceras* sp. indet. (1; CA 3786).

446.31 Shale, finely laminated, with occasional strings and masses of pyrites 0.60
Promicroceras capricornoides (Quenstedt) (7; C.49339, CA 3902-07), *Asteroceras* sp. indet. (1; CA 3035).

Zone of *Caenisites turneri*
Subzone of *Microderoceras birchi*

446.2 Cone-in-cone enveloped calcareous mudstone nodules 0.15

446.1 Shale 0.30
Promicroceras capricornoides (Quenstedt) (1; C.49335).

445 Hard calcified shale 0.13

444 Calcareous mudstone nodules 0.06

443.3 Shale, with a few calcareous mudstone nodules 1.37
Promicroceras capricornoides (Quenstedt) (10; C.49327-34).

443.2 Hard calcified shale 0.25
Promicroceras capricornoides (Quenstedt) (1; CA 3901).

443.1 Grey calcareous mudstone nodules 0.05

442.2 Hard partially calcified shale 0.48

442.1 Grey crystalline shelly limestone, weathering yellow-brown; lenticular or nodular in some places 0.08

441.3 Shale with occasional small calcareous mudstone nodules, especially at the middle of the bed 0.30

441.2 Harder calcified shale and shaly limestone 0.15
Microderoceras scoresbyi (Simpson) (1; C.49327).

441.1 Shale, with occasional calcareous mudstone nodules 0.41

440 Grey shaly limestone, weathering yellow-brown 0.13

439 Grey calcareous mudstone nodules 0.05

438 Shale 0.15

437 Harder partially calcified shale 0.10
Promicroceras capricornoides (Quenstedt) (3; C.49323-25).

436 Shale 0.61
Promicroceras capricornoides (Quenstedt) (13; C.49315-22, CA 3896-3900), *Arnioceras* sp. indet. (1; CA 2938).

435 Hard calcified shale and shaly limestone 0.15
Caenisites cf. *turneri* (J. de C. Sowerby) (2; CA 3211-12), ?*Caenisites* sp. indet. (4; CA 3213-16), ?*Arnioceras* sp. indet. (2; CA 2937).

434 Grey calcareous mudstone nodules 0.06

433.3 Shale, with impersistent calcified patches and thin shaly limestones 0.91
Microderoceras birchi (J. Sowerby) (5; C.49314, CA 3976-79; Pl. 5, fig. 7), *Caenisites turneri* (J. de C. Sowerby) (24; CA 3187-3210; Pl. 2, figs 3, 5), *Caenisites brooki* (J. Sowerby) (4; CA 3183-86).

Subzone of *Caenisites brooki*

433.2 Harder calified shale, with limestone lenses 0.11

433.1 Shale, with occasional small calcareous mudstone nodules and cone-in-cone structures 0.15

432 Grey shaly limestone, weathering yellow-brown, nodular in the lower half, and shelly in places 0.10

431.3 Shale, with some thin lenses and patches of shelly limestone, especially in the upper part 0.86
Caenisites brooki (J. Sowerby) (2; CA 3181-82), *Arnioceras* sp. indet. (1; lost).

431.2 Hard, grey, shelly limestone, nodular in the lower half; some masses of pyrites 0.08
Caenisites cf. *brooki* (J. Sowerby) (5; CA 3179-80, 3 lost).

431.1 Shale, with a few thin lenses of limestone in the upper part 0.30
430 Hard, pyritous, shelly, grey limestone, weathering yellow-brown 0.08
Arnioceras sp. indet. (1; lost).
429.8 Shale, with 0.06 m thick calcareous mudstone nodules in the top half 0.15
429.7 Flat lenses of hard, grey, crystalline limestone 0.03

Zone of *Arnioceras semicostatum*
Subzone of *Euagassiceras sauzeanum*

429.64 Grey calcareous mudstone nodules 0.05
Arnioceras semicostatum (Young & Bird) (1; CA 2913), *Coroniceras (Arietites) alcinoe* (Reynès) (2; CA 2803-04; Pl. 1, fig. 8).
429.63 Shale, with thin lenses of shaly limestone, especially at the top of the lower third 0.61
429.62 Occasional grey calcareous mudstone nodules in shale 0.05
Arnioceras semicostatum (Young & Bird) (4; CA 2909-12).
429.61 Shale, with small sideritic mudstone nodules, and occasional much larger 'cheese' doggers up to 2 m diameter 0.61
Arnioceras semicostatum (Young & Bird) (2; CA 2907-08).
429.5 Grey limestone, shaly in places, weathering yellow-brown, with small nodules on its upper surface 0.08
429.4 Shale, containing many small grey calcareous mudstone nodules 0.08
Arnioceras semicostatum (Young & Bird) (1; lost).
429.3 Shale, with very occasional calcareous mudstone nodules 0.36
429.2 Thin continuous or nodular grey limestone, shaly in places 0.03
429.1 Shale 0.18
Arnioceras obliquecostatum (Zieten) (1; lost), *Arnioceras* sp. indet. (2; CA 2935-36).
428 Shale, with lenses or a continuous band of grey shaly limestone in the top third, and calcareous mudstone nodules in the lower third 0.15
Arnioceras semicostatum (Young & Bird) (5; CA 2902-06).
427.3 Shale 0.38
Arnioceras semicostatum (Young & Bird) (4; CA 2898-2901).
427.2 Irregular band of hard grey shaly limestone, weathering brown 0.15
Arnioceras semicostatum (Young & Bird) (4; CA 2895-97), *Coroniceras (Arietites)* sp. indet. (1; CA 2805).
427.1 Shale, with some lenses of shaly limestone, and a few large 'cheese' doggers of sideritic mudstone 0.71
Arnioceras sp. indet. (1; CA 2934).
426.2 Hard grey shaly limestone, weathering brown, with a rough top surface; forms a conspicuous scar landward of Pseudo Low Balk (bed 424.2); many *Gryphaea* 0.05
Coroniceras (Arietites) alcinoe (Reynès) (1; CA 2802), *Arnioceras semicostatum* (Young & Bird) (10; CA 2885-94), *Arnioceras* sp. indet. (1; CA 2933).
426.1 Hard calcified shale, weathering brown 0.15
Arnioceras semicostatum (Young & Bird) (3; CA 2882-84), *Euagassiceras* sp. indet. (1; CA 2973).
425.7 Shale, with a few indurated patches 0.15
425.6 Grey calcified shale, weathering brown 0.11
Arnioceras semicostatum (Young & Bird) (9; CA 2873-81).
425.5 Shale; very occasional large calcareous mudstone 'cheese' doggers 0.15
Arnioceras semicostatum (Young & Bird) (16; CA 2857-72), *Arnioceras miserabile* (Quenstedt) (2; CA 2919-20).
425.4 Grey calcified shale, weathering brown 0.11
Arnioceras sp. indet. (1; CA 2932).
425.3 Shale 0.15
Arnioceras sp. indet. (1; CA 2931).
425.2 Grey calcified shale, weathering brown 0.11
Arnioceras sp. indet. (1; CA 2930).
425.1 Shale, with a few indurated patches 0.52
Euagassiceras sp. indet. (2; CA 2971-72), *Arnioceras* sp. indet. (11; CA 2921-29).
424.3 Calcified shale, harder in the upper half; occasional small calcareous mudstone nodules 0.61
Euagassiceras sp. indet. (3; CA 2968-70), *Arnioceras semicostatum* (Young & Bird) (18; CA 2839-56), *Arnioceras miserabile* (Quenstedt) (3; CA 2916-18), *Coroniceras (Arietites) alcinoe* (Reynès) (1; C.41310).
424.2 Shale, partially calcified in the top half; this middle division of bed 424 forms the scar 'Pseudo Low Balk' which emerges immediately landward of Low Balk (bed 422.2) 0.30
Arnioceras semicostatum (Young & Bird) (10; CA 2829-38; Pl. 1, fig. 2), *Arnioceras miserabile* (Quenstedt) (2; CA 2914-15).
424.1 Shale, partially calcified near the top 0.61
423 Shale, no subdivisions observed 1.58
422.2 Hard blue-grey flaggy limestone, weathering brown, with a rough top surface; slightly micaceous; forms the capping of

	the very conspicuous scar Low Balk	0.10
	Euagassiceras resupinatum (Simpson) (21; CA 2942-62; Pl. 1, fig. 5).	
422.1	Hard grey micaceous calcified shale, weathering brown	0.30
	Euagassiceras resupinatum (Simpson) (1; CA 2941).	
421.4	Hard partially calcified shale, micaceous and with strings of pyrites in places; a few harder calcified lenses near the top	0.91
	Arnioceras semicostatum (Young & Bird) (31; CA 2806-28, CA 2974-81), *Euagassiceras resupinatum* (Simpson) (2; CA 2939-40), *Euagassiceras* sp. indet. (5; CA 2963-67).	
421.3	Shale; forms a terrace on the scar due to a harder band at the top	0.46
421.2	Shale; forms a terrace due to a harder band at the top	0.69
	Euagassiceras sp. indet. (1; lost).	
421.1	Shale; forms a terrace due to a harder band at the top	0.91
	Euagassiceras sp. indet. (2; lost), *Arnioceras* sp. indet. (1; lost).	
420	Hard grey flaggy limestone passing down into grey shale; slightly micaceous and pyritous; full of bivalves in places; forms a dip slope 25 m wide and a scarp face 0.13 m high	1.75
419	Hard grey calcified shale, slightly micaceous; dip slope 1 m wide, and scarp face 0.13 m high	0.13
418	Hard grey partially calcified shale; slightly micaceous; forms a terrace 4 m wide, ending seaward in a scarp face 0.46 m high; the lowest bed exposed at low water of the lowest spring tides	0.60

LITHOSTRATIGRAPHY

The Lower Lias of Robin Hood's Bay is 163.74 m thick and belongs to the Redcar Mudstone and the lower part of the Staithes Sandstone Formations. These names were introduced as formations by Powell (1984: 53) and Howard (1985: 262), and details of their definitions were given by Cox *et al.* (1998: 35, 39). Fig. 18 is a complete vertical section of the succession of the Lower Lias in Robin Hood's Bay, showing the changes in lithology, the lithological divisions and the main features of significance formed by the harder beds, some of which have received formal names; bed thicknesses are drawn to scale on this figure, giving a visual indication of the relative thicknesses of the subzones and lithostratigraphical divisions.

Staithes Sandstone Formation (beds 591–601.2 and higher)

Consists of sandstones, that are mid to pale grey, fine to medium-grained, micaceous, with grey siltstone bands and some beds of silty shales; nodules of argillaceous limestone occur in the shales and are occasionally sideritic; there is much bioturbation, cross-bedding and ripple marked bedding, especially in the sandstones.

The type area is in Robin Hood's Bay. The formation is somewhat transitional from the underlying Redcar Mudstone Formation, but a convenient marker bed that defines the lower boundary just south of Castle Chamber is bed 591, the Oyster Bed, which is a hard, calcified, silty shale or argillaceous sandstone, containing many oysters and other fossils. Above this level the amounts of silt and sand are higher than lower in the sequence and hard and soft sandstones are frequent. The formation has no subdivisions and extends up into the lower half of the Upper Pliensbachian. The Lower Pliensbachian (ie. Capricornus and Figulinum Subzones) part of the formation is 12.74 m thick.

Redcar Mudstone Formation (beds 418–590; 151 m thick)

Consists of mudstones and shales, grey, soft and well-bedded, but some beds are indurated due to calcification, and there are some harder siltstones; thin beds of shelly limestone occur in the lower part, and nodules of calcareous or sideritic mudstone occur, especially in the upper part; pyritized nodules or irregular aggregations of iron pyrites occur at some horizons.

Although the name is derived from the Lower Lias exposures at Redcar to the north-west, and the lower boundary is defined in the BGS Felixkirk Borehole (Cox *et al.* 1998: 35), the type section consists of the whole sequence exposed in Robin Hood's Bay below the base of the Staithes Sandstone Formation. Here the lithology is more argillaceous than in the Staithes Sandstone Formation, though different parts are variously more calcareous, siliceous, pyritous or ferruginous, and they form the basis of the following four members:

4. Ironstone Shale Member.
3. Pyritous Shale Member.
2. Siliceous Shale Member.
1. Calcareous Shale Member.

These members were introduced as 'Shales' by Buckman (1915: 61) for lithological divisions in Robin Hood's Bay below the 'Sandy Series' (= Staithes Sandstone Formation), and he based them on groups of the ammonite zones that he applied to the succession. His zones can be linked to beds in his detailed sections, but they are not the same as the ammonite zones recognized now, and in any case it is not satisfactory to base lithological divisions on the ranges of palaeontological zones. No formal definitions have been given to these divisions, though Hesselbo & Jenkyns (1995: 114–135) applied them informally to the succession, and placed boundaries between them at appropriate levels in the succession, all of which are followed here. The four members are defined formally here, and their type sections are in Robin Hood's Bay.

Ironstone Shale Member (beds 527–590; 62.73 m thick). Mudstones and shales, grey, soft, with some beds of micaceous silty shales, many grey sideritic mudstone nodules, weathering red on the outside, and a few calcareous mudstone nodules. The nodules are scattered sparsely through the shale, but are more often developed at single horizons, either scattered or as near-continuous beds. The distinctive beds of red-weathering nodules have frequently been referred to as 'ironstones', but they are better described as sideritic mudstones.

The base is defined at the bottom of bed 527 in Robin Hood's Bay, which is a prominent continuous bed of sideritic mudstone weathering red-brown. Although sideritic mudstone nodules occur at several

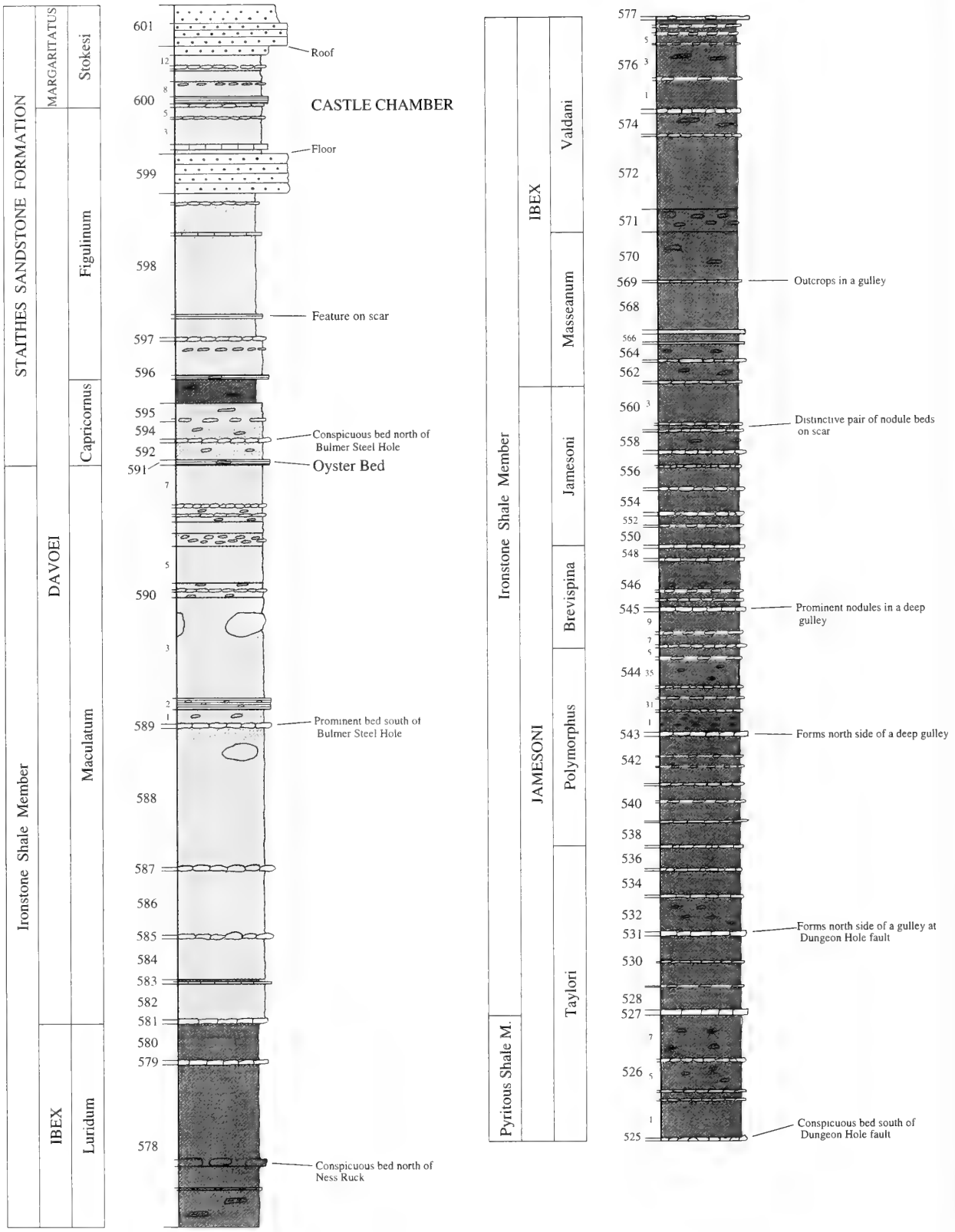

Fig. 18 Vertical section of the Lower Lias of Robin Hood's Bay, showing the main lithological features, relative thickness of all the beds, and named beds and other beds that form prominent features on the foreshore.

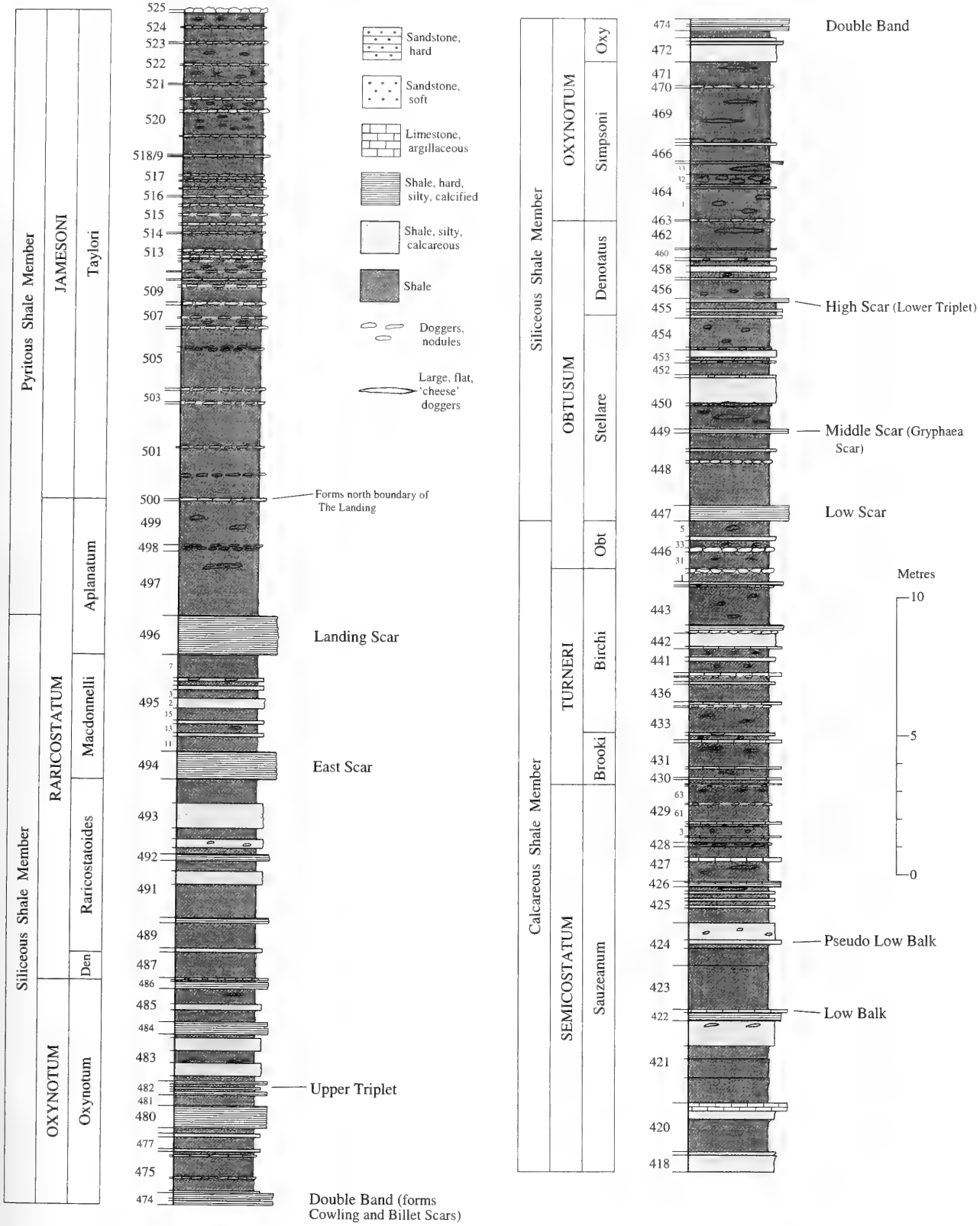
Pyritous Shale Member
Siliceous Shale Member
JAMESONI
RARICOSTATUM
OXYNOTUM
Taylori
Aplanatum
Macdonnelli
Raricostatoides
Den
Oxynotum
525
524
523
522
521
520
518/9
517
516
515
514
513
509
507
505
503
501
500
499
498
497
496
495
494
493
492
491
489
487
486
485
484
483
482
481
480
477
475
474
Sandstone, hard
Sandstone, soft
Limestone, argillaceous
Shale, hard, silty, calcified
Shale, silty, calcareous
Shale
Doggers, nodules
Large, flat, 'cheese' doggers
Forms north boundary of The Landing
Landing Scar
East Scar
Upper Triplet
Double Band (forms Cowling and Billet Scars)
Siliceous Shale Member
Calcareous Shale Member
OXYNOTUM
OBTUSUM
TURNERI
SEMICOSTATUM
Oxy
Simpsoni
Denotatus
Stellare
Obt
Birchi
Brooki
Sauzeanum
474
472
471
470
469
466
464
463
462
460
458
456
455
454
453
452
450
449
448
447
446
443
442
441
436
433
431
430
429
428
427
426
425
424
423
422
421
420
418
Double Band
High Scar (Lower Triplet)
Middle Scar (Gryphaea Scar)
Low Scar
Pseudo Low Balk
Low Balk
Metres
10
5
0

lower horizons down as far as bed 500 and those of bed 525 are especially conspicuous, pyrites is very common at most horizons up to bed 526.7 but does not occur higher. So the strong sideritic mudstone of bed 527 is a good base for this member. Such sideritic mudstone nodules and occasional continuous beds are a feature of the whole thickness of the member up to the base of the Staithes Sandstone Formation. Several of them form prominent features on the scars, eg. beds 527, 531, 543, 545, 559 and 560.2 (a distinctive pair of nodule beds), 569, 578.4 and 589.

Pyritous Shale Member (beds 497–526; 26.18 m thick). Consists of dark grey, soft and micaceous shales, with many calcareous and/or sideritic mudstone nodules; there are many nodules or irregular masses of iron pyrites, especially in the lower part. This member is similar to the Ironstone Shale Member in containing both calcareous and sideritic mudstone nodules, but it also contains much iron pyrites as irregular nodules or masses of crystals.

The base is defined here as the bottom of bed 497 in Robin Hood's Bay. This is the horizon at which the sand and silt content almost disappears and calcification is much diminished, leaving the beds above as softer shales. Iron pyrites is common at many horizons, appearing variously as irregular masses or strings of pyrites, or pyrite-rich concretions, and many of the fossils are partly pyritized in these beds. The softness of the shale leads to this part of the succession forming the wettest and lowest part of the bay relative to sea level.

Siliceous Shale Member (beds 447–496; 38.74 m thick). Dark-grey shales, interbedded with much harder and lighter-coloured beds of calcified mudstones, silts and fine sandstones; a few nodules and doggers of calcareous or sideritic mudstone occur. This member forms the series of hard calcified beds alternating with soft shales that is typical of the lower part of the succession in Robin Hood's Bay. Red-weathering sideritic nodules are now scarce, and most of the harder beds are calcareous cemented muds and silts, in which the arenaceous content is higher than in the underlying Calcareous Shale Member. Large, circular 'cheese' doggers of hard argillaceous limestone, containing vertically orientated cystals of calcite, occur at several horizons in both this member and the Calcareous Shale Member below. Such doggers are generally up to only about 10 cm thick, but they can reach 2.5 m in diameter; they occur at 7 levels between beds 450 and 471.

The base is defined here at the bottom of bed 447 (Low Scar) in Robin Hood's Bay. This is the first prominent bed of very hard calcified shale or argillaceous limestone that has a significant sand content. Sand and silt occur in many of the hard calcified shales or sandstones at horizons up to the base of the Pyritous Shale Member. Most of the prominent 'scars' in the bay are formed of beds in this member – ie. Low Scar, Middle Scar (Gryphaea Scar), High Scar (Lower Triplet), Double Band (Cowling Scar and Billet Scar), Upper Triplet, East Scar and Landing Scar.

Calcareous Shale Member (beds 418–446; 23.35 m thick). Dark-grey shales, interbedded with hard, calcified, silty mudstones; doggers of calcareous mudstone and some beds of limestone also occur; cone-in-cone enveloped calcareous mudstone nodules also occur at several horizons. This member is less arenaceous than the Siliceous Shale Member, the hard beds now having no sand and less silt, and the hardness being due mainly to calcification. The very prominent Low Balk and the less prominent Pseudo Low Balk are formed by limestones or highly calcified shales. Large 'cheese' doggers, similar to those in the Siliceous Shale Member, are found at three levels in beds 425–429.

In Robin Hood's Bay the base has to be placed at the lowest horizon exposed, ie. at the base of bed 418. If it is thought that the base should coincide with the base of the Redcar Mudstone Formation, then it must be defined at the same level (ie. 288.87 m depth) in the BGS Felixkirk Borehole (Cox *et al.* 1998: 35).

EXPOSURES IN ROBIN HOOD'S BAY NOW

The extent of the foreshore exposures of the solid geology on the north Yorkshire coast has always depended on the vagaries of shifting sand and boulder cover, algal growth, barnacle growth, and major cliff falls, all caused or cleared away by the actions of tides and storms. But in the last 25 years much more extensive, and possibly more permanent, sand, boulder, algal and barnacle cover, and mussel beds have made major inroads into the amount of rock exposed in some areas. Especially serious on some of the scars are mussel beds that trap mud and silt to form a thick, impenetrable cover that completely obscures the rock underneath. At the end of the 1990s the foreshore exposures were largely obscured from Way Foot at the bottom of Robin Hood's Bay Town northwards to just south of Dungeon Hole. In fact there are few or no exposures of beds 497–525 owing to the sand and seaweed cover, which has possibly been exacerbated by the high concrete seawall built to protect Robin Hood's Bay in 1975. That seawall covers the cliff face of the same beds, so that they are not now exposed in either the cliff face or on the foreshore. Exposures improve upwards from bed 526, especially north of the Dungeon Hole fault, though there is still much algal growth and large areas are covered by loose boulders. Around the north side of the bay in the top half of Map 1 (Fig. 5) the foreshore continues to be washed clean by tides and storms and exposures are still good. Exposures seaward and south of Boggle Hole (Map 3; Fig. 8) are also better, and they are good in front of Peter White Cliff (Map 4; Fig. 11). The lowest beds on the latter map, especially from bed 430 down to below Low Balk have always suffered from algal cover, of which *Laminaria* is a significant factor at those low sea-levels, but barnacle growth is also very pronounced and makes observations difficult on some beds.

For most of the past two centuries the foreshore of Robin Hood's Bay has been largely clear of such cover, and collectors from Young & Bird in the 1820s, Phillips, Simpson, Tate & Blake, the Geological Survey in 1880–1910, up to Bairstow in the period from 1928 to the 1950s (see Fig. 7) were able to make significant fossil collections from all the beds. In particular, most of them obtained large specimens of *Apoderoceras* from the Taylori Subzone of beds 501 to 526. No such specimens can be collected today. The foreshore was largely clean in 1969 when Bairstow conducted a field party from the William Smith Jurassic Symposium to the Bay, but deterioration proceeded rapidly from the early 1970s. Bairstow's work could not be repeated today, at least for the beds on Map 2 (Fig. 6) from Robin Hood's Bay town northwards to the top of that map.

CORRELATION WITH PREVIOUS DESCRIPTIONS

The Lower Lias of Robin Hood's Bay was mentioned by Young & Bird (1822, 1828) and Phillips (1829, 1875), and a few ammonites from the bay were figured by them, but their descriptions were not in sufficient detail to be correlated with the work in this paper. Prior to Bairstow's work, detailed descriptions were published by Simpson (1868, 1884), Tate & Blake (1876) and Buckman (1915), all of whom numbered their beds from the top downwards. After Bairstow prepared his maps and stratigraphical descriptions, detailed accounts

of the geology of parts of the bay were published by Howarth (1955), Phelps (1985) and Hesselbo & Jenkyns (1995). The tables of Figs 19 and 20 give bed-by-bed correlation columns for all these schemes in as much detail as is possible; the columns of subzones in both figures are the subzones as determined in this paper.

Simpson first described the beds in 1868 (Simpson, 1868: 53–56), but in his later work (Simpson, 1884: xvii–xxii) there are more details at some horizons, and the Simpson columns in the tables are based on his later work. Tate & Blake (1876: 63–65, 73–75, 79–81, 91, 92, 109, 110) described the beds in greater detail, and in many parts of the succession their beds correspond closely with those in the present paper, though they omitted about 3 m of strata within their group Jam.30–Jam.32. Tate & Blake (1876: 79, 91–2) also duplicated part of the succession in their descriptions, inasmuch as their Jamesoni beds 1–7 are the same as their Capricornus beds 28–33 (these are shown in Fig. 19 as Jam.1–Jam.7 only).

The Geological Survey's description of the succession first appeared in the memoir of Fox-Strangways & Barrow (1882: 4–10), where the beds were described in detail but not numbered, and the ammonites that they listed for individual beds are not accurately determinable in modern terms. The same description was used by Buckman (1915: 67–74) in his appendix to the 2nd edition of that memoir: the same basic data was used for the succession, but the beds were sometimes combined into thicker units and were now given numbers; lithological names were given to a few of the beds, and Buckman's determinations of the ammonites and zonal divisions were added. Buckman's 1915 description of the sequence is used for Figs 19 and 20, rather than the original 1882 description.

Howarth (1955: 155) described beds upwards from the bottom of the Upper Pliensbachian; the equivalence of his beds 1–6 are shown at the top of Fig. 19, with bed 1 being the same as beds 600.5 and 600.6, while the equivalence of a few lower beds that were given roman numbering in the upper part of the Figulinum Subzone is indicated in the detailed stratigraphical section above (p. 98).

Phelps (1985: fig. 4) described the succession in the Davoei and upper part of the Ibex Zones in detail. When the vertical tabular section of his fig. 4 is compared at the same scale with the tabular section of Fig. 18 here, good correlations can be made from his top bed near the top of the Figulinum Subzone down to his bed 4b (= bed 567) in the Masseanum Subzone, and at the bottom it seems fairly certain that his bed 1 is the same as bed 561. Phelps (1985: pl. 1, figs 1, 3, pl. 2, figs 1, 6, 8) figured five ammonites from his beds 21, 23, 37, 47 and 63, the identifications of which are discussed below (pp. 141–144) in the description of the ammonite genus *Aegoceras*.

Hesselbo & Jenkyns's (1995) sequence of the Lower Lias of Robin Hood's Bay was based on new observations made by them. Their bed numbers are original from the bottom of the sequence up to their bed 121 at the base of the Masseanum Subzone, then higher up they used the bed numbers of Phelps (1985), and finally the bed numbers of Howarth (1955) upwards from the top of the Figulinum Subzone. Although their descriptions and measurements were new, above bed 121 their identification and use of Phelps' bed numbers is difficult to interpret at some horizons, especially in the Ibex Zone, so in Fig. 19 the correlation of Phelps' beds 1–65 is based on Phelps' original description of that sequence, not on Hesselbo & Jenkyns' re-interpretation of it. However, from the base of the sequence up to bed 121, Hesselbo & Jenkyn's description can be readily correlated with that of this paper at most levels, and is shown as their beds 1–121 in the relevant columns of Figs 19 and 20. The main areas of uncertainty are at the bottom of the succession below their bed 23 (=bed 447), though it appears likely that their bed 5 has been correctly identified as bed 422 (Low Balk), in their beds 73–94 in the Taylori Subzone, that are difficult to correlate in detail, and in beds 113–121 in the Brevispina and Jamesoni Subzones. In the upper part of the sequence between beds 102 and 116, a strikingly similar pattern can be seen by comparing Hesselbo & Jenkyns' tabular section side-by-side with that of Fig. 17; eg. bed 102 = bed 527; 104 = 531; 112 = 543; 114, lower part = 545, and it is probable that bed 116 is the same as bed 547. Bed 1 of Phelps has already been correlated with bed 561, so this leaves Hesselbo & Jenkyns' beds 117–121 (4.5 m thick) as eqivalent to Bairstow beds 548–560 (6.3 m thick), but there are some differences in thickness and they are not correlatable in detail. The position of the subzone boundaries given by both Phelps and Hesselbo & Jenkyns differ in detail from those determined for this paper, except for the upper parts of the Raricostatum and Davoei Zones.

In addition to the previous descriptions in the works listed above, Getty measured and collected ammonites from the Oxynotum and Raricostatum Zones in the bay. The stratigraphical part of his work is only available in his unpublished thesis (Getty, 1972), but many of the ammonites he collected were described in his revision of the family Echioceratidae (Getty, 1973), and they are in the collections of the Natural History Museum. His stratigraphical sequence of ammonites and biostratigraphical divisions are very similar to those of Bairstow as determined here.

BAIRSTOW'S AMMONITE COLLECTION

More than 2360 ammonites were collected by Bairstow. The majority were obtained in the years 1927–1935, but small numbers of specimens were added up to about 1970. In addition there are a few specimens that were given to him by other collectors: the majority came from Dr J. Coggin Brown, who collected well-preserved ammonites at Robin Hood's Bay in the period 1940–1960 (on retiring to north-east England after working for the Geological Survey of India). Bairstow checked the horizons of the specimens given to him with great care, and only those that he was satisfied came from definitely identifiable beds are included amongst those listed in this paper. All Bairstow's ammonites are preserved in collections of the Department of Palaeontology, The Natural History Museum, London, and most have been given Museum registration numbers, in addition to the collecting numbers given by Bairstow. The identifiable Liparoceratidae were registered for Spath's (1938) catalogue of that family, and received some of the numbers in the series C.38871–C.39579; some of the Eoderoceratidae were registered in the late 1950s in the series C.49314–C.49431; the remainder of the collection was registered in 2000 with the numbers CA 2744–CA 4608. The three nautiloids in his collection have the numbers CN 86, 87 and 93.

In 1928 Bairstow consulted with S.S. Buckman, a year or two before his death, who had expressed interest in the ammonites he was collecting in the bay. From his earlier work on ammonites collected by the Geological Survey, Buckman knew that the succession up to the top of the Sinemurian was exposed in both the north-western and south-eastern parts of the bay. The sequences of ammonites that Bairstow was obtaining in the two outcrops that are up to 3 km apart seemed to Buckman to be a good opportunity to test his hemeral theory[1], and he advised Bairstow to record the geographical position,

[1]Briefly, Buckman's theory of hemera was that every species of ammonite reached its acme of abundance at a unique time that did not overlap with the acme of any other species. By discovering the order in which ammonites reached their acme, a sequence of 'hemerae' could be constructed, which would be smaller and finer divisions than ammonite subzones and would be applicable over wide areas. Contemporary palaeontologists were sceptical of the theory, and work by many palaeontologists during the following 70 years has shown that the hemeral theory is not valid.

SIMPSON 1868, 1884	TATE & BLAKE 1876	BUCKMAN 1915	HOWARTH 1954 PHELPS 1995	THIS PAPER	SUBZONES
ML r_1	Mar.30	Dom.30	6	601.1	Stokesi
ML r_2-t	Mar.31	Dom.31	5	600.13	
				600.12	
		Dom.32	4	600.11	
	Mar.32	Dom.33	3	600.8-.10	
			2	600.7	
	Mar.33		1	600.6	
		Dom.34		600.5	Figulinum
			65	600.4	
			64	600.3	
ML u_1	Mar.34	Ch.1	63	600.2	
ML u_2-x	Mar.35	Ch.2	62	600.1	
	Cap.1	Ch.3	59-61	599	
	Cap.2	Ch.4	58	598.35	
			57	598.34	
			56	598.33	
			55	598.32	
	Cap.3-4		54	598.31	
	Cap.5		53	598.2	
	Cap.6		48-52	598.1	
	Cap.7			597	
	Cap.8			596.2-.3	
				596.1	Capricornus
	Cap.9-10		47	595.2	
			46	595.1	
			45	594	
			44	593	
	Cap.11	Ch.5	42, 43	592	
ML y_1-y_2	Cap.12		41	591	
ML y_3-LL b	Cap.13-15$_1$	Ch.6	40	590.7	Maculatum
			39	590.66	
			35-38	590.61-.65	
			34	590.5	
	Cap.15$_2$			590.43	
			33	590.42	
	Cap.16		30-32	590.41	
				590.3	
LL c_1, c_2	Cap.17		29	590.2	
LL c_3	Cap.18		28	590.1	
LL d_1	Cap.19		27	589	
LL d_2	Cap.20		25, 26	588	
LL e_1	Cap.21			587	
LL e_2	Cap.22		24	586	
LL f_1	Cap.23		23	585	
LL f_2	Cap.24		22	584	
LL g_1			21	583.2	
	Cap.25			583.1	
LL g_2	Cap.26		20	582	
LL h_1	Cap.27		19	581	
LL h_2	Jam.1		18	580	
LL i_1	Jam.2		17	579	Luridum
LL i_2-r (part)	Jam.3		16	578.5	
	Jam.4		15	578.4	
	Jam.5		14	578.3	
	Jam.6			578.2	
	Jam.7			578.1	
	Jam.8	Ch.7		577	
	Jam.9		13	576.4-.9	
			12	576.1-.3	
	Jam.10		11	575	
	Jam.11		10	574	Valdani
	Jam.12		9	573	
	Jam.13		8	572	
	Jam.14-16		7	571	
	Jam.17	Ch.8	6	570	
	Jam.18		5	569	Mass.
	Jam.19		4c	568	

SIMPSON 1868, 1884	TATE & BLAKE 1876	BUCKMAN 1915	PHELPS 1985 HESSELBO & JENKYNS 1995	THIS PAPER	SUBZONES
LL i_2-r (part)	Jam.19	Ch.8	4b	567	Masseanum
			4a	564-66	
	Jam.20		3	563	
	Jam.21		2	562	
	Jam.22		1	561	
	Jam.23		117-121	560.3	Jamesoni
				560.1-.2	
	Jam.24			559	
	Jam.25			558	
	Jam.26			557	
	Jam.27			556	
	Jam.28			555	
	Jam.29			554	
	Jam.30-32			550-553	
				548, 549	Brevispina
			115, 116	547	
				546.5	
			114	546.1-.4	
				545	
	Jam.33		113	544.6-.9	
				544.1-.5	
LL s_1	Jam.34	Ch.9	112	543	Polymorphus
LL s_2	Jam.35		111	542	
	Jam.36		110	541	
	Jam.37		109	540	
	Jam.38		108	539	
	Jam.39			538	
			107	536, 537	
LL t_1	Jam.40			535	
LL t_2	Jam.41			534	
LL u_1	Jam.42		106	533	
LL u_2	Jam.43		105	532	
LL v_1	Jam.44		104	531	
LL v_2	Jam.45	Ch.10	103	530.2-.3	
LL w_1				530.1	
LL w_2				528, 529	
LL x_1	Jam.46		102	527	
LL x_2-y_2	Jam.47	Ch.11	101	526.7	Taylori
			100	526.6	
			99	526.5	
			98	526.2-.4	
			97	526.1	
	Jam.48	Ch.12	96	525	
	Jam.49		95	522-24	
			94	521	
			93	520	
	Jam.50		92	519	
	Jam.51			518	
	Jam.52		91	517	
	Jam.53		90	516	
	Jam.54$_1$	Ch.13	89	513.7-515	
			88	513.2-.6	
			87	511-513.1	
			86	509.2-510	
			85	509.1	
			84	508	
			83	507	
			82	506	
			81	505.3	
			80	505.2	
			77-79	505.1	
			76	504	
			73-75	501.3-503	
	Jam.54$_2$	Ch.14		501.2	
	Jam.55	Ch.15		501.1	

Fig. 19 Correlation of the bed numbers used in this paper for the Lower Pliensbachian with divisions used in previous descriptions of the Lower Lias of Robin Hood's Bay; the subzones in the right hand columns are those determined in this paper. See text for details of the sources of the previous descriptions.

SIMPSON 1868, 1884	TATE & BLAKE 1876	BUCKMAN 1915	HESSELBO & JENKYNS 1995	THIS PAPER	SUBZONES
LL z_1	Jam. 56	Ch. 16	72	500	Aplanatum
LL z_2	Jam. 57	Ch. 17	71	499	
	Jam. 58	Ch. 18	70	498	
	Jam. 59	Ch. 19			
	Jam. 60	Ch. 20	69	497	
LL 1_1	Ox. 1		68	496	
LL 1_2-13	Ox. 2	Ch. 21	67	495.7	Macdonnelli
			66	495.3-.6	
			65	495.15-.2	
			64	495.11-.14	
	Ox.3		63	494	
	Ox. 4		62	493.5	Raricostatoides
			61	493.4	
			60	493.1-.3	
	Ox. 5		59	492	
	Ox. 6-12		58	491	
			57	490	
			56	489	
			55	488	
			54	487	Den.
			53	486.3	Oxynotum
				486.1-.2	
			52	485	
			51	484	
			50	483.4-.5	
			49	483.1-.3	
	- - - ? - - -	- - - ? - - -	48	482	
	Ox. 13		47	480-81	
	Ox. 14			479	
	Ox. 15	Ch. 22	46	478	
	Ox. 16		45	477	
	Ox. 17			476	
	Ox. 18	Ch. 23	44	475.4-.6	
	Ox. 19			475.3	
	Ox. 20	Sin. 1		475.1-.2	
LL 14_1	Ox. 21_1	Sin. 2	43	474.3	
	Ox. 21_2			474.2	
	Ox. 22			474.1	
LL 14_2	Ox. 23	Sin. 3	42	472.3-473	
LL 15_1	Ox. 24			472.2	
LL 15_2	Ox. 25			472.1	Simpsoni
				471	
	Ox. 26		41	470	
	Ox. 27		40	469	
			39	468	
LL 16_1	Ox. 28	Sin. 4	38	467	
LL 16_2	Ox. 29			466.3-.5	
LL 17_1				466.2	
LL 17_2				466.1	
LL 18_1	Ox. 30		37	465	
LL 18_2	Ox. 31			464.3	
LL 19_1				464.2	
LL 19_2				464.1	
LL 20_1			36	463	

SIMPSON 1868, 1884	TATE & BLAKE 1876	BUCKMAN 1915	HESSELBO & JENKYNS 1995	THIS PAPER	SUBZONES
LL 20_2	Ox. 31	Sin. 5-8	35	462	Denotatus
LL 21_1			34	461	
LL 21_2				458-60	
	Ox. 32			457	
	Ox. 33		33	456	
	Ox. 34	Sin. 9	32	455.5	
	Ox. 35			455.2-.4	
				455.1	Stellare
			31	454	
	Ox. 36	Sin. 10	30	453.3	
	Ox. 37			453.1-.2	
			29	452	
	Ox.38, 39		28	450.3-451	
			27	450.1-.2	
LL 22_1	Ox.40		26	449	
LL 22_2	Ox.41		25	448.5	
			24	448.1-.4	
LL 23_1	Ox. 42	Sin. 11	23	447	
LL 23_2-26	Ox. 43		22	446.5	Obtus.
	Ox. 44			446.4	
	Ox. 45			446.3	
			21	446.2	Birchi
	Buckl. 1		20	446.1	
	Buckl. 2			445	
				444	
			19	443.3	
			18	443.1-.2	
	Buckl. 3		17	442.2	
	Buckl. 4			442.1	
	Buckl. 5			441	
	Buckl. 6		16	440	
	Buckl. 7			438-39	
	Buckl. 8			437	
				436	
			15	435	
			14	433.3-434	
	Buckl. 9			433.1-.2	Brooki
	Buckl. 10-21	Sin. 12		432	
				431.3	
			13	431.2	
			12	429.7-431.1	
				429.6	Sauzeanum
			11	429.5	
			9, 10	429.1-.4	
		Sin. 13		426-28	
				425	
			8	424.3	
			6, 7	424.1-.2	
				423	
LL 27_1			5	422.2	
				422.1	
LL 27_2			3, 4	421	
			1, 2	420	
				418-19	

Fig. 20 Correlation of the bed numbers used in this paper for the Sinemurian with divisions used in previous descriptions of the Lower Lias of Robin Hood's Bay; the subzones in the right hand columns are those determined in this paper. See text for details of the sources of the previous descriptions.

as well as the stratigraphical horizon, of all his specimens. Bairstow did this by drawing 17 datum lines on his copies of the maps (ie. they are not on the originals in King's College, Cambridge). Each was a straight line crossing the foreshore from the base of the cliff to the seaward edge of the scar; most cross the foreshore approximately at right angles to the cliff, but a few cross at an oblique angle. Originally he chiselled marks on the outcrops to record the exact position of each datum line, but all such marks have long since disappeared. Each ammonite he collected was related to the nearest point on a datum line by pacing yards (0.9 m) from the intersection of the line

with the bottom of the cliff, then yards at right angles to the line up to the position of the ammonite. By these means the geographical position of each ammonite was recorded to approximately the nearest square yard. This information, which is not included in this paper, occurs on many of the original specimen labels that are with the ammonites in his collection.

In 1957 Bairstow prepared a bed-by-bed list of the identifications of every ammonite in his collection. This is a large manuscript amounting to 390 pages. Not only is it a list of the specimens then in the collection (over the years a small number had decayed or were lost), but its main value is as a record of the identifications made by Dr L.F. Spath. He saw the specimens as Bairstow collected them, and made identifications that date mainly from the period 1927–40, while a few were checked or reidentified by him up to 1956. In preparing the list of ammonites for this paper, all the identifications were verified, mainly in order to produce a consistent set of determinations from which the account of the biostratigraphy could be prepared, but also to revise the generic attributions of the species according to modern usage of the various genera. In general Spath's identifications were found to be accurate, and only a few needed revision. The only previous publication of any of Spath's identifications was in his catalogue of the Liparoceratidae (Spath, 1938), where all the Robin Hood's Bay Liparoceratidae collected up to 1937 were listed by register number.

SYSTEMATIC DESCRIPTION OF THE AMMONITES AND NAUTILOIDS

This section is not intended be a full description of the ammonites in the Sinemurian and Lower Pliensbachian of Robin Hood's Bay, but all ammonites that have been figured before are included in a list in systematic order, and this gives an indication of their synonymies. All the Robin Hood's Bay ammonites that have been described or figured by the following authors are included: J. Sowerby and J. de C. Sowerby (1812–1846), Young & Bird (1822, 1828), Phillips (1829, 1835, 1875), Brown (1837, 1889), Simpson (1843, 1855, 1884), Blake (1876), Wright (1878–82), Hyatt (1889), Buckman (1909–30), Spath (1923*b*, 1924, 1925*a*, 1938, 1956), Trueman & Williams (1925), Jaworski (1931), Howarth (1955, 1962), Dean *et al* (1961), Howarth & Donovan (1964), Guérin-Franiatte (1966), Getty (1973), Donovan & Forsey (1973), Schlegelmilch (1976, 1992), Phelps (1985), Dommergues (1987) and Dommergues & Meister (1992).

All the ammonites listed are from Robin Hood's Bay, except where indicated otherwise, and the beds from which the type and figured specimens might have come are identified with varying degrees of confidence, as indicated in the list; register numbers are given, where known. The list also shows the data on which the identifications in the paper are based (eg. by giving references to the type specimens in most cases, including those that are not Yorkshire specimens). 56 of the better preserved ammonites in Bairstow's collection are figured to illustrate the identifications and the contents of some of the subzones. Further discussion of synonymies, identifications and distribution in the zones and subzones is found in the section on Biostratigraphy, and more details of the identifications of the type specimens of some species can be found in Howarth (1962). All measurements are in millimetres (mm); D = diameter, Wh = whorl height, Wb = whorl breadth, U = diameter of the umbilicus.

Order **AMMONOIDEA** Zittel, 1884
Suborder **PHYLLOCERATINA** Arkell, 1950
Family **JURAPHYLLITIDAE** Arkell, 1950
Genus ***TRAGOPHYLLOCERAS*** Hyatt, 1900

Tragophylloceras numismale (Quenstedt, 1845) Pl. 1, fig. 1

1843 *Ammonites huntoni* Simpson: 41.
1845 *Ammonites heterophyllus numismalis* Quenstedt: 100, pl. 6, figs 4a, b, 5a, b, *non* figs 3a, b, 5c (figs 5a, 5b, from Germany, designated lectotype by Buckman, 1912: *viii*).
1855 *Ammonites nanus* Simpson: 38.
1921 *Tragophylloceras huntoni* (Simpson); Buckman: pl. 219 (paratype or holotype, WM 477; ?from bed 517 or 520).
1926 *Tragophylloceras nanum* (Simpson); Buckman: pl. 679 (holotype, WM 472; from bed 517 or 520).
1964 *Tragophylloceras numismale* (Quenstedt); Howarth & Donovan: 295, pl. 48, fig. 5 (BM C.67766; from bed 517 or 520).

RANGE. Beds 505.2–544.5, Taylori to Polymorphus Subzones; 17 specimens.

Tragophylloceras loscombi (J. Sowerby, 1817)

1817 *Ammonites loscombi* J. Sowerby: 185, pl. 183.
1843 *Ammonites ambiguum* Simpson: 8.
1843 *Ammonites robinsoni* Simpson: 42.
1910 *Rhacoceras ambiguum* (Simpson); Buckman: pl.16 (holotype, WM 89; ?from bed 569).
1914 *Tragophylloceras loscombi* (J. Sowerby); Spath: 336, pl. 49, fig. 1 (holotype, from Dorset).
1921 *Tragophylloceras robinsoni* Buckman: pl. 220 (paratype, WM 478; ?from bed 569).
1964 *Tragophylloceras loscombi* (J. Sowerby); Howarth & Donovan: 301, pl. 49, figs 4–7 (from Dorset).

RANGE. Found in bed 569 only, Masseanum Subzone; 2 specimens.

REMARKS. This single specimen high in the Masseanum Subzone is at a lower horizon than specimens in Dorset, where they have not been recorded from below the Luridum Subzone (Howarth & Donovan, 1964: 293, 302).

Suborder **LYTOCERATINA** Hyatt, 1889
Superfamily **LYTOCERATACEAE** Neumayr, 1875
Family **LYTOCERATIDAE** Neumayr, 1875
Genus ***LYTOCERAS*** Suess, 1865

Lytoceras fimbriatum (J. Sowerby, 1817) Pl. 1, fig. 3

1817 *Ammonites fimbriatus* J. Sowerby: 145, pl. 164.
1919 *Fimbrilytoceras fimbriatum* (J. Sowerby); Buckman: pl. 130A–C (from Dorset).

RANGE. Beds 570–578.5, Ibex Zone; 25 specimens. Two *Lytoceras* of indeterminate species were found in beds 568 (top) and 584.

REMARKS. *Lytoceras fimbriatum* is confined to the Ibex Zone in Robin Hood's Bay, except for one poorly preserved specimen in bed 584 (Maculatum Subzone) that can only be determined as *Lytoceras* sp. indet. Many of those in the Ibex Zone are large and well-preserved, and one of the best specimens is figured in Pl. 1, fig. 3. Sowerby's figured specimen, now lost, was from Dorset.

Suborder **AMMONITINA** Zittel, 1884
Superfamily **PSILOCERATACEAE** Hyatt, 1867
Family **PSILOCERATIDAE** Hyatt, 1867

Blocks of limestone containing *Psiloceras, Caloceras* and other Hettangian and Lower Sinemurian ammonites are sometimes found loose in Robin Hood's Bay, and species have been described by several authors as coming from 'Robin Hood's Bay'. They are not from the inter-tidal exposures (the lowest of which is in the upper part of the Semicostatum Zone), but are derived from Glacial Drift nodules that are widespread in the bay and were exploited by 19th century collectors.

Genus ***PSILOCERAS*** Hyatt, 1867

Psiloceras erugatum (Phillips, 1829)

1829 *Ammonites erugatus* Phillips: 163, pl. 13, fig. 13; also Phillips, 1835: 135, pl. 13, fig. 13; and Phillips, 1875: 270, pl. 13, fig. 13.
1962 *Psiloceras erugatum* (Phillips); Howarth: 99, pl. 14, fig. 2 (holotype, BM 37982, from 'Robin Hood's Bay').

Psiloceras* aff. *sampsoni (Portlock, 1843)

1879/81 *Aegoceras planorbis* (J. Sowerby); Wright: 308 (1881), pl. 14, figs 1, 2 (1879) (SM J18216, from 'Robin Hood's Bay').

Genus ***CALOCERAS*** Hyatt, 1870

Caloceras belcheri (Simpson, 1843)

1843 *Ammonites belcheri* Simpson: 12.
1910 *Caloceras belcheri* (Simpson); Buckman: pl. 17 (holotype, WM 101, from Robin Hood's Bay).
1879/81 *Aegoceras belcheri* (Simpson); Wright: 313 (1881), pl. 15, figs 7, 8 (1879) (SM J18217, from Robin Hood's Bay), 9.
1976 *Psiloceras (Caloceras) johnstoni* (J. de C. Sowerby); Schlegelmilch, 1976: 106, pl. 5, fig. 8 (WM 101).

Caloceras convolutum (Simpson, 1855)

1855 *Ammonites convolutus* Simpson: 43 (*non Ammonites convolutus* Schlotheim, 1820).
1910 *Caloceras convolutum* (Simpson); Buckman: pl. 18 (holotype, WM 491, from Robin Hood's Bay).

Caloceras wrighti Spath, 1924

1880/81 *Aegoceras belcheri* (Simpson); Wright: 313 (1881), pl. 19, figs 1, 2 (1880) (holotype, from North Cheek, Robin Hood's Bay, ?lost).
1924 *Caloceras wrighti* Spath: 191 (*nom. nov.* for Wright's figured specimen).

Family **SCHLOTHEIMIDAE** Spath, 1923
Genus ***SCHLOTHEIMIA*** Bayle, 1878

Schlotheimia redcarensis (Young & Bird, 1822)

1822 *Ammonites redcarensis* Young & Bird: 248, pl. 14, fig. 13; also Young & Bird, 1828: 258, pl. 14, fig. 10.
1925 *Schlotheimia redcarensis* (Young & Bird); Buckman, pl. 608 (neotype, WM 314; if from Robin Hood's Bay, as labelled, it must be from Glacial Drift).

Genus ***SAXOCERAS*** Lange, 1924

Saxoceras aequale (Simpson, 1855)

1855 *Ammonites aequalis* (Simpson): 49.
1925*a* *Saxoceras aequale* (Simpson); Spath: 204, fig. 4 (drawing of holotype, BM 18109).
1962 *Saxoceras aequalis* Howarth: 100, pl. 14, fig.3 (holotype, BM 18109, from Robin Hood's Bay or Redcar, more probably the latter).

Genus ***ANGULATICERAS*** Quenstedt, 1883

Angulaticeras sulcatum (Simpson, 1843)

1843 *Ammonites sulcatus* Simpson: 55 (*non Ammonites sulcata* Lamarck, 1822).
1911 *Schlotheimia sulcata* (Simpson); Buckman: pl. 38 (holotype, WM 743; ?from beds 461–464).
1976 *Angulaticeras sulcatum* (Simpson); Schlegelmilch: 112, pl. 8, fig. 7 (WM 743).

RANGE. Six small examples of *Angulaticeras* sp. indet. were found in beds 461–464.33 and 485.2, Denotatus to Oxynotum Subzones.

Genus ***Macrogrammites*** Buckman, 1928

Macrogrammites antiquatum (Simpson, 1855)

1855 *Ammonites antiquatus* Simpson: 36.
1927 *Schlotheimia antiquata* (Simpson); Buckman, 1927, pls 718A, B (holotype, WM 79/80); if this holotype is a large smooth outer whorl of the Hettangian genus *Macrogrammites* as identified by Buckman (1928: on caption to pl. 718A* [re-issue of 1927, pl. 718A]), then it comes from Glacial Drift in Robin Hood's Bay, or from Redcar; it is not from beds exposed in Robin Hood's Bay.

Family **ARIETITIDAE** Hyatt, 1875
Subfamily **ARIETITINAE** Hyatt, 1875
Genus ***CORONICERAS*** Hyatt, 1867
Subgenus ***ARIETITES*** Waagen, 1869

Coroniceras (Arietites) alcinoe (Reynès, 1879)
Pl. 1, fig. 8

1879 *Ammonites alcinoe* Reynès: pl. 23, figs 7, 8, 9–11 (neotype, from France).
1955 *Pararnioceras alcinoe* (Reynès); Donovan: 14.

RANGE. Beds 424.3–429.64, Sauzeanum Subzone; 5 specimens.

Coroniceras (Arietites) validanfractum (Simpson, 1855)

1855 *Ammonites validanfractus* Simpson: 95.
1962 *Coroniceras validanfractum* Howarth: 101, pl. 14, figs 4 (holotype, WM 282), 5 (paratype, WM 530); similarly preserved specimens have been found at Redcar, but not at Robin Hood's Bay; this species is close to *C. (A.) alcinoe* (Reynès).

Coroniceras (Arietites) obesulus (Blake, 1876)

1876 *Arietites obesulus* Blake: 284, pl. 5, fig. 2 (lectotype, SM J34800, from Robin Hood's Bay); also very similar to *C. (A.) alcinoe* (Reynès).

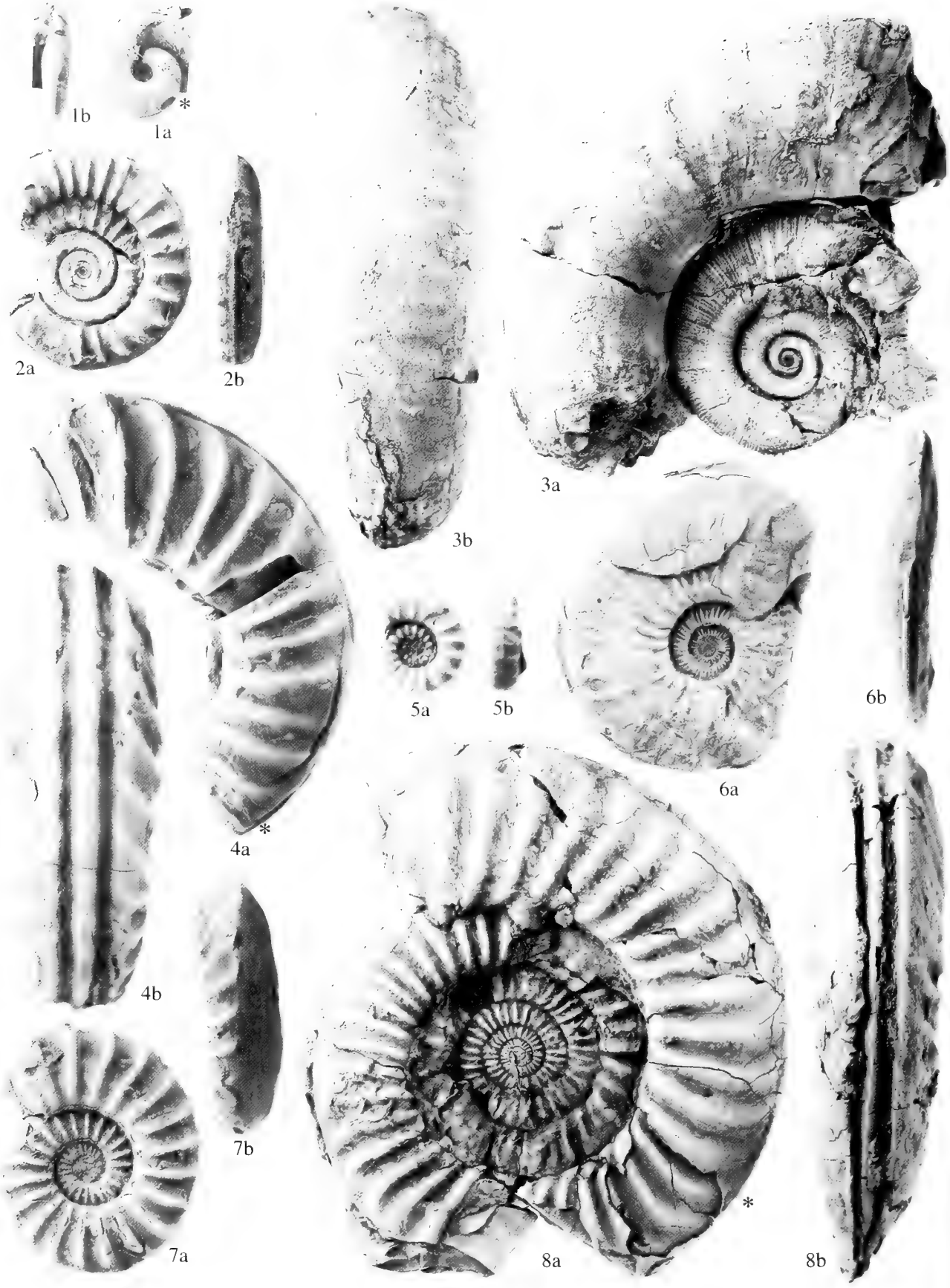
1b
1a
*
2a
2b
3b
3a
4a
*
5a
5b
6b
6a
4b
7b
7a
8a
*
8b

?*Coroniceras (Arietites) radiatus* (Simpson, 1843)

1843 *Ammonites radiatus* Simpson: 47 (*non Ammonites radiatus* Bruguière, 1789).
1911 *Arietites radiatus* (Simpson); Buckman: pl. 35 (holotype, WM 304, possibly from beds 426–429, but it is only 12 mm diameter and is not identifiable).

Coroniceras (Arietites) cf. *planaries* (Reynès, 1879)

1878/81 *Arietites nodulosus* (Young & Bird); Wright: 288 (1881), pl. 6, figs 2, 3 (1878) (C.1880, possibly from beds 426–429).

Genus ***ARNIOCERAS*** Hyatt, 1867

Arnioceras semicostatum (Young & Bird, 1828)

Pl. 1, fig. 2

1828 *Ammonites semicostatus* Young & Bird: 257, pl. 12, fig. 10.
1855 *Ammonites vetustus* Simpson: 88.
1876 *Arietites semicostatus* (Young & Bird); Blake: 288, pl. 5, fig. 4a (upper figure, BM C.17935; lower figure, BM C.17934 (?malformation); both from Redcar).
1876 *Arietites differmis* (Emmrich); Blake: 289, pl. 6, fig. 3 (C.17933, possibly from Redcar).
1889 *Arnioceras semicostatum* (Young & Bird); Hyatt: 165, pl. 2, figs 12, 13 (from 'Whitby', presumably from Robin Hood's Bay).
1918 *Arnioceras semicostatum* Buckman: pl. 112 (holotype, WM 924).
1925*a* *Arnioceras semicostatum* (Young & Bird); Spath: 329, fig. 10a (BM C.86a).
1931 *Arnioceras semicostatum* (Young & Bird); Jaworski: 111, pl. 5, fig. 1 (WM 924).
1956 *Arnioceras semicostatum* (Young & Bird); Spath: 153, pl. 10, figs 6 (BM C.25651), 7 (BM C.17933).
1961 *Arnioceras semicostatum* (Young & Bird); Dean *et al.*: pl. 65, fig. 4 (BM C.25651).
1962 *Arnioceras vetustum* (Simpson); Howarth: 103, pl. 15, fig. 2 (holotype, GSM 26404, ?from bed 421 or 424).
1976 *Arnioceras semicostatum* (Young & Bird); Schlegelmilch: 138, pl. 21, fig. 4 (WM 924).

RANGE. Beds 421.4–429.64, Sauzeanum Subzone; 118 specimens.

REMARKS. Jaworski's (1931: pl. 5, fig. 1) enlarged figure of the holotype is much better than Buckman's (1918) figure. Older collections contain many well-preserved *Arnioceras semicostatum* from limestone nodules. Such good specimens were not found by Bairstow and they have sometimes been considered to come from Glacial Drift, but judging from the preservation it is possible that they came from nodules near the top of bed 421.4 or from beds 424.2 or 424.3. Although *Arnioceras* persists elsewhere into the overlying Brooki and Birchi Subzones, all the well-preserved Robin Hood's Bay specimens appear to have come from these limestone nodules of the Sauzeanum Subzone. One of the better examples in Bairstow's collection is figured in Pl. 1, fig. 2.

The range of *Arnioceras* is extended down to bed 421.1 and up to beds 430–436 by six specimens of indeterminate species found by Bairstow.

Arnioceras acuticarinatum (Simpson, 1855)

1855 *Ammonites acuticarinatum* (Simpson): 94)
1911 *Arnioceras acuticarinatum* (Simpson); Buckman: pl. 40 (holotype, WM 295; ?from beds 421–424).
1931 *Arnioceras acuticarinatum* (Simpson); Jaworski: 126, pl. 5, fig. 2 (WM 295).
1976 *Arnioceras acuticarinatum* (Simpson); Schlegelmilch, 1976: 138, pl. 21, fig. 3 (WM 295).

REMARKS. The best figure of the holotype is that of Jaworski, and such a well-preserved specimen might have come from beds 421–424. Its more finely ribbed inner whorls possibly separate it from *A. semicostatum*.

Arnioceras miserabile (Quenstedt, 1856)

1856 *Ammonites miserabilis* Quenstedt: 71, pl. 8, fig. 7.
1876 *Aegoceras nigrum* Blake: 274, pl. 6, fig. 6 (lectotype, BM C.17889, possibly from bed 424.2 or 424.3).
1884 *Ammonites miserabilis* Quenstedt; Quenstedt: 106, pl. 13, figs 27–30.
1925*a* *Arnioceras nigrum* (blake); Spath: 329, fig. 10b (BM 50150c, possibly from bed 424.2 or 424.3).
1966 *Arnioceras miserabile* (Quenstedt); Guérin-Franiatte: 254, pl. 136, figs 1 (neotype, from Germany, original of Quenstedt, 1884: pl. 21, fig. 27), 2–4 (from Germany and France).
1976 *Arnioceras miserabile* (Quenstedt); Schlegelmilch: 49, pl. 21, fig. 5 (neotype).

RANGE. Beds 424.2–425.5, Sauzeanum Subzone; 7 specimens.

Genus ***VERMICERAS*** Hyatt, 1889

Vermiceras multanfractum (Simpson, 1855)

1855 *Ammonites multanfractus* Simpson: 95.
1962 *Vermiceras multanfractum* (Simpson); Howarth: 101, pl. 14, fig. 6 (neotype, WM 281); not found by Bairstow, possibly derived from Glacial Drift in Robin Hood's Bay.

PLATE 1

Fig. 1 *Tragophylloceras numismale* (Quenstedt). Bed 505.2, CA 2744.
Fig. 2 *Arnioceras semicostatum* (Young & Bird). Bed 424.2, CA 2830.
Fig. 3 *Lytoceras fimbriatum* (J. Sowerby). Bed 576.4, CA 2778, × 0.6; the large outer whorl is part of the body chamber.
Fig. 4 *Asteroceras confusum* Spath. Bed 446.32, CA 3010.
Fig. 5 *Euagassiceras resupinatum* (Simpson). Bed 422.2, CA 2948.
Fig. 6 *Eparietites impendens* (Young & Bird). Bed 461, CA 3228.
Fig. 7 *Aegasteroceras sagittarium* (Blake). Bed 456, CA 3124.
Fig. 8 *Coroniceras (Arietites) alcinoe* (Reynès). Bed 429.64, CA 2803, × 0.6; the asterisk marks the probable end of the phragmocone.
All figures natural size, except Figs 3 and 8.
Where determinable the position of the end of the phragmocone is marked with an asterisk (*) on all specimens figured in the plates.

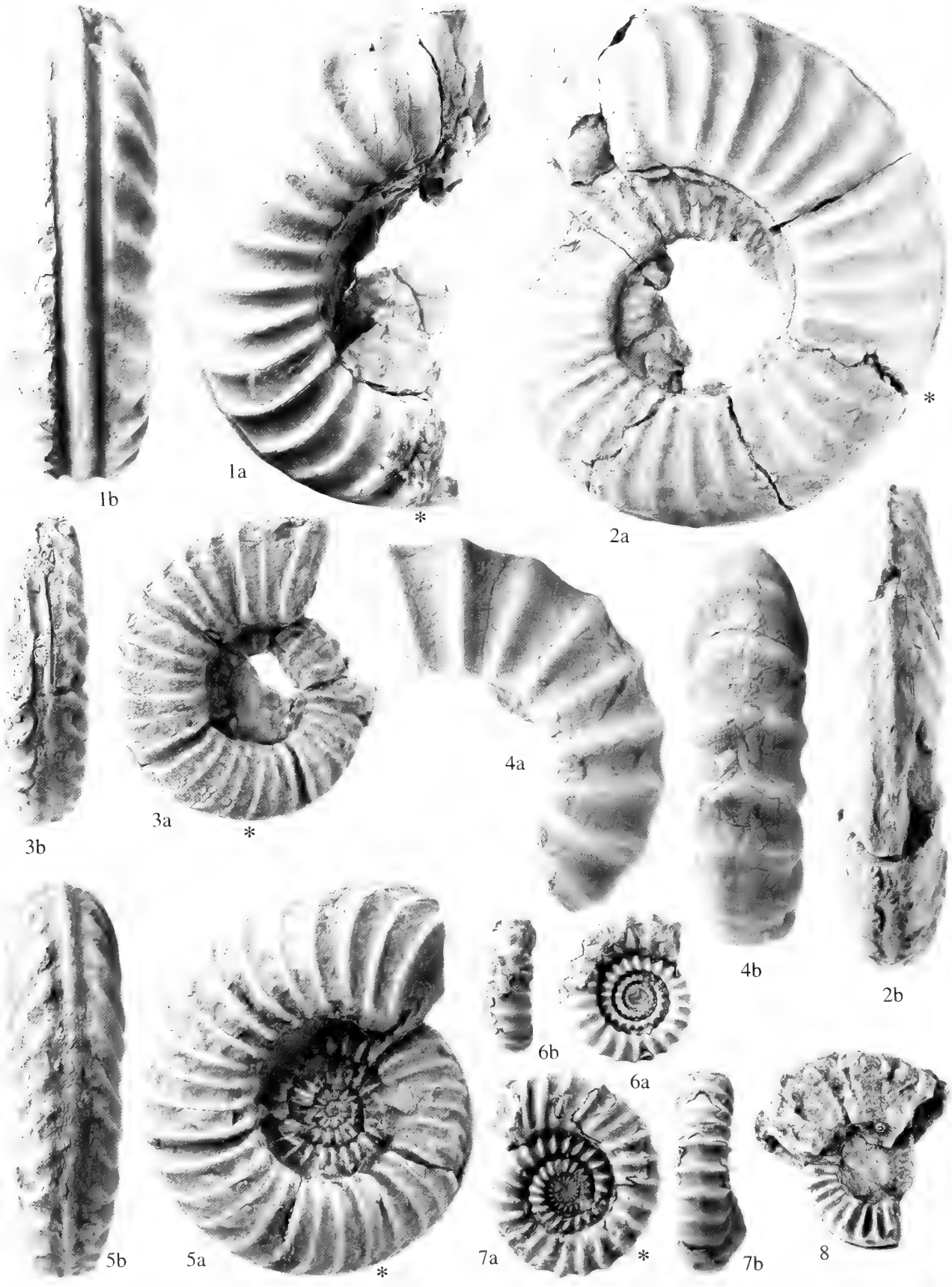
1b
1a
*
2a
*
3b
3a
*
4a
4b
2b
5b
5a
*
6b
6a
7a
*
7b
8

Subfamily **AGASSICERATINAE** Spath, 1924
Genus ***AGASSICERAS*** Hyatt, 1875

Well-preserved *Agassiceras scipionianum* (d'Orbigny) and the smaller, smoother species *A. personatum* have been figured before from Robin Hood's Bay and are common in old collections, but none were found by Bairstow. *Agassiceras* mainly characterizes the Scipionianum Subzone, just below the lowest horizon exposed in Robin Hood's Bay, so, although it is possible that some of them came from beds 421 or 422, it is more likely that they were derived from Glacial Drift.

Agassiceras personatum (Simpson, 1843)

1843 *Ammonites personatus* Simpson: 9.
1920 *Agassiceras personatum* (Simpson); Buckman: pl. 187, figs 1, 2 (holotype, WM 2125), 3, 4 (paratype WM 67).

REMARKS. A small smooth species.

Agassiceras scipionianum (d'Orbigny, 1844)

1844 *Ammonites scipionianus* d'Orbigny: 207, pl. 51, figs 7, 8.
?1855 *Ammonites illatus* Simpson: 39 (*non Ammonites illatus* Simpson, 1843: 10).
1876 *Arietites scipionianus* (d'Orbigny); Blake: 287, pl. 5, fig. 3 (BM C.17909; locality not recorded, but the preservation is like that of other specimens from Robin Hood's Bay).
1961 *Agassiceras scipionianum* (d'Orbigny); Dean *et al.*: pl. 65, fig. 3 (BM 37909).
?1962 *Agassiceras illatum* (Simpson, 1855, *non* 1843); Howarth: 102, pl. 15, fig. 1 (holotype, WM 84).
1994 *Agassiceras scipionianum* (d'Orbigny); Fischer: 53, pl. 16, figs 1 (lectotype), 2 (both from France).

Agassiceras decipiens (Spath, 1923)

1923*b* *Aetomoceras decipiens* Spath: 72.

REMARKS. Spath's three syntypes are BM C.22067a, C.22067b and a specimen at the top of the block WM 67 as figured by Buckman (1920: pl. 187, fig. 3), all from Robin Hood's Bay. Of these, C.22067a is here designated lectotype; it is similar to *A. scipionianum* (d'Orbigny), but has slightly more ribs.

Genus ***EUAGASSICERAS*** Spath, 1924

Euagassiceras resupinatum (Simpson, 1843)

Pl. 1, fig. 5

1843 *Ammonites resupinatus* Simpson: 15.
1844 *Ammonites sauzeanus* d'Orbigny: 304, pl. 95, figs 4, 5.
1855 *Ammonites transformatus* Simpson: 91.
1889 *Coroniceras sauzeanum* (d'Orbigny); Hyatt: 184, pl. 6, figs 4, 6–9.
1909 *Agassiceras resupinatum* (Simpson); Buckman: pl. 6 (holotype, WM 96; ?from bed 421 or 422).
1913 *Agassiceras transformatum* (Simpson); Buckman: pl. 75 (holotype, WM 279, ?from bed 421 or 422).
1913 *Defossiceras defossum* (Simpson, 1843); Buckman: pl. 76 (WM 103, a paralectotype, presumably also from beds 421–422; see Donovan & Forsey (1973: 13) for interpretation of *Defossiceras* and its type species).
1994 *Euagassiceras sauzeanum* d'Orbigny; Fischer: 84, pl. 16, fig. 3 (holotype, from France).

RANGE. Beds 421.4–426.1, Sauzeanum Subzone; 38 specimens, of which the best preserved are in beds 421 and 422.

REMARKS. Typical examples of *Euagassiceras* occur in beds 421 and 422, and it is likely that the holotypes of Simpson's species *E. resupinatum* and *E. transformatum* are from those beds; both species are synonyms of *E. sauzeanum* (d'Orbigny, 1844), and *E. resupinatum* (Simpson, 1843) is the senior name for this species.

Subfamily **ASTEROCERATINAE** Spath 1946
Genus ***ASTEROCERAS*** Hyatt, 1867

Asteroceras obtusum (J. Sowerby, 1817)

1817 *Ammonites obtusus* J. Sowerby: 151, pl. 167.
1966 *Asteroceras obtusum* (J. Sowerby); Guérin-Franiatte: 294, pl. 170 (lectotype, Oxford University Museum, OUM J.1194, from Charmouth, Dorset).

RANGE. One specimen in bed 446.32, Obtusum Subzone. A single *Asteroceras* sp. indet. in bed 446.31 is the lowest recorded *Asteroceras* in Robin Hood's Bay.

Asteroceras confusum Spath, 1925

Pl. 1, fig. 4; Pl. 2, fig. 1

1880/81 *Arietites obtusus* (J. Sowerby); Wright: 293 (1881), pl. 21, figs 3, 4 (1880) (holotype of *Asteroceras confusum* Spath).
1925*a* *Asteroceras confusum* Spath: 300.
1966 *Asteroceras confusum* Spath; Guérin-Franiatte: 296, pl. 172 (holotype, BM C.2223, from Bredon, Worcestershire).

RANGE. Five specimens in beds 446.32 and 446.33, Obtusum Subzone.

REMARKS. *A. confusum* has thicker whorls and more prominent grooves bordering the keel on the venter than *A. obtusum*.

Asteroceras stellare (J. Sowerby, 1815)

1815 *Ammonites stellaris* J. Sowerby: 211, pl. 93.
1880/81 *Arietites stellaris* (J. Sowerby); Wright: 295 (1881), pl. 22, figs 3–5 (1880) (lectotype, BM 43969a, from Dorset).
1882 *Aegoceras sagittarium* (Blake); Wright: 355, pl. 52, figs 1–

PLATE 2
Fig. 1 *Asteroceras confusum* Spath. Bed 446.32, CA 3011, × 0.6.
Fig. 2 *Asteroceras blakei* Spath. Bed 452, CA 2990, × 0.5.
Figs 3, 5 *Caenisites turneri* (J. de C. Sowerby). Bed 433.3. **3,** CA 3194. **5,** CA 3197; the asterisk marks the probable end of the phragmocone.
Fig. 4 *Aegasteroceras crassum* Spath. Bed 458.2, CA 3048; a body chamber fragment.
Fig. 6 *Gagaticeras neglectum* (Simpson). Bed 468, CA 3326; probably wholly septate.
Fig. 7 *Gagaticeras exortum* (Simpson). Bed 468, CA 3292; the asterisk marks the probable end of the phragmocone.
Fig. 8 *Eparietites bairstowi* sp. nov. **Paratype,** bed 455.5, CA 3218; probably wholly septate.
All figures natural size, except Figs 1 and 2.

3 (BM C.3124, a large specimen that is very similar to specimens from bed 451; it is more involute and has higher whorls than *sagittarium*).

1961 *Asteroceras stellare* (J. Sowerby); Dean *et al.*: pl. 67, fig. 2 (lectotype, BM 43969a, from Dorset).

RANGE. Beds 447–451, Stellare Subzone; 19 specimens.

REMARKS. *A. stellare* is a large species, and is more involute and has more massive whorls than *A. obtusum*.

Asteroceras blakei Spath, 1925 Pl. 2, fig. 2

1925*a* *Asteroceras blakei* Spath: 264, fig. 5 (holotype, BM C.19991; from beds 452–455.4, probably 452–53).

1925*a* *Asteroceras marstonense* Spath: 267, fig. 7 (holotype, BM 37948, probably from bed 452 or 453).

RANGE. Beds 452–455.4, Stellare and Denotatus Subzones; 29 specimens.

REMARKS. *A. blakei* occurs at a higher stratigraphical level, and is more involute and more compressed than *A. obtusum*. *A. marstonense* is a synonym, and its holotype comes from Robin Hood's Bay despite being named after Marston Magna, Somerset.

Genus ***AEGASTEROCERAS*** Spath, 1925

Aegasteroceras sagittarium (Blake, 1876) Pl. 1, fig. 7

1876 *Aegoceras sagittarium* Blake: 276, pl. 7, figs 2A (lectotype, SM J18230), 2B (paralectotype, BM C.17881).

1880/82 *Aegoceras acuticostatum* Wright: 371 (1882), pl. 35, figs 1–3 (1880) (holotype, SM J18230); objective synonym of *Aegoceras sagittarium* Blake, 1876.

1882 *Aegoceras sagittarium* Blake; Wright: 355, pl. 52, figs 4, 5 (BM C.1873); pl. 52A, figs 3, 4 (BM C.1873), 5 (BM C.1874), 6 (BM C.1875).

1925*a* *Aegasteroceras simile* Spath: 265, fig. 6a (holotype, BM C.26687).

1966 *Aegasteroceras simile* Spath; Guérin-Franiatte: 310, pl. 189 (BM C.26687).

1966 *Aegasteroceras sagittarium* (Blake); Guérin-Franiatte: 312, pl. 192, fig. 1 (SM J18230).

RANGE. Beds 454.1–458.1, Stellare and Denotatus Subzones; 123 specimens; all the figured ones are from beds 454.2 or 456, probably the latter.

Aegasteroceras crassum Spath, 1925 Pl. 2, fig. 4

1882 *Aegoceras sagittarium* Blake; Wright: 355, pl. 52A, figs 1, 2 (BM C.1922, from bed 458.2 or 458.3, holotype of *Aegasteroceras crassum* Spath, 1925).

1925*a* *Aegasteroceras crassum* Spath: 266.

RANGE. Beds 449–458.3, Stellare and Denotatus Subzones; 9 specimens.

Genus ***CAENISITES*** Buckman, 1925

Caenisites turneri (J. de C. Sowerby, 1824) Pl. 2, figs 3, 5

1824 *Ammonites turneri* J. de C. Sowerby: 75, pl. 452, upper figure.

1879/81 *Arietites turneri* (J. de C. Sowerby); Wright: 292 (1881), pl. 12, fig. 4 (1879) (lectotype, BM 43973a, from Glacial Drift, Norfolk).

1956 *Euasteroceras turneri* (J. de C. Sowerby); Arkell: 760, pl. 31, fig. 1 (BM 43973a).

1961 *Caenisites turneri* (J. de C. Sowerby); Dean *et al.*: pl. 66, fig. 2 (from Bredon Hill, Worcestershire).

RANGE. From beds 433.3 and 435, Birchi Subzone; 26 specimens.

Caenisites brooki (J. Sowerby, 1818)

1818 *Ammonites brooki* J. Sowerby: 203, pl. 190.

1961 *Caenisites brooki* (J. Sowerby); Dean *et al.*: pl. 66, fig. 1 (BM C.5606, from Charmouth, Dorset).

1966 *Caenisites brooki* (J. Sowerby); Guérin-Franiatte: 325, pl. 210 (holotype, OUM J.16020, from Lyme Regis, Dorset).

RANGE. From beds 431.2–433.3, Brooki and Birchi Subzones; 11 specimens.

REMARKS. One of those from bed 431.3 is notable in being extremely large: before removal from the rock, it was measured by Bairstow as 585 mm diameter. The outer part was not recovered, but the portion now preserved in the collection is 445 mm diameter and has a massive, almost smooth outer half whorl with keel and grooves on the venter. The inner whorls are covered in matrix and probably crushed.

Genus ***EPARIETITES*** Spath, 1924

Eparietites impendens (Young & Bird, 1828) Pl. 1, fig. 6; Pl. 4, fig. 1

1828 *Ammonites impendens* Young & Bird: 266.

1855 *Ammonites denotatus* Simpson: 76.

1855 *Ammonites tenellus* Simpson: 97.

1876 *Arietites impendens* (Young & Bird); Blake: 290, pl. 6, fig. 7 (BM C.17936).

1878/81 *Arietites collenoti* (d'Orbigny); Wright: 304 (1881), pl. 6 (1878), fig. 1 (BM C.1881; probably from bed 464.32), pl. 22B, figs 1–3 (holotype of *Ammonites denotatus*, SM J3273).

1912 *Arietites tenellus* (Simpson); Buckman: pl. 54 (holotype, WM 293, probably from bed 461 or 464.32).

1912 *Arietites denotatus* (Simpson); Buckman: pls 67A, B (holotype, SM J3273).

1919 *Arietites impendens* (Young & Bird); Buckman: pl. 120 (holotype, WM 292, from bed 462 or 464.1).

1961 *Eparietites denotatus* (Simpson); Dean *et al.*: pl. 66, fig. 4 (BM C.17936).

RANGE. Beds 457–464.32, Denotatus and Simpsoni Subzones; 57 specimens; all the figured specimens are from beds 461–464.

REMARKS. Both *denotatus* and *tenellus* are synonyms of *E. impendens;* the best type specimen is the holotype of Simpson's *denotatus*, but it is clearly the same as the holotype of Young & Bird's *impendens*, and the holotype of *tenellus* differs only in having the crushed-flat type of preservation that is common at some horizons.

Eparietites bairstowi sp. nov. Pl. 2, fig. 8; Pl. 3

HOLOTYPE. CA 3217, from bed 455.2, lower part of Denotatus Subzone.

PARATYPES. CA 3218 and 3219, from bed 455.5, lower part of Denotatus Subzone.

DIAGNOSIS. An evolute species of *Eparietites* in which the umbili-

cal width is 38–40% of the diameter; the whorls are quickly expanding and massive, the whorl breadth is large, and the venter is tricarinate-bisulcate, but loses the sulci at the largest sizes; inner whorls have radial ribs and small ventro-lateral tubercles, but all ornament fades by 230 mm diameter.

DESCRIPTION. Before removal from the rock, Bairstow measured the holotype as having a crushed outer whorl ending at 480 mm ('19 inches') diameter. At that size it was probably complete, but the part he collected in 1933 is solid and uncrushed up to the end of the phragmocone at 330 mm diameter, followed by a short portion at the begining of the crushed body-chamber ending at about 350 mm diameter. Slightly more than one whorl up to the end of the phragmocone is preserved, to which is attached a small portion of the upper part of the side of the next inner whorl. These whorls are massive, rapidly expanding, moderately evolute, and have a whorl section in which the whorl sides converge slightly towards the tricarinate-bisulcate venter, which has a strong central keel. Moderately strong radial ribs fade and disappear three-quarters of a whorl before the end of the phragmocone, and the remaining whorls are smooth.

The larger paratype (CA 3218) consists of inner whorls up to 40 mm diameter, but only a quarter of a whorl up to 25 mm is well preserved. This has quadrate, moderately evolute whorls with a tricarinate-bisulcate venter, and strong straight radial ribs up to small ventro-lateral tubercles; the ribs then bend strongly forwards on the side of the venter and join the lateral keels.

The smaller paratype (CA 3219) consists of small inner whorls up to only 12.5 mm diameter. Its whorl shape, ribs and tubercles are similar to those of the larger paratype.

MEASUREMENTS (in mm)

	D	Wh	Wb	U
CA 3217	342	116 (0.34)	90 (0.26)	136 (0.40)
CA 3217	265	92 (0.35)	67 (0.25)	101 (0.38)

REMARKS. This is the oldest *Eparietites* and is more evolute than any of the succeeding species. The large holotype has massive whorls, with a quadrate whorl section in which the whorl sides converge only slightly towards the venter, a large whorl breadth, and a tricarinate-bisulcate venter; the sulci bordering the central keel on the venter slowly disappear at the largest sizes. *E. impendens* occurs higher up at Robin Hood's Bay and has much more compressed and involute whorls, the umbilical width being 22–24% of the diameter compared with 38–40% in *E. bairstowi*.

Many *Eparietites* occur in the Denotatus Subzone in the top 0.5 m of the Frodingham Ironstone at Scunthorpe, Lincolnshire. Specimens attain very large sizes, some in the NHM collections being up to 600 mm diameter. Most of the smaller specimens are *E. impendens*, but the larger specimens belong mainly to the more evolute species *Eparietites undaries* (Quenstedt), in which the umbilical width is 27–34% of the diameter (Guérin-Franiatte, 1966: 319). There is also one good example of *E. bairstowi* in the Frodingham Ironstone: it is a quarter whorl uncrushed fragment, wholly septate, with a whorl height and breadth of 103.5 and 69.3 mm respectively, and is closely similar to the Robin Hood's Bay holotype at the same size.

Genus ***EPOPHIOCERAS*** Spath, 1924

Epophioceras landrioti (d'Orbigny, 1849)

1849 *Ammonites landrioti* d'Orbigny: 213.
1907 *Ammonites landrioti* d'Orbigny; Thevenin: 94, pl. 7, figs 4, 5 (holotype, from the Obtusum Zone, France).
1966 *Epophioceras landrioti* (d'Orbigny); Guérin-Franiatte: 329, pl. 217 (holotype).

RANGE. Beds 446.5–448.11, Obtusum and Stellare Subzones; 3 specimens. A single *Epophioceras* sp. indet. was found in bed 446.4.

Family **ECHIOCERATIDAE** Buckman, 1913
Genus ***PALAEOECHIOCERAS*** Spath, 1929

Palaeoechioceras sp. indet.

1973 *Palaeoechioceras* sp.; Getty: 9, pl. 1, figs 1 (BM C.79680), 5 (BM C.79678), 9 (BM C.79679); all from bed 467.

RANGE. Bed 467, Simpsoni Subzone; 3 specimens.

Genus ***GAGATICERAS*** Buckman, 1913

REMARKS. In Robin Hood's Bay examples of *Gagaticeras* are found only in beds 467–470, the top half of the Simpsoni Subzone. Although they are divided here into *G. neglectum* with medium to coarse ribs, *G. finitimum* with finer ribs, *G. exortum* with strongly rursiradiate ribs, and *G. gagateum* with markedly depressed whorls, larger collections of better specimens might suggest that there are fewer than four species present.

Gagaticeras gagateum (Young & Bird, 1828)

1828 *Ammonites gagateus* Young & Bird: 255, pl. 12, fig. 7.
1876 *Aegoceras gagateum* (Young & Bird); Blake: 275, pl. 6, fig. 8 (BM C.17883, from bed 467).
1880/82 *Aegoceras gagateum* (Young & Bird); Wright: 364, pl. 37, figs 8, 9 (BM C.2228, probably from bed 467).
1913 *Gagaticeras gagateum* (Young & Bird); Buckman: pl. 78 (holotype, WM 104, from bed 467).
1919 *Gagaticeras funiculatum* Buckman: pl. 122 (holotype, BM C.41783).
1962 *Gagaticeras gagateum* (Young & Bird); Howarth: 102, pl. 14, fig. 6 (WM 744, paratype of *Ammonites multanfractus* Simpson, 1855).
1976 *Gagaticeras gagateum* (Young & Bird); Schlegelmilch: 138, pl. 21, fig. 7 (WM 104).

RANGE. Occurs only in bed 467, Simpsoni Subzone; 2 specimens; has strongly depressed whorls.

Gagaticeras exortum (Simpson, 1855) Pl. 2, fig. 7

1855 *Ammonites exortus* Simpson: 44.
1855 *Ammonites integricostatus* Simpson: 46.
1910 *Echioceras exortum* (Simpson); Buckman: pl. 19, figs 2, 3 (neotype (designated Howarth, 1962: 106), WM 645).
1912 *Androgynoceras integricostatum* (Simpson); Buckman: pl. 47 (holotype, WM 92).

RANGE. Beds 467–70, Simpsoni Subzone; 15 specimens; characterized by markedly rursiradiate ribbing.

Gagaticeras neglectum (Simpson, 1855) Pl. 2 fig. 6

1855 *Ammonites neglectus* Simpson: 45.
1914 *Parechioceras neglectum* (Simpson); Buckman: pl. 101 (holotype, WM 98).
1976 *Gagaticeras neglectum* (Simpson); Schleglemilch: 138, pl. 21, fig. 8 (WM 98).

RANGE. Beds 467-70, Simpsoni Subzone; 77 specimens; the holotype came from bed 468 or 470; has medium to coarse ribbing.

Gagaticeras finitimum (Blake, 1876)

1876 *Aegoceras* (?) *finitimum* Blake: 273, pl. 6, fig. 9.
1914 *Parechioceras finitimum* (Blake); Buckman: pl. 100A (holotype, SM J3280, possibly from bed 468).

RANGE. Beds 467 and 468, Simpsoni Subzone; 11 specimens; finely ribbed.

Genus ***ECHIOCERAS*** Bayle, 1878

Echioceras raricostatum (Zieten, 1831)

1831 *Ammonites raricostatus* Zieten: 18, pl. 13, fig. 4.
1855 *Ammonites cereus* Simpson, 1855: 47.
1912 *Echioceras cereum* (Simpson); Buckman: pl. 49 (holotype, WM 461).
1973 *Echioceras raricostatum* (Zieten); Getty: 13, pl. 1, fig. 7 (neotype, designated Getty, from Württemberg, Germany).

PLATE 3
Eparietites bairstowi sp. nov. **Holotype,** bed 455.2, CA 3217, × 0.48.

REMARKS. Examples of *Echioceras* with strongly depressed whorls and coarse ribs were not found by Bairstow, and the horizon of Simpson's holotype WM 461 is not known; presumably it ought to have come from the Raricostatoides Subzone.

Echioceras raricostatoides (Vadasz, 1908) Pl. 4, fig. 2

1908 *Arietites raricostatoides* Vadasz: 373.
1925 *Echioceras fulgidum* Trueman & Williams: 717, pl. 1, fig. 12 (BM C.17424, possibly from bed 489).
1973 *Echioceras raricostatoides* (Vadasz); Getty: 13, pl. 1, fig. 12 (neotype, designated by Getty, from Nancy, France).

RANGE. Beds 488–491.1, Raricostatoides Subzone; 15 specimens.

REMARKS. The very well preserved specimen from bed 489 figured in Pl. 4, fig. 2 has a closely similar rib-density to that of the neotype shown in Getty's (1973: 15, fig. 3) graph. The more densely ribbed species *E. aeneum* Trueman & Williams, *Echioceras laevidomum* (Quenstedt; Schleglemilch, 1976: pl. 21, fig. 12, lectotype) which has modified ribbing at large whorl sizes, and *E. pauli* (Dumortier, 1867: pl. 29, figs 5, 6), all said to occur in the lowest part of the Raricostatoides Subzone by Getty (1973: 14), were not identified amongst Bairstow's material.

Echioceras intermedium (Trueman & Williams, 1925)

1925 *Pleurechioceras intermedium* Trueman & Williams: 720, pl. 2 fig. 2 (holotype, BM C.26787, from bed 493.
1973 *Echioceras intermedium* (Trueman & Williams); Getty: 16, pl. 3, fig. 1 (BM C.79684, from bed 493).

RANGE. Beds 491.2 and 493.2, Raricostatoides Subzone; 7 specimens.

Genus ***LEPTECHIOCERAS***, Buckman 1923

Leptechioceras macdonnelli (Portlock, 1843)

1843 *Ammonites macdonnelli* Portlock: 134, pl. 29A, fig. 12.
1880/81 *Arietites nodotianus* (d'Orbigny); Wright: 301 (1881), pl. 37, figs 3, 4 (1880) (holotype of *Ammonites macdonnelli* Portlock, from Larne, northern Ireland, Ulster Museum no. K8117).
1923 *Leptechioceras macdonnelli* (Portlock); Buckman: pl. 443 (BM C.41756, from Cheltenham).
1961 *Leptechioceras macdonnelli* (Portlock); Dean *et al.*: pl. 67, fig. 6 (BM C.41756, from ?Larne, Co Antrim, northern Ireland).
1973 *Leptechioceras macdonnelli* (Portlock); Getty: 16.

RANGE. Beds 494–495.7, Macdonnelli Subzone; 5 specimens.

REMARKS. The earliest examples in bed 494 are identified as *L.* aff. *macdonnelli* because reduced ribbing persists onto their outer whorls, which do not become as smooth as in the later specimens from beds 495.13 and 495.7. Nevertheless, in those early specimens the ribs are more reduced than in *L. nodotianum* (d'Orbigny, 1843; Fischer, 1994: 48, pl. 20, fig. 4, holotype), *L. charpentieri* (Schafhäutl, 1847; Getty, 1973: pl. 2, fig. 6, lectotype) or *L. meigeni* (Hug, 1899), all of which are more strongly ribbed throughout.

Genus ***PALTECHIOCERAS*** Buckman, 1924

Paltechioceras planum (Trueman & Williams, 1925)

1925 *Leptechioceras planum* Trueman & Williams: 731, pl. 2, fig. 5 (holotype, from Radstock, Somerset).
1926 *Leptechioceras planum* Trueman & Williams; Buckman: pl. 696 (holotype refigured).

RANGE. Beds 493.3–493.5, Raricostatoides Subzone; 5 specimens.

Paltechioceras tardecrescens (Hauer, 1856) Pl. 4, figs 3, 6

?1855 *Ammonites aureolus* Simpson: 94.
1856 *Ammonites tardecrescens* Hauer: 20, pl. 3, figs 10–12.
1876 *Arietites tardecrescens* (Hauer); Blake: 285, pl. 5, figs 5 (?BM C.17879, from bed 498), 5b (?BM C.17898).
1889 *Caloceras aplanatum* Hyatt: 146, figs 23, 24 (on p. 147).
1889 *Arnioceras tardecrescens* (Hauer); Hyatt: 168, pl. 2, fig. 19.
?1914 *Echioceras aureolum* (Simpson); Buckman: pl. 96 (lectotype, designated by Donovan (1958: 24), GSM 26402, from bed 497); ?senior synonym of *P. tardecrescens*.
1926 *Metechioceras aplanatum* (Hyatt); Buckman: pl. 640 (holotype, MCZ 80 (Museum of Comparative Zoology, Cambridge, Massachussets), from bed 498).
1961 *Paltechioceras aplanatum* (Hyatt); Dean *et al.*: pl. 68, fig. 2 (BM 37999, from bed 498).
1973 *Paltechioceras aplanatum* (Hyatt); Getty: 21, pl. 4, fig. 1 (BM C.17898, from bed 498).
1973 *Paltechioceras tardecrescens* (Hauer); Getty: 21, pl. 4, fig. 2 (lectotype, designated Getty, from Adneth, Saltzburg, Austria).
1992 *Paltechioceras tardecrescens* (Hauer); Dommergues & Meister: 221, figs 5(1)–5(4) (from bed 497).

RANGE. Beds 497–499, Aplanatum Subzone; 228 specimens.

REMARKS. *P. tardecrescens* is abundant in beds 497 and 498; those in bed 498 are up to 175 mm diameter and are preserved in limestone nodules (Pl. 4, fig. 6), and many of the previously figured specimens undoubedly came from this bed (including the holotype of Hyatt's species *aplanatum*). Most of the specimens in bed 497 are much smaller pyritized whorls up to about 40 mm diameter (Pl. 4, fig. 3), though there are a few crushed and partly pyritized fragments of larger whorls up to 90 mm diameter. The lectotype of *P. aureolum* (Simpson, 1855; Buckman, 1914: pl. 96) is pyritized like most specimens in bed 497 and can be matched closely with several of them (eg. CA 3456 and 3480); it is only 25 mm diameter, but *Ammonites aureolus* Simpson, 1855, might be a senior synonym of *Paltechioceras tardecrescens* (Hauer, 1856). In addition, two specimens were found at the base of bed 499 and 0.08 m above the base of that bed respectively.

Paltechioceras regustatum Buckman, 1914

1911 *Echioceras aureolum* (Simpson); Buckman: pl. 28 (paralectotype of *Ammonites aureolus* Simpson, WM 872, from bed 497).
1914 *Paltechioceras regustatum* Buckman: 96c.
1973 *Paltechioceras aureolum* (Simpson); Getty: 20, pl. 5, figs 3 (holotype of *Echioceras regustatum* Buckman, GSM 26439, from bed 496 or 497), 4 (BM C.79681, from bed 497).

RANGE. Beds 496 and 497, Aplanatum Subzone; 18 specimens.

REMARKS. *P. regustatum* is the second and less common species of *Paltechioceras* in the Aplanatum Subzone, and is represented by a few poorly preserved specimens in bed 496 and two in bed 497; it has much more widely spaced ribs than *P. tardecrescens* at diameters of more than 25 mm. Two larger examples figured by Getty (1973: pl. 5, figs 3, 4) as *P. aureolum* are 50 and 64 mm diameter respectively, and the latter

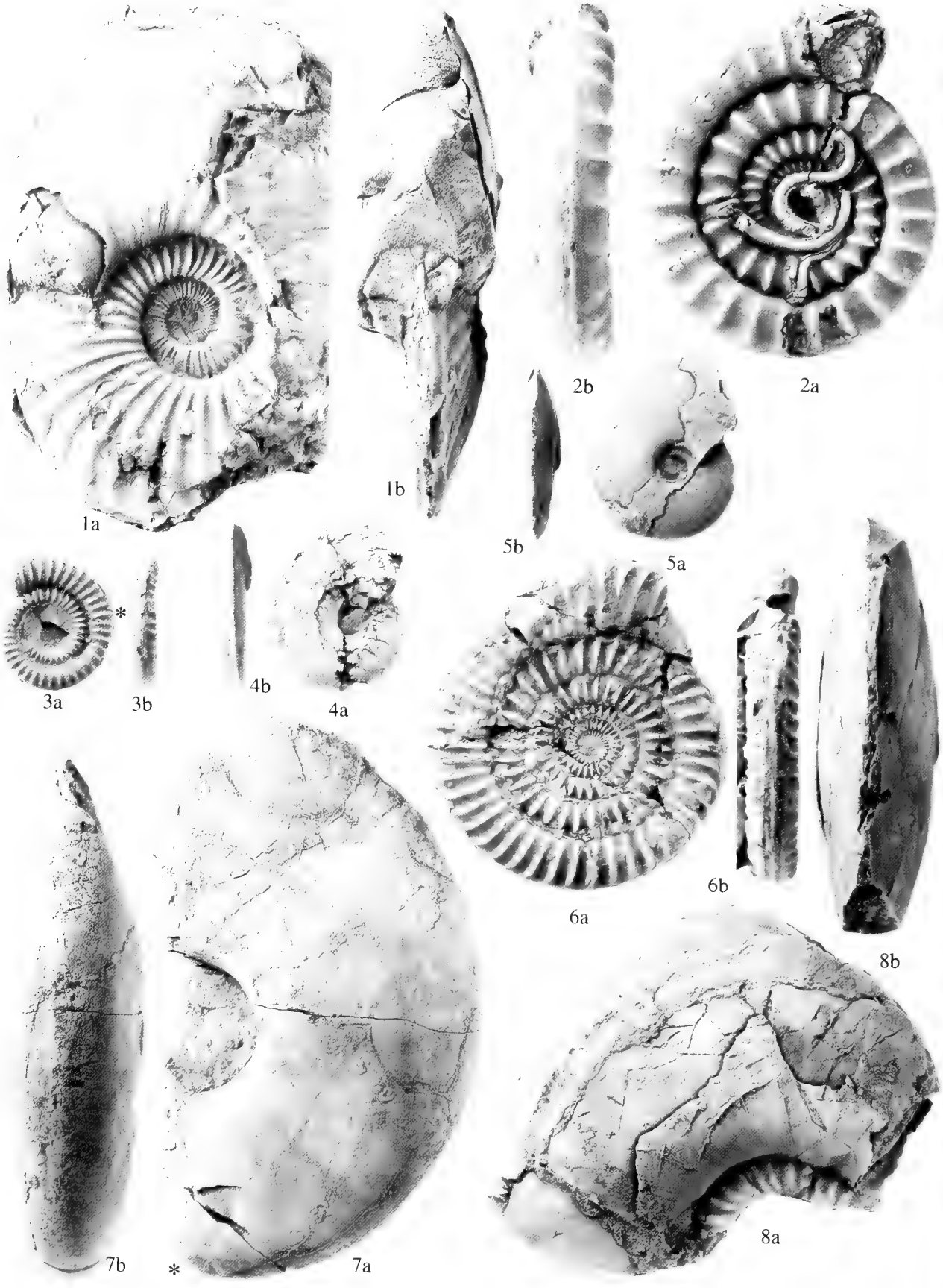
1a
1b
2b
2a
5b
5a
3a
*
3b
4b
4a
6a
6b
8b
7b
*
7a
8a

was said to be from bed 497 (Getty, 1973: 20, 'Tate & Blake's Jamesoni Zone bed 60'). The former of Getty's specimens is the holotype of *P. regustatum* (Buckman, 1914), and this seems to be the correct specific name for the less densely ribbed *Paltechioceras* in beds 496 and 497, because the lectotype of *P. aureolum* has the same rib density as in *P. tardecrescens*, of which it might be a senior synonym.

Family **OXYNOTICERATIDAE** Hyatt, 1867
Genus ***OXYNOTICERAS*** Hyatt 1867

REMARKS. Determination of species of *Oxynoticeras* in the Simpsoni Subzone presents many problems: Simpson (1843, 1855) proposed the specific names *simpsoni, limatus, bucki, flavus* and *lens*, and Spath (1925*a*) proposed the name *eboracense*, all for specimens from beds 467 or 468 (the type specimens of *aliaenum* and *dejectum*, both of Simpson, 1855, are lost and the names are not usable). The name *simpsoni* has date and page priority, and is frequently used for these ammonites. However, Spath's *eboracense* also has a well-preserved type specimen, and if this represents a species different from *O. simpsoni*, then it differs only by its more compressed whorls up to 40 mm diameter. But the many examples of *Oxynoticeras* in beds 467 and 468 show a large amount of variation in whorl compression and rib strength on whorls up to 50 mm diameter, and there are no larger ammonites that can be identified as *O. 'eboracense'* in having more compressed whorls than *O. simpsoni* at large sizes. *O. bucki* (Simpson, 1843) and *O. lens* (Simpson, 1855) are clearly the same as *O. eboracense*, of which they are senior synonyms; *O. flavum* and *O. limatum*, both of Simpson, 1843, are smaller and have slightly thicker whorls like those of *O. simpsoni*. The lectotype of *O. collenoti* (d'Orbigny, 1844; figured by Fischer, 1994: 85, pl. 17, fig. 3) is also very similar to the types of *lens* and *eboracense*.

Larger collections of better preserved specimens will be needed to determine whether these *Oxynoticeras* can really be divided into more than one species, so in this paper all the specimens in beds 463–472.1 are identified as *O. simpsoni*.

Oxynoticeras simpsoni (Simpson, 1843) Pl. 4, figs 5, 8

1843 *Ammonites simpsoni* Simpson: 37.
1843 *Ammonites limatus* Simpson: 41.
1843 *Ammonites bucki* Simpson: 42.
1843 *Ammonites flavus* Simpson: 43.
?1855 *Ammonites lens* Simpson: 80.
1876 *Amaltheus simpsoni* (Simpson); Blake: 291, pl. 8, fig. 4 (BM C.17903).
1881/82 *Amaltheus simpsoni* (Bean); Wright: 392 (1882), pl. 47 (1881), figs 4, 5 (SM J18231), 6, 7 (SM J18232).
1912 *Oxynoticeras flavum* (Simpson); Buckman: pl. 55 (holotype, WM 481).
1912 *Oxynoticeras limatum* (Simpson); Buckman: pl. 56, fig. 1 (holotype, WM 480).
1912 *Aetomoceras simpsoni* (Simpson); Buckman: pls 66A, B (holotype, WM 813).
1920 *Oxynoticeras bucki* (Simpson); Buckman: pl. 165A (holotype, WM 479a).
1925*a* *Oxynoticeras eboracense* Spath: 108, 110, figs d, e (holotype, BM C.18060).
1925*a* *Oxynoticeras simpsoni* (Simpson); Spath: 110, figs f, g (BM 37998).
1961 *Oxynoticeras simpsoni* (Simpson); Dean *et al.*: pl. 67, fig. 4 (BM C.17903).
?1962 *Gleviceras lens* (Simpson); Howarth: 105, pl. 15, fig. 3 (holotype, GSM 26405).
1976 *Oxynoticeras bucki* (Simpson); Schlegelmilch: 140, pl. 22, fig. 12 (WM 479a).

RANGE. Beds 463–470, Simpsoni Subzone; 63 specimens.

REMARKS. All the figured specimens listed in the synonymy above probably came from beds 467 or 468. *O. simpsoni* is a distinctive species that has a larger umbilicus and thicker whorls than *O. oxynotum* and similar species. In Robin Hood's Bay it overlaps in stratigraphical range with *Eparietites impendens*, from which it differs mainly in whorl section: *E. impendens* has a differentiated ventral keel, flanked by narrow flat areas then angled ventro-lateral shoulders, and a vertical umbilical wall and rounded umbilical edge; in *O. simpsoni* the venter is either lanceolate or fastigate with no angles at the umbilical shoulders and without a differentiated keel, and the broad umbilical wall typically slopes at a low angle and merges gradually into the side of the whorl. *E. impendens* has ribs at least on the inner whorls; most *O. simpsoni* are smooth, though some early examples retain ribs on small inner whorls.

The lowest *O. simpsoni* with no ventro-lateral angles at the side of the keel occurs in bed 463, where there are two large examples: one is part of a solid body-chamber ending at about 340 mm diameter; the other is 380 mm diameter and has half a whorl of body-chamber, but is crushed and less well-preserved. A large fragment from bed 464.33 is septate up to at least 256 mm diameter. A smaller *O. simpsoni* from bed 464.32 is figured in Pl. 4, fig. 8, which has ribbing on its inner whorl at about 80 mm diameter, and a small specimen from bed 468 is also figured (Pl. 4, fig. 5).

Oxynoticeras oxynotum (Quenstedt, 1843) Pl. 4, fig. 4

1843 *Ammonites oxynotus* Quenstedt: 161.
1843 *Ammonites polyophyllus* Simpson: 39.
1845 *Ammonites oxynotus* Quenstedt; Quenstedt: 98, pl. 5, fig. 11 (holotype).
1884 *Ammonites oxynotus* Quenstedt; Quenstedt: 175, pl. 22, fig. 29 (holotype).
1909 *Oxynoticeras polyophyllum* (Simpson); Buckman: pl. 8 (holotype, WM 739).

PLATE 4

Fig. 1 *Eparietites impendens* (Young & Bird). Bed 462, CA 3243.
Fig. 2 *Echioceras raricostatoides* Vadasz. Bed 489, CA 3393; wholly septate.
Figs 3, 6 *Paltechioceras tardecrescens* (Hauer). **3,** bed 497, CA 3572. **6,** bed 498, CA 3616; probably wholly septate.
Fig. 4 *Oxynoticeras oxynotum* (Quenstedt). Bed 481, CA 3716; wholly septate.
Figs 5, 8 *Oxynoticeras simpsoni* (Simpson). **5,** bed 468, CA 3692; wholly septate. **8,** bed 464.32, CA 3652, × 0.8; the outer whorl is part of the body chamber.
Fig. 7 *Gleviceras doris* (Reynès). Bed 476, CA 3726, × 0.6.
All figures natural size, except Figs 7 and 8.

1961 *Oxynoticeras oxynotum* (Quenstedt); Dean *et al.*: pl. 66, fig.5 (holotype, Geol.-Pal. Institut, Tubingen, from Württemberg, Germany).

RANGE. Beds 472.1–481, Oxynotum Subzone; 4 specimens.

REMARKS. The lowest *Oxynoticeras* that are more involute and flat-whorled than *O. simpsoni* occur in bed 472.1, which is therefore the base of the Oxynotum Subzone. Better preserved *O. oxynotum* occur higher up in beds 475.3 and 481 (Pl. 4 fig. 4), and there are several fragments of *Oxynoticeras* sp. indet. from beds 480, 482 and 483 consisting of large compressed whorls up to 260 mm diameter that have acute venters and complex suture-lines.

Other species of *Oynoticeras*:

?*Oxynoticeras aliaenum* (Simpson, 1855: 85).
?*Oxynoticeras dejectum* (Simpson, 1855: 85).

The type specimens of both Simpson's species are lost, and the species are not identifiable.

Genus ***GLEVICERAS*** Buckman, 1918

Gleviceras doris (Reynès, 1879) Pl. 4, fig. 7

1879 *Ammonites doris* Reynès: pl. 41, figs 13–15 (probably from France).
1914 *Oxynoticeras doris* (Reynès); Pia: 7, 30, pl. 1, fig. 1; pl. 8, fig. 1.

RANGE. Beds 476 and 485.2, Oxynotum Subzone; 3 specimens.

Gleviceras guibalianum (d'Orbigny, 1844)

1844 *Ammonites guibalianus* d'Orbigny: 259, pl. 73, figs 1–4.
1973 *Gleviceras subguibalianum* (von Pia) (*sic*); Donovan & Forsey: 9, pl. 2, fig. 1 (lectotype of *Ammonites guibalianus* d'Orbigny, designated by Donovan & Forsey, from Nantua, France).
1994 *Gleviceras guibalianum* (d'Orbigny); Fischer: 66, pl. 17, fig. 2 (lectotype refigured).

RANGE. Beds 484.1–499, Oxynotum to Aplanatum Subzones; 14 specimens.

REMARKS. Most specimens are large body-chambers, or fragments thereof, up to 300 mm diameter.

Genus ***PARACYMBITES*** Trueman & Williams, 1927

Paracymbites dennyi (Simpson, 1843)

1843 *Ammonites dennyi* Simpson: 9.
1843 *Ammonites arctus* Simpson: 10.
1909 *Oxynoticeras dennyi* (Simpson); Buckman: pl. 7, figs 1 (lectotype, WM 470), 2, 3 (two paralectotypes).
1911 *Oxynoticeras arctum* (Simpson); Buckman: pl. 36 (holotype, WM 471).
1966 *Paracymbites dennyi* (Simpson); Donovan: 315, pl. 53, figs 5–12 (from Oxfordshire and Gloucestershire).

REMARKS. As revised by Donovan (1966), the holotype of this species should have come from the lower part of the Raricostatum Zone in Robin Hood's Bay, but no examples were found by Bairstow.

Genus ***PAROXYNOTICERAS*** von Pia, 1914

Paroxynoticeras salisburgense (Hauer, 1856)

1856 *Ammonites salisburgensis* Hauer: 47, pl. 13, figs 1–3 (lectotype, designated Donovan & Forsey (1973: 9), from Adneth, Austria).
1914 *Paroxynoticeras salisburgense* (Hauer); Pia: 18, 73, pl. 1, fig. 2; pl. 7, fig. 22; pl. 13, fig. 12.

RANGE. Two probable examples of this species were found in bed 474.3, Oxynotum Subzone.

Genus ***RADSTOCKICERAS*** Buckman, 1918

REMARKS. As well as the two species described below, two very large fragments of *Radstockiceras* sp. indet. were found in beds 544.4 and 544.6; both are about 350 mm diameter and one of them is septate up to about 300 mm diameter; a poorly preserved specimen was also found in bed 548.

In their revision of the holotype of *Radstockiceras buvignieri*, Donovan & Guérin-Franiatte (in Fischer, 1994: 68) said that *Radstockiceras* was a late oxynoticeratid that appeared in the Jamesoni Zone (from the evidence of Tutcher & Trueman, 1925: 598, 642) and was not present in the Raricostatum Zone (which was the supposed horizon at Radstock of Buckman's (1918: 288) holotype of the type species of *Radstockiceras*). However, the four large examples from bed 494 described below are a genuine record of *Radstockiceras* from the Macdonnelli Subzone, Raricostatum Zone, whatever may be held to be their specific determination.

PLATE 5

Fig. 1 *Radstockiceras buvignieri* (d'Orbigny). Bed 494, CA 3744, × 0.6; wholly septate.
Fig. 2 *Xipheroceras dudressieri* (d'Orbigny). Bed 446.33, C.49336; the asterisk marks the probable end of the phragmocone.
Fig. 3 *Promicroceras planicosta* (J. Sowerby). Bed 451, CA 3927.
Fig. 4 *Radstockiceras sphenonotum* (Monke). Bed 544.4, CA 3758; wholly septate.
Fig. 5 *Xipheroceras ziphus* (Zieten). Bed 451, CA 3784; wholly septate.
Fig. 6 *Cymbites laevigatus* (J. de C.Sowerby). Bed 448.1, CA3763; 6a, b, × 1; 6c, d, × 3; the last septa at the position shown are approximated and probably adult.
Fig. 7 *Microderoceras birchi* (J. Sowerby). Bed 433.3, CA 3977, × 0.5; a complete (?adult) specimen with a body chamber nearly 1½ whorls long.
Fig. 8 *Apoderoceras subtriangulare* (Young & Bird). Bed 501.1, CA 3981; a septate fragment.
Fig. 9 *Eoderoceras armatum* (J. Sowerby). **Neotype**, probably from bed 497, C.67323, × 0.75.
All figures natural size, except Figs 1, 6c, 6d, 7 and 9.

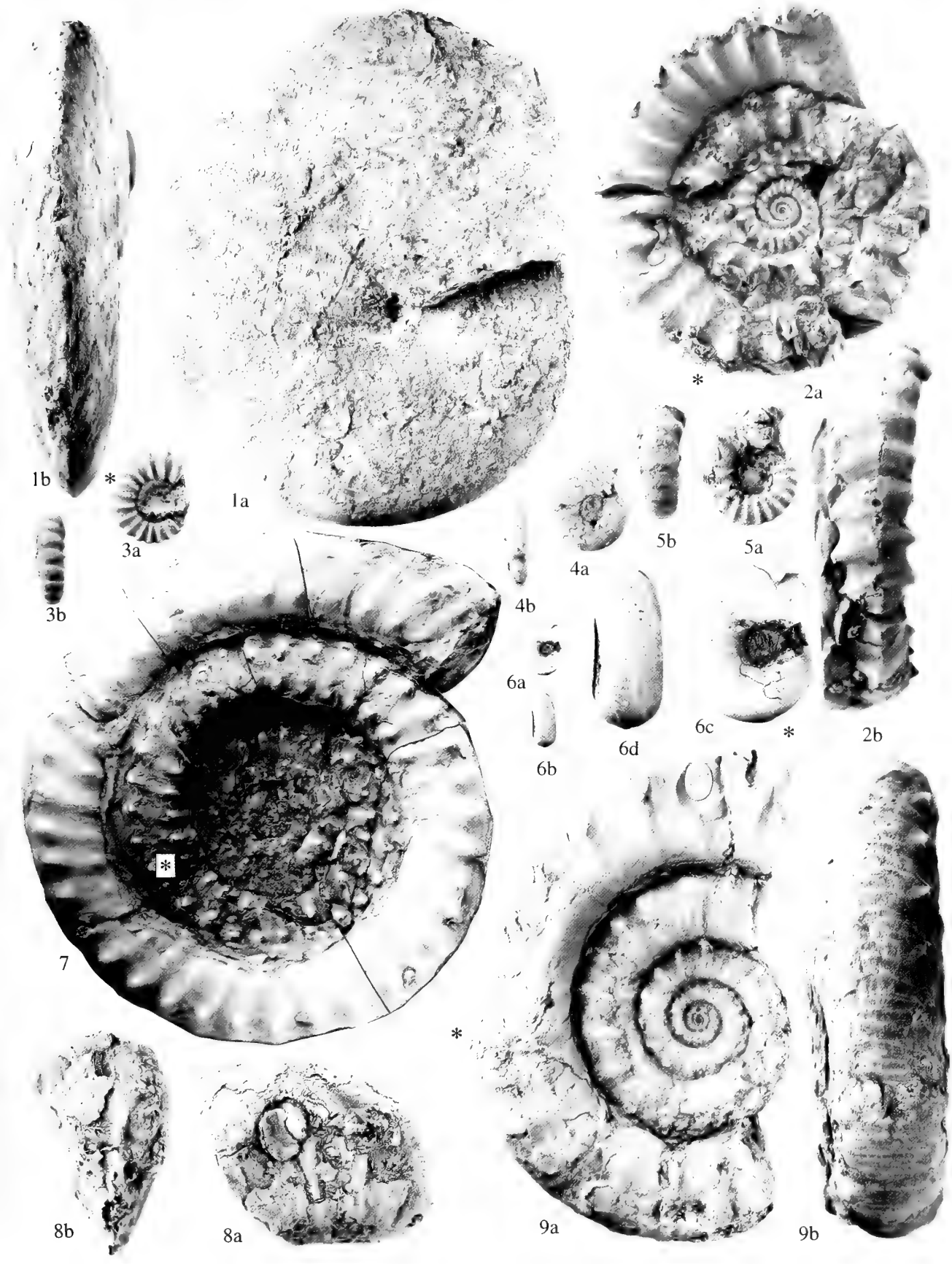
1b
1a
2a
3a
3b
4a
4b
5b
5a
6a
6b
6c
6d
2b
7
8b
8a
9a
9b

Radstockiceras buvignieri (d'Orbigny, 1844) Pl. 5, fig. 1

1844 *Ammonites buvignieri* d'Orbigny: 261, pl. 74, figs 1–3.
1855 *Ammonites complanosus* Simpson: 79, 80.
1855 *Ammonites retentus* Simpson: 84.
1920 *Retenticeras retentum* (Simpson); Buckman: pl. 166 (holotype, GSM 26401).
1962 *Metoxynoticeras complanosum* (Simpson); Howarth: 105, pl. 15, fig. 4 (holotype, WM 239, now lost).
1992 *Radstockiceras complanosum* (Simpson); Schlegelmilch: 60. pl. 54, fig. 2 (WM 239).
1994 *Radstockiceras buvignieri* (d'Orbigny); Fischer: 67, pl. 21, fig. 3 (holotype, from Breux, Meuse, France).

REMARKS. Occurs in beds 494, Macdonnelli Subzone, 505.2, Taylori Subzone, and 544.7, Brevispina Subzone; 7 specimens.

MEASUREMENTS (in mm)

	D	Wh	Wb	U
CA 3744	167.0	94.5 (0.57)	42.0 (0.25)	7.0 (0.04)
CA 3744	138.5	79.0 (0.57)	33.5 (0.24)	6.3 (0.05)

REMARKS. The four examples obtained from bed 494 are all large specimens of 145–250 mm diameter preserved in grey limestone. The best one (Pl. 5, fig. 1) is wholly septate up to its maximum size of 168 mm diameter. The single specimen from bed 505.2 is a well-preserved fragment of a part of a whorl, with whorl height 72 mm and whorl breadth 27 mm (if the whorl height is 0.57 of the diameter, then the whorl breadth is 0.21 of the diameter). One of the two pyritized specimens found in bed 544.7 is 25 mm diameter and is similar to the holotype of '*Retenticeras*' *retentum* figured by Buckman (1920: pl. 166). With their very small umbilici (4–5% of the diameter) and compressed whorl sections (whorl breadth 21–25% of the diameter), all appear to be genuine examples of *Radstockiceras buvignieri*, of which the holotype (Fischer, 1994: 67, pl. 21, fig. 3 – 178 mm diameter, 99 (0.56), 37 (0.21), 6 (0.03)) has closely similar characters. The holotype of Simpson's species *complanosum*, and the almost identical specimen BM 37960 (from Robin Hood's Bay), undoubtedly belong to the same species, but it is difficult to identify their horizons – they could have come from any of the beds 494, 505 and 544.

Radstockiceras sphenonotum (Monke, 1888) Pl. 5, fig. 4

1888 *Ammonites sphenonotus* Monke: 228, pl. 2/3, fig. 14 (holotype, from Germany).
1914 *Oxynoticeras sphenonotum* (Monke); Pia: 65, pl. 7, fig. 12.

RANGE. Beds 542.1–544.4, Polymorphus Subzone; 8 specimens.

REMARKS. The best preserved specimen occurs in bed 544.4 (Pl. 5, fig. 4).

Family **CYMBITIDAE** Buckman, 1919
Genus ***CYMBITES*** Neumayr, 1979

Cymbites laevigatus (J. de C. Sowerby, 1827) Pl. 5, fig. 6

1827 *Ammonites laevigatus* J. de C. Sowerby: 135, pl. 570, fig. 3.
1957 *Cymbites laevigatus* (J. de C. Sowerby); Donovan: 413, figs 1–8 (topotypes (the holotype is lost), from Brooki to Stellare Subzones, Dorset coast).

RANGE. Beds 446.5–464.1, top Obtusum to Simpsoni Subzones; 15 specimens; 2 specimens of *Cymbites* sp. indet. occur slightly higher in beds 464.32 and 464.33.

REMARKS. The main species present in Robin Hood's Bay is *C. laevigatus*, but a more compressed species with obsolete ribbing, eg. *C. fastigatus* Schindewolf (1961: 211, pl. 30, figs 8–10), may also be present amongst the small specimens determined as *Cymbites* sp. indet. in the Denotatus and Simpsoni Subzones.

Superfamily **EODEROCERATACEAE** Spath, 1929
Family **EODEROCERATIDAE** Spath, 1929
Genus ***MICRODEROCERAS*** Hyatt, 1871

Microderoceras scoresbyi (Simpson, 1843)

1843 *Ammonites scoresbyi* Simpson: 12.
1911 *Xipheroceras scoresbyi* (Simpson); Buckman: pls 39A, B (holotype, WM 173), C (topotype, GSM 23616), both probably from bed 441.2.

RANGE. One specimen found in bed 441.2, Birchi Subzone.

REMARKS. This single specimen differs from *M. birchi* in having higher and thicker whorls that are slightly less evolute.

Microderoceras birchi (J. Sowerby, 1820) Pl. 5, fig. 7

1820 *Ammonites birchi* J. Sowerby: 121, pl. 267.
1961 *Microderoceras birchi* (J. Sowerby); Dean *et al.*: pl. 66, fig. 3 (BM 67973, from the Dorset coast).
1973 *Microderoceras birchi* (J. Sowerby); Donovan & Forsey: 10, pl. 1, fig. 1 (lectotype, BM 43923, from the Dorset coast).

RANGE. Found only in bed 433.3, Birchi Subzone; 5 specimens.

REMARKS. The five large specimens in bed 433.3 have typical very evolute whorls, with bituberculate ribs up to the end of the largest specimen at 235 mm diameter, and considerable variation in whorl thickness. The specimen figured in Pl. 5, fig. 7 appears to have a complete body-chamber nearly 1½ whorls long, ending in an (?adult) aperture at 210 mm diameter.

Genus ***XIPHEROCERAS*** Buckman, 1911

Xipheroceras dudressieri (d'Orbigny, 1845) Pl. 5, fig. 2

1845 *Ammonites dudressieri* d'Orbigny: 325, pl. 103, figs 1, 2.
1926b *Xipheroceras dudressieri* (d'Orbigny); Spath: 172, pl. 9, fig. 6 (BM C.2235a, a typical example from the Obtusum Subzone, Dorset).
1994 *Xipheroceras dudressieri* (d'Orbigny); Fischer: 91, pl. 19, fig. 3 (from Mulhausen, France).

RANGE. One specimen in bed 446.33, Obtusum Subzone.

Xipheroceras ziphus (Zieten, 1830) Pl. 5 fig. 5

1830 *Ammonites ziphus* Zieten: 6, pl. 5, fig. 2 (holotype, BM 62590, from Heiningen, Württemberg, Germany).
1926 *Xipheroceras ziphus* (Zieten); Buckman: pl. 732 (GSM 47832, coarsely ribbed inner whorls, from the Obtusum Subzone, Dorset).
1928 *Xipheroceras revertens* Buckman: pls 772A, B (a typical large example of *X. ziphus* from the Obtusum Subzone, Dorset).

1973 *Xipheroceras planicosta* Buckman; Donovan & Forsey: 9, pl. 3, figs 1, 2 (GSM 25033, Obtusum Zone, Dorset).

RANGE. Beds 446.4–453.1, Obtusum and Stellare Subzones; 7 specimens.

REMARKS. In addition to those listed above, single examples of *Xipheroceras* sp. indet. occur in beds 446.32, 453.2 and 453.3.

Genus ***BIFERICERAS*** Buckman, 1913

Bifericeras bifer (Quenstedt, 1845)

1845 *Ammonites bifer* Quenstedt: Quenstedt: 83, pl. 4, fig. 14 (from Württemberg, Germany).
?1925*a* *Ophideroceras ziphoides* Spath: 138–40, figs 1, 2a, 2b (from low in the Oxynotum Subzone, Mill Beck Nab, Robin Hood's Bay; originally in Hull Museum, but now destroyed; see Donovan & Forsey, 1973: 16).
1957 *Bifericeras bifer* (Quenstedt); Söll: 402, pl. 19, figs 1–7 (from Württemberg, Germany).
1976 *Bifericeras bifer* (Quenstedt); Schlegelmilch: 58, pl. 25, fig. 3 ('neotype', from Württemberg, Germany).
1990 *Bifericeras bifer* (Quenstedt); Hollingworth *et al.*: 165, pl. 2, figs 1–12 (BM C.93398–93409, from the Oxynotum Subzone, Somerset).

RANGE. Bed 483.1, Oxynotum Subzone; 5 specimens. The destroyed holotype of *Ophideroceras ziphoides* Spath might have been a large example of *Bifericeras bifer*.

Bifericeras vitreum (Simpson, 1855)

1855 *Ammonites vitreus* Simpson: 46.
1924 *Microceras vitreum* (Simpson); Buckman: pl. 529 (holotype, WM 462, possibly from bed 486.2).
1976 *Bifericeras vitreum* (Simpson); Schlegelmilch: 146, pl. 25, fig. 9 (WM 462).

RANGE. One specimen in bed 486.2, Oxynotum Subzone.

Bifericeras donovani Dommergues & Meister, 1992

Pl. 8, fig. 3

1992 *Bifericeras donovani* Dommergues & Meister: 223, figs 5(8)–5(10), figs 7(1), 7(2), 7(3) (holotype), 7(4)–7(11) (all from nodules in the lower part of bed 501.1 at Wine Haven).

RANGE. Occurs only in bed 501.1, base of Taylori Subzone; 18 specimens.

Genus ***CRUCILOBICERAS*** Buckman, 1920

Crucilobiceras densinodulum Buckman, 1923

Pl. 6, fig. 1

1876 *Aegoceras obsoletum* (Simpson); Blake: 276, pl. 7, fig. 1 (BM C.17939, from bed 486.3).
1923 *Crucilobiceras densinodulum* Buckman: pl. 442 (holotype, from Lyme Regis, Dorset).
1926*b* *Crucilobiceras ornatilobatum* Spath: 176, pl. 11, fig. 1 (holotype, from Lyme Regis, Dorset).

RANGE. Beds 486.3–488, Densinodulum and Raricostatoides Subzones; 19 specimens.

REMARKS. The well-preserved *C. densinodulum* in beds 486.3 (Pl. 6, fig. 1) are unituberculate (ie. have ventro-lateral but no prominent umbilical-lateral tubercles), are moderately to finely ribbed on the inner whorls, and are characteristically much more compressed than *C. densinodum* (Oppel). Small specimens or inner whorls of *C. densinodulum* are very similar to '*Bifericeras (Hemimicroceras)' subplanicosta* (Oppel, 1856) and the relationship between the two (eg. a macroconch/microconch pair or size difference only) has yet to be resolved.

Genus ***EODEROCERAS*** Spath, 1925

Eoderoceras armatum (J. Sowerby, 1815)

Pl. 5, fig. 9; Pl. 8, fig. 2

1815 *Ammonites armatus* J. Sowerby: 215, pl. 95.
1843 *Ammonites anguiformis* Simpson: 17.
1843 *Ammonites owenensis* Simpson: 25.
1855 *Ammonites miles* Simpson: 65.
1880/82 *Aegoceras armatum* (J. Sowerby); Wright: 340 (1882), pl. 28 (1880), figs 1, 2 (SM J18222), 3–5 (SM J18223), both from beds 497–99; *non* pl. 29, =*Eoderoceras pugnax* (Buckman, 1914: 103c).
1911 *Deroceras miles* (Simpson); Buckman: pl. 44 (holotype, WM 162, from bed 498 or 499).
1912 *Deroceras anguiforme* (Simpson); Buckman: pl. 64 (holotype, WM 86, from beds 497–99).
1912 *Deroceras owenense* (Simpson); Buckman: pl. 65 (holotype, WM 476, from beds 497–99).
1926*b* *Deroceras eusculptum* Spath: 175, pl. 10, fig. 3 (BM C.26907, from Lyme Regis, Dorset).
1992 *Eoderoceras* gr. *miles* (Simpson); Dommergues & Meister: 231, figs 5(5), 5(7) (from bed 497).
2000 *Eoderoceras armatum* (J. Sowerby); Blau *et al.*: 269, figs 4 (1–7), 5 (1, 3, 5), 6 (1), 7, 8 (from NW Germany).

RANGE. Beds 494–499, Macdonnelli and Aplanatum Subzones; 62 specimens.

TYPE SPECIMEN. BM C.67323, Sowerby Collection, from Robin Hood's Bay, probably from bed 497, is here designated neotype.

MEASUREMENTS (in mm)

	D	Wh	Wb	U
BM C.67323	128.0	32.0 (0.25)	31.5 (0.25)	69.8 (0.54)
BM C.67323	102.0	27.4 (0.27)	–	53.3 (0.52)

REMARKS. Sowerby (1815: 215) stated that many examples of his species, including the specimen that he figured, which was collected by Mr. Strangewayes, came from 'the great Alum-clay formation at Whitby' (a stratigraphical term that was used by Sowerby, Young & Bird, Sedgwick and others for beds that included ones as low as the Upper Sinemurian/Lower Pliensbachian clays). Sowerby did not mention any other locality in his original description, so it is not possible to agree with Spath's (1925*a*: 137, 167) statements that 'the true *D. armatum* apparently does not occur in Yorkshire', and 'Sowerby's type is not preserved in the BM . . . and has always seemed to me to be more like a Charmouth than a Whitby specimen', nor with Donovan's (1958: 32) opinion that 'Sowerby's type specimen . . . was almost certainly obtained from the Dorset coast'. It is not permissible to transfer the type locality to Dorset on the opinion that the Yorkshire specimens are morphologically different from those in Dorset, or the belief that the pyritic preservation and frequency of decay perceived from Sowerby's figure are more reminiscent of Dorset examples. The Yorkshire specimens are not morphologically different from those in Dorset (two especially fine

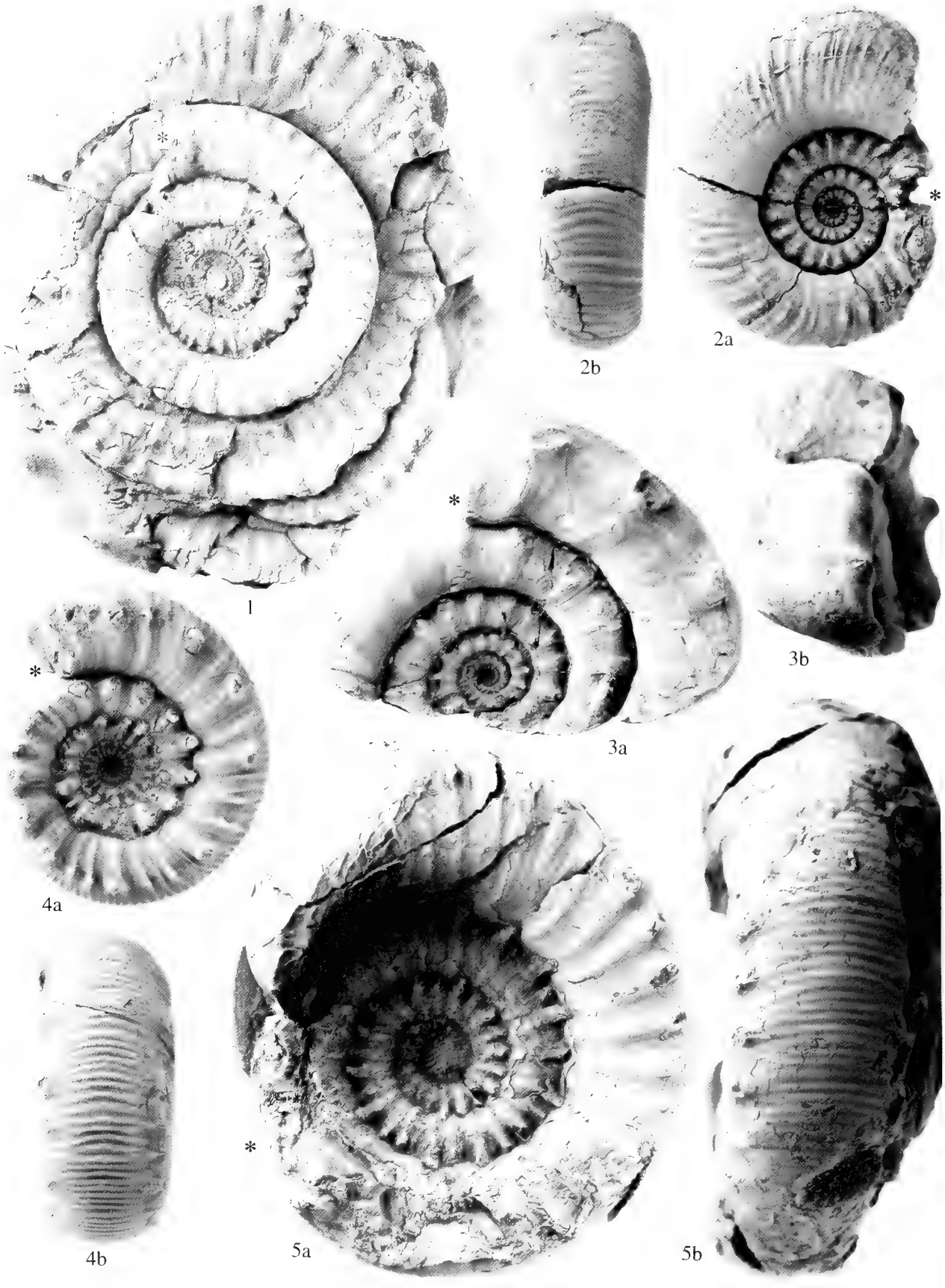
*
1
2b
2a
*
*
3a
3b
*
4a
4b
*
5a
5b

Yorkshire specimens had been figured by Wright, 1880: pl. 28), and there are many Yorkshire examples preserved in iron pyrites, especially in beds 497 and 499, which are also subject to decay, though less readily than the Dorset ones.

After Spath wrote about the species in 1925, the remaining ammonites in the Sowerbys' collections were obtained by The Natural History Museum in 1935, and amongst them is a medium to large example (BM C.67323) of *Eoderoceras armatum* from Robin Hood's Bay, which might even have been one of Sowerby's original syntypes. At 132 mm diameter it is slightly larger than Sowerby's figure of a 117 mm diameter specimen (assuming that his figure is natural size), but it does not differ in any morphological feature from that figure, and the part now missing at the beginning of the final whorl was once present, judging from remaining traces of old glue. There are some patches of pyritic preservation on the inner whorls, which fortunately do not appear to be subject to decay. As a possible original syntype, and a definite topotype, it is a close morphological match with Sowerby's figured specimen and is clearly the best neotype that can now be selected. It presents an unexpected opportunity to finally settle the identity of this frequently quoted species.

The neotype (Pl. 5, fig. 9) consists of 6–6½ septate whorls up to about 110 mm diameter, followed by a quarter of a whorl of body chamber ending at 132 mm diameter. The whorls are very evolute, the whorl section is near-circular and the umbilical wall and edge are evenly rounded. There are many fine indistinct radial ribs between stronger periodic lateral ribs that end in prominent ventro-lateral tubercles. Ribs of moderate strength cross the venter, curving gently forwards, and there are 3–5 such ribs between adjacent ventro-lateral tubercles. There are no umbilical tubercles.

In Robin Hood's Bay there are a few specimens in the Macdonnelli Subzone, then the species becomes much more common in the Aplanatum Subzone, with 44, 8 and 7 examples collected by Bairstow from beds 497, 498 and 499 respectively. The highest in bed 499 is 0.15 m below the top, and only 0.23 m below the top of the Sinemurian. Six specimens were found lower in bed 499 (0.15–0.37 m above the base), and the best preserved of them is figured in Pl. 8, fig. 2; the latter has a phragmocone ending at ca. 68 mm diameter at the position indicated on the figure, then it has a body-chamber 1.125 whorls long ending at a final aperture at ca. 125 mm diameter (the final 0.35 whorls are detached and poorly preserved, and are not figured). There is no overlap between *Eoderoceras* and *Apoderoceras*, and the lowest example of the latter genus occurs in bed 501.1 just 0.36 m above the highest *Eoderoceras*.

Eoderoceras hastatum (Young & Bird, 1828) Pl. 6, fig. 3

1828 *Ammonites hastatus* Young & Bird: 261, pl. 14, fig. 3.
1914 *Deroceras hastatum* (Young & Bird); Buckman: pls 102A, B (?holotype, WM 661, from bed 493.2).
1914 *Deroceras impavidum* Buckman: pl. 104 (holotype, WM 166; probably from bed 493.2).

RANGE. Found only in bed 493.2, Raricostatoides Subzone; 4 specimens.

REMARKS. *E. hastatum* has more depressed whorls and more widely spaced ventro-lateral tubercles than *E. armatum* which occurs at higher levels. The specimen figured here (Pl. 6, fig. 3) is very like the holotype in having striate ribs angled strongly backwards from the umbilical edge, and the almost identical holotype of Buckman's species *impavidum* probably came from the same bed 493.2.

Other species of *Eoderoceras:*

?*E. diversum* (Simpson, 1843: 13); Blake, 1876: 282, pl. 8, fig. 3 (SM J34799); Howarth, 1962: 107, pl. 15, fig. 9 (SM J34799, neotype). The neotype represents a highly evolute, serpenticone species, which might be an *Eoderoceras*, but no specimens were found by Bairstow.

Genus ***PROMICROCERAS*** Spath, 1925

Promicroceras planicosta (J. Sowerby, 1814) Pl. 5, fig. 3

1814 *Ammonites planicosta* J. Sowerby: 167, pl. 73.
1822 *Ammonites aureus* Young & Bird: 248, pl. 13, fig. 6) (type specimen lost).
?1843 *Ammonites siphuncularis* Simpson: 46.
?1912 *Androgynoceras siphunculare* (Simpson); Buckman: pl. 48 (holotype, WM 485, from beds 451–454).
1925*a* *Promicroceras planicosta* (J. Sowerby); Spath: 299–302, fig. 8f.
1925*a* *Promicroceras aureum* (Young & Bird); Spath: 301, fig. 8d (BM 17160, possibly from 451).
1926*b* *Promicroceras planicosta* (J. Sowerby); Spath: 171, pl. 9, figs 1 (BM C.26337), 7 ('neotype', BM C.2235b); both from Charmouth, Dorset.

RANGE. Beds 446.33–454.1, Obtusum and Stellare Subzones; 290 specimens.

REMARKS. The current interpretation of *Promicroceras planicosta* may not be satisfactory. After lengthy discussion, Spath (1925*a*: 299–302) selected as neotype the specimen BM C.2235b (T. Wright Colln, 1887) from Charmouth, Dorset (almost certainly from bed 85), even though Sowerby (1814: 167) said that his main specimens came from Marston Magna, and it is highly probable that the original block of specimens that he figured (Sowerby, 1814: pl. 73, now lost) came from the Marston Marble at Marston Magna, Somerset. Spath (1925*a*: 305) then created a new species, *P. marstonense*, for the form at Marston Magna, using as holotype a specimen (BM 43914b) from Sowerby's syntypes of *P. planicosta*. The selection of a Charmouth specimen as neotype of *P. planicosta* was unfortunate, and may be invalid because there were Marston Magna specimens available amongst the original syntypes. The designation of a Marston Magna specimen as neotype (or lectotype) would have been much more in accordance with Sowerby's original concept of his species. In any case, the forms of *Promicroceras* at Charmouth and Marston Magna appear to be very close and the two names are probably

PLATE 6

Fig. 1 *Crucilobiceras densinodulum* Buckman. Bed 486.3, CA 3828; the body chamber is exactly one whorl long.

Fig. 2 *Apoderoceras aculeatum* (Simpson). Bed 526.5, CA 4031.

Fig. 3 *Eoderoceras hastatum* (Young & Bird). Bed 493.2, CA 3895, × 0.6; suture-lines that probably mark the end of the phragmocone are visible exactly one whorl before the aperture.

Figs 4, 5 *Apoderoceras subtriangulare* (Young & Bird). **4,** bed 520.7, CA 4018; probably a complete adult microconch, with a body chamber exactly one whorl long and a slightly contracted final aperture. **5,** bed 502, CA3990; the asterisk marks the probable end of the phragmocone.

All figures natural size, except Fig. 3.

synonyms. Two other names that are probably also synonyms of *P. planicosta* are *P. perplanicosta* (Spath, 1925*a*: 269; 1926*b*, 172, pl. 9, fig. 2) and *P. precompressum* Spath (1926*b*, 173, pl. 9, fig. 5), both from beds 83 or 85 at Charmouth.

Promicroceras capricornoides (Quenstedt, 1883)

1883 *Ammonites capricornoides* Quenstedt: 129, pl. 17, fig. 11 (from Württemberg, Germany).
1926*b* *Promicroceras capricornoides* (Quenstedt); Spath: 172, pl. 9, fig. 3 (from the Turneri Zone, Charmouth, Dorset).

RANGE. Beds 436–446.32, Birchi and basal Obtusum Subzones; 39 specimens.

REMARKS. *P. capricornoides* is slightly more involute, has a more rapidly increasing whorl height and slightly fewer ribs than *P. planicosta*.

Family **COELOCERATIDAE** Haug, 1910
Genus ***APODEROCERAS*** Buckman, 1921

REMARKS. Identification of the horizons from which the Yorkshire type and figured specimens were obtained is especially uncertain in *Apoderoceras*. The originals of *A. subtriangulare* and its two synonyms (*A. hamiltoni* and *A. spicatum*) could have come from any of beds 502, 504–07 509, 520 and 522, all of which contain many large fragments of outer whorls as well as a few more complete specimens like the original of *A. 'hamiltoni'*. Similarly, the originals of *A. aculeatum* and its three synonyms (*A. decussatum, A. mutatum* and *A. leckenbyi*) could have come from any of beds 523–526.

Apoderoceras subtriangulare (Young & Bird, 1822)
Pl. 5, fig. 8; Pl. 6, figs 4, 5

1822 *Ammonites subtriangularis* Young & Bird: 250, pl. 12, fig. 4.
1843 *Ammonites hamiltoni* Simpson: 27.
1843 *Ammonites spicatus* Simpson: 28.
1913 *Deroceras subtriangulare* (Young & Bird); Buckman: pl. 71 (holotype, WM 927).
1914 *Deroceras spicatum* (Simpson); Buckman: pl. 103 (holotype, WM 920).
1924 *Apoderoceras hamiltoni* (Simpson); Buckman: pls 530A, B (both are the holotype, WM 165).
1992 *Apoderoceras* sp. indet.; Dommergues & Meister: 232, fig. 5(6) (from nodules at the middle of bed 501.1, Wine Haven).

RANGE. Beds 501.1–522.1, Taylori Subzone; 41 specimens.

REMARKS. The lowest examples of *Apoderoceras* are three specimens in bed 501.1. Two are very small cadicones, one large enough to have ventro-lateral tubercles, while the third (Pl. 5, fig. 8) is part of one side of a whorl at a whorl height of 35 mm that has obscure radial ribs and striae and pointed ventro-lateral tubercles. It is identical with *A. subtriangulare* at a similar size, and is important for fixing the base of the Taylori Subzone at this level.

Large *A. subtriangulare* up to 350 mm diameter, with large ventro-lateral spines and broad flat venters occur in bed 502 and at many more horizons up to bed 522.1. Most are fragments of outer whorls with nothing to link them to the few inner whorls, but an example in bed 507.1 (CA 4006) has both inner and outer whorls, and proves that small inner whorls like those in Pl. 6, fig. 5 and the very well-preserved specimen of Pl. 6, fig. 4 develop into the massive outer whorls with broad flat venters and very large ventro-lateral spines that are characteristic of *A. subtriangulare*. The holotype of *A. subtriangulare* (Buckman, 1913: pl. 71) is a fragment of such a large outer whorl. Of the two Simpson species that are placed in synonymy, the holotype of *A. spicatum* (Buckman, 1914: pl. 103) is a very similar fragment of a large outer whorl, though the broad flat venter is not shown because only one side is preserved, while the holotype of *A. hamiltoni* (Buckman, 1924: pl. 530) is one of the few specimens that show inner and outer whorls preserved in the same individual. [Note the remarkable resemblance of Pl. 6, fig. 4 to a depressed-whorled species of the Toarcian genus *Peronoceras*, eg. *P. perarmatum* (Young & Bird), Howarth, 1978: pl. 4, fig. 7; the latter differs only in having well-defined ribs on the side of the whorl, compared with the poor, irregular or striate ribs on the inner whorls of *Apoderoceras subtriangulare*].

Apoderoceras aculeatum (Simpson, 1843)
Pl. 6, fig. 2: Pl. 7, fig. 1

?1843 *Ammonites marshallani* Simpson: 24.
1843 *Ammonites decussatus* Simpson: 25.
1843 *Ammonites aculeatus* Simpson: 27.
1855 *Ammonites mutatus* Simpson: 63.
1876 *Aegoceras aculeatum* (Simpson); Blake: 278, pl. 7, fig. 4 (BM C.17878).
1880/82 *Aegoceras leckenbyi* Wright: 344 (1882), pl. 30 (1880), figs 1–3 (lectotype of *leckenbyi* (designated Howarth, 1962: 109), SM J18224), figs 4–7 (paralectotype of *leckenbyi*, also holotype of *decussatum*, SM J18225).
1913 *Deroceras aculeatum* (Simpson); Buckman: pls 72A–C (paratype, WM 177; the holotype is lost).
1914 *Deroceras mutatum* (Simpson); Buckman: pl. 105 (holotype, GSM 26406).
1962 *Apoderoceras decussatum* (Simpson); Howarth: 109, pl. 16, fig 1 (holotype, SM J18225).
?1962 *Apoderoceras marshallani* (Simpson); Howarth: 109, pl. 15, fig. 5 (holotype, WM 468); the holotype is only 16 mm diameter, and although it could be a very small example of *A. aculeatum*, Simpson's species is not accurately determinable.

RANGE. Beds 523–526.6, Taylori Subzone; 15 specimens. There are also single specimens of *Apoderoceras* sp. indet. in beds 526.7 and 529.

REMARKS. Specimens from beds 523–526 differ from *A. subtriangulare* in beds 501–522 in having the outer whorls more rounded, with evenly arched whorl sides and venter, no definite ventro-lateral angle, and smaller ventro-lateral tubercles on the inner whorls. These stratigraphically higher specimens belong to the species *A. aculeatum* (Simpson), of *A. decussatum* and *A. leckenbyi* are synonyms (*Ammonites aculeatum* and *A. decussatum* are both of Simpson, 1843, and therefore have equal priority; the name for the species was selected by Blake (1876: 278), who, as 'First Reviser' (ICZN Code, art. 24.2), chose *aculeatum* as the name for the species). *A. marshallani*, another Simpson name of the same date (1843), is probably also a synonym, but the holotype is too small to be definitely identifiable, and *A. mutatum* (Simpson, 1855) and *A. leckenbyi* (Wright, 1880) are two more synonyms, judging from their well-preserved type specimens.

The specimen figured in Pl. 7, fig. 1 is a fairly large, wholly septate example of *A. aculeatum* and Pl. 6, fig. 2 has well-preserved inner whorls showing much smaller ventro-lateral tubercles than in *A. subtriangulare* (cf. inner whorls of Pl. 6, fig. 5).

Other species of *Apoderoceras:*

1. ?*Apoderoceras sinuatum* (Simpson, 1855: 62); Buckman, 1914:

pl. 94 (holotype, WM 160). No specimens resembling this holotype were found by Bairstow.

2. ?*A. armiger* (Simpson, 1855: 66 (*non Ammonites armiger* J. de C. Sowerby, 1840)); Howarth, 1962: 107. From Simpson's description this was probably an *Apoderoceras*, but the type specimen is lost and the species is not identifiable.

Genus ***HYPERDEROCERAS*** Spath, 1926

REMARKS. Bairstow found only one poorly preserved example (CA 4053) of *Hyperderoceras* sp. indet. in bed 540.1 (Polymorphus Subzone). This shows parts of inner whorls at 15–50 mm diameter that have strong ribs and ventro-lateral tubercles, followed by septate fragments of larger whorls with a quadrate whorl section, where both whorl height and breadth are 50–60 mm, ie. they are not compressed like *Epideroceras* at this size. Any of the following four Simpson species might have come from this horizon, but the Bairstow specimen is not specifically identifiable:

1. *Hyperderoceras mamillatum* (Simpson, 1843: 28 (*non Ammonites mamillatus* Schlotheim, 1813)); Howarth, 1962: 108, pl. 15, fig. 6 (neotype (designated by Howarth, 1962: 108), WM 2102).
2. *H. validum* (Simpson, 1855: 39); Blake, 1876: 278, pl. 7, fig. 3 (SM – ?holotype); Buckman, 1913: pl. 83 (holotype, SM J3275).
3. *H. retusum* (Simpson, 1855: 62); Buckman, 1913: pl. 82 (holotype, WM 184).
4. *H. nativum* (Simpson, 1855: 68); Buckman, 1913: pl. 84 (holotype, WM 931).

Family **PHRICODOCERATIDAE** Spath, 1938
Genus ***PHRICODOCERAS*** Hyatt, 1900

REMARKS. Species of *Phricodoceras* show a considerable amount of variation in rib-density, in the development of lateral tubercles, and in overall size of the tubercles. The specimens from Robin Hood's Bay suggest that a sparsely-ribbed species, here identified as *P. taylori*, occurs in the lower half of the Taylori Subzone, while a more densely-ribbed species, *P. cornutum*, occurs in the upper half of the subzone. Tubercle strength depends to some extent on preservation, and in any species tubercles are more prominent when the shell is preserved, compared with their appearance on internal moulds. The Robin Hood's Bay specimens are identified below mainly according to their rib-density, but tubercles are accorded some significance when they are especially large.

Phricodoceras taylori (J. de C. Sowerby, 1826)

1826 *Ammonites taylori* J. de C. Sowerby: 23, pl. 514, fig. 1 (holotype, lost (originally in Norwich Museum), from Glacial Drift, Happisburgh, north Norfolk, perhaps derived from the Yorkshire coast).
1855 *Ammonites quadricornutus* Simpson: 71.
1884 *Ammonites quadricornutus* Simpson: 106.
1911 *Phricodoceras quadricornutum* (Simpson); Buckman: pl. 33 (holotype, WM 495; possibly from beds 501–517, lower than *P. cornutum*).

RANGE: Beds 501.3–524.1, Taylori Subzone; 8 specimens.

REMARKS. *P. taylori* occurs in the lower and middle parts of the Taylori Subzone at Robin Hood's Bay, where the poorly preserved specimens have the widely spaced ribs (12–13 per whorl at 50 mm diameter) that are typical of the species. The holotype of *Ammonites quadricornutus* has the same rib-density, and the strength of the tubercles is similar to that shown in Sowerby's figure of *taylori*, even after allowances are made for slightly different modes of preservation.

Phricodoceras cornutum (Simpson, 1843) Pl. 7, fig. 2

1843 *Ammonites cornutus* Simpson: 31.
1855 *Ammonites cornutus* Simpson: 71.
1884 *Ammonites taylori* J de C. Sowerby; Simpson: 105 (including *Ammonites cornutus* which Simpson now considered to be a synonym).
1911 *Phricodoceras cornutum* (Simpson); Buckman: pl. 32 (holotype, WM 185).
1976 *Phricodoceras cornutum* (Simpson); Schlegelmilch: 152, pl. 28, fig. 1 (WM 185).

RANGE: Beds 524.3–530.2, Taylori Subzone; 8 specimens.

REMARKS. *P. cornutum* occurs higher in the Taylori Subzone than *P. taylori*, and differs from the latter in having more ribs (17–20 per whorl at 50 mm diameter) and smaller tubercles.

Phricodoceras nodosum (Quenstedt, 1846)

1846 *Ammonites taylori nodosus* Quenstedt: 136, pl. 9, fig. 21 (holotype, from Württemberg, Germany) (*non Ammonites nodosus*, Bruguière, 1789).
1961 *Phricodoceras* aff. *taylori* (J. de C. Sowerby); Dean *et al.*: pl. 68, fig. 5 (BM C.17981, probably from bed 520).
1980 *Phricodoceras nodosum* (Quenstedt); Schlatter: 78, pl. 6, figs 5, 6 (from Württemberg, Germany).

RANGE. A single specimen in bed 520.5, Taylori Subzone.

REMARKS. All the specimens listed above have the same rib-density as *P. taylori*, but they have much more prominent tubercles. Even on the internal mould the tubercles appear to be genuinely much larger, as can be seen on the specimen figured by Dean *et al* (1961), which has both shell and internal mould preserved on different portions of the shell.

Genus ***EPIDEROCERAS*** Spath, 1923

REMARKS. The only examples of *Epideroceras* found by Bairstow were parts of two specimens in bed 542.4, Polymorphus Subzone. They are fragments of large septate whorls, with compressed whorl sections at 45–60 mm whorl height, a rounded venter, and radial ribs, but no tubercles. They are too fragmentary and poorly preserved to be specifically identified. The following Simpson species might have come from bed 542.4:

Epideroceras sociale (Simpson, 1855: 39); Blake, 1876: 278, pl. 7, fig. 6 (SM collection); Buckman, 1914: pl. 95 (holotype, WM 68).

Family **POLYMORPHITIDAE** Haug, 1887
Genus ***GEMMELLAROCERAS*** Hyatt, 1900

SYNONYMS. *Tubellites* Buckman, 1924; *Leptonotoceras* Spath, 1925.

REMARKS. *Gemmellaroceras* has been divided in two subgenera: *Gemmellaroceras* s.s., in the Jamesoni Zone and younger beds, in which the first lateral lobe is trifid, and an earlier Raricostatum to basal Jamesoni Zone subgenus *G. (Leptonotoceras)*, in which the first lateral lobes are bifid (Dubar & Mouterde, 1961: 237; Geczy, 1976: 73–75). In Robin Hood's Bay *Gemmellaroceras* ranges from the top part of the Macdonnelli Subzone up to near the top of the Taylori Subzone. Most specimens belong to the very small species *G. tubellum* (Simpson) (the type species of *Tubellites* Buckman, 1924), and those specimens that

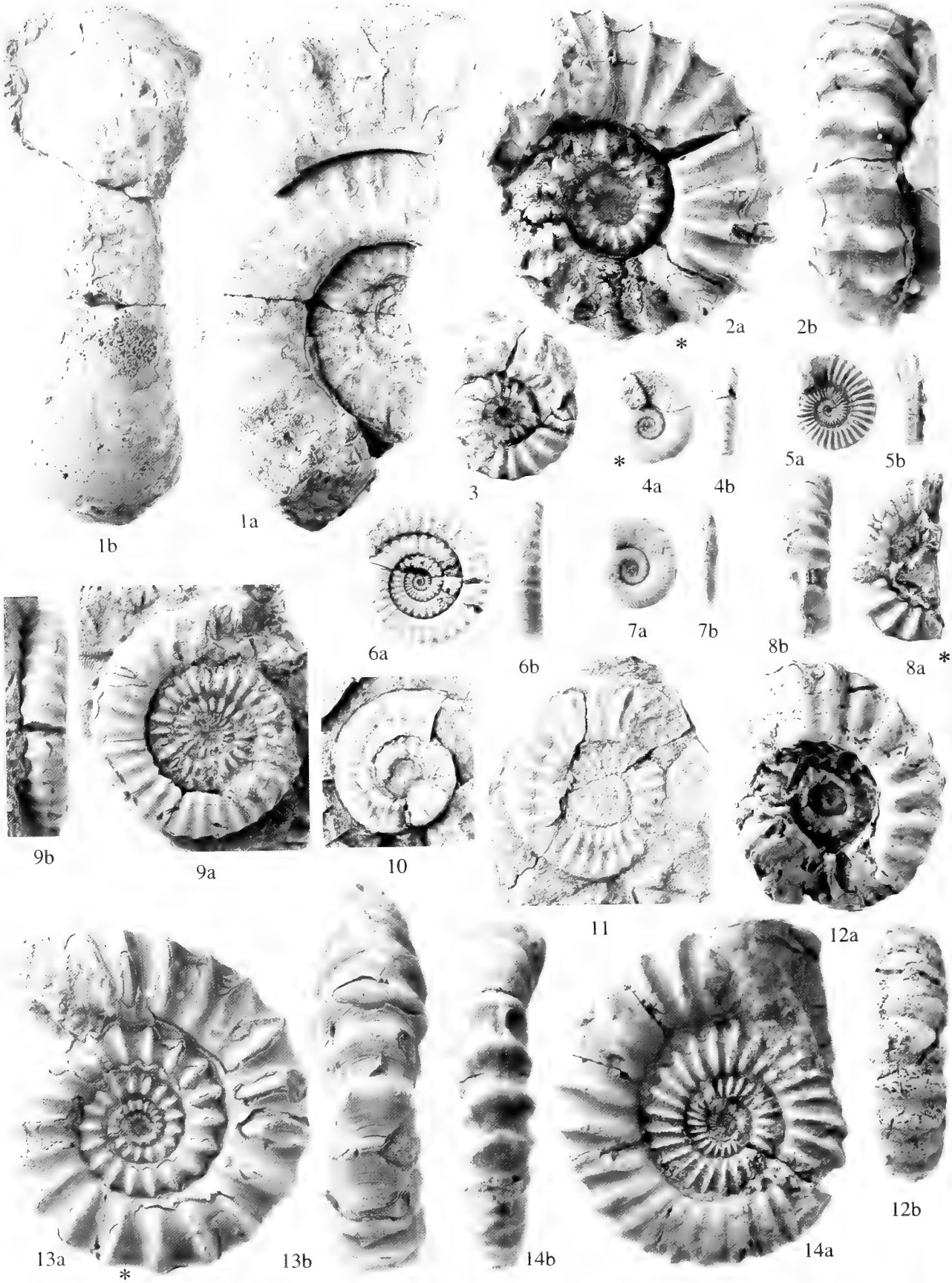
1b
1a
2a
*
2b
3
*
4a
4b
5a
5b
6a
6b
7a
7b
8b
8a
*
9b
9a
10
11
12a
12b
13a
*
13b
14b
14a

are large enough to have divided first lateral lobes appear to have the bifid lobes of *Leptonotoceras*. However, many of the specimens are very small and the largest (in bed 501.2) is only 19 mm diameter. In the top part of the Taylori Subzone at Robin Hood's Bay the much larger species *Gemmellaroceras rutilans* has the trifid first lateral lobes of *Gemmellaroceras* s.s. Whether this division into subgenera is real, or is a function of the size to which species grow and therefore the complexity attained by their suture-lines, has still to be resolved.

Gemmellaroceras tubellum (Simpson, 1855)

1855 *Ammonites tubellus* Simpson: 42.
1876 *Aegoceras tubellum* (Simpson); Blake: 279, pl. 5, fig. 7.
1924 *Tubellites tubellus* (Simpson); Buckman: pl. 491 (holotype, WM 981; ?probably from bed 497 or 498).

RANGE. Beds 495.7–505.1, Macdonnelli to Taylori Subzones; 104 specimens.

RANGE. After its first appearance in the top bed of the Macdonnelli Subzone, *G. tubellum* becomes much more common in the Aplanatum and bottom of the Taylori Subzones.

Gemmellaroceras rutilans (Simpson, 1843) Pl. 7, fig. 4

1843 *Ammonites rutilans* Simpson: 45.
1962 *Polymorphites rutilans* (Simpson); Howarth: 110, pl. 15, figs 7 (neotype (designated Howarth, 1962: 110), WM 95), 8 (WM 94); both probably from bed 526.1 or 530.1.

RANGE. Beds 526.1 and 530.1, Taylori Subzone; 4 specimens.

REMARKS. *G. peregrinum* (Haug, 1887: 114, pl. 4, fig. 5) is a very similar (?or identical) species that occurs in the upper part of the Taylori Subzone in Dorset (bed 108), where specimens attain large sizes of up to 90 mm diameter.

Genus ***POLYMORPHITES*** Haug, 1887

Polymorphites caprarius (Quenstedt, 1856) Pl. 7, fig. 9

1856 *Ammonites caprarius* Quenstedt: 131, pl. 16, fig. 1 (holotype, from Balingen, Württemberg, Germany; BM C.55358 is a cast of this specimen).
1885 *Ammonites caprarius* Quenstedt: Quenstedt: 244, pl. 30, figs 40, 41 (holotype refigured).
1976 *Platypleuroceras caprarium* (Quenstedt); Schlegelmilch: 63, pl. 29, fig. 5 (holotype refigured).
1980 *Polymorphites caprarius* (Quenstedt); Schlatter: 92.

RANGE. Beds 538–542.5, Polymorphus Subzone; 87 specimens.

REMARKS. There seems to be no doubt that Quenstedt's figure of 1885 (pl. 30, fig. 41) is a drawing of the same specimen that he figured in 1856 (pl. 16, fig. 1). This specimen (Geological Institute, Tübingen University, Ce 5/30/41) was figured again by Schlegelmilch (1976); it is the holotype. Schlegelmilch's (1976: 63) designation of this specimen as neotype was not necessary. One of Bairstow's better preserved specimens from bed 539 is figured in Pl. 7, fig. 9.

Polymorphites trivialis (Simpson, 1843) Pl. 7, fig. 7

1843 *Ammonites trivialis* Simpson: 10.
1876 *Amaltheus trivialis* (Simpson); Blake: 292, pl. 5, figs 6a (BM C.17891), 6b–d.
1912 *Polymorphites trivialis* (Simpson); Buckman: pl. 53, figs 1, 1a, 1b (the lectotype, WM 105, now lost), figs 2, 3 (paralectotypes).

RANGE. Beds 542.4–546.3, Polymorphus and Brevispina Subzones; 84 specimens.

REMARKS. Many examples of *P. trivialis* are found in beds 544.35–544.9 at the top of the Polymorphus and bottom of the Brevispina Subzones, and it is highly probable that the type specimens came from 544.35, 544.4, 544.5 or 544.9.

Polymorphites bronni (Roemer, 1836) Pl. 7, fig. 5

1836 *Ammonites bronni* Roemer: 181, pl. 12, fig. 8 (holotype, from north Germany).
1884 *Ammonites bronni* Roemer; Quenstedt: 245, pl. 30, figs 44, 46, 48 (from Württemberg, Germany).
1976 *Polymorphites bronni* (Quenstedt); Schlegelmilch: 62, pl. 28, fig. 8 (original of Quenstedt, 1885: pl. 30, fig. 48).
1980 *Polymorphites bronni* (Quenstedt); Schlatter: 82, pl. 7, fig. 1, pl. 11, fig. 5 (from Württemberg, Germany).

RANGE. Beds 554–560.3, Jamesoni Subzone; 36 specimens.

REMARKS. Occurs in the upper half of the Jamesoni Subzone, and it differs from *P. trivialis* and *P. polymorphus* in having consistently stronger ribbing, small ventro-lateral tubercles and a mid-ventral keel. The Robin Hood's Bay specimens have been identified from Schlatter's (1980: 82) interpretation of the species.

Polymorphites polymorphus (Quenstedt, 1845) Pl. 7, fig. 3

1845 *Ammonites polymorphus quadratus* Quenstedt: 87, pl. 4, fig. 9 (lectotype, from Germany, designated by Donovan & Forsey, 1973: 12).
1961 *Polymorphites polymorphus* (Quenstedt); Dean *et al.*: pl. 68, fig. 4 (from Gloucestershire).

PLATE 7

Fig. 1 *Apoderoceras aculeatum* (Simpson). Bed 524.3, CA4022, × 0.5; wholly septate up to the aperture at ca. 210 mm diameter.
Fig. 2 *Phricodoceras cornutum* (Simpson). Bed 525, CA 4070.
Fig. 3 *Polymorphites polymorphus* (Quenstedt). Bed 555, CA 4317.
Fig. 4 *Gemmellaroceras rutilans* (Simpson). Bed 526.1, CA 4178; approximated adult septa occur at the position marked three-quarters of a whorl before the aperture.
Fig. 5 *Polymorphites bronni* (Roemer). Bed 560.3 (below the top 0.08 m), CA 4226; wholly septate.
Fig. 6 *Platypleuroceras aureum* (Simpson). Bed 546.2, CA 4480; the body chamber appears to be exactly one whorl long.
Fig. 7 *Polymorphites trivialis* (Simpson). Bed 544.35, CA 4326; wholly septate.
Fig. 8 *Aegoceras (A.) maculatum* (Young & Bird) var. *atavum* Spath. Bed 583.2, C.38874.
Fig. 9 *Polymorphites caprarius* (Quenstedt). Bed 539, CA 4237; a complete microconch, with a body chamber about two-thirds of a whorl long.
Figs 10, 11 *Tropidoceras futtereri* Spath. **10,** bed 560.3 (in the top 0.08 m), CA 4544. **11,** bed 568, CA 4545.
Figs 12, 13 *Aegoceras (A.) maculatum* (Young & Bird). **12,** bed 581, C.41307. **13,** bed 590.61, C. 38883.
Fig. 14 *Aegoceras (Oistoceras) sinuosiforme* Spath. Bed 598.1, C.38930.
All figures natural size, except Fig. 1.

1973 *Polymorphites polymorphus* (Quenstedt); Donovan & Forsey: 11, 12.
1980 *Polymorphites polymorphus* (Quenstedt); Schlatter: 84, pl. 7, fig. 2 (from Württemberg, Germany).

RANGE. Found only in bed 555, Jamesoni Subzone; 2 specimens.

REMARKS. Although the lectotype of *P. polymorphus*, as validly designated by Donovan & Forsey (1973: 12), is probably lost, Schlegelmilch's (1976: 61) designation of a 'neotype' is not valid because it is radically different in morphology from the lost lectotype. That specimen (Schlegelmilch, 1976: pl. 28, fig. 3) is the original of Quenstedt, 1885, pl. 30, fig. 9, and represents a round-whorled, striate species of *Polymorphites*, which was described as *P. lineatus* (Quenstedt, 1845) by Schlatter (1980: 86).

The relationship between *P. trivialis* (Simpson, 1843) and *P. polymorphus* (Quenstedt, 1845) remains to be clarified: both have wide ranges of morphological variation, and they may be synonyms. *P. trivialis* is abundant in the lower half of the Brevispina Subzone, but two examples of *P. polymorphus* (Pl. 7, fig. 3) that are identical with the specimen figured by Dean *et al.* (1961: pl. 68, fig. 4) and Schlatter (1980: pl. 7, fig. 2) were found in bed 555 in the Jamesoni Subzone. They have broad whorls, widely spaced ribs and ventro-lateral tubercles that are characteristic of the most strongly ornamented forms of both species.

Genus ***PLATYPLEUROCERAS*** Hyatt, 1867

Platypleuroceras brevispina (J. de C. Sowerby, 1827)

1827 *Ammonites brevispina* J. de C. Sowerby: 106, pl. 556, fig. 1.
1843 *Ammonites ripleyi* Simpson: 11.
1880/82 *Aegoceras brevispina* (J. de C. Sowerby); Wright: 361 (1882), pl. 32, fig. 2, 3 (1880) (holotype, BM 43915, from Pabba, Inner Hebrides, Scotland).
1909 *Uptonia ripleyi* (Simpson); Buckman: pl. 2 (holotype, WM 106, probably from beds 544.7–546.4).
1961 *Platypleuroceras brevispina* (J. de C. Sowerby); Dean *et al.*: pl. 69, fig. 1 (holotype).

RANGE. From beds 544.6–550, Brevispina and Jamesoni Subzones; 83 specimens.

Platypleuroceras obsoleta (Simpson, 1843)

1843 *Ammonites obsoletus* Simpson: 23.
1882 *Aegoceras brevispina* (J. de C. Sowerby); Wright: 361, pl. 50, figs 13, 14 (BM C.3126).
1914 *Uptonia obsoleta* (Simpson); Buckman: pl. 92 (holotype, WM 157).

RANGE. A single specimen in bed 544.7, Brevispina Subzone.

REMARKS. This is a single poorly preserved specimen with many ribs and ventro-lateral tubercles which is not good enough to elucidate the horizon of Simpson's larger and better preserved holotype.

Platypleuroceras aureum (Simpson, 1855) Pl. 7, fig. 6

1855 *Ammonites aureus* Simpson: 44 (*non Ammonites aureus* Young & Bird, 1822).
?1855 *Ammonites tenuispina* Simpson: 69 (the holotype is lost – see Howarth, 1962: 111).
1909 *Platypleuroceras aureum* (Simpson); Buckman: pl. 3 (holotype, WM 107, from bed 546.2 or 546.5).

RANGE. Beds 546.1–546.5, Brevispina Subzone; 23 specimens.

REMARKS. *P. aureum* is a more evolute species than *P. brevispina*, and is bituberculate (ie. both umbilical and ventro-lateral tubercles are well developed). A small, typical specimen is figured in Pl. 7, fig. 6.

Genus ***UPTONIA*** Buckman, 1897

Uptonia jamesoni (J. de C. Sowerby, 1827)

1827 *Ammonites jamesoni* J. de C. Sowerby: 105, pl. 555, fig. 1.
?1855 *Ammonites ignotus* Simpson, 1855: 61.
?1910 *Uptonia ignota* (Simpson); Buckman: pl. 21 (holotype, WM 159).
1973 *Uptonia jamesoni* (J. de C. Sowerby); Donovan & Forsey: 12, pl. 4, fig. 3 (neotype, BM C.40426, designated by Donovan & Forsey, 1973: 12, from Pabba, Inner Hebrides, Scotland).

RANGE. Beds 550–560.3, Jamesoni Subzone; 23 specimens.

REMARKS. Many of the 23 specimens in the Jamesoni Subzone are typical examples of the species, but they are mostly fragmentary, and none are preserved well enough to be figured.

Uptonia lata (Quenstedt, 1845)

1845 *Ammonites jamesoni* J. de Sowerby, var. *latus* Quenstedt: 88, pl. 4, fig. 1 (holotype, from Württemberg, Germany).
1980 *Uptonia lata* (Quenstedt); Schlatter: 113, pl. 12, figs 3, 4 (from Württemberg, Germany).

RANGE. Beds 558 and 560.3, Jamesoni Subzone; 6 specimens.

REMARKS. A more involute species than *U. jamesoni*, with much finer ribbing; identified according to Schlatter's (1980: 113) interpretation of Quenstedt's species.

Genus ***TROPIDOCERAS*** Hyatt, 1867

Tropidoceras futtereri Spath, 1923 Pl. 7, figs 10, 11

1923*a* *Tropidoceras futtereri* Spath: 8.
1928 *Tropidoceras futtereri* Spath; Spath: 228, pl. 16, fig. 8 (holotype, BM C.23687, from bed 118b, Charmouth, Dorset).

RANGE. Single specimens in beds 560.3 (top) and 568 (base), Masseanum Subzone.

Tropidoceras masseanum (d'Orbigny), var. *rotundum* (Futterer, 1893)

1893 *Cycloceras masseanum* (d'Orbigny), var. *rotundum* Futterer: 330, pl. 12, figs 3, 4 (holotype, from Württemberg, Germany).
1980 *Tropidoceras masseanum* (d'Orbigny) *rotundum* (Futterer); Schlatter: 138, pl. 19, fig. 4, pl. 20, figs 1, 2 (from Württemberg, Germany).

RANGE. Found only at the boundary of beds 567 and 568, Masseanum Subzone; 11 specimens.

Genus ***PARINODICERAS*** Trueman, 1918

REMARKS. Although considered by Spath (1938: 81) to be a subgenus of *Liparoceras*, *Parinodiceras* (including its synonym *Platynoticeras*) is now thought to have been derived from *Polymorphites* and is therefore placed in the family Polymorphitidae (Donovan, 1981: 111, 138).

Parinodiceras parinodum (Quenstedt, 1884)

1884 *Ammonites striatus parinodus* Quenstedt: 225, pl. 28, fig. 16.
1938 *Liparoceras (Parinodiceras) parinodum* (Quenstedt); Spath: 82, pl. 6, fig. 5 (from Radstock, Somerset), pl. 25, figs 1, 4, 5 (all from Württemberg, Germany).
1976 *Liparoceras (Parinodiceras) parinodum* (Quenstedt); Schlegelmilch: 67, pl. 32, fig. 3 (lectotype, from Ofterdingen, Württemberg, Germany).

RANGE. Beds 546.3, 548 and 554, Brevispina and Jamesoni Subzones; 3 specimens.

Family **LIPAROCERATIDAE** Hyatt, 1867
Genus ***LIPAROCERAS*** Hyatt, 1867
Subgenus ***LIPAROCERAS*** Hyatt, 1867

Liparoceras (L.) cheltiense (Murchison, 1834)

1834 *Ammonites cheltiensis* Murchison: 20, fig. 1.
1904 *Liparoceras cheltiense* (Murchison); Buckman: pls 67, 67a (holotype, BM 74955a, from Gloucestershire).
1938 *Liparoceras cheltiense* (Murchison); Spath: 46.

RANGE. Two specimens in bed 562, Masseanum Subzone.

Liparoceras (L.) heptangulare (Young & Bird, 1828)

1828 *Ammonites heptangularis* Young & Bird: 263, pl. 14, fig. 1.
1914 *Liparoceras heptangulare* (Young & Bird); Buckman: pls 108A–C (holotype, WM 170, probably from bed 575).
1938 *Liparoceras heptangulare* (Young & Bird); Spath: 59. pl. 7, fig. 1 (BM C.2685, possibly from bed 575).

RANGE. Single specimens in beds 571, 575 and 577, Valdani Subzone; the best preserved is in bed 577.

Liparoceras (L.)* cf. *naptonense Spath, 1938

1938 *Liparoceras naptonense* Spath: 63, pl. 6, fig. 1, pl. 9, fig. 7, pl. 10, fig. 6 (holotype, BM C.12638, from Napton, Warwickshire), pl. 14, fig. 6, pl. 16, fig. 10 (all from Warwickshire or Leicestershire).

RANGE. Single specimens in beds 580 and 582.3, Luridum and Maculatum subzones.

Liparoceras (L.) divaricosta (Trueman, 1919) Pl. 8, fig. 1

1919 *Androgynoceras divaricosta* Trueman: 278, pl. 22, fig. 1 (holotype, BM C.38326, from Lincolnshire).
1938 *Liparoceras divaricosta* (Trueman); Spath: 68, pl. 5, fig. 1 (holotype).

RANGE. A single specimen in bed 596.3, Figulinum Subzone.

Genus ***AEGOCERAS*** Waagen, 1869
Subgenus ***AEGOCERAS*** Waagen, 1869

Aegoceras (A.) maculatum (Young & Bird, 1822) Pl. 7, figs 12, 13

1822 *Ammonites maculatus* Young & Bird: 248, pl. 14, fig. 12.
1828 *Ammonites maculatus* Young & Bird; Young & Bird: 259, pl. 14, fig. 9.
1829 *Ammonites arcigerens* Phillips: 163, pl. 13, fig. 9.
1835 *Ammonites arcigerens* Phillips; Phillips: 135, pl. 13, fig. 9.
1875 *Ammonites arcigerens* Phillips; Phillips: 270, pl. 13, fig. 9.
1880/82 *Aegoceras maculatum* (Young & Bird); Wright: 368 (1882), pl. 34 (1880), figs 1–3 (SM J18227), 4–7 (SM J18228).
1912 *Androgynoceras maculatum* (Young & Bird); Buckman: pls 45A, B (holotype, WM 493; from bed 590.61)
1938 *Androgynoceras maculatum* (Young & Bird); Spath: 126, pl. 20, fig. 6 (BM C.17752, from bed 590.61).
1938 *Androgynoceras maculatum* (Young & Bird), var. *rigida*; Spath: 126, pl. 19, figs 2 (BM C.28175, from bed 590.61), 13 (BM C.24601, from bed 590).
1961 *Androgynoceras maculatum* (Young & Bird); Dean *et al.*: pl. 70, fig. 4 (BM C.17752; from bed 590.61)
1962 *Androgynoceras arcigerens* (Phillips); Howarth: 112, pl. 16, fig. 5 (holotype, BM 17139; from bed 590.61).
1976 *Androgynoceras (A.) maculatum* (Young & Bird); Schlegelmilch: 162, pl. 33, fig. 9 (WM 493).
1985 *Androgynoceras (Beaniceras) luridum* (Simpson); Phelps: 350, pl. 1, fig. 3 (from bed 583).
1985 *Androgynoceras (Aegoceras) sparsicosta* (Trueman); Phelps: 351, pl. 1, fig. 1 (from bed 585).
1985 *Androgynoceras (Aegoceras) maculatum* (Young & Bird); Phelps: 350, pl. 2, fig. 8 (probably from bed 590.61).

RANGE. Beds 581–590.63, Maculatum Subzone; 35 specimens.

REMARKS. Ammonites in bed 590.61 have a distinctive style of preservation, where the dark brown or black shell of the ammonite has small near-circular patches of white calcite; such a well-preserved example is figured in Pl. 7, fig. 13. This type of preservation does not occur at any other level and allows the horizon of many of the figured specimens, including the holotype, to be identified precisely, as given in the list of figured specimens above. The lowest specimens in bed 581 are typical examples of the species, being much larger and more developed than is found in transitions from *Aegoceras (Beaniceras) luridum*. The latter transitions are represented by two specimens in bed 583.2 determined as *A. (A.) maculatum* var. *atavum* (see discussion below). The specimen from bed 583 figured by Phelps as *A. (Beaniceras) luridum* is also an *A. maculatum*; it has ribs on the venter that are bold and well developed and are not much reduced on a nearly flat venter as in *B. luridum*.

Phelps (1985: 351) divided the Maculatum Subzone into a lower 'Sparsicosta Zonule' and an upper 'Maculatum Zonule'. His lower division was based on the range of ammonites in the lower part of the Subzone that have low rib densities on their inner whorls of 16–18 ribs per whorl, and were identified as *Androgynoceras (Aegoceras) sparsicosta* (Trueman). Such rib densities are not different from the rib densities of *Aegoceras maculatum*, and in any case *sparsicosta* is not an appropriate name for them. The real *Androgynoceras sparsicosta* (Trueman) (holotype figured Spath, 1938: pl. 5 fig. 7) is a species that develops swollen, quickly expanding whorls and has sharply bituberculate ribs from a diameter of about 25 mm. These features are typical of the genus *Androgynoceras*, and Phelps' (1985: pl. 1, fig. 1) 58 mm diameter ammonite from the lower part of the Maculatum Subzone does not show such features – it is a typical *Aegoceras maculatum*, as are all the specimens in Bairstow's collection. Subdivision of the Maculatum Subzone on the basis of these ammonites is not followed here.

Aegoceras (A.) maculatum (Young & Bird), var. ***atavum*** Spath, 1938 Pl. 7, fig. 8

1938 *Androgynoceras maculatum* (Young & Bird), var. *atavum* Spath: 127, pl. 20, fig. 3 (from Gloucestershire).

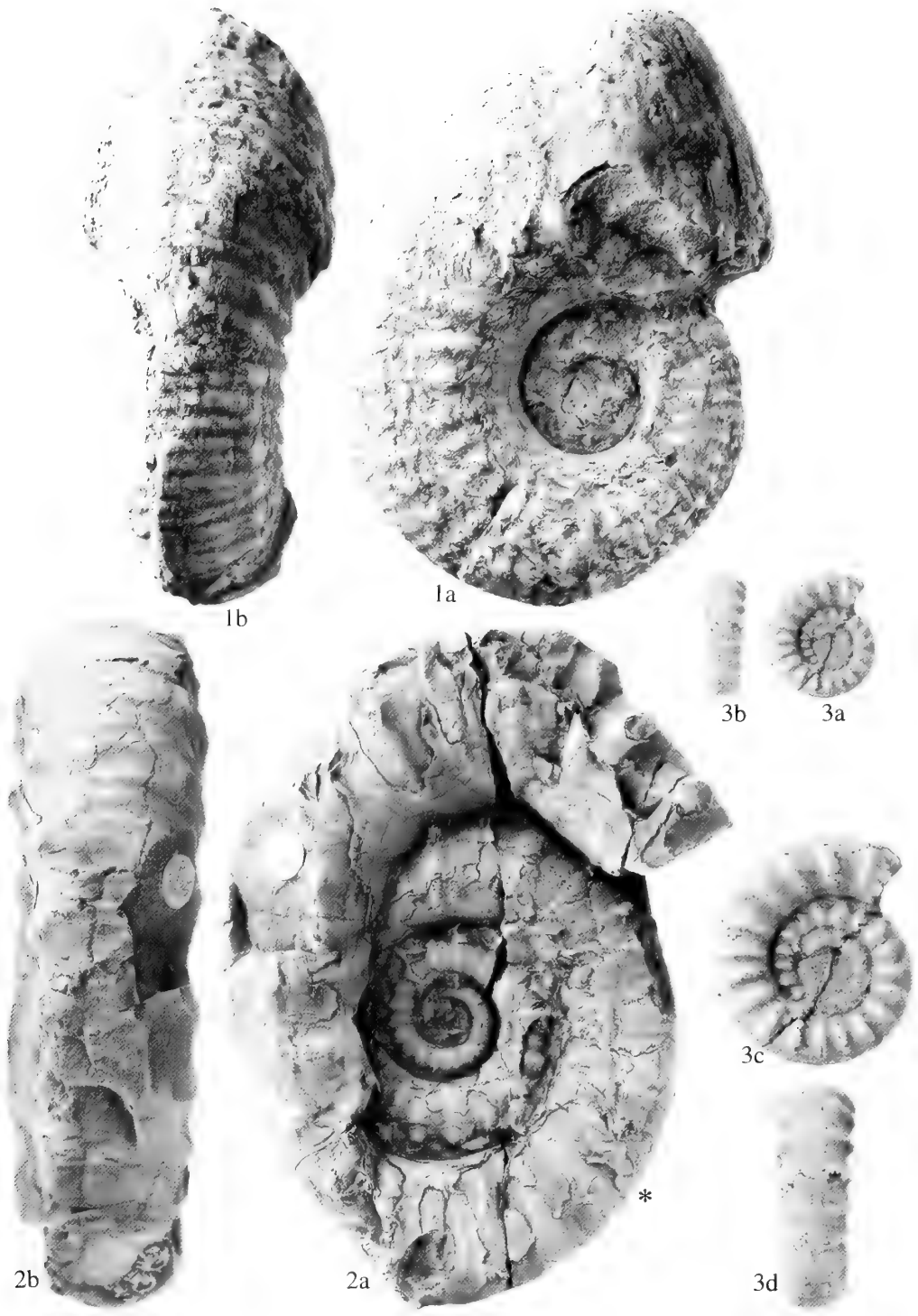

PLATE 8

Fig. 1 *Liparoceras (L.) divaricosta* (Trueman). Bed 596.3, C.39455, × 0.67; wholly septate.

Fig. 2 *Eoderoceras armatum* (J. Sowerby). Bed 499, near Bay Town, 0.18 m above base of bed, CA 3885, × 1.

Fig. 3 *Bifericeras donovani* Dommergues & Meister. Bed 501.1, near Bay Town, 0.22 m above base of bed, CA 3804; **3a, 3b,** × 1; **3c, d,** × 2; wholly septate.

RANGE. Two specimens in bed 583.2, Maculatum Subzone.

REMARKS. This record is based on two specimens (C.38873-74) from bed 583.2 that were determined by Spath (1938: 133) as belonging to his var. *atavum*; two other specimens in the same bed (C.348871-72) are typical of the normal variety of *maculatum*. C.38873-74 are both only 34 mm diameter, possibly nearly adult, with reduced ribbing on the nearly flat venter (Pl. 7, fig. 8). The whorl breadth is not as large as in Spath's (1938: 127, pl. 20, fig. 3) type of his variety, but otherwise they are closely similar. Spath (1938: 128) himself remarked that an alternative place for such specimens might be in the genus *Beaniceras*, and it is possible that bed 583.2 might be the horizon from which the holotype of *Aegoceras (Beaniceras) luridum* was obtained (SM J3274, figured Dean *et al.*, 1961: pl. 69, fig. 6). That holotype is somewhat larger (46 mm diameter), more complete and better preserved than Bairstow's specimens, and no others that are as well-preserved have been found in beds 578–583. Spath's determination as var. *atavum* for these Bairstow collection ammonites is retained here.

Aegoceras (A.) maculatum (Young & Bird), var. *leckenbyi* Spath, 1938

1938 *Androgynoceras maculatum* (Young & Bird), var. *leckenbyi*; Spath: 126, pl. 13, fig. 2 (C.3741, from bed 590.1).
1938 *Androgynoceras maculatum* (Young & Bird), var. *arcigerens* (Phillips); Spath: 126, pl. 20, fig. 5 (from Dorset).

RANGE. A single specimen in bed 590.1, Maculatum Subzone.

REMARKS. This variety is kept distinct from the normal type of *A. maculatum* only because it develops massive whorls with '*Liparoceras*-type' of ornamentation at sizes of more than 100 mm diameter. Bairstow's specimen is 120 mm diameter, and a Dorset specimen with similar whorls at 120–150 mm diameter was figured by Spath (1938: pl. 20, fig. 5) as *A. maculatum* var. *arcigerens* (Phillips).

Aegoceras (A.) lataecosta (J. de C. Sowerby, 1827)

1827 *Ammonites lataecosta* J. de C. Sowerby: 106, pl. 556, fig. 2.
1880/82 *Aegoceras lataecosta* (J. de C. Sowerby); Wright: 365 (1882), pl. 32, fig. 1 (1880) (holotype, BM 43916, from Drift, locality unknown).
1938 *Androgynoceras lataecosta* (J. de C. Sowerby); Spath: 135, pl. 19, figs 4 (holotype, BM 43916), 6 (BM C.38562, from Staithes, Yorkshire).

RANGE. Single specimens in beds 591 and 594, Capricornus Subzone.

Aegoceras (A.) artigyrus (Brown, 1837)

1837 *Ammonites artigyrus* Brown: 26, pl. 19, fig. 5.
1843 *Ammonites defossus* Simpson: 15
1855 *Ammonites defossus* Simpson: 48
1884 *Ammonites defossus* Simpson: 78
1889 *Ammonites artigyrus* Brown: 20, pl. 19, fig. 5.
1938 *Androgynoceras artigyrus* (Brown); Spath: 158, pl. 14, fig. 5, pl. 18, fig. 1, pl. 23, figs 3 (holotype, Manchester Museum LL.230, possibly from bed 593), 12, 14.
1973 *Aegoceras maculatum* (Young & Bird); Donovan & Forsey: 14, pl. 4, fig. 1 (SM B11945, paralectotype of *Ammonites defossum* Simpson, 1843).
1973 *Aegoceras (Oistoceras)* cf. *figulinum* (Simpson); Donovan & Forsey: 14, pl. 4, fig. 2 (SM B11946, lectotype of *Ammonites defossum* Simpson, 1843, designated by Donovan & Forsey).
1985 *Androgynoceras (Aegoceras) capricornus* (Schlotheim), morphotype *A. artigyrus*; Phelps: 352, pl. 2, fig. 6.

RANGE. Found by Bairstow only in bed 593, Capricornus Subzone, 4 specimens, but Phelps' figured specimen is from bed 595.2.

REMARKS. Donovan & Forsey's (1973: 14) designation of the Robin Hood's Bay specimen SM B11946 as lectotype of *Ammonites defossus* Simpson, 1843, has consequences for the position of both the genus *Defossiceras* Buckman, 1913, and Simpson's species *defossus*. That lectotype and the paralectotype (SM B11945), also figured for the first time by Donovan & Forsey, are closely similar to each other, and both have robust, quickly expanding whorls and moderately fine ribs on the inner whorls. The robust whorls are not like the slender whorls of *Oistoceras* at similar sizes, and the ribs are more closely spaced on the inner whorls than in *Aegoceras (A.) maculatum*. The ribs are projected slightly forwards on the venter of both lectotype and paralectotype of *defossus*, but a varying amount of projection of the ribs on the venter occurs in Capricornus Subzone species of *Aegoceras (A.)*, though it is never as pronounced as in the later subgenus *Oistoceras*. The holotype of *A. (A.) artigyrus* figured by Spath (1938) has similarly robust whorls, the same rib-density on the inner whorls and similar slight forward projection of the ribs on the venter. This is considered here to be the best place for *defossus*, and places the genus *Defossiceras* as a junior synonym of *Aegoceras (A.)* (ie. not a synonym of the subgenus *Oistoceras*), and the species *defossus* as a junior synonym of *Aegoceras (A.) artigyrus*.

Subgenus ***BEANICERAS*** Buckman, 1913

Aegoceras (Beaniceras) luridum (Simpson, 1855)

1855 *Ammonites luridus* Simpson: 46.
1913 *Beaniceras luridum* (Simpson); Buckman: pl. 73 (holotype, SM J3274).
1961 *Beaniceras luridum* (Simpson); Dean *et al.*: pl. 69, fig. 6 (holotype, SM J3274, possibly from bed 583.2) (see description of Maculatum Subzone, p. 150 below).

RANGE. Beds 578.1–580, Luridum Subzone; 8 specimens; possibly also from bed 583.2, Maculatum Subzone.

REMARKS. Although the eight specimens in beds 578 and 580 are crushed, they are much larger (up to 37 mm diameter) and more compressed than *A. (B.) centaurus* (d'Orbigny), and so can be confidently referred to *A. (B.) luridum*.

Subgenus ***OISTOCERAS*** Buckman, 1911

Aegoceras (Oistoceras) sinuosiforme Spath, 1938

Pl. 7, fig. 14

1938 *Oistoceras sinuosiforme* Spath: 167, pl. 18, fig. 6, pl. 19, fig. 7 (holotype, BM C.38564), pl. 26, figs 6, 7, 9 (all Spath's figured specimens are from Lincolnshire).

RANGE. Beds 596.2–598.1, Figulinum Subzone; 93 specimens.

REMARKS. *A.(O.) sinuosiforme* has more widely spaced ribs and much less well-developed chevrons on the venter than *A. (O.) figulinum*.

Aegoceras (Oistoceras) angulatum (Quenstedt, 1856)

1856 *Ammonites maculatus angulatus* Quenstedt: 121, pl. 14, fig. 12.
1885 *Ammonites maculatus angulatus* Quenstedt; Quenstedt: 270, pl. 34, fig. 11.

1938 *Oistoceras angulatum* (Quenstedt); Spath: 171, pl. 21, fig. 5 (from France), pl. 22, fig. 5 (from Lincolnshire), pl. 26, figs 10, 12 (both from Lincolnshire).
1976 *Androgynoceras (Oistoceras) angulatum* (Frebold, 1922) (*sic*); Schlegelmilch: 69, pl. 34, fig. 4 (from Germany).
1985 *Androgynoceras (Oistoceras) angulatum* (Quensedt); Phelps: 354, pl. 2, fig. 4 (from Germany).

RANGE. Bed 599, Figulinum Subzone; 1 specimen.

REMARKS. Quenstedt (1856: 121) had specimens from Metzingen and Iggingen, Germany, and he figured one from the former locality. So the original of Quenstedt (1884: pl. 34, fig. 11), refigured by both Schlegelmilch (1976: pl. 34, fig. 11) and Phelps (1985: pl. 2, fig. 4), is almost certainly a syntype and can be designated lectotype; its designation by Schlegelmilch as the neotype is not correct. *A. (O.) angulatum* is more evolute, has more slowly expanding whorls, has no ventro-lateral tubercles, and has fewer ribs on the inner whorls, than *A. (O.) figulinum*. The angle of the ribbing varies between rectiradiate and prorsiradiate in both species.

Aegoceras (Oistoceras) figulinum (Simpson, 1855)

1855 *Ammonites figulinus* Simpson: 47.
1855 *Ammonites omissus* Simpson: 47.
1876 *Aegoceras defossum* (Simpson); Blake: 282, pl. 8, fig. 9 (SM J17988, see Donovan & Forsey, 1973: 13).
1911 *Oistoceras figulinum* (Simpson); Buckman: pl. 26A (holotype, WM 115).
1911 *Oistoceras omissum* (Simpson); Buckman: pl. 27 (holotype, WM 502, now lost).
1938 *Oistoceras figulinum* (Simpson); Spath: 162, pl. 19, fig. 10 (BM C.17988), pl. 22, fig. 8 (BM 37973a).
1938 *Oistoceras omissum* (Simpson); Spath: 170, pl. 21, fig. 3 (BM 38561).
1955 *Oistoceras* aff. *figulinum* (Simpson); Howarth: 161, pl. 11, fig. 4 (SM J35968, from bed 600.4).
1976 *Androgynoceras (Oistoceras) figulinum* (Simpson); Schlegelmilch: 69, pl. 34, fig. 3 (WM 115, holotype).
1985 *Androgynoceras (Oistoceras) figulinum* (Simpson); Phelps: 353, pl. 2, fig. 1 (from bed 600.2).
1987 *Oistoceras figulinum* (Simpson); Dommergues: pl. 11, figs 5, 6.

RANGE. Beds 600.2 and 600.4, Figulinum Subzone; 20 specimens.

REMARKS. This is the most highly developed species of *Oistoceras*, which has fine ribs on the inner whorls, small ventro-lateral tubercles, and well-developed chevrons in the ribs that are connected together into a rudimentary pseudo-keel along the middle of the venter.

Other species of *Oistoceras* from Yorkshire:

1. *A. (O.) curvicorne* (Schloenbach, 1863); Spath, 1938: 164, pl. 19, fig. 11 (BM C.19228; indeterminate inner whorls), pl. 22, fig. 9 (BM C.6235); both of Spath's figured specimens were probably from Staithes, not Robin Hood's Bay.
2. ?*A. (O.) anguliferum* (Phillips, 1829: 163, pl. 13, fig. 19: 1835: 135, pl. 13, fig. 19; 1875: 270, pl. 13, fig. 19); the type specimen is lost, and Phillips' figure cannot be interpreted.

Genus ***ANDROGYNOCERAS*** Hyatt, 1867

Androgynoceras heterogenes (Young & Bird, 1828)

1828 *Ammonites heterogenes* Young & Bird: 264, pl. 14, fig. 7.
1880/82 *Aegoceras heterogenum* (Young & Bird); Wright: 370 (1882), pl. 35, figs 4–6, (1880) (SM J18229), pl. 36, figs 1–4 (1880) (BM C.1870).
1912 *Androgynoceras heterogenes* (Young & Bird); Buckman: pl. 46 (holotype, WM 195).
1938 *Androgynoceras heterogenes* (Young & Bird); Spath: 113, pl. 13, figs 7a (BM C.19225), 7b (BM C.38457), pl. 20, fig. 2 (BM C.38496, as var. *gigas*, from bed 590.61).

RANGE. Maculatum Subzone: Bairstow found single specimens in beds 583.2 and 588, but BM C.38496 definitely came from bed 590.61, and the other figured specimens are probably from bed 590.63.

Order **NAUTILOIDEA**
Family **NAUTILIDAE** d'Orbigny, 1840
Genus ***CENOCERAS*** Hyatt, 1883

Cenoceras striatus (J. Sowerby, 1817)

1817 *Nautilus striatus* J. Sowerby: 183, pl. 182 (3 figures, all syntypes, from Dorset).
1829 *Ammonites annularis* Phillips: 163, pl. 12, fig. 18; 1835: 134, pl. 12, fig. 18; 1875: 263, pl. 12, fig. 8.
1855 *Ammonites heterogeneus* Simpson: 33.
1956 *Cenoceras striatus* (J. Sowerby); Kummel: 362, pl. 3, figs 1, 2 (BM 43852, from Dorset).
1962 *Cenoceras heterogeneum* (Simpson); Howarth: 96, pl. 13, fig. 1 (holotype, WM 442).
1962 *Cenoceras annulare* (Phillips); Howarth: 96, pl. 13, fig. 2 (holotype, WM 62).

RANGE. Bairstow found single specimens in beds 464.32, 468 (both Simpsoni Subzone) and 505.1 (Taylori Subzone).

BIOSTRATIGRAPHY

In the description below the ammonite distribution and the placement of the boundaries are discussed for all the zones and subzones in Robin Hood's Bay. Additionally, it is noteworthy that Wine Haven at the south-eastern end of the bay has recently been proposed as the world standard for the definition of the base of the Pliensbachian Stage.

The scheme of ammonite zones used here is based on that regularized by Dean, Donovan & Howarth (1961), with a few later refinements to the details of some of the definitions. Cariou & Hantzpergue (1997) used the same scheme of divisions for the Sinemurian and Lower Pliensbachian in eastern France and the central Mediterranean area. The distribution of the ammonites, on which the biostratigraphical divisions are based, is shown in detail in Figs 21, 22, 24 and 25, which give the number of specimens of each species found in each bed, and a visual indication of the range of each species.

LOWER SINEMURIAN

SEMICOSTATUM ZONE, Sauzeanum Subzone, beds 418–429.64. No ammonites were found in beds 418–420, which are the first 2.48 m of strata exposed above the lowest level to which the tide ever falls in Robin Hood's Bay. Above this, *Euagassiceras* occurs up to about the middle of the subzone, and *Coroniceras (Arietites) alcinoe* occurs in a broad middle part of the subzone; both are

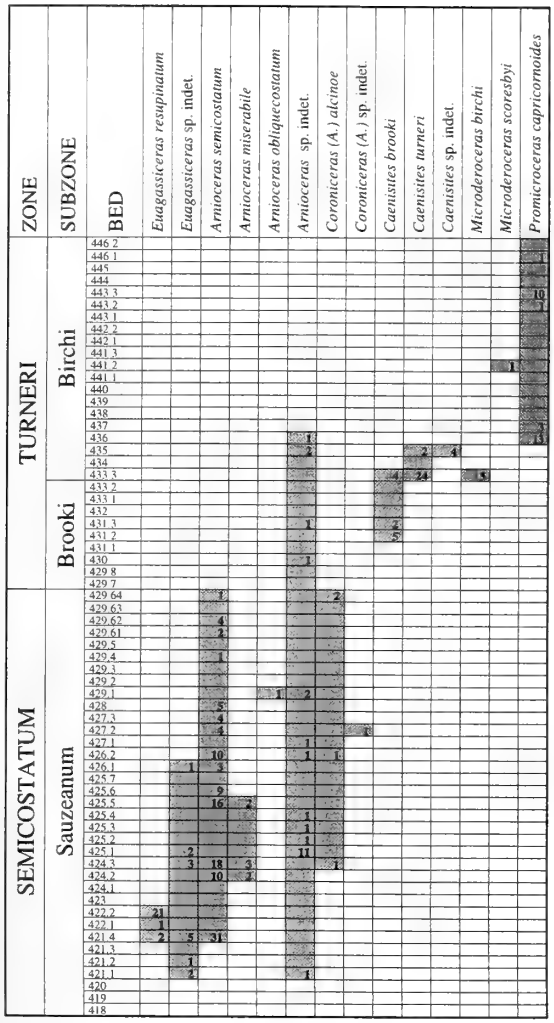

Fig. 21 Distribution of ammonites in the Lower Sinemurian of Robin Hood's Bay.

characteristic of the Sauzeanum Subzone. *Arnioceras semicostatum* is common through most of the subzone.

TURNERI ZONE, Brooki Subzone, beds 429.7–433.2. The only ammonites found in the beds that are allocated to this subzone are seven *Caenisites brooki* in the middle part and two *Arnioceras* sp. indet. in the middle and lower beds. *Caenisites brooki* probably only occurs in the upper or top part of the subzone (Dean *et al.*, 1961: 453), and the ammonite *Caenisites preplotti* Spath, which is characteristic of the base of the subzone, does not occur in Robin Hood's Bay. So the Brooki Subzone has to be defined according to the boundaries of the adjoining subzones: the highest occurring *Coroniceras (Arietites) alcinoe* in bed 429.64 at the top of the Sauzeanum Subzone defines the base of the Brooki Subzone at the bottom of bed 429.7, and the appearance of *Microderoceras birchi* in bed 433.3 at the base of the Birchi Subzone defines the top of the Brooki Subzone at the top of bed 433.2.

Birchi Subzone, beds 433.3–446.2. This subzone is generally considered to correspond to the range of *Microderoceras*: five *M. birchi* occur in bed 433.3, so defining the base of the subzone, and a single *M. scoresbyi* occurs in bed 441.2 at the middle of the subzone. The top of the subzone is delimited by the appearance of the first *Asteroceras* at the base of the Obtusum Zone. *Caenisites brooki* persists into the basal bed (433.3) of the Birchi Subzone, and the same bed also contains 24 examples of *Caenisites turneri*. *Promicroceras capricornoides* appears just above the lowest part and extends to the top of the subzone. There are no other ammonites in the subzone.

UPPER SINEMURIAN

OBTUSUM ZONE, Obtusum Subzone, beds 446.31–446.5. The base of both zone and subzone is drawn at the first appearance of a single *Asteroceras* in bed 446.31; that specimen is a definite example of the genus, but is not specifically determinable. The only specimen of *A. obtusum* that was found occurs in the overlying bed 446.32, and *A. confusum* is more common in beds 446.32 and 446.33. *Promicroceras capricornoides* persists into the lowest two beds of the Obtusum Subzone, then is immediately replaced by *P. planicosta* for the remainder of the subzone; the two species do not overlap. Other ammonites are *Xipheroceras dudressieri* (confined to the subzone) and *X. ziphus*, *Epophioceras landrioti* in the upper half and *Cymbites laevigatus* at the top of the subzone.

Stellare Subzone, beds 447–455.1. The base of the subzone is placed at the first appearance of the distinctive index species *Asteroceras stellare*, which ranges up to the middle of the subzone, and the top is limited by the first *Eparietites* at the base of the Denotatus subzone. In the upper half of the subzone the index species is replaced by *Asteroceras blakei*, which persists into the overlying subzone. *Aegasteroceras crassum* appears at about the middle of the subzone, then *A. sagittarium* occurs in the top part. *Promicroceras planicosta* is very common in all but the highest beds of the subzone, and 262 specimens were collected by Bairstow. Other ammonites in the subzone are *Cymbites laevigatus, Xipheroceras ziphus, and Epophioceras landrioti* near the base.

Denotatus Subzone, beds 455.2–462. The base of this subzone is placed at the first appearance of the genus *Eparietites*, ie. the new species *E. bairstowi*, which is more evolute and has thicker and more massive whorls than any other *Eparietites*. The main species ranging through the middle and upper parts and up into the Simpsoni Subzone is *E. impendens*. From the subzone below *Asteroceras blakei, Aegasteroceras crassum* and *A. sagittarium* persist into the bottom and middle parts of the Denotatus Subzone. *Cymbites laevigatus* occurs throughout the subzone, and the Schlotheimid *Angulaticeras* sp. indet. occurs in the top two beds.

OXYNOTUM ZONE, Simpsoni Subzone, beds 463–471. The base of the subzone is placed at the first appearance of the index species *Oxynoticeras simpsoni* in bed 363, where there are two large specimens that show typical characters of the species; there are four more specimens in bed 464.3, poorly preserved examples in beds 465 and 466, then the species becomes common in bed 467 and 468 in the mid to upper part of the subzone.

From the subzone below, *Eparietites impendens* persists into beds 463–464.32, where it overlaps with *O. simpsoni* in the bottom 1.68 m of the Simpsoni Subzone. In fact at its highest level in bed 464.32 there are many typical *E. impendens*. A similar overlap between *E. impendens* and *O. simpsoni* is also found in the top part of the Frodingham Ironstone near Scunthorpe, Lincolnshire.

Gagaticeras is characteristic of the upper half of the Simpsoni Subzone, from bed 467 upwards, where there are many specimens belonging to four species. *Palaeoechioceras* occurs in bed 467, and

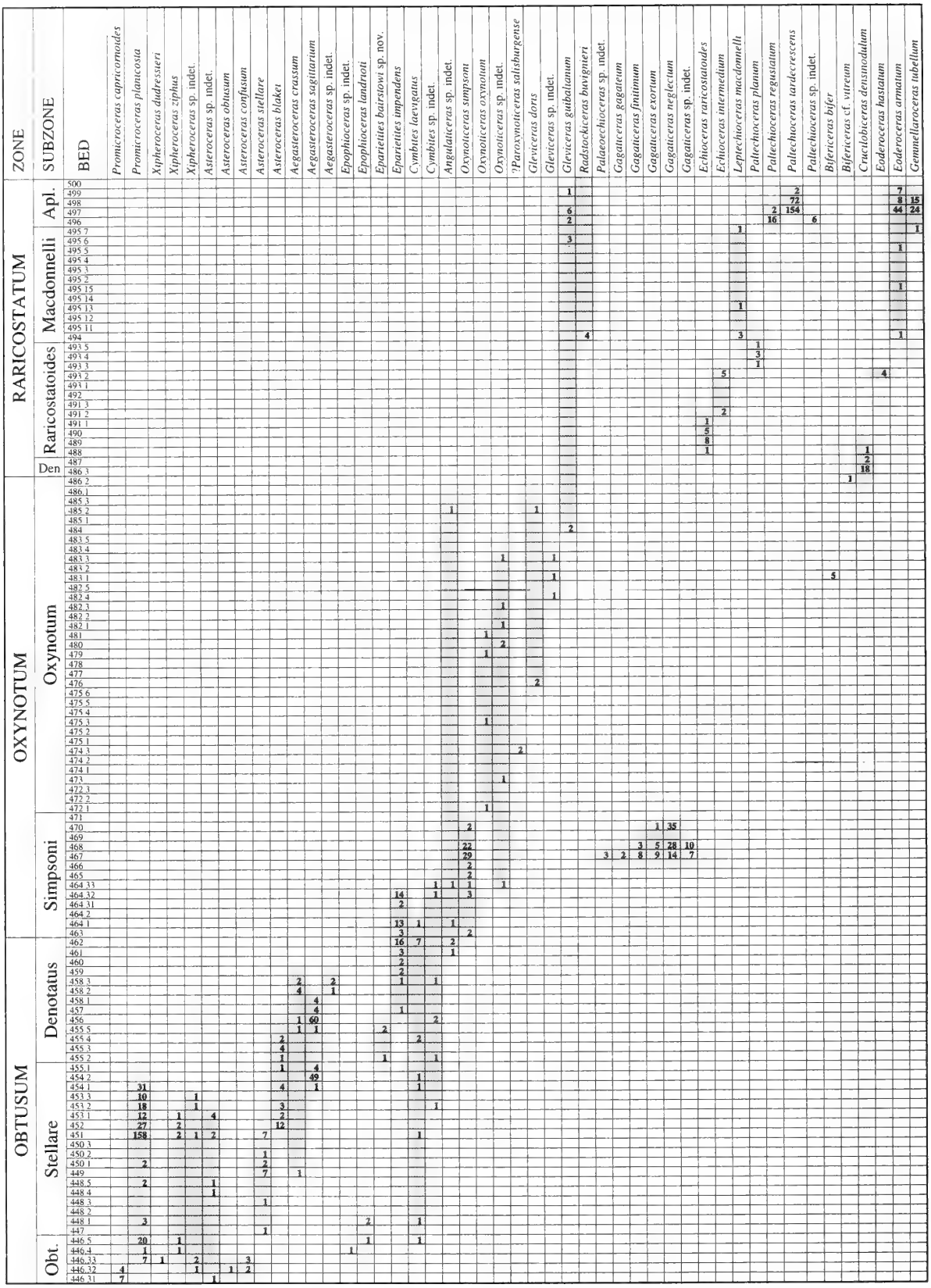

Fig. 22 Distribution of ammonites in the Upper Sinemurian of Robin Hood's Bay.

Cymbites laevigatus and *Angulaticeras* sp. indet. occur in the lower half of the subzone.

Oxynotum Subzone, beds 472.1–486.2. More involute and compressed *Oxynoticeras* like *O. oxynotum* rather than *O. simpsoni* first occur in bed 472.1, so the base of the subzone is placed at that level. Better specimens occur higher in the subzone, as well as fragments of large specimens. Other oxynoticeratids present are two possible specimens of *Paroxynoticeras salisburgense* in the lower half, and *Gleviceras doris* and *G. guibalianum* in the upper half of the subzone. *Angulaticeras* sp. indet., *Bifericeras bifer* and *B.* cf. *vitreum,* also occur in the upper half of the subzone.

RARICOSTATUM ZONE, Densinodulum Subzone, beds 486.3 and 487. The base of the subzone is placed at the first appearance of *Crucilobiceras* in bed 486.3 and the top is limited by the first occurrence of *Echioceras* in bed 488 marking the base of the Raricostatoides Subzone. So the Densinodulum Subzone consists only of the 1.0 m thick beds 486.3 and 487. *C. densinodulum* is abundant in bed 486.3, but there are no other ammonites in the subzone.

Raricostatoides Subzone, beds 488–493.5. The base of the subzone is placed at the first appearance of *Echioceras*: *E. raricostatoides* in the basal one-third of the subzone is followed by *E. intermedium* in the middle part, then by *Paltechioceras planum* in the upper one-third of the subzone. *Crucilobiceras densinodulum* persists from the subzone below into the basal bed, and the only other ammonite in the subzone is *Eoderoceras hastatum* in the upper part.

Macdonnelli Subzone, beds 494–495.7. This subzone is based on the range of the index species *Leptechioceras macdonnelli,* which occurs in the top and bottom beds and does not range higher. The earliest *Eoderoceras armatum* occurs in the bottom bed, and the first Polymorphitid, *Gemmellaroceras tubellum,* occurs in the top bed. The only other ammonites present are the Oxynoticeratids *Gleviceras guibalianum* near the top of the subzone and *Radstockiceras buvignieri* in the bottom bed. The latter record seems to be the first provable occurrence of *Radstockiceras* in the Raricostatum Zone.

Aplanatum Subzone, beds 496–500. The base of the subzone is placed at the first occurrence of *Paltechioceras regustatum,* and *P. tardecrescens* (of which *P. aplanatum* is a synonym) becomes abundant in the middle and upper parts of the subzone. *Paltechioceras* first occurs in the top part of the Raricostatoides Subzone, but the genus is much more common in the Aplanatum Subzone and does not range higher. Another ammonite that is characteristic of the Aplanatum Subzone is *Eoderoceras armatum,* which first appears as rare examples in the Macdonnelli Subzone, but becomes much more common in the Aplanatum Subzone; it ranges up to 0.15 m below the top of bed 499, but it does not occur higher and does not overlap with *Apoderoceras* in the Taylori Subzone. *Gemmellaroceras tubellum* is common in the middle part, and *Gleviceras guibalianum* occurs in the lower part of the subzone.

LOWER PLIENSBACHIAN

The exposures at the base of the cliff in Wine Haven, Robin Hood's Bay, have recently been proposed as the Global Stratotype Section and Point (GSSP) for the base of the Pliensbachian Stage (Hesselbo *et al.,* 2000). The sequence across the Sinemurian/Pliensbachian boundary is sufficiently expanded and rich in ammonites here to be suitable for such an important global reference section. Hesselbo *et al.*'s (2000: 604, fig. 4) stratigraphical sequence is closely similar to the sequence described here, as are their ammonite records and identifications. Their bed 73 at the base of the Pliensbachian is the same as bed 501 here (see the correlation table of Fig. 19), and their photograph (Hesselbo *et al.* 2000: fig. 3) shows the nodules of their bed 72 (=bed 500 here) and the basal reference point of the Pliensbachian low in the cliff at Wine Haven.

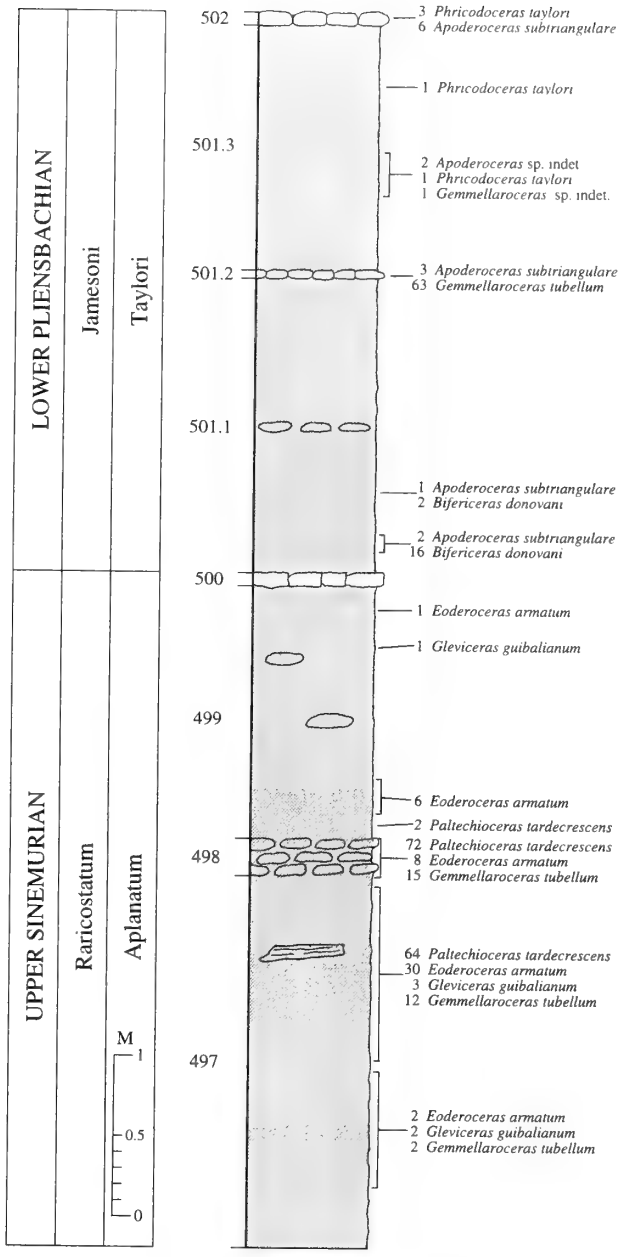

Fig. 23 The distribution of ammonites close to the Sinemurian/Pliensbachian boundary in Robin Hood's Bay. The ammonites listed include those collected from the exposures across the boundary at both Wine Haven and the foreshore immediately east of Robin Hood's Bay town; there are no significant differences in the distribution of ammonites at the two exposures.

Fig. 23 shows details of the stratigraphical distribution of Bairstow's ammonites at the Sinemurian/Pliensbachian boundary. The first ammonites to occur above the boundary are 16 *Bifericeras donovani* Dommergues & Meister (one is figured in Pl. 8, fig. 3) and

two *Apoderoceras subtriangulare* (Young & Bird) (Pl. 5, fig. 8) 0.13–0.22 m above the bottom of bed 501.1. Hesselbo *et al.* (2000) did not find ammonites in the 1.8 m of strata below the base of the Pliensbachian (ie. in the nodules of bed 500 and the shales of bed 499). Bairstow did not find ammonites in bed 500, but he collected six specimens of *Eoderoceras armatum* from bed 499 in the middle of the bay near Robin Hood's Bay town. These are well-preserved, readily identifiable examples of the species (one is figured in Pl. 8, fig. 2), and Bairstow's records show that they were collected 0.15–0.37 m above the base of that bed. A single *E. armatum*, less well-preserved than those lower down, but still readily identifiable with that species, was collected from Wine Haven high in bed 499, only 0.15 m from the top. The thickness of strata across the Sinemurian/Pliensbachian boundary from which no ammonites have been collected is thus reduced to only 0.36 m.

JAMESONI ZONE, Taylori Subzone, beds 501.1–537. The base of the subzone (and the Jamesoni Zone, and the Pliensbachian Stage) is placed at the bottom of bed 501.1, which contains the lowest occurrence of the characteristic genus *Apoderoceras*, and this is the only horizon at which *Bifericeras donovani* Dommergues & Meister occurs. *Phricodoceras taylori* and other species of *Phricodoceras* are present through much of the subzone and do not range higher. Many examples of *Gemmellaroceras tubellum* are found near the base of the subzone, and the larger species *G. rutilans* occurs in the top part. A single specimen of *Radstockiceras buvignieri* was also

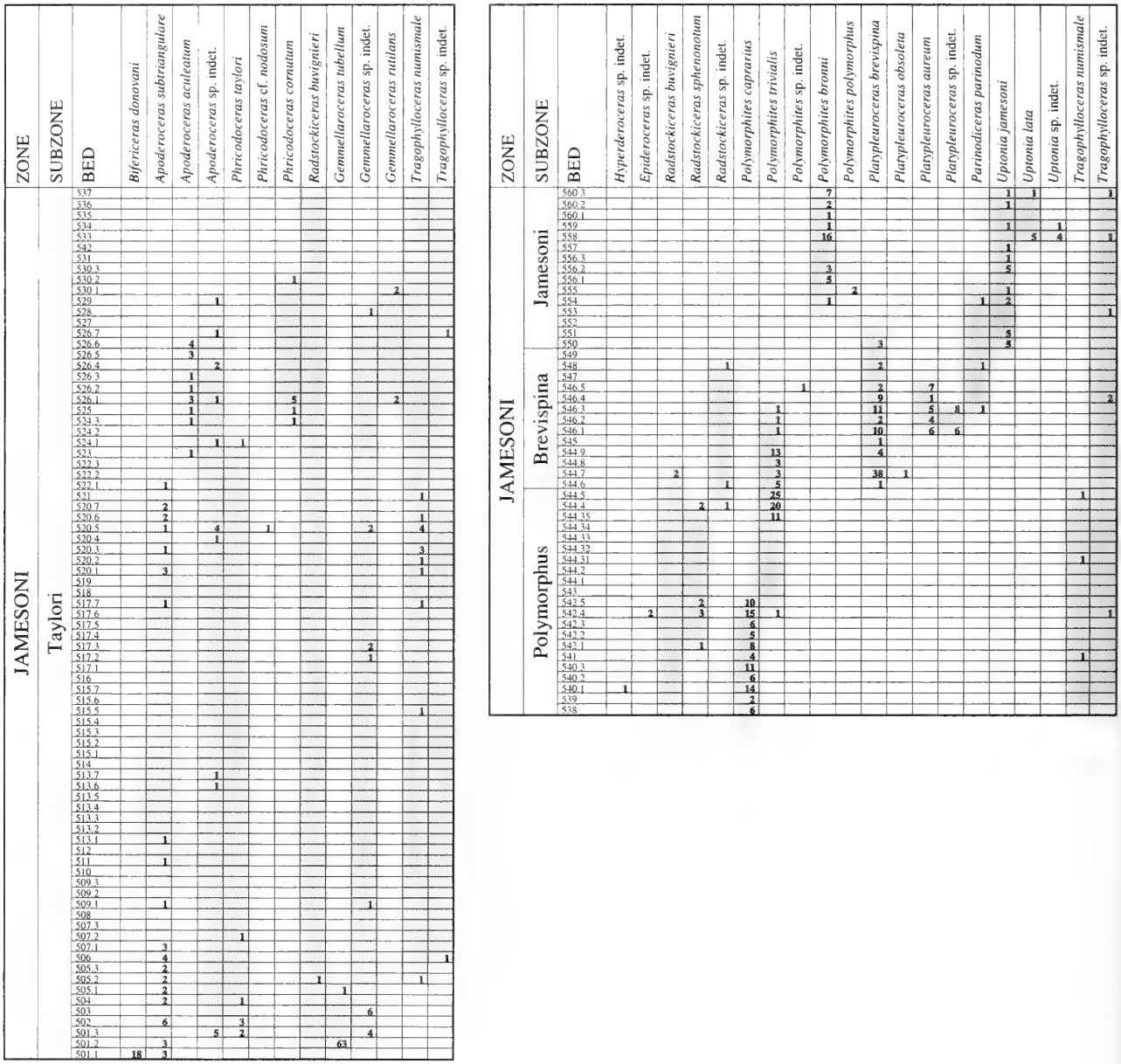

Fig. 24 Distribution of ammonites in the Jamesoni Zone, Lower Pliensbachian, of Robin Hood's Bay.

found in the subzone, along with widely scattered specimens of *Tragophylloceras numismale*.

Polymorphus Subzone, beds 538–544.5. The first appearance of *Polymorphites* marks the base of this subzone. The earliest species is *P. caprarius* which occurs in the bottom half of the subzone, followed by *P. trivialis* in the upper half. The latter species extends into the Brevispina Subzone, and other species occur in the Jamesoni Subzone. The only other ammonites in this subzone in Robin Hood's Bay are the last examples of *Tragophylloceras numismale*, a single *Hyperderoceras* sp. indet. low in the subzone and the oxynoticeratid genus *Radstockiceras:* the small species *R. sphenonotum* is confined to the Polymorphus Subzone, and another much larger fragment of a *Radstockiceras* was found in bed 544.4 near the top of the subzone.

Brevispina Subzone, beds 544.6–549. The base is placed at the first appearance of *Platypleuroceras brevispina,* which is common throughout the subzone and extends up to its highest occurrence in the basal bed of the Jamesoni Subzone. Many of those in beds 544 and 546 are large, crushed and fragmentary, though they show the

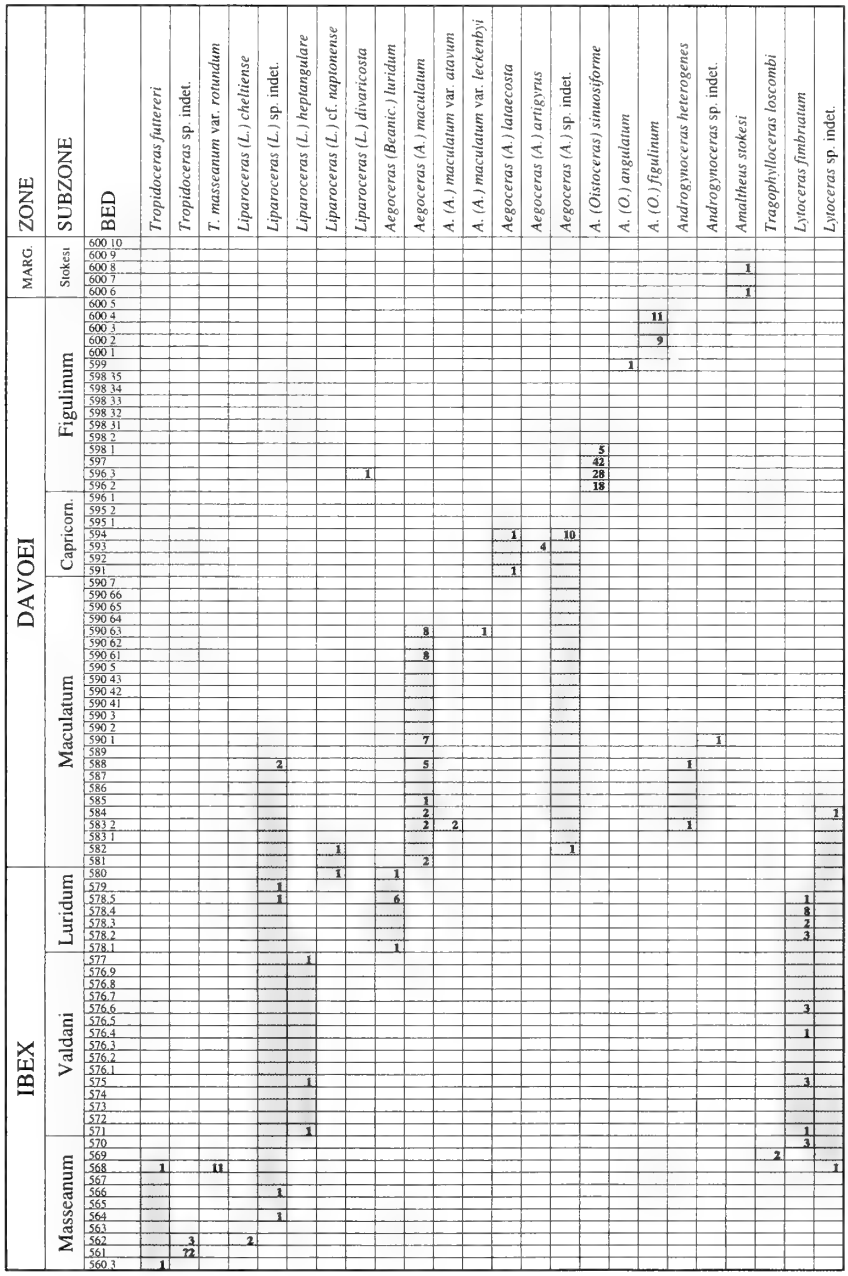

Fig. 25 Distribution of ammonites in the Ibex and Davoei Zones, Lower Pliensbachian, and in the base of the Margaritatus Zone, Upper Pliensbachian, of Robin Hood's Bay.

typical features of the species. The more evolute *P. aureum* occurs in the middle part of the subzone, and the more finely ribbed *P. obsoleta* is represented by only one specimen in Bairstow's collection from the lower part of the subzone. *Polymorphites trivialis* is common in the lower and middle parts of the subzone, and there are rare occurrences of *Radstockiceras, Parinodiceras* and *Tragophylloceras*.

Jamesoni Subzone, beds 550–560.3 (except the top 0.08m). The base of the Jamesoni Subzone is placed at the first occurrence of *Uptonia jamesoni* in bed 550, and the index species then extends through the full thickness of the subzone, to which it is confined. The more finely ribbed *U. lata* occurs less commonly in the upper half of the subzone, and *Polymorphites bronni* is also characteristic of the upper half of the subzone. The only other ammonites in the subzone are the highest occurring specimens of *Platypleuroceras brevispina* in bed 550, *Polymorphites polymorphus* at the middle of the subzone, and rare examples of *Parinodiceras* and *Tragophylloceras*.

IBEX ZONE, Masseanum and Valdani Subzones, beds 560.3 (top 0.08 m)–577. These two subzones are delimited according to the distribution of species of *Tropidoceras* and *Acanthopleuroceras*: *Tropidoceras* occurs in both subzones and *Acanthopleuroceras* only in the Valdani Subzone. Unfortunately ammonites are rare in this interval in Robin Hood's Bay, and the few examples of these genera are not well-preserved. None, however, have the definite bituberculate ribs of *Acanthopleuroceras*, so they all have to be identified as *Tropidoceras*, in which umbilical tubercles are much reduced or absent. The lowest example (Pl. 7, fig. 10) from the top 0.08 m of bed 560.3 and another (Pl. 7, fig. 11) from near the bottom of bed 568 are best determined as *T. futtereri* (Spath), while several specimens from the boundary of beds 567 and 568 have the much more massive ribs at larger sizes and the more widely spaced ribs of *T. masseanum* (d'Orbigny), var. *rotundum* (Futterer). The base of the Masseanum Subzone (and of the Ibex Zone) is placed 0.08 m below the top of bed 560.3 to include this earliest *T. futtereri*, and bed 568 probably belongs to the same subzone.

In the absence of *Acanthopleuroceras* there is no good evidence for the position of the base of the Valdani Subzone, so it is placed provisionally at the bottom of bed 571 from the occurrence of *Liparoceras (L.) heptangulare*. There are two more specimens of that species in beds 575 and 577. According to Spath (1938: 59) *L. (L.) heptangulare* might be confined to the Valdani Subzone (ie. Spath's 'Centaurus Subzone'), so its presence in beds 571–577 (7.66 m thick) suggests that they are probably of Valdani Subzone age.

The only other ammonites in either subzone are two *Liparoceras (L.) cheltiense* low in the Masseanum Subzone, one *Tragophylloceras loscombi* high in the same subzone, and *Lytoceras fimbriatum* in the upper part of the Masseanum Subzone and throughout the Valdani Subzone. The latter species becomes more common in the Luridum Subzone.

Luridum Subzone, beds 578.1–580. The presence of eight *Aegoceras (Beaniceras) luridum* in beds 578.1, 578.5 and 580 is sufficient evidence to refer beds 578 to 580 to the Luridum Subzone. Other ammonites in this subzone are a single *Liparoceras (L.)* cf. *naptonense*, two *Liparoceras (L.)* sp. indet. and 14 examples of *Lytoceras fimbriatum*.

DAVOEI ZONE, Maculatum Subzone, beds 581–590.7. The base of this zone and subzone is placed at the bottom of bed 581 which contains the lowest *Aegoceras (A.) maculatum* (Pl. 7, fig. 12). Two more, typical, examples occur in bed 582.3, then there are many well-preserved specimens at higher levels, especially in beds 590.61 and 590.63. Other ammonites in the Maculatum Subzone are *A. (A.) maculatum* vars *atavum* and *leckenbyi*, *Liparoceras (L.)* cf. *naptonense*, *Androgynoceras heterogenes* and *Lytoceras* sp. indet. See remarks on the identification of *Aegoceras maculatum* (p. 141) for discussion of the division of the Maculatum Subzone into smaller units.

Capricornus Subzone, beds 591–596.1. The base of the subzone is placed at earliest occurrence of *Aegoceras (A.) lataecosta* in bed 591. This is 1.83 m above the highest *A. (A.) maculatum* in bed 590.63, but the intervening strata (beds 590.64–590.7) did not yield any ammonites and are retained in the Maculatum Subzone. The only other ammonites in the subzone are *A. (A.) artigyrus*, which has more massive whorls and coarser ribbing than *lataecosta*, and a number of poorly preserved *Aegoceras (A.)* sp. indet.

Figulinum Subzone, beds 596.2–600.5. This subzone is based on the range of the subgenus *Oistoceras*. The index species, *Aegoceras (Oistoceras) figulinum*, occurs in beds 600.2 and 600.4 near the top of the subzone, but the base of the subzone is placed at the lowest appearance of *A. (O.) sinuosiforme* in bed 596.2. This and *A. (O.) angulatum* in bed 600.2 have more widely spaced ribs than *figulinum*, especially on the inner whorls. The only other ammonite in the subzone is a single *Liparoceras (L.) divaricosta* in bed 596.3 (Pl. 8, fig. 1).

The top of the subzone is limited by the base of the Stokesi Subzone (Margaritatus Zone, Upper Pliensbachian), which is placed at the first appearance of *Amaltheus stokesi* in bed 600.6. There are other examples of *A. stokesi* in bed 600.8 and at higher levels in the Stokesi Subzone. *Aegoceras (Oistoceras) figulinum* and *Amaltheus stokesi* are confined to their respective subzones in Robin Hood's Bay and their ranges do not overlap.

ACKNOWLEDGEMENTS. I wish to thank the late Leslie Bairstow for entrusting me with his unfinished manuscripts in the hope that I would be able to complete them in a form suitable for publication. Mrs L.M. Spencer kindly helped me to retrieve those manuscripts when he left his London home in 1985. Thanks are also due to Mr. Peter Jones of King's College, Cambridge, for information about Bairstow during his time at that college, to Rosalind Moad for allowing me to examine the original copy of Bairstow's 1930 Fellowship Dissertation, which is held in the Archive Centre at King's College, and to Professor D.T. Donovan for reading the manuscript and suggesting several significant improvements.

REFERENCES

Arkell, W. J. 1956. *Jurassic geology of the world*. xv + 806 pp. Edinburgh and London, Oliver and Boyd.

Bairstow, L. 1948. Robin Hood's Bay and Fylingdales Moor. *In,* Versey, H.C. & Hemingway, J.E. *Guide to Excursion C.2, North-east Yorkshire*: 8–10. International Geological Congress, 18th session, Great Britain 1948.

—— 1953. Lower Lias. *In,* Sylvester-Bradley, P.C. *A stratigraphical guide to the fossil localities of the Scarborough District.* The Natural History of the Scarborough District, **1:** 41–44. Scarborough Field Naturalist Society.

—— 1969. Lower Lias. *In,* Hemingway, J.E., Wright, J.K. & Torrens, H.S. (editors), *International Field Symposium on the British Jurassic; excursion guide no. 3, NE Yorkshire:* C24–28. University of Keele.

Blake, J.F. 1876. *Class Cephalopoda*: 261–330, pls 1–8. *In,* Tate, R. & Blake, J.F. 1876. *The Yorkshire Lias*. viii + 475 pp., 19 pls. London.

Blau, J., Meister, C., Ebel, R. & Schlatter, R. 2000. Upper Sinemurian and Lower Pliensbachian ammonite faunas from Herford-Diebrock area (NW Germany). *Paläontologische Zeitschrift,* **74:** 259–280, 13 figs.

Boer, G. de 1974. Physiographic evolution. Pp. 271–292. *In,* Rayner, D.H. & Hemingway, J.E. (editors), *The geology and mineral resources of Yorkshire*. Yorkshire Geological Society.

Brown, T. 1837–49. *Illustrations of the Fossil Conchology of Great Britain and Ireland, with descriptions and localities of all the species*. viii + 275 pp., 98 pls. London. [Pp. 1–36, pls 1–30, 35, 37 were issued in 1837].

—— 1889. *An atlas of the Fossil Conchology of Great Britain and Ireland, with descriptions of all the species*. 2nd edition. iv + 117 pp., 98 pls. London.

Buckman, S.S. 1909–1930. *Yorkshire Type Ammonites*, **1, 2,** and *Type Ammonites*, **3–7**. 790 pls. London.

—— 1915. A Palaeontological classification of the Jurassic rocks of the Whitby district; with a zonal table of the ammonites. *In*, Fox-Strangways, C. & Barrow, G. The geology of the country between Whitby and Scarborough, pp. 59–102. *Memoirs of the Geological Survey of Great Britain*.

Cariou, E & Hantzpergue, P. (editors). 1997. Biostratigraphie du Jurassique ouest-européen et méditerranéen: zonations parallèles et distribution des invertébrés et microfossiles. *Bulletin de la Centre Recherche Elf Exploration Production, Mémoire* **17:** 440 pp., 42 pls.

Cox, B.M., Sumbler, M.G. & Ivimey-Cook, H.C. 1998. A formational framework for the Lower Jurassic of England and Wales (onshore area). *British Geological Survey, Onshore Geology Series, Research report*, no. RR/99/01: 65 pp.

Dean, W.T., Donovan, D.T. & Howarth, M.K. 1961. The Liassic ammonite zones and subzones of the north-west European Province. *Bulletin of the British Museum (Natural History), Geology*, **4:** 435–505, pls 63–75.

Dommergues, J-L. 1987. L'evolution chez les Ammonitina du Lias moyen (Carixien, Domérien basal) en Europe occidentale. *Documents des Laboratoires de Géologie de Lyon*, **98:** 296 pp., 12 pls.

—— **& Meister, C.** 1992. Late Sinemurian and early Carixian ammonites in Europe with cladistic analysis of sutural characters. *Neues Jahrbuch für Geologie und Paläontologie*, **185:** 211–37.

Donovan, D.T. 1955. Révision des éspèces décrites dans la 'Monographie des Ammonites' (Lias inférieur) de P. Reynès. *Mémoires de la Société géologique de France*, (N.S.) **73:** 47 pp., 2 pls.

—— 1957. Notes on the species *Cymbites laevigatus* (J. de C. Sowerby) and on the genus *Cymbites* Neumayr. *Geological Magazine*, **94:** 413–420.

—— 1958. The Lower Liassic ammonite fauna from the fossil bed at Langeneckgrat, near Thun (Median Prealps). *Schweizerische Paläontologische Abhandlungen*, **74** (2): 58 pp., 7 pls.

—— 1966. The Lower Liassic ammonites *Neomicroceras* gen. nov. and *Paracymbites*. *Palaeontology*, **9:** 312–18, pl. 53.

—— 1981. Superfamilies Psiloceratacеae and Eoderoceratacеae. Pp. 109–113, 136–138, *In*, Donovan, D. T., Callomon, J.H. & Howarth, M.K. 1981. Classification of the Jurassic Ammonitina. *Systematics Association, London, Special volume*, no. 18: 101–155. London, Academic Press.

—— **& Forsey, G.F.** 1973. Systematics of Lower Liasssic Ammonitina. *The University of Kansas Paleontological Contributions*, **64:** 20 pp., 4 pls.

Dubar, G. & Mouterde, R. 1961. Les faunes d'Ammonites du Lias moyen et supérieur. Vue d'ensemble et bibliographie. *In*, Colloque sur le Lias français, Chambery 1960. *Mémoires du Bureau Recherches Géologiques et Minières*, **4:** 236–244, 263–69.

Dumortier, E. 1867. *Études paléontologiques sur les dépôts jurassiques du Bassin du Rhône*: part 2, Lias inférieur. 252 pp., 50 pls. Paris.

Fischer, J.-C. 1994. *Révision critique de la Paléontologie Française d'Alcide d'Orbigny*. Vol. 1, *Céphalopodes Jurassiques*. xii + 340 pp, 90 pls. Paris.

Fox-Strangways, C. & Barrow, G. 1882. The geology of the country between Whitby and Scarborough. *Memoirs of the Geological Survey of England and Wales*. 60 pp.

—— **&** —— 1915. The geology of the country between Whitby and Scarborough. Second edition, with a chapter on the palaeontological classification of the local Jurassic rocks, by S.S. Buckman. 144 pp. *Memoirs of the Geological Survey of England and Wales*.

Futterer, K. 1893. Die Ammoniten des mittleren Lias von Östringen. *Mitteilungen der grossherzoglich Badischen Geologischen Landesanstalt, Heidelberg*, **2:** 277–343, pls 8–13.

Géczy, B. 1976. *Les Ammonitines du Carixian de la Montagne du Bakony*. 223 pp., 39 pls. Budapest.

Getty, T. A. 1972. *Revision of the Jurassic ammonite family Echioceratidae*. Unpublished thesis, University of London.

—— 1973. A revision of the generic classification of the family Echioceratidae (Cephalopoda, Ammonoidea) (Lower Jurassic). *The University of Kansas Paleontological Contributions*, **63:** 32 pp., 5 pls.

Guérin-Franiatte, S. 1966. *Ammonites du Lias inférieur de France. Psiloceratidae: Arietidae*. **1:** 455 pp.; **2:** 231 pls. CNRS Ed., Paris.

Hauer, F.R. von. 1856. Über die Cephalopoden aus dem Lias der nordöstlichen Alpen. *Denkschriften der Mathematisch-Naturwissenschaftlichen Classe der Kaiserlichen Akademie der Wissenschaften, Wien*. **11:** 86 pp., 25 pls.

Haug, E. 1887. Über die 'Polymorphitidae', eine neue Ammonitenfamilie aus dem Lias. *Neues Jahrbuch fur Mineralogie, Geologie und Paläontologie, Stuttgart*, **1887** (2): 89–163, pls 4, 5.

Hesselbo, S.P. & Jenkyns, H.C. 1995. A comparison of the Hettangian to Bajocian successions of Dorset and Yorkshire. *In*, Taylor, P.D. (editor), *Field Geology of the British Jurassic*: 105–150. Geological Society of London.

——, **Meister, C. & Gröcke, D.R.** 2000. A potential global stratotype for the Sinemurian-Pliensbachian boundary (Lower Jurassic), Robin Hood's Bay, UK; ammonite faunas and isotope stratigraphy. *Geological Magazine*, **137:** 601–607.

Hollingworth, N.T.J., Ward, D.J., Simms, M.J. & Clothier, P. 1990. A temporary exposure of Lower Lias (Late Sinemurian) at Dimmer Camp, Castle Cary, Somerset, south-west England. *Mesozoic Research*, **2:** 163–180, 4 pls.

Howard, A.S. 1985. Lithostratigraphy of the Staithes Sandstone and Cleveland Ironstone formations (Lower Jurassic) of North-east Yorkshire. *Proceedings of the Yorkshire Geological Society*, **45:** 261–275.

Howarth, M.K. 1955. Domerian of the Yorkshire coast. *Proceedings of the Yorkshire Geological Society*, **30:** 147–175, pls 10–13.

—— 1962. The Yorkshire type ammonites and nautiloids of Young and Bird, Phillips, and Martin Simpson. *Palaeontology*, **5:** 93–127, pls 13–19.

—— 1978. The stratigraphy and ammonite fauna of the Upper Lias of Northamptonshire. *Bulletin of the British Museum (Natural History), Geology*, **29:** 235–288, pls 1–9.

—— 1996. Obituary: Leslie Bairstow (1907–1995). *Annual Report of the Geological Society of London*, **1995:** 16–17.

—— **& Donovan, D. T.** 1964. *Ammonites of the Liassic family Juraphyllitidae in Britain*. Palaeontology, **7:** 286–305, pls 48, 49.

Hyatt, A. 1889. Genesis of the Arietidae. *Smithsonian Contributions to Knowledge, Washington*, no. 673: xi + 238 pp., 14 pls.

Jaworski, E. 1931. *Arnioceras geometricum* Oppel 1856 und verwandte Spezies nebst einem Anhang über *Ammonites natrix* v. Schlotheim 1820. *Neues Jahrbuch fur Mineralogie, Geologie und Paläontologie, Stuttgart, Beilage Band*, **65:** 83–140, pls 2–6.

Kent, P.E. 1974. Structural history. Pp. 13–28, *In*, Rayner, D.H. & Hemingway, J.E. (editors), *The geology and mineral resources of Yorkshire*. Yorkshire Geological Society.

Kummel, B. 1956. Post-Triassic nautiloid genera. *Bulletin of the Museum of Comparative Zoology*, **114** (7): 321–494, 28 pls.

Monke, H. 1888. Die Liasmulde von Herford in Westfalen. *Verhandlungen des naturhistorischen Vereines der preussischen Rheinlande, Westfalens und des Reg.-Bezirks Osnabrück*, **45** (5): 125–294, pl. 2/3.

Murchison, R.I. 1834. *Outline of the geology in the neighbourhood of Cheltenham*. 40 pp., 1 pl. Cheltenham.

Orbigny, A. d'. 1842–51. *Paléontologie française. Terrains oolitiques ou jurassiques*. **1:** *Céphalopodes*. 642 pp., 234 pls. Paris.

—— 1849. *Prodrome de Paléontologie stratigraphique universelle des animaux mollusques et rayonnés*, **1:** lx + 396 pp. Paris.

Phelps, M.C. 1985. A refined ammonite biostratigraphy for the middle and upper Carixian (*ibex* and *davoei* Zones, Lower Jurassic) in North-West Europe and stratigraphical details of the Carixian-Domerian boundary. *Geobios*, **18:** 321–361.

Phillips, J. 1829. *Illustrations of the Geology of Yorkshire; or, a description of the strata and organic remains of the Yorkshire coast*. xvi + 192 pp., 14 pls. York.

—— 1835. *Illustrations of the Geology of Yorkshire; or, a description of the strata and organic remains. Part 1 – The Yorkshire coast*. 2nd edition. xii + 184 pp, 23 pls. London.

—— 1863–1909. A monograph of British Belemnitidae. *Monographs of the Palaeontographical Society*, London: 136 pp., 36 pls.

—— 1875. *Illustrations of the Geology of Yorkshire; or, a description of the strata and organic remains. Part 1 – The Yorkshire coast*. 3rd edition, edited by R. Etheridge. xii + 354 pp., 28 pls. London.

Pia, J. von. 1914. Untersuchungen über die Gattung *Oxynoticeras* und einige damit zusammenhängende allgemeine Fragen. *Abhandlungen der Kaiserlich königlichen geologischen Reichsanstalt, Wien*, **23:** iv + 179 pp., 13 pls.

Portlock, J. E. 1843. *Report on the Geology of the county of Londonderry, and of parts of Tyrone and Fermanagh*. xxxi + 784 pp., 54 pls. Dublin and London.

Powell, J.H. 1984. Lithostratigraphical nomenclature of the Lias Group in the Yorkshire Basin. *Proceedings of the Yorkshire Geological Society*, **45:** 51–57.

Quenstedt, F.A. 1843. *Das Flözgebirge Württembergs*. iv + 558 pp. Tübingen.

—— 1845–49. *Petrefactenkunde Deutschlands. Die Cephalopoden*. Pp. 1–104, pls 1–6 (1845); 105–184, pls 7–14 (1846); 185–264, pls 15–19 (1847); 265–472, pls 20–29 (1848); 473–580, pls 30–36 (1849). Tübingen.

—— 1856–58. *Der Jura*. Pp. 1–576, pls 1–72 (1856); 577–824, pls 73–100 (1857); 825–842 (1858). Tübingen.

—— 1882–1885. *Die Ammoniten des Schwäbischen Jura. I, Der Schwarze Jura (Lias)*. Pp. 1–48, pls 1–6 (1882); 49–96, pls 7–12 (1883); 97–240, pls 13–30 (1884); 241–440, pls 31–54 (1885). Tübingen.

Reynès, P. 1879. *Monographie des Ammonites*. Atlas, 58 pls. Marseilles and Paris.

Roemer, F.A. 1835–36. *Die Versteinerungen des Norddeutschen Oolithen-Gebirges*. Pp. 1–74 (1835); 75–218 (1836); 16 pls. Hannover.

Schindewolf, O.H. 1961. Die Ammoniten-gattung *Cymbites* im Deutschen Lias. *Palaeontographica*, **117A:** 193–232, pls 29–31.

Schlatter, R. 1980. Biostratigraphie und Ammonitenfauna des Unter-Pliensbachium im Typusgebiet (Pliensbach, Holzmaden und Nürtingen, Württemberg, Südwestdeutschland). *Stuttgarter Beiträge zur Naturkunde*, (B) **65:** 261 pp., 25 beilagen, 23 pls.

Schlegelmilch, R. 1976. *Die Ammoniten des süddeutschen Lias*. 212 pp., 52 pls. Stuttgart & New York.

—— 1992. *Die Ammoniten des süddeutschen Lias; 2, neubearbeitete und ergänzte Auflage*. 241 pp., 58 pls. Stuttgart, Jena & New York.

Simpson, M. 1843. *A monograph of the ammonites of the Yorkshire Lias*. 60 pp. London.

—— 1855. *The fossils of the Yorkshire Lias; described from Nature*. 149 pp. London and Whitby.

—— 1868. A guide to the geology of the Yorkshire coast. 64 pp. Whitby.

—— 1884. *The fossils of the Yorkshire Lias; described from Nature*. 2nd edition, xxiii + 256 pp. London and Whitby.

Söll, H. 1957. Stratigraphie und Ammonitenfauna des mittleren und oberen Lias-ß (Lotharingien) in Mittel Württemberg. *Geologisches Jahrbuch*, **72:** 367–434, pls 17–20.

Sowerby, J. 1812–22. *The Mineral Conchology of Great Britain*: vols 1–3, 4 (part): pls 1–383. London.

Sowerby, J. de C. 1823–46. *The Mineral Conchology of Great Britain;* vols 4 (part)–7: pls 384–648. London.

Spath, L.F. 1914. On the development of *Tragophylloceras loscombi* (J. Sowerby). *Quarterly Journal of the Geological Society of London*, **70:** 336–362, pls 48–50.

—— 1923*a*. Correlation of the Ibex and Jamesoni Zones of the Lower Lias. *Geological Magazine*, **60:** 6–11.

—— 1923*b*. The ammonites of the Shales-with-Beef. *Quarterly Journal of the Geological Society of London*, **79**: 66–88.

—— 1924. The ammonites of the Blue Lias. *Proceedings of the Geologists' Association*, **35:** 186–211, pl.18.

—— 1925*a*–26*a*. Notes on Yorkshire ammonites. *The Naturalist, Hull*, **1925:** 107–112, 137–141, 167–172, 201–206, 263–269, 299–306, 327–331, 359–364; **1926:** 45–49, 137–140, 169–171, 265–268, 321–326.

—— 1926*b*. The Black Marl of Black Ven and Stonebarrow in the Lias of the Dorset coast. Part 2, Palaeontology. *Quarterly Journal of the Geological Society of London*, **82:** 165–179, pls 9–11.

—— 1928. The Belemnite Marls of Charmouth, a series in the Lias of the Dorset coast. V, The ammonites. *Quarterly Journal of the Geological Society of London*, **84:** 222–232, pls 16, 17.

—— 1938. *A catalogue of the ammonites of the Liassic family Liparoceratidae*. British Museum (Natural History), London. 191 pp., 26 pls.

—— 1956. The Liassic ammonite faunas of the Stowell Park Borehole. *Bulletin of the Geological Survey of Great Britain*, **11:** 140–164.

Tate, R. & Blake, J.F. 1876. *The Yorkshire Lias*. viii + 475 pp., 19 pls. London.

Thevenin, A. 1907. Types du Prodrome de Paléontologie de d'Orbigny. *Annales de Paléontologie*, **2:** 89–96, pls 7, 8.

Trueman, A.E. 1919. The evolution of the Liparoceratidae. *Quarterly Journal of the Geological Society of London*, **74:** 247–298, pls 21–25.

—— **& Williams, D.M.** 1925. Studies in the ammonites of the family Echioceratidae. *Transactions of the Royal Society of Edinburgh*, **53** (3) (34): 699–739, pls 1–4.

Tutcher, J. W. & Trueman, A. E. 1925. The Liassic rocks of the Radstock district, Somerset. *Quarterly Journal of the Geological Society of London*, **81:** 595–662, pls 38–41.

Vadasz, M. E. 1908. Die Unterliassiche Fauna von Alsórákos im Komitat Nagyküküllö. *Mitteilungen aus dem Jahrbuche der Königlich Ungarischen Geologischen Reichsanstalt*, **16** (5): 309–406, pls 6–11.

Versey, H.C. 1939. The Tertiary history of east Yorkshire. *Proceedings of the Yorkshire Geological Society*, **23:** 302–314, pl. 15.

Withers, T.H. 1933. On the Decapod Crustacean *Aeger laevis* (Blake). *Annals and Magazine of Natural History*, **11:** 159–162, pl. 4, figs 1–3.

Wright, T. 1878. A monograph on the Lias ammonites of the British Islands. Part 1: 1–48, pls 1–8. *Monographs of the Palaeontographical Society*, London (Publication no. 147, part of vol.32 for 1878).

—— 1879. A monograph on the Lias ammonites of the British Islands. Part 2: 49–164, pls 9–18. *Monographs of the Palaeontographical Society*, London (Publ. no.154, part of vol.33 for 1879).

—— 1880. A monograph on the Lias ammonites of the British Islands. Part 3: 165–264, pls 19–40. *Monographs of the Palaeontographical Society*, London (Publ. no.160, part of vol.34 for 1880).

—— 1881. A monograph on the Lias ammonites of the British Islands. Part 4: 265–328, pls 22A, 22B, 41–48. *Monographs of the Palaeontographical Society*, London (Publ. no.165, part of vol.35 for 1881).

—— 1882. A monograph on the Lias ammonites of the British Islands. Part 5: 329–400, pls 49–52, 52A, 53–69. *Monographs of the Palaeontographical Society*, London (Publ. no.173, part of vol.36 for 1882).

Young, G.M. & Bird, J. 1822. *A Geological Survey of the Yorkshire Coast: describing the Strata and Fossils occurring between the Humber and the Tees, from the German Ocean to the Plain of York*. 336 pp., 17 pls. Whitby.

—— **&** —— 1828. *Ibid*. 2nd edn., enlarged. 368 pp., 17 pls. Whitby.

Zieten, C.H. von. 1830–33. *Die Versteinerungen Württembergs*. Pp. 1–16, pls 1–12 (1830); 17–32, pls 13–24 (1831); 33–64, pls 25–48 (1832); 65–102, pls 49–72 (1833). Stuttgart.

Bulletin of The Natural History Museum
Geology Series

Earlier Geology *Bulletins* are still in print. The following can be ordered from Cambridge University Press or Intercept (addresses on inside front cover). Where the complete backlist is not shown, this may also be obtained from the same addresses.

Volume 51

No. 1 A synopsis of neuropteroid foliage from the Carboniferous and Lower Permian of Europe—The Upper Cretaceous ammonite *Pseudaspidoceras* Hyatt, 1903, in north-eastern Nigeria—The pterodactyloids from the Purbeck Limestone Formation of Dorset. 1995. Pp. 1–88. **£37.50**

No. 2 Palaeontology on the Qahlah and Simsima Formations (Cretaceous, Late Campanian-Maastrichtian) of the United Arab Emirates-Oman Border Region—Preface—Late Cretaceous carbonate platform faunas of the United Arab Emirates-Oman border region—Late Campanian-Maastrichtian echinoids from the United Arab Emirates-Oman border region—Maastrichtian ammonites from the United Arab Emirates-Oman border region—Maastrichtian nautiloids from the United Arab Emirates-Oman border region—Maastrichtian Inoceramidae from the United Arab Emirates-Oman border region—Late Campanian-Maastrichtian Bryozoa from the United Arab Emirates-Oman border region—Maastrichtian brachiopods from the United Arab Emirates-Oman border region—Late Campanian-Maastrichtian rudists from the United Arab Emirates-Oman border region. 1995. Pp. 89–305. **£37.50**

Volume 52

No. 1 Zirconlite: a review of localities worldwide, and a compilation of its chemical compositions—A review of the stratigraphy of Eastern Paratethys (Oligocene–Holocene)—A new protorichthofenioid brachiopod (Productida) from the Upper Carboniferous of the Urals, Russia—The Upper Cretaceous ammonite *Vascoceras* Choffat, 1898 in north-eastern Nigeria. 1996. Pp. 1–89. **£43.40**

No. 2 Jurassic bryozoans from Baltów, Holy Cross Mountains, Poland—A new deep-water spatangoid echinoid from the Cretaceous of British Columbia, Canada—The cranial anatomy of *Rhomaleosaurus thorntoni* Andrews (Reptilia, Plesiosauria)—The first known femur of *Hylaeosaurus armatus* and re-identification of ornithopod material in The Natural History Museum, London—Bryozoa from the Lower Carboniferous (Viséan) of County Fermanagh, Ireland. 1996. Pp. 91–171. **£43.40**

Volume 53

No. 1 The status of '*Plesictis*' *croizeti*, '*Plesictis*' *gracilis* and '*Lutra*' *minor:* synonyms of the early Miocene viverrid *Herpestides antiquus* (Mammalia, Carnivora)—*Baryonyx walkeri,* a fish-eating dinosaur from the Wealden of Surrey—The Cretaceous-Miocene genus *Lichenopora* (Bryozoa), with a description of a new species from New Zealand. 1997. Pp. 1–78. **£43.40**

No. 2 Ordovician trilobites from the Tourmakeady Limestone, western Ireland—Ordovician Bryozoa from the Llandeilo Limestone, Clog-y-fran, near Whitland, South Wales—New Information on Cretaceous crabs. 1997. Pp.79–139. **£43.40**

Volume 54

No. 1 The Jurassic and Lower Cretaceous of Wadi Hajar, southern Yemen—Ammonites and nautiloids from the Jurassic and Lower Cretaceous of Wadi Hajar, southern Yemen. 1998. Pp. 1–107. **£43.40**

No. 2 Caradoc brachiopods from the Shan States, Burma (Myanmar)—A review of the stratigraphy and trilobite faunas from the Cambrian Burj Formation in Jordan—The first Palaezoic rhytidosteid: *Trucheosaurus major* (Woodward, 1909) from the late Permian of Australia, and a reassessment of the Rhytidosteidae (Amphibia, Temnospondyli)—The rhynchonellide brachiopod *Isopoma* Torley and its distribution. 1998. Pp.109–163. **£43.40**

Volume 55

No. 1 Latest Paleocene to earliest Eocene bryozoans from Chatham Island, New Zealand. 1999. Pp. 1–45. **£43.40**

No. 2 A new stylophoran echinoderm, *Juliaecarpus milnerorum*, from the late Ordovician Upper Ktaoua Formation of Morocco—Late Cretaceous-early Tertiary echinoids from northern Spain: implications for the Cretaceous-Tertiary extinction event. 1999. Pp 47–137. **£43.40**

Volume 56

No. 1 A review of the history, geology and age of Burmese amber (Burmite—A list of type and figured specimens of insects and other inclusions in Burmese amber—A preliminary list of arthropod families present in the Burmese amber collection at The Natural History Museum, London—The first fossil prosopistomatid mayfly from Burmese amber (Ephemeroptera; Prosopistomatidae)—The most primitive whiteflies (Hemiptera; Aleyrodidae; Bernaeinae subfam. nov.) from the Mesozoic of Asia and Burmese amber, with an overview of Burmese amber hemipterans—A new genus and species of Lophioneuridae from Burmese amber (Thripida (=Thysanoptera): Lophioneurina),—*Burmapsilocephala cockerelli*, a new genus and species of Asiloidea (Diptera) from Burmese amber—Phantom midges (Diptera: Chaoboridae) from Burmese amber—An archaic new genus of Evaniidae (Insecta: Hymenoptera) and implications for the biology of ancestral evanioids—Digger Wasps (Hymenoptera, Sphecidae) in Burmese Amber—*Electrobisium acutum* Cockerell, a cheiridiid pseudoscorpion from Burmese amber, with remarks on the validity of the Cheiridioidea (Arachnida, Chelonethi). 2000. Pp. 1–83. **£43.40**

No. 2 *Terebratula californiana* Küster, 1844, and reappraisal of west coast north American brachiopod species referred to the genus *Laqueus* Dall, 187—Late Campanian-Maastrichtian corals from the United Arab Emirates-Oman border region—*Rhombocladia dichotoma* (M'Coy, 1844) [Fenestrata, Bryozoa]: designation of a lectotype—The Gough's Cave human fossils: an introduction—The Creswellian (Pleistocene) human axial skeletal remains from Gough's Cave (Somerset, England)—The Creswellian (Pleistocene) human lower limb remains from Gough's Cave (Somerset, England). 2000. Pp. 85–161. **£43.40**

Volume 57

No. 1 Fossil pseudasturid birds (Aves, Pseudasturidae) from the London Clay—*Novocrania*, a new name for the genus *Neocrania* Lee & Brunton, 1986 (Brachiopoda, Craniida), preoccupied by *Neocrania* Davis, 1978 (Insecta, Lepidoptera)—The Creswellian (Pleistocene) human upper limb remains from Gough's Cave (Somerset, England)—Gough's Cave 1 (Somerset, England): a study of the hand bones—A revision of the English Wealden Flora, III: Czekanowskiales, Ginkgoales & allied Coniferales. 2001. Pp. 1–82. **£43.40**

No. 2 The Cenozoic Brachiopod *Terebratula*: its type species, neotype, and other included species—Gough's Cave 1 (Somerset, England): a study of the pectoral girdle and upper limbs—Systematic affinity of *Acroporella assurbanipali* Elliott (Dasycladaceae), with notes on the genus *Neomeris* Palynological zonation of Mid-Palaeozoic sequences from the Cantabrian Mountains, NW Spain: implications for inter-regional and interfacies correlation of the Ludford/Přídolí and Silurian/Devonian boundaries, and plant dispersal patterns. 2001. Pp. 83–162. **£43.40**

Volume 58

No. 1 Gough's Cave 1 (Somerset, England): a study of the axial skeleton—Upper Ordovician brachiopods from the Anderken Formation, Kazakhstan: their ecology and systematics. 2002. Pp. 1–80. **£43.40**

CONTENTS

CAMBRIDGE
UNIVERSITY PRESS

0968-0462(200211)58:2;1-6

Bulletin of The Natural History Museum
GEOLOGY SERIES
Vol. 58, No. 2, November 2002

S. 186 A

THE NATURAL HISTORY MUSEUM
9 JUL 2003
PRESENTED
PALAEONTOLOGY LIBRARY

Bulletin of
The Natural History
Museum

Geology Series

VOLUME 58 SUPPLEMENT 26 JUNE 2003

The *Bulletin of The Natural History Museum* (formerly: *Bulletin of the British Museum (Natural History)*), instituted in 1949, is issued in four scientific series, Botany, Entomology, Geology (incorporating Mineralogy) and Zoology.

The Geology Series is edited in the Museum's Department of Palaeontology

Keeper of Palaeontology:	Dr N. MacLeod
Editor of Bulletin:	Dr M.K. Howarth
Assistant Editor:	Mr C. Jones

Papers in the *Bulletin* are primarily the results of research carried out on the unique and ever-growing collections of the Museum, both by the scientific staff and by specialists from elsewhere who make use of the Museum's resources. Many of the papers are works of reference that will remain indispensable for years to come. All papers submitted for publication are subjected to external peer review before acceptance.

SUBSCRIPTIONS *Bulletin of the Natural History Museum*, Geology Series (ISSN 0968-0462) is published twice a year (one volume per annum) in June and November. Volume 58 will appear in 2002. The 2002 subscription price (excluding VAT) of a volume, which includes print and electronic access, is £88.00 (US $155.00 in USA, Canada and Mexico). The electronic-only price available to institutional subscribers is £79.00 (US $140.00 in USA, Canada and Mexico).

ORDERS Orders, which must be accompanied by payment, may be sent to any bookseller, subscription agent or direct to the publisher: Cambridge University Press, The Edinburgh Building, Shaftesbury Road, Cambridge CB2 2RU, UK; or in the USA, Canada and Mexico: Cambridge University Press, Journals Department, 40 West 20th Street, New York, NY 1011-4211, USA. EU subscribers (outside the UK) who are not registered for VAT should add VAT at their country's rate. VAT registered members should provide their VAT registration number. Japanese prices for institutions (including ASP delivery) are available from Kinokuniya Company Ltd, P.O. Box 55, Chitose, Tokyo 156, Japan. Prices include delivery by air. Postmaster: send address changes in USA, Canada and Mexico to: Bulletin of the Natural History Museum. Geology Series, Cambridge University Press, 110 Midland Avenue, Port Chester, New York, NY 105783-4930. Claims for missing issues should be made immediately on receipt of the subsequent issues.

Orders and enquiries for issues prior to 2002 should be sent to: Intercept Ltd., P.O. Box 716, Andover, Hampshire SP10 1YG, *Telephone*: (01264) 334748, *Fax*: (01264) 334058, *Email*: intercept@andover.co.uk, *Internet*: http:/www.intercept.co.uk

ADVERTISING Apply to the Publisher. Address enquiries to the Advertising Promoter.

COPYRIGHT AND PERMISSIONS This journal is registered with the Copyright Clearance Center, 222 Rosewood Drive, Danvers, MA 01923, USA. Organizations in the USA who are also registered with CCC may therefore photocopy material (beyond the limits permitted by Section 107 and 108 of US Copyright law) subject to payment to CCC of the per-copy fee of $16.00. This consent does not extend to multiple copying for promotional or commercial purposes. Code 0968-0462/2002 $16.00. ISI Tear Sheet Service, 3501 Market Street, Philadelphia, PA 19104, USA, is authorised to supply single photocopies of separate articles for private use only. Organizations authorised by the UK Copyright Licensing Agency may also copy material subject to the usual conditions. For all other use, permission should be sought from Cambridge University Press.

No part of this publication may otherwise be reproduced, stored or distributed by any means without permission in writing from Cambridge University Press, acting for the copyright holder.

Copyright © 2003 The Natural History Museum

ELECTRONIC ACCESS This journal is included in the Cambridge Journals Online service which can be found at: http://journals.cambridge.org

For further information on other Press titles access http://uk.cambridge.org or http://us.cambridge.org

World list abbreviation: *Bull. nat. Hist. Mus. Lond.* (Geol.)

ISSN 0968–0462

The Natural History Museum
Cromwell Road
London SW7 5BD

Geology Series
Vol. 58, Supplement, pp. 1–81
Issued 26 June 2003

Typeset by Ann Buchan (Typesetters), Middlesex
Printed by University Press, Cambridge

Bull. nat. Hist. Mus. Lond. (Geol.) **58**(supp): 1–21 Issued 26 June 2003

Gough's Cave 1 (Somerset, England): a study of the pelvis and lower limbs

THE NATURAL HISTORY MUSEUM
PRESENTED
PALAEONTOLOGY LIBRARY

ERIK TRINKAUS
Department of Anthropology, Campus Box 1114, Washington University, St. Louis, MO 63130, USA

SYNOPSIS. The lower limb remains of Gough's Cave 1 retain most of the pelvis, both femora, one complete tibia and portions of the other, sections of both fibulae, two tarsals and three metatarsals. They are those of a largely average European Mesolithic young adult male. Overall diaphyseal robusticity is generally similar to that of other Mesolithic specimens, even though the fibula and third metatarsal appear gracile. Musculo-ligamentous attachment areas are generally weakly marked. The proximal femora and the femoral diaphyses exhibit a clear asymmetry, especially in their neck-shaft angles and diaphyseal dimensions, which is is accompanied in the pelvis by a greater degree of left iliac lateral flare. These aspects are associated with a pelvis that combines several distinctly male characteristics with an overall pelvic aperture shape which is female.

INTRODUCTION

The Gough's Cave 1 skeleton retains a largely complete pelvis (which has been permanently articulated), both femora very well preserved, most of the right tibia and fibula, portions of the left tibia and fibula, the complete right talus and cuboid, and three complete metatarsals. As such, Gough's Cave 1 retains essentially complete anatomy on at least one side from the L5-S1 articulation to the talo-calcaneal articulation, with additional data from the subtalar skeleton.

MATERIALS

The description of the Gough's Cave 1 lower limb remains includes extensive osteometrics (Tables 1–5, 10, 11, 16–21). To evaluate some of these dimensions and the resultant proportions, comparative summary statistics (as available) are included for other European Mesolithic remains. These include remains from the sites of Arene Candide, Los Azules, Bichon, Birsmatten, Bottendorf, Riparo Continenza, Culoz, Gramat, Grotte des Enfants, Hoëdic, Holmegård, Koelbjerg, Kosor Glas, Loschbour, Moita do Sebastião, Molara, Mondeval, Muge (N = ≤57), Obercassel, Parabita, Le Peyrat, Le Rastel, Rochereil, Romanelli, Romito, Riparo Tagliente, San Teodoro, Sejrø, Téviec, Unseburg, Uzzo, Vaegensø, Vatte di Zambana, and Veryier 1 (Pittard & Sauter, 1946; Graziosi, 1947; Combier & Genet-Varcin, 1959; Barral & Primard, 1962; Genet-Varcin *et al.*, 1963; Patte, 1968; Cremonesi *et al.*, 1972; Ferembach, 1976; Paoli *et al.*, 1980; Holliday, 1995; Holt, 1999; Churchill, pers. comm.). These comparative remains vary in age from terminal Paleolithic to well within the western European Mesolithic, approximately between 12,000 and 6,000 years B.P. They should bracket reasonably well the Gough's Cave 1 remains in age.

The most detailed metrics are available for the Gramat, Hoëdic, Rochereil and Téviec remains, but the other specimens fill out the samples for the more commonly reported measurements (e.g., long bone lengths and diaphyseal diameters). For diaphyseal metrics, the femoral (proximal and midshaft), tibial (proximal) and fibular (midshaft) samples are dominated by the large sample from Muge. Consequently, when the Muge sample is significantly different from the remainder of this 'Mesolithic' sample, summary statistics for it are provided in addition to those for the total sample.

Of the 39 comparative specimens other than those from Muge, 26 are male, 12 are female and 1 has unknown sex. In the Muge femoral sample (the largest sample for the bones providing relevant data), 33 are male and 24 are female. This is therefore a male biased sample, but given the probable male sex of Gough's Cave 1, this is not inappropriate.

METHODS

The majority of the metric comparisons involve traditional osteometrics and associated indices. For these, the values for Gough's Cave 1, the total 'Mesolithic' sample, and the male Mesolithic samples are provided as mean ± standard deviation in the appropriate text position. Except for Gough's Cave 1, right and left values were averaged prior to computing the sample summary statistics.

In addition, it is appropriate to include cross-sectional geometric parameters (cross-sectional areas and second moments of area) into the description and analysis of the long bone diaphyses of fossil hominids. Consequently, these data are included for Gough's Cave 1 in the description of the femoral and tibial diaphyses (Tables 6, 8, 12, 14). Comparative data are less abundant. They have been generated for the full femoral and tibial diaphyses (five sections each) by S.E. Churchill and myself for most of the Mesolithic remains from Gramat, Hoëdic, Rochereil and Téviec; additional data for the proximal and midshaft femur and midshaft tibia are available from B. Holt (1999) (see Tables 7, 9, 13, 15 for sample sizes).

All of the Gough's Cave 1 and most of the comparative Mesolithic cross sections were reconstructed using transcriptions of the subperiosteal contours and interpolations of the endosteal contours from anterior, posterior, medial and lateral cortical thicknesses. These were done at 20%, 35%, 50%, 65% and 80% of biomechanical length, as preservation permitted. The subperiosteal contours were taken using silicone putty molds [using Cuttersil Putty Plus (Heraeus Kulzer Inc.)] perpendicular to the diaphyseal axis, which were then transcribed onto paper. Cortical thicknesses were measured on antero-posterior and medio-lateral radiographs of the diaphyses, correcting for parallax using the subperiosteal diameters. The endosteal contours were manually interpolated using the cortical thickness rectangle to limit their extent and the subperiosteal contours as a guide. The resultant cross sections were digitized and cross-sectional geometric parameters were computed using a PC-DOS version

© The Natural History Museum, 2003

(Eschman, 1992) of SLICE (Nagurka & Hayes, 1970). All sections were digitized twice and the results averaged.

From this, six primary measurements were computed. These included total subperiosteal (TA) and cortical (CA) areas, from which medullary area (MA) can be computed, as well as the second moments of area relative to the antero-posterior (I_y) and medio-lateral (I_x) axes, the maximum second moment of area (I_{max}), and the perpendicular to I_{max} (I_{min}). The polar moment of area (J, or I_p), a measure of torsional rigidity and overall strength, is the sum of any two perpendicular second moments of area (usually $I_{max} + I_{min}$, but also equal to $I_x + I_y$)

For a few of the Mesolithic comparative specimens, subperiosteal contour molds were unavailable. For these, the cross-sectional parameters were computed using standard ellipse formulae (Runestad *et al.*, 1993) from the subperiosteal diameters and cortical thicknesses. Given the antero-posterior and medio-lateral orientations of the radiographs, the resultant cross-sectional measures include only cross-sectional areas and antero-posterior (I_x) and medio-lateral (I_y) second moments of area, plus the polar moment of area computed as the sum of I_x and I_y. For these, the resultant computed values were corrected for parallax and non-ellipse shapes of the cross-sections using least squares regressions between the radiographically determined measurements and the cross-sectional values obtained from digitizing the same sections of the other Mesolithic femora or tibiae.

To assess proportions in the Gough's Cave 1 diaphyses using cross-sectional parameters, three shape indices were computed, percent cortical area (%CA: (CA/TA) × 100), I_x/I_y (as a ratio) and I_{max}/I_{min} (also as a ratio). The last two assess diaphyseal shape at the cross section locations, the former with respect to the anatomical axes and the latter with respect to the axis of maximum bending rigidity. The second is especially appropriate in the proximal femoral diaphysis and along the tibial diaphysis, given varying degrees of torsion in the proximal epiphyses of these bones.

To assess robusticity, and hence to scale the cross sectional parameters to appropriate body size and beam characteristics (Ruff *et al.*, 1993), cortical areas (as a reflection of axial loading levels) and polar moments of area (as a measure of resistance to bending and torsional loads) should be plotted against appropriate powers of long bone lengths adjusted for variance in body laterality and crural indices. Cortical areas should scale to body mass, which is proportional to femoral length cubed (Ruff *et al.*, 1993). Polar moments of area should scale to body mass times beam length, all raised to the four-thirds power (Ruff *et al.*, 1993). In other words, for the femur $J \propto (FL^3 \times FL)^{4/3} = FL^{16/3}$ and for the tibia $J \propto (FL^3 \times TL)^{4/3} = FL^4 \times TL^{4/3}$.

However, given the apparently similar degrees of body laterality and crural indices across these European terminal Upper Paleolithic and Mesolithic samples, as is expected by theoretical considerations (Ruff, 1991) and supported by current data (Holliday, 1995; Holliday & Churchill, 2003), it is appropriate to simply scale logged cortical areas and logged polar moments of area against logged bone length. Since this approach avoids determining the actual allometric scaling coefficient for each of these bones, it is employed here.

In addition, even though comparative data are not available, metatarsal midshaft cross-sectional geometric measures are provided (Table 20). They were computed from radiographically determined subperiosteal diameters and cortical thicknesses using ellipse formulae (Runestad *et al.*, 1993) after the radiographic measurements were corrected for parallax using the osteometrically determined diaphyseal diameters.

Fig. 1 Ventral (left) and dorsal (right) views of the sacrum; × 0.75.

PELVIC REMAINS

Inventory

The pelvis is conserved fully articulated, with the two coxal bones in articulation with the sacrum and with each other at the pubic symphysis (Figs 1–5). As a result, overall dimensions and proportions are readily ascertainable, but the configurations of the sacroiliac and pubic symphyseal surfaces are not observable. In addition, there is a bolt transversely through the sacroiliac articulations, the S2 and the dorsal ilia which maintains the pelvis in articulation. It is only apparent on the external ilia just dorso-cranial of the dorsal greater sciatic notches.

Despite minor abrasion to several of the margins, there is no apparent distortion to any of these bones, and adhering matrix is thin and scattered. This makes morphological observations on them highly reliable.

Sacrum. The sacrum is largely complete from the cranial S1 to the caudal S5, with minor abrasion to several of the edges. The primary areas of abrasion are across the sacral promontory producing a rounded margin, and on most of the S1 cranial disk surface and the cranial surfaces of the alae. There is also minor surface bone loss along the edges of the sacro-iliac articulations, but it is largely obscured by their articulations with the ilia. There is also a rounded hole dorso-ventrally through the S2 body, the result of a bolt placed through it for the previous mounting of the articulated skeleton in the Gough's Cave Museum.

Right Coxal Bone (No. 1.1/23). The right coxal bone is essentially intact. There is abrasion to the ventro-caudal ischio-pubic ramus margin just ventral of the ischial tuberosity, to the internal margin of the mid iliac crest, and along the superior auricular margin extending on to the dorsal arcuate line. In addition, the middle of the iliac fossa has an area of adhering matrix and a small hole (maximum diameter: 6.5mm) in the middle of that area. All of the iliac crest is present, even though it is partially fused.

Left Coxal Bone (No. 1.1/24). The left coxal bone is similarly intact without distortion. It shares the same abrasion to the ventro-caudal margin of the ischio-pubic ramus just ventral of the ischial tuberosity and to the cranial margin of the auricular surface and adjacent arcuate line. In addition, there is a notch of bone missing from the ventral ilium just below the anterior superior iliac spine, and there is a large hole (31.8mm dorso-ventral and 23.0mm cranio-caudal) in the middle of the iliac fossa. The iliac crest is present ventrally, but it was (at least partially) unfused between the iliac pillar and the iliac tuberosity and is absent from that portion of the ilium.

Pelvic Morphology

Sacrum (Table 1; Fig. 1). The Gough's Cave 1 sacrum retains five clear sacral vertebrae. In this they follow the pattern of the majority of recent humans (Schultz, 1930). Despite damage in the regions of the auricular surfaces, it appears that the lateral portions of the sacrum and their dorsal neural arches were fully fused at the time of death. However, the bodies remain largely separate across their ventral margins. The degree of fusion of the sacral bodies and the pattern of fusion (from caudal to cranial) primarily reflects the young adult age of the individual and not an unusual pattern or degree of sacral fusion.

The ventral length of the Gough's Cave 1 sacrum of ca.123.7mm is large for a recent human (Radlauer, 1908). In combination with a mean femoral bicondylar length of 436.0mm, it provides a length index of ca.28.4. This value high for a recent human sample (Warren, 1897; Trinkaus, 1983) but it is only slightly above a Mesolithic sample mean (27.6 ± 2.2, N = 14) and very close to the mean of a Mesolithic male sample (28.0 ± 2.2, N = 11).

Table 1 Osteometrics of the Gough's Cave 1 sacrum.

Ventral height chord (M-2)[1]	(123.7)
Ventral height arc (M-1)	(131.5)
Ventral S1 height chord[2]	(32.2)
Ventral S2 height chord	30.2
Ventral S3 height chord	25.9
Ventral S4 height chord	21.8
Ventral S5 height chord	19.5
Dorsal height chord (M-3)	124.7
Antero-cranial breadth (M-5)	(110.0)
Mid sacral breadth (M-9)	83.0
Base dorso-ventral diameter (M-18)	(29.0)
Base transverse diameter (M-19)	46.2
Base sagittal angle[3]	81°
Base/S1 sagittal angle[4]	60°
Canal dorso-ventral diameter (M-16)	17.6
Canal transverse diameter (M-17)	30.6

[1] (M-xx) refers to the equivalent measurement in R. Martin's *Lehrbuch der Anthropologie* (see Bräuer, 1988).
[2] Cranio-caudal distance between the cranial and caudal margins of each ventral body.
[3] The angle, in the median sagittal plane, between the tangent to the S1 vertebral disk surface and the ventral height chord from S1 to S5.
[4] The angle, in the median sagittal plane, between the tangent to the S1 vertebral disk surface and the ventral surface of S1.

The maximum antero-cranial breadth of the Gough's Cave 1 sacrum (ca.110.0mm) is moderate compared to other Mesolithic remains, and it provides an index against ventral height of 88.9. This value is only slightly below that of a highly variable Mesolithic sample (91.4 ± 8.9, N = 16) and removing the three females from the sample moves the mean close to the Gough's Cave 1 value (Mesolithic males: 89.8 ± 8.4, N = 13).

The sacrum presents a modest degree of ventral concavity, as is indicated by an index of the ventral chord to the ventral arc of ca.94.1. This index is well above the mean of a Euroamerican male sample [85.8 ± 4.7, N = 50 (Tague, 1989)]. However, it is quite close to means of 93.3 for both Mesolithic samples (pooled sex sample: ± 2.5, N = 9; males: ± 2.6, N = 8). Most of the curvature present is in the vicinity of S4, with only a slight concavity cranial of the S3/S4 articulation.

The sacral foramina are all present and prominent. They are slightly larger on the left side, primarily in cranio-caudal height, but present no unusual features.

The cranial surface of the S1 is notable for the degree of caudal slope of the alae, from the lateral margins of the S1 body to the cranial margins of the auricular surfaces (or their estimated positions given damage). The degree of downward slope is indicated by a cranio-caudal distance of 21.0mm between the promontory and a line between the intersections of the arcuate lines and the auricular surfaces. In a parallel way, the S5 body extends caudally from its lateral portions, down to a clearly delimited body surface for the Cx1 articulation.

The sacral hiatus extends cranially to the level of the S3/S4 intervertebral body articulation. In two recent human samples, Euroamericans and Afroamericans, about a third of the individuals have the hiatus extend cranially to the cranial S4 or above [34.3%, N = 519 and 30.4%, N = 694 respectively (Trotter & Lanier, 1945)], making this pattern in Gough's Cave 1 relatively common.

Ilia (Table 2; Fig. 2). The Gough's Cave 1 ilia present relatively smooth surfaces but with generally clear markings for the various

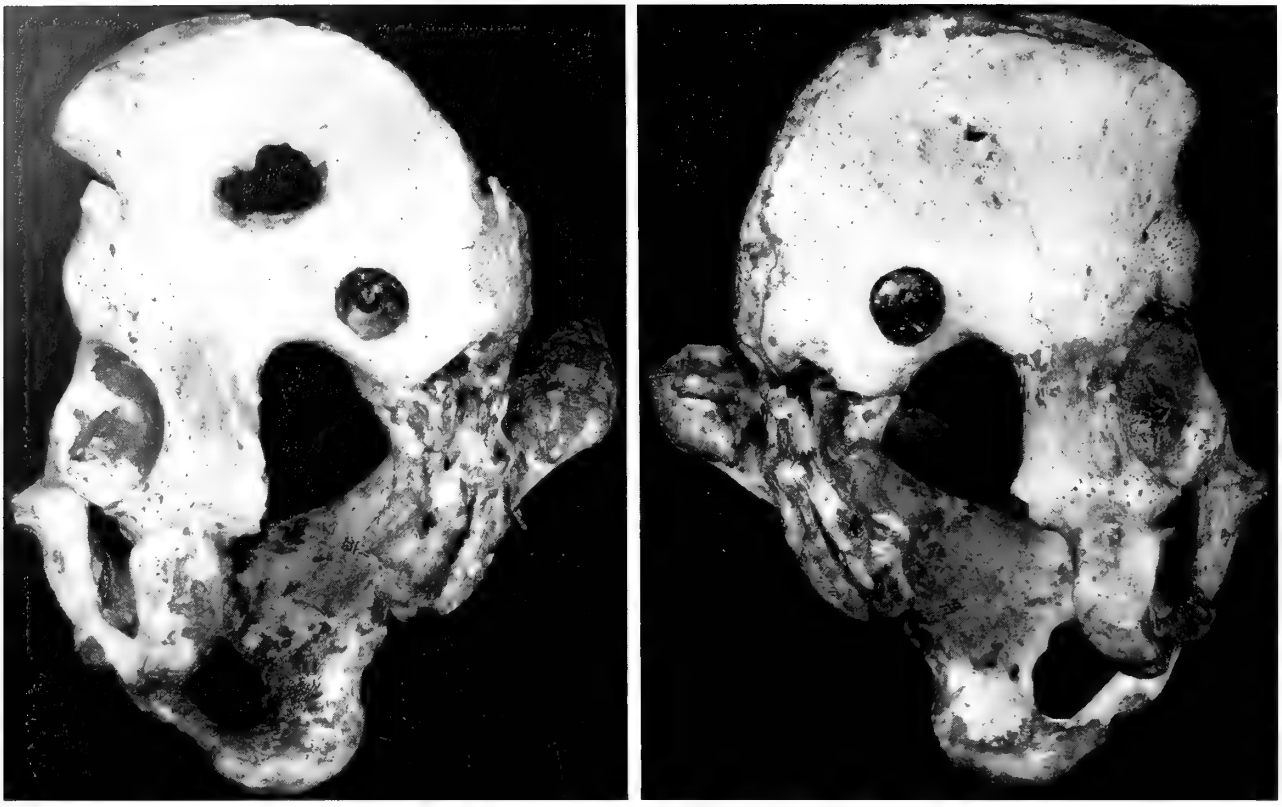

Fig. 2 Dorso-lateral views of the left and right ilia and ischia, with the caudal sacrum; × 0.44.

Table 2 Osteometrics of the Gough's Cave 1 ilia, acetabulae and greater sciatic notches.

	Right; 1.1/23	Left; 1.1/24
Iliac blade height (M-10)	100.0	100.9
Iliac blade depth (M-11)	9.2	(8.0)
Superior iliac breadth (M-12)	166.0	164.5
Inferior iliac breadth[1]	119.4	(113.0)
Arcuate line chord[2]	–	59.0
Arcuate line subtense[3]	–	3.5
Acetabular height[4]	53.8	53.5
Acetabular depth[5]	24.0	26.1
Acetabulo-sciatic breadth[6]	35.6	35.2
Greater sciatic notch height[7]	54.6	(50.0)
Greater sciatic notch breadth[8]	40.9	42.2

[1] Maximum direct length around the anterior inferior iliac spine and the posterior inferior iliac spine.
[2] Anterior margin of the auricular surface to the point on the arcuate line where a line, perpendicular to the arcuate line and passing through the depth of the psoas groove below the anterior inferior iliac spine, meets the arcuate line (Ruff, 1995).
[3] Maximum subtense from the arcuate line chord to the arcuate line.
[4] Acetabular margin height from the margin adjacent to the anterior inferior iliac spine to the most distant point on the inferior acetabulum, measuring only on the subchondral bone of the acetabulum proper.
[5] Maximum depth from the height chord to the subchondral bone.
[6] Miminum distance from the postero-lateral margin of the acetabulum to the ischial margin of the greater sciatic notch.
[7] Direct distance from the middle of the ischial spine to the middle of the posterior inferior iliac spine.
[8] Direct distance from the middle of the posterior inferior iliac spine to the posterior ischial margin of the greater sciatic notch, taken perpendicular to the ischial margin between the notch itself and the ischial spine.

muscular attachments. Externally, the gluteal abductor surfaces show little relief. One can perceive a *M. gluteus minimus* line curving from the iliac crest to the greater sciatic notch region, and there is smooth vertical ridging on the surface dorsal of that line. Internally, there is erosion on both sides but the preserved areas are evenly concave and smooth. The iliac portions of the arcuate lines are rounded angles from the acetabular area to the auricular surfaces.

The cranial surfaces of the greater sciatic notches are smooth bilaterally. The right one, however, presents a prominent pre-auricular sulcus, with some rugosity but mostly resorptive bone. The well-preserved left one, in contrast, is smooth with no trace of a pre-auricular sulcus.

The iliac crest is moderately developed where it is preserved, with minimal rugosity. Similarly, the anterior superior iliac spine is modest in its development, producing only a small concavity in lateral view between it and the anterior inferior iliac spine (at least on the right side, where the bone is intact). The anterior inferior iliac spines are prominent and thick, but there is no lateral rotation of the spines or internal concavity to them. Yet, they are accompanied by a distinct sulcus between them and the acetabular margin, ca.1.5mm wide on each side. The attachment area for the long head of *M. rectus femoris* is evident but not accompanied by marked rugosity or surface bone resorption.

Ischia (Table 3; Figs 2, 3). The ischial tuberosities are generally smooth with prominent proximal depressions for the insertions of *Mm. semimembranosus*. They are clearly differentiated from their adjacent acetabular margins as well as from the ventro-lateral surface

Fig. 3 Ventro-lateral view of the right ischiopubic region, with ventro-medial view of the left ischiopubic ramus; × 0.6.

Table 3 Osteometrics of the Gough's Cave 1 ischio-pubic regions.

Pubic length[1]	90.4	90.2
Acetabulo-symphyseal length[2]	65.5	70.1
Ventral pubic ramus thickness[3]	11.0	11.4
Symphyseal height (M-18)	41.7	42.4
Symphyseal breadth (M-19)	20.2	21.7
Symphyseal body breadth[4]	23.7	24.0
Obturator foramen length (M-20)	62.2	61.5
Obturator foramen breadth (M-21)	36.6	37.2
Ischial length[5]	87.0	86.8
Ischial tuberosity breadth[6]	27.2	28.5
Ischio-pubic ramus height[7]	–	16.2
Ischio-pubic ramus thickness[8]	–	8.2
Ischio-pubic chord[9]	102.8	(102.0)
Arcuate line chord[10]	–	125.0

[1] Direct distance from the middle of the acetabulum to the medial symphysis.
[2] Direct distance from the medial symphysis to the nearest point on the acetabular marrgin (McCown & Keith, 1939).
[3] Minimum thickness from the sulcus for the obturator vessels and nerve to the middle of the cranial surface of the superior pubic ramus (Trinkaus, 1983).
[4] Minimum distance from the middle of the pubic symphysis to the adjacent obturator foramen margin.
[5] Mid-acetabular point on the superior margin of the acetabular notch to the furthest point on the ischial tuberosity.
[6] Maximum breadth of the muscle attachment area on the tuberosity.
[7] Minimum dimension of the ramus, measured in an supero-dorsal to infero-ventral direction, parallel to the ventro-lateral surface of the ramus.
[8] Minimum dimension of the ramus, measured perpendicular to the ramus height.
[9] Direct distance between the dorsal end of the ischial spine and the inferior margin of the pubic symphysis [Tague (1989) measurement MD].
[10] Direct distance along the arcuate line from where it meets the anterior margin of the auricular surface to where it meets the pubic symphysis [Tague (1989) measurement KO].

of the ischium along the obturator foramen. There is a slight development of ridged bone between the dorso-cranial corners of the tuberosities and the ischial spines for the bursae of each *Mm. obturator internus*, especially on the left side. However, the sulci for each *Mm. obturator internus* do not impinge on the tuberosities, as in many recent and Late Pleistocene humans (Trinkaus, 1996). This is accompanied by a strong lateral rotation of the tuberosities, such that their primary muscular surfaces are almost in the same planes as the external ilia.

The tips of the ischial spines are absent, but they appear to have been curved inwards and moderately robust.

Pubic bones (Table 3; Fig. 3). The pubic bones present prominent pubic tubercles for the inguinal ligaments, accompanied by clear, angled but not cresting pectineal lines, extending from adjacent to the acetabulae to the symphysis. The ventral margins of the superior pubic rami are moderately thick (11.0 and 11.4 mm), and end ventrally in rounded but downwardly curved margins. The symphyseal bodies are narrow.

The internal surfaces of the symphyseal bodies and the ischio-pubic rami are smooth with only a hint of musculo-ligamentous attachments, but the cranial two-thirds of the external ischio-pubic rami have strong muscular markings and are ventrally flared.

Acetabulae (Table 2). There is little of note on the acetabulae except for a large pit on each of the subchondral bone surfaces in the middle of the weight bearing portion (the middle of the iliac portion between the anterior inferior iliac spine and the iliac pillar). The details of it are obscured on the left side by adhering matrix, but on the right side it is accompanied by a large vascular groove between it and the acetabular notch plus a smaller pit 19.0mm ventral of it immediately below the anterior inferior iliac spine.

Pelvis as a Whole (Table 4; Figs 4, 5). The articulated Gough's Cave 1 pelvis presents a largely symmetrical outline. The only real right-to-left contrast is in the degree of iliac flare, in which the left ilium is more laterally and less vertically oriented. The only other visual difference, the apparently more open sub-pubic angle on the right side, is the product of postmortem abrasion to the right ischio-pubic ramus.

The completeness of the Gough's Cave 1 pelvis permits comparisons of some 'obstetric' dimensions to those of at least recent human samples (Tague, 1989). In particular, comparisons are made to Euroamerican males, matching sex and approximate geographic origin. The pelvic funneling index of Gough's Cave 1 (outlet (bituberous) breadth vs. inlet breadth: 79.2) is essentially the same as the mean of the recent Euroamerican male sample (78.8 ± 7.9, N = 50), and similar to the means of Afroamerican and Amerindian male samples and well below the means of similar female samples (Tague, 1989). However, the inlet, midplane and outlet shape indices (dorso-ventral vs. transverse diameter) of Gough's Cave 1 (100.0, 115.0 and 104.2 respectively) contrast with those of the Euroamerican male sample (79.0 ± 7.9, 133.4 ± 6.9, 111.1 ± 14.1; N = 50). In this, Gough's Cave 1 has a much rounder pelvic inlet, one which is hyperfemale. Its midplane index is low for either males or females, and its outlet proportions are between the means of the Euroamerican male and female samples. These proportions therefore combine with several other aspects of its pelvic morphology in indicating a relatively female-like but male pelvis.

Table 4 Osteometrics of the Gough's Cave 1 articulated pelvis.

Pelvic inlet antero-posterior diameter (M-23)	125.0
Pelvic midplane antero-posterior diameter[1]	112.0
Pelvic outlet antero-posterior diameter[2]	103.2
Bi-iliac breadth (M-2)	274.0
Pelvic inlet transverse breadth (M-24)	125.0
Articular bi-acetabular breadth (M-7)	126.0
Minimum bi-acetabular breadth (M-7(1))	115.0
Bi-spinous breadth (M-8)	97.4
Bi-tuberous (outlet) breadth[3]	99.0
Sub-pubic angle (M-33)	64°

[1] Direct distance from transverse ventral line between fourth and fifth sacral vertebral bodies to dorsomedial margin of the inferior pubic symphysis [Tague (1989) measurement CD].
[2] Direct distance from the ventral apex of the fifth sacral vertebra to the dorso-medial margin of the inferior pubic symphysis [Tague (1989) measurement DE].
[3] Minimum distance between the two ischial tuberosities.

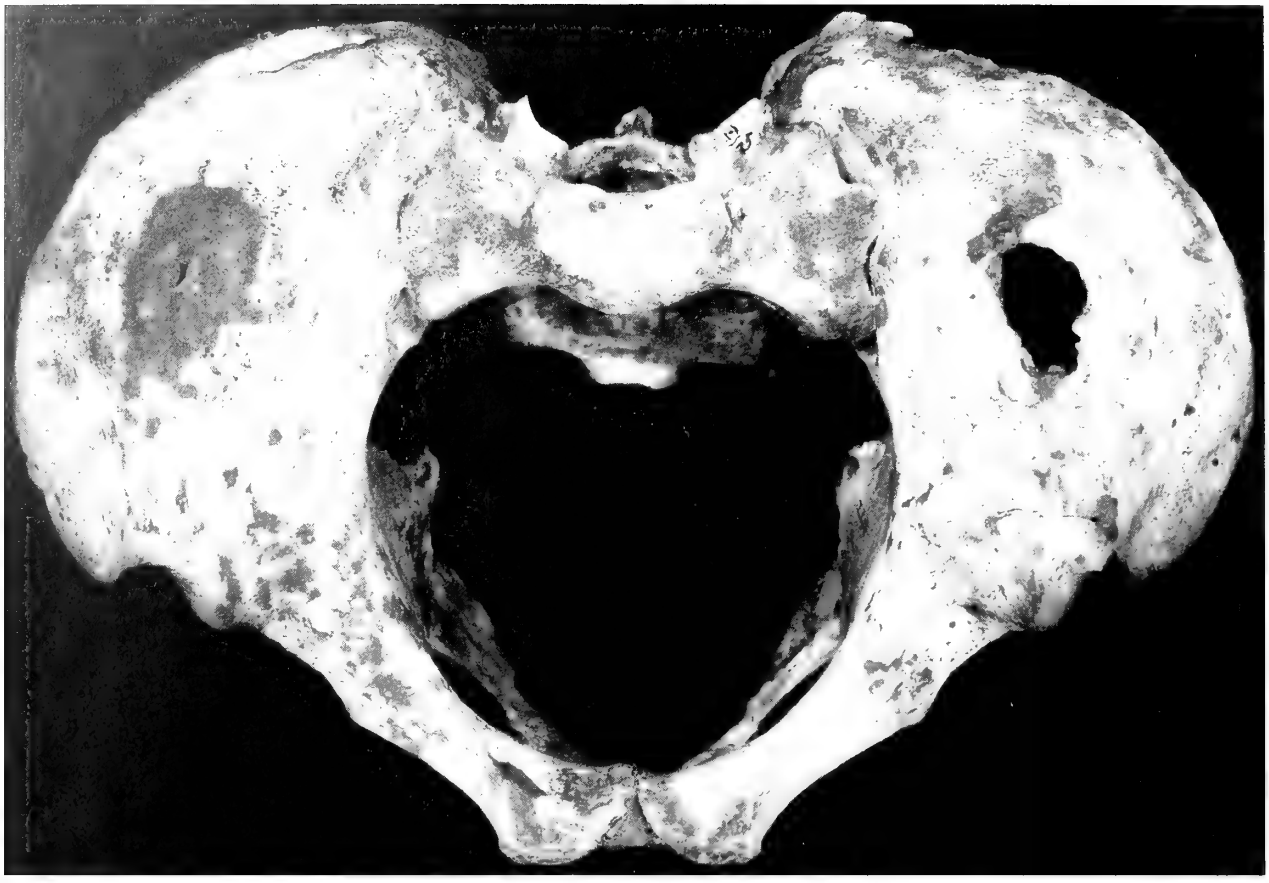

Fig. 4 Cranial view of the articulated Gough's Cave 1 pelvis; × 0.6.

Fig. 5 Ventral view of the articulated Gough's Cave 1 pelvis; × 0.6.

FEMORA

Inventory

Right (No. 1.1/35)
The right femur is essentially complete. There is minor damage to the anterior head margin over an area 15.3mm proximo-distal by 17.0mm antero-posterior, and there was abrasion to the medial margin of the medial condyle which obscures the medial articular margin. In addition, there is matrix adhering to the intertrochanteric crest combined with surface bone damage.

Left (No. 1.1/34)
The left femur is a complete bone with trivial edge abrasion to the condyles, and a loss of surface bone to the postero-proximal head over an area 21.5 by 19.0 mm.

Morphology

The Gough's Cave 1 femora are long, slender and relatively straight bones, with moderate muscular markings. This is combined with moderately sized articulations (Figs 6, 7).

The maximum and bicondylar lengths of the two bones differ

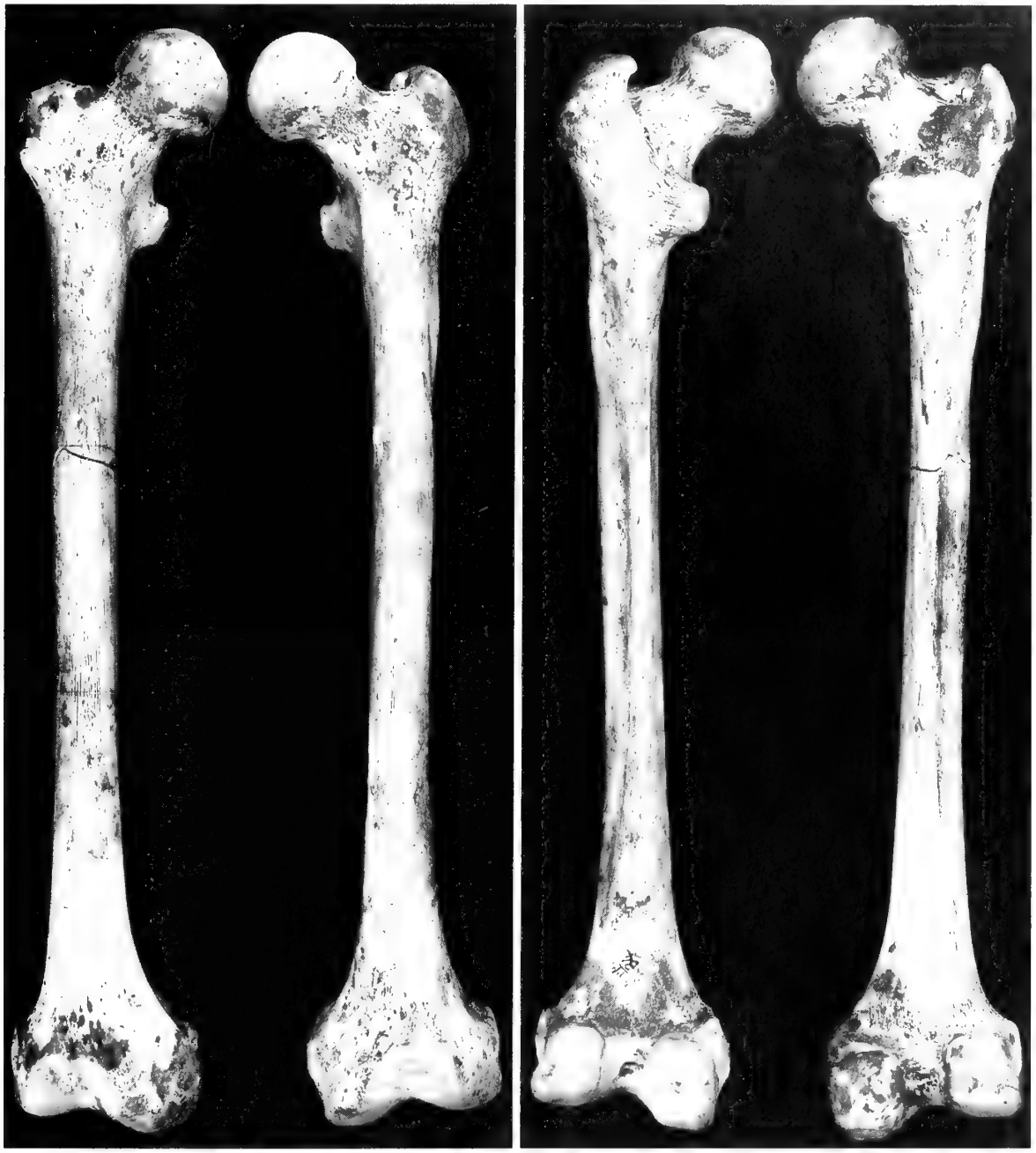

Fig. 6 Anterior (left) and posterior (right) views of the Gough's Cave 1 femora; × 0.4.

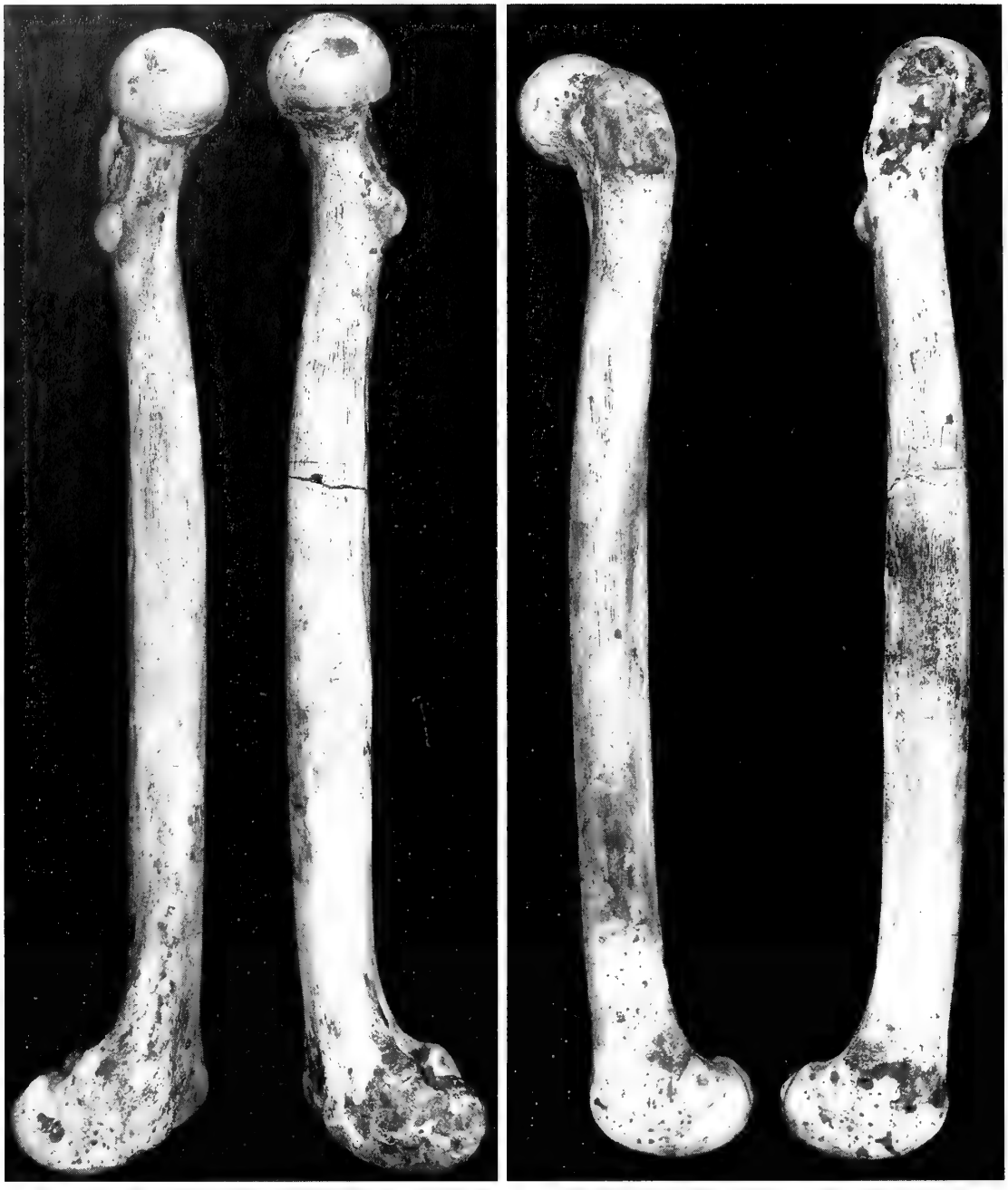

Fig. 7 Medial (left) and lateral (right) views of the Gough's Cave 1 femora; × 0.4.

slightly, with the right interarticular lengths being ca.6.0mm longer (Table 5). However, all of this difference is contained within the proximal epiphyses, since the bicondylar trochanteric lengths are identical and the left maximum trochanteric length is slightly longer.

Diaphyses (Tables 5, 6, 8; Figs 6, 7)

The diaphyses are straight medio-laterally with the minimum breadth near midshaft. The femora have moderate anterior curvature, as is indicated by subtense/chord indices of 3.1 and 2.9 versus 3.4 ± 0.7 (N = 16) for a Mesolithic sample and 3.5 ± 0.6 (N = 10) for a Mesolithic male sample. It is produced primarily by an anterior angulation in the mid-proximal diaphysis with relatively straight more proximal and distal diaphyseal profiles. As a result, the positions of the maximum subtenses are 43.9% and 39.7% of the chords from their proximal ends, values which are only slightly below the means of variable Mesolithic (46.0 ± 9.0, N = 15) and Mesolithic male (47.1 ± 10.4, N = 9) samples.

The diaphyses exhibit clear asymmetry near midshaft with the right side being larger. This is reflected in larger right side midshaft diameters (Table 5). It is more evident in cross–sectional measures (Tables 6, 8), which exhibit a 6.7% asymmetry in cortical area and a 16.9% asymmetry in the polar moment of area [% asymmetry =

Table 5 Length measurements of the Gough's Cave 1 femora and osteometrics of the femoral diaphyses .

	Right	Left
Maximum length (M-1)	443.0	437.5
Bicondylar length (M-2)	439.0	433.0
Trochanteric length (M-3)	423.0	424.5
Bicondylar trochanteric length (M-4)	413.0	413.0
Biomechanical length[1]	415.3	408.0
Midshaft antero-posterior diameter (M-6)	33.7	30.2
Midshaft medio-lateral diameter (M-7)	24.8	23.8
Midshaft circumference (M-8)	92.0	85.5
Subtrochanteric antero-posterior diameter (M-10)[2]	28.2	27.6
Subtrochanteric medio-lateral diameter (M-9)	31.5	31.7
Subtrochanteric circumference	94.0	93.0
Anterior curvature chord (M-27)	303.0	295.0
Anterior curvature subtense	9.5	8.5
Anterior curvature subtense position[3]	133.0	117.0

[1] Distance parallel to the diaphyseal axis between the intersection of that axis with the proximal neck (just medial of the greater trochanter) and the average of the positions along the diaphyseal axis of the distal condyles (Ruff & Hayes, 1983).
[2] The subtrochanteric diameters are taken as the maximum medio-lateral dimension (usually close to the antero-medial to postero-lateral plane of anteversion) and the antero-posterior diameter perpendicular to that medio-lateral one.
[3] Distance from the proximal end of the chord to the position of the maximum subtense.

Table 6 Cross-sectional second moments of area of the Gough's Cave 1 femoral diaphyses (in mm^4 and degrees).

	Right	Left
20% AP second moment of area (I_x)	35927.1	29219.4
20% ML second moment of area (I_y)	39249.1	35295.2
20% Maximum second moment of area (I_{max})	40399.9	36884.4
20% Minimum second moment of area (I_{min})	34776.2	27630.1
20% Polar moment of area (J)	75176.1	64514.5
20% Angle of I_{max} (theta)	27°	25°
35% AP second moment of area (I_x)	35539.9	28073.8
35% ML second moment of area (I_y)	20315.4	20642.1
35% Maximum second moment of area (I_{max})	35629.1	28972.0
35% Minimum second moment of area (I_{min})	20226.3	19743.9
35% Polar moment of area (J)	55855.4	48715.9
35% Angle of I_{max} (theta)	94°	108°
50% AP second moment of area (I_x)	39160.3	28671.0
50% ML second moment of area (I_y)	21418.6	21693.3
50% Maximum second moment of area (I_{max})	40129.3	30867.6
50% Minimum second moment of area (I_{min})	20449.5	19496.7
50% Polar moment of area (J)	60578.8	50364.3
50% Angle of I_{max} (theta)	103°	116°
65% AP second moment of area (I_x)	39874.0	29467.0
65% ML second moment of area (I_y)	23495.7	22797.5
65% Maximum second moment of area (I_{max})	41309.5	31796.8
65% Minimum second moment of area (I_{min})	22060.2	20467.7
65% Polar moment of area (J)	63369.7	52264.5
65% Angle of I_{max} (theta)	106°	117°
80% AP second moment of area (I_x)	30878.2	30129.1
80% ML second moment of area (I_y)	31956.3	31368.4
80% Maximum second moment of area (I_{max})	33380.3	34249.7
80% Minimum second moment of area (I_{min})	29454.2	27247.8
80% Polar moment of area (J)	62834.5	61497.5
80% Angle of I_{max} (theta)	37°	40°

((max – min)/max) × 100]. In contrast, in the proximal diaphysis, even though the right side continues to be larger, the level of asymmetry is much less, with cortical area exhibiting 4.8% asymmetry and the polar moment of area providing only a 2.1% contrast.

The lineae asperae are smooth along the entire lengths of the bones, which is possibly the product of the young adult age of the individual. They are along prominent pilasters for most of the middle half to two-thirds of the diaphysis. The pilasters are formed by antero-posteriorly convex medial surfaces but distinctly antero-posteriorly concave lateral surfaces. This results in a sulcus along the lateral pilaster especially in the midshaft region. The lineae asperae taper off gradually disto-medially, ending in moderate adductor tubercles.

The prominence of the Gough's Cave 1 pilasters is evident by their pilastric indices of 135.9 and 126.9. Both of them, and especially the right one, are well above the means of Mesolithic (109.5 ± 10.6, N = 52) and Mesolithic male (113.0 ± 9.2, N = 34) samples. This is further and better illustrated, albeit with smaller comparative samples, by the Gough's Cave 1 I_x/I_y and I_{max}/I_{min} ratios (Table 7) along the middle third of the diaphysis (the 35%, 50% and 65% sections). Again, the right femur is more pilastric than the left one.

Proximally, the markings in the pectineal region are very light, and they are bordered laterally by small but rugose gluteal tuberosities (Fig. 8). Neither gluteal tuberosity is projecting or concave, and there is no trace of hypotrochanteric fossae. The right tuberosity fades out proximally, but the left one leads to a small tubercle at the proximo-distal level of the lesser trochanter. The modest dimensions of the Gough's Cave 1 gluteal tuberosities are demonstrated by comparisons of their maximum breadths. The absolute breadths (8.2 and 8.4 mm) are below the means Mesolithic (11.6 ± 1.9 mm, N = 17) and especially Mesolithic male (12.3 ± 1.9 mm, N = 10) samples. This is further illustrated by indices between the gluteal tuberosity breadths and the geometric means of the associated subtrochanteric diaphyseal diameters – the mean of the resultant values of 27.5 and 28.4 for Gough's Cave 1 are 1.91 and 1.98 standard deviations below the means respectively of Mesolithic (42.3 ± 7.5, N = 17) and Mesolithic male (43.0 ± 7.6, N = 10) samples.

The gluteal buttresses are pronounced, with distinct sulci formed anteriorly and posteriorly. The right one is covered posteriorly by the gluteal tuberosity, but the left gluteal tuberosity covers only the medial half of the buttress. Nonetheless, the subtrochanteric diaphyses of Gough's Cave 1 are relatively round compared to those of most Mesolithic femora. Its meric indices of 89.5 and 87.1 are 2.49 and 2.84 standard deviations above the means respectively of pooled Mesolithic (74.6 ± 5.5, N = 85) and Mesolithic male (75.8 ± 4.4, N = 50) samples. However, the large sample Muge has significantly lower meric indices (73.0 ± 4.8, N = 55) than the remainder of the Mesolithic sample ($P < 0.001$). Yet even using only non-Muge Mesolithic remains for the comparison still places the Gough's Cave 1 femora 1.93 standard deviations from the mean (77.5 ± 5.6, N = 30). Similarly, the proximal diaphyseal (80%) I_{max}/I_{min} ratios are 2.43 and 2.70 standard deviations below the means of respective Mesolithic samples (Table 7).

Table 7 Comparative femoral second moment of area diaphyseal shape indices, I_x/I_y and I_{max}/I_{min}, for Gough's Cave 1 and Mesolithic samples. For Mesolithic samples, mean ± SD is given.

I_x/I_y	Gough's Cave 1: Right; Left	Mesolithic Sample	Mesolithic Males
20%	0.92; 0.83	0.66 ± 0.08; N = 16	0.68 ± 0.07; N = 10
35%	1.75; 1.36	1.01 ± 0.15; N = 14	1.02 ± 0.20; N = 8
50%	1.83; 1.32	1.18 ± 0.23; N = 55	1.20 ± 0.22; N = 37
65%	1.70; 1.29	1.00 ± 0.21; N = 15	1.08 ± 0.17; N = 9
80%	0.97; 0.96	0.77 ± 0.20; N = 52	0.79 ± 0.19; N = 34
I_{max}/I_{min}			
20%	1.16; 1.33	1.58 ± 0.19; N = 13	1.54 ± 0.18; N = 8
35%	1.76; 1.47	1.20 ± 0.12; N = 11	1.26 ± 0.12; N = 6
50%	1.96; 1.58	1.33 ± 0.19; N = 45	1.33 ± 0.19; N = 30
65%	1.87; 1.55	1.32 ± 0.26; N = 12	1.25 ± 0.13; N = 7
80%	1.13; 1.26	1.90 ± 0.29; N = 41	1.87 ± 0.25; N = 27

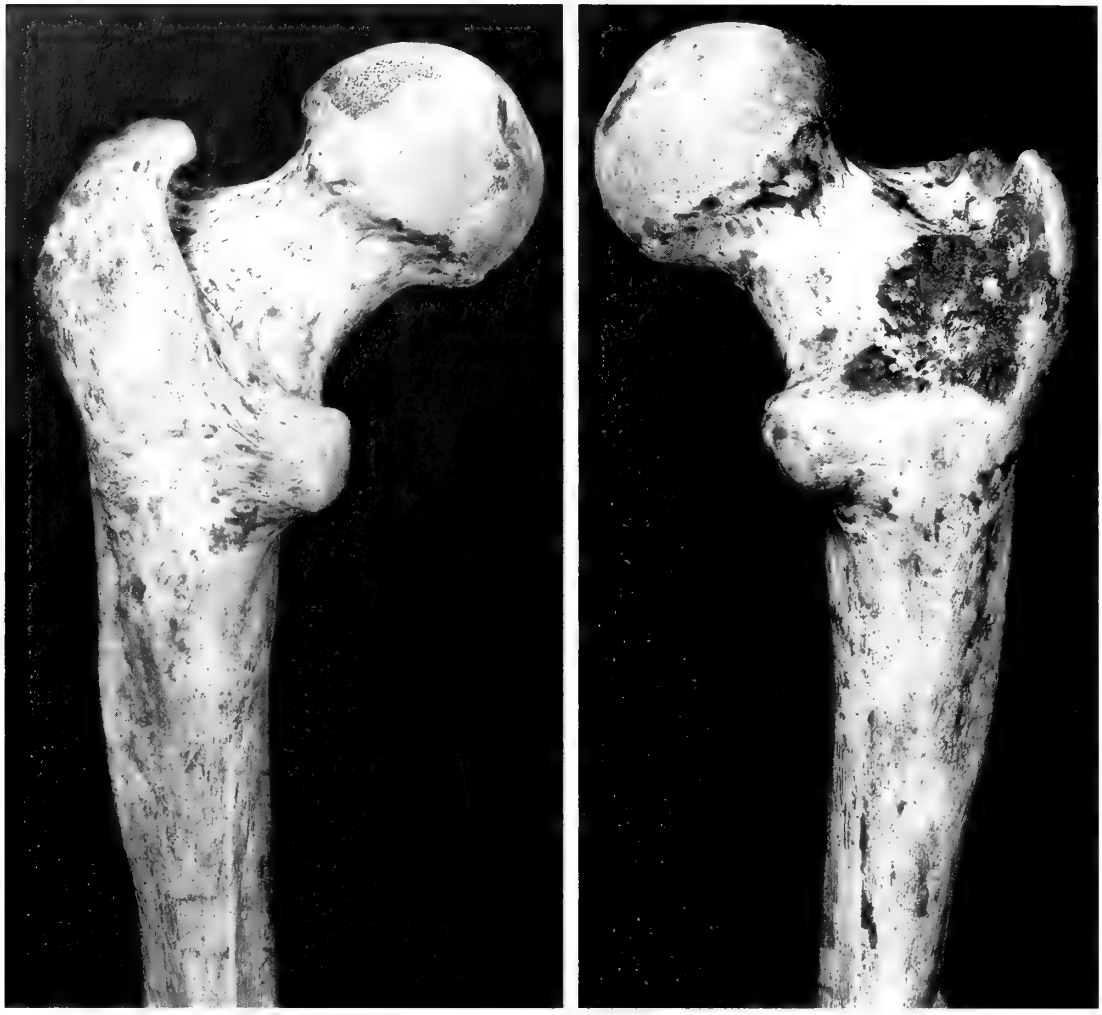

Fig. 8 Proximo-posterior view of the Gough's Cave 1 femora; × 0.8 (enlargement of Fig. 6, top right).

Table 8 Cross-sectional area measures of the Gough's Cave 1 femoral diaphyses (in mm^2).

	Right	Left
20% Total area (TA)	806.3	751.3
20% Cortical area (CA)	390.4	343.3
20% Medullary area (MA)	415.9	408.0
35% Total area (TA)	612.0	562.8
35% Cortical area (CA)	390.4	417.9
35% Medullary area (MA)	221.6	144.9
50% Total area (TA)	595.3	552.9
50% Cortical area (CA)	507.2	473.3
50% Medullary area (MA)	88.1	79.6
65% Total area (TA)	618.8	572.5
65% Cortical area (CA)	544.1	479.5
65% Medullary area (MA)	74.7	93.0
80% Total area (TA)	668.0	668.8
80% Cortical area (CA)	433.4	412.7
80% Medullary area (MA)	234.6	256.1

The overall robusticity of the femoral diaphyses can be compared to those of relatively large samples of European Mesolithic femora using its midshaft external diameters [$((AP \times ML)^{1/2}$ / bicondylar length) × 100]. The resultant indices are 6.6 and 6.2 for Gough's Cave 1, the right one of which is on the means of Mesolithic (6.5 ± 0.4, N = 47) and Mesolithic male (6.6 ± 0.4, N = 31) samples and the left one only slightly below them. In this, the large Muge sample has a significantly (P = 0.002) lower mean (6.3 ± 0.2, N = 19), but its inclusion or deletion from the Mesolithic sample has little effect on the relative position of Gough's Cave 1.

Table 9 Comparative femoral percent cortical area (%CA = (CA/TA) × 100) for Gough's Cave 1 and Mesolithic samples.

	Gough's Cave 1: Right; Left	Mesolithic Sample	Mesolithic Males
20%	48.4; 45.6	48.2 ± 4.1; N = 16	47.3 ± 3.6; N = 10
35%	63.8; 74.3	67.3 ± 5.8; N = 14	65.1 ± 3.3; N = 8
50%	85.2; 85.6	79.0 ± 6.9; N = 55	77.9 ± 6.3; N = 37
65%	87.9; 83.6	86.3 ± 2.6; N = 15	85.7 ± 2.7; N = 9
80%	64.9; 61.7	77.6 ± 8.3; N = 52	78.1 ± 6.8; N = 34

Using midshaft cross-sectional measures, the percent cortical areas largely cluster close to the Mesolithic comparative means; only the 80% one is relatively low, significantly so with respect to the Mesolithic male sample (Table 9). Plots of the midshaft cortical area and polar moment of area versus powers of femoral length (Fig. 9) largely support the pattern seen in the robusticity indices; Gough's

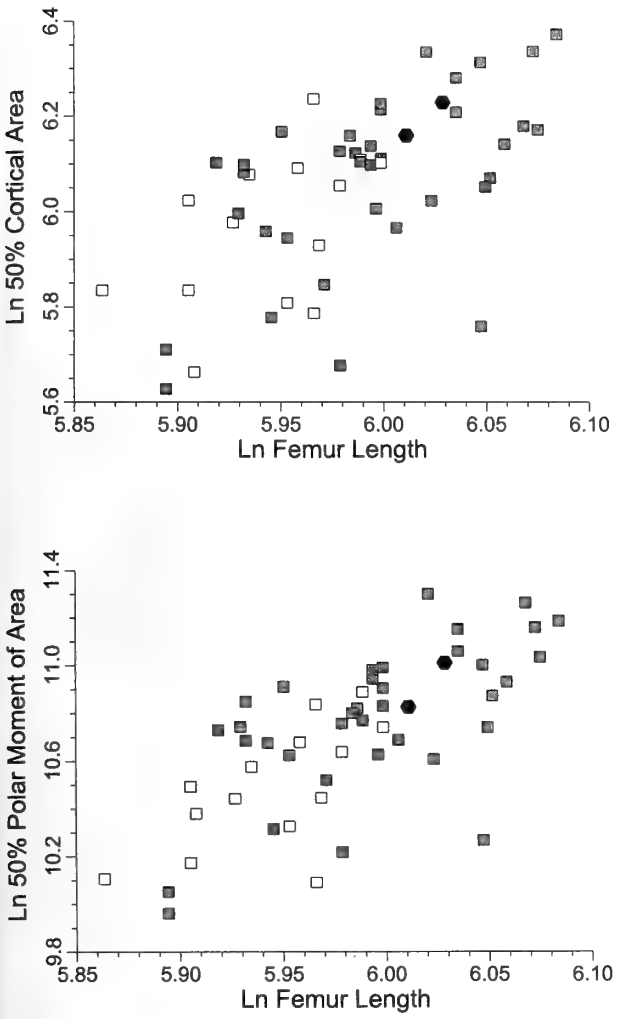

Fig. 9 Plots of the Gough's Cave 1 femoral midshaft logged cross-sectional parameters vs. ln length (see text). Solid hexagons: Gough's Cave 1 right and left femora; gray squares: Mesolithic males; open squares: Mesolithic females.

Cave 1 is well within the Mesolithic distributions, close to the middles of the comparative sample distributions in both measures.

Proximal Epiphyses (Table 10; Fig. 10)

The proximal epiphyses present overall similar morphologies but contrast in several aspects of their proportions, some of which are reflected in the slight (ca.1%) length asymmetry. The heads are evenly rounded and each has a large fovea capitis placed slightly posterior on the head. There is no trace of an Allen's fossa on either femur. The right head is slightly larger, especially in the cranio-caudal direction (Table 10), but comparisons of their head sagittal diameters to femoral bicondylar length produce similar indices (10.9 & 10.7), in part due to the differences in femoral lengths. They are both very close to the means of Mesolithic (10.7 ± 0.5, N = 37) and Mesolithic male (10.8 ± 0.5, N = 26) samples.

On the left femur where is it preserved, there is a large obturator fossa with a large pit 12.5mm deep from its posterior edge. The intertrochanteric crest has clearly marked fibrous spicules running along it, from the capsular attachment, but the intertrochanteric lines on the anterior surfaces are faint. Both lesser trochanters are strongly medially projecting, and the greater trochanters have a clear lateral swelling below the *M. gluteus medius* insertion. The left greater trochanter also exhibits a strong beak at its proximo-medio-posterior margin.

The neck shaft angles of the two femora show a moderate degree of asymmetry, with the left one being 3° higher. Both of these angles (132° & 135°) are relatively high for foraging populations (Trinkaus, 1993) but not exceptional for a European Mesolithic sample (125.5° ± 5.9°, N = 22) or a male one (124.4° ± 5.4°, N = 15). However, the Gough's Cave 1 values nonetheless have z-scores of 1.36 and 1.68 respectively.

Of greater asymmetry are the anteversion angles, a modest 11° on the right side but a pronounced 30° on the left. This asymmetry in anteversion angles is reflected in direction but not in degree by the values for theta at the subtrochanteric level (37° and 40° respectively). In comparison, a variable Mesolithic sample provides anteversion angle values of 18.2° ± 9.0° (N = 18) and 18.3° ± 8.7° (N = 12) for males alone.

The relatively high neck-shaft angles of Gough's Cave 1 contribute in part to its relatively short biomechanical neck lengths, which provide indices relative to bicondylar length 8.4 and 9.2 for the anatomical biomechanical neck length and 14.4 and 15.5 for the trochanteric one. These are relative respectively to 9.6 ± 0.9 (N = 11) and 16.7 ± 1.0 (N = 10) for the Mesolithic sample and 9.5 ± 0.8 (N = 7) and 16.9 ± 0.7 (N = 6) for the male sample.

Table 10 Osteometrics of the Gough's Cave 1 femoral epiphyses.

	Right	Left
Head-neck length (M-14)	80.1	79.9
Anatomical biomechanical neck length[1]	37.0	40.0
Trochanteric biomechanical neck length[2]	63.0	67.0
Head sagittal diameter (M-19)	47.7	46.3
Head vertical diameter (M-18)	48.2	46.3
Neck circumference (M-17)	97.0	91.5
Neck-shaft angle (M-29)[3]	132°	135°
Anteversion angle (M-28)	11°	30°
Greater trochanter depth (M-26(1))	–	37.3
Gluteal tuberosity breadth[4]	8.2	8.4
Distal epicondylar breadth (M-21)	–	78.5
Bicondylar breadth[5]	(75.6)	76.6
Medial condylar breadth (M-21c)	(29.4)	29.6
Lateral condylar breadth (M-21e)	28.3	28.6
Bicondylar angle (M-30)	10°	10°
Medial patellar projection (M-24b)	60.7	58.9
Lateral patellar projection (M-22)	63.6	61.9
Median patellar projection[6]	59.0	58.9
Patellar surface circumference[7]	42.0	45.0
Patellar surface breadth (M-26(3b))	37.7	39.1
Patellar surface depth[8]	6.0	6.5
Patellar surface depth position[9]	13.6	13.6

[1] Distance perpendicular to the diaphyseal axis from that axis to the proximal tangent to the femoral head.
[2] Distance perpendicular to the diaphyseal axis from the proximo-distal tangent to the lateral greater trochanter to the proximal tangent to the femoral head (Lovejoy *et al.*, 1973).
[3] Taken in the anteversion plane of the femoral head and neck.
[4] Maximum breadth of the rugose area for the insertion of *M. gluteus maximus* on the proximal diaphysis (Trinkaus, 1976).
[5] Maximum breadth across the external medial and lateral condylar surfaces.
[6] Dorsal condylar plane to the tangent parallel to that dorsal plane within the deepest portion of the patellar sulcus.
[7] Articular arc in the patellar sulcus from the intercondylar margin to the proximal patellar surface.
[8] Maximum depth subtense to the sulcus floor, taken from the surface breadth.
[9] Position of the depth subtense from the lateral margin of the patellar surface.

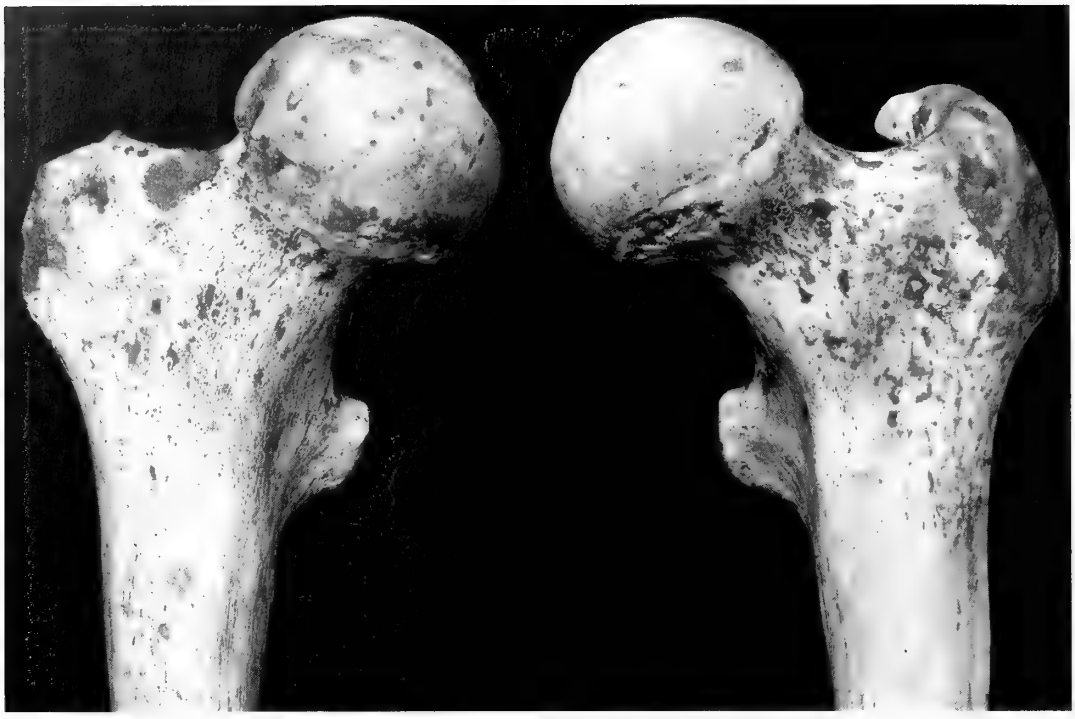

Fig. 10 Anterior view of the Gough's Cave 1 proximal femora; × 0.8 (enlargement of Fig. 6, top left).

Distal Epiphyses (Table 10)
There is little of note on the Gough's Cave 1 distal femoral epiphysis. The condyles are rounded with no evidence of femoral squatting facets. There is only a small rounded ridge along the supracondylar margin of the medial condyles, up to 3.5mm from the condylar surface on the left side where it is best preserved.

Their bicondylar angles of 10° each are well within Mesolithic ranges of variation (9.7° ± 3.1, N = 19; 8.8° ± 2.5°, N = 15 for males only), all of which are similar to those of recent humans (Tardieu & Trinkaus, 1994). The one measure of distal epiphyseal size for which reasonable Mesolithic comparative samples exist, epicondylar breadth versus bicondylar length, provides an index of 18.1. It suggests a modest but not unusually small epiphysis, given means of 18.8 for total (± 1.1, N = 19) and 18.9 for male (± 1.1, N = 14) Mesolithic samples.

TIBIAE

Inventory

Right (No. 1.1/27)
A complete bone with minor abrasion to the medial half of the posterior distal epiphysis and thin adhering matrix around the proximal epiphysis.

Left (No. 1.1/26)
The bone retains two pieces, a proximal posterior piece of the diaphysis with the abraded soleal line (maximum preserved length: ca.80.0mm) and a diaphyseal section with all of the surfaces just proximal of the distal epiphysis (maximum preserved length: ca.50.0mm). Both of the pieces are set in a plaster and papier-mâché reconstruction of the bone and attached to the left fibula (Fig. 11).

Morphology

Even though portions of both tibiae are present, meaningful morphological observations can be made primarily on the essentially complete right bone. Therefore, the following comments apply to the right bone except where noted otherwise.

Diaphysis (Tables 11, 12, 14; Figs 11, 12)
The right tibial diaphysis has a gently 'S'-curved, sharply angled anterior crest, which is bordered medially by a smooth and slightly convex medial diaphyseal surface. The lateral surface is convex between the interosseus crest and the anterior margin and concave between the crest and the postero-lateral corner along the proximal two-thirds of the diaphysis. Distal of there, it becomes fully convex. The postero-medial margin is rounded proximal of the meeting of the soleal line with that margin, near midshaft.

Both tibiae have a distinct but small flexor line, a crest between the origins of *M. tibialis posterior* and *M. flexor digitorum longus* on the proximal posterior diaphysis extending distally from the soleal line. On the right bone, it is raised from the subperiosteal surface along ca.78mm distally from the soleal line. The soleal line itself is a low rugose area proximal of the flexor line, 4.7mm wide near the flexor line and 5.3mm wide more proximally. Disto-medial of the flexor line, the soleal line becomes a slightly raised crest, extending to the medial side distally. The interosseus line is a distinct crest from the very proximal shaft to about midshaft, at which level it becomes blunt and blends in with the lateral diaphysis.

The nutrient foramen is located just medial of the flexor line, 37.5mm distal of the intersection of the two muscular lines.

The Gough's Cave 1 tibial diaphysis, like those of other Mesolithic humans, is distinctly platycnemic. Its cnemic index of 55.9 is even slightly below the means of Mesolithic (62.4 ± 5.8, N = 73) and Mesolithic male (61.8 ± 6.2, N = 46) samples. Moreover, its 35% to 80% I_{max}/I_{min} ratios are all higher than the means of Mesolithic

Table 11 Osteometrics of the Gough's Cave 1 right tibia.

Maximum length (M-1)	385.0
Medial total length (M-1b)	375.0
Medial articular length (M-2)	360.0
Biomechanical length[1]	360.5
Midshaft antero-posterior diameter (M-8)	34.3
Midshaft medio-lateral diameter (M-9)	21.3
Midshaft circumference (M-10)	87.5
Proximal antero-posterior diameter (M-8a)	38.1
Proximal medio-lateral diameter (M-9a)	21.3
Proximal circumference (M-10a)	94.0
Distal minimum circumference (M-10b)	77.0
Proximal epiphyseal maximum breadth (M-3)	76.1
Medial condyle breadth (M-3a)	34.5
Lateral condyle breadth (M-3b)	34.4
Medial condyle depth (M-4a)	46.7
Lateral condyle depth (M-4b)	40.9
Tuberosity projection[2]	48.0
Medial retroversion angle (M-12)	16°
Lateral retroversion angle	13°
Medial inclination angle (M-13)	11°
Lateral inclination angle	8°
Torsion angle (M-14)	20°
Distal maximum breadth (M-6)	49.1
Distal maximum depth (M-7)	40.3
Talar trochlear articular breadth[3]	30.0
Medial talar articular depth[4]	26.2
Lateral talar articular depth[5]	33.7

[1] The average distance, measured parallel to the diaphyseal axis, from the middle of the talar trochlear surface to the middle of each condyle (Ruff & Hayes, 1983).
[2] The distance perpendicular to the diaphyseal axis from the antero-posterior middle of the condyles to the coronal plane tangent to the anterior surface of the tibial tuberosity (Trinkaus, 1983).
[3] The medio-lateral breadth of the talar trochlear facet from the antero-posterior middle of the lateral margin to the middle of the curve between the trochlear and the medial malleolar facets (Trinkaus, 1983; Ruff, 1990).
[4] The minimum antero-posterior dimension of the talar trochlear facet taken adjacent to the medial malleolus (Trinkaus, 1983; Ruff, 1990).
[5] The maximum antero-posterior dimension of the talar trochlear facet taken adjacent to the fibular articulation (Trinkaus, 1983; Ruff, 1990).

Table 12 Second moments of area of the Gough's Cave 1 right tibial diaphysis (in mm^4 and degrees).

20% AP second moment of area (I_x)	14154.4
20% ML second moment of area (I_y)	12798.3
20% Maximum second moment of area (I_{max})	15461.6
20% Minimum second moment of area (I_{min})	11491.1
20% Polar moment of area (J)	26952.7
20% Angle of I_{max} (theta)	125°
35% AP second moment of area (I_x)	17618.5
35% ML second moment of area (I_y)	12738.0
35% Maximum second moment of area (I_{max})	21220.1
35% Minimum second moment of area (I_{min})	9136.4
35% Polar moment of area (J)	30356.5
35% Angle of I_{max} (theta)	119°
50% AP second moment of area (I_x)	29204.5
50% ML second moment of area (I_y)	15067.5
50% Maximum second moment of area (I_{max})	33212.7
50% Minimum second moment of area (I_{min})	11059.3
50% Polar moment of area (J)	44272.0
50% Angle of I_{max} (theta)	113°
65% AP second moment of area (I_x)	42160.0
65% ML second moment of area (I_y)	16796.3
65% Maximum second moment of area (I_{max})	46262.6
65% Minimum second moment of area (I_{min})	12693.7
65% Polar moment of area (J)	58956.3
65% Angle of I_{max} (theta)	111°
80% AP second moment of area (I_x)	58126.5
80% ML second moment of area (I_y)	32073.3
80% Maximum second moment of area (I_{max})	65287.7
80% Minimum second moment of area (I_{min})	24912.2
80% Polar moment of area (J)	90199.9
80% Angle of I_{max} (theta)	115°

Table 13 Comparative tibial second moment of area diaphyseal shape indices, I_{max}/I_{min}, for Gough's Cave 1 and Mesolithic samples.

	Gough's Cave 1	Mesolithic Sample	Mesolithic Males
20%	1.35	1.38 ± 0.25; N = 12	1.32 ± 0.22; N = 7
35%	2.32	2.23 ± 0.40; N = 13	2.19 ± 0.34; N = 8
50%	3.00	2.59 ± 0.46; N = 47	2.63 ± 0.47; N = 34
65%	3.64	2.89 ± 0.44; N = 16	2.86 ± 0.41; N = 10
80%	2.62	2.44 ± 0.46; N = 11	2.47 ± 0.53; N = 8

Table 14 Cross-sectional areas of the Gough's Cave 1 right tibial diaphysis (in mm^2).

20% Total area (TA)	480.2
20% Cortical area (CA)	224.1
20% Medullary area (MA)	256.1
35% Total area (TA)	432.5
35% Cortical area (CA)	299.5
35% Medullary area (MA)	133.0
50% Total area (TA)	491.1
50% Cortical area (CA)	375.8
50% Medullary area (MA)	115.3
65% Total area (TA)	566.8
65% Cortical area (CA)	404.4
65% Medullary area (MA)	162.4
80% Total area (TA)	793.7
80% Cortical area (CA)	432.5
80% Medullary area (MA)	361.2

Table 15 Comparative tibial percent cortical area (%CA = (CA/TA) × 100) for Gough's Cave 1 and Mesolithic samples.

	Gough's Cave 1	Mesolithic Sample	Mesolithic Males
20%	46.7	57.3 ± 4.8; N = 15	55.8 ± 3.9; N = 9
35%	69.2	81.0 ± 3.0; N = 16	80.8 ± 2.5; N = 10
50%	76.5	84.4 ± 5.0; N = 53	85.0 ± 4.4; N = 38
65%	71.4	68.6 ± 4.5; N = 16	68.2 ± 4.3; N = 10
80%	54.5	51.2 ± 5.0; N = 15	51.3 ± 5.4; N = 8

samples, with the 50% and especially the 65% ratios being well above those Mesolithic means (Table 13).

In terms of diaphyseal robusticity, the Gough's Cave 1 tibia on average is similar to those of other Mesolithic specimens. Its percent cortical area values are below Mesolithic means for the mid and distal diaphysis, but above those means in the proximal diaphysis (Table 15). A diaphyseal robusticity index (from the geometric mean of the midshaft diameters versus articular length) is 7.5 for Gough's Cave 1, which is very close to the means of Mesolithic (7.6 ± 0.6, N = 24) and Mesolithic male (7.8 ± 0.6, N = 17) samples. The plots of midshaft cortical area and polar moment of area versus appropriate powers of femoral or tibial and femoral length (Fig. 13) place Gough's Cave 1 clearly well within the Mesolithic ranges of variation is slightly below a number of those specimens.

Proximal Epiphysis (Fig. 14)

The tibial plateau presents small intercondylar spines, a distinctly concave medial condylar surface, and an evenly convex lateral condylar surface. There is a nearly horizontal fibular facet, with its maximum dimension of 20.2mm approximately medio-lateral and the minimum diameter of 14.5mm approximately antero-posterior. There is a clear sulcus for the *M. semimembranosus* tendon, but there is no smoothing of the bone in the sulcus for its insertion.

The tibial plateau is strongly rotated relative to the diaphysis, with a torsion angle of 20°. However, this value is close to the means of variable Mesolithic (22.7° ± 12.4°, N = 15) and Mesolithic male

Fig. 11 Anterior (left) and posterior (right) views of the Gough's Cave 1 tibiae and fibulae, with the heavily reconstructed left tibia and fibula shown only in anterior view; × 0.4.

(22.4° ± 9.9, N = 12) samples. The Gough's Cave 1 tibia also has clear retroversion of the condyles, with a medial retroversion angle of 15°. However, this value is also very close to the means of Mesolithic (15.3 ± 5.1°, N = 18) and Mesolithic male (15.0° ± 4.7°, N = 15) samples. All of these retroversion angles are normal for non-industrial recent humans (Trinkaus, 1975a).

Similarly, the overall dimensions of the tibial plateau, quantified by an index of maximum breadth versus articular length of 21.1 for Gough's Cave 1, is normal for Mesolithic samples (22.4 ± 1.8, N = 12, and 22.1 ± 1.5, N = 11 for males only). One feature in which the Gough's Cave 1 proximal tibia is further from the mean of the comparative samples is in relative tuberosity projection, or the posterior displacement of the tibial condyles from the tibial tuberosity (a measure of the *M. quadriceps femoris* moment arm through the patellar ligament). The Gough's Cave 1 value of 13.3 is significantly above the mean of a small Mesolithic pooled-sex sample (9.4 ± 1.4, N = 6), and still well above the mean of a male sample (10.5 ± 2.0, N = 4).

Distal Epiphysis

The Gough's Cave 1 tibial distal epiphysis is likewise unremarkable. Its talar trochlear articular surface, relative to tibial length, is similar in size to other Mesolithic tibiae. The index formed by the geometric mean of its breadth with the average of its depth measurements versus articular length is 8.3 – this value is close to the means for Mesolithic (8.1 ± 0.6, N = 23) and Mesolithic male (8.1 ± 0.6, N = 18) samples.

It does present a clear lateral squatting facet, 9.0mm wide and 3.7mm proximo-distal. There is no trace of a medial squatting facet or other rounding of the anterior articular margin.

Fig. 12 Medial (left) and lateral (right) views of the Gough's Cave 1 right tibia and fibula; × 0.4.

FIBULAE

Inventory

Right (No. 1.1/28)
The bone consists of a proximal section with the proximal epiphysis and the proximal half of the diaphysis, plus a distal section with the distal quarter of the diaphysis and the complete distal epiphysis. The two pieces are joined together by a plaster reconstruction of the mid-distal epiphysis (minimum gap: 47.8mm), and its reconstructed lengths (Table 16) are based on articulation with the complete right tibia.

Left (No. 1.1/26)
Most of the diaphysis lacking both epiphyses. The epiphyses are reconstructed in plaster and joined to the reconstructed left tibia. Maximum preserved length: 279.0mm.

Morphology

Even though both of the diaphyses are preserved, most of the morphological information and all of the osteometrics derive from the separated right fibula. Nonetheless, osteometric comparisons of the Gough's Cave 1 fibula are limited by poor preservation and limited published measurements for other European Mesolithic fibulae.

Diaphyses (Table 16; Figs 11, 12)
Both fibular diaphyses are very straight, with well formed angles for musculo-ligamentous attachments on all of the margins. On anterior view, the left one has a slight 'S' curve in the distal third, producing a slight lateral concavity just below midshaft – the right bone's reconstruction in this region (Fig. 11) may therefore be too straight.

Even though the various angles are clearly formed, none of them present clear rugosities. The primary evident muscular insertions

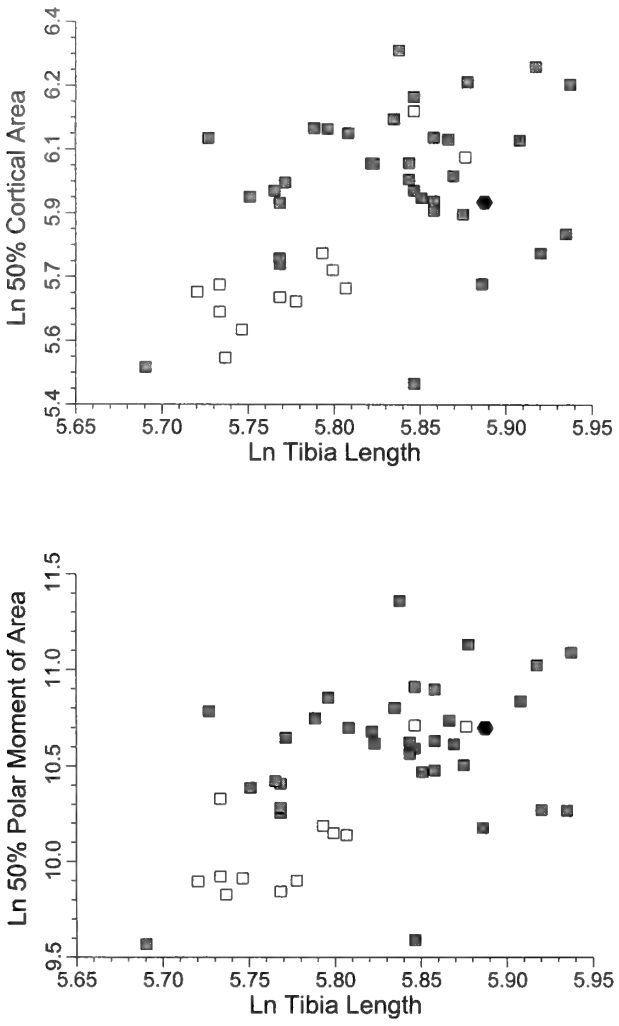

Fig. 13 Plots of the Gough's Cave 1 tibial midshaft logged cross-sectional parameters versus loggen tibial length. Solid hexagons: Gough's Cave 1 right and left femora; gray squares: Mesolithic males; open squares: Mesolithic females.

areas are the soleal line proximally (preserved on the right bone) and a broad area on the posterior midshaft (evident on both fibulae). The soleal line is a broad, rugose area, 13.5mm long and up to 12.7mm wide. It forms a slight depression and has a small lip medially. The right midshaft exhibits a broad rugose area ca.40.0mm long along the posterior surface. A similar but much less rugose area is present on the left diaphysis. The attachments for the distal interosseus (or tibio-fibular) ligaments are modest, spiraling from proximo-anterior to disto-posterior.

Morphometrically, the Gough's Cave 1 right fibula is similar to those of other Mesolithic humans. Its midshaft maximum to minimum diameter index of 133.6 is moderately below to the means of highly variable samples (Mesolithic: 141.6 ± 17.7, N = 40; Mesolithic males: 140.0 ± 18.6, N = 22). It is slightly less robust than most other Mesolithic fibulae, as indicated by an index between the geometric mean of its midshaft diameters and maximum length (Gough's Cave 1: 3.8; Mesolithic: 4.2 ± 0.6, N = 20; Mesolithic males: 4.2 ± 0.3, N = 13).

It is also possible, with smaller comparative samples, to assess its

Table 16 Osteometrics of the Gough's Cave 1 right fibula.

Maximum length (M-1)	(366.0)
Articular length (M-1a)	(356.0)
Midshaft maximum diameter (M-2)	15.9
Midshaft minimum diameter (M-3)	11.9
Midshaft circumference (M-4)	45.5
Neck maximum diameter	13.1
Neck minimum diameter	10.5
Neck circumference (M-4a)	37.0
Proximal epiphyseal medio-lateral diameter	29.8
Proximal epiphyseal antero-posterior diameter	24.4
Proximal tibial facet medio-lateral diameter	20.9
Proximal tibial facet antero-posterior diameter	18.2
Proximal articular angle[1]	111°
Distal maximum depth[2]	24.9
Distal articular depth[3]	19.5
Distal articular length[4]	22.7
Distal articular angle[5]	19°

[1] The angle between the antero-medial to postero-lateral plane of the proximal tibial facet and the diaphyseal axis.
[2] The maximum antero-posterior diameter of the epiphysis, measured parallel to the talar surface.
[3] The maximum antero-posterior diameter of the talar articular surface.
[4] The maximum proximo-distal diameter of the talar articular facet, measured parallel to the long axis of the facet.
[5] The angle in coronal plane of the talocrural articulation between the chord for the articular height and the diaphyseal axis.

neck proportions. A maximum to minimum diameter index of 124.8 for Gough's Cave 1 is relatively low (Mesolithic: 141.9 ± 13.2, N = 4). However, the size of its neck circumference vis-à-vis midshaft circumference (81.3) is close to the values for other Mesolithic fibulae (79.8 ± 2.2, N = 4).

Proximal Epiphysis

The right fibula preserves a large rounded head with a subcircular flat facet for the tibia. It is notable primarily for its development of a very large ossification of the proximal tibio-fibular ligament (Fig. 11). The crest is rounded on its medial margin, 22.8mm long (proximo-distally), 13.1mm thick, and projects ca.9.0mm from the adjacent head. Interestingly, there is no counterpart on the proximal tibia, only the tapering off of the modest interosseus line previously noted.

Distal Epiphysis

The right distal epiphysis generally smooth in its external surfaces. The digital fossa is modest in size, and the malleolar surface is gently convex in a proximo-distal direction. The angle between the proximo-distal chord of the articular surface relative to the diaphyseal axis (19°) falls close to means of variable Mesolithic (20.1° ± 6.5°, N = 7) and Mesolithic male (21.0° ± 6.4°, N = 5) samples.

TALUS

Inventory

Right (No. 1.1/29)

A complete bone, which has had holes drilled in the medial calcaneal surface and the sulcus tali for analytical samples.

Morphology

The right talus of Gough's Cave 1 (Table 17; Fig. 15) is a modest bone with generally smooth surfaces. In overall length relative to femoral length, it is very close to other Mesolithic specimens [12.6 versus 12.6 ± 0.4 for Mesolithic (N = 11) and male Mesolithic (N = 6) samples]. Similarly, its relative trochlear length (versus length)

Fig. 14 Views of the Gough's Cave 1 right tibial epiphyses. Left: posterior proximal epiphysis and diaphysis. Above right: proximal medial epiphysis. Below right: anterior distal epiphysis; × 0.8 (enlargement of parts of Figs 11, 12).

index of 65.1 is just below the means of variable Mesolithic (65.4 ± 4.1, N = 10) and male Mesolithic (65.3 ± 4.2, N = 6) samples. However, its trochlea is slightly narrower than those of most Mesolithic tali, since a trochlear breadth/length index provides a value of 79.1 for Gough's Cave 1, but means of 84.5 (± 7.5, N = 26) and 82.8 (± 6.3, N = 18) for pooled-sex and male only Mesolithic samples. Finally, its neck shaft angle of 23° falls in the middles of the ranges of Mesolithic (24.1° ± 4.4°, N = 7) and male Mesolithic (22.9° ± 3.5°, N = 6) samples.

On its talo-crural articulations, it presents several variants of the anterior trochlear margin (Table 18). There is a full anterior extension of the medial malleolar surface with an associated medial extension of the trochlear margin. The lateral trochlear margin likewise extends anteriorly, and abuts against a lateral squatting facet, the latter matching the one on the distal tibia.

Plantarly, the medial and anterior calcaneal facets are partially fused. They exhibit a non-articular wedge extending 7.8mm in from the sulcus tali, leading up to a clear fusion line 8.4mm long. In addition, the posterior 8.4mm of the margin between the anterior calcaneal facet and the talar head along the postero-medial portion of their border is open.

The bone lacks a clear sulcus tali facet on the anterior margin of the posterior calcaneal surface, but it presents rounding of that surface along its more anterior sulcus tali margin. In addition, there is a swelling of non-articular bone 14.7mm long in the antero-medial portion of the postero-medial end of the sulcus tali. It is up to 4.4mm wide, and it abuts against the posterior margin of the medial calcaneal facet, remaining separate from the posterior facet.

Finally, the posterior calcaneal facet has a persistent small sulcus 3.0mm long extending in near the posterior end of the postero-lateral margin of the facet. It is the result of incomplete fusion of the ossification center for the lateral posterior tubercle to the talus.

CUBOID

Inventory

Right (No. 1.1/30).
Complete undamaged bone.

Morphology

The right cuboid bone of Gough's Cave 1 (Table 19; Fig. 15) is a

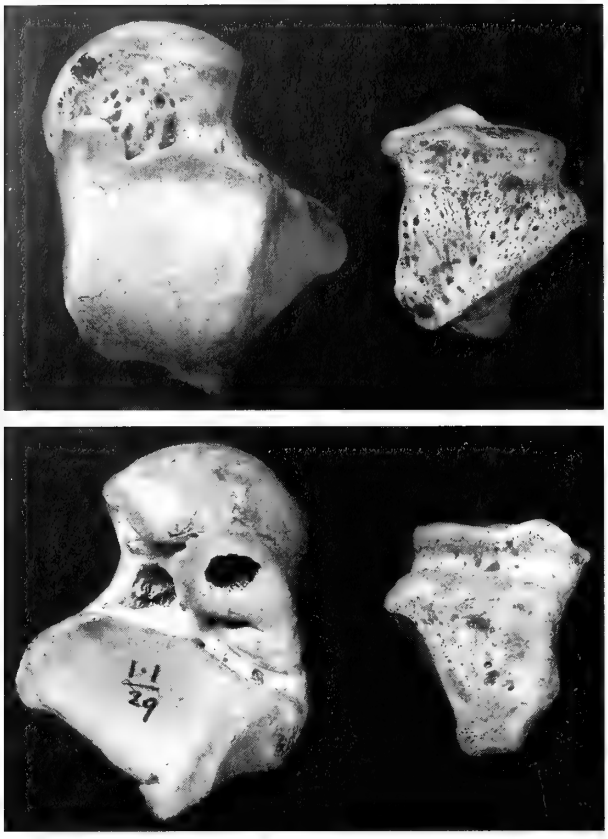

Fig. 15 Dorsal (above) and plantar (below) views of the Gough's Cave 1 right talus and cuboid bone; × 0.9.

Table 17 Osteometrics of the Gough's Cave 1 right talus.

Maximum (lateral) length[1]	60.5
Length (M-1)	55.0
Articular height (M-3b)	26.0
Articular breadth (M-2b)	46.7
Trochlear length (M-4)	35.8
Trochlear breadth (M-5)	28.3
Trochlear height (M-6)	11.4
Lateral malleolar height[2]	26.5
Lateral malleolar oblique height (M-7a)	28.0
Lateral malleolar breadth (M-7)	9.0
Lateral malleolar length[3]	29.5
Head and neck length (M-8)	20.0
Head length (M-9)	37.2
Head breadth (M-10)	21.6
Posterior calcaneal length (M-12)	35.0
Posterior calcaneal breadth (M-13)	23.5
Trochlear angle[4]	5°
Neck angle (M-16)	23°
Torsion angle (M-17)	34°
Posterior calcaneal angle (M-15)	41°
Subtalar angle[5]	59°

[1] Distance from the distal head to the proximal lateral tubercle parallel to the sagittal plane of the trochlea.
[2] Distance from plantar-lateral tip of the lateral malleolar surface to the highest point on the lateral malleolar arc, measured in the coronal and sagittal planes determined by the horizontal plane of the mid-trochlea.
[3] The antero-posterior maximum distance on the articular surface for the lateral malleolus (Day & Wood, 1968).
[4] Angle between the medial and lateral margins of the middle of the trochlea (Trinkaus, 1975b).
[5] Angle between the long axis of the subtalar joint (midline across the medial and posterior calcaneal surfaces) and the median sagittal plane of the trochlea (Trinkaus, 1975b).

Table 18 Discrete trait features of the Gough's Cave 1 right talus.

Calcaneal surface fusion	partial anterior & medial[1]
Anterior extension of the medial malleolar surface[2]	present
Medial extension of the trochlea	present
Lateral extension of the trochlea	present
Medial squatting facet	absent
Lateral squatting facet	present
Sulcus tali facet	absent
Sulcus tali margin rounding	present

[1] Partial fusion of the anterior and medial surfaces with a notch present along the sulcus tali margin (see Trinkaus, 1975a).
[2] For definitions of variations, see Barnett (1954) and Trinkaus (1975a).

Table 19 Osteometrics of the Gough's Cave 1 right cuboid.

Maximum length (M-1)	38.4
Medial length[1]	29.7
Lateral length (M-2)	13.5
Height[2]	26.6
Calcaneal height[3]	23.5
Calcaneal breadth[4]	30.0
Navicular height	11.2
Navicular breadth	5.8
Lateral cuneiform height	17.3
Lateral cuneiform breadth	13.2
Metatarsal 4/5 height	19.3
Metatarsal 4/5 breadth	28.5
Metatarsal 4 height	19.3
Metatarsal 4 breadth	12.7
Metatarsal 5 height	14.5
Metatarsal 5 breadth	15.8

[1] Minimum distance on the medial side between the calcaneal and metatarsal 4 facets.
[2] Maximum dorso-plantar height of the bone.
[3] All articular facet heights are the maximum dorso-plantar dimension of the articular facet in question.
[4] Articular facet breadths are the maximum medio-lateral dimensions for the calcaneal and metatarsal facets and the maximum proximo-distal dimensions for the navicular and lateral cuneiform facets.

relatively long bone that is strongly narrowed laterally. An index comparing its maximum length to that of the talus provides a value of 69.8, which is exceeded only by that of Le Peyrat 5 (70.9) in a small 80% male sample of Mesolithic cuboid bones (62.8 ± 5.0, N = 5). At the same time, its index of the lateral length to maximum (medial) length (35.2) is the lowest of the available Mesolithic indices (49.7 ± 8.3, N = 5), again approached only by the one from Le Peyrat 5 (35.8).

The non-articular surfaces of the bone are quite porous, and the articular surfaces themselves have generally distinct but rounded margins. There is a large facet for the navicular bone, which is separated from the calcaneal facet by 2.0mm of non-articular bone and blends into the lateral cuneiform facet with only a modest angle in the subchondral bone surface. The metatarsal 4 and 5 facets are partially separated by a vertical ridge, with the metatarsal 5 facet being distinctly wider but shorter.

The peroneal sulcus exhibits a lateral projection for the tendon of *M. peroneus longus*, but its surface shows no evidence of an articulation with a sesamoid bone.

METATARSALS

Inventory

Metatarsal 1 Right (No. 1.1/33). Complete bone.

Metatarsal 3 Right (No. 1.1/32). Complete bone.

Metatarsal 4 Right (No. 1.1/31). Complete bone.

Morphology

The three preserved metatarsal bones of the Gough's Cave 1 right foot present an unexceptional morphology, with relatively smooth surfaces and distinct articular facets. The metatarsal 1 presents a strongly twisted medial cuneiform facet and a large but smooth *M. peroneus longus* tubercle. Distally, it has a relatively flaring surface for the lateral sesamoid bone, and a clear lateral deviation of the head indicating hallux valgus.

Robusticity indices for the Gough's Cave 1 metatarsals (geometric mean of the midshaft diameters versus articular length) are similar to Mesolithic means for the first and fourth rays (metatarsal 1: 22.9 versus 23.0 ± 1.6, N = 5; metatarsal 4: 12.9 versus 13.1 ± 0.7, N = 5). The third metatarsal, however, has a robusticity index (12.2) which is two standard deviations below the mean of a Mesolithic comparative sample (13.4 ± 0.6, N = 5).

Fig. 16 Plantar (above), medial (below left) and lateral (below right) views of the Gough's Cave 1 right metatarsals; × 1.

Table 20 Length and midshaft diaphyseal measurements of the Gough's Cave 1 right metatarsals; in mm, unless otherwise noted.

	1	3	4
Maximum length	61.7	72.4	71.4
Articular length (M-1, M-2)	59.6	70.4	69.4
Midshaft height (M-4)	14.4	9.7	11.3
Midshaft breadth (M-3)	12.9	7.6	7.1
Total area (mm^2)	145.9	57.9	63.0
Cortical area (mm^2)	75.6	50.7	50.6
Medullary area (mm^2)	70.3	7.2	12.4
Dorso-plantar 2nd moment of area (I_x) (mm^4)	1438.1	331.0	472.1
Medio-lateral 2nd moment of area (I_y) (mm^4)	1174.9	207.2	193.7
Polar moment of area (mm^4)	2613.0	538.2	665.8

Table 21 Osteometrics of the Gough's Cave 1 right metatarsal epiphyses.

	1	3	4
Proximal maximum height (M-7)	30.1	21.0	19.0
Proximal maximum breadth (M-6)	21.6	14.3	13.1
Proximal articular height	30.1	20.7	18.6
Proximal articular breadth	16.8	13.6	11.9
Lateral cuneiform breadth[1]			2.3
Dorsal metatarsal 2 height[2]		8.7	
Dorsal metatarsal 2 breadth		9.2	
Plantar metatarsal 2 height		8.4	
Plantar metatarsal 2 breadth		4.8	
Metatarsal 3 height			10.6
Metatarsal 3 breadth			11.0
Metatarsal 4 height		11.3	
Metatarsal 4 breadth		11.9	
Metatarsal 5 height			10.3
Metatarsal 5 breadth			11.3
Distal height (M-9)	22.8	15.5	14.4
Distal maximum breadth (M-8)	21.9	10.5	11.1
Distal articular breadth	20.2	9.8	9.4
Distal medial height[3]	19.6		
Distal lateral height	20.9		
Torsion angle (M-11)	3°	14°	25°
Horizontal angle[4]		16°	21°
Vertical angle[5]		4°	15°
Horizontal head angle[6]	7°		

[1]Breadths of the secondary proximal metatarsal facets are all proximo-distal.
[2]Heights of the secondary proximal metatarsal facets are all dorso-plantar.
[3]Distal medial and lateral heights are from each hallucal sesamoid sulci to the dorsal margin of the metatarsal head.
[4]Angle between the coronal plane of the main metatarsal facet and the diaphyseal axis in the horizontal plane of the bone. A positive angle indicates a medial deviation of the facet.
[5]Angle between the coronal plane of the main metatarsal facet and the diaphyseal axis in the sagittal plane of the bone. A positive angle indicates a plantar deviation of the facet.
[6]Angle in the horizontal plane between the intersesamoid crest and the diaphyseal axis.

The relative lengths of the Gough's Cave 1 metatarsals can be assessed by comparing their articular lengths to talar length and femoral bicondylar length. In the first comparison, the first and third rays produce indices of 108.4 and 128.0, which are slightly shorter and longer respectively than the means of a Mesolithic sample (metatarsal 1: 113.6 ± 7.3, N = 5; metatarsal 3: 122.9 ± 11.8, N = 5). Comparing the same lengths to femoral length produces indices of 13.7 and 16.1, values which are similar to and slightly above the means of a Mesolithic sample (13.8 ± 0.8, N = 5 and 15.6 ± 1.1, N = 5 respectively).

SUMMARY

The lower limb remains of Gough's Cave 1 are therefore those of a largely average young adult male, compared to other European Mesolithic specimens. Overall diaphyseal robusticity is generally similar to that of other Mesolithic specimens, even though the fibula and third metatarsal appear relatively gracile. In general, however, musculo-ligamentous attachment areas are weakly marked, in terms of the prominence, size and rugosity of the various crests and tuberosities. The exceptions to this are the marked pilasters of the femora (but weak lineae asperae) and the large proximal tibio-fibular ligament crest on the right fibula.

The proximal femora and the femoral diaphyses exhibit a clear asymmetry, especially in their neck-shaft angles and diaphyseal dimensions. This asymmetry is accompanied, in the pelvis, by a greater degree of lateral flare of the left ilium. It is not possible to determine, given primarily preservation of only the right side below the knee, whether this asymmetry continued distally.

These aspects are associated with a pelvis that combines several distinctly male characteristics with an overall pelvic aperture shape which is female.

ACKNOWLEDGEMENTS. I would like to thank Chris Stringer for inviting me to participate in the Cheddar Man project. I am very grateful to Steve Churchill for taking over the description of the upper limb and axial remains, thereby relieving me of the need to sequence the ribs, and to Trent Holliday and Steve Churchill for dealing with issues of body size and proportions. Steve Churchill also collected lower limb osteometrics and generated the raw data for the Mesolithic comparative lower limb cross sections, and Erik Ozolins digitized all of them. The femoral and tibial cross-sectional geometry samples were greatly expanded through the work of Brigitte Holt. My participation in this project has been supported by the Interdisciplinary Research Fund of the Natural History Museum (London) and National Science Foundation grant SBR-9318702. To all of these individuals and institutions I am grateful. This paper was submitted and accepted for publication in October 1997.

REFERENCES

Barnett, C.H. 1954. Squatting facets on the European talus. *Journal of Anatomy*, London, **88**: 509–513.

Barral, L. & Primard, S. 1962. L'homme du Rastel. Commune de Peillon (A.-M.). *Bulletin du Musée d'Anthropologie Préhistorique de Monaco*, Monaco, **9**: 171–190.

Bräuer, G. 1988. Osteometrie. In: *Anthropologie I*. Stuttgart: Fischer Verlag. pp.160–232.

Combier, J., and Genet-Varcin, E. 1959. L'homme mésolithique de Culoz et son gisement. *Annales de Paléontologie*, Paris, **45**: 141–174.

Cremonesi, G., Parenti, R., & Romano, S. 1972. Scheletri paleolitici della Grotta delle Veneri presso Parabita (Lecce). *Atti della XIV Riunione Sci. dell'Istituto Italiano de Preistoria e Protoistoria*, Rome, pp.105–117.

Day, M.H. & Wood, B.A. 1968. Functional affinities of the Olduvai Hominid 8 talus. *Man*, London, **n.s. 3**: 440–455.

Eschman, P.N. 1992. *SLCOMM Version 1.6*. Albuquerque: Eschman Archeological Services.

Ferembach, D. 1976. *Mensurations individuelles des squelettes Mésolithiques de Moita do Sebastião (Muge – Portugal)*. Paris: Laboratoire d'Anthropologie Biologique de l'École Pratique des Hautes Études.

Genet-Varcin, E., Vilain, R., & Miquel, M. 1963. Une seconde sépulture mésolithique à Culoz (Ain). *Annales de Paléontologie (Vertébrés)*, Paris, **49**: 305–324.

Graziosi, P. 1947. Gli uomini paleolitici della Grotta di S. Teodoro (Messina). *Rivista Scienze preistoria*, Rome, **2**: 123–233.

Holliday, T.W. 1995. *Body Size and Proportions in the Late Pleistocene Western Old World and the Origins of Modern Humans*. Ph.D. Thesis, University of New Mexico.

—— **& Churchill, S.E.** 2003. Gough's Cave 1 (Somerset, England): an assessment of body size and shape. *Bulletin of the Natural History Museum, Geology*, **58**(supplement): 37–44.

Holt, B. 1999. *Biomechanical Evidence of Decreased Mobility in Upper Paleolithic and Mesolithic Europe*. Ph.D. Thesis, University of Missouri – Columbia.

Lovejoy, C.O., Heiple, K.G. & Burstein, A.H. 1973. The gait of *Australopithecus*. *American Journal of Physical Anthropology*, New York, **38**: 757–779.

McCown, T.D. & Keith, A. 1939. *The Stone Age of Mount Carmel II*. Oxford: Clarendon Press.

Nagurka, M.L. & Hayes, W.C. 1980. An interactive graphics package for calculating cross-sectional properties of complex shapes. *Journal of Biomechechanics*, Oxford, **13**: 59–64.

Paoli, G., Parrenti, R. & Sergi, S. 1980. Gli scheletri mesolitici della Caverna delle Arene Candide (Liguria). *Memorie dell'Istituto Italiano di Paleontologia Umama*, Rome, **3**: 33–154.

Patte, E. 1968. L'homme et la femme de l'Azilien de Saint Rabier. *Mémoires du Muséum National d'Histoire Naturelle*, Paris, Série C. **19**: 1–56.

Pittard, E. & Sauter, M.R. 1946. Un squelette magdalénien provenant de la station des Grenouilles (Veyrier, Haute Savoie). *Archives suisses d'Anthropologie Générale*, Geneva, **11**: 149–200.

Radlauer, C. 1908. Beiträge zur Anthropologie des Kreuzbeines. *Gegenbaurs Morphologisches Jahrbuch*, Leipzig, **38**: 323–447.

Ruff, C.B. 1990. Body mass and hindlimb bone cross-sectional and articular dimensions in anthropoid primates. *In*: Damuth, J. & MacFadden, B.J. (eds.), *Body Size in Mammalian Paleobiology: Estimation and Biological Implications*. New York: Cambridge Univ. Press. pp. 119–149.

—— 1991. Climate and body shape in hominid evolution. *Journal of Human Evolution*, London, **21**: 81–105.

—— 1995. Biomechanics of the hip and birth in early *Homo*. *American Journal of Physical Anthropology*, New York, **98**: 527–574.

—— **& Hayes, W.C.** 1983. Cross-sectional geometry of Pecos Pueblo femora and tibiae – A biomechanical investigation: I. Method and general patterns of variation. *American Journal of Physical Anthropology*, New York, **60**: 359–381.

——**, Trinkaus, E., Walker, A. & Larsen, C.S.** 1993. Postcranial robusticity in *Homo*, I: Temporal trends and mechanical interpretations. *American Journal of Physical Anthropology*, New York, **91**: 21–53.

Runestad, J.A., Ruff, C.B., Nieh, J.C., Thorington, R.W. & Teaford, M.F. 1993. Radiographic estimation of long bone cross-sectional geometric properties. *American Journal of Physical Anthropology*, New York, **90**: 207–213.

Schultz, A.H. 1930. The skeleton of the trunk and limbs of higher Primates. *Human Biology*, Detroit, **2**: 303–438.

Tague, R.G. 1989. Variation in pelvic size between males and females. *American Journal of Physical Anthropology*, New York, **80**: 59–71.

Tardieu, C. & Trinkaus, E. 1994. The early ontogeny of the human femoral bicondylar angle. *American Journal of Physical Anthropology*, New York, **95**: 183–195.

Trinkaus, E. 1975a. Squatting among the Neandertals: A problem in the behavioral interpretation of skeletal morphology. *Journal of Archaeological Science*, London, **2**: 327–351.

—— 1975b. *A Functional Analysis of the Neandertal Foot*. Ph.D. Thesis, Univ. of Pennsylvania.

—— 1976. The evolution of the hominid femoral diaphysis during the Upper Pleistocene in Europe and the Near East. *Zeitschrift für Morphologie und Anthropologie*, Stuttgart, **67**: 291–319.

—— 1983. *The Shanidar Neandertals*. New York: Academic Press.

—— 1993. Femoral neck-shaft angles of the Qafzeh-Skhul early modern humans, and activity levels among immature Near Eastern Middle Paleolithic hominids. *Journal of Human Evolution*, London, **25**: 393–416.

—— 1996. The *M. obturator internus* sulcus on Middle and Late Pleistocene human ischia. *American Journal of Physical Anthropology*, New York, **101**: 503–513.

Trotter, M. & Lanier, P.F. 1945. *Hiatus canalis sacralis* in American whites and negroes. *Human Biology*, Detroit, **17**: 368–381.

Warren, E. 1897. An investigation on the variability of the human skeleton: with especial reference to the Naqada race. *Philosophical Transactions of the Royal Society*, London, Series B, **189**: 135–227.

Bull. nat. Hist. Mus. Lond. (Geol.) **58**(supp): 23–35 Issued 26 June 2003

Human Dental Remains from Gough's Cave (Somerset, England)

DIANE E. HAWKEY
Department of Anthropology, Arizona State University, Tempe, AZ 85287-2402, USA

SYNOPSIS. The dental remains of nine individuals from Gough's Cave (Cheddar, Somerset) date from Late Pleistocene to the Holocene. Descriptions are provided for all individuals for crown and root morphology, odontometric data, dental pathology (caries, abscess, periodontal disease, enamel hypoplasia), calculus deposition, enamel pressure chipping, occlusal attrition, and evidence of intentional/occupational modification. The analytical focus is on seven individuals who date from the Late Upper Paleolithic/Mesolithic (Creswellian) culture periods. Comparative data from nine world populations suggest five trends: 1) Gough's Cave individuals have a morphologically simplified dental pattern similar to other Late Pleistocene/Early Holocene populations of North Europe, South/Southwest Asia and North Africa. 2) Within Europe, Gough's Cave is consistent in post-Pleistocene trend towards reduction in tooth size. 3) There is a temporal trend in the British Isles towards lateral incisor reduction, while maintaining stable molar tooth size. 4) Pathology, wear, and enamel pressure chipping are consistent with a hunter/gatherer lifeway, with one individual who may have occupationally related microtrauma. 5) No evidence occurs of any cleaning striations ('toothpick groves') as has been suggested for Neanderthals.

INTRODUCTION

Little is currently known about the dentition of Late Pleistocene/Early Holocene inhabitants of the British Isles. Excavations at Gough's Cave (Cheddar Gorge, Somerset) have recovered the dental remains for a minimum number of seven individuals dating to this time range. The remains have been radiocarbon dated to between 12,380 and 9,080 BP (Hedges *et al* 1991) and include 'Cheddar Man' (Gough's Cave 1), the most complete early human skeleton from Britain. Individuals from this time span date to the Upper Late Paleolithic/Mesolithic (Creswellian) culture periods. Dentition from two additional specimens (Gough's Cave 4 and 5) are more recent, dating to the Late Holocene. Gough's Cave 1, although dating to the Mesolithic time period, was included in analysis of the Upper Late Paleolithic group in order to maximize sample. While the sample is small the assumption is that the available data characterize individuals from early Gough's Cave.

The first part of this study describes all dental remains from Gough's Cave. Included are crown and root morphology, odontometric data, pathology (caries, abscess, periodontal disease, enamel hypoplasia), calculus deposition, enamel pressure chipping, occlusal attrition (wear), cultural treatment and intentional/occupational modification. The latter half of the study focuses specifically on the dentition from the Late Pleistocene/Early Holocene and provides a comparative analysis with other early and recent world populations.

General descriptions of the Gough's Cave skeletal and dental remains have been published elsewhere (Oakley *et al* 1971; Tratman 1975; Stringer 1985, 1990). This research is part of a larger series of forthcoming articles published in the Bulletin of the Natural History Museum that will present a detailed analysis of the material.

METHODS AND MATERIALS

Gough's Cave remains used in this study are currently housed at the Natural History Museum in London and were excavated in 1903, 1927–29, and 1986–87 (Davies 1904; Seligman & Parsons 1914; Keith & Cooper 1929; Cooper 1931; Currant *et al* 1989). Although Humphrey and Stringer (n.d.) argue for a numerically conservative approach, and suggest a minimum number of five individuals for the Late Pleistocene/Early Holocene group, the lack of any clear association between the dental elements (especially occlusion and enamel pressure chipping patterns) argues for a minimum number of seven individuals as presented in the current study (Table 1). The two more recent specimens (Gough's Cave 4 and 5) date to the Late Holocene.

Table 1 Gough's Cave specimen numbers, time period, age, sex, number of teeth with morphology data (includes root data and unerupted teeth), and number of teeth with odontometric data.

Specimen number	Time period	Age	Sex	Morphology (n = teeth)	Metrics (n = teeth)
87-25/87/49	Late Pleistocene	Adolescent	Unknown	27	18
87-103a	Late Pleistocene	Adult, mid-old	Unknown	1	1
87-139	Late Pleistocene	Adult, young-mid	Unknown	13	12
87-253	Late Pleistocene	Adult, young-mid	Male	10	5
89-001	Late Pleistocene	Adult, young	Unknown	1	1
Gough's Cave 6	Late Pleistocene	Adult, mid-old	Male	16	1
Gough's Cave 1	Early Holocene	Adult, young-mid	Male	27	20
Gough's Cave 4	Late Holocene	Adolescent	Unknown	6	1
Gough's Cave 5	Late Holocene	Adult, mid-old	Unknown	4	0
Total				105	59

© The Natural History Museum, 2003

The dental remains described here include three males (all Late Pleistocene/Early Holocene), with the remaining six of indeterminate sex. The Late Pleistocene/Early Holocene adults range in dental age from adolescent (n = 1), young adult (n = 1), young-middle adult (n = 3), middle-older adult (n = 2). The two Late Holocene individuals are an adolescent (Gough's Cave 4) and a middle-older age adult (Gough's Cave 5). Age determination for adolescents is based on eruption, degree of root formation, and occlusal wear. Adult age is based on degree of dental attrition, using the adolescent sample as a baseline.

Morphology: Crown and root morphology data for 105 teeth were collected using the Arizona State University Dental Anthropology System (Turner *et al* 1991). The Dental Anthropology System (DAS) consists of a series of rank-scaled reference plaques to score trait presence and degree of expression. When congenital absence of a tooth was suspected, the score was confirmed through use of radiographs. Data for two additional crown traits (to be added to DAS in the future) were collected: 1) maxillary premolar accessory ridge (Burnett *et al* 1996) and 2) upper premolar buccal style (Hawkey n.d.*a*).

For the purpose of analysis, the individual count was used (Turner & Scott 1977), a method that assumes the highest grade of expression for a given antimere best characterizes an individual's genotype for that trait. Thus, the score used for an individual is the highest grade observed between the two sides. In order to maximize sample size when only one side is present, the score for that side is used, and symmetry is assumed. Comparative key trait data for nine geographic populations were obtained from the literature and adjusted to reflect the DAS breakpoints for presence/absence following methodology used by Turner (1987). The key traits for a given tooth/feature are considered to be the most reliable population discriminators, and are scored for the teeth considered to be the least influenced by environmental factors according to the Field concept (Dahlberg 1945).

Metrics: Odontometric measurements for 59 teeth were taken using Helios needle-point calipers, calibrated to 0.05 mm. Each measurement was taken on three separate occasions and all were found to be within 0.05 mm difference. When discrepancies occurred, the results of the three measurements were averaged. The mesiodistal (MD) and buccolingual (BL) diameters of the maximum crown length and breadth were obtained, following the methods of Moorrees (1957). Teeth with observable interproximal wear were not measured for MD diameter. In addition, data for crown height of unworn teeth and complete root length were collected.

Asymmetry between right and left antimeres in both MD and BL diameters were assessed by paired samples t-test. A metric description of crown size and shape dimension was calculated by use of Crown Index, Crown Area, and Crown Module for all premolars and molars. Crown Index ([BL/MD] × 100) provides a measurement of relative crown breadth, with a score of 100 indicating that the BL and MD measurements are equal; a score greater than 100 denotes that the BL diameter is larger than the MD diameter. Crown Area (MDxBL) provides occlusal surface area, although it is assumed that the surface is rectangular. Crown Module ([MD+BL]/2) is calculated to indicate the average diameter of the tooth. While Crown Index provides some idea of occlusal shape, the Crown Module and Area describe the size of the crown. Incisor Breath (MD diameter I^2/MD diameter of I^1) was also determined because the MD ratio of the upper incisors has been proposed as useful in population affinity assessment (Lukacs 1985; Potter *et al* 1981).

When both sides were present, left side data were utilized for odontometric analysis. Due to the limited number of teeth available for analysis, right side measurements were used when the left side was absent (Goose 1963). Data from both sexes were pooled, because only three males could be identified reliably in the sample.

In order to characterize the population in a single figure, the Total Crown Area (sum of the mean crown area for all maxillary and mandibular teeth on one side) was calculated and presented as millimetres squared (mm^2). The Molar Crown Area for M1-M2 teeth (M1M2CA) was also calculated (sum of the Crown Area of maxillary and mandibular first and second molars on one side) in order to assess posterior tooth size. Ordinarily, the M3 is included in the calculation, but a lack of M3 data in the comparative samples necessitated use of only M1 and M2. The Penrose shape/size statistic (Penrose 1954) was used to assess dental metric population similarities based on both size and shape components; Corruccini (1973) has found the shape component to be particularly useful for population comparisons.

Pathology/occlusal attrition/crown chipping: Data for three forms of dental pathology (caries, abscessing, periodontal disease), calculus deposition and enamel hypoplasia were collected. Caries were scored for presence/location, following the definitions and procedures established by Koritzer (1977). An abscess was defined as a perforation of the alveolar bone connected to the root socket, while periodontal disease was noted in terms of degree of root exposure with antemortem erosion of the alveolar border (Turner *et al*, 1991). Calculus deposition was scored following Brothwell's (1981) definition of slight, medium, and heavy. Presence of enamel hypoplasia was scored as either chronic or acute episodes, in linear or pitting forms, with the dental age development estimate obtained from Schour and Massler's (1940) crown formation chart for U.S. Whites. Degree of occlusal attrition (wear) was noted for each tooth, following procedures established in DAS, with a score of '0' indicating no wear, '.5' as trace wear facets seen with 10x magnification, '1' has dentine exposed, '2' indicates cusps are worn away, '3' is exposed pulp, and '4' as functional root stump, with all or most of the enamel missing. Antemortem crown chipping (microtrauma) was determined through examination by a 10x hand lens to differentiate from post-mortem damage. Any presence of chipping was noted as to tooth and location on the tooth.

Other features: Any evidence of intentional dental modification (ablation, filing, inlay, staining), cleaning striations (brushing, interproximal 'toothpick' grooves), or occupational use of teeth were described.

SPECIMEN DESCRIPTIONS: LATE PLEISTOCENE/EARLY HOLOCENE

SPECIMEN. Gough's Cave 87-25/87/49 (including Specimens 009,120a, 120b, 165, 264b)

TIME PERIOD. Late Pleistocene (Late Upper Paleolithic)

DESCRIPTION. Individual is an older adolescent (approximately 15–18 years), based on eruption pattern and degree of occlusal wear. The specimen includes the left maxilla (87/25), right maxilla (87/87), and mandible (87/49), including the RI_1 (87/264b), LI_2 (87/102a), RP_3 (87/120b), LP_3 (87/165), and LP_4 (89/009). *Maxillary dentition:* Present are the $LRI^{1,2}$, LR^C, LP^3, retained deciduous lm^2, $LM^{1,2}$ and an unerupted LM^3. The RP^3, RP^4, $RM^{1,2,3}$ are missing postmortem and there is postmortem damage (chipping) on the occlusal edges of the $RI^{1,2}$ and the paracone of LM^2. *Mandibular dentition*: Teeth present are the RI_1, LI_2, LRP_3, LP_4, $LRM_{1,2}$, and unerupted

LRM_3. There is postmortem loss of the LI_1, RI_2, LR_C, and RP_4. There is no evidence of cultural treatment or modification of the teeth.

CROWN WEAR. All maxillary and mandibular anterior teeth present and all first molars exhibit slight to moderate (grade = 1) wear. All second molars have only wear facets present (grade = 0.5). All third molars are unerupted and lack wear.

ENAMEL PRESSURE CHIPPING. None occurs on either maxillary or mandibular teeth.

PATHOLOGY. No evidence occurs of caries, abscess, calculus, periodontal disease, or enamel hypoplasia on maxillary or mandibular teeth.

CROWN MORPHOLOGY. *Maxillary dentition:* LRI^1: labial curvature = 1, there is no winging. $LRI^{1,2}$: Absence of shovel, double shovel, interruption groove, tuberculum dentale. LRI^2 are not peg-shaped, or reduced. LR^C: lack shovel, double shovel, tuberculum dentale, mesial or distal accessory ridges. LP^3: lacks double shovel, accessory cusps, disto-sagittal ridge, enamel extension, odontome, MxPAR, or buccal style. LM^1: metacone = 4, hypocone = 5, lack of cusp 5. LM^2: metacone = 3.5, hypocone = 3, cusp 5 = 4 with the presence of cusp 6, (grade 1 on the UM5 plaque, with cusp 5 very much larger than cusp 6). Both molars lack Carabelli's trait, parastyle, and enamel extension. *Mandibular dentition:* RI_1 and LI_2: absence of shovel. LRP_3: lack enamel extension and odontome. RP_3: grade = 1 lingual cusp. LP_4: single lingual cusp (grade = 0). LRM_1: Y-5 pattern (cusp 5 = grade 5), protostylid = 1, enamel extension = 2, with absence of anterior fovea, cusp 7. LRM_2: + 5 pattern (cusp 5 = grade 3), with absence of deflecting wrinkle, distal and mid-trigonid crest, protostylid, cusp 7.

ROOT MORPHOLOGY. *Maxillary dentition*: LI^1: single root, with one radical. LI^2: single root with two radicals. L^C: single root with three radicals. LP^3: single root with two radicals. *Mandibular dentition*: All incisors, canines and premolars are single root teeth. RI_1: four radicals. LI_2: two radicals. RP_3: presence of Tomes' root (grade = 3), six radicals. LP_3: presence of Tomes' root, four radicals.

ODONTOMETRIC DATA

	crown dimensions MD	BL	crown height	root length	crown index	crown area	crown module
LI^1	9.28	7.85	–	12.20	–	–	–
RI^1	9.45	7.73	–	–	–	–	–
LI^2	7.38	7.23	–	12.95	–	–	–
RI^2	7.48	7.55	–	–	–	–	–
L^C	7.50	9.50	–	14.80	–	–	–
R^C	7.40	9.58	–	–	–	–	–
LP^3	6.43	9.28	–	10.00	144.32	59.67	7.86
LM^1	10.83	12.83	–	–	118.47	138.95	11.83
LM^2	10.23	13.23	–	–	129.33	135.34	11.73
dlm^2	9.48	11.50	–	–		–	–
RI_1	5.70	6.38	–	11.53			–
LI_2	6.23	7.03	–	13.48			–
LP_3	6.80	8.63	–	11.20	126.91	58.68	7.72
RP_3	6.78	8.90	–	11.18	131.27	60.34	7.84
LP_4	7.15	8.50	–	–	118.88	60.78	7.83
LM_1	11.58	11.15	–	–	96.29	129.12	11.37
RM_1	11.78	11.10	–	–	94.23	130.76	11.44
LM_2	11.90	10.43	–	–	87.65	124.12	11.17
RM_2	11.20	10.18	–	–	90.89	114.02	10.69

SPECIMEN. Gough's Cave 87-103a

TIME PERIOD. Late Pleistocene (Late Upper Paleolithic)

DESCRIPTION. An isolated LI^1 does not match any of the maxillary alveolar sockets present. There is perimortem damage to the distal third of the labial enamel surface. Occlusal wear and degree of root formation suggests the individual was middle-old age adult.

CROWN WEAR. Heavy wear occurs on the occlusal surface up to, but not exposing, the pulp chamber (grade = 3). An estimated loss of one-half of the total crown has occurred, with only the cervical one-half of the crown remaining.

ENAMEL PRESSURE CHIPPING. No evidence noted of antemortem chipping. Postmortem chipping occurs on the distal one-third of the labial crown surface.

PATHOLOGY. No carious activity is present in root or crown. No evidence occurs of enamel hypoplasia or calculus on the remaining cervical half of the crown.

CROWN MORPHOLOGY. Tooth is too worn to score for traits (labial curve, winging, shovel, double shovel, interruption groove, tuberculum dentale).

ROOT MORPHOLOGY. LI^1: single root, no radicals.

ODONTOMETRIC DATA

	crown dimensions MD	BL	crown height	root length	crown index	crown area	crown module
LI^1	–	6.98	–	6.30	–	–	–

SPECIMEN. Gough's Cave 87–139 [460-B-ALT; 301.0]

TIME PERIOD. Late Pleistocene (Late Upper Paleolithic)

DESCRIPTION. Specimen is of an adult maxilla, with complete alveolus and palate. Based on eruption and degree of occlusal wear, this individual is an adult, possibly young-middle age. Maxillary teeth present are the $LRI^{1,2}$, LR^C, LRP^3, RP^4, and $LRM^{1,2}$, with antemortem loss of LP^4. Postmortem damage occurred on the buccal surfaces of the LP^3, the LM^1 and LRM^2.The RM^3 is missing postmortem, and the LM^3 is congenitally absent. No evidence of cultural treatment or modification was found. Although Humphrey and Stringer (n.d.) suggest a possible association between this specimen and GC87–253, a lack of occlusion and lack of matching enamel pressure chipping patterns on the anterior dentition of GC87–253 argue against the two specimens representing a single individual.

CROWN WEAR. Slight-moderate, with heaviest wear on first molars (grade = 1.5), anterior teeth (grade = 1), and wear facets without dentine exposure (grade = 0.5) on the second molars.

ENAMEL PRESSURE CHIPPING. There is a minor degree of chipping on the disto-labial surfaces of LRI^1, the mesio-occlusal surfaces of LRI^2, and the buccal surface of L^C.

PATHOLOGY. Antemortem loss of LP^4 has occurred. No caries, abscessing, or calculus noted. Slight enamel hypoplastic pitting (acute episode) occurs near the CEJ on LI^2, LR^C, and RM^1. All remaining teeth do not display hypoplasia.

CROWN MORPHOLOGY. LRI^1: labial curvature = 1, tuberculum dentale = 1, absence of shovel, double shovel, interruption groove, and winging.; LRI^2: both teeth lack shovel, double shovel, interruption grooves, and are not peg/reduced shaped; RI^2 has tuberculum dentale = 2, (LI^2 is missing data) ; LR^C: absence of shovel, double shovel, tuberculum dentale, mesial accessory ridge; LRP^3: no double shovel on RP^3 (missing data for LP^3), lack of mesial/distal accessory cusps, disto-sagittal ridge, enamel extension, odontome, buccal style

on both teeth; RP^4: no accessory cusps, enamel extension, odontome, buccal style; RM^1: metacone = 4, hypocone = 4, absence of cusp 5, Carabelli's trait, parastyle, enamel extension; LM^1: hypocone = 4, lack of Carabelli's trait, enamel extension; RM^2: enamel extension = 1, absence of hypocone, cusp 5, Carabelli's trait; LM^2: metacone = 4, hypocone = 1, absence of cusp 5, Carabelli's trait.

ROOT MORPHOLOGY. Could not be determined.

ODONTOMETRIC DATA

	crown dimensions MD	BL	crown height	root length	crown index	crown area	crown module
LI^1	9.60	7.45	–	–	–	–	–
RI^1	9.90	7.33	–	–	–	–	–
LI^2	8.20	7.90	–	–	–	–	–
RI^2	7.85	7.28	–	–	–	–	–
L^C	8.13	9.85	–	–	–	–	–
R^C	7.95	9.98	–	–	–	–	–
LP^3	6.73	9.03	–	–	134.17	60.77	7.88
RP^3	6.03	–	–	–	–	–	–
RP^4	5.75	8.83	–	–	–	–	–
LM^1	–	12.20	–	–	–	–	–
RM^1	10.28	–	–	–	–	–	–
LM^2	9.75	–	–	–	–	–	–

SPECIMEN. Gough's Cave 87–253 [304.0]

TIME PERIOD. Late Pleistocene (Late Upper Paleolithic)

DESCRIPTION. Mandibular fragment of an adult male, consisting mainly of the right portion of the mandible, separated just distal to LI_2, and including the lower portion of the right ramus. There is postmortem loss of LRI_1,RI_2, RP_3. The RM_3 is congenitally absent. Mandibular teeth present are the LI_2 (89/003) R_C (87/263), RP_4 (89/002), and $RM_{1,2}$. There is no evidence of cultural treatment or modification. On the basis of occlusal wear and calculus deposition, this adult is estimated to be young-middle age.

CROWN WEAR. Slight-moderate, with heaviest wear (grade = 1.5) on the first molar and anterior teeth (grade = 1), and second molars with wear faceting, but no dentine exposure (grade = 0.5).

ENAMEL PRESSURE CHIPPING. None.

PATHOLOGY. No caries, abscessing, or periodontal disease occur. There is possible pitting on the buccal surface near CEJ on the R_C. A slight degree of calculus is present at the CEJ of all teeth.

CROWN MORPHOLOGY. LI_2: absence of shovel; RP_4:single lingual cusp (grade = 0), absence of odontomes, absence of buccal style; RM_1: Y-5 pattern (cusp 5 = grade 4), enamel extension present (grade = 2), absence of protostylid, cusp 7; RM_2: X-4 pattern, enamel extension present (grade = 3), absence of deflecting wrinkle, distal trigonid crest, mid-trigonid crest, protostylid, cusp 7.

ROOT MORPHOLOGY. All incisors, canines and premolars are single-rooted; LI_2: radicals = 2 ; R_C: radicals = 2; RP_4: radicals = 1.

ODONTOMETRIC DATA

	crown dimensions MD	BL	crown height	root length	crown index	crown area	crown module
LI_2	5.15	6.50	–	–	–	–	–
R_c	7.68	8.70	–	–	–	–	–
RP_4	6.58	8.33	6.08	13.53	126.60	54.81	7.46
RM_1	10.08	10.45	–	–	103.67	105.34	10.33
RM_2	10.15	10.58	–	–	104.24	107.39	10.37

SPECIMEN. Gough's Cave 89–001 [Area I/M102/701.0]

TIME PERIOD. Late Pleistocene (Late Upper Paleolithic)

DESCRIPTION. An isolated tooth, LP_4, that does not belong to the same individual as Gough's Cave 89–002 or 89–003, on the basis of morphology, metrics or degree of wear. Amount of occlusal wear and degree of root formation suggest a young adult.

CROWN WEAR. Slight wear facets (grade = 0.5) are on the buccal/occlusal surface, although no dentine is exposed.

ENAMEL PRESSURE CHIPPING. None.

PATHOLOGY. No caries or enamel hypoplasia, but a slight degree of calculus is present on the buccal and lingual surfaces of the cervical fourth of the crown.

CROWN MORPHOLOGY. Single lingual cusp (grade = 0), trace of buccal style (both mesial and distal), no odontome.

ROOT MORPHOLOGY. Single rooted, with three radicals.

ODONTOMETRIC DATA

	crown dimensions MD	BL	crown height	root length	crown index	crown area	crown module
LP_4	7.10	8.25	–	6.93	116.20	58.58	7.68

SPECIMEN. Gough's Cave #6

TIME PERIOD. Late Pleistocene: 11,700 ± 100 BP [OxA-2236] (Late Upper Paleolithic)

DESCRIPTION. An almost complete mandible (missing right ramus) of an adult male. Only the RM_2 is present. There is postmortem loss of $LRI_{1,2}$, LR_C, $LRP_{3,4}$, LRM_1, and LM_2. Both LRM_3 are congenitally absent. There is no evidence of cultural treatment or modification on the remaining tooth. The individual appears to be middle-old age on the basis of occlusal wear and amount of root exposure.

CROWN WEAR. Moderate wear (grade = 2) of dentine exposure on RM_2.

ENAMEL PRESSURE CHIPPING. None.

PATHOLOGY. No evidence for abscessing occurs. No caries, calculus, enamel hypoplasia present on remaining tooth, although there is a slight degree (1–2 mm) of root exposure.

CROWN MORPHOLOGY. RM_2: 4-cusped, lacking a protostylid, cusp 7.

ROOT MORPHOLOGY. All incisors, canines and premolars are single-rooted. Both first molars are two-rooted, although the root sockets of RM_1 indicate that the mesial root is slightly bifurcated (approximately a fourth of the total root length). The RM_2 is three-rooted and the socket for LM_2 has a mesial and distal root socket with a small auxiliary lingual root socket positioned just distal to the mesial alveolar socket, suggesting a 3-rooted tooth.

ODONTOMETRIC DATA

	crown dimensions MD	BL	crown height	root length	crown index	crown area	crown module
RM_2	12.03	10.90	–	–	90.61	131.13	11.47

SPECIMEN. Gough's Cave #1 ['Cheddar Man']

TIME PERIOD. Early Holocene: 9,080 ±150 BP [BM-525]; 9,100 ± 100 BP [OxA-814] (Mesolithic/Creswellian)

DESCRIPTION. Adult male with an almost complete mandible (missing left coronoid process and the left and right condyle) and an almost complete maxilla (missing the palate). *Maxillary teeth:* Present are the $LRM^{1,2,3}$ with postmortem loss of $RI^{1,2}$, R^C, RP^3, LRP^4. The remainder of the teeth ($LI^{1,2}$, L^C, LP^3) were damaged postmortem and observations were not made. *Mandibular teeth:* The $LRI_{1,2}$, LR_C, $LP_{3,4}$, and $LRM_{1,2,3}$ are present. Postmortem loss of $RP_{3,4}$ had occurred. There was no evidence of any cultural treatment or modification of the teeth. On the basis of eruption and occlusal wear, the individual was of young-middle age.

CROWN WEAR. Moderate to slight, with heaviest wear on LP_4, and RM_1 (grade = 1.5), remaining anterior teeth and LM_1 (grade = 1), and all remaining molars (grade = 0.5).

ENAMEL PRESSURE CHIPPING. RM^1: lingual portion of the hypocone.

PATHOLOGY. No evidence occurs of caries, abscessing, periodontal disease, enamel hypoplasia, or calculus.

CROWN MORPHOLOGY. *Maxillary teeth*: LRM^1: metacone = grade 4, hypocone = grade 4, absence of cusp 5, Carabelli's trait, parastyle, and enamel extension. RM^2: metacone = 4, hypocone = 3, cusp 5 = 3, with lack of Carabelli's trait, parastyle, enamel extension. LM^2: metacone = 4, hypocone = 1, with absence of cusp 5, Carabelli's trait, parastyle, and enamel extension. LRM^3: metacone = 3.5, hypocone = 1, with absence of cusp 5, Carabelli's trait, parastyle, enamel extension. Neither third molar exhibited a peg or reduced form. *Mandibular teeth:* All incisors lacked shovel. L_C: absence of distal accessory ridge. LP_3: lacked a lingual cusp (grade = A), and both $LP_{3,4}$ did not have enamel extension, or odontomes. LRM_1: have the Y-5 pattern (cusp 5 grade = 5), and lack protostylid, cusp 7, and enamel extension. LRM_2 and LM_3:have an X-4 pattern, with absence of deflecting wrinkle, distal and mid-trigonid crests, protostylid, cusp 7, and enamel extension. RM_3: has a Y-4 pattern and also lacks deflecting wrinkle, distal and mid-trigonid crest, protostylid, cusp 7. Because molars are slightly crowded, the torso-molar angle could not be assessed.

ROOT MORPHOLOGY. $RP_{3,4}$: single-rooted.

ODONTOMETRIC DATA

	crown dimensions MD	BL	crown height	root length	crown index	crown area	crown module
LM^1	10.80	11.53	–	–	106.76	124.52	11.17
RM^1	10.95	11.55	–	–	105.48	126.47	11.25
LM^2	10.00	11.68	7.18	–	116.80	116.80	10.84
RM^2	10.95	11.75	7.58	–	107.31	128.66	11.35
LM^3	8.33	11.13	7.50	–	133.61	92.71	9.73
RM^3	9.20	11.38	7.88	–	123.70	104.70	10.29
LI_1	4.65	5.60	–	–	–	–	–
RI_1	4.93	5.55	–	–	–	–	–
LI_2	5.15	6.08	–	–	–	–	–
RI_2	5.25	5.93	–	–	–	–	–
L_C	6.05	7.63	–	–	–	–	–
R_C	6.48	7.50	–	–	–	–	–
LP_3	6.40	7.33	–	–	114.53	46.91	6.87
LP_4	6.83	7.98	–	–	116.84	54.50	7.41
LM_1	11.03	10.28	–	–	93.20	113.39	10.66
RM_1	11.18	10.33	–	–	92.40	115.49	10.76
LM_2	10.03	9.80	8.13	–	97.71	98.29	9.92
RM_2	10.03	10.08	7.20	–	100.50	101.10	10.06
LM_3	10.68	10.00	8.18	–	93.63	106.80	10.34
RM_3	10.83	10.03	–	–	92.61	108.62	10.43

SPECIMEN DESCRIPTIONS: LATE HOLOCENE

SPECIMEN. Gough's Cave #4 [Cooper 1929 No. 7]

TIME PERIOD. Late Holocene

DESCRIPTION. Maxillary fragment separated along mid-line of a young-late adolescent individual. Age category was made on the basis of dental eruption, root formation and occlusal wear. The LM^1 is present, and the crown of the LM^3 is complete although unerupted, with the roots not yet formed. Postmortem loss occurred of $LI^{1,2}$, L^C, $LP^{3,4}$, LM^2.Alveolar sockets indicate the roots of $LP^{3,4}$ are completely formed, while the roots for LM^2 have not completely formed. There is no indication of cultural modification or treatment of the teeth.

CROWN WEAR. The LM^1 has slight wear faceting with no dentine exposure (grade = 0.5).

ENAMEL PRESSURE CHIPPING. None.

PATHOLOGY. No caries, abscessing, periodontal disease, or enamel hypoplasia present, although there is slight-moderate formation of calculus on the buccal surface near CEJ.

CROWN MORPHOLOGY. LM^1: metacone = 4, hypocone = 3.5, Carabelli's trait = 2, absence of cusp 5, and enamel extension. There is a very faint parastyle expression, although it is not the buccal pit form (grade 1) and the expression of the trait is too weak to classify it as grade 2, because it lacks a free apex.

ROOT MORPHOLOGY. $LI^{1,2}$, L^C, $LP^{3,4}$: single-rooted teeth.

ODONTOMETRIC DATA

	crown dimensions MD	BL	crown height	root length	crown index	crown area	crown module
LM^1	10.10	9.88	5.85	–	97.82	99.79	9.99

SPECIMEN. Gough's Cave #5 [Cooper 1929]

TIME PERIOD. Late Holocene

DESCRIPTION. Right mandibular fragment of an adult, with postmortem loss of R_C, $RP_{3,4}$, RM_2. The RM_1 is present. Degree of occlusal wear suggests middle-old age.

CROWN WEAR. The RM_1 is heavily worn, with the pulp chamber almost exposed (grade = 2.5).

ENAMEL PRESSURE CHIPPING. RM_1:buccal and mesio-buccal surfaces.

PATHOLOGY. No caries, abscessing, periodontal disease, or enamel hypoplasia, although a slight-moderate degree of calculus is present.

CROWN MORPHOLOGY. RM_1:absence of enamel extension.

ROOT MORPHOLOGY. R_C, $RP_{3,4}$: single-rooted teeth.

ODONTOMETRIC DATA. None available due to wear.

Table 2 Number of Gough's Cave individuals (Late Pleistocene/Early Holocene) with any morphological expression for a given trait.

Data are presented only for grades that were present in the sample. Traits lacking any morphological expression in the sample are winging (UI1), labial curvature (UI1), shovel (UI1-2, UC, LI1-2), double-shovel (UI1-2, UC, UP3), interruption groove (UI1-2), canine mesial accessory ridge (UC), canine distal accessory ridge (UC, LC), premolar distal accessory cusps (UP3-4), maxillary premolar accessory ridge (UP3 only), premolar buccal style (UP3-4), disto-sagittal ridge (UP3), odontomes (UP3-4, LP3-4), Carabelli's trait (UM1-2-3), parastyle (UM1-2-3), anterior fovea (UM1), deflecting wrinkle (LM2-3 only), distal trigonid crest (LM2-3 only), cusp 6 (LM1-2-3), cusp 7 (LM1-2-3), mid-trigonid crest (LM2-3 only).

All upper and lower incisors, canines and premolars are single-rooted. The only data available for molars are from a single individual who has both lower M1 (two-rooted) and a lower M2 (three-rooted).

Tuberculum Dentale

grade	UI1	UI2	UC
0	1	1	2
1	1	0	0
2	0	1	2
Total	2	2	4

Metacone

grade	UM1	UM2	UM3
3.5	0	1	1
4	3	2	0
Total	3	3	1

Upper Molar Cusp 5

grade	UM1	UM2	UM3
0	3	1	1
3	0	1	0
4	0	1	0
Total	3	3	1

Hypocone

grade	UM1	UM2	UM3
1	0	1	1
3	0	2	0
4	2	0	0
5	1	0	0
Total	3	3	1

Enamel Extension

grade	UP3	UP4	UM1	UM2	UM3
0	2	1	3	2	1
1	0	0	0	1	0
Total	2	1	3	3	1

Peg, Reduced, Congenital Absence

grade	UI2	UP4	UM3	LI1	LP4	LM3
+	3	2	2	5	6	2
-	0	0	1	0	0	1
Total	3	2	3	5	6	3

Lower Molar Cusp Pattern

grade	LM1	LM2	LM3
Y	3	0	1
X	0	2	0
+	0	1	0
Total	3	3	1

Premolar Lingual Cusp

grade	LP3	LP4
0	0	2
A	1	0
1	1	0
Total	2	2

Lower Molar Cusp Number

grade	LM1	LM2	LM3
4	0	3	1
5	3	1	0
Total	3	4	1

Lower Molar Cusp 5

grade	LM1	LM2	LM3
4	0	3	1
5	3	1	0
Total	3	4	1

Protostylid

grade	LM1	LM2	LM3
0	2	4	1
1	1	0	0
Total	3	4	1

Tomes' Root

grade	LP3
0	1
3	1
Total	2

RESULTS: LATE PLEISTOCENE/EARLY HOLOCENE REMAINS

Morphology: Grades for teeth with a given trait (number or individuals = 7, number of teeth = 97) are summarized in Table 2, and include root number data obtained from the alveolar socket when postmortem loss of a tooth occurred. In general, Gough's Cave individuals have a simplified, modern *Homo sapiens* dental pattern, and lack strong expression for almost all traits.

Presence/absence breakpoints for key tooth/trait combinations limit the sample available for analysis due to use of the individual count (number of key trait observations = 65). There is a lack of winging (0/2), shovel I^1 (0/2), double shovel I^1 (0/2), interruption groove I^2 (0/2), upper canine mesial accessory ridge, or 'Bushman's canine' (0/2), upper canine distal accessory ridge (0/1), disto-sagittal ridge or 'Uto-Aztecan premolar' P^3 (0/2), Carabelli's trait M^1 (0/3), cusp 5 M^1 (0/3), parastyle M^3 (0/1), enamel extension M^1 (0/4), greater than one lingual cusp P_4 (0/2), Y-groove M_2 (0/3), cusp 6 M_1 (0/3), cusp 7 M_1 (0/3), two-rooted lower canine (0/4), three-rooted lower molar (0/1), one-rooted M_2 (0/1), or upper/lower premolar odontomes (0/5). There are some instances of presence of tuberculum dentale I^2 (1/2), peg/reduced/congenital absence of M^3 (1/3), protostylid M^1 (1/3), Tomes' root P_3 (1/2). Higher frequencies were noted for presence of one-rooted P^3 (2/2), presence of hypocone M^2 (2/3) and four-cusped M_2 (3/4).

Metrics: Out of 58 teeth measured in the Late Pleistocene/Early Holocene sample, a total of 16 permanent maxillary teeth and 21 permanent mandibular teeth supplied data for the seven individuals, with the means summarized in Table 3. Fluctuating dental asymmetry in tooth size is present in the sample, although the results from paired t-tests between antimeres do not indicate significant differences statistically ($p = 0.05$). Only one individual (Gough's Cave 6) had all maxillary or mandibular molar teeth present. Crown Area in Gough's Cave 6 indicates an upper molar decrease from $M^1 > M^2 > M^3$. Lower molars follow a slightly different pattern of $M_1 > M_2 < M_3$.

The TCA for the Gough's Cave sample is 1,244 mm^2 (I1-M3) and 1,034 mm^2 (I1-M2), while the M1M2CA is 486 mm^2. There is a lack of reduction in lateral incisor MD diameters when compared to the MD measurement for the central incisors, with the incisor breadth (I^1: I^2) ratio of 0.83.

Pathology/occlusal attrition/crown chipping: All seven individuals could be assessed for pathology, although of these, three were represented by isolated teeth. There is an apparent lack of caries and abscessing in this series. Antemortem tooth loss (LP^4) occurred in only one individual (87/139). This same young adult also has the only instance of macroscopically observable enamel hypoplasia, an acute episode with pitting which occurs at the cemento-enamel junction (CEJ) of three teeth (I^1, ^{C}, M^1) during crown formation between three to five years of age. Although no periodontal pockets occur, one adult male (Gough's Cave 6) showed evidence of 1–2 mm of root exposure of M_2, the only tooth remaining, the rest having been lost postmortem. There does seem to be higher degree of calculus deposition (slight grades: confined to crown but not extending to the CEJ) occurring in two young-middle age adults (87-253, 89–001), including only one of the three identifiable males in the sample.

The degree of attrition in the sample is similar to other hunter/gatherer groups, in that the rate of wear is not excessive (i.e., the pulp chamber is not exposed before secondary dentine is formed to protect tooth integrity). Thus, the majority of wear seems likely to be age-related rather than occupational or due to highly abrasive diet. In

Table 3 Summarized odontometric data for Gough's Cave sample (Late Pleistocene/Early Holocene), including number of individuals (n), mean mesio-distal diameter (MD), mean bucco-lingual diameter (BL), standard deviation (sd) and mean crown area. Data are for the left side, with right side substituted when the left is missing. When only one tooth is available, data are presented in parentheses.

Tooth	n	Avg. MD	sd	n	Avg. BL	sd	Crown Area
UI1	2	9.44	0.23	3	7.43	0.44	70.14
UI2	2	7.79	0.58	2	7.57	0.47	58.97
UC	2	7.82	0.45	2	9.68	0.25	75.70
UP3	2	6.58	0.21	2	9.16	0.17	60.27
UP4	1	(5.75)	–	1	(8.83)	–	(50.77)
UM1	3	10.64	0.31	3	12.19	0.65	129.70
UM2	3	9.99	0.24	2	12.46	1.10	124.48
UM3	1	(8.33)	–	1	(11.13)	–	92.71
LI1	2	5.18	0.74	2	5.99	0.55	31.03
LI2	3	5.51	0.62	3	6.54	0.48	36.04
LC	2	6.87	1.15	2	8.10	0.85	55.65
LP3	2	6.60	0.28	2	7.98	0.92	52.67
LP4	4	6.92	0.26	4	8.27	0.22	57.23
LM1	3	10.90	0.76	3	10.64	0.44	115.98
LM2	4	11.03	1.09	4	10.50	0.34	115.82
LM3	1	(10.68)	–	1	(10.93)	–	(116.73)

adults, the wear on the anterior teeth is almost always grade 1 (some dentine exposed). There is one instance of an isolated upper incisor (87-103a) that is heavily worn (grade 3) although probably due to age-related wear consistent with older age. The maxillary first molars have a wear range of grades 1–1.5, with the lower molars experiencing slightly more wear (grades 1–2.5), although again, the type of wear suggests older adults. All erupted maxillary and mandibular second and third molars in the sample were only slightly worn (grade = 0.5).

The degree of wear may be correlated with instance of molar crown pressure chipping in at least one individual. In Gough's Cave 1, the RM^1, has an attrition score of grade 1, although the tooth exhibits chipping along the lingual surface of the hypocone; its antimere, LM^1, has the same amount of wear but lacks any evidence of pressure chipping. However, the mandibular counterparts to these two teeth indicate much heavier use of the right side, with the RM_1 wear grade of 1.5, (no chipping) while the LM_1 mirrors the lesser wear (no chipping) of the left maxillary molar. Two other individuals (87-253, Gough's Cave 6), have a high degree of attrition on the lower molars, but wear is not correlated with pressure chipping.

Specimen 87-139, a young-middle age adult, displays an attrition/chipping pattern that may be consistent with occupational use of the teeth. Crown microtrauma occurs on the maxillary incisors, between the right $I^{1,2}$, and the left $I^{1,2}$, and on the buccal surface of the left upper canine. The LP^4 was lost antemortem, and the LP^3 crown was damaged postmortem. The left side of the anterior dentition may have been utilized more in this adult; the R^C, $RP^{3,4}$, and $LRM^{1,2}$ did not display evidence of chipping. Because there are no instances of caries in the sample, the antemortem loss of LP^4 may be related to the degree and amount of pressure chipping found in the dentition of this specimen. Unfortunately, no mandibular dental remains for this adult were recovered.

Other Features: There is no evidence of cultural treatment (i.e., interproximal 'toothpick' grooves, enamel cleaning striations) or of intentional dental modification.

COMPARATIVE ANALYSIS

Results of this comparative analysis are based on a numerically limited series should be treated with caution. The analysis presented here suggests only possible trends present in the available data, and with the assumption that these few individuals from Gough's Cave are representative of the populations of the Late Pleistocene/Early Holocene British Isles.

Morphology: Table 4 presents a comparison of the Gough's Cave morphological data with the occurrence of 20 key traits in seven early populations: Upper Paleolithic-Neolithic North Europe (*ca.*32,000–4,000 BP), Mesolithic Nubia (*ca.* 18,000–12,000 BP), Iberomaurusian North Africa (*ca.* 16,700–10,500 BP), Epi–Paleolithic Levant Natufians (*ca.* 12,800–10,200 BP), Mesolithic–Neolithic South Asia (*ca.* 8,000 –2,800 BP), Neolithic-Bronze Age Lake Baikal (*ca.* 7,400–3,800 BP), and Jomon Japan (*ca.* 7,000–2,300 BP). The data are also compared with two historic pooled populations: North Europe, and Khoisan-speakers of sub-Saharan Africa. Results were compared with the Early World Average for each trait (Hawkey 1998) . Populations were then designated as having percentages higher than (H), lower than (L) or within five percent above or below the Early World Average (A). Because the Gough's Cave sample is so small numerically, the frequency of each trait is characterized as having total absence (0), less than or equal to 50 percent (+), or more than half the sample (++).

Among world populations, the Gough's Cave dental morphology seems most like other early world groups with a simplified dental pattern. Gough's Cave is most similar to Late Pleistocene/Late Holocene (Neolithic) North Europe, sharing trait frequencies of 83.3%. By historic times, Gough's Cave is still like Recent North Europe (72.2%), although there are differences in presence of tuberculum dentale, hypocone, Carabelli's trait, one-root P^3 , and cusp 7. The simplified dental pattern seen in Gough's Cave shares similarities with two other Late Pleistocene/Early Holocene world samples: Epi-Paleolithic Levant Natufians (70.0%) and North African Iberomaurusians (70.0%), and with the Early Holocene sites of South Asia (83.3 %) and Jomon (80.0%).

The sample is dentally unlike the Late Pleistocene sites of Nubia (42.1%), and the Late Holocene (Neolithic-Bronze Age) inhabitants of Lake Baikal (52.6%). If the Khoisan-speaking populations from modern sub-Saharan Africa are taken to represent the early sub-Saharan African dental pattern (Irish 1993, 1998), then Gough's Cave shares only 60% of key traits with this geographic group.

Only one archaic dental trait appears in the sample. Presence of P_3 Tomes' root occurred in one out of two individuals who could be scored for the trait. A study of more than 7,700 individuals (Turner & Hawkey 1991) found that the trait occurs most often in Africa, ranging from 20–50%, with the Late Pleistocene Nubian sample among the highest in the world (47%). North Europe averages 9%of trait presence, although the range can be quite broad (0–43%). The instance of Tomes' root in this sample, therefore, cannot exclude similarities with either European or African populations for the trait. However, the lack of expression in Gough's Cave of many other archaic traits found by Irish (1993, 1998) in the sub-Saharan African Dental Complex (i.e, high frequencies of upper canine mesial accessory ridge, Carabelli's trait M^1, cusp 7 M_1, presence of Y-groove pattern M_2, two-rooted P^3, and lack of congenital absence M^3) suggests that Gough's Cave is dentally unlike the African samples.

Surprisingly, Gough's Cave lacked any expression of Carabelli's trait (0/3), although the trait is often found to occur in high frequencies (80%) among modern British (Goose & Lee 1971). The trait is of little use by itself to differentiate at geographic population levels

Table 4 Results for 20 dental traits for Gough's Cave, seven Early populations, and two Recent populations (no. of individuals = 296-1494), compared with Early World average (based on nine geographic populations (North Asia, Nubia, Southeast Asia, Malaysia, South Asia, Early Eurasia, North Europe, Levant, and North American Paleo-Indian). Data for the Early World Average are taken from personal observations and literature (as cited in Hawkey 1998).

0 = absence of any expression; + = some expression (less than or equal to 50% of the sample); ++ = more than half the sample; L = less than 5% of the Early World Average ; A = within 5% more than or less than the Early World Average; H = more than 5% of the Early World Average. Similarities in trait expression percentage indicated in boldface. Gough's Cave score of "0" is similar to "0" and "L", while "+" is similar to "L" or "A". Scores of "++" would be equal to either "A" or "H".

Trait	Gough's Cave[1]	Early Jomon[2]	Early Baikal[3]	Early South Asia[4]	Early Levant[5]	Early Europe[6]	Recent Europe[7]	Early Nubia[8]	Early North Africa[9]	Recent Khoisan[10]	Early World Average
Wing	0	**A**	H	**L**	**0**	**0**	**L**	H	**L**	**A**	17.9%
Shov	0	**A**	H	H	**L**	**A**	**L**	H	**A**	H	28.2%
DbShov	0	**L**	H	**L**	**L**	**A**	**L**	**0**	**L**	**0**	19.5%
IG	0	H	H	H	**L**	**0**	—	**L**	H	**L**	27.7%
TD	+	**L**	**L**	**L**	H	H	H	**L**	**L**	**A**	48.0%
MAR	0	**L**	**A**	**0**	H	**A**	**0**	H	**A**	H	7.7%
Hypo	++	**A**	**H**	**H**	**H**	**A**	L	**A**	**H**	L	88.7%
UMC5	0	**A**	—	**A**	**L**	**L**	**L**	**A**	**A**	**A**	26.1%
Para	0	**A**	H	**A**	**A**	**0**	**A**	**0**	**A**	**A**	3.4%
Cara	0	**L**	**A**	**A**	**L**	**L**	H	H	H	H	28.3%
PRCA	+	**A**	**A**	**L**	H	—	—	—	**L**	H	16.3%
EnExt	0	**A**	**A**	**0**	**0**	**0**	**L**	H	**L**	**0**	14.4%
1RUP1	++	**H**	**H**	—	L	—	L	L	L	**H**	56.3%
PLC#	0	**A**	**A**	**L**	**A**	H	**L**	H	H	**A**	67.4%
Y	0	H	**L**	H	H	**L**	**L**	H	H	H	20.9%
6CLM1	0	H	H	**L**	**L**	**L**	**L**	**A**	**L**	**L**	26.0%
4CLM2	++	L	L	**H**	L	**H**	**H**	0	L	L	71.4%
Proto	+	**L**	H	**L**	**L**	H	**L**	H	**A**	**A**	22.6%
C7	0	**A**	H	**A**	**A**	**L**	H	**A**	**A**	H	6.8%
Tomes	+	**L**	**A**	—	**A**	**L**	**L**	H	**L**	A	21.3%
Totals		16/20 **80.0%**	10/19 **52.6%**	15/18 **83.3%**	14/20 **70.0%**	15/18 **83.3%**	13/18 **72.2%**	8/19 **42.1%**	14/20 **70.0%**	12/20 **60.0%**	

[1] Present study
[2] Turner 1987
[3] Turner 1987
[4] Hawkey 1977; Lukacs 1986
[5] Lipschultz 1996
[6] Alexandersen 1963; Beillard, cited in Brabant 1976; Brabant 1971, 1976; Brabant & Ketelbant 1975; Brabant et al. 1961; deTerra 1905; Haeussler 1996; Hellman 1928; Turner & Benjamin 1989; Turner & Hawkey 1991, 1998
[7] Axelsson & Kirveskari 1977; Brabant & Ketelbant 1975; Goose & Lee 1971; Guigui 1974; Hjelmman 1928; Kaczmarek 1981; Kirveskari 1974; Lavelle et al. 1970; Morris 1975; Morris et al. 1978; Pedersen 1949; Sauter & Moeschler 1960; Schwerz 1917; Scott 1973, 1977; Selmer-Olsen 1949; Turner & Benjamin 1989; Turner & Hawkey 1991, 1998; Zubov & Kaldiva 1979
[8] Irish 1993
[9] Irish 2000
[10] Irish 1993

(Turner & Hawkey 1998) however, with the range in modern North Europeans (29–80%) quite variable in terms of trait presence. Although presence of Carabelli's trait averages 43% in modern North Europe, the same percentage is found in North American Indians, and is often even higher (53%) in modern sub-Saharan and West Africans.

Thus, by the Late Pleistocene/Early Holocene, Gough's Cave shows the strongest dental similarity with Noth Europe, South/Southwest Asia and North Africa. They appear to be dentally unlike either East Africa (Nubia), South Africa (modern Khoisan), or North Asia (Baikal).

Metrics: While the amount of environmental influence on tooth size is debatable (Goose 1963; Hillson 1986; Kieser 1990; Lukacs 1985; Scott & Turner 1988, 1999), crown shape appears to be another reliable way to assess population affinity (Corruccini 1973). When compared with TCA results for earlier samples from Europe (Table 5) Gough's Cave is approximately 13% smaller than European Neanderthal dentition (based on I1-M3), but only 3% smaller than Late Upper Paleolithic Europeans. Gough's Cave is closest to other European Mesolithic populations, and have teeth 4% larger than Neolithic Europeans, and 10% larger than modern Europeans. The latter result supports the post-Pleistocene trend towards dental reduction, most likely due to relaxed selection for large tooth/body size (Brace & Mahler 1971; Wolpoff 1971).

Table 5 Temporal comparisons of Total Crown Area (TCA) for early to recent Europe. Gough's Cave value is calculated with M3 data to compare with published information. (Source for non-Gough's Cave sample: Brace *et al* 1991).

TCA (mm^2)I1-M3	Period
1415	Neanderthal
1267	Late Upper Paleolithic Europe
1237	Mesolithic Europe
1244	**Gough's Cave (Late Upper Paleolithic-Mesolithic)**
1196	Neolithic Europe
1127	Modern Europe

Table 6 Total Crown Area (TCA) for Gough's Cave (Late Pleistocene/Early Holocene) compared to early and modern populations. The TCA is calculated without M3 data. Samples that contain only males are indicated as M; pooled data for both sexes are designated as M&F.

TCA (mm^2) I1-M2	Area/Site	Sex	Source
1158	Nubia (Mesolithic East Africa)	M	Calcagno 1986
1103	Mahadaha (Mesolithic India)	M&F	Lukacs & Hemphill 1992
1054	Natufian (Epi-Paleolithic Levant)	M&F	Dahlberg 1960
1037	Mehrgarh (Neolithic Pakistan)	M&F	Lukacs 1985
1034	**Gough's Cave (Late Paleolithic-Mesolithic)**	**M&F**	**Present study**
981	Jomon (Early Japan)	M	Brace & Nagai 1982
981	Anglo-Saxon (Early Britain)	M	Lavelle 1968
966	Britain (Recent)	M	Lavelle 1968
910	Khoisan (Recent South Africa)	M	Haeussler *et al* 1989; van Reenan 1982

In order to compare Gough's Cave with published data for Holocene populations, the results are based on measurements for I1-M2 (Table 6). According to Brace (1980), differences of more than 100 mm^2 summed TCA are significant statistically, while differences of more than 50 mm^2 are probably significant. The TCA values for Gough's Cave are closest with the incipient agriculturalists of Neolithic Mehrgarh (Pakistan) with only 3 mm^2 difference, and Levant Natufians (20 mm^2). Four other populations were within 100 mm^2 difference: the Anglo-Saxons (53 mm^2), Jomon (53 mm^2), Recent Britain (68 mm^2) and Mesolithic Mahadaha in Indo-Gangetic India (69 mm^2). Gough's Cave TCA values are unlike those of Late Pleistocene Nubia (124 mm^2) and modern sub-Saharan Khoisan-speakers (124 mm^2).

A similar pattern appears in the Penrose *size* component (Table 7), with Levant Natufians (0.02), Mehrgarh (0.04) and Mahadaha (0.05) most similar to Gough's Cave. The component for Anglo-Saxon (0.33), Jomon (0.39), and Nubia (0.59) show less similarity. Recent Britain (0.97) and Khoisan (1.14) are least like Gough's Cave in occlusal crown size. The two groups that show closest similarity in Penrose *shape* are the Natufians (0.87) and Mehrgarh (0.97), mirroring the size component results. However, the remaining sample indicates moderate similarity (Jomon = 1.07, Nubia = 1.10, Mahadaha = 1.24, Khoisan = 1.34) with Anglo-Saxon (2.39) and Recent Britain (4.22) the most dissimilar to Gough's Cave in shape component.

The differences between the size and shape results may be due to several factors. The most likely explanation is that the size component results reflect sexual dimorphism in tooth size. Gough's Cave, Natufians, Mehrgarh and Mahadaha (the most similar in size component results) are all from pooled samples of males and females. All other data are from males only.

Table 7 Results of Penrose statistic (Shape/Size) for Gough's Cave sample (Late Pleistocene/Early Holocene) compared with eight other populations.

	Gough's Cave sample		
	Size component	Shape component	Combined statistic
Natufian (M&F)	0.02	0.87	0.89
Mehrgarh (M&F)	0.04	0.97	1.01
Mahadaha (M&F)	0.05	1.24	1.29
Anglo-Saxon (M)	0.33	2.39	2.72
Jomon (M)	0.39	1.07	1.46
Nubia (M)	0.59	1.10	1.69
Recent British (M)	0.97	4.22	5.19
Khoisan (M)	1.14	1.34	2.48

Another possibility is that the TCA and Penrose size statistic, both of which include anterior and posterior teeth, may reflect apportionment differences within populations (Harris & Rathbun 1991). Size differences between incisor/canine and premolar/molar fields within individuals may explain why Recent Britain appears so dissimilar to Gough's Cave in size component, yet so similar in TCA value. Incisor breadth ratio (Table 8) shows that Recent Britain has the most reduced lateral incisors (IB = 0.72) when compared to Gough's Cave (IB = 0.83), yet the molar crown area for M1M2 (Table 9) indicates the molars are similar in size for both groups.

When both metric and morphology differences are compared (Table 10) the data reveal the following consistent patterns:

1. Gough's Cave is most like early populations of South/Southwest Asia, including Pakistan (Mehrgarh) and the Levant (Natufians) in TCA and Penrose size/shape components.
2. Gough's Cave is also similar to other early North Europe populations (in TCA and DAS), although published data for North Europe were unavailable for Penrose size/shape analysis.
3. Both metric and morphology results suggest that Late Pleistocene East Africa (Nubia) and sub-Saharan Africans (modern Khoisan) are most dissimilar to Gough's Cave. The DAS morphological data for Late Pleistocene North Africans (Iberomaurusian) suggest a much closer dental similarity to Gough's Cave than other African regions.
4. Differences within the British Isles suggest Gough's Cave is unlike Anglo-Saxon (53 mm^2 difference) and Recent Britain (68 mm^2 difference) in TCA I1-M2 value, but more similar with Late Pleistocene North Europe (23 mm^2 difference, for available TCA I1-M3 data). Both size and shape components indicate Gough's Cave is dissimilar to Anglo-Saxon, and even less similar to Recent Britain. The DAS data, however, suggest close morphological similarities between Gough's Cave and early North Europe. The discrepancies may reflect temporal fluctuations in environment/subsistence, with the metric data more sensitive than morphology to these variables. In addition, sexual dimorphism and apportionment of tooth size may also have an effect.

Pathology/occlusal attrition/crown chipping: Lack of carious teeth, periodontal pathology and low instance of enamel defects in Gough's Cave is well within the range of other hunter/gatherer populations (Cook & Buikstra 1979; Leigh 1925; Turner 1979). The one individual with less than 2 mm of root exposure between CEJ and the alveolar border is not indicative of periodontal disease, but is most likely the result of further root eruption to compensate for attrition, and correlated with age (Clarke & Hirsch 1991). Similarly, there is one young adult with antemortem tooth loss, suggesting an occupationally related cause rather than due to carious activity or periodontal disease.

Table 8 Incisor Breadth ratio (IB) of upper central and lateral incisors compared with early and recent populations.

IB	Area/Site	Sex	Source
0.83	**Gough's Cave (Late Paleolithic-Mesolithic)**	M&F	**Present study**
0.83	Jomon (Early Japan)	M	Brace & Nagai 1982
0.80	Mehrgarh (Neolithic Pakistan)	M&F	Lukacs 1985
0.80	Mahadaha (Mesolithic India)	M&F	Lukacs & Hemphill 1992
0.80	Nubia (Mesolithic East Africa)	M	Calcagno 1986
0.78	Khoisan (Recent South Africa)	M	Haeussler *et al* 1989; van Reenan 1982
0.78	Anglo-Saxon (Early Britain)	M	Lavelle 1968
0.75	Natufian (Epi-Paleolithic Levant)	M&F	Dahlberg 1960
0.72	Britain (Recent)	M	Lavelle 1972

Table 9 Molar Crown Area calculated for upper and lower M1 and M2 (M1-M2CA) and compared to early and recent populations.

M1-M2CA(mm^2)	Area/Site	Sex	Source
536	Nubia (Mesolithic East Africa)	M	Calcagno 1986
503	Mahadaha (Mesolithic India)	M&F	Lukacs & Hemphill 1992
503	Natufian (Epi-Paleolithic Levant)	M&F	Dahlberg 1960
486	Mehrgarh (Neolithic Pakistan)	M&F	Lukacs & Hemphill 1991
486	**Gough's Cave (Late Paleolithic-Mesolithic)**	**M&F**	**Present study**
485	Britain (Recent)	M	Lavelle 1968
465	Jomon (Early Japan)	M	Brace & Nagai 1982
448	Anglo-Saxon (Early Britain)	M	Lavelle 1968
428	Khoisan (Recent South Africa)	M	Haeussler *et al* 1989; van Reenan 1982

Table 10 Comparisons of Gough's Cave metric and morphological data for TCA absolute mean difference (TCAD), Penrose Size (PEN SIZE), Penrose Shape (PEN SHAPE), and Morphology (DAS) ranked in terms of most similar to least similar.

Site/Area	TCAD	Site/Area	PEN SIZE	Site/Area	PEN SHAPE	Site/Area	DAS %
Mehrgarh	3	Natufian	0.02	Natufian	0.87	Early Europe	83.3
Natufian	20	Mehrgarh	0.04	Mehrgarh	0.97	Early S. Asia	83.3
Early Europe	23	Mahadaha	0.05	Jomon	1.07	Early Jomon	80.0
Jomon	53	Anglo-Saxon	0.33	Nubia	1.10	Recent Europe	72.2
Anglo-Saxon	53	Jomon	0.39	Mahadaha	1.24	Early Natufian	70.0
Recent Britain	68	Nubia	0.59	Khoisan	1.34	Early N. Africa	70.0
Mahadaha	69	Recent Britain	0.97	Anglo-Saxon	2.39	Recent S. Africa	60.0
Nubia	124	Khoisan	1.14	Recent Britain	4.22	Early Baikal	52.6
Khoisan	124					Early Nubia	42.1

Although an increase in the presence of calculus has been observed with the advent of Neolithic culture (Hildebolt & Molnar 1991), calculus deposits on the teeth are also found in populations with hunter-gatherer or mixed economies, and may actually be under-reported in archaeological specimens due to preservation or postmorten damage (Brothwell 1981). Evidence of phytoliths within the calculus deposits of Gough's Cave teeth has been recovered by K. Dobney of University of Bradford (reported in, Currant *et al* 1989). While the presence of phytoliths can introduce a somewhat abrasive element into the diet, the teeth of the Gough's Cave sample are not excessively worn. However, a hunter-gatherer subsistence strategy also includes a reliance on meat, an element that is not necessarily abrasive to the dentition (Hillson 1986). Thus, the presence of crown microtrauma in Gough's Cave may be at least partially related to subsistence, especially when grit and bone may be present in the diet (Turner & Cadien 1969).

Although caution should be used in a macroscopic analysis of enamel disturbances (Hillson & Brand 1997), it has been suggested that hunter/gatherers tend to be less severely affected by enamel hypoplasias (Cook & Buikstra 1979; Lukacs *et al* 1982), with the average age of onset between four to five years of age (Schulz & McHenry 1975). But the low instance of enamel hypoplasia in the Gough's Cave sample may not reflect a lack of nutritional stress, because there can be a variety of underlying causes (Goodman & Rose 1991). The Mesolithic site of Mahadaha, for example, exhibits a high frequency (64%) of enamel defects, although the population appears to be free of nutritional stress markers in the osseous remains (Lovell 1992). Some authors have suggested that the amount of stress seen in a population may be reflected in greater dental asymmetry (Bailit *et al* 1970), or even by significant tooth size variation within age groups (Guargliardo 1982), neither of which are especially apparent in the limited number of individuals from Gough's Cave.

Other features: An absence of evidence for either enamel cleaning striations or interproximal grooves, coupled with a lack of caries, periodontal pathology and only slight degree of calculus, suggest that the people of Gough's Cave did not need to practice a rigorous form of dental hygiene. Early teeth cleaning practices, however, have been noted in the Middle East, Asia, Africa, and North American Indians, who often utilized the frayed end of twigs to clean the teeth (Hawkey *et al* n.d.). Similarly there is even earlier evidence for interproximal grooves between the teeth, usually attributed to use of a 'toothpick' to remove irritating substances. These grooves have been reported for a variety of groups in Europe, dating from the Late

Paleolithic to the Bronze Age (Alexandersen 1978; Bennike 1985; Formicola 1988; Frayer & Russell 1987; Turner 1988), were noted in the Neolithic remains from Mehrgarh (Lukacs & Pastor 1988), and possibly in South African Late Pleistocene sites (Grine & Henshilwood 2002; Grine *et al* 2000).

The earliest evidence of intentional modification of the anterior teeth is the ablation seen at Minatogawa, dating to circa 18,000 years BP (Hanihara & Ueda 1982). In addition, intentional filing of the labial surface of incisors has been reported in early Holocene in South Asia (Kennedy *et al* 1981), and the practice of dental modification commonly occurs in Africa, the Americas, South Asia, Japan, Southeast Asia, Australia and Melanesia (Hawkey n.d *b*; Milner & Larsen 1991). There are no instances of intentional dental modification (ablation, filing, or inlay) in the Gough's Cave sample, a fact that is supported by ethnographic reports that suggest the later populations of Europe and the Middle East abhorred the loss of the anterior teeth (Guerini 1977; Kanner 1928).

There are only a few cases of possible dental modification in early Britain (Jackson 1915), from two sites ascribed to a Neolithic culture (Dog Holes cave in Lancashire, and Perthi Chwareu caves in North Wales). Jackson's description of the specimens remains unconvincing, however, as examples of intentional dental modification. There is an abnormal amount of wear on all four specimens, particularly those with loss of central incisors, and the loss may due to excessive attrition leading to exposure of the pulp chamber and premature exfoliation of the teeth. Interestingly, two of Jackson's specimens display antemortem loss of lower premolars; one individual from Gough's Cave has antemortem loss of LP^4. Because the loss seen in both Gough's Cave and two of Jackson's specimens are not anterior teeth, it is unlikely to be intentional dental modification. The antemortem tooth loss seen in Gough's Cave, in particular, is more likely due to activity-induced traumatic injury, a situation observed in populations as ecologically disparate as the Arctic (Merbs 1983) and Pakistan (Lukacs & Hemphill 1990).

CONCLUSIONS

Although the dental remains from Gough's Cave are from a numerically limited series, several trends are suggested, with the underlying assumption that dentition from these individuals accurately represent the Late Pleistocene/Early Holocene populations of the British Isles. It is cautioned , however, that the results are tentative and may reflect statistical fluctuations due to small sample size.

1) *Morphology*: The individuals from Gough's Cave have a simplified dental pattern, similar to the dentition of other Late Pleistocene/Early Holocene populations of North Europe, the Levant, and North Africa. They have similarities with two other groups, also with a simplified pattern: South Asia (Indodont pattern) and the Jomon (Sundadont pattern). They are dentally unlike populations of modern sub-Saharan Africa, Mesolithic Nubia, or the more complex Sinodont dentition of Lake Baikal. Gough's Cave lacks expression of any of the archaic traits, with the exception of P_3 Tomes' root.

2) *Metrics*: Gough's Cave dentition is more similar in crown size to other Mesolithic European populations, exhibiting a significant reduction in tooth size from European Neanderthals, consistent with the post-Pleistocene trend in dental reduction. Among the Late Pleistocene/Early Holocene comparative samples, Gough's Cave is most similar in dental crown size to early populations from the Levant, South/Southwest Asia, and North Europe, but unlike both early East Africa (Nubia) and modern sub-Saharan Africa (Khoisan). When both morphology and metric differences are compared, a similar pattern tends to occur, although no published metric data are available for North Africa (Iberomaurusian). There are temporal differences within the British Isles: Gough's Cave appears most similar to the North Europe sample dating to the approximately the same time period. Gough's Cave is less similar to Anglo-Saxon, with the Recent Britain sample even more dissimilar. A trend towards lateral incisor reduction occurs in later British populations, with Molar Crown Area remaining approximately the same as Gough's Cave. This finding may have some effect on the odontometric analysis, reflecting apportionment changes between the incisor/canine and premolar/molar fields with time.

3) *Pathology/occlusal attrition/crown chipping*: The dental pathology profile is consistent with that of a hunter-gatherer lifeway, with absence of caries, no periodontal disease, and low frequency of enamel hypoplasia. The diet was probably not particularly abrasive, because the teeth show evidence of a gradual progression of attrition with age, rather than evidence of excessive wear during adolescence. An almost complete absence of enamel hypoplasia, along with little dental size asymmetry suggest a relatively healthy population. This low incidence of enamel hypoplasia may indicate a lack of nutritional stress, similar to that noted by Kennedy *et al* (1986), for the Mesolithic site of Sarai Nahar Rai in India, where hunter/gatherer subsistence strategy and ecological conditions may well have provided an abundance of food resources. Given the absence of caries in these remains, it is probable that the only instance of antemortem tooth loss in one individual may be occupationally related, especially considering the excessive enamel microtrauma found on the anterior teeth.

4) *Other features*: Similar to other European populations, there is no convincing evidence of intentional dental modification. Although there have been some reports of interproximal 'toothpick' grooves and cleaning striations among European Neanderthal populations, the lack of these features in Gough's Cave individuals may be related to the low instance of caries, and the presence of only slight-moderate degree of supragingival calculus.

ACKNOWLEDGEMENTS: The author particularly wishes to thank Christopher B. Stringer and Louise T. Humphrey for their assistance (and patience). Special thanks are also due to Robert Kruszynski, Steven E. Churchill, and Christy G. Turner II. Dental morphology data for the South Asian samples were collected courtesy of funding from a National Science Foundation Dissertation Grant (# 9318334) and an American Institute of Indian Studies Junior Fellowship (1993–94).

REFERENCES

Alexandersen, V.V. 1963. Double-rooted human lower canine teeth. *In,* Brothwell, D.R. (editor), *Dental Anthropology*: 235–244. New York.

—— 1978. Approximale furchen bei Dänischen Mesolithischen und Neolithischen molaren. *Deutsche Zahnaerztliche Zeitschrift,* **33**: 213–215.

Axelsson, G. & Kirveskari, P. 1977. The deflecting wrinkle on the teeth of Icelanders and the Mongoloid Dental Complex. *American Journal of Physical Anthropology,* **47**:321–324.

Bailit, H., Workman, P.L., Niswander, J.K. & MacClean, C.J. 1970. Dental asymmetry

as an indicator of genetic and environmental stress in human populations. *Human Biology*, **42**: 626–638.

Bennike, P. 1985. *Paleopathology of Danish Skeletons*. Copenhagen.

Brabant, H. 1971 The human dentition during the Megalithic era. *In,* Dahlberg, A.A. (editor), *Dental Morphology and Evolution*: 283–297. Chicago.

—— 1976. Observations sur l'evolution de certaines dimensions coronaires des dents humaines. *Acta Stomatologica Belgica* **73**: 193–234.

—— **& Ketelbant, C.** 1975. Observations sur la frequence de certaines caractères mongoloides dans la denture permanente de la population belge. *Stomatologie et Odontologie*, **18:** 121–134.

—— **Sahly, A. & Bouyssou, M.** 1961. Etude des dents préhistorique les station archéologique des Metelles. *Stomatologie et Odontol*ogie **4:** 382–448.

Brace, C.L. 1980. Australian tooth-size clines and the death of a stereo-type. *Current Anthropology*, **21**: 141–164.

—— **& Mahler, P.E.** 1971 Post-Pleistocene changes in the human dentition. *American Journal of Physical Anthropology*, **34:** 191–204.

—— **& Nagai, M.** 1982. Japanese tooth size, past and present. *American Journal of Physical Anthropology*, **59:** 399–411.

—— **Smith, S.L. & Hunt, K.D.** 1991. What big teeth you had Grandma! Human tooth size, past and present. *In,* Kelley, M.A. & Larsen, C.S. (editors), *Advances in Dental Anthropology*: 33–57. New York.

Brothwell, D.R. 1981. *Digging Up Bones. Second Edition*. London and Oxford.

Burnett, S.E., Hawkey, D.E. & Turner, C.G. II 1996. Accessory ridges in maxillary premolars: a preliminary study of their occurrence in four populations. Abstract: *American Journal of Physical Anthropology*, **Suppl. 22:** 76.

Calcagno, J.M. 1986. Dental reduction in post-Pleistocene Nubia. *American Journal of Physical Anthropology*, **70**: 349–363.

Clarke, N.G. & Hirsch, R.S. 1991. Physiological, pulpal, and periodontal factors influencing alveolar bone. *In,* Kelley, M.A. & Larsen, C.S. (editors), *Advances in Dental Anthropology*: 241–266. New York.

Cook, D.C. & Buikstra, J.E. 1979. Health and differential survival in prehistoric populations: prenatal dental defects. *American Journal of Physical Anthropology*, **51:** 649–664.

Cooper, N.C. 1931. Report on a mandible from 'the caves', Cheddar. *Proceedings of the Somerset Archaeology and Natural History Society*, **76:** 57–58.

Corruccini, R.S. 1973. Size and shape in similarity coefficients based on metric characters. *American Journal of Physical Anthropology*, **38:** 743–754.

Currant, A.P., Jacobi, R.M. & Stringer, C.B. 1989. Excavations at Gough's cave, Somerset 1986–7. *Antiquity* **63:** 131–136.

Dahlberg, A.A. 1945. The changing dentition of man. *Journal of American Dental Association*, **32**: 676–680.

—— 1960. The dentition of the first agriculturalists (Jarmo, Iraq). *American Journal of Physical Anthropology*, **18:** 243–256.

Davies, H.N. 1904. The discovery of human remains under stalagmite in Gough's Cave, Cheddar, Somerset. *Report of the British Association for the Advancement of Science, 1904:* 569–70.

deTerra, M. 1905. *Beitrage zu einer Odontographie der Menschenrassen*. Inaugural dissertation, University of Zurich.

Formicola, V. 1988. Interproximal grooving of teeth: additional evidence and interpretation. *Current Anthropology*, **29:** 663–664.

Frayer, D.W. & Russell, M.D. 1987. Artificial grooves on the Krapina Neanderthal teeth. *American Journal of Physical Anthropology*, **74:** 393–405.

Goodman, A.H. & Rose, J.C. 1991. Dental enamel hypoplasias as indicators of nutritional status. *In,* Kelley, M.A. & Larsen, C.S. (editors), *Advances in Dental Anthropology*: 279–293. New York.

Goose, D.H. 1963. Dental measurement: an assessment of its value in anthropological studies. *In,* Brothwell, D.R. (editor), *Dental Anthropology*: 125–148. Oxford.

—— **& Lee, G.T.R.** 1971. The mode of inheritance of Carabelli's trait. *Human Biology*, **43:** 64–69.

Grine, F.E. & Henshilwood, C.S. 2002. Additional human remains from Blombos Cave, South Africa (1999–2000 excavations). *Journal of Human Evolution*, **42**: 293–302.

—— **Henshilwood, C.S. & Sealey, J.C.** 2000. Human remains from Blombos Cave, South Africa (1997–1998 excavations). *Journal of Human Evolution*, **38**: 755–765.

Guargliardo, M. 1982. Tooth size crown differences between age groups: a possible new indicator of stress in skeletal samples. *American Journal of Physical Anthropology*, **58:** 383–390.

Guerini, V. 1977. *A History of Dentistry*. Boston.

Guigui, R. 1974. *La Dentition des Eurasiens*. Doctoral thesis in Odontological Sciences, University of Paris.

Haeussler, A.M. 1996. *Dental Anthropology of Russia, Ukraine, Georgia, Central Asia: Evolution of Five Hypotheses for Paleo-Indian Origins*. Ph.D. dissertation, Arizona State University.

—— **Irish, J.D., Morris, D.H. & Turner, C.G. II** 1989. Morphological and metrical comparison of San and central Sotho dentitions from southern Africa. *American Journal of Physical Anthropology*, **78:** 115–122.

Hanihara, K. & Ueda, H. 1982. Dentition of the Minatogawa Man. *In,* Suzuki, H. & Hanihara, K. (editors), *The Minatogawa Man: The Upper Pleistocene Man from the Island of Okinawa*. University Museum Bulletin No. 19: 51–59. Tokyo.

Harris, E.F. & Rathbun, T.A. 1991. Ethnic differences in the apportionment of tooth sizes. *In,* Kelley, M.A. & Larsen, C.S. (editors), *Advances in Dental Anthropology*: 121–142. New York.

Hawkey, D.E. 1998. *Out of Asia: Dental Evidence for Affinity and Microevolution of Early/Recent Populations of India and Sri Lanka*. Ph.D. dissertation, Arizona State University.

—— n.d.*a*. Upper premolar buccal style: occurrence and scoring procedures. (In preparation).

—— n.d. *b*. .Dental modification in early South Asia. (In preparation).

—— **Merbs, C.F. & Tyson, R.A.** n.d.. Activity-induced dental wear: the effect of toothbrushing habits on the dentition as seen in biological supply specimens from modern India. (In preparation.)

Hedges, R., Housley, R., Bronk, C. & van Klinken, G. 1991. Radiocarbon dates from the AMS system: datelist 13. *Archaeometry*, **33**: 282–283.

Hellman, M. 1928. Racial characters in the human dentition. *Proceedings of the American Philosophical Society*, **67:** 157–174.

Hildebolt, C.F. & Molnar, S. 1991. Measurement and description of periodontal disease in anthropological study. *In,* Kelley, M.A. & Larsen, C.S. (editors), *Advances in Dental Anthropology*: 225–240. New York.

Hillson, S. 1986. *Teeth*. Cambridge.

Hillson, S. & Bond, S. 1997. Relationship of enamel hypoplasia to the pattern of tooth crown growth: a discussion. *American Journal of Physical Anthropology*, **104**: 89–103.

Hjelmman, G. 1928. *Morphologische Beobachtungen und den Zahnen der Finnen*. Acta Societatis Medicorum Fennicae 'Duodecim' Suomalaisen Laakariseuran Duodecim im Toimituksia To. XI, Fasc 1. Helsinki.

Humphrey, L. & Stringer, C. 2002. The human cranial remains from Gough's Cave (Somerset, England). *Bulletin of the Natural History Museum, London, Geology*, **58:** 153–168.

Irish, J.D. 1993. *Biological Affinities of Late Pleistocene Through Modern African Aboriginal Populations: The Dental Evidence*. Ph.D. dissertation, Arizona State University.

—— 1995. High frequency archaic dental traits in modern sub-Saharan African populations. Abstract: *American Journal of Physical Anthropology*, **Suppl. 20:** 117.

—— 1998. Ancestral dental traits in recent sub-Saharan Africans and the origins of modern humans. *Journal Human Evolution*, **34**:81–98.

—— 2000. The Iberomaurusian enigma: North African progenitor or dead end? *Journal Human Evolution*, **39**:393–410.

Jackson, J.W. 1915. Dental mutilations in Neolithic human remains. *Journal of Anatomy and Physiology*, **49:** 72–79.

Kaczmarek, M. 1981. Studies in the dental morphology of a modern Polish population. *Przeglad Antropologiczny*, **47:** 63–82.

Kanner, L. 1928. *Folklore of Teeth*. New York.

Keith, A. & Cooper, N. 1929. Report of human remains from Gough's cave, Cheddar. *Proceedings of the Somerset Archaeological and Natural History Society*, **74:** 118–121.

Kennedy, K.A.R., Lovell, N.C. & Burrow, C.B. 1986. *Mesolithic Human Remains from the Gangetic Plain: Sarai Nahar Rai*. South Asia Occasional Papers and Theses No.10. Ithaca.

—— **Misra, V.N. & Burrow, C.B.** 1981. Dental mutilation from prehistoric India. *Current Anthropology*, **22:** 285–286.

Kieser, J.A. 1990. *Human Adult Odontometrics: The Study of Variation in Adult Tooth Size*. Cambridge.

Kirveskari, P. 1974. *Morphological Traits in the Permanent Dentition of Living Skolt Lapps*. Turku.

Koritzer, R.T. 1977. An anthropological approach to the study of dental anthropology. *In,* Dahlberg, A.A. & Graber, T.M. (editors), *Orofacial Growth and Development*: 283–299. The Hague.

Lavelle, C.L.B. 1968. Anglo-Saxon and modern British teeth. *Journal of Dental Research*, **47:** 811–815.

—— 1972. Maxillary and mandibular tooth size in different racial groups and in different occlusal categories. *American Journal of Orthodontics*, **61:** 29–37.

—— **Ashton, E.H. & Flinn, R.M.** 1970. Cusp pattern, tooth size, and third molar agenesis in the human mandibular dentition. *Archives of Oral Biology*, **15:** 227–287.

Leigh, R.W. 1925. Dental pathology of Indian tribes of varied environmental and food conditions. *American Journal of Physical Anthropology*, **8:** 179–199.

Lipschultz, J.G. 1996. *Who were the Natufians? A Dental Assessment of their Population Affinities*. M.A. thesis, Arizona State University.

Lovell, N.C. 1992. Paleodemography. *In, Human Skeletal Remains from Mahadaha: A Gangetic Mesolithic Site*. South Asia Occasional Papers and Theses No.11: 139–156. Ithaca.

Lukacs, J.R. 1985. Tooth size variation in prehistoric India. *American Anthropologist*, **87:** 811–825.

—— 1986. Dental morphology and odontometrics of early agriculturalists from Neolithic Mehrgarh, Pakistan. *In,* Russell D.E, Santoro, J-P., & Sigogneau-Russell,

D. (editors), *Teeth Revisited: Proceedings of the Seventh International Symposium on Dental Morphology, Paris. Mem. Mus. Nat. Hist. Paris (serie C),* **53:** 305–319.

—— **& Hemphill, B.E.** 1990. Traumatic injuries of prehistoric teeth: new evidence from Baluchistan and Punjab Provinces, Pakistan. *Anthropologischer Anzieger,* **48:** 351–363.

—— **& Hemphill, B.E.** 1991. The dental anthropology of prehistoric Baluchistan: a morphometric approach to the peopling of South Asia. *In,* Kelley, M.A. & Larsen, C.S.(editors), *Advances in Dental Anthropology*: 77–119. New York.

—— **& Hemphill, B.E.** 1992. Dental Anthropology. *In, Human Skeletal Remains from Mahadaha: A Gangetic Mesolithic Site.* South Asia Occasional Papers and Theses No.11: 157–270. Ithaca.

—— **& Pastor, R.F.** 1988. Activity-induced patterns of dental abrasion in prehistoric Pakistan: evidence from Mehrgarh and Harappa. *American Journal of Physical Anthropology,* **76:** 377–398.

—— **Misra, V.N. & Kennedy, K.A.R.** 1982. *Bagor and Tilwara: Late Mesolithic Cultures of Northwest India. Volume I: The Human Skeletal Remains*. Pune.

Merbs, C.F. 1983. *Patterns of Activity-Induced Pathology in a Canadian Inuit Population*. Archaeological Survey of Canada Paper 119. Ottawa.

Milner, G.R. & Larsen, C.S. 1991. Teeth as artifacts of human behavior: intentional mutilation and accidental modification. *In,* Kelley, M.A. & Larsen, C.S. (editors), *Advances in Dental Anthropology*: 357–378. New York.

Moorrees, C.F.A. 1957. *The Aleut Dentition: A Correlative Study of Dental Characteristics in an Eskimoid People*. Cambridge.

Morris, D.H. 1975. Bushmen maxillary canine polymorphism. *South African Journal of Science,* **71:** 333–335.

—— **Dahlberg, A.A. & Glasstone-Hughes, S.** 1978. The Uto-Aztecan premolar: the anthropology of a dental trait. *In,* Butler, P.M. & Joysey, K.A.(editors), *Development, Function and Evolution of Teeth*: 69–79. London.

Oakley, K.P., Campbell, B.G. & Molleson, T.I. 1971. *Catalogue of Fossil Hominids II: Europe. British Natural History Museum.* London.

Pedersen, P.O. 1949. The East Greenland Eskimo Dentition: Numerical Variations and Anatomy. *Meddelelser om Grønland,* **142:** 1–244.

Penrose, L.S. 1954. Distance, size and shape. *Annals of Eugenics,* **18:** 337–343.

Potter, R.H.Y., Alcazaren, A.B., Herbosa, F.M. & Tomaneng, J. 1981. Dimensional characteristics of the Filipino dentition. *American Journal of Physical Anthropology,* **55:** 33–42.

Sauter, M.R. & Moeschler, P. 1960. Caracteres dentaires mongoloides chez les Burgondes de la Suisse occidentale a Saint-Prex. Vaud. *Archives des Sciences, Geneve,* **13:** 387–400.

Schour, I. & Massler, M. 1940. The development of the human dentition. *Journal of the American Dental Association,* **28:** 1153–1160.

Schulz, P.D. & McHenry, H. 1975. The distribution of enamel hypoplasia in prehistoric California Indians. *Journal of Dental Research,* **54:** 913.

Schwerz, F. 1917. Morphologische untersuchengen an zahnen von Alamannen aus dem V bix X Jahrhundert. *Archiv fur Anthropologie,* **(n.s.) 15:** 1–43.

Scott, G.R. 1973. *Dental Anthropology: A Genetic Study of American White Families and Variation in Living Southwest Indians*. Ph.D. dissertation, Arizona State University.

—— 1977. Classification, sex dimorphism, association and population variation of the canine distal accessory ridge. *Human Biology,* **49:** 453–469.

—— **& Turner CG II** 1988. Dental anthropology. *Annual Review of Anthropology,* **17:** 99–126.

—— **& Turner CG II** 1997. *The Anthropology of Modern Human Teeth: Dental Morphology and Its Variation in Recent Human Populations*. Cambridge.

Seligman, C.G. & Parsons, F.G. 1914. The Cheddar Man: A skeleton of Late Palaeolithic date. *Journal of the Royal Anthropological Institute,* **44:** 241–263.

Selmer-Olsen, R. 1949. *An Odontometrical Study on the Norwegian Lapps.* Skrifter Utgitt av det Norske Videnskaps-Akademi i Oslo, I. Mat Natturv Klasses, No. 3. Oslo.

Stringer, C. 1985. The hominid remains from Gough's Cave. *Proceedings of the University of Bristol Selaeological Society,* **17:** 145–152.

—— 1990. *Hominid Remains – an up-date: British Isles.* Bruxelles.

Tratman, E. 1975. Problems of 'the Cheddar Man', Gough's Cave, Cheddar, Somerset. *Proceedings of the University of Bristol Spelaeological Society,* **14:** 7–23.

Turner, C.G. II 1979. Dental anthropological indicators of agriculture among the Jomon people of central Japan. *American Journal of Physical Anthropology,* **51:** 619–636.

—— 1987. Late Pleistocene and Holocene populations of East Asia based on dental variation. *American Journal of Physical Anthropology,* **73:** 305–321.

—— 1988. Interproximal grooving of teeth: additional evidence and interpretation (comment). *Current Anthropology,* **29:** 664–665.

—— **& Benjamin, O.** 1989. World variation in three-rooted lower first permanent molars. Presented at the Eighth International Symposium on Dental Morphology, Jerusalem.

—— **& Cadien, J.D.** 1969. Dental chipping in Aleuts, Eskimos and Indians. *American Journal of Physical Anthropology,* **31:** 303–310.

—— **& Hawkey, D.E.** 1991. World variation in Tomes' root. Abstract: *American Journal of Physical Anthropology,* **Suppl. 12:** 175.

—— **& Hawkey, D.E.** 1998. Whose teeth are these? Carabelli's trait. *In,* Lukacs, J.R. (editor), *Human Dental Development, Morphology and Pathology. A tribute to Albert A. Dahlberg*. University of Oregon Anthropological Papers No. 54: 41–50. Eugene..

—— **& Scott, G.R.** 1977. Dentition of Easter Islanders. *In,* Dahlberg, A.A. & Graber, T.M. (editors), *Orofacial Growth and Development*: 229–249. The Hague.

—— **Nichol, C.R. & Scott, G.R.** 1991. Scoring procedures for key morphological traits of the permanent dentition: the Arizona State University Dental Anthropology System. *In,* Kelley, M.A. & Larsen, C.S. (editors), *Advances in Dental Anthropology*: 13–31. New York.

van Reenan, J.F. 1982. The effects of attrition on tooth dimensions of San (Bushmen). *In,* Kurtén, B.(editor). *Teeth: Form, Function, and Evolution*: 182–203. New York.

Wolpoff, M.H. 1971. *Metric Trends in Hominid Dental Evolution*. Case Western Reserve University Studies in Anthropology, No. 2.

Zubov, A.A. & Kaldiva, N.E. 1979. *Ethnic Odontology of the USSR*. Moscow.

Bull. nat. Hist. Mus. Lond. (Geol.) **58**(supp): 37–44 Issued 26 June 2003

Gough's Cave 1 (Somerset, England): an assessment of body size and shape

TRENTON W. HOLLIDAY
Department of Anthropology, Tulane University, New Orleans LA 70118, USA
STEVEN E. CHURCHILL
Department of Biological Anthropology and Anatomy, Duke University, Durham NC 27710, USA

Synopsis. Stature, body mass, and body proportions are evaluated for the Cheddar Man (Gough's Cave 1) skeleton. Like many of his Mesolithic contemporaries, Gough's Cave 1 evinces relatively short estimated stature (ca. 166.2 cm [5' 5']) and low body mass (ca. 66 kg [146 lbs]). In body shape, he is similar to recent Europeans for most proportional indices. He differs, however, from most recent Europeans in his high crural index and tibial length/trunk height indices. Thus, while Gough's Cave 1 is characterized by a total morphological pattern considered 'cold-adapted', these latter two traits may be interpreted as evidence of a large African role in the origins of anatomically modern Europeans.

INTRODUCTION

Reconstructed stature, body mass, and body shape are all variables of interest in any attempt to understand the paleobiology of prehistoric humans such as the 'Cheddar Man', or the Gough's Cave 1 specimen. The relative completeness of the Gough's Cave 1 postcranial skeleton allows each of these variables to be accurately reconstructed. Such variables are of interest both for evolutionary and non-evolutionary questions. For example, any body mass and/or stature differences between Mesolithic humans, such as Gough's Cave 1, and recent humans are unlikely to be evolutionary in nature. Nonetheless, they are of interest to paleobiologists since they may reflect the nutritional and overall health status of prehistoric populations. In contrast, body proportions vary among recent humans, presumably as the result of climatic selection. Yet body proportions appear to have a large genetic component, and, over evolutionarily short periods, since they are the result of apparently *long-term* climatic selection (based on migrant studies), they may provide evidence of population movements or migration from different climatic regimes (Holliday, 1997*a*).

Stature in Gough's Cave 1 is predicted from lower limb long bone lengths using Trotter and Gleser's (1958) standard formulae for Euroamericans (discussed in detail below). Body mass for the specimen is predicted using two methods outlined in Ruff *et al.* (1997). The first method involves computing the arithmetic average of predictions based on three separate body mass/femoral head diameter regressions derived from recent human skeletal material. In the second method, body mass is predicted from stature and bi-iliac breadth. In concert these two variables (stature and bi-iliac breadth) are known to provide an accurate estimate of body mass in living humans, and have an added advantage in that they are independent of the locomotor biomechanical stresses to which the femoral head is subject (Ruff *et al.*, 1997). Ruff's stature/bi-iliac breadth predictive formula is derived from data on living humans. Therefore, in order to use this method with fossils, stature was estimated using the Trotter and Gleser (1958) formulae, and a 5% correction factor was added to bi-iliac breadth to account for soft tissue. All formulae used to predict body mass were kindly provided by Prof. C.B. Ruff.

With regard to body shape or proportions, there are several means by which these features may be accurately reconstructed from skeletal remains; these means approximate some of the anthropometric data taken on living human subjects. The measures that are used in this study reflect the following: 1) intralimb proportions (i.e., relative lengths of the proximal and distal limb segments), 2) limb/trunk proportions, 3) body linearity relative to overall body mass, and 4) body breadth relative to stature. For all analyses, Gough's Cave 1 is compared to other Late Pleistocene and Early Holocene associated skeletons as well as to a large sample of recent humans from across the western Old World (Africa and Europe). The fossils have been placed into Mesolithic (< 10,000 BP), Late Upper Paleolithic (LUP; 11,000–19,000 BP), Early Upper Paleolithic (EUP; 20,000–28,000 BP) and Neandertal (> 30,000 BP) samples, while the recent humans have been placed into three geographical subsamples: Europe, North Africa and Sub-Saharan Africa. Detailed discussion of these samples is found in Holliday (1995).

BODY SIZE

Stature

For all samples, stature was predicted using Trotter and Gleser's (1958) formulae for the tibia and femur; if both bones were present, the mean of the two resultant predictions was used. Formulae for Euroamerican males were used for Gough's Cave 1 and all comparative samples, with the exception of the recent Sub-Saharan Africans and the European EUP, for whom African-American formulae were used. These regression formulae are more appropriate because these two groups have a demonstrably more 'tropically-adapted' body shape which is more similar to that of African-Americans (Holliday, 1997*a*).

Table 1 presents summary statistics for predicted stature among Gough's Cave 1 and the comparative samples. The Gough's Cave specimen has a predicted stature of 166.2 cm, which falls just below the Mesolithic male mean of 167.5 cm. His predicted stature is much shorter relative to recent European males; he falls below their 25th percentile. Importantly, predicted stature values for the fossils are similar to those given in Frayer (1984), who used many of the same specimens, but temporally subdivided his samples differently than has been done here. As an example of the similarity of results, Frayer's (1984) Mesolithic sample had a predicted male stature of 167.8 cm, almost identical to our mean of 167.5 cm. Also, his Upper Paleolithic male mean of 174.3 cm is somewhat (although not

© The Natural History Museum, 2003

Table 1 Summary statistics (mean, standard devition, number of specimens) for Gough's Cave 1, fossil and recent human male samples – predicted stature (in cm).

	Predicted stature
Gough's Cave 1	166.2
European Mesolithic	167.5, 4.8, 7
European Late Upper Palaeolithic	170.2, 6.6, 17
European Early Upper Palaeolithic	170.1, 7.9, 11
European Neandertals	166.7, 3.8, 4
Recent Europeans	171.6, 5.8, 311
Recent North Africans	167.4, 5.9, 75
Recent Sub-Saharans	164.7, 8.2, 62

statistically significantly) higher than our LUP and EUP means of 170.2 cm and 170.1 cm, respectively.

Not unexpectedly, our results suggest that stature in Europe is highest among Upper Paleolithic (both EUP and LUP) and recent Europeans. Neandertals and Mesolithic Europeans, on the other hand, are significantly shorter than recent Europeans (two-tailed *t* test, $p = 0.020$ and 0.048, respectively). These results are similar to those reported by Frayer *et al.* (1993) and Formicola & Giannecchini (1999). With regard to the Mesolithic sample, this reduction in stature may be due to a drop in dietary protein. Such a drop could have followed decreased reliance on big game following the reforestation of Europe, a phenomenon documented by archaeologists for many early Holocene hunter-gatherers (Straus *et al.*, 1980; Geddes *et al.*, 1986).

Note that among the recent human groups, stature appears to decrease as one moves toward the equator. This is likely a secondary consequence of a decrease in body mass associated with increasingly hotter, more tropical temperatures, following Bergmann's rule (see below).

Body Mass

Table 2 gives predicted body mass summary statistics for Gough's Cave 1 and the comparative male sample. Among the recent human samples, there is a clear decrease in body mass (based on either predictive method) from higher to lower latitudes. This reflects adherence of humans to Bergmann's (1847) ecological rule (discussed below). The Gough's Cave 1 specimen has a predicted body mass of 64.8 kg based on femoral head size, and a mass of 67.3 kg based on stature and bi-iliac breadth. It is noteworthy that despite the fact that the two methods use very different anatomical features, the two predictions deviate from each other by less than 4%. Note, also that across all groups, the mean body mass estimates using the non-biomechanical (stature/bi-iliac breadth) method are close to those derived from the femoral head. The greatest difference between the two methods is found among the EUP sample, whose body mass prediction based on stature and bi-iliac breadth is 5.8% higher than the one based on femoral head diameter. Note, too, that while the Neandertal sample appears to be characterized by high body mass, there is relatively little evidence for a subsequent change in body mass in Europe from the EUP to the present (a result consistent with the findings of Ruff *et al.*, 1997). As for the specimen of interest, Gough's Cave 1 is not atypical among early Holocene Europeans in mass; he falls slightly below the Mesolithic male mean based on the femoral head prediction, and slightly above the mean for the stature/bi-iliac breadth prediction. He, like most of his Mesolithic cohorts, is light relative to recent Europeans; his femoral head-predicted and bi-iliac breadth/femoral length predicted weights fall on the 29th and 37th recent European male percentiles, respectively.

Table 2 Summary statistics for Gough's Cave 1, fossil and recent human males – predicted body mass (in kg).

	Femoral Head Method	Stature/BIB Method
Gough's Cave 1	64.8	67.3
European Mesolithic	66.9, 7.2, 7	66.0, 2.3, 6
European Late Upper Palaeolithic	67.7, 6.6, 14	67.4, 8.2, 6
European Early Upper Palaeolithic	65.8, 10.0, 10	69.6, 7.3, 6
European Neandertals	82.9, 4.3, 4	79.3, –, 1
Recent Europeans	69.3, 7.3, 134	71.0, 7.4, 126
Recent North Africans	59.0, 7.6, 73	61.3, 5.5, 60
Recent Sub-Saharans	54.7, 8.5, 53	53.6, 8.6, 49

BODY SHAPE

Intralimb Proportions

Elongation of the distal limb segment relative to the proximal has been demonstrated to be associated with overall limb elongation in both the upper and lower limb (Meadows & Jantz, 1995), and is correlated with climatic variables (Roberts, 1978; Trinkaus, 1981). Distal limb segment elongation is typically quantified in the form of brachial (radius length/humeral length × 100) and crural (tibial length/femoral length × 100) indices. These skeletal measures are comparable to the anthropometric antebrachial index (forearm length/upper arm length × 100) and calf/thigh index (calf length/thigh length × 100), respectively, which are commonly taken on living people (Roberts, 1978).

Table 3 gives summary statistics for the brachial and crural indices of the Gough's Cave 1 specimen and fossil and recent human samples. Note that among the recent humans, the indices show a cline from lower to higher latitudes, with high indices in the former, and low indices in the latter. This is presumably the result of long-term climatic selection (discussed below). Within groups, male and female brachial and crural index values are similar (males do, however, tend to have higher brachial indices than females; Trinkaus, 1981; Holliday, 1995). Given the difficulty in assigning sex to some fossil specimens (as well as the already small size of the fossil sample), combined-sex means are given in Table 3. This does not affect the overall pattern, as will be evident below, when we discuss Gough Cave 1's relationship to other males from the comparative sample.

As is evident from Table 3, the Cheddar specimen, like other Late Pleistocene and early Holocene Europeans, has elongated distal limb segments in both the upper and lower limb. In fact, Gough's Cave 1 has indices not unlike the means of the recent African samples, and

Table 3 Summary statistics for Gough's Cave 1, fossil and recent human samples – brachial and crural indices.

	Brachial Index	Crural Index
Gough's Cave 1	77.1	88.9
European Mesolithic	77.5, 1.9, 10	85.5, 2.6, 10
European Late Upper Palaeolithic	78.6, 3.0, 17	85.1, 1.9, 22
European Early Upper Palaeolithic	77.9, 2.2, 17	85.4, 1.9, 13
European Neandertals	73.2, 2.5, 5	78.7, 1.6, 4
Recent Europeans	75.0, 2.5, 391	82.7, 2.4, 436
Recent North Africans	78.6, 2.4, 136	85.0, 2.3, 133
Recent Sub-Saharans	78.6, 2.8, 103	85.4, 2.4, 110

his crural index value actually falls above the Sub-Saharan African mean. It is not, however, too unusual to find a male European specimen today with a brachial index value equal to or higher than that of the Gough's Cave specimen; Gough's Cave 1 falls right on the 75th percentile for the recent European males (n = 239). However, his crural index would be extremely unusual in a sample of recent Europeans, since his value falls above the 99th percentile for recent European males (n = 273).

His values are not, however, unusual among European Mesolithic (nor Paleolithic) humans. His brachial index is virtually identical to the Mesolithic mean, and while his crural index is above the Mesolithic mean, one of the 10 Mesolithic specimens sampled (Téviec 11) has yet a higher crural index (89.1).

Limb/Trunk Proportions

The fact that limb/trunk proportions of modern humans covary with climate and geography has been documented for both skeletal (Holliday, 1995, 1997*a*) and anthropometric samples (via the relative sitting height index {sitting height/stature × 100}, Roberts, 1978). Given the largely complete (albeit poorly reconstructed) vertebral column of the Gough's Cave specimen, one can estimate skeletal trunk height (STH = summed dorsal vertebral elements T1-L5 + sacral ventral length; Franciscus & Holliday, 1992) as a body size or trunk length variable to which relative limb length may be assessed. As was done for the thoracic and lumbar vertebral column heights (Chuchill & Holliday, 2002), STH is estimated from those vertebral elements preserved in Gough's Cave 1, using a least-squares regression for a complete recent human series (n = 45). The formula used is: $Y = 1.086x - 1.806$; $r^2 = 0.998$, where x (partial trunk height, or PTH) is the summed dorsal body heights for T4-L5, sacral ventral length, and the ventral body height of T1. The 'reconstruction' for display of the specimen necessitated further estimation. Thoracic vertebrae 6 and 7 were glued together with a mock intervertebral disk between them; thus their combined dorsal height was measured and the height of the intervening 'disk' (2.9 mm) was subtracted, yielding 39.8 as the estimate of combined T6-T7 dorsal height. The combined height of T8-T9 (42.5) and T11-T12 (48.1) were estimated in the same manner. The predictive equation based on the above measurements yields an STH of 483.9 mm, with a SE of the estimate of 1.6 mm. The 95% confidence limits for the prediction are 480.6–487.2 mm, a span which is only 1.4% of the prediction itself, indicating that STH can be accurately predicted in Gough's Cave 1.

As discussed in Churchill & Holliday (2002), the height of Cheddar Man's vertebral column (as reflected in thoracic and lumbar column heights) was short for a Mesolithic male. Thus, it is not surprising that the Gough's Cave specimen possesses a short STH, as well. The specimen's STH of 483.9 falls well below (although within one standard deviation of) the Mesolithic male mean of 511.6 (n = 4), and only one Mesolithic male, the diminutive Hoëdic 9, has a shorter trunk. However, the most important question that remains is how Gough's Cave 1 compares in terms of limb length relative to trunk height. In order to elucidate these patterns, limb segment length (maximum humeral, radius and tibial length and femoral bicondylar length) to trunk height ratios were computed for the comparative fossil and recent human sample, and are compared to Gough's Cave 1 in Tables 4 and 5. Sexual dimorphism in these traits exists, but is minimal (Holliday, 1995); thus, as was done with the brachial and crural indices, Gough's Cave 1 is compared to combined-sex samples. As was evident in intralimb proportions, among recent humans there is a clinal distribution of limb/trunk ratios, with Sub-Saharan Africans exhibiting the highest mean indices, the Europeans the lowest, and North Africans intermediate between the two groups.

Table 4 Summary statistics for Gough's Cave 1, fossil and recent human samples – upper limb segment/trunk height ratios.

	HL/STH	RL/STH
Gough's Cave 1	66.7	51.5
European Mesolithic	61.7, 3.7, 7	47.9, 2.7, 7
European Late Upper Palaeolithic	61.2, 2.8, 15	48.3, 2.4, 12
European Early Upper Palaeolithic	69.1, 4.0, 8	55.0, 2.7, 7
European Neandertals	64.0, 1.5, 3	47.0, 0.2, 3
Recent Europeans	63.6, 3.4, 124	47.9, 2.8, 123
Recent North Africans	66.0, 3.8, 62	51.9, 3.4, 62
Recent Sub-Saharans	69.6, 4.1, 51	55.0, 4.0, 51

Table 5 Summary statistics for Gough's Cave 1, fossil and recent human samples – lower limb segment/trunk height ratios.

	FL/STH	TL/STH
Gough's Cave 1	89.7	79.8
European Mesolithic	87.4, 3.9, 7	74.0, 4.0, 7
European Late Upper Palaeolithic	86.6, 3.4, 15	73.6, 3.5, 13
European Early Upper Palaeolithic	96.0, 5.1, 7	84.0, 4.6, 6
European Neandertals	89.1, 0.0, 2	71.2, 1.0, 2
Recent Europeans	88.6, 4.4, 123	73.6, 4.3, 124
Recent North Africans	94.2, 5.5, 63	79.8, 4.9, 60
Recent Sub-Saharans	97.7, 7.5, 51	84.1, 6.5, 51

For the upper limb/trunk height ratios (Table 4), Gough's Cave 1 differs not only from recent Europeans, but from Late Upper Paleolithic (LUP) Europeans, as well. In fact, relative to trunk height, the Cheddar specimen is somewhat long-armed, and is most similar to the recent North Africans in this regard. He is less long-armed, however, than the average recent Sub-Saharan African or European Early Upper Paleolithic (EUP) humans. While the distribution of sample means provides an overall pattern of differences, we may still ask how unusual would upper limb/trunk height ratios equal to or greater than that of Gough's Cave 1 be among recent Europeans? An examination of the male European distribution provides some insight. For the humeral length/trunk height ratio, he falls on the 75% percentile of recent European males, while for the radius length/trunk height ratio, he falls above the 85% percentile. Thus while he does exhibit a positive deviation from the mean, sampling a recent European male who shares his upper limb/trunk height (or greater) values could be as common as 1 in 4.

The lower limb/trunk height ratios reveal a slightly different pattern (Table 5). The Cheddar specimen's femoral length/trunk height ratio is very similar to the recent European mean, while his tibial length/trunk height ratio is 2.5 standard deviations above the recent European mean – indicating that he has an extremely long tibia relative to the height of his trunk. His percentile placement among the recent Europeans males reflects this dichotomy; he falls on their 60th percentile for the femoral length index, and above the 94th percentile for the tibial length index. With regard to the recent Africans, he falls below the Sub-Saharan African mean for both indices, and below the North African FL/STH mean. His TL/STH value, however, is identical to the North African average.

In comparison with other European fossils, Gough's Cave 1 possesses a relatively longer femur than the mean of all but one fossil sample (the long-limbed EUP), although he falls well within the range of all but the short-limbed Neandertal samples. His high relative tibial length index, however, is somewhat more unusual in the sense that he exceeds the range of the LUP sample, and, additionally, he evinces the highest TL/STH index of the Mesolithic sample. In fact, with regard to relative tibial length, among the fossil groups only the long-limbed EUP sample exceeds his value.

Body Linearity Relative to Mass

Another body shape feature known to covary with climate is relative body linearity. In living populations, the weight: height, or ponderal, index is used as a measure of this relationship (e.g., Newman, 1961; Schreider, 1964, 1975; Eveleth, 1966; Hiernaux *et al.*, 1975). This relationship is most easily quantified skeletally via relative femoral head size (i.e., antero-posterior femoral head diameter/femoral bicondylar length × 100). This index should reflect relative linearity, since the femoral head is highly correlated with body mass, while femoral length is highly correlated with stature. This skeletal index was (not surprisingly) found to vary significantly between males and females, with males possessing relatively larger femoral heads than females (two-tailed t test, $p < 0.0001$), and thus Gough's Cave 1 is compared only to other males for this trait.

Table 6 reports the summary statistics for this trait among the comparative samples and the Cheddar specimen. Within the recent humans, there is a clear clinal pattern from Sub-Saharan Africa through North Africa and into Europe, such that the femoral head becomes relatively larger with increasing latitude (see also Ruff, 1994). With regard to fossil humans, note the extremely high indices exhibited by the male Neandertals. For this index, both Neandertal males (La Chapelle-aux-Saints 1 and La Ferrassie 1) fall beyond the 99th percentile of recent European males (n = 134). The other European fossils, including the Mesolithic males and the Gough's Cave 1 specimen himself are virtually identical to recent Europeans for this trait. Only the EUP sample slightly deviates from the European pattern of relatively large femoral heads; they are more similar to recent North Africans in that their femoral heads are somewhat smaller (although not as small as those of the Sub-Saharan Africans).

Body Breadth Relative to Stature

Bi-iliac breadth, or bi-cristal breadth, as it is sometimes called, is measured as the transverse diameter of the superior margin of the pelvic girdle. This raw measurement is correlated with climatic variables (Crognier, 1981; Ruff, 1994), but its fit with climate and/or geography significantly improves when it is scaled to a linear dimension of the body such as stature (Roberts, 1978; Ruff, 1991, 1993, 1994). For the samples presented here, stature is unknown, and therefore must be predicted from long bone length, e.g. femoral length. In such cases, then, predicted stature is each individual's femoral length subsequent to an arithmetic manipulation, (i.e., femoral length × slope, + Y-intercept). Such prediction formulae inevitably introduce error into the analysis, however, since biologically speaking, many individuals are expected to fall well above or well below the predictive line. Thus, to avoid the introduction of further error, stature is not predicted for this analysis, but rather, femoral length (which is highly correlated with stature) is used in its stead.

The first means by which the body breadth to height relationship can be investigated is via the computation of ratios – in this case, bi-iliac breadth / femoral bicondylar length × 100. Due to the fact that females have wider trunks relative to stature than do males, the values for this index are significantly different between the sexes (two-tailed t test, $p < 0.0001$), and therefore the Cheddar specimen is compared solely to males for this variable. Table 6 reports the summary statistics for the males in the comparative sample and the Cheddar specimen. Gough's Cave 1 lies well within 1 standard deviation of the Mesolithic, LUP and recent European male means. Likewise, his value is only 1.4 standard deviations above the North African mean. However, he falls over 3 standard deviations above the recent Sub-Saharan African mean; as discussed below, this group is characterized by some of the longest limbs and narrowest trunks of any humans. Interestingly, while based on extremely small samples, the earlier European fossil samples stand in marked contrast to each other and to recent Europeans. The Neandertals (albeit solely represented by the La Chapelle-aux-Saints 1 specimen) are characterized by an extremely high index, indicative of their broad body breadth relative to stature (Ruff, 1991, 1993, 1994; Trinkaus *et al.*, 1994). By way of contrast, the earliest modern European males (represented by 6 individuals) have low indices; in fact, their mean index falls between those of the North and Sub-Saharan Africans.

Table 6 Summary statistics for Gough's Cave 1, fossil and recent human males – femoral head/femoral length ratios (FHAP/FL) and bi-iliac breadth/femoral length ratios (BIB/FL).

	FHAP/FL	BIB/FL
Gough's Cave 1	10.7	63.3
European Mesolithic	10.7, 0.5, 6	62.1, 3.2, 6
European Late Upper Palaeolithic	10.8, 0.7, 15	61.2, 5.1, 10
European Early Upper Palaeolithic	10.1, 0.4, 10	56.6, 3.2, 6
European Neandertals	12.3, 0.4, 4	69.8, –, 1
Recent Europeans	10.6, 0.5, 134	61.2, 3.4, 126
Recent North Africans	9.9, 0.6, 72	57.3, 4.4, 60
Recent Sub-Saharans	9.5, 0.6, 53	52.6, 3.0, 49

A second means of evaluating relative body breadth has been used extensively by Ruff (1991, 1993, 1994), and involves plotting relative bi-iliac breadth indices, like those calculated above, against stature in bivariate space. Using this method, one can evaluate the relationship between the 'size-corrected' index and a measure of overall size (in Ruff's case, stature; here again, femoral length is used in its stead). Ruff has shown that among recent humans, there is little overlap among broad geographically circumscribed samples for this bivariate relationship, and thus this method could provide some insight into the relative position of the Cheddar specimen. Figure 1 is a scatter plot of the bi-iliac breadth/femoral length ratios regressed on femoral length for the recent Sub-Saharan Africans (squares), the recent Europeans (crosses) and Gough's Cave 1 (star). The lines fitted to the recent samples are least-squares regression

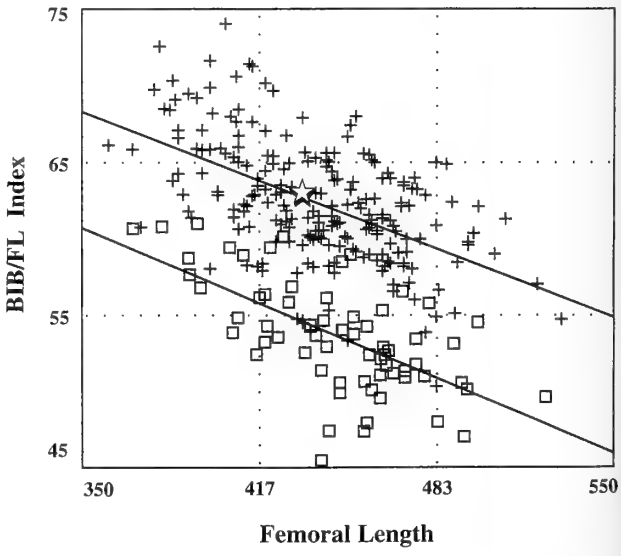

Fig. 1 Scatter plot of bi-iliac breadth/femoral length index on femoral length. Recent Europeans are indicated by crosses; recent Sub-Saharan Africans by squares. Gough's Cave 1 is indicated by a star. The lines for the two recent human samples are least-squares regression lines.

lines. As Ruff has found, there is good separation of the Europeans from the Sub-Saharan Africans throughout most of the size range. Informatively, Gough's Cave 1 falls squarely on the European regression line, far above the Sub-Saharan African line.

Multivariate Assessment of Body Shape

Any assessment of an individual's body size and proportions is at its base an assessment of that individual's total morphological pattern. While the individual analyses presented above when considered as a whole provide tantalizing clues as to the total morphological pattern of the Cheddar Man, these analyses are likely not as informative as would be a multivariate assessment based on the same morphological variables. In fact, a multivariate analysis may be expected to resolve some of the conflicting results obtained above. For example, in relative body linearity, relative body breadth and limb/trunk (excepting the tibia) proportions, the Gough's Cave specimen looks essentially like a recent European (albeit occasionally at the more linear end of the European range). In contrast, his tibia/trunk, brachial, and especially his crural index are more similar to those of more tropically-adapted groups (e.g., Africans).

What then, is the total morphological pattern of body size and shape exhibited by Gough's Cave 1? The way to discover this is to investigate overall body proportions in multivariate space, taking the variances and covariances of all the skeletal manifestations of body shape into account. Once this is done, Gough's Cave 1 will either continue to fall among recent Europeans, or he could possibly exhibit a somewhat different, more tropically-adapted pattern.

The variables to be used in the multivariate analysis and their abbreviations are found in Table 7. Note that these measurements are the same variables used to compute ratios and/or which were plotted in bivariate space. They should therefore provide an accurate reflection of total body shape. The method chosen for body shape extraction is that outlined by Mosimann and colleagues (Mosimann & James, 1979; Darroch & Mosimann, 1985; James & McCulloch, 1990). These morphometricians argue that an individual's overall size is best represented by the geometric mean of all the measurements taken on that individual. The geometric mean (or 'log size' as the authors denominate it) can then be used to create scale-free ratios, or 'shape' variables, between each of the individual's measurements and his geometric mean. The utility of the shape variables lies not in the 'removal' of size *per se*, but in the ability of the researcher to determine if there is a relationship between size and shape via correlation analyses. The application of this method to anthropological data sets is discussed in greater detail elsewhere (e.g., Falsetti *et al.*, 1993; Jungers *et al.*, 1995). In this study, since the primary interest is the body shape of Cheddar Man, discussion is limited to the analysis of shape variables. The variance-covariance matrix (VCM) of the shape variables for a combined sample of fossil and recent humans (n = 225), all of whom preserve the measurements in question, was computed and then subjected to principal components analysis (PCA).

Table 7 First two principal components of shape variables – fossil and recent humans.

	Eigenvector Coefficient I	II
Femoral A-P head diameter (FHAP)	0.305	–0.860
Bi-iliac breadth (BIB)	0.591	0.451
Femoral bicondylar length (FL)	–0.246	0.070
Humeral maximum length (HL)	–0.178	0.037
Tibial maximum length (TL)	–0.404	0.124
Radius maximum length (RL)	–0.421	–0.009
Skeletal trunk height (STH)	0.591	0.187
Eigenvalue	0.0094	0.0032
% total variance	58.25	19.63

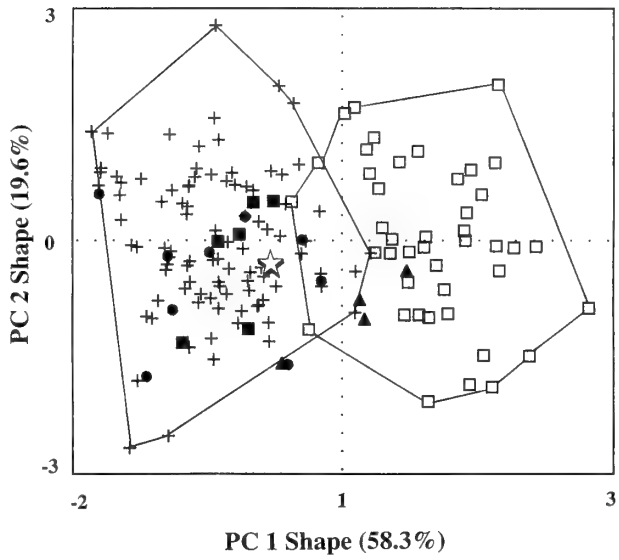

Fig. 2 Scatter plot of PC2 on PC1 (shape data). Crosses are recent Europeans, open squares are recent Sub-Saharan Africans, triangles are Early Upper Paleolithic, circles are Late Upper Paleolithic, closed squares are Mesolithic, star is Gough's Cave 1. Lines indicate range of the recent human samples.

The eigenvector coefficients and eigenvalues for the first two principal components of the log shape data are found in Table 7. The first principal component (PC1) accounts for 58.3% of the total shape variance, and contrasts limb segment length (particularly the distal segments) with femoral head diameter, bi-iliac breadth and skeletal trunk height. The PC scores along this axis are not significantly correlated with overall size (i.e., the geometric mean; $r^2 = 0.008$, $p = 0.1758$). PC1 is readily interpreted as a climatic adaptation component, since it separates heavier, less linear individuals (more cold-adapted) from lighter, more linear individuals (more heat-adapted). The second principal component (PC2) accounts for 19.6% of the shape variance and contrasts bi-iliac breadth and trunk height with femoral head diameter. The scores along this axis are correlated with log size ($r^2 = 0.18$, $p < 0.0001$), and this component tends to segregate males (who on average have large femoral heads and relatively narrow pelves) from the small femoral-head possessing and wider hip bearing females (albeit with considerable overlap).

Component scores for the European early modern fossils (including Gough's Cave 1), as well as the recent Sub-Saharan Africans and recent Europeans are plotted in Figure 2. Note that the separation of the groups is along the first principal axis. This axis contrasts individuals on the left, who possess short distal limbs, wide and relatively long trunks, and large femoral heads from those individuals on the right, who are characterized by relatively short and narrow trunks, long distal limb segments and smaller femoral heads. There is no separation of the groups (fossil or recent) along the second principal axis. Note that for the first principal component, there is relatively little overlap between the recent Sub-Saharan Africans (represented by open squares) and the recent Europeans (represented by crosses). Gough's Cave 1 (the star) and his contemporaries, the European Mesolithic specimens (indicated by dark squares) fall clearly among the recent Europeans, as do the LUP specimens

(indicated by circles). Only 2 of the 9 (22%) LUP specimens (Barma Grande 2 and Bichon 1) even fall in the region of overlap between the recent Sub-Saharan Africans and Europeans, and none of the Mesolithic sample does. In contrast, there is a tendency for the EUP specimens (indicated by triangles) to fall among the Sub-Saharan Africans and outside of the European sample range. This specific result is said to be indicative of a relatively recent African origin for the earliest modern Europeans, and is discussed in detail elsewhere (Holliday, 1995, 1997*a*). What is of most interest to this chapter is that the Gough's Cave specimen, despite possessing some 'non-typically' European traits, falls squarely among the Europeans in multivariate space, albeit toward the more linearly-built end of the distribution.

Discussion

Gough's Cave 1 is relatively unremarkable with regard to stature and body mass; he is small, yet similar to all European samples, save the heavier Neandertals. However, his body shape poses some interesting contrasts which need to be further explored. Among recent humans, clear differences in body shape manifest themselves among geographically-dispersed samples. In terms of relative sitting height, for example, some Australian Aboriginal and Sub-Saharan African groups evince mean relative sitting height indices as low as 47.0, while at the other extreme, many Inuit (Eskimo) samples evince mean indices of around 54.0 (Eveleth & Tanner, 1976). What this means is that among some of the more tropically-adapted groups worldwide, the head, neck and trunk comprise less than half (ca. 47% or less) of a person's stature. Yet another way of looking at this is that among these groups, the lower limb accounts for more than half (ca. 53+%) of a person's standing height. By way of contrast, among the Inuit and other cold-adapted groups, the head, neck and trunk make up well over half (ca. 54+%) of the average person's height, while the lower limbs make up considerably less than half (ca. 46% or less).

The explanation for empirical patterns such as the above is that they are due to climatic selection, and more specifically, reflect the adherence of recent humans to the ecological 'rules' of Bergmann (1847) and Allen (1877). These rules state that within a widespread species of warm-blooded animals, those in colder regions will tend to be heavier (Bergmann's rule) and evince shorter extremities (Allen's rule) than do their more tropical conspecifics. Theoretically, it is argued that we find this pattern because animals in cold regions minimize their surface area: volume ratio (SA:V) in order to better conserve body heat, since heat loss occurs through the skin (i.e., the animal's surface). On the other hand, heat loss in hot environments may be facilitated by increasing relative surface area. Changes in body size and shape can drastically affect the SA:V ratio, as discussed in Ruff (1994) and Holliday (1995).

But do these rules apply to fossil humans as well, or is this an over-extention of biological uniformitarianism? Limited fossil data suggest that prehistoric human populations were characterized by ecogeographical clines that were perhaps even steeper than those one finds today (Trinkaus, 1981, 1991; Stringer, 1989; Ruff, 1991, 1993, 1994). For example, the Kenyan Nariokotome *Homo erectus* skeleton (KNM-WT 15000) is said to be characterized by 'hyper-African' body proportions (Ruff and Walker, 1993), while European Neandertals are characterized by an extremely cold-adapted morphology (Trinkaus, 1981, 1986; Holliday, 1995, 1997*b*; Churchill, 1998).

How do the Gough's Cave 1 specimen and his contemporaries fit into this apparently climatically-driven geographical patterning? In order to address this question adequately, we must have at least some understanding of what the pattern in Europe was *before* the early Holocene, i.e., what was the temporal pattern of body proportions in the European Pleistocene? In other words, were there temporal trends in body shape during this time period? The answer is an emphatic 'yes'. There is actually more *temporal* variability in body shape in Pleistocene Europe than there is *spatial* variability in the world today.

We begin with the European Neandertals. They exhibit a clearly cold-adapted physique, including low brachial and crural indices, low limb/trunk ratios, extremely large femoral heads and wide trunks. Those who succeed them in the region, however, hominins differentially referred to as the 'Cro-Magnons' or the Early Upper Paleolithic (EUP) humans, exhibit the opposite pattern – high brachial and crural indices, high limb/trunk proportions, *relatively* smaller femoral heads and narrower trunks. Succeeding the Cro-Magnons are the Late Upper Paleolithic (LUP), and subsequent Mesolithic populations. These later two samples have, in this analysis, been divided at the Pleistocene/Holocene boundary, with the Mesolithic sample (including Gough's Cave 1) being restricted to the latter epoch. This division may be biologically insignificant, however, since for virtually all analyses – univariate, bivariate or multivariate, the LUP and Mesolithic samples more closely resemble each other than they do any other group, fossil or recent (see also Holliday, 1995, 1997*a*).

Combined or separate, the real question of interest is what was the pattern of body shape in LUP and Mesolithic humans? Importantly, the 'shared' morphology of these two samples (including the specimen of interest) is in some regards paradoxical (Holliday, 1999). Late Upper Paleolithic and Mesolithic specimens retain the high brachial and crural indices of their presumed ancestors, the 'Cro-Magnons'. Yet unlike the Cro-Magnons, they tend not to possess relatively narrow trunks, relatively small femoral heads, or high limb-trunk ratios. Gough's Cave 1, as a general rule, follows this pattern. Like his contemporaries, his brachial and crural indices are near the upper extreme of the recent European sample. Likewise, as with others from his time period, his limb/trunk proportions are within the European range, although his values for HL/STH, RL/STH and particularly his TL/STH indices are somewhat more extreme than those of average Europeans today. Recall that he falls on the 75th, 85th and 94th percentiles, respectively, of the recent European male sample for these traits. For the other traits (relative femoral head size and relative body breadth), however, he falls very near the recent European mean, and is distinctly different from recent Africans. In multivariate space, however, he lies within the European scatter, and beyond the range of recent Sub-Saharan Africans, as do his Mesolithic contemporaries and the majority of the LUP sample. By way of contrast, the EUP sample tends to cluster more closely with the recent Africans.

Both in scientific articles (Frayer, 1992; Frayer *et al.*, 1993) and the popular press (Shreeve, 1995), it has been pointed out that the retention of high brachial and crural indices among Late Upper Paleolithic and Mesolithic humans is problematic for Trinkaus' (1981) argument that these indices reflect elevated gene flow (or population dispersal) from Africa associated with the origins of modern humans. After all, these workers argue, the glacial cold of Europe should have modified, at least by the end of the Pleistocene, any previously incoming population toward a more cold-adapted morphology. Yet with regard to brachial and crural indices, the LUP sample have an even more extreme (almost 'hyper-tropical') morphology than their EUP forebears.

As pointed out in Holliday (1999), this argument shows the problems that can arise when single traits are studied in isolation[1]. In

[1]We can, for the sake of argument, consider the brachial and crural indices a single trait, since they tend to covary, and are likely influenced by the same gene complexes. Likewise, they are almost certainly influenced by the same environmental factors.

the modern world, high brachial and crural indices tend to be associated with longer limbs. Not only have Trinkaus (1981) and Meadows & Jantz (1995) documented this, but Roberts' (1978) relative forearm index (the anthropometric equivalent of the brachial index) is also positively associated with temperature, and thus tends to be found in absolutely longer-limbed groups. However, while the association between these indices and limb length is a very real one, there remains much variability in these features (Holliday, 1999). For example, among the global sample of recent humans used for this analysis, correlations between the brachial index and total arm length (humeral length + radius length), and between the crural index and total lower limb length (femoral + tibial length) are significant, but are not particularly high (for the former relationship, $r = 0.12$, $p = 0.0036$, $n = 631$; for the latter, $r = 0.15$, $p = 0.0001$, $n = 680$). Thus, while there is a clear tendency among recent humans for brachial and crural indices to increase with overall limb length, there is also considerable variability in limb length, and how that length is distributed between the proximal and distal segments (and see Holliday & Ruff, 2001). As a result, there is much overlap in distal limb segment length proportions among individuals from broad geographic regions (Holliday, 1999).

Nevertheless, when the brachial indices of recent Europeans are compared to Mesolithic and Late Upper Paleolithic samples, two-tailed *t* tests detect significant differences between the recent and fossil Europeans (Mesolithic vs. Recent, $p = 0.004$; LUP vs. Recent, $p = 0.0002$). The crural index yields similarly significant differences (Mesolithic vs. Recent, $p = 0.01$; LUP vs. Recent, $p < 0.0001$). It is difficult to imagine that these differences are due to mere sampling error in the fossil record.

Thus, we are faced with a dichotomy. In multivariate analyses of shape, Mesolithic and LUP samples (unlike their EUP forebears) cluster among recent Europeans, yet their brachial and crural indices are significantly higher. Importantly, however, this does not mean that their limbs are long. In fact, while brachial and crural indices remained elevated from the EUP through the Mesolithic, total limb length *reduced* (Frayer, 1980, 1981, 1984, 1992; Jacobs, 1983, 1985; Holliday, 1995, 1999).

What, therefore, do the high brachial and crural indices of the Late Upper Paleolithic and Mesolithic humans, including Gough's Cave 1, mean? As argued in Holliday (1999), this is a clear example of mosaic evolution. It seems likely that climatic selection due to the glacial cold of Europe modified what had been a more tropically-adapted physique into a more cold-adapted one. Yet selection acted more or less equally on both the proximal and distal limb segments, leaving the later humans with shorter limbs (and thus better adapted to the cold), but permitting them to retain their relatively long distal limb segments[2].

Whether some other type of selection was maintaining these high ratios in spite of overall reduction in limb length, or whether they were selectively neutral is uncertain. The most likely conclusion is that the brachial and crural indices are genetic markers linking the Late Upper Paleolithic and Mesolithic populations to their 'Cro-Magnon' forebears. The logical extension of this argument is that contra Frayer (1992) and Frayer *et al.* (1993), these indices are, as Trinkaus (1981) first posited, indicative of African genes in the early modern Europeans.

In sum, while the total morphological pattern of the Cheddar Man's body proportions is European-like, it is those features for which he differs from the modern European condition that are of the most interest. Specifically, it seems likely that his high brachial, crural indices, and TL/STH indices, reflective of relatively longer distal limb segments, are a retention from an earlier, largely African gene pool – a retention no longer seen in Europe today.

[2]At least over the time period observed – at some point, apparently subsequent to the Mesolithic, European brachial and crural indices decreased to approximate the condition seen today.

REFERENCES

Allen, J.A. 1877. The influence of physical conditions in the genesis of species. *Radical Review*, **1:** 108–140.

Bergmann, C. 1847. Ueber die Verhaltnisse der Warmeokonomie der thiere zu ihrer grosse. *Gottinger Studien*, **3:** 595–708.

Churchill, S.E. 1998. Cold adaptation, heterochrony, and Neandertals. *Evolutionary Anthropology*, **7:** 46–61.

—— **& Holliday, T.W.** 2002. Gough's Cave 1 (Somerset, England): A study of the axial skeleton. *Bulletin of the Natural History Museum London (Geology)*, **58:** 1–11.

Crognier, E. 1981. Climate and anthropometric variations in Europe and the Mediterranean area. *Annals of Human Biology*, **8:** 99–107.

Darroch, J.N. & Mosimann J.E. 1985. Canonical and principal components of shape. *Biometrika*, **72:** 241–252.

Eveleth, P.B. 1966. The effects of climate on growth. *Annals of the New York Academy of Science*, **134:** 750–759.

—— **& Tanner, J.M.** 1976. *Worldwide Variation in Human Growth*. International Biological Programme **8**. Cambridge.

Falsetti, A.B., Jungers, W.L. & Cole, T.M., III. 1993. Morphometrics of the callitrichid forelimb: A case study in size and shape. *International Journal of Primatology*, **14:** 551–572.

Formicola, V. & Giannecchini, M. 1999. Evolutionary trends of stature in Upper Paleolithic and Mesolithic Europe. *Journal of Human Evolution*, **36:** 319–333.

Franciscus, R.G. & Holliday, T.W. 1992. Hindlimb skeletal allometry in Plio-Pleistocene hominids with special reference to AL-288-1('Lucy'). *Bulletins et Mémoires de la Société d'Anthropologie de Paris*, n.s. **4**, série 22: 1–16.

Frayer, D.W. 1980. Sexual dimorphism and cultural evolution in the late Pleistocene and Holocene of Europe. *Journal of Human Evolution*, **9**: 399–415.

—— 1981. Body size, weapon use, and natural selection in the European Upper Paleolithic and Mesolithic. *American Anthropologist*, **83:** 57–73.

—— 1984. Biological and cultural changes in the European Late Pleistocene and Early Holocene. *In*: FH Smith & F Spencer (eds), *The Origins of Modern Humans: A World Survey of the Fossil Evidence*. New York, pp. 211–250.

—— 1992. Evolution at the European edge: Neanderthal and Upper Paleolithic relationships. *Préhistoire Européenne*, **2:** 9–69.

——, **Wolpoff, M.H., Thorne, A.G., Smith, F.H. & Pope, G.G.** 1993. Theories of modern human origins: The paleontological test. *American Anthropologist*, **95:** 14–50.

Geddes, D., Barbaza, M., Vaquer, J. & Guilaine, J. 1986. Tardiglacial and Postglacial in the eastern Pyrenees and western Langudoc (France). *In*: L.G. Straus (ed), *The End of the Paleolithic in the Old World*. BAR International Series **284**. Oxford.

Hiernaux, J., Rudan, P. & Brambati, A. 1975. Climate and the weight/height relationship in sub-Saharan Africa. *Annals of Human Biology*, **2:** 3–12.

Holliday, T.W. 1995. *Body Size and Proportions in the Late Pleistocene Western Old World and the Origins of Modern Humans*. Ph.D. thesis, University of New Mexico.

—— 1997*a*. Body proportions in Late Pleistocene Europe and modern human origins. *Journal of Human Evolution*, **32**: 423–448.

—— 1997*b*. Postcranial evidence of cold adaptation in European Neandertals. *American Journal of Physical Anthropology*, **104**: 245–258.

—— 1999. Brachial and crural indices of European Late Upper Paleolithic and Mesolithic humans. *Journal of Human Evolution*, **36:** 549–566.

—— **& Ruff, C.B.** 2001. Relative variation in human proximal and distal limb segment lengths. *American Journal of Physical Anthropology*, **116:** 26–33.

Jacobs, K.H. 1983. *Hominid Body Size, Body Proportions, and Sexual Dimorphism in the European Upper Paleolithic and Mesolithic*. Ph.D. Dissertation, University of Massachusetts, Amherst.

—— 1985. Evolution in the postcranial skeleton of late Glacial and early Postglacial European hominids. *Zeitschrift für Morphogie und Anthropologie*, **75:** 307–326.

James, F.C. & McCulloch, C.E. 1990. Multivariate statistical methods in ecology and systematics: Panacea or Pandora's box. *Annual Review of Ecology and Systematics*, **211:** 129–166.

Jungers W.L., Falsetti, A.B., & Wall, C.E. 1995. Shape, relative size and size-adjustments in morphometrics. *Yearbook of Physical Anthropology*, **38:**137–161.

Meadows, L. & Jantz, R.L. 1995. Allometric secular change in the long bones from the 1800s to the present. *Journal of Forensic Sciences* **40:** 762–767.

Mosimann, J.E. & James, F.C. 1979. New statistical methods for allometry with application to Florida Red-winged Blackbirds. *Evolution*, **33:** 444–459.

Newman, M.T. 1961. Biological adaptation of man to his environment: heat, cold, altitude, and nutrition. *Annals of the New York Academy of Science*, **91:** 617–633.

Roberts, D.F. 1978. *Climate and Human Variability*. 2nd edition. Menlo Park.

Ruff, C.B. 1991. Climate and body shape in hominid evolution. *Journal of Human Evolution*, **21:** 81–105.

—— 1993. Climatic adaptation and hominid evolution: The thermoregulatory imperative. *Evolutionary Anthropology*, **2:** 53–60.

—— 1994. Morphological adaptation to climate in modern and fossil hominids. *Yearbook of Physical Anthropology*, **37:** 65–107.

——, **Trinkaus, E. & Holliday, T.W.** 1997. Body mass and encephalization in Pleistocene *Homo*. *Nature*, **387:** 173–176.

—— **& Walker, A.** 1993. Body size and body shape. *In*: A. Walker & R. Leakey (eds), *The Nariokotome* Homo erectus *Skeleton*. Cambridge, MA, pp. 234–265.

Schreider, E. 1964. Ecological rules, body-heat regulation, and human evolution. *Evolution*, **18:** 1–9.

—— 1975. Morphological variations and climatic differences. *Journal of Human Evolution*, **4:** 529–539.

Shreeve, J. 1995. *The Neandertal Enigma: Solving the Mystery of Modern Human Origins*. New York.

Straus, L.G., Clark, G.A., Altuna, J. & Ortea, J.A. 1980. Ice-Age subsistence in northern Spain. *Scientific American*, **242:**142–152.

Stringer, C.B. 1989. Documenting the origin of modern humans. *In*: E. Trinkaus (ed) *The Emergence of Modern Humans: Biocultural Adaptations in the Later Pleistocene*. Cambridge, pp. 67–96.

Trinkaus, E. 1981. Neanderthal limb proportions and cold adaptation. *In*: C.B. Stringer (ed), *Aspects of Human Evolution*. London, pp. 187–224.

—— 1986. The Neandertals and modern human origins. *Annual Review of Anthropology*, **15:** 193–218.

—— 1991. Les hommes fossiles de la Grotte de Shanidar, Irak: Evolution et continuité parmi les hommes archaïques tardifs du Proche-Orient. *L'Anthropologie*, **95:** 535–572.

——, **Churchill, S.E. & Ruff, C.B.** 1994. Postcranial robusticity in *Homo*, II: Humeral bilateral asymmetry and bone plasticity. *American Journal of Physical Anthropology*, **93:** 1–34.

Trotter, M. & Gleser, G.G. 1958. A re-evaluation of estimation of stature based on measurements of stature taken during life and of long bones after death. *American Journal of Physical Anthropology*, n.s. **16:** 79–123.

Bull. nat. Hist. Mus. Lond. (Geol.) **58**(supp): 45–50 Issued 26 June 2003

Gough's Cave 1 (Somerset, England): an Assessment of the Sex and Age at Death

ERIK TRINKAUS
Department of Anthropology, Campus Box 1114, Washington University, St. Louis, MO 63130, USA
LOUISE HUMPHREY & CHRIS STRINGER
Department of Palaeontology, Natural History Museum, Cromwell Road, London SW7 5BD, U.K.
STEVEN E. CHURCHILL
Department of Biological Anthropology and Anatomy, Box 3170, Duke University Medical Center, Durham NC 27710, USA
ROBERT G. TAGUE
Department of Geography and Anthropology, Louisiana State University, Baton Rouge, LA 70803, USA

SYNOPSIS. The overall impression of the sexually dimorphic characteristics of Gough's Cave 1 is that the remains are those of a male. However, the specimen does present some 'female' features in the facial skeleton, the ischiopubic rami and pelvic apertures, combined with relatively small overall size, and an ambiguous greater sciatic notch morphology. Nevertheless, the various features employed for sexual diagnosis of Gough's Cave are predominantly those which indicate or strongly suggest that it is male, but this must be accompanied with the caveat that either this individual falls at the feminine end of the male range of variation or that the patterns of skeletal sexual dimorphism of the population from which it derived were modestly different from those of the mostly European and European-derived reference samples used for this assessment. In contrast to the ambiguities of sex determination for Gough's Cave 1, the various indicators of his age-at-death are highly consistent. All of them agree in placing Gough's Cave 1 between his late second decade and middle third decade. He was unlikely to have been younger than about 18 years, and most likely was not older than about 23 years at death.

INTRODUCTION

The remains of Gough's Cave 1 have been considered to be those of a 'young adult male' since Seligman & Parsons' (1914) original partial description of the remains (e.g., Oakley, 1971; Stringer, 1985). The original assessment of the age in the second half of the third decade was based on their observations of cranial sutures, postcranial epiphyses and dental attrition. The sex assessment was based entirely on comparisons of femoral proximal and distal epiphyseal dimensions to those of Medieval British remains. However, since the remains contain many more indicators of both sex and age, these need to be reconsidered.

SEX DETERMINATION

Overall Body Size

Overall body size can provide a good indication of sex, if the individual in question falls above or below the area of overlap between the sexes. For this, the two best indicators are femoral length and femoral head diameter, since the former correlates closely with stature and the latter with body mass.

The femoral lengths of Gough's Cave 1 (439.0 and 433.0 mm – the difference due largely to differences in neck-shaft angle), fall slightly above an overall European Mesolithic male mean (430.8 ± 19.5 mm, N = 35) and on either side of the mean of a European Mesolithic male sample without the large Muge sample (435.9 ± 20.3 mm, N = 21) (for comparative samples, see Trinkaus, 2003). However, the average femoral length of Gough's Cave 1 is only 1.23 standard deviations from an overall Mesolithic female mean (407.8 ± 22.9 mm N = 21) and only 0.90 standard deviations from the mean of a female sample without the Muge remains (416.2 ± 21.9 mm, N = 10).

Similarly, the sagittal femoral head diameters of Gough's Cave 1 (47.7 & 46.3 mm) are close to Mesolithic male means (46.3 ± 2.2 mm, N = 32; 47.0 ± 2.6 mm, N = 17 without Muge). Yet, the z-scores of the mean diameter (47.0 mm) relative to the female samples are 1.59 for the full sample (42.7 ± 2.7 mm, N = 15) and only 1.06 for the female sample without Muge (43.7 ± 3.1, N = 8).

Consequently, these size considerations support a male sex determination for Gough's Cave 1, but they are not conclusive by themselves relative to other skeletally sexed European Mesolithic remains.

The Pelvis

The pelvic remains of Gough's Cave 1 present a mixture of male and female features, plus ones that are ambiguous. Yet, the overall impression is that of a male pelvis with some female proportions.

The greater sciatic notches (Trinkaus, 2003: fig. 2) appear to be intermediate between the classic male semi-circular form and the more open female pattern. In addition, the right ilium, but not the left one, has a clear pre-auricular sulcus.

The ischiopubic rami (Trinkaus, 2003: fig. 3) are relatively thin and flare ventrally along their medial margins, a generally female feature (see Poulhés, 1947; Phenice, 1969). Yet, the small mediolateral breadth of the symphyseal body (obturator foramen margin to symphyseal surface), the thickness of the superior pubic ramus, the absence of a subpubic concavity, and the vertically elongated shape

© The Natural History Museum, 2003

Table 1 Results of pelvic discriminant function analysis for Gough's Cave 1.

Reference Sample	Female N	Male N	% Correctly Classified	Gough's Cave 1 Sex Assignment
Euroamericans				
pelvic variables	40	35	98.7%	male
pelvic and femoral variables	39	34	100%	male
Afroamericans				
pelvic variables	42	40	97.6%	male
pelvic and femoral variables	41	39	100%	female
Pooled Sample				
pelvic variables	113	123	95.8%	male
pelvic and femoral variables	107	116	98.7%	male

of the obturator foramen all indicate a male. This is supported by its subpubic angle (64°), which is very close to a recent Euroamerican male mean (63.7° ± 7.8°, N = 50) and well below that of a Euroamerican female sample (88.4° ± 8.5°, N = 50) (Tague, 1989) (other recent human samples exhibit similar mean angles and distributions for males and females (Tague, 1989)).

At the same time, the shape of the pelvic inlet is exceptionally round (Trinkaus, 2003: fig. 4), since its dorso-ventral and transverse diameters are equal, providing an index of ca.100. In contrast, a sample of Euroamerican male pelves has a mean index of 79.0 (± 7.9, N = 47) and a female sample has a mean of 83.1 (± 10.0, N = 47) (Tague, 1989). Its outlet index of 104.2 falls between the means of those male and female samples (111.1 ± 14.1, N = 44 and 99.8 ± 11.0, N = 46, respectively).

Given the mixed indications of these individual sex characteristics of the Gough's Cave 1 pelvis, we performed a discriminant function analysis of a series of measurements of the pelvis and femur in order to resolve the sex assessment of Gough's Cave 1. The measurements were selected for overall proportional coverage, preservation and body size indication. Those employed are: sacral ventral height and arc, sacral antero-cranial breadth, pelvic antero-posterior inlet, midplane and outlet diameters, bi-iliac breadth, pelvic inlet transverse breadth, minimum bi-acetabular breadth, bi-tuberous (outlet) breadth, sub-pubic angle, and maximum length and head diameter of the femur. The analyses were performed with just the pelvic dimensions and combining the pelvic and femoral dimensions.

These measurements were compared to three samples. The first was of Euroamericans with documented sex, given the geographical origins of Gough's Cave 1. The second is of Afroamericans of documented sex, given the slightly linear body build of Gough's Cave 1 (Holliday & Churchill, 2003). The last includes the first two samples, plus four samples of Amerindians with skeletally determined sex (see Tague (1989) for sample composition). The analyses were done first using only the modern human reference sample, and Gough's Cave 1 was then included to determine its affinities.

As can be seen in Table 1, Gough's Cave 1 is assigned to the male sample in all but one case, when the reference sample consists of Afroamericans and the femoral variables are included in the analysis. This single exception is almost certainly a result of the slightly linear proportions of the Gough's Cave specimen combined with the relatively tall stature of the individuals in that reference sample.

The Skull

The overall impression from the Gough's Cave 1 cranium is that of a male. Although we do not have other crania from the same population for comparison, the prominence and volume of the mastoid processes suggest that the cranium is that of a male. A further indication that the cranium is male is the presence of a pronounced crest on each suprameatal triangle, which extends the zygomatic process almost as far as the parietal notch. The cranium has marked temporal lines with both the upper and lower temporal lines extending to the lambdoid suture.

The appearance of the occipital is also that of a robust individual. It has marked superior and inferior nuchal lines and a well-defined external occipital crest. The area of the external occipital protuberance is partially obscured by sediment, but it is clearly not a prominent feature.

The sexually diagnostic features of the upper facial region and frontal bone are ambiguous. The right side of the glabella and right supraorbital margin are partially obscured by a pathological lesion. Based on what can be seen, the glabella is only moderately prominent and the supraorbital ridges are not particularly well-defined. The supraorbital margin is of moderate thickness and sharpness.

Relative to the overall impression from the cranium the mandible appears to be that of a more gracile individual (for a detailed description of mandibular morphology, see Humphrey & Stringer, 2002). The mental protuberance and mental tubercles are not particularly prominent. The gonial region is everted and the areas of attachment of the masseter and medial pterygoid are well defined.

Buikstra and Ubelaker (1994) emphasised five aspects of cranial morphology that can be useful for sex determination. Each feature is scored on a five-point scale, with higher values representing more robust masculine features. A score of 1 indicating a probable female, a score of 5 indicating a probable male and a score of 3 indicating that the feature is ambiguous. The scores for the Gough's cave cranium for each of the five sexually diagnostic structures are:

Robusticity of nuchal crest: 5; size of the mastoid process: 5; sharpness of the supraorbital margin: 2; prominence of the glabella: 3; and projection of the mental eminence: 2–3.

The skull therefore presents a mixture of robust and gracile characteristics. The most masculine features relate to the attachment of the nuchal and temporal musculature, while the supraorbital region and mandible present features that are not obviously masculine or feminine.

The Gough's Cave 1 cranium was compared metrically to a sample of European Mesolithic and Late Upper Palaeolithic crania (Humphrey and Stringer, 2002). The crania were measured according to the system devised by Howells (1973). A total of 39 cranial measurements were made of Gough's Cave and the comparative sample included only crania on which the same set of measurements could be taken. Principal components analysis of 39 cranial dimensions suggests that Gough's Cave 1 is male (Humphrey & Stringer, 2002). A stepwise discriminant analysis using the same comparative sample classifies Gough's Cave 1 as male (Humphrey & Stringer, 2002).

Summary Sex Assessment

The overall impression of the sexually dimorphic characteristics of Gough's Cave 1 is that the remains are those of a male. This is supported by posterior and posterolateral cranial features, long bone lengths, many discrete pelvic traits and particularly discriminant functional analysis of the pelvis. However, the specimen also presents a series of features that are generally considered to be female characteristics, including several features of the facial skeleton, the ischiopubic rami and the pelvic apertures. This is combined with its overall size being well within Mesolithic female ranges of variation, and its ambiguous greater sciatic notch morphology.

We feel that the various features employed for sexual diagnosis of Gough's Cave are predominantly those which indicate or strongly suggest that it is male, but this must be accompanied with the caveat that either this individual falls at the feminine end of the male range of variation or that the patterns of skeletal sexual dimorphism of the population from which it derived were modestly different from those of the mostly European and European-derived reference samples used for this assessment.

AGE ASSESSMENT

In their presentation of the Gough's Cave 1 remains, Seligman & Parsons (1914) make several references to its age at death, including 'the sutures are open both extra- and intra-cranially, a condition which would make us fairly sure that that the individual was under 30 years of age' (p. 255), 'the teeth in the lower jaw are very perfect and, although their possessor was probably between 24 and 28 years of age, show very little sign of grinding down' (p. 258), and 'a part of the left os innominatum has been preserved and shows that the epiphyseal line for the crest of the ilium is not completely closed' (p. 261). 'As all other available epiphyseal lines have disappeared in this skeleton we should say that death took place between the ages of 24 and 28, and this is quite in harmony with the evidence of the skull' (p. 261). Given the presence of a variety of other age indicators on the remains (of varying precision), a reassessment of these statements is in order.

The Skull

Parts of the basicranial region are missing so it is not possible to examine the area of the basi-occipital synchondrosis. However, most of the cranial vault sutures remain, permitting their assessment endocranially and ectocranially.

The reliability of cranial suture closure for age estimation is debated. Nevertheless, several different systems have been developed for estimating age at death from suture closure on the endocranial and ectocranial surfaces of the skull (e.g. Meindl & Lovejoy 1985, Perizonius 1984, Buikstra & Ubelaker 1994). Key *et al.* (1994) conducted a detailed investigation of cranial suture closure in 183 individuals of known age at death from the Christ Church, Spitalfields sample. Their study recorded the degree of closure at 54 different sites on the cranial vault. Key *et al.* (1994) demonstrated a high level of variability in suture closure with age in the Spitalfields sample. In particular, their study warned that open ectocranial sutures were found to occur with equal frequency at all ages, and should not be used as an indication of young age.

The degree of suture closure in Gough's Cave 1 was evaluated using the methods described by Key *et al.* (1994). Observations could be made at 24/36 ectocranial sites and at 14/18 endocranial sites. All except two of the recording positions could be scored on either the left or right side of the skull. Suture closure was scored as 0 at each of the sites examined. The conclusions of Key *et al.* (1994) suggest that this result does not provide any definitive evidence of age at death, and perhaps all that can be concluded in relation to the evidence from cranial suture closure in Gough's Cave 1 is that it does not conflict with other morphological indicators of a young age at death.

Table 2 Degrees of occlusal attrition in Gough's Cave 1, scored following the system of Molnar (1971).

		Right	Left
Maxilla	M^1	2	3
	M^2	2	2
	M^3	1	1
Mandible	I_1	3	3
	I_2	3	3
	C_1	3	3
	P_3	–	3
	P_4	–	2
	M_1	3	3
	M_2	2	2
	M_3	1	1

The Dentition

All of the teeth present in the upper and lower jaws are fully emerged into the tooth row, suggesting a minimum age at death of about 17 years (Smith 1991, table 1). Radiographs reveal that the roots of the mandibular third molars are complete and appear to be completely closed at the apex. The mean age of attainment of apical closure of the third molar in a recent North American sample is 20 years for males and 20.7 years for females (data from Moorrees et al. 1963, presented by Smith 1991). The minimum age of attainment of this stage is just over 16 years (mean – 2sd, for age of closure of distal root apex (Moorrees *et al.*, 1963).

It is also possible to assess the degree of wear as a general indication of age-at-death. The occlusal attrition scores, following Molnar (1971), are in Table 2. In this, 1 indicates an essentially unworn tooth, and 3 (the highest score for Gough's Cave 1) indicates that the cusp pattern is partially or completely obliterated and there are small dentine patches exposed. As can be seen, all of the anterior teeth and three of the first molars exhibit wear stage 3, the third molars exhibit wear stage 1, and the remaining teeth are in between.

Of particular relevance is the amount of wear on the third molars, which is minimal. Both mandibular third molars have slightly polished enamel, and there is a small wear facet on the mesio-buccal cusp of the right one. The difference in the amount of wear between the left and right teeth is consistent with the amount of wear on the other molars, which is higher on the right side than on the left. There is slight polishing on the upper third molars and a small wear facet on the mesio-lingual cusp of the upper right third molar. The amount of wear suggests that death occurred not long after the third molars came into occlusion. The evidence from the third molars is consistent with the relatively low level of wear on the first and second molars. Application of the Miles method (Miles 1978) for ageing using attrition on the mandibular molars indicates an age at death of between 18 and 24 years, with an age at the lower end of the scale being more likely.

The Axial Skeleton

The Vertebral Column

The indications of age-at-death in the vertebral column, as preserved and as observable given the partial articulation of the remains (originally for museum display), are as follows:

C6 or 7: Posterior tubercle of spinous process unfused.

T1: Posterior tubercle unfused.

T2 or 3: Posterior tubercle unfused.

T11: Posterior tubercle appears to be unfused.

T12: Posterior tubercle unfused, annular ring of the inferior surface is not fully fused.

L1: Posterior tubercle appears to be unfused.

L2: The tubercle of the spinous process is fused but the epiphyseal line is still open along its superior margin. The epiphyseal line between the secondary center of ossification of the inferior annular ring and the centrum is also evident (but is mostly closed and was undergoing obliteration at the time of death).

L3: The tip of the spinous process is fused but the epiphyseal line is still open along its superior edge. The inferior and superior annular rings appear to be fully fused to the centrum, with the epiphyseal lines completely obliterated.

S1–S2: Between the S1 and S2, the ventral bodies are fully separate, with a maximum gap between them of 2.3mm. Laterally and dorsally they remain unfused but the bone surfaces are in contact with each other.

S2–S3: There is clear contact but no evidence of fusion between S2 and S3 bodies.

S3–S4: There is clear contact but no evidence of fusion between S3 and S4 bodies.

S4–S5: The S4 and S5 bodies are fully fused, but the line between them is readily apparent.

S5–Cx1: There is no evidence of any bridging between the S5 and Cx1 bodies.

Summary. The secondary center of ossification for the inferior annular ring of the twelfth thoracic vertebra is unfused, and the inferior annular ring of the second lumbar vertebra is fused but the epiphyseal line remains visible. The superior and inferior annular rings of the third lumbar vertebra are clearly fused, and the epiphyseal lines are obliterated. Post-mortem damage to the bones and the presence of reconstructive materials and adherent matrix make the evaluation of the developmental state of the other vertebrae difficult. The dorsal tubercles of the spinous processes of the sixth cervical, first, second, eleventh and twelfth thoracic and first lumbar vertebrae are clearly unfused, suggesting a relatively young age at death for this individual.

Secondary centers of ossification in the vertebrae appear around puberty, and with the exception of the epiphyseal rings of the centra, are usually fused by the age of 18 years (Steele & Bramblett, 1988). Maturation of the annular rings usually begins prior to age 17 and is complete by the age of 25 (Steele & Bramblett, 1988). However, a considerable amount of individual variation exists in ages of fusion of the annular rings and other secondary centers in the vertebrae (McKern & Stewart, 1957). None of the preserved vertebrae shows any signs of osteophyte development, arthritis to the articular surfaces, or Schmorl's nodes (on the centra that can be examined), consistent with the death of this individual during the third decade.

The pattern and degree of fusion of the sacral vertebral bodies is normal for a young adult, and by reference to Euroamerican males indicates an age-at-death in the mid twenties (McKern & Stewart, 1957).

The Costal Skeleton

4 Right: The surface of the head is rough and irregular, likely representing the subchondral surface of the unfused secondary center of ossification for the head.

5 Right and Left: The secondary centers of ossification for the heads are only partially fused (and portions are missing).

6 Right and Left: The heads are incompletely fused and portions of them are missing.

7 Left: The secondary center of ossification for the head of the left rib is unfused and missing.

8 Right: The head is unfused and missing.

9 Right and Left: The centers of ossification for the heads are unfused and missing.

11 Right and Left: The heads are unfused and missing.

12 Right: The head appears to be unfused.

Summary. Most of the ribs preserving the proximal end have unfused or partially fused heads. The secondary centers of ossification for the articular tubercles are, without exception, fully fused in all the ribs retaining this region. Secondary centers for the head and tubercle generally appear around puberty and fuse between the ages of 18 and 24 (McKern & Stewart, 1957), beginning in the upper and lower end ribs and progressing towards the middle. Apparently the articular tubercles followed a more accelerated schedule of fusion than the rib heads in the Gough's Cave 1 skeleton. The developmental state of Cheddar Man's ribs suggests that he died in his late teens or early in his third decade.

The Upper Limbs

No degenerative changes are evident in any of the preserved upper limb articular surfaces, and all of the age-at-death indications are associated with the fusion and obliteration of the epiphyseal lines.

The Claviculae

Both lack the sternal epiphysis but have well preserved metaphyseal surfaces, making it clear that the sternal secondary centers of ossification were unfused.

The Right Scapula

All of the observable secondary centers of ossification are fully fused, and the epiphyseal lines are obliterated. These include the subcoracoid center, the infraglenoid center, the acromial center, and the vertebral border center (at least at the root of the spine – the only place this center can be evaluated). It is possible that the vertebral border – inferior angle center of ossification was not fully fused along its entire length, and that the preserved portion of the inferior angle represents an epiphyseal surface. Reconstructive materials obscure observation of the inferior angle, making evaluation of the state of fusion of the growth center difficult.

The Humeri

There is a very slight trace of an epiphyseal line on the anterior and medial surfaces of the proximal metaphysis just below the lesser tubercle and the articular surface of the head. The line is more apparent on the right humerus than on the left. On both humeri the line is largely obliterated on the dorsal and lateral surfaces. Even though the line is visible, the head is fully fused and the lines are near obliteration. Radiographically, a faint sclerotic line can be made out between the metaphysis and proximal epiphysis on the right humerus (despite considerable trabecular radio-opacity in the area). No such line can be distinguished amongst the trabeculae on the left

side. Distally, the epiphyses and the medial epicondyle secondary centers of ossification are fully fused and the lines obliterated (both on gross and radiographic examination) on both humeri.

The Ulnae

The proximal and distal epiphyses are fully fused. The lines between the olecranon secondary centers and the proximal shafts are obliterated (radiographically as well as on gross external examination). The left ulna has a closed but still (barely) visible epiphyseal line between the head and shaft. Sclerotic epiphyseal lines can be seen between the metaphyses and distal epiphyses of both ulnae, albeit more distinctly in the left ulna. The distal epiphyseal lines are more distinct in the antero-posterior than in the medio-lateral radiographs.

The Radii

The proximal (right and left) and distal (left) epiphyses are fully fused, and the epiphyseal lines are obliterated on gross examination. Radiographically, radiotranslucent lines can be faintly discerned on the right proximal and left distal radius in antero-posterior view.

The Hand Remains

The metacarpals and phalanges all exhibit complete fusion of the epiphyses externally.

Summary

With the exception of the proximal clavicles, all of the upper limb epiphyseal lines are either entirely fused and completely obliterated, or are essentially fused but still show a slight trace (mainly radiographically) of the fusion line. These age indicators are all in agreement, given normal variation, in assigning an age-at-death between approximately 18 and 25 years, with the absence of fusion in the proximal clavicle suggesting a maximum age estimate closer to 22 or 23 years (McKern & Stewart, 1957).

The Lower Limbs

The Pelvis

The symphyseal and auricular surfaces of the Gough's Cave 1 pelvis are completely obscured by its articulated state, so that the age-related metamorphosis of these surfaces cannot be employed for age assessment. However, the ilium and the ischium show clear age indicators. On the left ischium, the tuberosity epiphysis is unfused along the external margin from the middle of the tuberosity to the medial (pubic) end of the tuberosity; internally and proximally it is fully fused. On the right tuberosity, there is only a hint of a persistent fusion line externally, but it is partially obscured by matrix. Along the iliac crests, there is also partial fusion of the epiphyseal lines. On the right side, the crest is incompletely fused from the iliac pillar to the iliac tuberosity, being completely unfused near the pillar and tuberosity and partially fused between them. On the left side, the crest is unfused (and absent) from the iliac pillar to the ventral margin of the iliac tuberosity, and then partially fused along the tuberosity. Ventrally, there is a fusion line still apparent externally (but not internally) from the anterior superior iliac spine to the region of the pillar.

The Femora

There is no trace of the epiphyseal fusion lines on the femora externally, for the head, trochanters or condyles. Radiographically, the fusion lines are completely obliterated through the trabeculae for the heads, the greater trochanters and the right distal epiphysis. However, there is a hint of a line from the middle of the condyles to the epicondyles in the antero-posterior radiograph of the left distal femur.

The Tibiae and Fibulae

The right tibia and fibula also show no trace externally of fusion lines distinct from normal capsular attachment areas around their epiphyses. Distally, both have no trace of a fusion line radiographically, but proximally both of the these bones show a slight indication of the former fusion line. In the tibia, there is a hint of a condylar fusion line in antero-posterior view, and the trabeculae of the proximal fibula exhibit radiographically a head fusion line that is largely obliterated.

The Pedal Remains

The two lateral metatarsals have no retention of their head epiphyseal fusion lines, but the proximal metatarsal 1 still retains a slight indication of the base fusion line. It is apparent only in the medio-lateral radiographic view along the dorso-plantar middle third of the base.

Summary

The leg bone and pedal epiphyseal fusion, all of which is normally complete by late in the second decade, primarily indicates that this individual was no younger than the late second decade but is unlikely to be much older given the persistence of fusion lines radiographically around the knee and in the proximal metatarsal 1. The degree of fusion of the iliac crest, stages 1/2 of McKern & Stewart (1957), places Gough's Cave 1 most likely between the ages of 17 and 19 with the possibility of being as old as 22. The partial fusion of the ischial tuberosity suggests a similar age, most likely between 17 and 21 but unlikely to be older than about 22 years.

Summary Age Assessment

In contrast to the ambiguities of sexual determination of Gough's Cave 1, the various indicators of his age-at-death are highly consistent. All of them agree in placing Gough's Cave 1 between his late second decade and middle third decade. In this, the dentition suggests an age between about 18 and 24 years, the vertebrae suggest an age in the middle of the third decade, whereas the rib and appendicular epiphyses (including the pelvis) suggest an age between the late second and the early third decade. It therefore appears that Gough's Cave 1 was unlikely to have been younger than about 18 years at death, and most likely was not older than about 23 years at death.

REFERENCES

Buikstra, J.E. & Ubelaker, D.H. 1994. Standards for data collection from human skeletal remains. *Arkansas Archaeological Survey Report,* **44**.

Holliday, T.W. & Churchill, S.E. 2003. Gough's Cave 1 (Somerset, England): an assessment of body size and shape. *Bulletin of the Natural History Museum, Geology,* **58**(supplement): 37–44.

Howells, W.W. 1973. Cranial Variation in Man. *Papers of the Peabody Museum of Archaeology and Ethnology,* **67**: 1–259.

Humphrey, L. T. & Stringer, C. 2002. The human cranial remains from Gough's Cave (Somerset, England). *Bulletin of the Natural History Museum, Geology,* **58:** 153–168.

Key, C.A., Aiello, L.C. & Molleson, T. 1994. Cranial suture closure and its implications for age estimation. *International Journal of Osteoarchaeology,* **4**: 193–207.

McKern, T.W. & Stewart, T.D. 1957. Skeletal Age Changes in Young American Males. *Quartermaster Research and Development Center Technical Report EP-45.* Natick: Quartermaster Research & Development Command.

Meindl, R.S. & Lovejoy, C.O. 1985. Ectocranial suture closure: a revised method for the determination of skeletal age based on the lateral-anterior sutures. *American Journal of Physical Anthropology*, **68**: 47–56.

Miles, A.E.W. 1978. Teeth as an indicator of age in man. In: Butler, P.M. & Joysey, K.A. (editors), *Development, Function and Evolution of Teeth*: 455–462. London.

Molnar, S. 1971. Human tooth wear, tooth function and cultural variability. *American Journal of Physical Anthropology*, **34**: 175–190.

Moorrees, C.F.A., Fanning, E.A. & Hunt, E.E. 1963. Age variation of formation for ten permanent teeth. *Journal of Dental Research*, **42**: 1490–1502.

Oakley, K.P. 1971. British Isles. *In*, Oakley, K.P., Campbell, B.G. & Molleson, T.I. (editors), *Catalogue of Fossil Hominids II: Europe*, pp.15–43. London.

Perizonius, W.R.K. 1984. Closing and non-closing sutures in 256 crania of known age and sex from Amsterdam (AD 1883–1909). *Journal of Human Evolution*, **13**: 201–216.

Phenice, T.W. 1969. A newly developed visual method of sexing the os pubis. *American Journal of Physical Anthropology*, **30**: 297–301.

Poulhés, M.J. 1947. La branche ischio-pubienne: ses caractères sexuelles. *Bulletin et Mémoires de la Société d'Anthropologie de Paris*, (9) **6**: 191–201.

Seligman, C.G. & Parsons, F.G. 1914. The Cheddar Man: A skeleton of Late Palæolithic date. *Journal of the Royal Anthropological Institute*, **44**: 241–263.

Smith, B.H. 1991. Standards of human tooth formation and dental age assessment. *In*, Kelley, M.A. & Larsen, C.S. (editors), *Advances in Dental Anthropology*, pp. 143–68. New York.

Steele, D.G. & Bramblett, C.A. 1988. *The Anatomy and Biology of the Human Skeleton*. College Station, Texas.

Stringer, C.B. 1985. The hominid remains from Gough's Cave. *Proceedings of the University of Bristol Spelaeological Society*, **17**: 145–152.

Tague, R.G. 1989. Variation in pelvic size between males and females. *American Journal of Physical Anthropology*, **80**: 59–71.

Trinkaus, E. 2003. Gough's Cave 1 (Somerset, England): a study of the pelvis and lower limbs. *Bulletin of the Natural History Museum, Geology*, **58**(supplement): 1–21.

Bull. nat. Hist. Mus. Lond. (Geol.) **58**(supp): 51–58 Issued 26 June 2003

Gough's Cave, Cheddar, Somerset: Microstratigraphy of the Late Pleistocene/ earliest Holocene sediments

RICHARD I. MACPHAIL
Institute of Archaeology, University College London, 31-34, Gordon Sq., London, WC1H 0PY, UK
PAUL GOLDBERG
Department of Archaeology, Boston University, 675, Commonwealth Ave., Boston, Mass. 02215, USA

SYNOPSIS. Eleven thin sections of Late-glacial and early Holocene sediments from Gough's Cave were investigated by soil micromorphology in order to complement analyses of contemporary faunal and human remains. Despite the paucity of continuous vertical and lateral stratigraphic sequences, which were the result of cave exploitation during the first half of the twentieth century, we were able to elucidate site formation processes relating to both Late-Glacial environmental conditions and the burial environment affecting human remains.

INTRODUCTION

During 1987–1989 the Late Pleistocene (c. 12 ka bp) to earliest Holocene cave sediments at Gough's Cave, Cheddar, Somerset, were studied in conjunction with archaeological, human bone and faunal studies by R. Jacobi, A. Currant, and C. Stringer (Natural History Museum)(Jacobi, 1985, 1991; Currant *et al.*, 1989; Stringer, 1990, 2000; Currant, 1991). Sedimentological investigations, like the excavations, suffered from having only relict and fragmentary deposits to study, on account of the general removal of most of the cave fill during the opening up of the cavern during the first part of the twentieth century (Donovan, 1955). We therefore focused our attention upon extant sediment sequences dispersed within the upper part of the cave with Late Pleistocene deposits: i) Areas I and III of the North Wall of the cave, ii) the 'Skeleton Rift', iii) a cemented, early Holocene stalagmite on the 'South Wall', and iv) an earliest Holocene sequence in the 'Sand Hole'.

METHODS

Field

Undisturbed samples were collected during the excavations from North Wall Areas I (samples 44 and 59, G and H) and III (sample E), the 'Skeleton Rift' (sample D), cemented (Holocene) stalagmite on the 'South Wall' (sample F), and an earliest Holocene sequence in the 'Sand Hole' (samples A, B and C)(Table 1; Fig. 1). Samples were impregnated with an epoxy resin and manufactured into ~8 × 6 cm size thin sections at the Natural History Museum, London.

Eleven thin sections were made from Gough's Cave and were described according to Bullock *et al.* (1985) and Courty *et al.* (1989). They were viewed at a number of magnifications ranging from x1, up to x400 under a polarising microscope, employing plane polarised light (PPL), crossed polarised light (XPL), oblique incident light (OIL), and ultra-violet (blue) light (UVL) (cf. Stoops, 1996). The combined use of these different types of illumination permit a large number of identifications, such as apatite (bone, guano and coprolites) which autofluoresce under UVL. The authors also made use of comparative material of Pleistocene cave sediments (e.g., Courty *et al.*, 1989), including nearby Middle Pleistocene Westbury-sub-Mendip (Somerset) and Late Pleistocene King Arthur's Cave in the Wye Valley (ApSimon *et al.*, 1992; Macphail and Goldberg, 1999). In addition, the number of soil micromorphological investigations of palaeosols dating to the Dimlington Stadial, Windermere Interstadial and Loch Lomond Stadial has increased greatly since this original work was done at Gough's Cave. These include a number of chalky colluvial Allerød palaeosols (Rendzinas) from Kent (Macphail and Scaife 1987, Fig. 2.4; Preece *et al.*, 1995), a ranker from West Sussex (Macphail 1995) and a palaeosol formed in scree outside King Arthur's Cave (Macphail *et al.* 1999).

RESULTS AND INTERPRETATIONS

Soil micromorphological descriptions and findings are summarised in Table 1 and illustrated in Figs 1–7. In order to simplify presentation of the findings we have grouped the results and associated interpretations.

Pleistocene Deposits

Pleistocene deposits overlying the widespread, unfossiliferous, basal conglomerate are composed of gravels overlain by silt-rich sediments (Fig. 1) that represent an identifiable depositional/post-depositional sequence. We can broadly refine these characterisations as follows: 1) bedded silts, sands and gravels; 2) the formation of banded fabrics with associated link cappings; and 3) reworked and disrupted silts and sands; 4) minor biological reworking by roots and fauna, and 5) inwashing of silts and dusty clay.

Bedded silts (Fig. 2), sands and gravels (Fig. 4) are broadly related to an upward fining sequence associated with phreatic flow within the main chamber of the cave (cf. Gillieson, 1996, Fig. 5.3). These depositional episodes are tied to fluctuating/diminishing water flow events within the overall karstic system that give rise to a sequence of cobbles (e.g., the basal conglomerate; not sampled here), gravels (sample 59, Table 1), sand (samples G, H, D, E, I and 59), and mud (samples B and C). Very thick phreatic sands and gravels also typify the Middle Pleistocene basal fill at Westbury-sub-Mendip Cave (Macphail and Goldberg, 1999) and comparable karstic settings (e.g., Goldberg and Sherwood, 1994).

© The Natural History Museum, 2003

Fig. 1 Field photo of Gough's Cave, Area 3, lower red silts, sample I. Note faint traces of bedding next to the sampling box (8 × 6.5 cm); cf. Fig. 2.

At Gough's Cave, the basic sedimentary sequence has been modified by a number of post-depositional processes to produce different micro-sedimentary fabrics. For example, the banded fabrics/link capping features (Table 1) are the typical result of ice lensing produced by alternate freezing and thawing (Romans and Robertson, 1974; van Vliet-Lanöe, 1985, 1986). Extreme modification by freezing and thawing results in the fragmentation and chaotic mixing of the beds and link capping features, and infilling with impure clay and silt (Macphail, 1999) (Fig. 4).

Fig. 2 Macrophotograph of whole thin section of sample I (cf. Fig. 1). Shown here are interbedded beds of elutriated silts (Si) and clay (C). Width of photo is 6.5 cm.

Biological activity is also recorded at Gough's Cave, forming channels and vughs through likely rooting and faunal burrowing. Finally, in this sequence many of these voids have been coated with dusty clay that implies renewed fluid transport vertically through the sediments (see below).

Sand Hole (Pleistocene to earliest Holocene)

Here the sequence commences with the deposition of cave muds (sample C) that accumulated in the base of the Sand Hole. These muds are composed of clay with clasts of redeposited clay (Fig. 5) and accumulated under conditions of low energy ponding. These deposits have reticulate b-fabrics induced by minor shrinking and swelling that reflect alternating periods of wetting and drying. It is possible that these muds are the finest deposits within the cave system, recording the end member of the upward fining sequence present in the main chamber. It is likely that this red clay owes its ultimate origin to the weathering of the Carboniferous Limestone, and is a form of transported ßeta B clay (Duchaufour, 1977).

In the Sand Hole, the sequence continues with the 'Laminated Stalagmite' and the 'Frog Earth' (Figs 6, 7). The laminated stalagmite is composed of cryoclastically produced fallen limestone clasts and clay beds, which are both partially cemented by micrite originating from drip. These deposits are succeeded by muds containing large numbers of frog bones that appear to be typical of early Holocene faunas (Currant, NHM, pers. comm.).

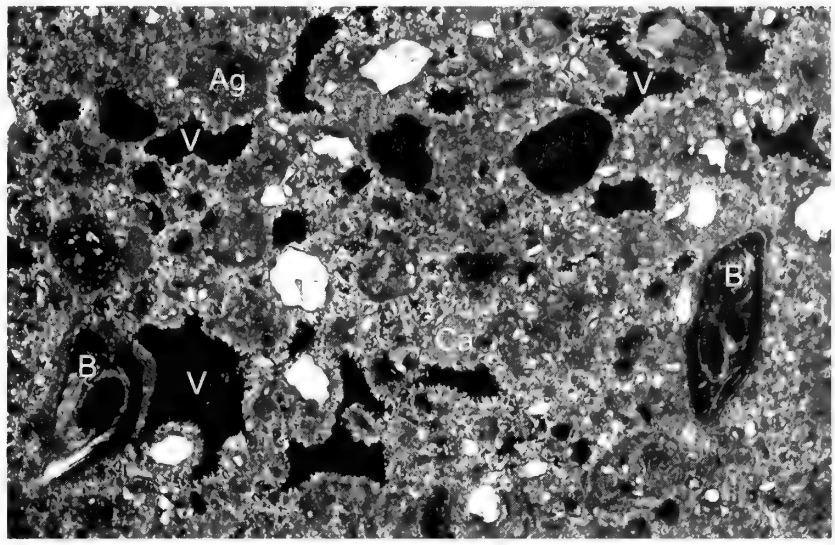

Fig. 3 Gough's Sample D (Table 1), consisting of rounded bone (B) and clayey sediment aggregates (Ag) in a calcareous silty clay. Note secondary porosity (V) composed of channels and vughs that feature secondary calcite carbonate growth. XPL; width of photo is ca. 5.4 mm.

DISCUSSION

It has not been an easy task to reconstruct the sedimentary history of Gough's Cave, because the micro-sedimentary evidence by necessity, has been gathered from the small (max. 40 mm thick) pockets of sediment that remain on the extreme edges of the main cave, and the mainly early Holocene sequence in the Sand Hole.

The sequence at Gough's is quite localized and built up from non-continuous exposures within the cave, and so must be considered as yielding only a partial history of the cave. The sedimentary sequence commences with the deposition of the conglomerate, followed by sands and gravels that fine upwards to the red silts, with muds being restricted only to the Sand Hole (Table 1). This Late Glacial accumulation lasted from about 12,000 to 10,500 ^{14}C years bp, and seems to be roughly correlated with the Windermere Interstadial (ca. 13,000 to 11,000 ^{14}C years bp) through to the Loch Lomond Stadial (11,000 to 10,000 ^{14}C years bp). Human skeletal remains occurred within the red silts and were variably coated with silty clay through to sand and fine gravel (Currant and Stringer, NHM, pers. comm.). The bones (Stringer, 2000) that date to ca. 13,000 to 11,500 radiocarbon years ago would thus appear to be *in situ* and contemporary with the lower energy deposition of the upward fining sequence.

This phreatic period appears to be contemporary with both Upper Palaeolithic activity and the Windermere Interstadial (Table 2). The formation of the conglomerate can perhaps be best related to

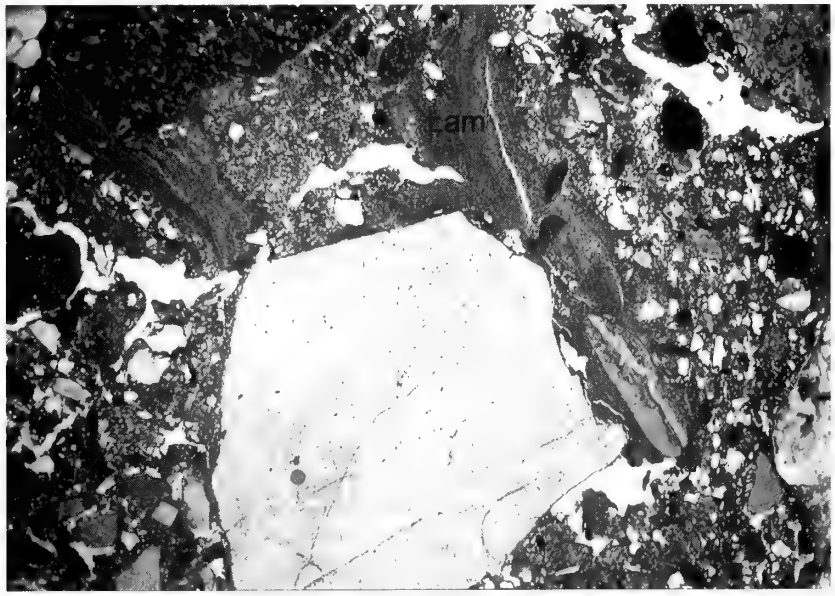

Fig. 4 Sample B from Gough's Cave (Table 1). Macroview of laminated silts and clays over conglomerate, the basal deposit. Width of photo ca. 1.1 cm.

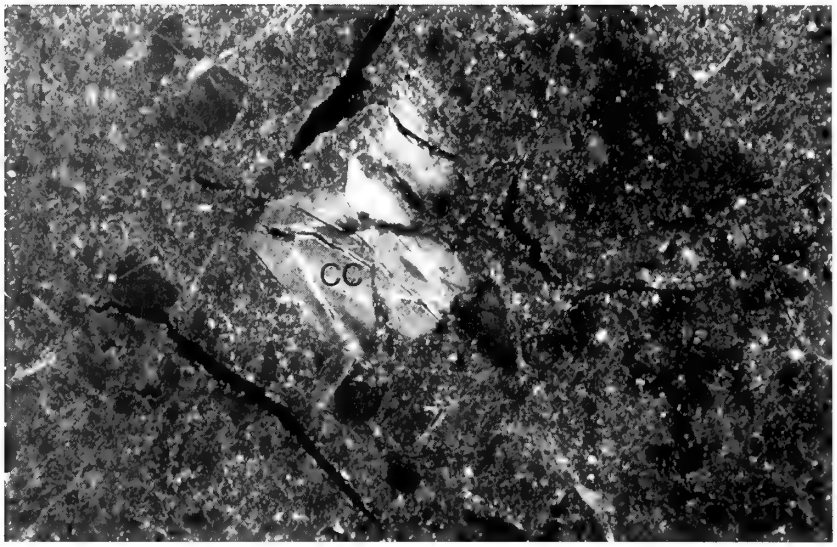

Fig. 5 Sample C from the sand hole, a basal clay deposit including a locally reworked clay (CC). Note the reticulate birefringent fabric which is indicative of minor shrinking and swelling reflecting alternate periods of wetting and drying. Width of photo ca. 5.4 mm.

cryoclastic activity and high energy phreatic flow occurring near the last glacial maximum. It is likely that diminishing phreatic flow and the upward fining sedimentary sequences situated at the sampled margins of the cave, occurred from the end of the Devensian (Oldest Dryas) to the Windermere Interstadial (Bølling/Allerød). This interval was contemporary with Upper Palaeolithic activity that led to the deposition of human skeletal remains in sediments that were once well-bedded (Fig. 2). It seems likely that the ice lensing activity noted in sample H, could be related to occasional cold conditions continuing into the Interstadial. The presence of humans is totally unrecorded at this period in the samples from Areas I and III and the Skeleton Rift, but a breccia remnant ('reindeer stalagmite') from the just below the cave roof does include some charcoal, as seen in thin section.

The mild conditions of the Windermere Interstadial are best recorded, albeit weakly, by biological activity producing an enhanced porosity pattern of channels and vughs (e.g., in samples 44 and D; Fig. 3). Other contemporary sites in southern England have produced longer sedimentary sequences. For example, a number of chalky colluvial deposits have been described from Kent and the Isle of Wight (e.g. Preece *et al.*, 1995). These are soil-sediments, with biological activity and pedogenesis being recorded through slightly enhanced amounts of organic matter, and in places, by concentrations of earthworm granules that indicate ephemeral land surfaces (Preece *et al.*, 1995). At King Arthur's Cave, Herefordshire, a very thin and weakly humic soil horizon was identified through soil micromorphology and chemistry (Macphail *et al.*, 1999). This soil

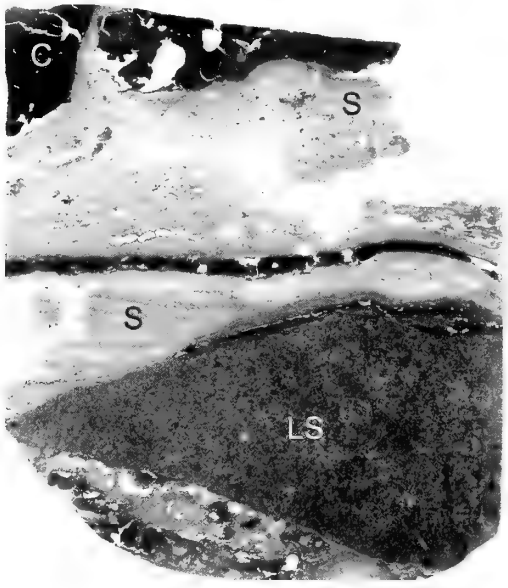

Fig. 6 Sample A3 composed of laminated stalagmite (S) overlying fallen limestone clast (LS) with stringers of red clay (C). Width of photo is ca. 4 cm.

Fig. 7 Sample A (Frog Earth) in sand hole showing clay beds (C) with included bone (B) capped by an iron-stained stalagmite deposit (S). Width of photo is ca. 4 cm.

had formed in Late Devensian scree produced from limestone, and was itself sealed by further scree dating to the ensuing Loch Lomond Stadial. Thus the dominance of sedimentation over 'pedogenic' and post-depositional effects, as at Gough's Cave is typical of Windermere Interstadial sites. One exception is the interstadial soil at Westhampnett, West Sussex, where a very thin *in situ* humic ranker had formed under a likely coniferous woodland cover (Macphail, 1995).

At Gough's Cave the renewed cold conditions of the Windermere Stadial are apparently recorded in the major disruption of sedimentary bedding and previously formed banded fabrics/linked cappings. This cold climate produced chaotic mixing of the deposits and resulted in the infilling of void space with impure clay and silts and clays (Figs 3, 4). Some channels and vughs formed previously by biological activity are coated and infilled, clearly revealing that the period of inwashing post-dated this activity (Table 2). Some of the clayey sediment adhering to the skeletal remains could thus be of the same origin, the orientation of the bones also possibly reflecting this period of disruption. For example, in the well-preserved Upper Palaeolithic occupation cave deposits at Arene Candide, Liguria, Italy, once- horizontal hearths were disrupted by this (Younger Dryas) freezing and thawing (Macphail *et al.*, 1994).

At the Sand Hole, the lowermost clay deposits (Fig. 5) appear to have been little affected by the Loch Lomond Stadial, but rather seem to reflect sedimentation strongly associated with faunal activity during the Late Pleistocene-Early Holocene transition. Typical of earliest Holocene deposits, speleothem formation dominated sedimentation in the Sand Hole, with the moist conditions possibly also favouring the contemporary amphibian fauna (Currant, NHM, pers. comm.).

CONCLUSIONS

This study of the sediment micromorphology enabled us to identify the sedimentary sequence that was contemporaneous with the human occupation/Windermere Interstadial, in spite of the paucity of a continuous sequence of cave sediments. Specifically, we were able to demonstrate an upward fining sedimentary sequence, pene-contemporary with both cool and mild climatic effects. The last led to ephemeral biological activity, and is consistent with a number of other contemporary, sediment-dominated sites in southern England. The investigation also showed that not only sediments but also the skeletal remains themselves were likely influenced by localised post-depositional processes (minor reworking, fine sediment inwash), dating to the cooler conditions of the Loch Lomond Stadial (?). In the Sand Hole, the transition between the Windermere Interstadial/Loch Lomond Stadial and the earliest Holocene, is recorded in the sediments. This detailed microstratigraphic approach exemplified here appears to offer the ability to extract the maximum sedimentary information from disparate and discontinuous deposits within a sedimentary system.

ACKNOWLEDGEMENTS. We gratefully acknowledge a grant from Natural History Museum Interdisciplinary Research Fund and the help of Chris Jones for making the thin sections; some thin sections were made at the Institut National Agronomique, Paris-Grignon (M. A. Courty and N. Fedoroff). The help and encouragement of Chris Stringer, Andy Currant and Roger Jacobi is very much appreciated as well as those of others of the excavation team who facilitated this study. We also thank the anonymous referee for their comments.

REFERENCES

ApSimon, A. M., Donovan, D. T., Scott, K. & Smart, P. L. 1992. King Arthur's Cave, Whitchurch, Herefordshire: a reassessment. *Proceedings of the University of Bristol Spelaeological Society*, **19**: 183–249.

Bullock, P., Fedoroff, N., Jongerius, A., Stoops, G. & Tursina, T. 1985. *Handbook for Soil Thin Section Description*. Waine Research Publications, Wolverhampton.

Courty, M. A., Goldberg, P. & Macphail, R.I. 1989. *Soils and Micromorphology in Archaeology*. Cambridge Manuals in Archaeology. Cambridge University Press, Cambridge.

Currant, A. 1991. A Late Glacial Interstadial mammal fauna from Gough's Cave, Somerset, England. *In,* Barton, R.N., Roberts A. & Roe D. (editors), *The late Glacial in north-west Europe: human adaptation and environmental change at the end of the Pleistocene.* CBA Research Report **77:** 48–50.

——, Jacobi, R. & Stringer, C. 1989. Excavations at Gough's Cave, Somerset 1986–7. *Antiquity,* **63**: 131–136.

Donovan, D. 1955. The Pleistocene deposits at Gough's Cave, Cheddar, including an account of recent excavations. *Proceedings of the University of Bristol Spelaeological Society,* **7**: 76–104.

Duchaufour, P. 1977. *Pedology*. George Allen & Unwin, London.

Gillieson, D. 1996. *Caves: Processes, Development, Management*. Blackwell, Oxford.

Goldberg, P. & Sherwood, S. 1994. Micromorphology of Dust Cave Sediments: some preliminary results. *Journal of Alabama Archaeology*, **40**, 56–64.

Jacobi, R. 1985. The history and literature of Pleistocene discoveries at Gough's Cave, Cheddar, Somerset. *Proceedings of the University of Bristol Spelaeological Society,* **17**: 102–115.

——1991. The Creswellian, Creswell and Cheddar. In R.N. Barton, A. Roberts & D. Roe (eds) *The late Glacial in north-west Europe: human adaptation and environmental change at the end of the Pleistocene.* CBA Research Report, **77:** 128–140.

Macphail, R.I. 1995. Report on the soils at Westhampnett bypass, West Sussex: with special reference to the micromorphology of the late-glacial soil and Marl at Area 3. Unpublished report to Wessex Archaeology, Southampton.

—— 1999. Sediment micromorphology. *In,* Roberts M. B. & Parfitt S. A. (editors), Boxgrove, A Middle Pleistocene Hominid Site at Eartham Quarry, Boxgrove, West Sussex. *English Heritage Archaeological Reports, London.,* **17:** 118–148.

——, Crowther, J. & Cruise, G. M., 1999. King Arthur's Cave: soils of the Allerød palaeosol. Unpublished report to N. Barton, Oxford Brookes University.

—— & Goldberg, P. 1999 *The Soil Micromorphological Investigation: Westbury-sub-Mendip, Somerset.* Pp. 59–86, *In,* Andrews, P., Stringer, C. B. & Currant, A. (editors), *Westbury Cave: the Natural History Museum Excavations 1976–1984.* Western Academic & Specialist Press Ltd., Bristol.

——, Hather, J., Hillson, S. & Maggi, R. 1994. The Upper Pleistocene deposits at Arene Candide: Soil micromophology of some samples from the Cardini 1940–42 Excavation. *Quaternaria Nova, Rome*, **IV**: 79–100.

—— & Scaife, R.G. 1987. *The geographical and environmental background. In,* Bird, J. & Bird, D.G. (editors), *The Archaeology of Surrey to 1540,* pp. 31–51. Surrey Archaeological Society, Guildford.

Preece, R.C., Kemp, R.A. & Hutchinson, J.N. 1995. A Late-glacial colluvial sequence at Watcombe Bottom, Ventnor, Isle of Wight, England. *Journal of Quaternary Science,* **10(2)**: 107–121.

Romans, J. C. C. & Robertson, L. 1974. Some aspects of the genesis of alpine and upland soils in the British Isles. *In,* Rutherford, G. K. (editor), *Soil Microscopy,* pp. 498–510. Limestone Press, Kingston, Ontario.

Stoops, G. 1996. Complementary techniques for the study of thin sections of archaeological materials. *In,* Castelletti, L. & Cremaschi, M. (editors), *XIII International Congress of Prehistoric and Protohistoric Sciences Forli-Italia-8/14 September 1996.* A.B.A.C.O., Forlì, pp. 175–182.

Stringer, C. 1990. *Hominid remains – an up-date: British Isles.* 40 pp. Universite Libre, Bruxelles

—— 2000. The Gough's Cave human fossils: an introduction. *Bulletin of the British Museum (Natural History), Geology,* **56:** 135–139.

Van Vliet-Lanöe, B. 1985. Frost effects in soils. Pp. 117–158, *In,* Boardman, J. (editor), *Soils and Quaternary Landscape Evolution.* John Wiley & Sons, Chichester.

—— 1986. Micromorphology. Pp. 91–96, *In,* Callow, P. & Cornford, J. M. (editors), *La Cotte de St. Brelade, 1961–1978.* Geo Books, Norwich.

Table 1 Selected soil micromorphological observations.

Area/Context/ Unit	Sample	Relative Depth (m)	Field	Micromorphology
'Sand Hole'				
'Frog earth'	A upper	-	0-0.19 m: Yellowish red (5YR4/6) sandy loam.	*Structure*: Massive, intermixed coarse silts and fine sand with thin beds and very coarse infills of silty clay; coarse vughy porosity. Very abundant sand-size bone, coprolite and possible fish bones; occasional long (3 cm) amphibian? bones; vertebra? also present; inclusions of stalagmite. Microfabric: C:F, 80:20, speckled brown (PPL), medium to high interference colours (close porphyric, crystallitic b-fabric; XPL), orange brown (OIL); rare charcoal.
'Laminated stalagmite'	A lower	0.11-0.27	0.19-0.41 m: pink (5YR7/4) laminated stalagmite.	*Structure*: Very finely (200 µm) bedded stalagmite with coarse limestone inclusions and silty clay bands. Likely lichen/algal stalagmite growth. Lower part contains few very leached bone fragments, otherwise sterile. Microfabric: whitish to cloudy grey (PPL), high to very high interference colours (crystallitic b-fabric); white to greyish brown (OIL); very abundant pseudomorphs of plant material in places. Porous basal stony layer features abundant micritic (with clay staining) coatings.
'Brown Clay'	B	0.42-0.47	0.41-0.49 m: reddish brown (5YR5/4) clay, with whitish patches (bone ghosts?); clay mixed with stalagmite and blackened, possible reindeer bones.	Lower part of this massive and heterogeneous clay is sterile except for rare plant fragments, while the upper part is rich in very fine to coarse sand-size, very pale bone, with 'vole' teeth. Under UVL, the bone has a whitish grey autofluorescence; pores within the bone are also infilled with dirty clay. The sediment is also characterised by a patchy autofluorescence under UVL, and a partially closed vughy porosity. Microfabric: C:F, 80:20; dominant (clast supported) angular small stone size limestone and calcite, common angular to subrounded fine to medium sand and silt-size quartz; speckled brown and greyish brown (PPL), moderate to high interference colours (close porphyric, crystallitic b-fabric; XPL), bright orange brown (OIL); frequent (15%) coarse packing voids, with many clayey/calcitic coatings in the lower part and many dark red clay coatings in upper part.
'Red Clay'	C; 2 thin sections	0.50-0.66	0.49-0.90+ m: yellowish red (5YR4/6) 'sterile'? clay over limestone blocks.	*Structure*: Dense massive, with rare interconnecting channels, fine bone and occasional plant fragments and possible *in situ* roots. At the base, cracks are present alongside rare plant fragments and many sand-size red clay papules (Fig. 2); C:F, 20:80; silt-size quartz, and rare very fine sand; speckled dark yellow/reddish brown (PPL), low interference colours (open porphyric, reticulate b-fabric; XPL), orange brown (OIL).
South Wall				
'Reindeer stalagmite'	F; 2 thin sections	-	Post stalagmite brown silt and charcoal, over stalagmite containing a reindeer tooth and charcoal.	*Structure*: Massive with disrupted beds and many closed vughs. Poorly sorted with stone size, angular limestone and sand-size quartz; charcoal, many bones and occasional teeth; C:F, 60:40; common to dominant stone inclusions (some limestone showing etching), with frequent to common medium sand of quartz and flint, with very few fine sand size to gravel size bone – some brown stained some leached and rounded (ex-regurgitation pellets?), possible teeth fragments; occasional sand size rounded charcoal; patchy grey and brown (PPL), medium and high interference colours (gefuric and open porphyric, crystallitic b-fabric, XPL), grey and pale brown (OIL); many 1-8 mm thick silty clay pans (width of slide); abundant brown clayey micritic hypocoatings on voids and embedding large clasts.
North Wall				
Area 1 (1987)				
Red Silt	44	0-0.15	Red Silt.	*Structure*: Massive to weakly coarse platy; *Porosity*: lower 20 mm ~5% voids, with fine channels and vughs; uppermost 25 mm 15-20% voids of coarse, smooth-walled vughs and channels. *Mineral*: C:F, 85:15 in lower 20 mm with horizontal fine (200 µm) bands of 100:00 (elutriated) very dominant silt to fine sand size angular quartz (and mica); with frequent fine, medium and coarse sand size quartz, limestone (also calcite); poorly rounded fragments of clay pans, clay/soil granules, sediment papules. Top 25 mm: dominant very coarse sand size quartz, quartzite, ferruginous nodules, etched calcite

continued ...

Table 1 *continued*

				clay/soil granules, sediment papules. Top 25 mm: dominant very coarse sand size quartz, quartzite, ferruginous nodules, etched calcite and weathered limestone. Inclusions of silt size pale yellowish autofluorescent material (UVL) representing reworked phosphatic coprolitic material. Fine mineral is composed of very dominant pale brown, dotted (PPL), low interference colours (close porphyric speckled b-fabric, XPL), pale orange brown (OIL). Very little organic matter. *Pedofeatures*: very abundant textural pedofeatures. Lower 20 mm: very abundant intercalations, occasional very dusty clay void coatings; in upper 25 mm very abundant, very dusty/impure clay void coatings; coatings on all void surfaces and ped faces; fabric pedofeatures composed of abundant inclusions of banded dusty clay/link capping material as fragments.
Gravels over conglomerate	59	-	Gravels.	*Structure*: massive. *Porosity*: 10-20% voids generally coarse channels and vughs. *Mineral*: C:F, 85:15 (silts) to 95:5 (gravels). Common gravel to very coarse sand size limestone (subangular to angular); various rounded/weathered aragonite, with flint/chert, siltstone, etc. Common silt size and fine sand size quartz with very few mica. Fine material composed of pale brown, speckled (PPL), low interference colors (close porphyric, speckled b-fabric, XPL), pale brown orange (OIL). No obvious organic matter. *Pedofeatures*: very abundant intercalations, dusty/impure clay void coatings, pans, 'micro-channel infills'. Very abundant banded fabric of clean silts.
Area 1 (L.102 metre square)				
Red Silt	G	0-0.095	Red silt beneath cave roof.	As Sample 44. Massive, very fine and coarse banded material with lamina fabric; generally closed vughs. An upward fining sequence of coarse silt to fine silty and clay. Contains rare plant fragments as well as phosphate clasts.
Red Silt	H	0.33-0.40	Red silt beneath cave roof, over conglomerate.	As Sample 44. Massive/fine banded, composed of strongly elutriated coarse silts with few mixed in coarse clayey fragments and sand size material. Top of sample contains a gravel and silt band.
Skeleton Rift				
Red Silt	D	0-0.17	0-0.05 m: Red silt beneath cave roof. 0.05+ m: Conglomerate.	As Samples 44 and 59. Massive with coarse banded silts. Upwards, deposit is composed of gravel-rich silts with stone-sized angular to subangular limestone clasts. Deposit is poorly sorted, mainly silt size material, with common sand, strongly disrupted banded fabric of dusty clay and silt pans with included sand. Inclusions of likely fragmented link cappings as sand size clasts; rounded bone present.
Area 3				
Red Silt	E	0-0.16	0-0.16 m: Red silt beneath cave roof (concrete floor) over conglomerate.	As Sample 44. Breccia; massive with few vughs and fine channels. Highly compact sediment; weakly to moderately impregnated with calcium carbonate; poorly sorted mixture of stone size, subangular limestone and a matrix of dominantly silt size quartz, mica and calcite. Also includes coarse sand size quartz, weathered limestone, fossils and speleothem. Patchy iron staining and depletion; possible occasional charcoal stuck to the roof. Few included, embedded/coated grains. Occasional thin to thick, very dusty to impure coatings.
Red Silt	I	0-0.16	0-0.16 m: Red silt beneath cave roof (concrete floor) over conglomerate.	Massively banded silts and clays with repeated graded beds. Some fine channeling at the top. Most of porosity in the form of packing voids.

Table 2 Tentative summary of sedimentary activity in Gough's Cave as reconstructed from soil micromorhpology.

Age (^{14}C yrs bp x 1000)	Period	Deposition	Post-Deposition	Comments
9				
10	Early Holocene	Formation of stalagmite and frog bone-rich muds in the Sand Hole	Stalagmite formation.	Climatic amelioration associated with warm and moist conditions (cf. frogs).
11-10	Loch Lomond Stadial (Younger Dryas)	Accumulation of breccia sediments in Sand Hole	Patchy formation of banded fabric and link capping, accompanied in places by physical mixing. Washing of impure clay into voids.	Renewal of cold conditions leading to freezing and thawing associated with increased meltwater activity.
13 to 11	Windermere Interstadial (Bølling/Allerød)	Upward fining sequence from gravels and sands through to the Red Silt; deposition of mud in the Sand Hole	Ephemeral biological activity producing channels and vughs. Localized ice lensing in the lowermost Red Silt.	Increased moderation in climate. Diminishing phreatic flow, possibly accompanied by ice-lensing in the early stages
16 to 13	Devensian (Oldest Dryas)	Formation of Conglomerate		Cryoclastic activity accompanied by high energy phreatic flow.

Bull. nat. Hist. Mus. Lond. (Geol.) **58**(supp): 59–81 Issued 26 June 2003

Cannibalism in Britain: Taphonomy of the Creswellian (Pleistocene) faunal and human remains from Gough's Cave (Somerset, England)

P. ANDREWS
The Natural History Museum, Cromwell Road, London SW7 5BD, UK
Y. FERNÁNDEZ-JALVO
Museo Nacional de Ciencias Naturales, 28006 Madrid, Spain

SYNOPSIS. Human induced damage is the main taphonomic modification observed on the fossil bone assemblage of Gough's cave. Fossils from this site are very fragmentary, showing abundant cut-marks, percussion marks and peeling. Some specimens, however, are complete (ribs, vertebrae, carpal-tarsal bones and phalanges), but these elements are characterised by low marrow content where breakage to open the bone is not needed. Human remains recovered from this site show similar butchering patterns to other animals suggesting skinning, dismembering, defleshing and marrow extraction activities. Excavations during the 1986–1987 seasons showed that the human remains appear at the site randomly mixed with animal bones, with no specific distribution or arrangement of human bones. The evidence from this distribution indicates equal treatment of human and animal remains, and the analysis of cut-marks and other modifications suggests that both humans and animals were accumulated as the discarded food remains of the human population. This is interpreted as nutritional cannibalism. One exception to this is seen in the slight differences in skull treatment compared with other sites, suggesting a possible element of ritual cannibalism (cf Fontbrégoua, the French Neolithic site, ca 4000 BC).

INTRODUCTION

Human remains from Gough's cave (Cheddar) have been recovered during several excavation seasons. They were found together with abundant remains of other vertebrate animals and stone tools from Oxygen Isotope Stage 2 deposits, and most come from the Late Pleistocene interstadial, 11,500–13,000 radiocarbon years ago (Stringer 2000).

The early excavations during the late 1920's and early 1950's took place over a wide area of the cave, and although abundant fossil remains were recovered, no record was kept of the bone distributions. A joint excavation undertaken by the University of Lancaster and The Natural History Museum (UL-NHM) was much more restricted in extent, with most of the bones coming from about one cubic metre of fine gravel and silt between a large rock and the north wall of the cave during 1986–92 (Stringer 2000). These were excavated, however, with much greater precision, and records of the fossils and stratigraphy were kept in meticulous detail, so that more information is available from this small area than for the whole of the previous, much more extensive, excavations. In addition, fossils recovered by this recent excavation have been found to refit with remains recovered by the earlier, indicating that it is the same fossil bone assemblage. The UL-NHM seasons have been essential in interpreting the site formation and the type of cannibalism practised by *Homo sapiens* about 12,000 years ago.

Cannibalism among humans has been a *taboo* topic and is still today a controversial aspect of human behaviour. By definition, a cannibal is a person or animal that eats any type of tissue of another individual of its own kind. Permissive tolerance of human cannibalism has traditionally occurred when referred to 'primitive' societies, but critical reviews such as Arens, (1979) have been sceptical of cannibalism claims based on written references or oral tradition. Taphonomic studies of bone remains of the victims have been the only way to validate some claims for cannibalism (Villa *et al.*, 1986a, 1986b; White, 1992; Turner and Turner, 1999; Fernández-Jalvo *et al.* 1999; Degusta, 1999, Defleur *et al.* 1999). The oldest case confirmed as cannibalistic practice among humans was described at the early Pleistocene site of Gran Dolina (TD6, Atapuerca, Burgos, Spain), but a recent study has discovered cut-marks on a right zygomaticomaxillary specimen from the Plio-Pleistocene site of Sterkfontein (South Africa) that may suggest an earliest case of human damage on human remains (Travis *et al*, in press). According to these authors, cut-marks appear on areas of ligament and muscle insertions, suggesting cuts were made on purpose to cut meat. Surprisingly this is the only specimen showing butchering marks, absent on the remaining 763 macro-mammalian fossil specimens, including the rest of the hominid remains recovered from the site.

Cut-marks are of great significance in coming to an understanding of prehistoric human behaviour, but on their own they cannot be used as direct evidence of cannibalism. Cut-marks may appear on human skeletons as result of mortuary rituals, practices still current today, where human carcasses are defleshed but meat or marrow is not consumed. Cuts may be frequent on these skeletons, although cannibalism is absent. Sometimes carcasses are defleshed and meat or organs eaten as result of rituals in relation to beliefs or religion. The identification of nutritional cannibalism, in contrast to ritual, is based on a combination of indicators, the main criterion of which is the comparison of human and animal remains from the same archaeological context. If a human population was living by hunting, and it did not distinguish between animal and human prey, the processing marks left on the bones of both human and animal should be the same. Turner (1983) has given several criteria for recognising nutritional cannibalism, but the most basic criteria by Villa *et al.* (1986a, pg 431) are as follows:

© The Natural History Museum, 2003

1. Similar butchering techniques in human and animal remains. Frequency, location and type of verified cut-marks and chop-marks on human and animal bones must be similar, allowing for anatomical differences between humans and animals.
2. Similar patterns of long bone breakage that might facilitate marrow extraction.
3. Identical patterns of post-processing discard of human and animal remains.
4. Evidence of cooking; if present, such evidence should indicate comparable treatment of humans and animal remains.

Previous work on Gough's cave material has come to contradictory conclusions. Cook (1986) attributed cut-marks on human remains to natural damage produced by trampling, with the exception of an adult mandible (Gough's cave 6) that shows evidence for deliberate human activity related to post mortem removal of the tongue. Apart from this human fossil, Cook found equivocal cut-marks on animal bones from the site that indicates dismembering activities. Cook, therefore, concluded that cannibalism was absent at Gough's cave. In contrast to this, Currant, Jacobi and Stringer (1989) consider that there is no doubt about human processing of parts of the body at or close to the time of death based on the new material from the 1987 collections. Similarly, Charles (1998) suggests cannibalism was the key factor based on the intermixing of human with animal bones in the deposits.

It is our intention here to show the results of a taphonomic analysis of Gough's Cave fossil remains. Both human and animal bones will be treated equally so that their modifications can be compared with a view to seeing if the agents responsible for the animal bones are the same as those responsible for the human bones. We will focus particularly on the evidence of cut-marks, which are present on both, to see if there is any difference in distribution and/or type of cut-marks. In addition, we will examine features of bone fracture and bone distribution that may contribute to the hypothesis of human cannibalism at the site.

METHODS AND MATERIAL

The fossil material here analysed consists of 240 human and other animal fossil bone fragments. These are in the collection of the Natural History Museum in London. In addition, there are a number of fossil bones at the local museum in Cheddar Gorge that we have not had the opportunity of studying and have therefore not been included. Both human and animal fossil bones have been examined with the aid of a binocular microscope. Some specimens were analysed using scanning electron microscopy (SEM), an ISI ABT55 SEM-fitted with an environmental chamber, operating in the back-scattered electron emission mode at 20 kV, which is housed at The Natural History Museum (London). This type of microscope enables specimens to be directly analysed with no necessity for coating (Taylor, 1986).

Breakage has been analysed following the method of Villa and Mahieu (1991):

1. Number of fractures.
2. Fracture angle: oblique/right/mixed (oblique and right).
3. Fracture outline: transverse/curved-V-shaped/intermediate/ longitudinal.
4. Fracture edge: smooth/jagged.
5. Shaft circumference: 1, circumference is <½ of the original; 2, circumference is > ½of the original; 3, complete
6. Shaft fragmentation: 1, shafts < ¼ of original length; 2, length between ¼ and ½ of original length; 3, length between ½ and ¾ of original length; 4, length >¾ of original length (complete).

Unfortunately, most remains from the study collection had been glued together and traits of fracture angle, fracture outline and fracture edge could not always be identified and quantified. Other fracture traits such as peeling (White, 1992), percussion pits (Blumenschine & Selvagio, 1988), adhering flakes (White, 1992) and conchoidal percussion scars (Blumenschine 1988) were recorded as present or absent.

Bone surface modifications attributed to human action were identified as tool-induced modifications such as incisions, scrape marks, chop-marks, hammer/anvil striations. Emplacement of cut-marks and identification of the muscles or tendons affected by the cuts were recorded. Post-depositional surface modifications were identified as weathering, desquamation, trampling marks, polishing, rounding, gnawing or tooth marks. Post-burial modifications recorded were manganese oxide stains, concretion (cemented sediment heavily attached to the fossil), soil corrosion or root-marks.

Tooth marks were described and measured separately for all anatomical items following Andrews and Fernández-Jalvo (1997):

a. Carnivore pits on bone surface (minimum dimension)
b. Carnivore gnawing on bone surface (transverse measurement of grooves)
c. Carnivore pits on articular surfaces.
d. Carnivore punctures on spiral breaks
e. Carnivore punctures on transverse breaks
f. Carnivore punctures on split shafts
g. Multiple molar pits made by multi-cuspid teeth.
h. Carnivore punctures on intact bone edges

RESULTS

The results of the taphonomic analysis are displayed in Table 1. The main taphonomic modifications that affect these fossils is human activity as seen at this table.

Species represented

The Gough's cave human material consists of both crania and postcrania. The former indicate the presence of five individuals, two adults, two adolescents and one child (Stringer 2000). The adults are represented by a calotte, part of a second calotte and two maxillae and two mandibles. The adolescents are represented by a cranium, two maxillae and one mandible, again suggesting two individuals. The child has a single calvaria. Depending on how the adolescent material is associated, there is a minimum of five individuals in the Gough's Cave deposits (Stringer 2000, Humphrey & Stringer 2002).

The taxonomic identification of the non-human collection analysed here has been done by A.Currant, R.M.Jacobi and C.Stringer. The species found are *Equus ferus*, *Cervus elephas, Bos primigenius, Sus scrofa, Lepus timidus.* The most abundant species represented in the study collection are the equids (Table 1), with 132 specimens, and this compares with 88 human and 42 cervids. Only two bone fragments of bovid, an astragalus and a tarsal, have been recovered from the study collection, and one fragment each of rabbit (tibia) and suid (mandible) species. The latter species have some impact marks, but they are too few to come to any conclusions about their nature and origin, and so our analyses here will concentrate on the modifications of the three common groups, one of which of course are the humans.

Table 1 Summary of taphonomic modifications seen on the fossil bones from Gough's Cave. Modifications are shown for each major postcranial element, which are listed in column 1. The total number of specimens (**N**) for each element is in column 2, and in column 3 the distribution of modifications by human action is shown for four taxonomic categories: human (**h**), equid (**e**), cervid (**c**) and indeterminate large mammal (**m**). The same distribution is shown for six types of modifications in the remainder of the table as explained in the text.

Anatomical element	Total N	N				Cut-marks				Percussion marks				Concoidal scars				Adhered flakes				Removed flakes				Peeling			
		h	e	c	m	h	e	c	m	h	e	c	m	h	e	c	m	h	e	c	m	h	e	c	m	h	e	c	m
Cranial	4	2	0	2		2	0	0		2	0	0		0	0	0		0	0	0		2	0	0		2	0	0	
Hemi-maxillae	9	2	3	4		2	2	2		2	2	2		0	0	0		0	1	0		0	0	0		0	1	0	
Hemi-mandible	27	6	12	9		2	3	2		0	9	4		0	0	0		0	0	1		0	0	0		1	3	1	
Hyoid	1	0	1	0		0	1	0		0	1	0		0	0	0		0	0	0		0	0	0		0	0	0	
Clavicle	3	3	0	0		3	0	0		0	0	0		0	0	0		0	0	0		0	0	0		1	0	0	
Humeri	6	6	0	0		4	0	0		3	0	0		1	0	0		1	0	0		1	0	0		0	0	0	
Radii	6	5	1	0		1	1	0		3	1	0		0	0	0		0	0	0		0	1	0		1	0	0	
Ulnae	5	4	1	0		2	1	0		1	1	0		0	0	0		1	0	0		0	0	0		2	0	0	
Scapulae	4	4	0	0		4	0	0		1	0	0		0	0	0		0	0	0		0	0	0		2	0	0	
Ribs	45	40			5	20			5	8			3	0			0	0			0	0	0	0	0	8			0
Vertebrae	19	7	7	5		3	6	2		1	1	0		0	0	0		0	0	0		0	0	0		2	0	0	
Pelves	2	0	2	0		0	2	0		0	0	0		0	0	0		0	0	0		0	0	0		0	0	0	
Femurs	1	1	0	0		0	0	0		1	0	0		0	0	0		0	0	0		0	0	0		0	0	0	
Fibula	1	1	0	0		1	0	0		0	0	0		0	0	0		1	0	0		0	0	0		0	0	0	
Tibiae	8	1	3	4		0	2	3		1	1	1		0	1	0		0	0	0		0	0	1		1	0	0	
Long bones	3	2	0	1		1	0	1		1	0	0		0	0	0		0	0	1		0	0	0		0	0	0	
Patellae	1	0	1	0		0	0	0		0	0	0		0	0	0		0	0	0		0	0	0		0	0	0	
Carpo-tarsal	35	0	28	7		0	12	3		0	1	0		0	0	0		0	1	0		0	0	0		0	0	0	
Metapodial	35	5	24	6		0	12	6		1	19	2		0	4	0		0	0	0		0	1	1		1	0	0	
Phalanges	54	6	49	4		0	29	2		0	27	2		0	0	0		0	0	0		0	0	0		0	0	0	
Totals	269	90	132	42	5	45	71	21	5	25	63	11	3	1	5	0	0	3	2	2	0	3	2	2	0	21	4	1	0

Skeletal elements

Anatomical elements of humans and other large mammals (horses and deer) recorded at the site suggest some differences between element representation. In general terms, human skeletons are better represented than are those of any of the other large mammals. Human skeletons show a relatively high abundance of cranial remains, ribs, scapulae, and arms (Table 1). In contrast, vertebrae are notable for their near absence, despite the abundance of ribs that were found in association (although not articulation) at the site. There is also a peculiar absence of pelves, carpo-tarsal bones and phalanges which are relatively abundant among horses or deer. Similarly, cranial elements, especially mandibles, are also abundant for both horses and deer, but while metapodials and phalanges are abundant, most limb bones are poorly represented. Horses have an extraordinarily high abundance of phalanges, which are not generally common in human occupation sites. Skeletal element proportions are summarized in Table 2.

Anatomical elements: limb bones

Five upper limb bones from Gough's cave have moderately complete shafts, three clavicles, one humerus and two radii and ulnae. These were recovered in a fragmentary state but reconstructed in the laboratory. For example ulna M54066 is made up by six fragments that make up most of the right ulna (Churchill 2001) and it has a possible antimere in M54067. Two of the clavicles are antimeres, and the four scapulae have been interpreted as representing two males and one female individuals. All have cut-marks, sometimes extensive. The lower limb bones are similarly fragmentary, with no complete bones. There are four left femora, although only one was

Table 2 Skeletal proportions of the anatomical elements recorded for 6 humans, 10 equids and 6 cervids from Gough's cave. Skeletal elements are shown on the left, and percentage occurrences of elements based on numbers present (N_a) divided by numbers of that element present in the skeleton (N_t) multiplied by the MNI.

	Human			Equid			Cervid		
		N_a	N_t		N_a	N_t		N_a	N_t
skull	50%	3	1	0%	0	1	33%	2	1
hemi-maxilla	17%	2	2	15%	3	2	33%	4	2
hemi-mandible	50%	6	2	60%	12	2	75%	9	2
hyoid	0%	0	1	10%	1	1	0%	0	1
clavicle	25%	3	2	0%	0	0	0%	0	0
humerus	50%	6	2	0%	0	2	0%	0	2
radius	42%	5	2	5%	1	2	0%	0	2
ulna	33%	4	2	5%	1	2	0%	0	2
scapula	33%	4	2	0%	0	2	0%	0	2
rib	28%	40	24	0%	0	36	3%	5	26
vertebra	7%	10	25	2%	7	32	3%	5	28
pelvis	0%	0	2	10%	2	2	0%	0	2
femur	42%	5	2	0%	0	2	0%	0	2
fibula	8%	1	2	0%	0	2	0%	0	2
tibia	75%	9	2	15%	3	2	33%	4	2
patella	0%	0	2	5%	1	2	0%	0	2
carpo-tarsal	0%	0	28	11%	28	26	5%	7	22
metapodial	4%	5	20	60%	24	4	25%	6	4
phalange	0%	1	56	41%	49	12	3%	4	24
long bones		2			0			1	
Total number	8%	90	179	10%	132	134	6%	47	128
MNI	6			10			6		

seen, so that at least four individuals are indicated. All four left femora are dyaphysis fragments that represent small individuals, and in addition there is a right proximal femur and fragments of diaphysis from a larger sized individual (Trinkaus 2000), so that the MNI indicated by the femur is five. Nine tibia fragments indicate four individuals, two large and two small (Trinkaus 2000), but only one was seen.

Humerus: There are six fragments of humeri, all of them from a single human individual. The shafts are split longitudinally (shaft circumference category 1, shaft fragmentation categories 1 and 2 according to Villa and Mahieu 1991). The ends are absent, with only one split fragment of shaft near the neck of the head (GC'87, no.12). Cut-marks appear on four of the six fragments of humerus (67%). Cuts run obliquely along the shaft clustered or isolated covering rugose surfaces or muscle attachments (*deltoid* crest, *triceps* insertion or *brachialis* muscle). One of the specimens (GC'87, no.12) preserves the area near the head, and it is here where a cut runs transversally across the humerus on the attachment of *teres minor*. Distally in the same fragment there are also scraping marks near the fracture edge. The scraping marks probably resulted from the removal of soft tissues that could have absorbed the blow when breaking the bone to extract the marrow (Binford, 1981). Three of these cut-marked fragments of humerus also show percussion marks along the broken edges. Some of these fragments also have conchoidal scars, adhered flakes and/or removed flakes, also located on the broken edge. Only one fragment of humerus has weathering in stage 1 (Behrensmeyer, 1978) and two are affected by trampling, but none of them have tooth marks.

Summary of humeri. Total 6 specimens, all human.
Cut-marks: 4 specimens (2 on fossils from the 1987 collections)
Percussion marks: 3 specimens (2 on fossils from the 1987 collections)
Conchoidal scars: 1 specimen (1 on fossils from the 1987 collections)
Adhered flake: 1 specimen
Removed flake: 1 specimen

Ulna: There are five fragments of ulna, four of them from humans (2 rights, 2 lefts, 2MNI) and one from a horse. The human fragments of ulna consist of longitudinal splits, as seen on the humeri, but several fragments have been refitted so that they now form most of the bone circumference (3 of them have circumference category 3 according to the classification of Villa and Mahieu, 1991). Two of the ulnae have cuts on the surface, running obliquely to the length of the

Fig. 1 **A,** Left human ulna GC87-209, midshaft fragment with part of the lateral aspect of the shaft. Cut-marks run obliquely across the posterior ridge (i.e. along the bottom of the shaft), and another concentration occurs more distally (not shown here). There is extensive peeling at the proximal end, on the left as shown here, and three massive percussion impact marks can be seen medially, along the upper edge of the bone as viewed here. There is also an adhered flake on the lateral aspect. **B,** Six fragments making up most of right human ulna M54066 (GC202, 243, 119c). Fractures are mixed, smooth, and fragmentation 3/4. Breakage appears to be natural with no percussion marks and no cut-marks. **C,** Proximal radius and ulna GC89-071&073 of *Equus ferus*. Cut-marks are seen on the olecranon process. **A,** × 1.6; **B,** × 0.5; **C,** × 0.7.

bone and probably related to the insertion of the *flexor* muscles. Percussion marks and adhered flakes have also been observed on one of these two damaged ulnae (GC'87 209) along the broken edge. Both ulnae show clear evidence of peeling, one on the proximal broken edge (Fig. 1A). The other two fragments of ulna which have not been damaged by human action have been refitted from several small split shafts found several metres apart from each other, in one case all the fragments coming from the 1987 excavation (M54066), and in the other, some fragments coming from the 1987 excavation and refitted with old 1927 excavation fragments (M54067). The proximal end of the right ulna M54066 (Fig. 1B) has lateral crushing of the head. No cut-marks or percussion marks have been distinguished on either of these two ulnae. One ulnae fragment (GC'50 420) is weathered in stage 1 or 2 and has dispersed manganese on its surface.

The only horse ulna-radius (GC'87 73) has only the proximal end preserved (circumference category 3, length category 1, Villa and Mahieu 1991). The heads of both the ulna and the radius are extensively cut and show percussion marks (Fig. 1C) and a flake has been removed from the interosseous space between ulna and radius. Percussion marks are present on the olecranon.

Summary of ulnae. Total 5 specimens, 4 humans, 1 equid
Cut-marks: 3 specimens (2 human, 1 equid) (1on fossils from the 1987 collections)
Percussion marks: 2 specimens (1 human, 1 equid) (1 on fossils from the 1987 collections)
Adhered flakes: 1 specimen (human) (from the 1987 collections)
Removed flakes: 1 specimen (1 equid)
Peeling: 2 specimens (human) (from the 1987 collections)

Radius: There are five fragments of all of them humans. There are two with proximal articulations with complete circumference, category 2 and 3 (Villa and Mahieu, 1991) and more than the half of the length of the bone. Specimens M54071 and GC'87 74 are refitted shafts (5 and 7 respectively) of split shaft fragments, open longitudinally and mostly category 1 shaft circumference. Only one of these radii has cut-marks (Fig. 2A). These cuts were formerly interpreted as decorative engraving. They appear on the lateral surface along the length of the bone, bordering the origin of the *flexor pollicis longus*, but there is no muscle attachment along this part of the shaft (between the ulna and the radius). On the SEM we could observe that each group of incisions is actually a single compound mark made by a single stroke (Fig. 2B). Directionality is the same in every set (Fig. 2B), and it appears to be the result of filleting, removal of the muscle progressively along the shaft. With regard to breakage, two of the radii have percussion marks, which are distributed along the longitudinal broken edge. One of the radii also shows large percussion marks on the anterior and posterior edges. Peeling is seen on M54071 on at least three joint fragments. This specimen has many percussion impacts mainly along broken edges, and there are at least two large impact scars along the anterior side and one impact pit on the posterior surface.

Summary of radii. Total 6 specimens, 5 human, 1 equid
Cut-marks: 2 specimens (1 human, 1 equid) (1 from the 1987 collections)
Percussion marks: 4 specimens (3 human, 1 equid)

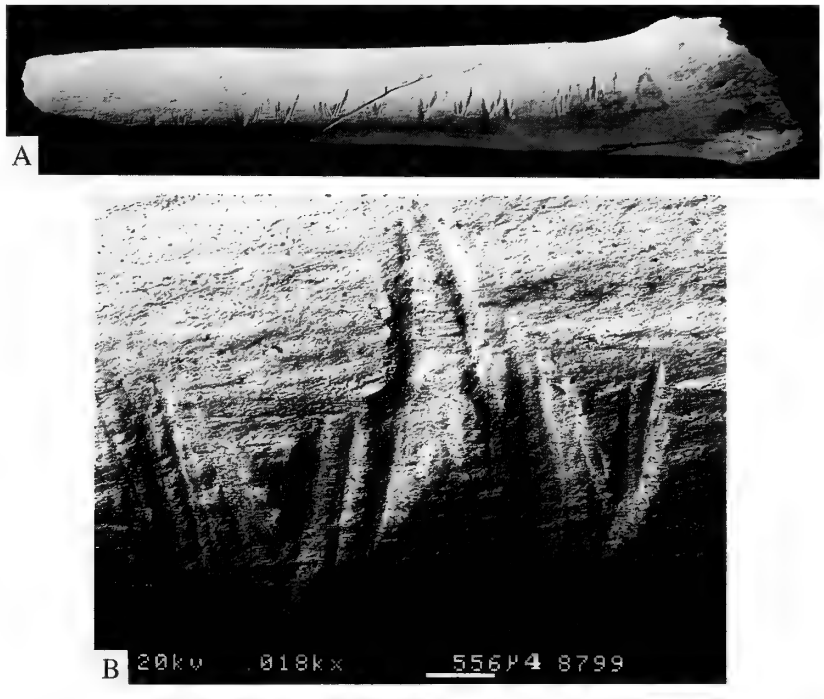

Fig. 2 **A,** Right human radius GC87-74. Partial diaphysis with the anterior surface preserved for most of it length. Extensive cutmarks are present on the lateral surface, which is the side of the shaft away from the ulna where there are no muscle attachments, but in addition there are a few cut-marks proximally (on the left as seen here) on the supinator insertion. These marks have been interpreted as engraving, but all of the 'groups' of incisions are actually compound marks made by single strokes, with consistent directionality towards the superior aspect of the shaft. This is interpreted as filleting of the arm muscles progressively along the shaft. **B,** Scanning electron micrograph of GC87-74 cut-marks. Notice that marks are made by the same stone tool edge and made with a sawing motion that follows the same direction for all cuts along the bone shaft. **A,** × 1.1.

Fig. 3 **A,** Distal articulation of tibia M50017, left distal tibia of Rangifer tarandus. This articulates with astragalus M49914, and both have matching cut-marks, probably for disarticulation of the foot. **B,** Distal tibia, no number, of *Equus ferus*, with cut-marks on the distal turberosity and oblique break, circumference 3, of the shaft. **C,** Right distal tibia of *Equus ferus*, GC87-4. The distal articular surface is intact. The shaft is broken with oblique fracture, circumference 3. There are cut-marks on the lateral ridge of the distal tubersosity and carnivore chewing just proximal to the cut-marks, but they do not overlap and so their relative times of occurrence are unknown. There are extensive percussion marks on all surfaces of the shaft in the region of the oblique break, with a conchoidal scar posteriorly (on the right side of the break as viewed here). Finally, there is a network of shallow rootmarks on the shaft. **A,** × 1; **B,** × 0.65; **C,** × 0.6.

Removed flakes: 1 specimen (1 equid)
Peeling: 1 specimen (1 human)

Femur: We only saw one fragment of human femur, although five individuals are apparently represented in the collection (Trinkaus 2000). The femur fragment we saw is a split fragment of shaft (no ends, circumference category 1, length category 1, Villa and Mahieu, 1991) with strongly developed linea aspera. It does not have cut-marks but it has percussion marks. These percussion marks are along the linea aspera, 3 grouped together.

Fibula: There is only one fragment, which has been identified as human. It is part of the shaft having a circumference category 2 and length category 2 (Villa and Mahieu 1991). It has cuts near the end of attachment of the *soleus* muscle indicating dismembering activities, and evidence of breakage provided by an adhered flake depressed into the cavity.

Tibia: There are nine human tibia fragments, but we only saw one fragment, plus three of equid and four of cervid. One of the cervid tibiae has tooth marks on the surface. They are chewing marks on anatomical edges (tooth marks type c following to Andrews and Fernandez-Jalvo, 1997) measuring 1.4 and 0.9 mm (average 1.15mm). The human tibia fragment is a longitudinally split section of shaft

with no ends (circumference category 1 and length category 1). In contrast to this all animal tibiae have circumferences category 3 and length between 1 and 2 (according to Villa and Mahieu, 1991). It is apparent from this that the animal bones are preserved differently from the human long bones. There are no cut-marks on the human tibia fragment, but percussion marks are present. On the animal bones, cuts appear on 5 of the 7 distal ends of tibiae. The cuts are related to the articulation of the tibia with the tarsals, on the distal ends (Fig. 3A), or on the posterior and/or anterior surfaces (Fig. 3B), and all are related to dismembering the ankle joint. The distal end of another equid tibia with a small part of the shaft shows cuts on the lateral maleolus, probably also related to cutting the short and long lateral ligaments when dismembering the foot. Another distal end with a small part of the shaft of cervid also has cuts on the shaft, but this time they appear on the opposite side of the shaft from percussion marks (see below).

With regard to fracture, the human tibia has peeling on one of the ends and percussion impact scars on the edge of the longitudinal breakage. This suggests there were several impacts on the bone to open the bone longitudinally and expose the marrow. One of the equid tibiae (GC'87-4, Fig. 3C) has a conchoidal scar on the posterior midshaft and extensive percussion marks all round the shaft. Two of the four cervid tibiae show percussion marks. One of them (M50019) has percussion marks on the opposite side of cuts, which suggests that the latter could be anvil marks as result of blows on the bone. The other (M50017) has a flake removed on the lateral side near the broken edge and a percussion impact mark on the plantar side, near the articulation (Fig. 3A). M50017 has also trampling marks running transversally.

Summary of tibiae. Total 8 specimens 1 human, 3 equid, 4 cervid
Cut-marks: 5 specimens (2 equid, 3 cervid) (1 each of cervid and equid from the 1987 collections)
Percussion marks: 3 specimens (1 human, 1 equid from the 1987 collections)
Conchoidal scars: 1 specimen (equid from the 1987 collections)
Removed flakes: 1 specimen (cervid)
Peeling: 1 specimen (human from the 1987 collections)

Long bones (indet.): There are three fragments of long bones two of them identified as humans and the third as cervid, though the anatomical elements could not be specified. One of the human split shafts has oblique cuts and percussion marks on the edge of the fracture. The cervid shaft is formed by two longitudinally split fragments, having several cuts running transversally along the edge, and an adhered flake between the joint fracture of both fragments.

Anatomical elements: hands and feet

Calcaneus: There are eight calcanei, seven of them are from equids and only one of cervid. Cut-marks are present on five specimens (4 equids and 1 cervid):
4 on the lateral side of the calcaneus along the plantar and the dorsal surfaces (4 equids)
2 on the upper edge of the calcis (2 equids)
1 on the medial side distally and on upper surface (equid)
1 on the dorsal side close to the articulation with the astragalus (1 cervid)

Cuts are related to plantar ligament and lateral and medial ligaments, with the cutting directed at dismembering the ankle joint.

Four calcanei are chewed, three of them very heavily (Fig. 4A). Puncture marks are superimposed over cut-marks and percussion marks on one of these calcanei (M50029), which indicates that carnivore activity occurred after human. Chewing marks are pits on the surface (type a, average 2.0mm, N = 6), grooves on surface (type b, average 1.6mm, N = 7) and only one of type c (1.5 mm) and one of type h (3mm).

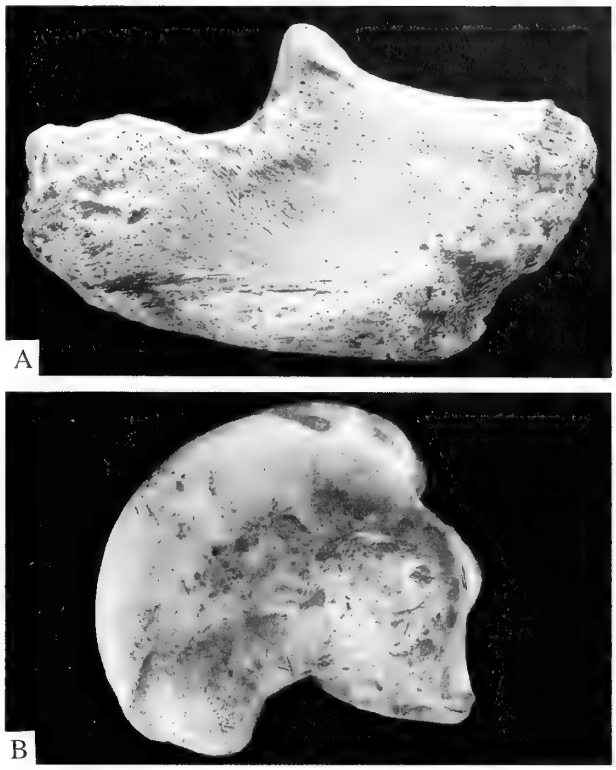

Fig. 4 **A,** Left calcaneus M50029 of *Equus ferus*. Much of the calcis has been damaged by extensive percussion marks on both sides, and there is a cluster of cut-marks along the upper edge just posterior to he articular surface. **B,** Medial view of left astragalus of *Equus ferus*, M49843. Cut-marks are present in three clusters, one on the medial edge of the medial condyle, the second on the medial surface of the body, both seen here, and the third on the upper edge of the lateral condyle. Both figures, × 0.9.

Summary of calcanei. Total 8 specimens, 7 equid, 1 cervid
Cut-marks: 5 specimens (4 equids, 1 cervids).
Percussion: 1 specimen (1 equid)

Astragalus: there are ten specimens of equid astragali (left 5, right 5, MNI 5) and five cervid astragali. Nearly all specimens are complete. Cut-marks are present on five of the equid astragali and two of the cervid astragali:
5 astragali have cuts on the medial condyle, medial side (3 equids and 2 cervids)
4 astragali have cuts on the medial surface of the body, and on the proximal and/or distal tuberosities (2 equids, 2 cervids)
2 astragali have cuts on the central trochlear ridge (1 equid, 1 cervid)
1 equid astragalus has cuts on the lateral condyle, medial side
2 astragali have cuts on the lateral side of the lateral condyle (1 equid, 1 cervid)
1 equid astragalus has cuts on the posterior surface of the body.

Cut-marks are most abundant at the medial condyle and medial surface of the body (Fig. 4B). The medial surface bears on its distal part a large tuberosity and on its proximal part a smaller one for the

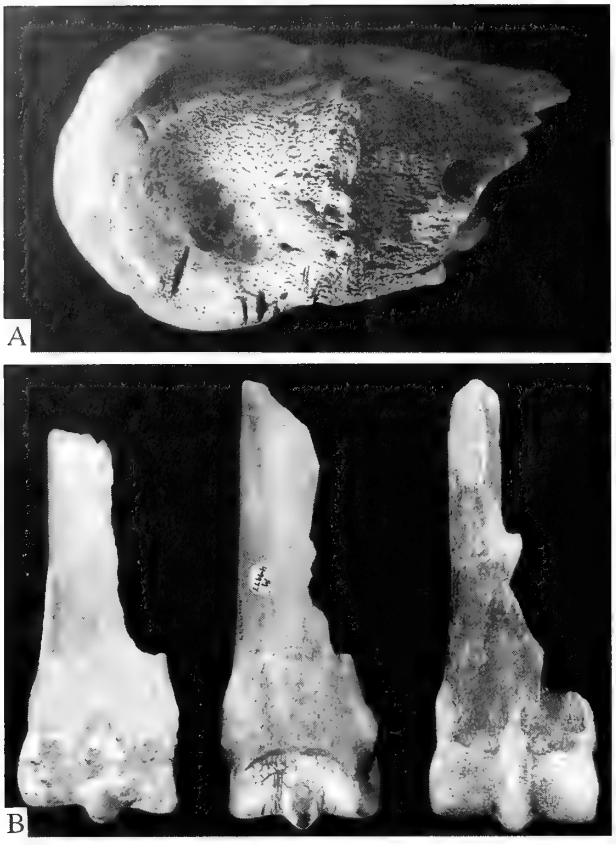

Fig. 5 **A,** Distal metapodial of *Equus ferus*, M50043. Deeply incised cut-marks can be seen around the edge of the articular surface. **B,** Three distal metapodials of *Equus ferus*, from left to right ventral view of M49834, dorsal views of M49977 & 49950. In each case, the shaft is split up to the articular surface with oblique fractures, curved, smooth, and shaft circumference 2. On M49834 there are cut-marks on the terminal end of the central ridge of the trochlea and a conchoidal scar on the dorsal side of the oblique fracture (not seen here); M49977 has percussion marks on the central ridge of the trochlea, visible here on the dorsal aspect as discolouration of the articular surface, conchoidal scars along the oblique break, and cut-marks on the shaft; M49950 also has cut-marks on the shaft along the ridge bordering the post-articular sulcus and conchoidal scars along the oblique break, and there are extensive percussion marks on the distal (terminal) part of the articular surface. These modifications appear to be concerned with breakage of the shaft for extraction of marrow and disarticulation of the foot. **A,** × 0.7; **B,** × 0.4.

attachment of the medial ligament of the hock joint. Cuts are therefore aimed at disarticulating the tarsal bones and tibia. Most of the marks were distributed in clusters of short incisions but no chops or percussion marks have been recorded. The lateral surface is smaller and has a wide rough fossa in which the lateral ligament is attached, and only isolated incisions have been found on the lateral trochlea. No human activity has been observed on these bones, so that there is no evidence of percussion or conchoidal scars. There is also no evidence of peeling, flakes removed or adhered flakes.

Carnivore chewing marks are present on two specimens, one of them heavily chewed (M50003, lacking cut-marks). The chewing marks are mainly on the articulation with the calcaneus (type b, average 1.9mm, N = 2 and type c, average 2.8mm, N = 14)

Summary of astragali. Total 15 specimens, 10 equid, 5 cervid Cut-marks: 7 specimens (5 equid, 2 cervid).

Third tarsals: Seven specimens of equid tarsals have been seen, all complete. Cut-marks are present only on two specimens, transverse incisions across the dorsal surface. Three of the tarsals are slightly cracked by weathering, and two have manganese stains.

Other podials: There are a magnum and a scaphoid of equid, two naviculars (1 equid, 1 cervid) and a central tarsal of horse, all of them complete. Human-induced damage is evident on the scaphoid that has cut-marks on the dorsal surface, and on the central tarsal that bears an adhered flake on a lateral broken surface on the articular dorsal ridge. All of them are slightly cracked on surface.

Metapodials: There are five human metatarsals, twenty four metapodials of equids and six of cervids. They have mostly come from the earlier excavations, with only three of the human metapodials coming from the 1987 excavations.

Human metapodials are mainly shafts, sometimes with one end. They have no cut-marks on their surface or articulations. Animal metapodials are all distal ends, except for 13 lateral metapodials of equid that are complete. All human and equid lateral metapodials have length category 3 (almost complete). Medial metapodials have circumference almost complete with the exception of three of them that have circumference 2, but they have length values that are mostly category 1 (less than 1/4th of the length) or category 2 (less than half of the original length) (Villa and Mahieu 1991). Cut-marks are present on 18 of the 30 animal metapodials (6 cervids, 12 equids), but they have been found on none of the humans. Cuts are located on the trochlea, all round the articulation (Fig. 5A) or on the dorsal/ventral surfaces close to the articulation. Medial metapodials of horse have a consistent pattern of breakage (Fig. 5B) indicated by breakage on the shaft close to the distal articular end and extensive percussion marks providing similar bone fragments.

Human metatarsals are all crushed on one or both ends. The ends show evidence of chewing marks, peeling or percussion marks on the edge of the articulation. Two human metapodials appear chewed (a 5th and a 2nd left), although no actual clear puncture mark can be measured. The 2nd left human metatarsal shows strong similarities with a suid rib experimentally chewed by humans (Fig. 6). In contrast to this, no carnivore tooth marks have been recorded on any other animal metapodial surface.

With regard to lateral metapodials of equids, they show similar crushing on articular ends to that seen in humans. Lateral horse metapodials have a consistent pattern with percussion marks on proximal ends on the outer (lateral) surfaces and only rarely on the inner articular surface with the medial metapodial (only 1 specimen). Percussion marks appear on one specimen distally as well. Sometimes, percussions are associated with chop marks (2 cases) and/or cut-marks (3 cases) transversally to the length of the bone. Percussion marks are located on the lateral tuberosity of the proximal end. One of the bones has three chewing marks, type b averaging 1.4mm, N = 3.

The length of metapodials is variable, but none has been split longitudinally. Percussion marks on 21 of the metapodials, however, are located at one side (ventral or dorsal) or distributed on lateral, ventral and dorsal surfaces or, more exceptionally on the articulation. A distal metapodial of cervid has a percussion triangular shape as observed in mandibles (see below). Some metapodials have been seen to have scratches on the opposite side of percussion marks, probably as result of anvil effect on the bone during breakage. Four metapodials show conchoidal scars and flakes removed on the broken edge.

Fig. 6 **A,** a suid metapodial; and **B,** a second left human metatarsal, GC87-30. The suid metapodial was experimentally chewed by humans. The extensive fracturing of the proximal ends, with depressed flakes of bone and splaying of the ends, is extremely similar in both bones, and may indicate human chewing on the metatarsal from Gough's Cave; × 1.2.

Only three metapodials have trampling marks and five have evidence of wet abrasion. One metapodial is weathered in stage 3 or 4 and two are in stage 1 or 2. Manganese oxide stains affects 10 of the 35 metapodials.

Summary of metapodials. Total 35 specimens, 5 human, 24 equid, 6 cervid
Cut-marks: 18 specimens (12 equids, 6 cervids).
Percussion: 22 specimens (1 human from the 1987 collection, 19 equids (11 lateral metapodials), 2 cervids)
Conchoidal scars: 4 specimens (4 equids)
Flakes removed: 2 specimens (1 equid, 1 cervid)
Peeling: 1 specimen (1 human)

Phalanges: There are 22 proximal phalanges, one human, 20 horse and one cervid. The only human phalanx here studied is from the hand and it has the proximal end smashed and the distal end intact. This is similar to patterns observed in the human collection of Atapuerca, Mancos and the Anasazi pueblos (Andrews & Fernandez-Jalvo 1997).

Most horse proximal phalanges are intact except for M49945, which has the proximal end removed by heavy percussion impacts. A flake has been removed on the medial edge, and the shaft is cracked both longitudinally and transversely with percussion marks on the broken edge. Another horse phalanx (M49788) is complete, but shows very heavy percussion marks on ventral (palmar) surface: two multiple marks on the distal articular surface (Fig. 7B) and two extensive percussion marks on the proximal articular end. In general, percussion marks may occur on the lateral, dorsal or ventral surfaces, as well as proximal and distal ends. Cut-marks are oblique to the length of the shaft on both dorsal and especially on ventral surfaces (Fig. 7A). Carnivore chewing appear on two phalanges (M 49787) showing four carnivore pits on the surface (type a, average 1.7mm, N = 4), grooves on the surface (type b, average 1.4mm, N = 14), and eight carnivore pits on articular surfaces (type c, average 1.65mm, N = 8). The average width of carnivore gnawing grooves that affect the proximal phalanx M49958 is 0.72mm. Manganese staining affects eight proximal horse phalanges on the surface. There is no evidence of water damage observed on other phalanges from this study collection. The only proximal cervid phalanx is longitudinally broken with grooves and percussion marks on both sides of the fracture. Cuts affect the phalanx on the dorsal surface and on the articulation.

There are 13 middle phalanges, 11 of horse and two of cervid. Fewer cut-marks and percussion marks are present on the middle phalanges, and where they occur they tend to be at the end of the bones near the articular surfaces. Two of the horse phalanges show percussion marks, but both of them are complete. One of them (M49921) has extensive percussion all around the dorsal (proximally on articular surface) and lateral surfaces. The horse phalanx labelled as number 23 from the excavations of 1987 shows also extensive percussion marks on the dorsal surface. Cut-marks are abundant and very marked on M50030 (Figs 7B, 7C) affecting dorsal and ventral surfaces on the shafts, proximal and distal ends and articular surfaces. Manganese stains cover all over the surface of three medial horse phalanges. Both second phalanges of cervid are complete. Phalanx M49758 shows deep cuts on the ventral side on the shaft and a couple of small incisions on the lateral side of the articulation (distal end).

There are 18 terminal phalanges of horse and one of cervid. Eleven of the horse phalanges have percussion marks and cut-marks on the flexor surface, hoof surface and dorsal surface (Fig. 8). Six of horse and the cervid phalanges have no modifications. Cuts on the ventral side affect the deep flexor tendon, although this would seem to be an uncommon area of cutting related to dismemberment of the hoof. Two horse phalanges (M49959, M49879) show water damage.

Summary of phalanges. Total 54 specimens, 1 human, 49 equid, 4 cervid
Cut-marks: 31 specimens (29 equid,. 2 cervid)
Percussion marks: 29 specimens (27 equid, 2 cervid)

Anatomical elements: axial skeleton

Ribs: The human ribs from Gough's Cave are attributed to three individuals (Churchill 2000). The first individual has lightly constructed ribs and must have been relatively small. The associations between ribs are based on size, curvature and morphology of the iliocostal line, which is superoinferiorly compressed in this individual (Churchill 2000). The heads of all but one rib are missing from this individual, perhaps because it represents an immature individual. The ribs of the second individual are more robust, with heavier muscle markings, and again the heads are missing from all but one rib. The ribs from these two individuals were found in partial association during the 1986–1987 excavation, in close proximity although not articulated (Fig. 9, data from 1987 excavation). A third individual is represented by six fragments forming parts of three ribs from the left side, and a further ten fragments that could not be further identified are also present (Churchill 2000). The 40 human ribs contrast with only five of large mammal. Individual two is the more complete, with 18 ribs, 6 of them complete. Individual one has 16 ribs, 6 of them complete. Human induced damage on the ribs is very extensive (Table 3), with 30 of the 45 total number of ribs (animal and human) showing human-induced damage. Of the

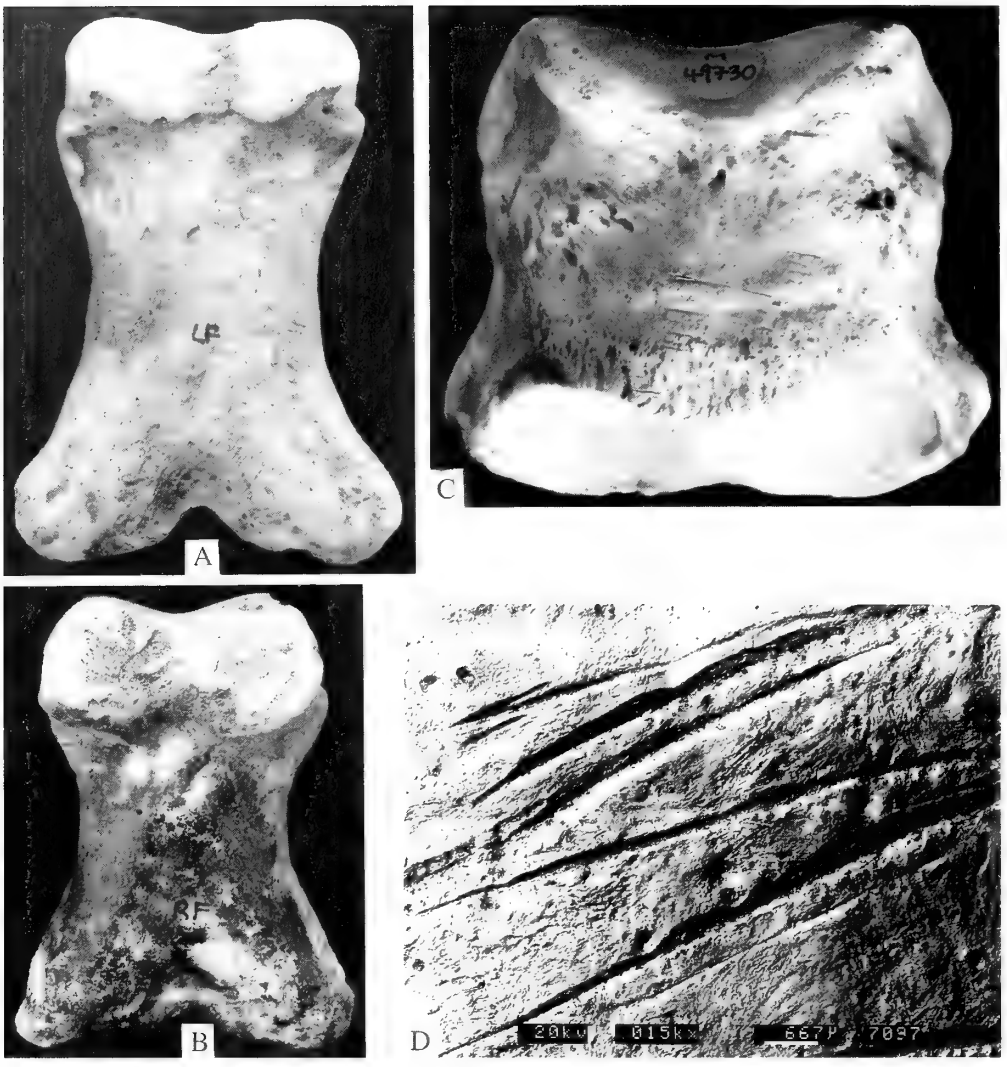

Fig. 7 **A,** First phalanx of *Equus ferus* M49730. Two areas of cut-marks are present, both on the ventral surface, one laterally and the other proximally. **B,** First phalanx of *Equus ferus* M49788. Very heavy percussion marks are present on the ventral (palmar) surface of the distal articulation, seen as two rosette-shaped multiple marks with a single additional mark laterally, and at the proximal end there are two extensive areas of percussion damage ventrally, on either side of the proximal articular surface and extending round on to this surface. **C,** Middle phalanx of *Equus ferus*, M50030. A series of distinct cut-marks cross the dorsal surface on the shaft and the medial edge of the distal articular surface. **D,** SEM micrographs of a set of stone tool cut-marks of a second phalanx of equid (M49999). These marks are related to meat filleting. The cut-marks are characterised by V-shaped sections, microstriations running linearly along the length of the cut, lateral and more superficial cut ('shoulder effect' Shipman and Rose 1981) and irregular displaced bone on the side of the striations caused by resistance of the bone to the cut friction ('herzinian cones' Bromage and Boyde, 1984). **A,** × 0.9; **B,** × 0.85; **C,** × 1.3.

unmarked ribs, only 2 of the 15 are complete. Cut-marks are present on 25 of the ribs and occur on the shafts as well as both caudal and sternal ends. Extensive peeling is seen on the human ribs, sometimes on both ends of the fragment and sometimes also on the shaft at the inferior border or broken edges. Percussion marks are frequent on most of the ribs (Fig. 10B).

There is one case of percussion damage on associated human ribs that suggest that this activity took place when the ribs were still anatomically joined together. There are two percussion/chop marks that coincide between the inferior border of rib 5 and the superior border of rib 6 of individual 2 (Fig. 10 B). In addition there is a massive chop mark on the superior border of rib 5 coinciding with a percussion mark on the inferior border of rib 4 from the same individual. Rib 4 also has extensive peeling all along the inferior border on the outer surface (Fig. 11). The inner surfaces of the ribs are affected by cut-marks on 5 human ribs from both individual 1 and 2, and similar marks are seen on a large mammal rib that also bears percussion marks. In any case, the outer surface of the ribs is the most affected area by intensive cutting, percussion and peeling.

Cut-marks on ribs are mainly oblique to the long axis of the bone, but also longitudinal and sometimes transverse around the head of the ribs on both animal (Fig. 12A) and human ribs (Fig. 12B). Scratches related to anvil-hammerstone effect have also been observed on at least two ribs. Fig. 13 shows the actual number of cut-marks found on all human ribs from Gough's Cave.

Tooth marks are recorded on only two human ribs, but they could

Table 3 Human induced modifications observed on ribs and clavicles. The ribs are identified to individual 1 or 2, their number and left or right. Modifications are shown according to their position on the bones (internal surface, outer surface, caudal end, mid-haft, sternal end, and inferior or superior borders). Modifications are identified as c = cutmark; p = peeling; perc = percussion/chop marks. Sequences of modifications are given in order of importance.

Register number: RIBS	Identity	Side	Internal surface	Outer surface	Caudal	Shaft	Sternum	Inferior	Superior
M54016	human; ind.2	1st L		c		c			
M54017	human; ind.2	2nd L		p/c		p/c		p	c
M54018	human; ind.2	3rd L		p	p				
M54019	human; ind.2	4th		c/p/perc		p/perc	c	perc/p	c
M54020	human; ind.2	5th L		perc		perc		perc	perc
M54021	human; ind.2	7th L		(chop)/c/p	c/perc/p	perc(chop)		perc	
M54022	human; ind.2	6th L (2/3 rib)		perc/c	c	perc(chop)	c		perc(chop)
M54023	human; ind.2	8th-9th L (head rib)		c	c			c	
M54024	human; ind.2	8th-9th L (body frag)		c		c			
M54025	human; ind.2	8th-9th L (body frag)							
M54026	human; ind.2	2nd R (1/2 body)							
M54027	human; ind.2	3rd R		perc		perc			
M54028	human; ind.2	4th R		c/p/perc		perc	c/p		chop
M54029	human; ind.2	5th R		c/perc	perc		c	perc	
M54030	human; ind.2	6th R (part body)		c		c			c
M54031	human; ind.2	7th-9th R (head of rib)	c		c				
M54032	human; ind.2	10th R (part body)							
M54001	human; ind.1	1st L		c	c			c	c
M54002	human; ind.1	2nd L (caudal end)							
M54003	human; ind.1	3rd L (caudal end)		p		p		p	
M54004	human; ind.1	4th L							
M54005	human; ind.1	5th L		c			c		
M54006	human; ind.1	6th L							
M54007	human; ind.1	7th-9th L (frag blade)		c/perc		c			perc
M54008	human; ind.1	12th L		p					
M54009	human; ind.1	2nd R	c		c			c	
M54010	human; ind.1	4th R	c			c			
M54011	human; ind.1	5th R							
M54012	human; ind.1	6th R (caudal end)	c	c	c			c	c
M54013	human; ind.1	7th-9th R (shaft)							
M54014	human; ind.1	11th R	c	c	c		c	c	c
M54015	human; ind.1	12th R (part blade)		c/p		c/p		p	c
M54033	human								
M54034	human			c			c	c	c
M54035	human								
M54036	human								
M54038	human								
M54040	human								
M54041	human								
M54052	human	2 indet. fragments							
GC'86 28	equid-cervid			c			c		c
GC'86 28	equid-cervid	L		perc/c		perc/c		p	
	equid-cervid			perc/c	perc	c			
GC'89 3	equid-cervid		perc/c	c	perc/c			p	
GC'90 184	equid-cervid			c					
CLAVICLES									
M54053	human	L	c	c	c	c	c	c	c
M54054	human	R		c/p	p		c	scraping	
M54055	human	R	c	c	c			c	c

not be measured. It is possible that these chewing marks could be human in origin (1 human rib). Carnivore chewing has also been recorded on one deer rib, type a average 1.9, N = 6, and type b average 1.3, N = 5. Trampling marks have been seen on 4 human ribs. Six ribs are weathered, but only to stage 1. One of the human ribs is affected by weathering on the outer side but the inner side looks fresh. Manganese oxide stains are present on one large mammal rib, and one human rib has root-marks on its surface.

Summary of ribs. Total 45 specimens, 40 human, 5 large mammal

Cut-marks: 25 specimens (20 humans, 5 large mammals)
Percussion: 11 specimens (8 humans, 3 large mammals)
Peeling: 8 specimens (8 humans)

Clavicles: There are three specimens of human clavicle, two of them almost complete (Fig. 14). They have cut-marks on both the inner and outer surfaces, caudal, shaft and sternum surfaces, and on both the inferior and superior edges (Table 3). There are no percussion marks, anvil-hammerstone scratches, conchoidal or flakes that may suggest breakage of this anatomical element, though peeling is

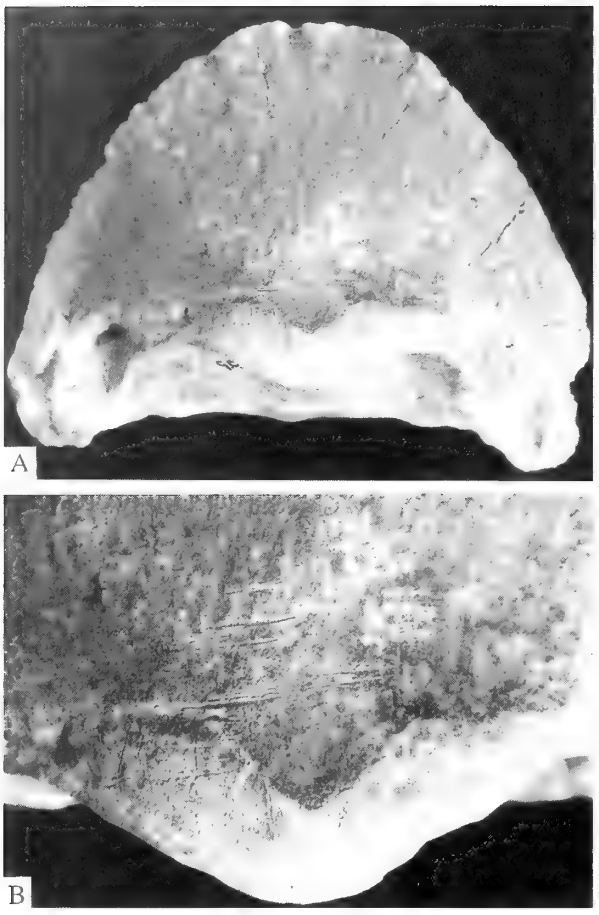

Fig. 8 Two views of distal phalanges of *Equus ferus*. **A,** dorsal view, with transverse cut-marks across the body and dorsal edge of the proximal articulation; **B,** an enlarged view of these cut-marks. **A,** × 1.1; **B,** × 2.2.

present in one of the clavicles (M54054) on the caudal outer surface indicating bending of the bone to dismember or detach the clavicle. Scraping also occurs on this clavicle.

Vertebrae: There are ten human vertebrae in the Gough's Cave material. Most of these were cervical vertebrae, but there were four fragments of thoracic vertebrae, three neural arches and part of one body. It is possible that nine of the vertebrae could be from a single individual (Churchill 2000), and since they were found with the two partial sets of ribs it is likely that they came from one of these individuals. We were able to study seven of the vertebrae (1 axis, 3 cervicals and 3 thoracics), seven of equid (1 atlas, 1 axis, 4 cervicals and sacrum). There are five cervid vertebrae (3 cervicals, 1 thoracic and the 1st caudal). Most vertebrae are affected by human induced damage (Fig. 15), with only two human and two cervid vertebrae that are intact and undamaged. Neural arches are broken in two of the human vertebrae. The vertebral bodies from humans, equids and cervids have cut-marks or percussion marks, especially on the anterior part of the body. The human axis (M54042, Fig. 16A) has cuts on the anterior side of the body along the insertion of the *stylohyoid* muscle (Fig. 16B). Most transverse processes on human, equid, and cervid vertebrae are broken or cut on the posterior part of the vertebra. One human vertebra shows peeling on the transverse processes. The laminae of the vertebrae, especially those of equids, but also of humans and cervids, are also broken (peeled apart in humans) or cut on one side or all round the spinous process.

Tooth marks are abundant on the vertebrae, with five specimens showing chewing or tooth marks, but only a few of these were clear enough to be measured on the equid sacrum. The type of tooth marks are pits on bone surface (a, average 2mm, N = 2), grooves on bone surfaces (b, average 1.6 mm, N = 4), and tooth print (g, 2.9 + 2.9, total length 7.9 mm). Trampling marks have been seen on two cervid vertebrae and manganese oxide stains on three vertebrae of equid.

Summary of vertebrae. Total 19 specimens, 7 human, 7 equid, 5 cervid
Cut-marks: 11 specimens (3 human, 6 equid, 2 cervid)
Percussion: 2 specimens (1 human, 1 equid)
Peeling: 2 specimens (2 human)
Tooth marks: 5 specimens (4 equid, 1 cervid chew mark)

Anatomical elements: flat bones

Pelvis: Two equid pelves are the only specimens found of this element. One specimen has the ileum and part of the acetabulum preserved, the other is almost complete with the pubis recently broken. Cut-marks (Fig. 17) are concentrated along the spine and along the posterior edge on the dorsal side of the ileum, as well as on the ridge below the acetabulum, and chop marks are present on the spine near the acetabulum. The most complete pelvis has cut-marks on similar areas but also including the ischium on both sides (dorsal and ventral). Trampling occurs extensively on one of the pelves, and manganese oxide stains occur on both. Both pelves also have carnivore damage, mainly on the ischium and ventral side of the ileum proximal edge. Types of tooth marks are as follows (Andrews & Fernandez-Jalvo 1997): a (pit marks on bone surface) average 1.5 mm, N = 5; b (grooves on bone surface) average 1.5 mm, N = 4; c (punctures on anatomical borders) average 3.5 mm, N = 2.

Summary of Pelves. Total 2 equid specimens
Cut-marks: 2 specimens

Scapula: The scapula is also poorly represented in the collection, with just four fragments from humans. Cut-marks and scraping marks are extensive on all four scapula fragments. The scapula M54057 which was partially recovered in 1927 has been completed by refitting fragments recovered in 1987. The cuts are mixed on most scapulae with trampling marks (Fig. 18A). Some incisions are definitively human made because they bend without interruptions and pass over and around curvatures in the bone. They are present on both dorsal and ventral sides. Cuts also occur over areas protected by the curvature of the bone (eg. between acromium and the scapula neck; Fig. 18B). In these positions, trampling is impossible because they are deeply recessed, and further the marks are deeply incised, which is not usual in trampling marks (Andrews & Cook 1985). Cuts show a random distribution by direction related to the strong muscle attachments. Scrapes occur on the deeply concave angle between the spine and the infraspinatous fossa. Peeling occurs laterally on two specimens (M54057 and M54059) and the latter also has percussion marks on the spine, probably as result of dismembering processes of the humerus from the scapula. Only one scapula (M54057) shows evidence of weathering which is located along the infraglenoid tubercles along the lateral margin, indicating the scapula was resting with the spine down in the soil.

Summary of scapulae. Total 4 specimens all human
Cut-marks: 4 specimens
Percussion: 1 specimen
Peeling: 2 specimens

Fig. 9 The Gough's Cave excavation showing some of the human ribs in individual 2 being excavated beneath the overhang of the side wall.

Anatomical elements: Cranial

Mandibles: There are three adult human mandibles in the collection, counted as six hemi-mandibles, 12 specimens of equids, and 9 of cervid. All the mandibles are heavily damaged. The equid mandibles consist either of symphysis (50%) or alveolar fragments (50%) with no inferior border or ascending ramus. Most mandibles have some of the premolars and molars *in situ*. Cervid mandibles show a similarly highly destructive pattern, with broken fragments consisting only of portions of alveolus with no inferior border or ascending ramus. The only exception to this pattern is shown in Fig. 19, where a cervid mandible is shown with a dental series and diastema complete to the symphysis. Most mandibles of cervid (56%), but also some horses (33%), show percussion marks on the lingual side, some of them with massive damage (Fig. 19B). Also common are cut-marks on the buccal side (Fig. 19A). Such strength applied to the mandible has produced severe damage, not only to the mandible, but also to most of the teeth, which are seriously crushed (Fig. 19B). It is further peculiar that three of the cervid mandibles and one of the horse mandibles have a triangular shaped percussion mark (Fig. 19B), also seen on a distal metapodial of cervid (M49832). The triangular percussion mark is quite deep, suggesting a forceful stroke.

Human mandibles are also heavily damaged in a similar way, although they have no percussion marks. A complete human mandible (M54137b) has both ascending rami broken. The right hemi-mandible has extensive peeling on the ascending ramus, possibly related to breakage of the articular condyle, and slight breakage is seen along the inferior border close to the mandibular angle (lower angle of the mandible). The left hemi-mandible has the ascending ramus broken in the region of the temporal muscle insertion. (coronoid process) and the articular condyle. Another hemi-mandible shows deep incisions at the ascending ramus (Fig. 20A) probably inflicted as a result of masseter muscle removal.

A third human mandible (M54130a) shows extensive cuts on the lingual surface of the body (along the *linea mylohyoidea*) and also on the buccal side, and there are percussion marks on the buccal side as well. The left ascending ramus is broken at the articular condyle and the right ascending ramus is missing. The inferior border on both sides of the mandible is broken, and peeling is evident on the left side along the fracture edge. Cuts are also present on the symphysis on the lingual side (*fossa digastrica* and *spina mentalis*) (Fig. 20B). It is remarkable that one horse symphysis also shows cuts on the inner margin of the symphysis (Fig. 20C) similar to that seen on humans. This evidence is reinforced by the recovery of the hyoid of a horse that has percussion marks and is extensively cut.

Trampling is evident on equid and cervid mandibles. Weathering has been detected on three mandibles (two of horses and one of deer) at stage 1 and 2/3 on one of the horses. Manganese covers four of the deer and horse mandibles, with the three deer mandibles are heavily stained.

Summary of hemi-mandibles. Total 27 specimens: 6 human, 12 equid, 9 cervid
Cut-marks: 6 specimens (4 human, 3 equid, 2 cervid)
Percussion: 13 specimens (9 equid, 4 cervid)
Adhered flakes: 1 specimen (1 cervid)
Peeling: 5 specimens (1 human, 3equid, 1 cervid)

Fig. 10 **A,** Three human ribs from individual 2, numbering from the top ribs 4, 5 & 6. The inferior border of rib 4 (M54019) has several percussion/chop marks, notably one about one third the way from the caudal end; the superior border of rib 5 (M54020) has a chop mark opposite this mark on rib 4, and it has two percussion/chop marks on its inferior border; the superior border of rib 6 (M554022) has a chop mark opposite the first and a percussion pit opposite the second. These are shown in context in Fig. 11. **B,** Rib of *Cervus/Equus* (GC86-28) with head intact and much of the shaft, with extensive cut-marks along the superior border and percussion marks on the inferior border. **A,** × 0.7; **B,** × 0.55.

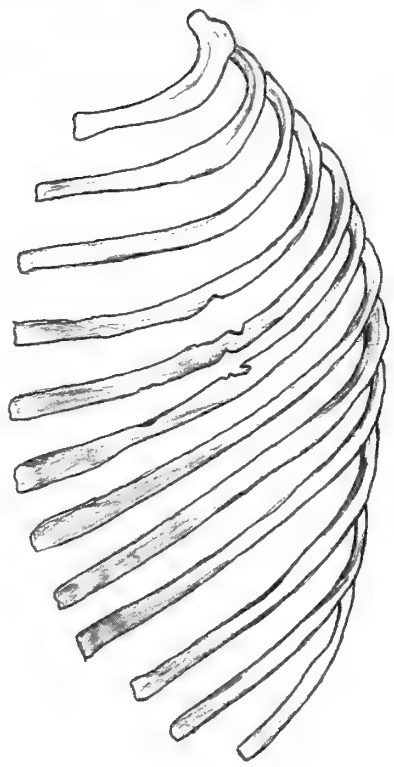

Fig. 11 Drawing of left rib cage with the percussion and chop marks of ribs 4, 5 & 6 shown in the context of the whole rib cage.

Fig. 12 **A,** Caudal end of *Rangifer tarandus* rib, no number, with cut-marks running transversely across the neck of the rib close to the articular facet of the tubercle. **B,** Caudal end of a human rib, M54009, with both ends broken and cut-marks running transversely across the neck of the rib and into the articular facet of the tubercle. **A,** × 1.3; **B,** × 1.4.

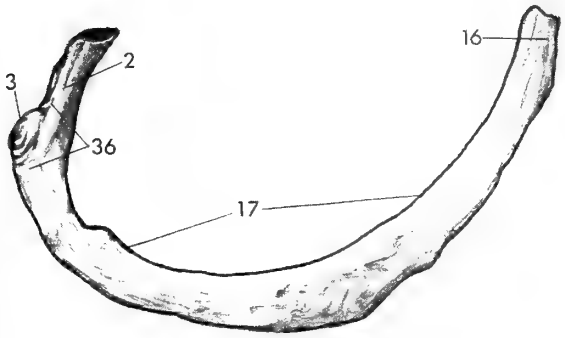

Fig. 13 Generalized view of human rib showing the numbers of cut-marks found on all human ribs from Gough's Cave, and their distribution on the rib.

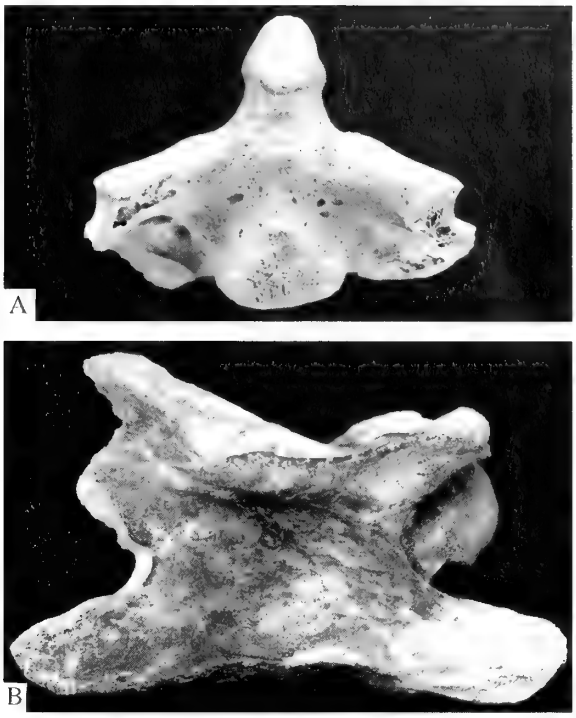

Fig. 15 **A,** Axis vertebra M54042. Numerous cut-marks are present on this bone, particularly along the anterior surface of the body of the vertebra (i.e. on the front of the body, not the back). The conformation of these cut-marks is shown in Fig. 16. There are also cut-marks superiorly next to the articular surface connecting to the atlas vertebra, and in this region there is also peeling of the bone on the lateral aspects on both sides of the articulations. **B,** Cervical vertebra of *Equus ferus* (M50068) with cut-marks along lateral-ventral surface. Cut-marks are short and concentrated along the anatomical edge probably related to the detachment between vertebrae. **A,** × 1.2; **B,** × 0.65.

Maxillae: There are two human palates, and three half-maxillae of equid and four of cervid. Two human half-maxillae, with both zygomatics broken, are from the same individual (M54130b), and they fit with mandible M54130a described above (Fig. 21A). The muscle insertions of the nose and lips (levator muscles and the zygomatic and masseter muscles) are affected by cut-marks on the human specimen, which also has cut-marks on the front of the palate. Apart from cuts, the nasomaxillary bone is heavily modified around the lips and nose, and this is similar to cut-marks seen on the buccal surfaces of the molars (Figs 22, 23) as it is observed in other cannibalistic sites (Atapuerca in Spain, Fontbrégoua in France and

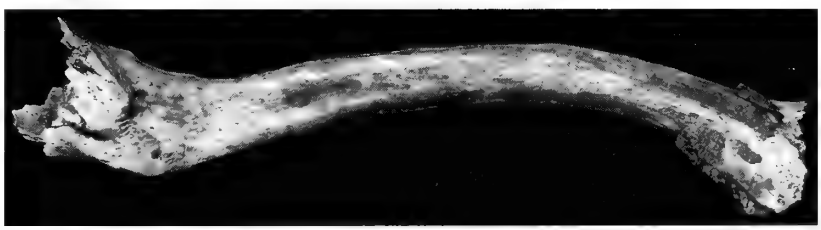

Fig. 14 Right clavicle M54055 diaphysis. Cut-marks are present in two places, two marks on the deltoid insertion and two also where the *cortoclavicular* ligament attaches to the shaft of the clavicle; × 1.

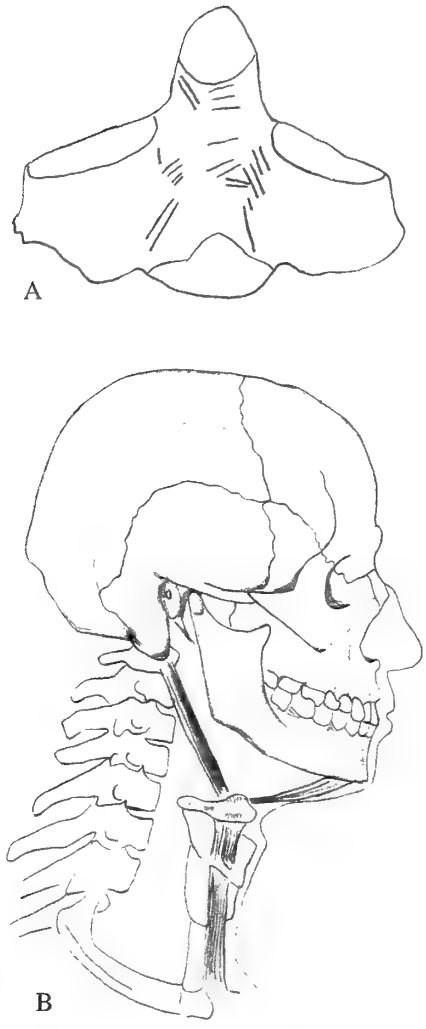

Fig. 16 **A,** Human axis vertebra M54042 showing the conformation of the cut-marks along the anterior surface. This is the area of attachment of the anterior longitudinal ligament, and in addition the superior marks are probably related to the detachment of the axis from the atlas, and the posterior marks to the detachment of the axis from the third cervical vertebra; × 1.2. **B,** Schematic drawing of human skull and upper vertebrae showing the disposition of two muscles that insert on the internal surface of the mandibular symphysis (digastric muscle) and the back of the skull (stylohyoid muscle).

Anasazi pueblos in States). Breakage of the zygomatic arches is necessary in order to remove the *temporalis* muscle so as to open the vault for access to the brain tissues.

Other animal maxillae are heavily broken, with only alveolar fragments and few premolar and molar preserved *in situ*. Horses show percussion marks on buccal and lingual sides, or only on the buccal. Cut-marks have not been seen on the bone of horse maxillae, but there are two specimens that show oblique cuts on the buccal side of the premolar/molar toothrow (Figs 21B, 22). Extensive percussion marks appear on both the lingual and the buccal sides of horse maxillae, and one specimen has adhered flakes also on both sides. It is interesting to note that one horse maxilla has peeling on the palate.

Fig. 17 Innominate of *Equus ferus* M50028. This bone has been extensively modified, with loss of the extremities and many trampling marks on both surfaces. There are many carnivore tooth marks on the upper border of the ilium, and four chop marks are also present crossing the spine near the superior border of the ilium. More inferiorly there are numerous cut-mark incisions concentrated along the spine; × 0.8.

With regard to cervids there are cuts only on the buccal side of the maxilla, along the dental series (Fig. 21C). Percussion marks on the lingual side have only been seen on one cervid specimen. No teeth have cut-marks on cervid maxillae, but the teeth are heavily crushed on the lingual side or broken.

Summary of hemi-maxillae: Total 9 specimens, 2 human, 3 equid, 4 cervid
Cut-marks: 6 specimens (2 human, 2 equid, 2 cervid)
Percussion: 6 specimens (2 human, 3 equid, 1 cervid)
Adhered flakes: 1 specimen (1 equid)
Peeling: 1 specimen (1 equid)

Skull: There are three human calottes (frontal, parietal and most part of the occipital) of an adult, adolescent and child. The adult skull is almost complete, although the face is missing (broken at the orbital region and maxilla), and a frontal fragment. There are two cervid skulls, both broken but there is no conclusive evidence of human damage. One of the cervid skulls shows weathering at a stage 1.

The human calottes show similar patterns to each other regarding cut-marks and percussion marks. Extensive and long cut-marks are present on the temporal insertions of the parietal bones on both sides (Figs 24A, C). Many cuts are also present on the frontal bones (Fig. 25) and on the supraorbital ridges (insertions of the *orbicular* and *superciliary* muscles), as well as in the eye sockets to extract the eyes (Fig. 24B). On the occipital bones, cuts are also seen along the

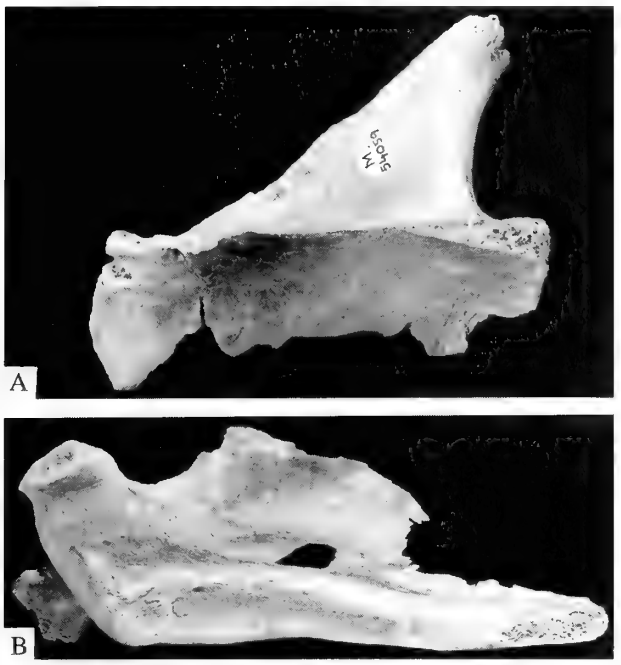

Fig. 18 **A,** Left scapula with the spine and part of the inferior blade of M54059. There are many trampling marks mixed in with cut-marks, and it is sometimes hard to distinguish them. Numerous scrapes occur in the deeply concave angle between the spine and the infraspinous fossa, with percussion marks on the edge of the inferior border. There are also percussion marks and peeling on the acromion process. The scrape marks are not straight, bending without interruption over and around curves in the bone surface, and they cut across several incisions perpendicular to the general trend of the scrapes, the cut-marks clearly preceding the scrapes. In the angle between the acromion and the scapular neck, cranial orientation, there are two oblique and deep incisions not visible on this view but similar to the ones in M54056. **B,** Right scapula M54056. Two incisions, one deep and the other shallow, are present in the angle between the acromion and the neck of the scapula, and in addition several cut-marks are present in the inferior angle of the scapular blace at the insertion of teres major. **A,** × 0.9; **B,** × 0.65.

sutures with the parietal bones, covering the insertion area of the *trapezius* and *sternocleidomastoid* muscles (Figs 24D, 25B). Percussion marks appear superimposed on cut-marks on the parietal bones at both sides (Fig. 24C) and cuts appear interrupted by the broken edges. Incipient peeling has been seen on the zygomatic arches, and some removed flakes on the broken edges (i.e. left side of the sphenoid bone and occipital bones).

Summary of skulls. Total 5 specimens = 3 human and 2 cervid)
Cut-marks: 2 specimens (2 human)
Percussion: 2 specimens (2 human)
Removed flakes: 2 specimens (2 humans)
Peeling: 2 specimens (2 human)

DISCUSSION

Large mammal species diversity recorded at Gough's cave is quite poor, with most remains assigned to three species of large mammals, *Homo sapiens*, *Equus ferus* and *Rangifer tarandus*.

The human skeletal element proportions are generally higher than those of any of the other large mammals. Ribs and cranial remains are the best represented for humans, but paradoxically, vertebrae are rare, whereas for the animal bones ribs are almost absent but vertebrae and especially phalanges and metapodials are much better rbepresented. Phalanges in particular are not commonly represented in human occupation sites. The relative abundances of anatomical elements suggest a type of selection for large mammal skeletons for heads and distal limbs, in contrast to human skeletons, for which elements from the thorax (except vertebrae), heads and arms have been selected.

The cranial skeleton is the most extensively damaged anatomical element, both in humans and large mammals (equids and cervids). Human skulls and faces at Gough's Cave have a higher intensity of cut-marks than are present on non-human animals, but contrasting with this, two of the human skulls are almost complete. Skull completeness differs greatly from site to site where cannibalism has been considered to be nutritional (i.e. TD6-*Aurora Stratum*, Spain), the Neandertal site of Moula-Guercy (France Defleur, *et al.*, 1999), or modern ones where fire is involved such as Native American sites

Fig. 19 **A,** lingual, and **B,** buccal views of deer mandible (*Rangifer tarandus*), M49821. The buccal view shows numerous cut-marks along the diastema, and the lingual view shows one and possibly two percussion marks near the alveolar border; both × 0.5.

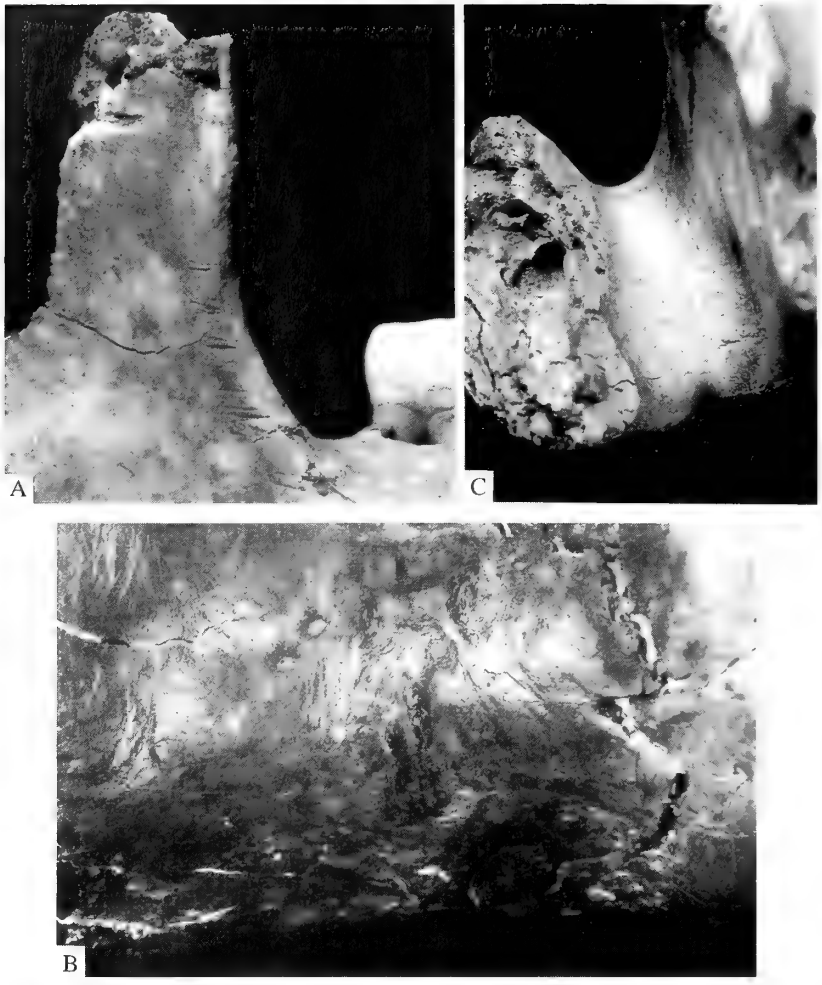

Fig. 20 **A,** Human mandible (GC'87) showing deep incisions on the ascending ramus as a result of dismemberment of the mandible probably inflicted as a result of *masseter* muscle removal. **B,** Detail of cut-marks on human mandible M54130a. The cuts are on the mandibular symphysis on the lingual side along the internal ridge, at the insertion of the *digastric* muscle. **C,** Mandible of *Equus ferus* M49848. Cut-marks are on the mandibular symphysis on the lingual side, and on the lingual border of the mandibular body close to the alveolar margin and on the lingual border of the diastema. **A,** × 2; **B,** × 3; **C,** × 1.2.

(USA, Turner and Turner, 1999; White, 1992), Navatu (Fiji Islands, Degusta, 1999). At all these sites, damage to the human skulls is great and it is interpreted as the result of gaining access to the brain. The only other cannibalistic site where human skulls are relatively complete is at Fontbrégoua (French Neolithic) where Villa *et al.* (1986a&b) interpreted it as an element of skull ritual treatment. We agree with this interpretation in relation to the Gough's Cave material because completeness of skulls, even where they have been damaged by percussion and intensive cutting, is an exception to the general pattern of the Gough's Cave assemblage. Animal skulls are notable for their absence, and most other skeletal elements, with the exception of the limb extremities and some of the human ribs, are all broken. The human skulls stand out as the most intact groups of bones that by their nature are relatively easily broken by post-depositional processes.

The jaws in particular have been heavily broken and cut. Most large mammal jaws recovered from the site consist of alveolar fragments, with or without teeth. Teeth are damaged by crushing, especially in cervids, but also in humans. There is a peculiar butchering technique observed on these specimens consisting of intensive cutting on the buccal side, and strong percussion marks on the lingual side. These suggest dismemberment of the mandible and cutting of the muscles of mastication and the lip depressors. Cut-marks lingually, particularly on the symphysis in the digastric area on both equids and humans, indicate removal of the tongue. Cut-marks have also been found on the enamel of horse upper molars on the buccal side. These cuts have also been observed at other sites such as Abric Romani (~40,000 BP. Barcelona, Spain), and here they have been interpreted as cutting of facial muscle attachments to extract the cheek.

Damage is also seen on human jaws with breakage of zygomatic arches on the upper jaws, and inferior borders and ascending ramii of mandibles. Similar destruction of human remains also appears at Native American sites (White, 1992; Turner and Turner, 1999), Fontbrégoua (Villa *et al*, 1986 a, b) and especially at TD6-*Aurora Stratum* (Fernández-Jalvo *et al.*, 1999), where no complete cranial element (skull vault, mandible or maxilla) has yet been found. Some authors have considered that this degree of intensive damage of faces

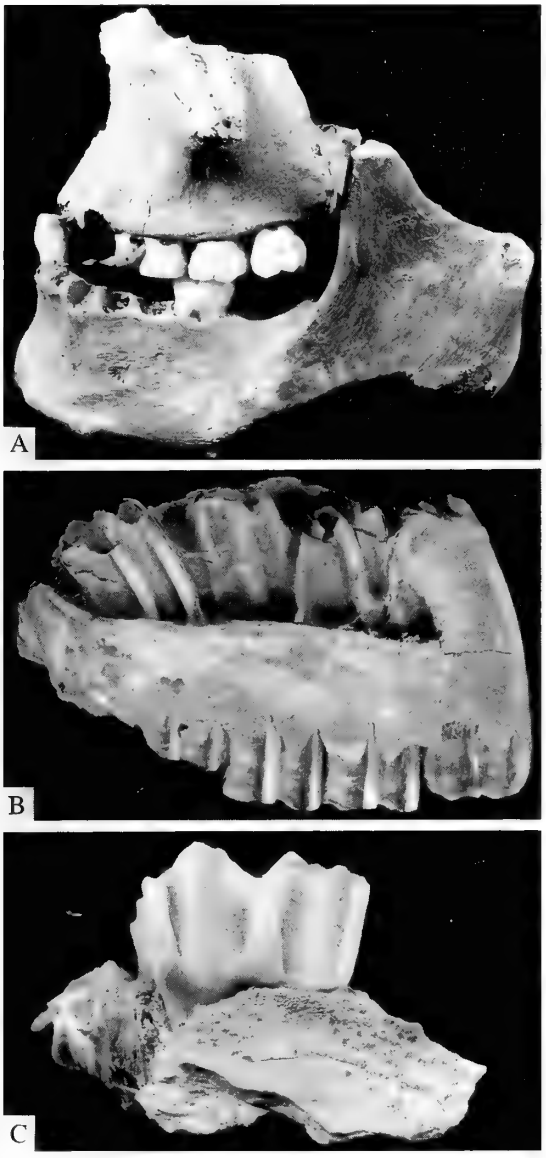

Fig. 21 **A,** Human maxilla (M54130a) and mandible (M54130a) from a young individual. The jaws are heavily damaged by percussion and cutting. The maxilla has both zygomatic arches broken and extensive cuts on the *masseter* insertion, as well as on the face above the canines where the lips attach, and on the palate. Cuts on the mandible are present on both lingual and buccal sides of the mandible. Also in the area of the medial *pterygoid* insertion and coronoid process the inferior border is broken and the ascending ramus broken. **B,** Maxilla of horse *Equus ferus*, GC89-061. The body of the maxilla is broken, with several percussion marks along the broken edge and one on the undamaged surface of the bone. There are also two sets of cut-marks passing diagonally across the buccal sides of the teeth which are shown in the next figure. **C,** Maxilla of red deer M49981, with cut-marks just below the alveolar margin on both the buccal and lingual surfaces. **A,** × ??; **B,** × 0.5; **C,** × 1.2.

and jaws is evidence of violence and destructive intent of mutilation of a possible enemy (Turner and Turner, 1992). In Gough's Cave, large mammal jaws have similar degrees of destruction to human jaws and faces and, we therefore do not consider this evidence as indication of human-to-human violence.

Cook (1986) also rejected any interpretation of violence on the Gough's Cave assemblage. Cook's critical review of the marks recorded on these fossils led her to interpret most marks on the human bones as being due to trampling (Andrews & Cook 1985, Cook 1986). In fact, Cook considered as the only firm evidence of deliberate human interference some marks on the buccal surface and inferior border of the adult mandible (M54130, Gough's 6). Cook (1986) considered these marks as related to removal of the tongue. It is remarkable that one horse mandible has also cuts on the inner inflexion of the symphysis (Fig. 20C), similar to the location on the human jaw (Fig. 20B), and this also suggests extraction of the tongue. Intensive cuts (and percussions) on an equid hyoid could indicate the same thing, as well as cuts on the anterior side of the human axis body (see Fig. 16) where hyoid ligaments attach.

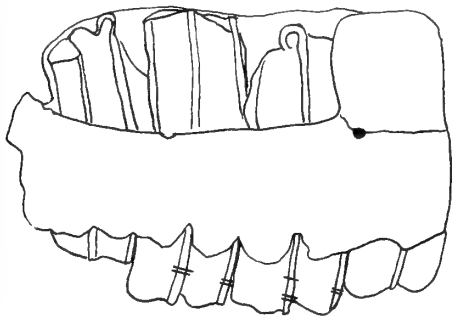

Fig. 22 Drawing of maxilla of horse *Equus ferus*, GC89-061, showing the locations of the two sets of cut-marks running along the buccal side of the crowns of the teeth. The marks appear to be lined up in two series running obliquely down mesially.

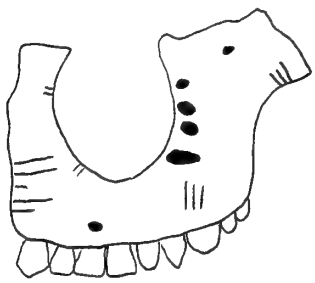

Fig. 23 Oblique frontal view of M54130, juvenile maxilla showing the location of cut-marks on the frontal aspect around the lips and nose and on the zygomatic.

No fragments of equid skulls have been recovered from Gough's Cave. Skull fragments of cervids (a calvaria and a frontal fragment) have no conclusive evidence of human-induced damage. In contrast to this, the two human skulls are heavily damaged by cut-marks and later percussion marks, but despite this, both were recovered almost complete. The adult calvaria was found virtually in one piece, but the

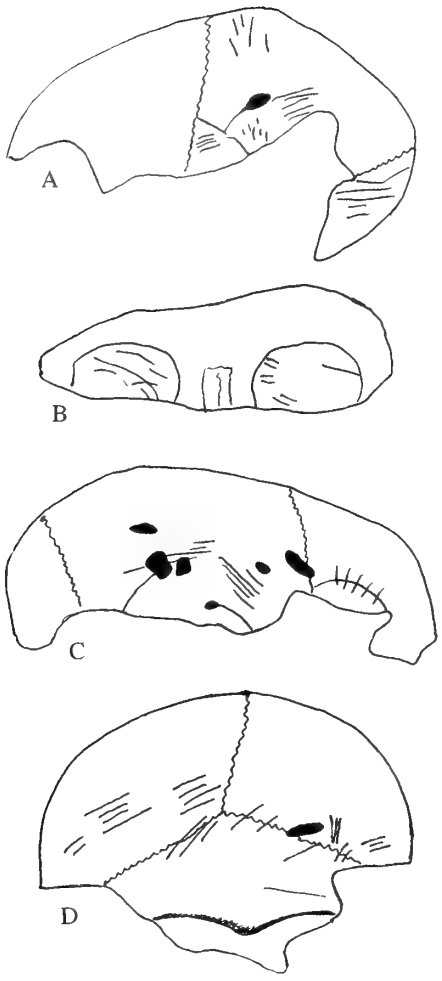

Fig. 24 Four views of human calvaria. **A,** lateral view of child's skull M54141 showing cut-marks and one percussion mark causing extensive cracking of the skull. **B,** frontal view showing cut-marks inside the orbits. **C,** lateral view of skull 460a, showing percusssion marks superimposed on cut-marks along the temporal muscle insertion. **D,** back view of the same skull showing extensive cut-marks in the broken occipital region.

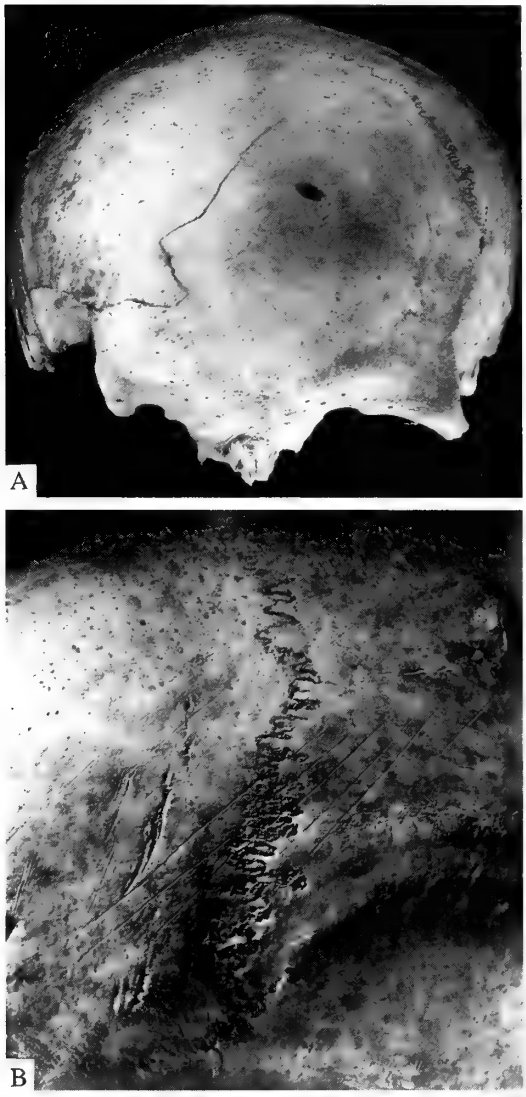

Fig. 25 **A,** Frontal view of the GC87 calotte showing cut-marks low down on the frontal bone. **B,** detail of the parietal (left) and occipital bones of the same calotte showing the cut-marks in this region. **A,** × 0.6; **B,** × 1.1.

child calvaria was fragmented by post-depositional damage, due to the greater fragility of its bones. This is in contrast to traits observed at the site of Atapuerca (TD6-*Aurora Stratum*, Spain) where mandibles and skulls of both humans and non-humans were highly broken, and cuts appeared on areas related to dismembering rather than skinning. In the light of taphonomic analyses of the Atapuerca TD6-*Aurora Stratum* fossil assemblage, the cause of cannibalism was considered to be purely nutritional, and probably gastronomic (Fernández-Jalvo, *et al.*, 1999).

Southwest Native Amerindian sites (White, 1992; Turner and Turner, 1999) have many skull fragments found mixed with complete skulls. These skulls, however, have evidence of heating which would make the face and head muscle attachments easier to remove. The use of fire has also been identified at the human sample of the Navatu Fijian assemblage (Degusta, 1999), and burning is focused on the head (41%) compared to post-cranial elements (16%). More significantly, the effects of fire are seen more commonly on human remains than on other taxa. In this case, however, Navatu skulls appear highly broken.

The Neolithic site at Fontbrégoua (France) has human skulls that are more complete than non-human skulls (with the exception of bovids). This contrasts with the Native American and Fijian sites. In addition, burning has not been detected on the fossil bones, and this has been interpreted as a case of ritual treatment of skulls and exocannibalism (Villa *et al.*, 1986b). Completeness of human skulls at Gough's cave is quite peculiar due to the fact that they are highly damaged by percussion marks. These contradictory results (strong damage and completeness) may suggest that the skulls were carefully treated to preserve them complete, in contrast to the rest of the skeleton and other animals at the site.

Ribs of both human and large mammals are extensively affected by human induced damage. Cut-marks, percussion marks and peeling

are frequent and affect both inner and outer surfaces of the ribs, and some other ribs are also heavily damaged by chop marks. Cut-marks on the inner surfaces have been interpreted as due to evisceration (Diez et al. 1999). Cuts and chop marks on adjacent ribs shows that the damage was inflicted while the rib cage was more or less intact, and the purpose must have been to gain access to the thoracic cavity while at the same time dismembering the ribs. The concentration of marks near the heads of the ribs suggests that the aim was to separate the ribs from the vertebrae (see Fig. 13, above). On the other hand, many of the ribs remained intact, with no further damage, and the ribs from individuals 1 and 2 were discarded within a very small area of the cave. Damage observed on the ribs thus suggests the commonest processes operating on both animal human bodies was dismemberment, filleting and possibly evisceration.

Vertebrae of all taxa recorded at Gough's cave have similar types of damage induced by humans. Cuts appear on similar sides and damage of the transverse or spinous processes are similar. Peeling only occurs on human vertebrae. The human axis and the equid atlas both show cuts on the articulation with the adjacent vertebrae in order to dismember the neck and head. The cuts observed on the front (ventral) of the human axis body are matched by cuts on the hyoid bone and may have been related to detachment of the hyoid. In summary, vertebrae show clear evidences of dismemberment activities, both in humans and non-human skeletons.

Human vertebrae are scarce at Gough's Cave and this is in agreement with Turner's (1983) observations that a characteristic of cannibalism is that vertebrae are usually missing. Turner explains the low representation of vertebrae as a result of having first been crushed on an anvil stone to then the fragments boiled to facilitate oil extraction. He suggests this hypothesis based on ethnographic descriptions of the boiling of animal bones for marrow extraction. Scarcity or absence of vertebrae has been observed among the Prehistoric American Southwest from Arizona (e.g.: Pollaca Wash, Leroux Wash, House of Tragedy, Canyon Butte, Chaco Canyon and others studied by Turner and colleagues 1970–1999) and at the Anasazi pueblo of Mancos (White, 1992), as well as at the French Neolithic of Fontbrégoua (Villa *et al*, 1986a,b), Navatu of Fijian groups (Degusta, 1999), and French Neanderthals (Defleur & White, 1999). Turner & Turner (1995) observed that vertebrae were absent or crushed at the prehistoric and historic Arizona sites. On the other hand, vertebrae are not scarce at the Atapuerca (TD6-*Aurora* Stratum) human assemblage among the early Europeans (Fernández-Jalvo et al. 1999), but here there is no evidence of fire. Villa, *et al* (1985) did not find evidence of fire at Fontbrégoua, and absence of vertebrae was considered as due to humans having moved the discarded bones into 'amas' (discard features). No evidence of burnt bones at Gough's Cave has been observed, but there is similar pattern of breakage and cutting between human and non-human vertebrae.

Four human scapulae, three clavicles and two horse pelves have been recorded at Gough's Cave as the only flat bones. Both scapulae and pelves are intensively damaged by cut-marks and percussion marks. The damage is mainly related to areas of muscle attachments, for example the muscle attachment of *rectus femoris* on the ilium. In the case of scapulae, which all come from humans, they also show peeling as evidence of stripping muscle from the scapula. All cuts found on the scapulae were interpreted by Cook (1986) as the natural effect of trampling processes (notably specimens M54059 and M54056). The cut-marks on these specimens, however, are deeply incised, their positions are often on protected areas of the bone that cannot be reached by sediment grains, and finally most of the cuts are located on areas associated with muscle attachments. They are also concentrated around the glenoid fossa, suggesting disarticulation of the shoulder joint, and they are seen on the muscle attachment areas of *trapezium, triceps, subscapular, teres major* and *teres minor* muscles. In contrast to this, if trampling were the only agent of modification that produced striations, it would be expected that the most salient angles of the scapula, such as the scapular spine or the outer edge of the coracoid process, should be most heavily damaged (Andrews & Cook 1985, Olsen & Shipman 1989). They are not cut, but on the contrary the cut-marks are on the inner angles of these processes. This leads us to the conclusion that the cuts were human-made, although it is certainly true that there are trampling marks as well as cut-marks. On the clavicles, cut-marks are related to muscle attachments, for example the *sternocleidomastoid* on M54054) and the *costoclavicular* ligament, indicating the purpose was dismemberment of the joints.

Most cut-marks on long bones, both on human and on animal, are related to muscle attachment or articular surfaces, indicating dismembering activities. There is also a case of filleting (a right human radius split shaft) with cuts that are not related to muscle attachment. Breakage to open the marrow is more evident on large bones (i.e. femora, humeri, tibiae) than on bones with no marrow content (i.e. radii, ulnae and fibulae). Most long bones, either human or animal bones, show strong percussion marks that occur extensively along the shafts and broken edges, and sometimes percussion marks are seen related to anvil marks. Repeated blows to the shaft are seen on some bones, for example on the human tibia. Adhered flakes, removed flakes, peeling and conchoidal scars related to longitudinal breakage of the bone most probably came about as the result of extracting the marrow content in the bone. Peeling occurs only on human bones (two ulnae, a radius, and a tibia fragment), but it is absent on other animal long bones. Binford (1981) considers scraping and peeling to be linked to the preparation of the bone for subsequent breakage and marrow extraction, since soft tissues might absorb much of the force when the attempt is made to break the bone. On the other hand, Díez *et al.* (1999) considered that periosteum extraction may also be an end in itself, aimed at getting at all of the animal's nutrients. Breakage to open the marrow is more evident on large bones (i.e. femurs, humeri, tibiae) than in no marrow content bones (i.e. radii, ulnae and fibulae). Most long bones, either human or animal bones, and broken edges, and sometimes percussion marks related to anvil marks.

Wrist and ankle bones are present only for large mammals, mostly horse. On these skeletal elements, cut-marks occur most frequently on calcanei (5 out of 8 specimens). Cut-marks on calcanei are mainly located on the calcis, on plantar and dorsal edges, as well as on the articulation between calcaneus and astragalus. Just one calcaneus has a chop mark and it is located on the calcis. Astragali have more cuts on the medial side of the condyle or on the trochlea related to the medial ligament. The other carpal-tarsal bones are damaged on the dorsal sides at the position of the dorsal ligament. In all cases the main purpose appears to be to cut ligaments connecting the lower leg and the metapodials. One central tarsal has an adhered flake on a broken surface on the articular dorsal ridge, probably due to dismemberment.

There are a few human metatarsals, all crushed on the ends but without cut-marks. Lateral metapodials of equids are also crushed on their articular ends as seen on humans. Some human metapodials could have human chewing (Fig. 6). Metapodials are much more abundant in the case of non-human mammals, more than a 50% of them with cut-marks, mainly located on the articulations (Fig. 5A), suggesting dismemberment of the joints. Medial metapodials of horse have a consistent pattern of breakage (Fig. 5B) that has produced great consistency of preservation of the metapodials, and this is probably the result of marrow extraction.

Most phalanges come from equids, with only one of human

Table 4 Surface damage induced by humans and other taphonomic agents at Gough's Cave. The human-induced damage is shown in the top part of the table, and all different types of modification are shown combined in the lower part for comparison with non-human taphonomic modifications

Human induced damage	Cut-marks	Percussion marks	Conchoidal scar	Adhered flakes	Removed flakes	Peeling	Overall human
human	48.9%	26.1%	1.1%	3.4%	3.4%	22.7%	69.3%
equid	37.1%	31.8%	3.8%	1.5%	1.5%	3.0%	73.5%
cervid	50.0%	23.8%	0.0%	4.8%	4.8%	0.0%	57.1%
large-mammal indet	100.0%	100.0%	60.0%	0.0%	0.0%	0.0%	100.0%
Taphonomic damage	Overall human	Trampling	Weathering	Mn oxides	Root-marks	Chewing	
human	69.3%	8.0%	9.1%	2.3%	1.1%	2.3%	
equid	73.5%	3.0%	17.4%	1.5%	0.8%	1.5%	
cervid	57.1%	14.3%	4.8%	21.4%	0.0%	4.8%	
large-mammal indet	100.0%	0.0%	20.0%	20.0%	0.0%	40.0%	

phalanx and four of cervid. Cut-marks and percussion marks appear near the articular surfaces, suggesting dismemberment activities. Terminal phalanges are only known for horse and they have cut-marks at both the palmar and dorsal sides, which is uncommon. Human phalanges are rare and have no cut-marks at cannibalistic sites, like Mancos, Fontbrégoua, Navatu (Turner & Turner, 1990; Villa *et al.* 1986a and 1986b ; White, 1992, Degusta, 1999), and now also Gough's Cave. In contrast to this, there are 16 phalanges from six individuals (5%), some of them cut (19%), at the Atapuerca site (Fernandez et al. 1999). The Neanderthal site of Moula-Guercy (France) has few phalanges too, 9 from 5 individuals, but four of them were cut (44%) and two smashed (22%).

Human-induced damage is the most frequent modification observed on the fossil bones recovered from Gough's Cave (Table 4). Percentages of modifications produced by humans are high, much higher than at other sites where cannibalism has been taphonomically studied (Fig. 25) with the exception of Fontbrégoua (Villa et al. 1986a&b). For instance, nearly half the modifications on fossil bones of both human and non-human species are cut-marks. The high percentage is partly the result of the refitting of bones before the taphonomic analysis was carried on. Weathering, manganese oxide stains, root-marks, chewing do not have a special relevance at the site (Table 5). Chewing mark measurement indicate a small carnivore sized like fox: average tooth mark sizes are1.8mm (N = 23) for surface pits (category a of Andrews & Fernandez-Jalvo 1997); 1.5mm (N = 36) for striations of diaphysis surface (category b); and 2.4mm (N = 25) for punctures on articular ends. These values are similar to those found for a sample of recent sheep bones chewed by foxes (Andrews & Armour-Chelu 1998). Most fossils affected by chewing are complete, and chewing is not related to broken edges (types **d**, **e** or **f**). These traits strongly suggest that the carnivores chewing the bones of the Gough's Cave fossil assemblage could not break the bone but could only chew the surfaces of the bones.

One of the difficulties in analysing the taphonomy of the Gough's Cave assemblage is that much of it comes from old excavations where bone distribution were not recorded. Fortunately, the 1986–87 excavations recorded these data and showed that human and non-human skeletal elements were randomly mixed (Fig. 9). There was also a very high density of finds per square meter, which appears to be proportionally higher than from the old excavations, but it should be noted that the 1986–87 excavations were close to an overhanging wall in the cave, and the higher concentration of remains may be due to preferential preservation in this area protected by the wall. One final point is that no evidence of burning or cooking has been found at Gough's Cave fossil assemblage.

CONCLUSIONS

The single most important conclusion arising out of our analyses is that the butchering techniques observed on human and non-human skeletons at Gough's Cave are similar, apart from differences arising out of differences in body weight. All activities associated with human butchering have been recorded on human and non-human skeletons (Table 5). Peeling, a type of fracture similar to bending a fresh twig between two hands, provides a specific breakage pattern, but it only occurs on human (with the exception of large mammal jaws), and this is related to the lighter body weight and size of humans.

The one major exception to this is the difference in skull completeness. The survival of relatively complete human skulls, despite extensive cut-marks and percussion damage seen on the skulls, indicates special treatment, for in all other cases these processes have resulted in high degrees of breakage, even when the bones thus broken were more robust than thin-walled human skulls. This suggests there may be a ritual element in the treatment of human skulls.

Human and non-human jaws have a high degree of breakage, and the location of cut-marks suggests tongue extraction on both humans and horses. Ribs of both human and large mammals are extensively damaged. Cut-marks and percussion damage suggest dismembering, filleting and evisceration. Vertebrae show clear evidence of dismemberment activities, both in humans and non-human skeletons, although peeling on the vertebrae is restricted to humans.

Table 5 Butchering activities identified at Gough's Cave

		Equid	Cervid	Homo
CRANIAL	Dismembering	•	•	•
	Filleting	•	•	•
	tongue extraction	•		•
	Skinning			•
AXIAL	Dismembering	•	•	•
	Filleting	•		•
	Marrow extraction			
	Evisceration	•	•	•
LIMBS	Dismembering	•	•	•
	Filleting			•
	Marrow extraction	•	•	•
	Periosteum removal	•		•
EXTREMITIES	Dismembering	•	•	•
	Filleting			
	Marrow extraction	•		
	Periosteum removal			

Similarly, peeling only occurs on lightly built long bones (e.g.: human radii and ulnae) with low marrow content. Most large long bones show strong percussion marks that occur extensively along the shafts to extract the marrow content in the bone. Long bones have cut-marks related to dismembering activities (filleting in humans) and periosteum removal shown by the location of scraping marks. Flat bones (human scapulae and horse pelves) are intensively damaged in areas of strong muscle attachment. Human metapodials also show similarities with lateral metapodials of equids, both of which have crushed articular ends.

Taking into account the high similarities in butchering techniques seen on both human and non-human bones, further similar patterns of long bone breakage for marrow extraction, and identical patterns of post-processing discard of human and animal remains in the Gough's Cave sediments, we conclude that this is a case of nutritional cannibalism.

ACKNOWLEDGEMENTS. We are grateful to Chris Stringer, Andrew Currant and Robert Jacobi for offering us the study of Gough's Cave fossil assemblage, and for help and information about the site and the fauna. The study was supported by the European Communities grant (ENV4-CT96-5043) to YFJ.

REFERENCES

Andrews, P. & Cook, J. 1985. Natural modifications to bones in a temperate setting. *Man,* **20**: 675–691.

—— **& Fernández-Jalvo, Y.** 1997. Surface modifications of the Sima de los Huesos fossil humans. *J. Hum. Evol,.* **33:** 191–217.

Arens W. 1979. *The Man Eating Myth: Anthropology and Anthropophagy.* Oxford: Oxford University Press.

Behrensmeyer, A.K. 1978. Taphonomic and ecologic information from bone weathering. *Paleobiology,* **4:** 150–162.

Binford, L.R. 1981. *Bones. Ancient Men and Modern Myths.* New York: Academic Press.

Blumenschine, R.J. 1988. An experimental model of the timing of hominid and carnivore influence on archaeological bone assemblages. *J. Archaeol. Sci.,* **15:** 483–502.

—— **& Selvagio, M.M.** 1988. Percussion marks on bone surfaces as a new diagnostic of hominid behavior. *Nature,* **333**: 763–765.

Bromage, T.G. & Boyde, A. 1984. Microscopic criteria for the determination of directionality of cutmarks on bone. *Am.J. Phys. Anthrop.,* **65**: 359–366

Cook, J. 1986. Marked human bones from Gough's cave, Somerset. *Proc. Univ. Bristol Spelaeol. Soc.,* **17**: 275–285.

Charles, R. 1998. Cresswell, Cheddar and Paviland. *Current Archaeology,* **160**: 131–135.

Churchill, S. 2000. The Creswellian (Pleistocene) human axial skeletal remains from Gough's Cave (Somerset, England). *Bull. Nat. Hist. Mus. Lond. (Geol.),* **56:** 141–154.

—— 2001. The Creswellian (Pleistocene) human upper limb remains from Gough's Cave (Somerset, England). *Bull. Nat. Hist. Mus. Lond. (Geol.),* **57:** 7–24.

Currant, A.P.; Jacobi, R.M. & Stringer, C. 1989. Excavations at Gough's Cave, Somerset 1986–7. *Antiquity,* **63**: 131–136

Defleur, A., White, T., Valensi, P., Slimak, L. & Crégut-Bonnoure, E. 1999. Neanderthal cannibalism at Moula-Guercy, Ardèche, France. *Science,* **286**: 128–131.

Degusta, D. 1999. Fijian Cannibalism: osteological evidence from Navatu. *Am. J. Phys. Anthrop.,* **110**: 215–241.

Díez, J.C., Fernández-Jalvo, Y., Rosell, J. & Cáceres I. 1999. The site formation (Aurora Stratum, Gran Dolina, Sierra de Atapuerca, Burgos, Spain). *J. Hum. Evol.,* **37**: 623–652.

Fernández-Jalvo, Y., Díez, J.C., Cáceres, I. & Rosell, J. 1999. Human cannibalism in the early Pleistocene of Southern Europe (Sierra de Atapuerca, Burgos, Spain). *J. Hum. Evol.,* **37**: 591–622.

Flinn, L.; Turner, C.G.II & Brew, A. 1976. Additional evidence for cannibalism in the Southwest: the case of LA 4528. *Am. Antiquity,* **41**: 308–318.

Olsen, S. & Shipman, P. 1988. Surface modification on bone: trampling versus butchery. *J. Archaeol. Sci.,* **15**, 535–553.

Shipman P. & Rose, J. 1983. Early hominid hunting, butchering and carcass-processing behaviours: approaches to the fossil record. *J. Anthrop. Archaeol.,* **2**, 57–98.

Stringer, C. 2000. The Gough's Cave human fossils: an introduction. *Bull. Nat. Hist. Mus. Lond. (Geol.),* **56**: 135–139.

Taylor, P.D. 1986. Scanning electron microscopy of uncoated fossils. *Paleontology,* **29**, 689–690.

Trinkaus, E. 2000. The Creswellian (Pleistocene) human lower limb remains from Gough's Cave (Somerset, England). 2000 *Bull. Nat. Hist. Mus. Lond. (Geol.),* **56:** 155–161.

Turner, C.G. II. 1983. Taphonomic reconstruction of human violence and cannibalism based on mass burials in the American Southwest. In G. LeMoine & S. MacEachern (editors) *Carnivores, Human Scavengers and Predators: a Question of Bone Technology.* Proceedings of the XV Annual Conference of The Archaeological Association of the University of Calgary.

—— 1988. Another prehistoric Southwest mass human burial suggesting violence and cannibalism: Marshview Hamlet, Colorado. In: (G.T.Gross and A.E. Kane, compilers) *Dolores Archaeological Program: Aceramic and Late Occupations at Dolores,* 81–83 Bureau of Reclamation. Denver, Colorado.

—— 1993. Cannibalism in Chaco Canyon: the channel pit excavated in 1926 at Small House Ruin by Frank H.H. Roberts, Jr. *Am.J.Phys. Anthrop.,* **91**, 421–439.

—— **& Morris, N.T.** 1970. A massacre at Hopi. *Am. Antiquity,* **35**, 320–331.

—— **& Turner, J. A.** 1990. Perimortem damage to human skeletal remains from Wupatki National Monument, northern Arizona. *Kiva,* **55**, 187–212.

—— **&** —— 1992. The first claim for cannibalism in the Southwest: Walter Hough's 1901 discovery at Canyon Butte Ruin 3, Northeastern Arizona. *Am. Antiquity,* **57** (4), 661–682

—— **&** —— 1995. Cannibalism in the prehistoric American Southwest: occurrence, taphonomy, explanation and suggestions for standardized world definition. *Anthropol.Sci.,* **103**, 1–22.

—— **&** —— 1999. *Man Corn: Cannibalism and Violence in the Prehistoric American Southwest.* University of Utah Press. Salt Lake City.

Villa, P., Bouville, C., Courtin, J., Helmer, D.. Mahieu, E., Shipman, P., Belluomini, G. & Branca, M. 1986a. Cannibalism in the Neolithic. *Science,* **233**, 431–437.

——**, Courtin, J., Helmer, D., Shipman, P. Bouville, C. & Mahieu, E.** 1986b. Un cas de cannibalisme au Néolithique. *Gallia Préhistoire,* **29**, 143–171.

—— **& Mahieu E.** 1991. Breakage patterns of human long bones. *J.hum.Evol.,* **21**, 27–48.

White T.D. 1992. *Prehistoric Cannibalism at Mancos 5MTUMR-2346* Princeton: Univ. Press, Princeton, NJ.

Bulletin of The Natural History Museum
Geology Series

Earlier Geology *Bulletins* are still in print. The following can be ordered from Intercept (address on inside front cover). Where the complete backlist is not shown, this may also be obtained from the same address.

Volume 36

No. 1 Middle Cambrian trilobites from the Sosink Formation, Derik-Mardin district, south-eastern Turkey. W.T. Dean. 1982. Pp. 1–41, 68 figs. **£5.80**

No. 2 Miscellanea

British Dinantian (Lower Carboniferous) terebratulid brachiopods. C.H.C. Brunton. 20 figs.

New microfossil records in time and space. G.F. Elliott. 6 figs.

The Ordovician trilobite *Neseuretus* from Saudi Arabia, and the palaeogeography of the *Neseuretus* fauna related to Gondwanaland in the earlier Ordovician. R.A. Fortey & S.F. Morris. 10 figs.

Archaeocidaris whatleyensis sp. nov. (Echinoidea) from the Carboniferous Limestone of Somerset and notes on echinoid phylogeny. D.N. Lewis & P.C. Ensom. 23 figs.

A possible non-calcified dasycladalean alga from the Carboniferous of England. G.F. Elliott. 1 fig.

Nanjinoporella, a new Permian dasyclad (calcareous alga) from Nanjing, China. X. Mu & G.F. Elliott. 6 figs, 1 table.

Toarcian bryozoans from Belchite in north-east Spain. P.D. Taylor & L. Sequeiros. 10 figs, 2 tables.

Additional fossil plants from the Drybrook Sandstone, Forest of Dean, Gloucestershire. B.A. Thomas & H.M. Purdy. 14 figs, 1 table.

Bintoniella brodiei Handlirsch (Orthoptera) from the Lower Lias of the English Channel, with a review of British bintoniellid fossils. P.E.S. Whalley. 7 figs.

Uraloporella Korde from the Lower Carboniferous of South Wales. V.P. Wright. 3 figs. 1982. Pp. 43–155. **£19.80**

No. 3 The Ordovician Graptolites of Spitsbergen. R.A. Cooper & R.A. Fortey. 1982. Pp. 157–302, 6 plates, 83 figs, 2 tables. **£20.50**

No. 4 Campanian and Mastrichtian sphenodiscid ammonites from southern Nigeria. P.M.P. Zaborski. 1982. Pp. 303–332, 36 figs. **£4.00**

Volume 37

No. 1 Taxonomy of the arthrodire *Phlyctaenius* from the Lower or Middle Devonian of Campbellton, New Brunswick, Canada. V.T. Young. 1983. Pp. 1–35, 18 figs. **£5.00**

No. 2 *Ailsacrinus* gen. nov., an aberrant millericrinid from the Middle Jurassic of Britain. P.D. Taylor. 1983. Pp. 37–77, 48 figs, 1 table. **£5.90**

No. 3 Miscellanea

Glossopteris anatolica Sp. nov. from uppermost Permian strata in south-east Turkey. S. Archangelsky & R.H. Wagner. 14 figs.

The crocodilian *Theriosuchus* Owen, 1879 in the Wealden of England. E. Buffetaut. 1 fig.

A new conifer species from the Wealden beds of Féron-Glageon, France. H.L. Fisher & J. Watson. 10 figs.

Late Permian plants including Charophytes from the Khuff formation of Saudi Arabia. C.R. Hill & A.A. El-Khayal. 18 figs.

British Carboniferous Edrioasteroidea (Echinodermata). A.B. Smith. 52 figs.

A survey of recent and fossil Cicadas (Insecta, Hemiptera-Homoptera) in Britain. P.E.S. Whalley. 11 figs.

The Cephalaspids from the Dittonian section at Cwm Mill, near Abergavenny, Gwent. E.I. White & H.A. Toombs. 20 figs. 1983. Pp. 79–171. **£13.50**

No. 4 The relationships of the palaeoniscid fishes, a review based on new specimens of *Mimia* and *Moythomasia* from the Upper Devonian of Western Australia. B.G. Gardiner. 1984. Pp. 173–428. 145 figs. 4 plates. 0 565 00967 2. **£39.00**

Volume 38

No. 1 New Tertiary pycnodonts from the Tilemsi valley, Republic of Mali. A.E. Longbottom. 1984. Pp. 1–26. 29 figs. 3 tables. 0 565 07000 2. **£3.90**

No. 2 Silicified brachiopods from the Viséan of County Fermanagh, Ireland. (III) Rhynchonellids. Spiriferids and Terebratulids.

C.H.C. Brunton. 1984. Pp. 27–130. 213 figs. 0 565 07001 0. **£16.20**

No. 3 The Llandovery Series of the Type Area. L.R.M. Cocks. N.H. Woodcock, R.B. Rickards, J.T. Temple & P.D. Lane. 1984.

Pp. 131–182. 70 figs. 0 565 07004 5. **£7.80**

No. 4 Lower Ordovician Brachiopoda from the Tourmakeady Limestone, Co. Mayo, Ireland. A. Williams & G.B. Curry. 1985.

Pp. 183–269. 214 figs. 0 565 07003 7. **£14.50**

No. 5 Miscellanea

Growth and shell shape in Productacean Brachiopods. C.H.C. Brunton.

Palaeosiphonium a problematic Jurassic alga. G.F. Elliott.

Upper Ordovician brachiopods and trilobites from the Clashford House Formation, near Herbertstown, Co. Meath, Ireland. D.A.T. Harper, W.I. Mitchell, A.W. Owen & M. Romano.

Preliminary description of Lower Devonian Osteostraci from Podolia (Ukrainian S.S.R.). P. Janvier.

Hipparion sp. (Equidae, Perissodactyla) from Diavata (Thessaloniki, northern Greece). G.D. Koufos.

Preparation and further study of the Singa skull from Sudan. C.B. Stringer, L. Cornish & P. Stuart-Macadam.

Carboniferous and Permian species of the cyclostome bryozoan *Corynotrypa* Bassler, 1911. P.D. Taylor.

Redescription of *Eurycephalochelys*, a trionychid turtle from the Lower Eocene of England. C.A. Walker & R.T.J. Moody.

Fossil insects from the Lithographic Limestone of Montsech (late Jurassic-early Cretaceous), Lérida Province, Spain. P.E.S. Whalley & E.A. Jarzembowski. 1985. Pp. 271–412, 162 figs. 0 565 07004 5. **£24.00**

Volume 39

No. 1 Upper Cretaceous ammonites from the Calabar region, south-east Nigeria. P.M.P. Zaborski. 1985. Pp. 1–72. 66 figs. 0 565 07006 1. **£11.00**

No. 2 Cenomanian and Turonian ammonites from the Novo Redondo area, Angola. M.K. Howarth. 1985. Pp. 73–105. 33 figs. 0 565 07006 1. **£5.60**

No. 3 The systematics and palaeogeography of the Lower Jurassic insects of Dorset, England. P.E.S. Whalley. 1985. Pp. 107–189. 87 figs. 2 tables. 0 565 07008 8. **£14.00**

No. 4 Mammals from the Bartonian (middle/late Eocene) of the Hampshire Basin, southern England. J.J. Hooker. 1986. Pp. 191–478. 71 figs. 39 tables. 0 565 07009 6. **£49.50**

Volume 40

No. 1 The Ordovician graptolites of the Shelve District, Shropshire. I. Strachan. 1986. Pp. 1–58. 38 figs. 0 565 07010 X. **£9.00**

No. 2 The Cretaceous echinoid *Boletechinus*, with notes on the phylogeny of the Glyphocyphidae and Temnopleuridae. D.N. Lewis. 1986. Pp. 59–90. 11 figs. 7 tables. 0 565 07011 8. **£5.60**

No. 3 The trilobite fauna of the Raheen Formation (upper Caradoc), Co. Waterford, Ireland. A.W. Owen, R.P. Tripp & S.F. Morris. 1986. Pp. 91–122. 88 figs. 0 565 07012 6. **£5.60**

No. 4 Miscellanea I: Lower Turonian cirripede—Indian coleoid *Naefia*—Cretaceous–Recent Craniidae—Lectotypes of Girvan trilobites—Brachiopods from Provence—Lower Cretaceous cheilostomes. 1986. Pp. 125–222. 0 565 07013 4. **£19.00**

No. 5 Miscellanea II: New material of *Kimmerosaurus*—Edgehills Sandstone plants—Lithogeochemistry of Mendip rocks—Specimens previously recorded as teuthids—Carboniferous lycopsid *Anabathra*—*Meyenodendron*, new Alaskian lepidodendrid. 1986. Pp. 225–297. 0 565 07014 2. **£13.00**

Volume 41

No. 1 The Downtonian ostracoderm *Sclerodus* Agassiz (Osteostraci: Trematapididae), P.L. Forey. 1987. Pp. 1–30. 11 figs. 0 565 07015 0. **£5.50**

No. 2 Lower Turonian (Cretaceous) ammonites from south-east Nigeria. P.M.P. Zaborski. 1987. Pp. 31–66. 46 figs. 0 565 07016 9. **£6.50**

No. 3 The Arenig Series in South Wales: Stratigraphy and Palaeontology. I. The Arenig Series in South Wales. R.A. Fortey & R.M. Owens. II. Appendix. Acritarchs and Chitinozoa from the Arenig Series of South-west Wales. S.G. Molyneux. 1987. Pp. 67–364. 289 figs. 0 565 07017 7. **£59.00**

No. 4 Miocene geology and palaeontology of Ad Dabtiyah, Saudi Arabia. Compiled by P.J. Whybrow. 1987. Pp. 365–457. 54 figs. 0 565 07019 3. **£18.00**

Volume 42

No. 1 Cenomanian and Lower Turonian Echinoderms from Wilmington, south-east Devon. A.B. Smith, C.R.C. Paul, A.S. Gale & S.K. Donovan. 1988. 244 pp. 80 figs. 50 pls. 0 565 07018 5. **£46.50**

Volume 43

No. 1 A Global Analysis of the Ordovician–Silurian boundary. Edited by L.R.M. Cocks & R.B. Rickards. 1988. 394 pp., figs. 0 565 07020 7. **£70.00**

Volume 44

No. 1 Miscellanea: Palaeocene wood from Mali—Chapelcorner fish bed—*Heterotheca* coprolites—Mesozoic Neuroptera and Raphidioptera. 1988. Pp. 1–63. 0 565 07021 5. **£12.00**

No. 2 Cenomanian brachiopods from the Lower Chalk of Britain and northern Europe. E.F. Owen. 1988. Pp. 65–175. 0565 07022 3. **£21.00**

No. 3 The ammonite zonal sequence and ammonite taxonomy in the *Douvilleiceras mammillatum* Superzone (Lower Albian) in Europe. H.G. Owen. 1988. Pp. 177–231. 0 565 07023 1. **£10.30**

No. 4 Cassiopidae (Cretaceous Mesogastropoda): taxonomy and ecology. R.J. Cleevely & N.J. Morris. 1988. Pp. 233–291. 0565 07024 X. **£11.00**

Volume 45

No. 1 Arenig trilobites—Devonian brachiopods—Triassic demosponges—Larval shells of Jurassic bivalves—Carboniferous marattialean fern—Classification of Plectambonitacea. 1989. Pp. 1–163. 0 565 07025 8. **£40.00**

No. 2 A review of the Tertiary non-marine molluscan faunas of the Pebasian and other inland basins of north-western South America. C.P. Nuttall. 1990. Pp. 165–371. 456 figs. 0 565 07026 6. **£52.00**

Volume 46

No. 1 Mid-Cretaceous Ammonites of Nigeria—new amphisbaenians from Kenya—English Wealden Equisetales—Faringdon Sponge Gravel Bryozoa. 1990. Pp. 1–152. 0 565 070274. **£45.00**

No. 2 Carboniferous pteridosperm frond *Neuropteris heterophylla*—Tertiary Ostracoda from Tanzania. 1991. Pp. 153–270. 0565 07028 2. **£30.00**

Volume 47

No. 1 Neogene crabs from Brunei, Sabah & Sarawak—New pseudosciurids from the English Late Eocene—Upper Palaeozoic Anomalodesmatan Bivalvia. 1991. Pp. 1–100. 0 565 07029 0. **£37.50**

No. 2 Mesozoic Chrysalidinidae of the Middle East—Bryozoans from north Wales—*Alveolinella praequoyi* sp. nov. from Papua New Guinea. 1991. Pp. 101–175. 0 565 070304. **£37.50**

Volume 48

No. 1 *'Placopsilina' cenomana* d'Orbigny from France and England—Revision of Middle Devonian uncinulid brachiopod—Cheilostome bryozoans from Upper Cretaceous, Alberta. 1992. Pp. 1–24. **£37.50**

No. 2 Lower Devonian fishes from Saudi Arabia—W.K. Parker's collection of foraminifera in the British Museum (Natural History). 1992. Pp. 25–43. **£37.50**

Volume 49

No. 1 Barremian—Aptian Praehedbergellidae of the North Sea area: a reconnaissance—Late Llandovery and early Wenlock Stratigraphy and ecology in the Oslo Region, Norway—Catalogue of the type and figured specimens of fossil Asteroidea and Ophiuroidea in The Natural History Museum. 1993. Pp. 1–80. **£37.50**

No. 2 Mobility and fixation of a variety of elements, in particular, during the metasomatic development of adinoles at Dinas Head, Cornwall—Productellid and Plicatiferid (Productoid) Brachiopods from the Lower Carboniferous of the Craven Reef Belt, North Yorkshire—The spores of *Leclercqia* and the dispersed spore morphon *Acinosporites lindlarensis* Riegel: a case of gradualistic evolution. 1993. Pp. 81–155. **£37.50**

Bulletin of The Natural History Museum
Geology Series

Earlier Geology *Bulletins* are still in print. The following can be ordered from Cambridge University Press or Intercept (addresses on inside front cover). Where the complete backlist is not shown, this may also be obtained from the same addresses.

Volume 50

No. 1 Systematics of the meliceritidid cyclostome bryozoans; introduction and the genera *Elea*, *Semielea* and *Reptomultelea*. 1994. Pp. 1–104. **£37.50**

No. 2 The brachiopods of the Duncannon Group (Middle-Upper Ordovician) of southeast Ireland. 1994. Pp. 105–175. **£37.50**

Volume 51

No. 1 A synopsis of neuropteroid foliage from the Carboniferous and Lower Permian of Europe—The Upper Cretaceous ammonite *Pseudaspidoceras* Hyatt, 1903, in north-eastern Nigeria—The pterodactyloids from the Purbeck Limestone Formation of Dorset. 1995. Pp. 1–88. **£37.50**

No. 2 Palaeontology on the Qahlah and Simsima Formations (Cretaceous, Late Campanian-Maastrichtian) of the United Arab Emirates-Oman Border Region—Preface—Late Cretaceous carbonate platform faunas of the United Arab Emirates-Oman border region—Late Campanian-Maastrichtian echinoids from the United Arab Emirates-Oman border region—Maastrichtian ammonites from the United Arab Emirates-Oman border region—Maastrichtian nautiloids from the United Arab Emirates-Oman border region—Maastrichtian Inoceramidae from the United Arab Emirates-Oman border region—Late Campanian-Maastrichtian Bryozoa from the United Arab Emirates-Oman border region—Maastrichtian brachiopods from the United Arab Emirates-Oman border region—Late Campanian-Maastrichtian rudists from the United Arab Emirates-Oman border region. 1995. Pp. 89–305. **£37.50**

Volume 52

No. 1 Zirconlite: a review of localities worldwide, and a compilation of its chemical compositions—A review of the stratigraphy of Eastern Paratethys (Oligocene–Holocene)—A new protorichthofenioid brachiopod (Productida) from the Upper Carboniferous of the Urals, Russia—The Upper Cretaceous ammonite *Vascoceras* Choffat, 1898 in north-eastern Nigeria. 1996. Pp. 1–89. **£43.40**

No. 2 Jurassic bryozoans from Baltów, Holy Cross Mountains, Poland—A new deep-water spatangoid echinoid from the Cretaceous of British Columbia, Canada—The cranial anatomy of *Rhomaleosaurus thorntoni* Andrews (Reptilia, Plesiosauria)—The first known femur of *Hylaeosaurus armatus* and re-identification of ornithopod material in The Natural History Museum, London—Bryozoa from the Lower Carboniferous (Viséan) of County Fermanagh, Ireland. 1996. Pp. 91–171. **£43.40**

Volume 53

No. 1 The status of '*Plesictis*' *croizeti*, '*Plesictis*' *gracilis* and '*Lutra*' *minor:* synonyms of the early Miocene viverrid *Herpestides antiquus* (Mammalia, Carnivora)—*Baryonyx walkeri*, a fish-eating dinosaur from the Wealden of Surrey—The Cretaceous-Miocene genus *Lichenopora* (Bryozoa), with a description of a new species from New Zealand. 1997. Pp. 1–78. **£43.40**

No. 2 Ordovician trilobites from the Tourmakeady Limestone, western Ireland—Ordovician Bryozoa from the Llandeilo Limestone, Clog-y-fran, near Whitland, South Wales—New Information on Cretaceous crabs. 1997. Pp.79–139. **£43.40**

Volume 54

No. 1 The Jurassic and Lower Cretaceous of Wadi Hajar, southern Yemen—Ammonites and nautiloids from the Jurassic and Lower Cretaceous of Wadi Hajar, southern Yemen. 1998. Pp. 1–107. **£43.40**

No. 2 Caradoc brachiopods from the Shan States, Burma (Myanmar)—A review of the stratigraphy and trilobite faunas from the Cambrian Burj Formation in Jordan—The first Palaezoic rhytidosteid: *Trucheosaurus major* (Woodward, 1909) from the late Permian of Australia, and a reassessment of the Rhytidosteidae (Amphibia, Temnospondyli)—The rhynchonellide brachiopod *Isopoma* Torley and its distribution. 1998. Pp.109–163. **£43.40**

Volume 55

No. 1 Latest Paleocene to earliest Eocene bryozoans from Chatham Island, New Zealand. 1999. Pp. 1–45. **£43.40**

No. 2 A new stylophoran echinoderm, *Juliaecarpus milnerorum*, from the late Ordovician Upper Ktaoua Formation of Morocco—Late Cretaceous-early Tertiary echinoids from northern Spain: implications for the Cretaceous-Tertiary extinction event. 1999. Pp 47–137. **£43.40**

Volume 56

No. 1 A review of the history, geology and age of Burmese amber (Burmite—A list of type and figured specimens of insects and other inclusions in Burmese amber—A preliminary list of arthropod families present in the Burmese amber collection at The Natural History Museum, London—The first fossil prosopistomatid mayfly from Burmese amber (Ephemeroptera; Prosopistomatidae)—The most primitive whiteflies (Hemiptera; Aleyrodidae; Bernaeinae subfam. nov.) from the Mesozoic of Asia and Burmese amber, with an overview of Burmese amber hemipterans—A new genus and species of Lophioneuridae from Burmese amber (Thripida (=Thysanoptera): Lophioneurina),—*Burmapsilocephala cockerelli*, a new genus and species of Asiloidea (Diptera) from Burmese amber—Phantom midges (Diptera: Chaoboridae) from Burmese amber—An archaic new genus of Evaniidae (Insecta: Hymenoptera) and implications for the biology of ancestral evanioids—Digger Wasps (Hymenoptera, Sphecidae) in Burmese Amber—*Electrobisium acutum* Cockerell, a cheiridiid pseudoscorpion from Burmese amber, with remarks on the validity of the Cheiridioidea (Arachnida, Chelonethi). 2000. Pp. 1–83. **£43.40**

No. 2 *Terebratula californiana* Küster, 1844, and reappraisal of west coast north American brachiopod species referred to the genus *Laqueus* Dall, 187—Late Campanian-Maastrichtian corals from the United Arab Emirates-Oman border region—*Rhombocladia dichotoma* (M'Coy, 1844) [Fenestrata, Bryozoa]: designation of a lectotype—The Gough's Cave human fossils: an introduction—The Creswellian (Pleistocene) human axial skeletal remains from Gough's Cave (Somerset, England)—The Creswellian (Pleistocene) human lower limb remains from Gough's Cave (Somerset, England). 2000. Pp. 85–161. **£43.40**

Volume 57

No. 1 Fossil pseudasturid birds (Aves, Pseudasturidae) from the London Clay—*Novocrania*, a new name for the genus *Neocrania* Lee & Brunton, 1986 (Brachiopoda, Craniida), preoccupied by *Neocrania* Davis, 1978 (Insecta, Lepidoptera)—The Creswellian (Pleistocene) human upper limb remains from Gough's Cave (Somerset, England)—Gough's Cave 1 (Somerset, England): a study of the hand bones—A revision of the English Wealden Flora, III: Czekanowskiales, Ginkgoales & allied Coniferales. 2001. Pp. 1–82. **£43.40**

No. 2 The Cenozoic Brachiopod *Terebratula*: its type species, neotype, and other included species—Gough's Cave 1 (Somerset, England): a study of the pectoral girdle and upper limbs—Systematic affinity of *Acroporella assurbanipali* Elliott (Dasycladaceae), with notes on the genus *Neomeris* Palynological zonation of Mid-Palaeozoic sequences from the Cantabrian Mountains, NW Spain: implications for inter-regional and interfacies correlation of the Ludford/Přídolí and Silurian/Devonian boundaries, and plant dispersal patterns. 2001. Pp. 83–162. **£43.40**

Volume 58

No. 1 Gough's Cave 1 (Somerset, England): a study of the axial skeleton—Upper Ordovician brachiopods from the Anderken Formation, Kazakhstan: their ecology and systematics. 2002. Pp. 1–80.

No. 2 The Lower Lias of Robin Hood's Bay, Yorkshire, and the work of Leslie Bairstow—The human cranial remains from Gough's Cave (Somerset, England). 2002. Pp. 81–168. **£43.40**

CONTENTS

CAMBRIDGE
UNIVERSITY PRESS
www.cambridge.org

0968-0462(200306)58+;1-L

Bulletin of The Natural History Museum

GEOLOGY SERIES

Vol. 58, Supplement, June 2003


Riley Dunn & Wilson Ltd